

**DEVELOPING CRITERIA TO ASSESS THE RESISTANCE AND
HYDROLOGIC STABILITY OF DESERT SPRINGS IN THE FACE OF A
CHANGING CLIMATE**

by

Zachary P. Meyers

A Dissertation

Submitted to the Faculty of Purdue University

In Partial Fulfillment of the Requirements for the degree of

Doctor of Philosophy



Department of Earth, Atmospheric, and Planetary Sciences

West Lafayette, Indiana

August 2020

**THE PURDUE UNIVERSITY GRADUATE SCHOOL
STATEMENT OF COMMITTEE APPROVAL**

Dr. Kenneth Ridgway, Chair

Department of Earth, Atmospheric, & Planetary Sciences, Purdue University

Dr. Marty Frisbee

Department of Earth, Atmospheric, & Planetary Sciences, Purdue University

Dr. Laura Rademacher

Department of Geological and Environmental Sciences, University of the Pacific

Dr. Brian Hedlund

School of Life Sciences, University of Nevada, Las Vegas

Dr. Marc Caffee

Department of Physics and Astronomy & Department of Earth, Atmospheric, & Planetary Sciences,
Purdue University

Approved by:

Dr. Daniel Cziczo

I dedicate this dissertation to Jordyn, Noah, Carolyn, and Sara- true friends and collaborators that have supported and inspired me throughout this process.

That deep silence has a melody of its own, a sweetness unknown amid the harsh discords of the world's sounds. – Paul Brunton

ACKNOWLEDGMENTS

My time at Purdue has been one of growth and development, academically and personally. My ability to complete this dissertation would not have been possible without numerous individuals and means of support.

This research was primarily funded by the National Science Foundation (NSF) Grants EAR 1516127 and EAR 1516698 under the project, “Collaborative Research: Tectonic and climatic forcing of hydrological systems in the southern Great Basin: Implications for ancient and future aquatic system resilience”. I have also received support from the Purdue Graduate School and the EAPS department in the form of the Purdue Doctoral Fellowship and the Bilsland Dissertation Fellowship. External awards have made additional research opportunities possible. I would like to acknowledge the Daryll Leap Hydrogeology Grant, the Terry R. West Scholarship, and the Chevron Cooperation Scholarship for providing me with additional support that allowed me to conduct extra studies and travel to my study area. During the IES project we also received support from numerous permitting agencies which made all this work possible. I would like to acknowledge the Los Angeles Department of Water & Power, Inyo National Forest, Ash Meadows National Wildlife Refuge, the Bureau of Land Management, and the Spring Mountains National Recreation Area, Humboldt-Toiyabe National Forest, I would especially like to acknowledge Death Valley National Park (specifically, Genni, Richard, and Josh) for their help and cooperation in allowing access and sampling permissions in remote and sensitive locations in the park, providing assistance to equipment and sample storage, and helping with additions of new springs.

I would like to start by thanking my primary advisor and mentor, Dr. Marty Frisbee. Marty and I have come a long way together and I will always be grateful to him for giving me the opportunity to work and become a collaborator on this project. In doing so, he unknowingly fostered a deep connection and respect that I now have for both deserts and springs, two things I had rarely thought about before this experience. To me, this is an invaluable gift and will likely shape the rest of my life. Marty also taught me the value of asking probing scientific questions, how to think creatively, and the importance of calm, peaceful observation and contemplation of the landscape. I am thankful to Marty for always providing me with guidance, direction, and a “playing field” for my research, yet letting me shape the dissertation of my choosing. I have come

away from my graduate experience with a deep respect for Marty's tenacious curiosity and unique ability as a scientist to ask the right questions.

Secondly, I would like to thank Dr. Laura Rademacher, who served as an unofficial co-advisor to me on this project. I'm grateful to Laura for always listening when I needed to talk. Laura always provided the most thoughtful, reasoned advice, both on research and in personal matters. Though she may not know it, Laura's consummate professionalism has taught me to think more about inclusion and how my actions (or nonactions) can impact others. I really cannot thank Laura enough for her mentorship and friendship. From a research perspective, not only did Laura's past (and ongoing) work have a profound effect on me, but Laura's demand for excellence undoubtedly improved this dissertation.

Each of my other committee members have been integral components of this dissertation and of my academic development while at Purdue. It has been a real pleasure to work collaboratively with Dr. Brian Hedlund. While he may never forgive me for leading him on two death marches (extremely long and brutal hikes) during fieldwork in the Death Valley area, collaborating with he and Don Sada on this project has been extremely innovative and exciting from a scientific perspective. I have really enjoyed spending so much time in the field learning from Brian and becoming a little bit more familiar with his expertise.

Dr. Ken Ridgway's classes were a rude awakening and a rough transition from my undergraduate curriculum, but *Basin Analysis* and *Crustal Tectonics* were truly some of the best classes I have ever had. Ken got me thinking about large scale, regional tectonics in a whole new conceptual way and really developed my confidence in this area. Without his instruction, navigating the geology of the southern Basin and Range would have been a lot more difficult. From an academic perspective, I can think of very few classes that were more influential and Ken is truly one of the best lecturers I have had the privilege of learning from.

I would like to thank Dr. Marc Caffee for coming on board to my committee in my fourth year. Dr. Caffee helped immensely in shepherding our ^{36}Cl samples through PRIME lab and providing instrumental expertise in areas such as ^{36}Cl cycling in vegetation and the application of bomb-pulse tracers to hydrologic applications here in Indiana. Feedback that Dr. Caffee provided during my preliminary exam and committee meetings was instrumental in improving this dissertation.

I would like to thank all of the members of the IES hydro-bio team, specifically Ariel Friel, Khaled Pordel, John Umek, and Don Sada for field assistance and excellent collaboration. We embarked together on a challenging, interdisciplinary project and though we suffered a countless number of popped tires, scraped vehicles (cringe), and sandy boots, we came out of this project with some really interesting and novel results.

Much of the inspiration and energy funneled into this dissertation stems from highly positive interactions with my immediate peers and friends within the EAPS department. I would like to specifically mention my labmates Noah Stewart-Maddox, Carolyn Gleason, and Jordyn Miller who not only put up with my craziness, but accepted me for it. Together, the four of us had an unforgettable trip to the Panamints and I was fortunate enough to share amazing field experiences individually with the three of the them. I would also like to thank Will Odom, Sara Warix, and Mario Caccia for their unwavering friendship and support during the past five years.

Lastly, I would like to thank my family, specifically my parents (Tilden and Venetia), my brother (Alex), and my sister and her husband (Jane and Hodie). My parents have never given up on me and always encouraged me to do my best. I have been extremely lucky to have such a support system throughout this process. The older I get, the more I appreciate how fortunate I am. I cannot wait to spend more time with all of you.

TABLE OF CONTENTS

LIST OF TABLES	15
LIST OF FIGURES	16
ABSTRACT.....	31
CHAPTER 1. INTRODUCTION	32
1.1 Spring systematics	32
1.2 The importance of desert springs.....	34
1.3 Desert springs are in decline.....	36
1.4 Motivation and overarching question	40
1.5 Site Description.....	42
1.5.1 Study Area Extent and Regional Geography.....	42
1.5.2 Geologic Overview	42
1.5.3 Climate and Hydrology.....	46
1.6 Organization of the Dissertation	47
1.7 Chapter Descriptions.....	47
1.8 References.....	51
CHAPTER 2. AN ALTERNATIVE DATA PREPROCESSING METHOD FOR GENERATING GEOCHEMICAL CLUSTERS FROM MAJOR ION DATA.....	60
2.1 Abstract.....	60
2.2 Introduction.....	61
2.2.1 What is useful about water chemistry data?	61
2.2.2 Why do people cluster or group water chemistry data?	61
2.2.3 What are the different types of clustering and what are their strengths?.....	62
2.2.4 What are the problems with current clustering workflows and what will be gained by this study?	63
2.3 Methods.....	65
2.3.1 Workflow using traditional methodology.....	65
2.3.2 Alternative data preprocessing methodology	67
2.3.3 Case Studies.....	68
2.3.3.1 Owens Valley (CA).....	68

2.3.3.2 The Spring Mountains (NV)	71
2.4 Results.....	72
2.4.1 Owens Valley Case Study	72
2.4.1.1 Traditional Preprocessing Results	74
2.4.1.1 Alternative Preprocessing Results	76
2.4.2 Spring Mountains Case Study	77
2.4.2.1 Traditional Preprocessing Results	77
2.4.2.2 Alternative Preprocessing Results	81
2.5 Discussion.....	82
2.5.1 Owens Valley Case Study	82
2.5.2 Spring Mountains Case Study	84
2.5.3 Commentary on both methods and case study results	86
2.6 Conclusions.....	88
2.7 References.....	90
CHAPTER 3. OLD GROUNDWATER BUFFERS THE EFFECTS OF A MAJOR DROUGHT IN GROUNDWATER-DEPENDENT ECOSYSTEMS OF THE EASTERN SIERRA NEVADA (USA)	95
3.1 Abstract.....	95
3.2 Introduction.....	95
3.3 Methods.....	102
3.3.1 Study area and spring sampling.....	102
3.3.2 General chemistry collection and analysis	103
3.3.3 Tritium collection and analysis.....	103
3.3.4 Chlorine-36 collection and analysis.....	103
3.3.5 Age partitioning.....	104
3.3.6 Vegetation indices for monitoring GDEs	105
3.3.7 Extraction and smoothing of NDVI data and creation of NDVI metrics	106
3.4 Results and Discussion	107
3.4.1 Drought progression in Owens Valley and the effect on streamflow.....	107
3.4.2 The origin of salinity in Owens Valley spring waters	108
3.4.3 ³⁶ Cl/Cl in spring waters and vegetation.....	110

3.4.4	Comparison of vegetation metrics and age partitions.....	112
3.4.5	Spring vegetation supplied by modern groundwater affected the most	115
3.5	Conclusions.....	116
3.6	References.....	117
CHAPTER 4. THE EFFECT OF SPATIAL SCALE AND TIME ON GEOCHEMICAL		
EVOLUTION INFERRED FROM SPRINGS IN THE SOUTHEASTERN SIERRA NEVADA,		
USA: REVISITING GARRELS AND MACKENZIE (1967).....		
		123
4.1	Abstract.....	123
4.2	Introduction.....	124
4.3	Study Area	127
4.3.1	Regional geography.....	127
4.3.2	Climate and precipitation.....	127
4.3.3	Hydrology.....	129
4.4	Geology.....	129
4.4.1	General overview.....	129
4.4.2	Bishop AOI.....	131
4.4.2.1	Wheeler Crest	131
4.4.2.2	Mount Tom and the Tungsten Hills.....	133
4.4.2.3	Bishop Tuff.....	133
4.4.3	Big Pine AOI	133
4.4.3.1	Warren Bench.....	136
4.4.3.2	Birch Mountain.....	136
4.4.4	Independence AOI.....	136
4.4.4.1	Lookout Point	137
4.4.4.2	Seven Pines.....	137
4.4.5	Lone Pine AOI.....	137
4.4.5.1	The Mount Whitney Intrusive Suite	138
4.4.5.2	The Alabama Hills.....	138
4.5	Methods.....	139
4.5.1	Field sampling procedures.....	139
4.5.2	Stable isotopes of water ($\delta^2\text{H}$ and $\delta^{18}\text{O}$).....	141

4.5.3	General chemistry	142
4.5.4	$^{87}\text{Sr}/^{86}\text{Sr}$ analyses and rock leaching of $^{87}\text{Sr}/^{86}\text{Sr}$	142
4.5.5	Tritium (^3H).....	143
4.5.6	Chlorine-36 (^{36}Cl).....	144
4.5.7	Noble Gases.....	144
4.5.8	Radiocarbon (^{14}C).....	146
4.5.9	Geochemical modeling	149
4.5.10	Partitioning young and old groundwater with ^3H , ^{36}Cl , and ^{14}C	151
4.6	Results.....	152
4.6.1	Field observations.....	152
4.6.2	Stable isotope observations.....	154
4.6.3	General Chemistry	156
4.6.4	Saturation indices, stability diagrams, and inverse geochemical models.....	163
4.6.5	Chloride, Chloride/Bromide, and Chlorine-36.....	165
4.6.6	Strontium and $^{87}\text{Sr}/^{86}\text{Sr}$	166
4.6.7	Noble gas and radiocarbon trends among all springs.....	170
4.6.8	Age partitioning and spring residence times	176
4.6.9	Age partitioning trends	178
4.7	Discussion.....	181
4.7.1	Spring sourcing and contributing areas	181
4.7.1.1	Spring temperature	181
4.7.1.2	Stable isotopes of spring waters as indicators of the geographic extent of recharge	181
4.7.1.3	Noble gas recharge parameters	182
4.7.2	The influence of local geology on geochemistry.....	183
4.7.3	Excess calcium in intermediate scale groundwaters.....	185
4.7.4	The influence of groundwater residence time	186
4.8	Conclusions.....	191
4.9	References.....	191

CHAPTER 5. EXAMINING LANDSCAPE PLACEMENT AND EMERGENCE MECHANISM AS CONTROLS ON SPRING HYDROCHEMICAL CHARACTERISTICS AND ECOLOGICAL COMMUNITY STRUCTURE.....	199
5.1 Abstract.....	199
5.2 Introduction.....	200
5.3 Methods.....	205
5.3.1 Defining the regional study area.....	205
5.3.2 Creation of a regional geochemical spring dataset.....	206
5.3.3 Recent sampling efforts.....	209
5.3.4 Topographic analysis and indices.....	210
5.3.4.1 Elevation data acquisition and processing.....	210
5.3.4.2 Creating a topographic classification.....	211
5.3.4.3 Quantitative analysis and indices.....	214
5.3.4.3.1 Elevation and slope.....	214
5.3.4.3.2 Topographic Wetness Index (TWI).....	214
5.3.4.3.3 Relative elevation.....	215
5.3.4.3.4 Curvature.....	215
5.3.5 Identifying springs emerging at fault zones.....	218
5.3.6 BMI analysis and indices.....	218
5.3.6.1 Non-metric multidimensional scaling (NMDS) analysis.....	220
5.3.6.2 Ecological metrics and indices.....	221
5.4 Results.....	222
5.4.1 Relationship between qualitative spring landscape placement classification and hydrochemical characteristics.....	222
5.4.2 Relationship between quantitative topographic metrics and hydrochemical characteristics.....	223
5.4.3 Relationship between emergence mechanism and hydrochemical characteristics..	230
5.4.4 NMDS results.....	232
5.4.5 Relationships with hydrochemical characteristics and ecological indices.....	236
5.5 Discussion.....	238
5.5.1 Systematic trends with landscape placement and hydrochemical characteristics ...	238

5.5.2	Scaling relationships and factors controlling BMI community structure	239
5.5.3	Conceptual model of spring systems in the southern Great Basin	240
5.6	Conclusions.....	242
5.7	References.....	244
CHAPTER 6. IS TEMPORAL VARIABILITY AN INDICATOR OF GROUNDWATER		
RESIDENCE TIME? TALES FROM THE SOUTHERN GREAT BASIN.....		
6.1	Abstract.....	253
6.2	Introduction.....	254
6.2.1	Temporal variability in hydrologic studies.....	254
6.2.2	A lack of temporal variability studies of groundwater	255
6.2.3	Why study temporal variability in spring?	257
6.2.4	Goals of the study and overarching research question	258
6.3	Methods.....	262
6.3.1	Site description	262
6.3.2	Sampling.....	265
6.3.2.1	Discharge temperature.....	265
6.3.2.2	Major ions	266
6.3.2.3	Trace elements.....	266
6.3.2.4	Strontium isotopes.....	267
6.3.2.5	Stable isotopes.....	267
6.3.2.6	Age-dating environmental tracers (^3H , ^{14}C , ^{36}Cl).....	269
6.3.3	Examining variability	270
6.3.3.1	Standard deviation and coefficient of variation.....	270
6.3.3.2	Principal Component Analysis (PCA) and Hierarchical Clustering Analysis (HCA)	271
6.4	Results.....	272
6.4.1	Discharge temperature	272
6.4.2	Major ions	276
6.4.3	Trace elements	282
6.4.4	$^{87}\text{Sr}/^{86}\text{Sr}$ variability	285
6.4.4.1	$^{87}\text{Sr}/^{86}\text{Sr}$ regional framework.....	285

6.4.4.3 $^{87}\text{Sr}/^{86}\text{Sr}$ variability	286
6.4.5 Stable isotopes of water ($\delta^2\text{H}$ and $\delta^{18}\text{O}$)	288
6.4.5.1 Regional framework	288
6.4.5.2 Overall variability and (lack of) correlations.....	291
6.4.5.3 Temporal water stable isotope variability within Ash Meadows	293
6.4.5.4 Isotopic shifting over time	295
6.4.6 Age-dating environmental tracers.....	298
6.4.7 Variability matrix: synthesis of results	301
6.5 Discussion	304
6.5.1 Overall springs are very stable	304
6.5.2 Springs that show changes across multiple variables	307
6.5.3 Ecological significance of highly variable springs	311
6.5.4 Stable isotope variability: response to a drought, long-term shifting, or other?.....	315
6.6 Conclusions.....	318
6.7 References	319
CHAPTER 7. CONCLUSIONS AND RECOMMENDATIONS	329
7.1 Epilogue	329
7.2 Synthesis and Recommendations.....	330
7.2.1 Alternative preprocessing methodology for geochemical clustering	331
7.2.2 Metrics that describe spring resistance	332
7.2.3 Metrics that are related to groundwater residence time.....	333
7.2.3.1 Extending Feth et al. (1964) and Garrels and Mackenzie (1967).....	333
7.2.3.2 Spring landscape position and emergence mechanism.....	334
7.2.3.4 Spring temporal variability.....	335
7.2.4 An invaluable baseline.....	337
7.2.5 A synthesis of spring vulnerability metrics	337
7.3 References.....	338

LIST OF TABLES

Table 4.1. Petrologic data for likely plutons supporting flow to springs in Owens Valley (CA).	140
Table 4.2. Additional units supporting springflow that do not have petrologic data.....	141
Table 4.3. Locations and field geochemical data for springs in Owens Valley (CA).	154
Table 4.4. General chemistry data and geochemical groupings for Owens Valley springs.	162
Table 4.5. Raw isotope data, corrected radiocarbon ages, and age partition distinctions for Owens Valley springs.	170
Table 4.6. Raw noble gas data and derived parameters from Noble90 for the Owens Valley springs.	173
Table 6.1: Table showing springs included in temporal analyses. An “X” denotes whether a spring was sampled enough for a particular metric to be included in temporal analysis. The total number of springs analyzed for a particular metric is shown in the last row.....	273

LIST OF FIGURES

- Figure 1.1. Chart showing residence time coverage of environmental tracers. Figure reproduced as published in Cartwright et al. (2017). 34
- Figure 1.2. Conceptual diagram showing how desert springs are integral components to many aspects of human life and to ecological systems. 35
- Figure 1.3. Examples of spring disturbance. A) Buck Spring (IES-006) altered by the construction of a spring box. B) Kiup Spring (IES-004) showing restoration efforts to increase native vegetation after disturbance. C) Warm Spring A (IES-031) disturbed by livestock grazing. D) China Garden Spring (IES-035) disturbed by introduction of non-native species. 37
- Figure 1.4. Figures showing the effects of climate change in the southern Great Basin since 1970. A) Temperature anomalies in the southern Great Basin since 1970 from NOAA (<https://www.ncdc.noaa.gov/cag/>) for 37.3° N, 118.7° W. B) Changes in annual precipitation since 1970 at three representative peaks in the southern Great Basin from PRISM (Parameter-elevation Regressions on Independent Slopes Model) data (<https://prism.oregonstate.edu/explorer/>): 1) Mt Tom (eastern Sierra Nevada), 2) Telescope Peak (Panamint Range), and 3) Mt Charleston (Spring Mountains) (PRISM Climate Group, Oregon State University, <http://prism.oregonstate.edu>, created 21 Feb 2020). 39
- Figure 1.5. Bar graph (top) and regional map (bottom) showing the timing and distribution of spring sampling across the southern Great Basin. 41
- Figure 1.6. Map showing simplified geologic units and major structural features of the study region. Adapted from Lutz et al. (2017). 45
- Figure 2.1. Conceptual diagram showing common analysis pathways when using water chemistry data for hydrological reconnaissance. Preliminary analysis of water chemistry data often falls under three categories; graphical, multivariate, and geospatial. Subcategory headings show specific plots, techniques, or algorithms associated with each category. Finding ways to combine multiple analysis pathways can be very powerful and elicit hidden information. For example, the program *Geostiff* (Boghici and Boghici, 2001) combines graphical and geospatial methods. In this paper we present an approach which combines graphical and multivariate methods (i.e., uses concepts of graphical tools in inform multivariate data preprocessing treatment). Results from this approach can then be imported into a geospatial platform to explore spatial relationships. 63
- Figure 2.2. Conceptual diagram showing a generalized interpretation of a “patterned” or “sequential” workflow commonly used to evaluate water chemistry data. This workflow has a lot of steps to ensure quality control and robustness. One problem, however, is that changes in data preprocessing have a large effect on the results derived from multivariate analysis, thus affecting the rest of the workflow. 65
- Figure 2.3. Simplified geologic map of the eastern Sierra Nevada in Owens Valley, CA. Spring sample locations are marked on the map. Springs are symbolized by shape to indicate data preprocessing technique and by color to indicate the geochemical group. Traditional preprocessing groups are show as triangles while alternative preprocessing groups are shown as circles. Lines on

the map indicate geologic cross sections (see Chapter 4). Regional boxes on the map around the springs indicate areas where we present an additional figure to zoom in on the geologic connections to springs (Figure 2.5)..... 70

Figure 2.4. This figure summarizes the geochemical differences between the traditional (OVT) and alternative (OVA) preprocessing results for springs in Owens Valley. OVT results are presented in section A and OVA results are presented in section B. Each section contains a dendrogram with the agglomerative clusters shaded by color. The phenon lines depict where the dendrograms are cut. Every spring has an associated stiff diagram and a point in the Piper diagram. Boxes next to the stiff diagrams show TDS ranges for each group of springs..... 73

Figure 2.5. Zoomed-in geologic maps associated with the boxes in Figure 2.3. Spring locations are denoted and springs are symbolized by shape (preprocessing technique) and color (geochemical group). White dotted lines indicate connection of Group OVA-1 springs to Penn-Permian metasedimentary roof pendants directly upgradient. 75

Figure 2.6. This plot is similar to Figure 2.4 and shows the geochemical clustering results for the Spring Mountain springs using traditional (SMT) and alternative (SMA) preprocessing methods. SMT results are depicted as triangles and shown in subplots A, B, and C. SMA results are depicted as circles and shown in subplots E, F, and G. Each preprocessing method depicts a dendrogram showing all springs, the pheneon line, and the resulting agglomerative clusters shaded by color. We also include geologic maps showing all samples symbolized by preprocessing type and geochemical group. The geologic map legend is shown in Subplot 2.6G. The geologic map in subplot 2.6B shows minor faults and a cross section line associated with the cross section in subplot 2.6D. The inset geologic map in subplot 2.6B shows a simplified geologic map. The geologic map in subplot 2.6F shows the major thrust faults. The inset map in subplot 2.6F shows a shaded DEM with 500m contour lines to show elevation (meters). Subplots 2.6C and 2.6G show stiff diagrams of the cluster centroids and Piper diagrams showing all samples shaded by geochemical group. We interpret the geochemical relationships among cluster centroids with annotations between stiff diagrams in Figure 2.6G. The cross section in Subplot 5D is adapted from Page et al., (2005) and Warix et al., (2020). 78

Figure 2.7. Histograms of specific conductance for Owens Valley springs (left) and Spring Mountain springs (right) used in the clustering analysis. The Spring Mountain springs more closely resemble a normal distribution..... 83

Figure 2.8. Stacked histograms of SMT springs (top) and SMA springs (bottom) showing the number of springs emerging from a geologic unit in each geochemical group. Colors on the stacked histograms are associated with the geologic units in the legend and in the Spring Mountains geologic map. Overall, SMA geochemical clusters are more closely associated to the emergence geology than the SMT geochemical clusters. 86

Figure 2.9. Conceptual figure showing a suggested workflow based on the findings from this study. 89

Figure 3.1. Birds-eye imagery (Google Earth, 2019) and complementary field photographs of spring-dependent vegetation along the eastern Sierra Nevada in Owens Valley (CA). Drought evasive vegetation, present around springs and the riparian areas surrounding streams, is green and lush in contrast to drought tolerant vegetation on alluvial slopes (Elmore et al., 2003). A & B

correspond to IES-043, South Harry Birch Spring. C & D correspond to the confluence area of IES-037 & IES-038, Wells Meadow. 98

Figure 3.2. The inset map shows the study area, the Mono-Owens Lake watershed (HUC 180901), shaded in white in the regional context of CA and NV. The dark grey area within HUC 180901 represents the area depicted in the larger map. The larger map depicts orthoimagery of the Owens Valley region within the Mono-Owens Lake watershed (outlined in black) lying east of the Sierra Nevada and west of the southern extent of the Basin and Range. OL represents the Owens Lake subwatershed of HUC 180901 and CL represents the Crowley Lake subwatershed. Light blue circles represent spring sampling locations from a spring 2016 hydrological field campaign. Bishop Creek, a major stream draining the Sierra Nevada, is shown in cyan. A hydrograph for Bishop Creek spanning the duration of the drought is shown in Figure 3.4. Known faults are shown by the small black lines and streams are shown by the small blue lines. Contour lines representing 2000m, 3000m, and 4000m are shown in the red, orange, and yellow lines, respectively..... 100

Figure 3.3. Example NDVI time series extracted from Landsat 7 multispectral imagery of an “old” (IES-031) and a “young” (IES-029) spring. The blue circles represent the Raw 32-Day Composite NDVI data prior to smoothing. The black line represents a smoothed fit of the data using a moving window, weighted, least-squares approach to temporal NDVI smoothing used by the USGS (Swets et al., 1999). Annual peak NDVI values are shown by the red circles. In the lower figures, a trendline is displayed showing the linear regression fitted to annual peak NDVI over the course of the drought. The slope of this line is one of our calculated metrics designed to measure spring groundwater-dependent vegetation response to drought duration. 107

Figure 3.4. Combined watershed drought severity area plot and hydrograph (Bishop Creek) for the duration of the drought. Stacked area plot depicts the drought summary for HUC 180901 from 2011-2017. The drought summary shows the percent area of the watershed experiencing different levels of drought intensity as defined by the USDM (U.S. Drought Monitor: <http://droughtmonitor.unl.edu/>). D0, D1, D2, D3, and D4 stand for Abnormally Dry, Moderate Drought, Severe Drought, Extreme Drought, and Exceptional Drought, respectively. Below, a hydrograph for Bishop Creek, a major stream draining the Eastern Sierra crest, is shown during the same interval. 109

Figure 3.5. Spring samples are represented by the blue circles. A) Relationship between log Cl⁻ concentration and Cl⁻/Br⁻ ratio for spring waters. Springs below the black line are indicative of natural waters unaffected by halite dissolution (Cl⁻/Br⁻ ≤ ~300). Two springs well above the line are Boron Spring A (IES-027) and Boron Spring B (IES-025). B) Relationship between log Cl⁻ concentration and log ³⁶Cl/Cl. Preanthropogenic background ³⁶Cl/Cl ratios in groundwater from Davis et al. (2003) are shown in the blue bounding box. Springs dilute with respect to chloride have elevated, bomb-pulse ³⁶Cl/Cl. C) Relationship between ³⁶Cl/Cl ratio and ³H (TU). This plot shows separation and potential mixing lines between submodern, bomb-pulse, and modern spring waters based on ³⁶Cl/Cl ratios and ³H concentration. 111

Figure 3.6. Bar plot combining residence time environmental tracer data with the results of metrics derived from NDVI time series analysis. Sampled springs are shown on the x-axis and are ordered from lowest tritium concentration on the left to highest tritium concentration on the right. Tritium values (in TU) are also displayed by the blue bars. The left to right trend approximately corresponds to increased amounts of young water. Springs within the solid black box have a TU < 0.2 and are binned as “old”. The coral bars represent the linear regression fitted to the slope of

annual peak NDVI from 2011-2016 $\times 10^5$. The grey bars represent the standard deviation in annual peak NDVI from 2011-2016 $\times 10^2$. $^{36}\text{Cl}/\text{Cl}$ ratios $\times 10^{-15}$ are shown in the black boxes. IES-026, which is interpreted as receiving part of its flow from leakage along the LAA is more susceptible to reductions in surface water flow (Figure 3.4) and has the highest values for both metrics. Notice that while the other “young” springs have elevated $^{36}\text{Cl}/\text{Cl}$ ratios indicative of bomb pulse waters, IES-026 has a low value consistent with modern precipitation. Overall, the “young” springs with $\text{TU} > 0.2$ and bomb-pulse $^{36}\text{Cl}/\text{Cl}$ ratios exhibit greater interannual variability in their spring-related vegetation and persistent peak NDVI decline over the course of the drought than the springs with smaller amounts of modern water. The dotted lines intersecting the “young” springs represent the maximum metrics observed in the old springs and provide a means of comparison between the two groups..... 113

Figure 3.7. Boxplots summarizing the results for “old” and “young” spring water bins from Figure 3.6. The central mark in each box represents the median value. The bottom and top extent of each box represent the 25th and 75th percentiles, respectively. The whiskers extend to the maximum and minimum data points not considered outliers. Outliers are represented by the “+” symbols. As given in Figure 3.6 and summarized in this plot, springs classified as “old” had less negative slopes and smaller standard deviations of peak NDVI over the course of the drought when compared to the “young” springs. The chloride boxplot excludes IES-025, a basinal brine with 264 mg/L, from the “young” springs..... 116

Figure 4.1: Conceptual model for geochemical evolution at intermediate scales as shown by mountain block and mountain front springs. Geochemical overprinting by basinal brines and alluvial material can obscure the relationship between flowpath length, residence time, and geochemical evolution. A) Feth (1964) and Garrels and Mackenzie (1967) provide a conceptual model at local scales describing the processes controlling chemical evolution from ephemeral to perennial springs in the Sierra Nevada (CA). Rademacher et al. (2001) and (2005) quantified the relationship between residence time and chemical evolution at local scales showing linear evolutionary trends with mineral weathering and residence time (inset “Local”). B) At intermediate, mountain block scales this relationship is hard to quantify and poorly understood (inset “Intermediate”). 126

Figure 4.2.: Map showing locations and sample IDs (IES-###) of sampled springs in Owens Valley, CA within the Crowley Lake and Owens Lake watersheds. Eastern and western map boundaries correspond to watershed divides. Map outline location within California is highlighted on the inset map. Elevation data for the study area was acquired from The National Map (TNM), a part of the USGS National Geospatial Program..... 128

Figure 4.3.: Simplified geologic map of Owens Valley with major petrologic compositions and significant geologic units (e.g., the Bishop Tuff) grouped by color. This geologic map was created by simplifying units across 10 geologic quadrangles. For granitic plutons, color ranges from light pink (alaskite) to dark purple (mafic rocks like diorite, quartz diorite, and hornblende gabbro). This color scheme is adapted from Bateman (1964). Spring locations are symbolized by their spring geochemical groupings. Four geologic areas of interest (AOIs) are shown in the black rectangles. Cross section lines are shown in the black lines across each geologic AOI. These lines correspond to cross sections in Figure 4.5..... 132

Figure 4.4.: Zoomed-in geologic maps showing geologic AOIs, springs symbolized by geochemical grouping, and hypothesized connections (white dashed lines) to Group 4 springs (blue

squares) from Paleozoic metasedimentary roof pendants (blue geologic units). A) Bishop AOI with Wheeler Crest, Mount Tom, Tungsten Hills subregions shown, B) Big Pine AOI with Warren Bench and Birch Mountain subregions shown C) Independence AOI with Lookout Point and Seven Pines subregions show, and C) Lone Pine AOI with Mt Whitney Intrusive Suite and Alabama Hills subregions shown..... 134

Figure 4.5.: Simplified geologic cross sections across transects outlined in Figure 3. The cross sections are described as follows: A) A transect across the Pine Creek Pendant into Round Valley, CA. Cross section adapted from Bateman et al. (1963), B) A transect through the Big Pine AOI from north of Birch Mountain to Crater Mountain. Cross section adapted from Bateman et al. (1963), C) Simplified cross section through metasedimentary roof septa and Spook Pluton near Independence, CA. IES-028, IES-042, and IES-043 likely source units featured in this cross section. Cross section adapted from Moore et al. (1963), D) Simplified cross section of the geologic AOI near Lone Pine, CA. Springs IES-021, IES-022, IES-023, IES-024 are likely influenced by the Mount Whitney Intrusive Suite and Alabama Hills biotite monzogranite. Cross section adapted from Stone et al. (2000). 135

Figure 4.6: Map showing the study area, Owens Valley, CA, bounded by the Sierra Nevada to the west and the White-Inyo Mountains to the east. A USA mean temperature raster developed by the USGS (O'Donnell and Ignizio, 2012) is draped over a hillshade constructed from a digital elevation model. Values of mean annual temperature and surface elevation were extracted from random points within the bounding region (black box) to create a synthetic environmental lapse rate (ELR). 147

Figure 4.7: Annual environmental lapse rate (ELR) (blue line) for the study area created from random points (black circles) shown in Figure 4.6. A linear regression was fitted to the ~6,000 points to create the ELR. Lines of 90% confidence for the regression are shown by the red dotted line..... 148

Figure 4.8: Environmental tracer plots from USGS NWIS groundwater samples (wells and springs) in the Crowley Lake and Owens Lake watersheds. A) Linear regression fitted to a plot of $\delta^{13}\text{C}$ versus ^{14}C activity for 94 samples. The intersection of this regression with a horizontal reference line of 100 pmc was used as a plausible endmember for $\delta^{13}\text{C}$ of soil gas. The value found at this intersection was ~15‰. B) Relationship between ^3H and ^{14}C activity for USGS NWIS groundwater samples..... 149

Figure 4.9: Spring discharge temperature versus spring elevation. Springs are symbolized by the black squares. The local environmental lapse rate (ELR) based on average annual temperature is shown as the blue reference line. The majority of springs fall above the local ELR which can be interpreted as indicative of some geothermal heating from groundwater circulation. B) Spring elevation is plotted against distance to the eastern regional divide, the crest of the Sierra Nevada. Distance to divide is used since spring flowpaths cannot be delineated similar to streams/surface water..... 153

Figure 4.10: Dual isotope plots showing $\delta^{18}\text{O}$ versus $\delta^2\text{H}$ for spring waters from this study (IES) and Owens Valley spring and well waters from the USGS Water Quality Portal (USGS). IES springs are shown in the circles and USGS waters are shown in the triangles. A) Waters from both datasets are plotted with four different reference lines; 1) a local meteoric water line from Friedman (2002) (dashed black line), 2) the global meteoric water line (GMWL) from Craig (1961), 2) a

local groundwater line (LGWL) fitted to USGS samples, and 4) a local spring water line fitted to IES samples. B) Dual isotope plot ($\delta^{18}\text{O}$ versus $\delta^2\text{H}$) with USGS and IES samples colored by geographic region within Owens Valley. Samples in the north near Bishop are isotopically depleted while samples in the south near Lone Pine are more isotopically enriched. 155

Figure 4.11: Poor relationships exist between water stable isotopes ($\delta^2\text{H}$ and $\delta^{18}\text{O}$) and elevation, even when separated by geographic area, precluding the use of $\delta^2\text{H}$ and $\delta^{18}\text{O}$ as recharge elevation tracers. Springs are symbolized by geographic region within Owens Valley. 155

Figure 4.12: Piper diagram showing geochemical compositions of spring waters. Springs are symbolized by geochemical grouping 156

Figure 4.13: Relationships between specific conductance and solute concentrations for major cations and anions for Owens Valley spring waters. Ca^{2+} and HCO_3^- have the highest coefficients of determinate for predicting specific conductance (R^2 of 0.73 and 0.88, respectively). These trends are indicative of plagioclase weathering as a major control on solute compositions. 157

Figure 4.14: Geochemical relationships among weathering derived solutes for Owens Valley spring waters. Springs are symbolized by geochemical grouping A) Relationship between calcium and magnesium ion concentrations in sampled spring waters. Springs are well below the 1:1 $\text{Mg}^{2+}:\text{Ca}^{2+}$ line representative of hornblende weathering. B) Relationship between calcium and bicarbonate ion concentrations C) Relationship between magnesium/potassium ion ratios and calcium/sodium ion ratios in sampled spring waters. The trend line expected for biotite weathering for $\text{Mg}^{2+}/\text{K}^+$ (~ 3) is shown by the blue line. The expected $\text{Ca}^{2+}/\text{Na}^+$ weathering ratio for granitic plutons in Owens Valley (Table 4.1) ($\text{An}_{28}\text{-An}_{36}$) is bounded for reference in the grey box. D) Relationship between dominant anions (HCO_3^- and SO_4^{2-} meq/L) and cations (Ca^{2+} and Mg^{2+} meq/L). All samples fall below the 1:1 reference line indicative of equal contributions from carbonate and silicate weathering. Group 4 springs lie the closest to the 1:1 line. E) Relationship between mol % SiO_2 and mol % Ca. Reference lines for predicted weathering trends are shown for 1) calcite dissolution and plagioclase to smectite weathering in a 1:1 ratio, 2) plagioclase to smectite weathering, and 3) plagioclase to kaolinite weathering. F) Relationship between mol % Ca and mol % Na. Predicted weathering trends for An_{25} and An_{45} plagioclase are shown. Plots E & F adapted from Pretti and Stewart (2002). 160

Figure 4.15: Diagram showing the log activity of SiO_2 vs log ratio $\text{Ca}^{2+}/(\text{H}^+)^2$ for Owens Valley spring water samples. Springs are symbolized by geochemical grouping. Mineral stability fields are bounded by the black lines. The majority of springs reside in the kaolinite stability field. . 164

Figure 4.16: Results from NETPATH inverse geochemical modeling from NADP precipitation to spring geochemical compositions. Positive mol transfers indicate dissolution and negative mol transfers indicate precipitation. In instances where multiple models were found, the average of mol transfers is shown. Successful model solutions do not exist without including calcite in these models. Group 4 springs are indicated by the rectangular bounding box. These springs require large mol transfers (% wise) of calcite to successfully model their geochemical compositions. 165

Figure 4.17: A) Relationship between log Cl^- concentration and Cl^-/Br^- ratios in spring waters. Springs below the black line are indicative of natural waters unaffected by halite dissolution. Two springs well above the line are Boron Spring A (IES-027) and Boron Spring B (IES-025). B) Relationship between log Cl^- concentration and log $^{36}\text{Cl}/\text{Cl}$. Preanthropogenic background $^{36}\text{Cl}/\text{Cl}$

ratios in groundwater from Davis et al. (2003) shown in the grey bounding box. Springs dilute with respect to chloride have elevated, bomb-pulse $^{36}\text{Cl}/\text{Cl}$. C) Relationship between $^{36}\text{Cl}/\text{Cl}$ ratio and ^3H (TU). This plot shows separation and mixing between submodern, bomb-pulse, and modern spring waters based on $^{36}\text{Cl}/\text{Cl}$ ratio and ^3H 167

Figure 4.18: Relationships with $^{87}\text{Sr}/^{86}\text{Sr}$, geochemistry, and inverse modeling results for sampled spring waters. Springs are symbolized by geochemical grouping. For plots B-F rock leachate values for Sierra Nevada granitoids are symbolized by the black Xs. A) Relationship between strontium and calcium ion concentrations in sampled spring waters. Springs emerging on the western flank of the Alabama Hills are geochemically distinct from other Group 1 waters. B) Relationship between $^{87}\text{Sr}/^{86}\text{Sr}$ and $\text{Ca}^{2+}/\text{Sr}^{2+}$ ionic ratios in spring waters. C) Mols transfers of carbonate/(plagioclase + carbonate) from inverse geochemical models versus $^{87}\text{Sr}/^{86}\text{Sr}$. The expected strontium ratio for Owens Valley granites (0.706-0.708) is shown in the pink shaded area. The estimated strontium ratio for Paleozoic roof pendants is shown in the blue shaded area. D) Average plagioclase mol transfer from inverse geochemical models versus $^{87}\text{Sr}/^{86}\text{Sr}$. E) Average kaolinite mol transfer (negative for precipitation) from inverse geochemical models versus $^{87}\text{Sr}/^{86}\text{Sr}$. F) Relationship between silica (as SiO_2) and $^{87}\text{Sr}/^{86}\text{Sr}$ 169

Figure 4.19: Trends with radiocarbon, noble gas, and temperature data. A) Shows poor trend between $\delta^{13}\text{C}$ (‰) versus ^{14}C activity (pmc) for Owens Valley spring waters. B) Relationship between bicarbonate concentration and ^{14}C activity (pmc) for Owens Valley spring waters. C) Relationship between ^{14}C activity and $^3\text{He}/^4\text{He}$ ratio normalized to the $^3\text{He}/^4\text{He}$ ratio of air (R/R_a). Springs with lower R/R_a ratios have lower ^{14}C activities. D) Relationship between lithium concentration (ppb) and R/R_a . There is a strong correlation with the exception of Group 3 waters. E) Relationship between spring discharge temperature and R/R_a . Spring waters with lower R/R_a ratios, interpreted to be circulating deeper and at increased flowpath lengths in order to accumulate excess ^4He , have increased discharge temperatures. F) ^3H - ^3He age versus spring temperature. As apparent age increases, spring temperature increases. Group 3 waters fall off the trendline. 174

Figure 4.20: A) Ne/He elemental ratio vs R/R_a . These data define a mixing line between radiogenic and atmospheric endmembers for spring water samples. IES-029, which emerges near Red Mountain in the vicinity of the Big Pine Volcanic Field, is well above this mixing line. B) Relationship between ^{14}C activity and terrigenic ^4He . Petrologic differences in granitic rocks, and subsequent differences in uranium and thorium contents in the rock matrix, likely lead to differences between accumulated $^4\text{He}_{\text{terr}}$ and ^{14}C activity. 175

Figure 4.21: Shows recharge temperature solved at 100m increments from the elevation of the spring emergence to the local high elevation point. Intersection with the environmental lapse rate can be used to estimate recharge elevation (H) and calculate recharge temperature when H is unknown as shown by Zuber et al. (1995), Aeschbach-Hertig et al. (1999), Doyle et al. (2015), and Peters et al. (2018). 176

Figure 4.22: Field photos (March 2016) showing spring emergence conditions for IES-021, IES-022, and IES-023. Samples for ^{14}C analysis were collected from these springs despite seepy, diffuse, and low discharge emergence conditions. While ^3H results for all three springs were all ≤ 0.11 TU, ^{14}C activities were all measured as > 95 pmc. While ^3H is not susceptible to atmospheric contamination or equilibration, we interpret the ^{14}C activities to be contaminated and thus not representative of the actual residence times of these spring waters..... 178

Figure 4.23: Boxplots showing geochemical and isotopic differences between “young” and “old” spring waters. The central mark on each box plot represents the median value while the bottom and top of each box represent the 25th and 75th percentiles, respectively. Whiskers extend to minimum and maximum values not considered to be outliers. Outliers, if applicable, are shown by the red crosses. Differences between young and old waters are shown for spring discharge temperature (A), chloride concentration (B), total dissolved solids (C), plagioclase weathered from NETPATH inverse geochemical models (D), ⁸⁷Sr/⁸⁶Sr (E), Ca²⁺/Sr²⁺ (F), ³He/⁴He ratio normalized to the ³He/⁴He ratio of air (R/R_a) (G), and noble gas recharge temperature computed using the median elevation method (H)..... 180

Figure 4.24: Geochemical evolution among Group 4 waters scales with inferred residence time and temperature. Spring temperature, ³⁶Cl/Cl, and R/R_a show linear trends with geochemical evolution. ³H and ¹⁴C activity have more convoluted relationships with geochemical evolution. ³H is nonunique and there are a variety of factors that can affect radiocarbon activities outside other than the decay of the parent radionuclide. 188

Figure 4.25: Complementary figure to Figure 4.24. Figure shows geochemical evolution with increasing groundwater residence time for Group 1 spring waters in the Lone Pine AOI and the Bishop AOI as well as Group 4 spring waters..... 189

Figure 4.26: Results from inverse geochemical models showing mol transfers of plagioclase vs mol transfers of biotite for Owens Valley spring waters. In cases where more than one geochemical model, error bars represent minimum and maximum mol transfers of plagioclase and biotite from inverse geochemical models. Springs without error bars only have one viable model. Springs are symbolized by color for geochemical grouping and symbolized by size based on ³H concentrations. “Old” waters have more plagioclase and biotite weathered compared to “young” spring waters. Group 2 and Group 3 spring waters fall off the general trendline for mineral weathering, perhaps indicative that these springs are not weathering Mesozoic granitoids like Group 1 and Group 4 waters. 190

Figure 5.1. Map showing the study area for this paper, the structurally extended terrain of the southern Great Basin of the United States. The study area is bounded by the dotted line in the Google Earth orthoimagery capture (Google Earth, 2020) and by the shaded grey area within the inset map. The blue circles show locations of mapped springs, which are distributed across all landscape positions and landform types (e.g., mountains, bajadas, playas, etc.) throughout the study area. The Sierra Nevada, other than the eastern slope, is shaded in yellow and excluded from analysis in this paper as it is not part of the southern Great Basin. 205

Figure 5.2. Flowchart showing the methodological workflow described in the paper. There are three main sections of the analysis: 1) database creation, 2) topographic analysis consisting of both qualitative and quantitative classification and metrics, and 3) ecological analysis..... 208

Figure 5.3. Map of the study area showing the IES springs (circles) symbolized by landscape position classification. Springs with associated BMI data are indicated by the inset black triangles within the circles. 210

Figure 5.4. Map and associated table showing qualitative topographic classification of the study area derived by combining K1 classification (Kapos et al., 2000) with MoRAP classification (True, 2002). Class names (e.g., Nival, High Mountain, Mountain, Low Mountain-Bajada, Valley Floor,

and Playa and isolated basins) were renamed to better characterize the study area and conform to prior classifications from Sada and Thomas (2015). 213

Figure 5.5. Diagram showing the following topographic metrics used in this study: A) Surface elevation, B) Slope, C) Curvature, D) Topographic Wetness Index (TWI), and E) Relative Elevation. For the purposes of clarity, curvature and TWI are both shown at the watershed scale for a catchment draining the western Panamint Range. Relative elevation is shown at both the local neighborhood (100 cell radius) and regional neighborhood (400 cell radius) scales. 217

Figure 5.6. A) Map of the study area showing major geologic contacts. B) Map of the study area showing synthesized mapped fault locations in California (Jennings et al., 1977) and Nevada (Stewart and Carlson, 1978). C) Map of the study area showing major faults. There are six types of major faults identified in the study area: 1) anticlines, 2) low-angle normal faults (LANF), 3) syncline, 4) normal, 5) reverse, and 6) strike-slip..... 219

Figure 5.7. Example BMI plot showing relationship between NMDS distance and similarity.. 220

Figure 5.8 Boxplots showing systematic trends in spring temperature, specific conductance, radiocarbon activity (percent modern carbon), and delta carbon 13 with landscape placement classifications. The central mark in each box represents the median value. The bottom and top extent of each box represent the 25th and 75th percentiles, respectively. The whiskers extend to the maximum and minimum data points not considered outliers. Outliers are represented by the “+” symbols. 223

Figure 5.9. Spring discharge temperature is plotted against elevation (meters), slope (degrees), TWI (unitless), curvature (unitless), and relative elevation (meters; 400 cell neighborhood) and symbolized by qualitative landscape placement class. On each plot, springs from the regional dataset are plotted as squares and springs from recent sampling efforts, the IES dataset, are plotted as circles. 226

Figure 5.10 Spring specific conductance is plotted against elevation (meters), slope (degrees), TWI (unitless), curvature (unitless), and relative elevation (meters; 400 cell neighborhood) and symbolized by qualitative landscape placement class. On each plot, springs from the regional dataset are plotted as squares and springs from recent sampling efforts, the IES dataset, are plotted as circles. 227

Figure 5.11. Spring radiocarbon activity is plotted against elevation (meters), slope (degrees), TWI (unitless), curvature (unitless), and relative elevation (meters; 400 cell neighborhood) and symbolized by qualitative landscape placement class. On each plot, springs from the regional dataset are plotted as squares and springs from recent sampling efforts, the IES dataset, are plotted as circles. 228

Figure 5.12. Plots of elevation versus radiocarbon activity, specific conductance, and spring discharge temperature for springs in the entire study area and two representative mountain blocks, the Funeral-Grapevine Mountains (light blue squares) and the Spring Mountains (dark blue squares). 229

Figure 5.13. Boxplots comparing radiocarbon activity and spring temperature at “fault-controlled” and “non fault-controlled” springs..... 231

Figure 5.14. Boxplots showing comparison of spring temperature and percent modern carbon for springs emerging at different types of major faults (e.g., Figure 5.6C)..... 232

Figure 5.15. NMDS plot of BMI community structure with springs symbolized by landscape placement classification (Top). Boxplots symbolized by landscape placement classification showing systematic trends in temperature, specific conductance, tritium concentration, and radiocarbon activity for the IES springs (Bottom). These trends correspond to similar trends shown in the regional dataset (e.g., Figure 5.8). 234

Figure 5.16. (Top) NMDS plot of BMI community structure with springs symbolized by groundwater residence time grouping. (Bottom) 3-D scatter plot showing spring concentrations of ^3H , $^{36}\text{Cl}/\text{Cl}$ (*10-15), and ^{14}C (fMC) symbolized by spring residence time grouping..... 235

Figure 5.17. Plots showing linear relationships of hydrochemical characteristics (e.g., temperature and specific conductance) and elevation with total BMI richness (# of taxa) and Shannon Diversity. Two outliers, IES-019 & IES-020, are excluded from the SPC plots..... 236

Figure 5.18. Plots showing trends with tolerance indices (e.g., % intolerant taxa, % tolerant taxa, and HBI) and hydrochemical characteristics. Springs are symbolized by landscape placement classifications..... 237

Figure 6.1: Conceptual figure adapted from Plummer et al. (2001) showing the primary research question driving this study; is there a continuum where geochemical and isotopic signals are continually attenuated at longer timescales and increased spatial scales (i.e. larger aquifer volume)? 257

Figure 6.2: Historical drought index comparison between March 2016 and March 2017 for the desert southwest region of the United States (<https://droughtmonitor.unl.edu/>). In March 2016, large portions of the study area were classified under “Exceptional” or “Extreme” drought condition. A year later, the majority of the region changed to a “No Drought” classification. Sampling for this study started during March 2016 and continued through the summer of 2019. 259

Figure 6.3: Conceptual model showing the hypothesis of the relationship among topographic position, flowpath transience, and temporal variability in physical, geochemical, and isotopic analytes. Illustrated flowlines are conceptual. I hypothesize that increased temporal variability in both hydrochemical and isotopic analytes will inversely correlate with groundwater residence time (i.e., springs with elevated temporal variability will have shorter residence times and correspond to higher topographic positions within the study region). Major climate events such as significant drought or a historic snowpack year will cause increased variability in local-scale, high elevation flowpath distributions that will be dampened at increasing spatial scales..... 261

Figure 6.4: Map showing the study area boundary and springs selected for repeat sampling. Springs are annotated by their Integrated Earth Systems (IES) number (e.g. IES-001). Green, teal, coral, yellow, and orange circles represent springs in the Spring Mountains, Ash Meadows, Death Valley, WMAR, and Owens Valley focus areas, respectively. The inset map shows the location of the study area within the context of the western United States. The inset bar chart shows the number of springs sampled as a part of each repeat sampling event. Abbreviations on the map are as follows; SN – Sierra Nevada, OV- Owens Valley, WM- White Mountains, SV- Saline Valley, DV- Death Valley, PR-Panamint Range, AM- Ash Meadows, SM- Spring Mountains..... 264

Figure 6.5: Time-series plots of discharge temperature at repeat springs separated out by focus area(A-F): A) Spring Mountains, B) Ash Meadows, C) Death Valley, D) WMAR, E) southern Owens Valley, F) northern Owens Valley. The majority of springs (21/34) have very stable discharge temperatures (i.e., $SD < 1.0^{\circ}C$). Moving temporal averages of mean daily temperature for local weather stations are included in each plot. Photos of selected springs are included for the purposes of discussion and can be identified by associating the symbol in the upper left-hand corner of the photo to the symbol in the subplot legend. Springs that are highly variable (e.g., IES-002, IES-019, IES-036, etc.) tend to mimic changes in mean annual air temperature. 274

Figure 6.6: Subplots showing metrics of temperature temporal variability (i.e., standard deviation and the coefficient of variance) versus mean spring discharge temperature. Springs are symbolized by color according to focus area and symbolized by shape according to emergence condition. Springs symbolized as squares meet one of three conditions, either they are very low discharge springs, seeps with shallow pools, or springs with modifications that promote diel/seasonal fluctuations due to ambient air temperature or sunlight (e.g., open barrel modification). Springs that show significant deviations are annotated and many of these springs have inset photos in Figure 6.5. Springs symbolized as circles are either unmodified, have high discharge, or have modifications (e.g., a downstream weir) that do not promote diel/seasonal temperature changes. 275

Figure 6.7: Figure showing Stiff diagrams for IES springs over three consecutive sampling events to illustrate the geochemical similarity in repeat spring samples over time. Overall, changes in spring geochemical compositions are very slight. 277

Figure 6.8: Hierarchical clustering analysis emphasizing solute magnitude (i.e., traditional preprocessing). Only one spring, IES-043, contains one geochemical sample that clusters with samples from another spring and is shaded in red. 279

Figure 6.9: Hierarchical clustering analysis emphasizing solute proportion (i.e., alternative preprocessing). Only three springs, IES-011, IES-026, and IES-043 have samples that cluster on a branch with another spring over time and are shaded in red. 280

Figure 6.10: Principal Component Analysis (PCA) plot of geochemical variance of 10 major solutes for springs over the study interval. The 10 major solutes and their corresponding vector magnitudes are symbolized in the inset biplot. PCA 1 and PCA 2 control 84.8% of the overall temporal variance. The majority of springs, symbolized by the annotated cluster, exhibit very limited geochemical temporal variability (i.e., the chemical compositions of the major cations and anions are very stable over time). One major takeaway from this figure is that even though there are some springs that exhibit more variability than others over time, even the most variable springs do not change considerably. This point is illustrated by the Stiff diagrams included for IES-014 (which falls within the very minimal variance bubble) and IES-043, which has a very positive score on PCA 1. While IES-043 clearly exhibits more temporal variability in chemical composition from March 2016-October 2017, the degree of change is still fairly minimal considering it is the most variable spring in the dataset. 281

Figure 6.11: Boxplots showing statistical distributions of coefficient of variation for different solutes by study area. For each boxplot, the central line of the box represents the median. The upper and lower extents of the box represent the 75th and 25th percentiles, respectively. Whiskers extending from the upper and lower portions of the box indicate the spread of all data not considered outliers.

Outlier samples are shown by the red crosses. The solutes shown on the x-axis are the same variables that were used in the PCA analysis of major ion geochemical variation. The study area and number of samples are described for each boxplot. The inset table shows focus area (group) averages in ^3H , ^{14}C and spring discharge temperature to allow comparison between these key metrics and boxplot spread. Broadly speaking, the most variable regional boxplots correspond to the focus areas with colder waters, shorter residence times, and more local flowpath distributions (i.e., Owens Valley and the Spring Mountains). Major outliers are IES-019 in Death Valley and IES-043 in Owens Valley. 283

Figure 6.12: Similar to Figure 6.10, this figure is a PCA plot of trace element variability. Springs are symbolized as circles and colored by focus area. An inset biplot shows the vector magnitude of each variable and how PCA space relates to trace metal temporal variation. Because trace element concentrations were below the detection limit for most analytes, only 5 variables (As, B, Fe, Li, Mo) were used to understand which springs exhibit minimal variation, which springs display the most temporal variability, and how changes in trace metal concentration over time are related. 284

Figure 6.13: Plot showing $^{87}\text{Sr}/^{86}\text{Sr}$ as a function of $1/\text{Sr}^{2+}$. Springs are shaded by focus area. The associated bar chart on the right shows whole-rock ranges for focus areas and geologic units in the region from Wasserburg et al. (1964), Pretti and Stewart (2003), Paces et al., (2007), Hirt (2007), and Chapman (2015). 285

Figure 6.14: Time series plots of $^{87}\text{Sr}/^{86}\text{Sr}$ in spring waters. The results are separated into three panels to maximize the y-axis limits. The measurement uncertainty for $^{87}\text{Sr}/^{86}\text{Sr}$ is 0.00005 and is shown by the y-axis error bars. WMAR and Death Valley springs are shown in subplot “A” while Spring Mountains and Owens Valley springs are shown in subplots “B” and “C”. Overall there is very little temporal variation, however because the measurement uncertainty is minimal, small changes in $^{87}\text{Sr}/^{86}\text{Sr}$ (e.g., IES-004) can provide insight into changes in flowpath distribution. 287

Figure 6.15: Plot showing Sr^{2+} coefficient of variation (%) versus $^{87}\text{Sr}/^{86}\text{Sr}$ standard deviation for spring waters. The majority of spring have $^{87}\text{Sr}/^{86}\text{Sr}$ standard deviations below the analytical uncertainty (grey box). Five springs have $^{87}\text{Sr}/^{86}\text{Sr}$ standard deviations greater than the analytical uncertainty. IES-043 appears to be the only spring where changes in spring $^{87}\text{Sr}/^{86}\text{Sr}$ can potentially be attributed to temporal variations in Sr^{2+} 288

Figure 6.16: A general understanding of the spatial distribution of $\delta^{18}\text{O}$ and $\delta^2\text{H}$ in groundwater and the mechanisms driving $\delta^{18}\text{O}$ and $\delta^2\text{H}$ variation throughout the region is first needed prior to understanding the possible mechanisms for temporal variation. Geographic, climatic, and topographic factors all contribute to variations in $\delta^{18}\text{O}$ and $\delta^2\text{H}$ in groundwater throughout the study area, Geographic factors are seen in subplot “A” where isotopic composition of springs waters in Owens Valley is more closely related to geographic position within the valley (easting or northing) rather than elevation. Specifically, isotopes are highly depleted in the Round Valley area west of Bishop. Moving south and eastward toward the Alabama Hills region, spring water isotopes are more enriched (Chapter 4). Climatic factors driving isotopic variation are shown in subplot “B”. Waters discharging currently at Ash Meadows, Furnace Creek, and the Grapevine Springs complex have a unique isotopic signature reflective of Pleistocene recharge. An example of isotopic fractionation driven by topography and recharge type is shown in subplot “C”. In the Spring Mountains, groundwater that is locally isotopically light or depleted is interpreted to be

sourced from cold, snowmelt recharge while springs discharging isotopically heavier water are dependent on lower elevation recharge, more rain, or a monsoonal moisture source. 290

Figure 6.17: Plot and associated correlation matrix showing water isotope variability results. The plot shows the standard deviation of $\delta^{18}\text{O}$ versus the standard deviation of $\delta^2\text{H}$ ($R^2 = 0.17$) for springs sampled more than four times during the sampling period. The darker shaded region represents the average analytical uncertainty for $\delta^{18}\text{O}$ and $\delta^2\text{H}$ from while the lighter shaded region represents 2X the analytical uncertainty. The correlation matrix results show that we do not observe any significant correlations with spring standard deviations of $\delta^2\text{H}$ and $\delta^{18}\text{O}$ and physical, geochemical, or isotopic metrics indicative of groundwater flow system stability (i.e., springhead elevation, discharge temperature, or groundwater residence time indicators)..... 292

Figure 6.18: Boxplots showing statistical distributions of $\delta^{18}\text{O}$ and $\delta^2\text{H}$ standard deviation separated out by focus area. For each boxplot, the central line of the box represents the median. The upper and lower extents of the box represent the 75th and 25th percentiles, respectively. Whiskers extending from the upper and lower portions of the box indicate the spread of all data not considered outliers. Outlier samples are shown by the red crosses. 292

Figure 6.19: Map of the Ash Meadow region showing all known springs in Ash Meadows (small blue circles) and springs sampled as a part of IES sampling efforts (large teal circles). Strontium values from this study and Peterman et al. (1992) are shown in gold and blue callouts, respectively. Fault lines are shown throughout the area, with dotted lines indicating approximate fault location. Stiff diagrams are show for the IES springs with a corresponding key in the legend. Note the difference in strontium and chemistry between the southernmost three springs, including IES-014, and the rest of the springs. 294

Figure 6.20: Subplots showing temporal stable isotope variation in springs at Ash Meadows National Wildlife Refuge. The figure on the left shows water stable isotope values over time symbolized by shape for each IES spring in Ash Meadows. Error bars represent the analytical uncertainty for each sample. The figure on the right shows water stable isotope values at Ash Meadows over time symbolized by color for each sampling campaign. Rather than cluster by spring (left), stable isotope values in the Ash Meadows flow system appear to cluster by sampling event (right). This finding has potential implications for groundwater movement and connectivity between springs in the Ash Meadows flow system despite the fact that the springs emerge at different faults and there are areas within the flow system that appear to receive flow from varying aquifer sources. 295

Figure 6.21: Plots showing temporal increases in $\delta^{18}\text{O}$ and $\delta^2\text{H}$ in the study area over the sampling interval (March 2016- June 2019). Springs are symbolized by IES number. Y-axis error bars represent the analytical uncertainty of each sample. 296

Figure 6.22: Histogram subplots showing counts of the direction and magnitude of the slope fitted to the linear regression of $\delta^{18}\text{O}$ and $\delta^2\text{H}$ over the sampling period. All but three springs had positive $\Delta\delta^2\text{H}/\text{day}$ slope over the sampling period (upper plot). All but one spring had a positive $\Delta\delta^{18}\text{O}/\text{day}$ slope over the sampling period (lower plot). 297

Figure 6.23: Plot of $\delta^{18}\text{O}$ versus $\delta^2\text{H}$ of springs ($n = 13$) that were never missed sampling during seven of the larger field campaigns. Springs are shaded by sampling event. Boxplots on each axis provide a statistical summary of change from the initial March/May 2016 sampling trip until June

2019. Areas of significant change in Owens Valley and the Spring Mountains are annotated on the plot. 298

Figure 6.24: Plots showing ^3H standard deviation (TU) versus ^3H (left) and ^{14}C activity (fmc) right. Springs with elevated ^3H and more modern ^{14}C activities have larger ^3H standard deviations even though the analytical uncertainty is within the same range (0.09-0.11 TU) for all samples. One sample, IES-034, is an outlier relative to the rest. 299

Figure 6.25: Plots showing standard deviation of ^{14}C (fmc) versus standard deviation of $\delta^{13}\text{C}$ (left) and mean tritium concentration (right). Both factors appear to exhibit some control on ^{14}C variability. However, IES-019, IES-010, IES-011, and IES-014 have relatively large standard deviations in ^{14}C (fmc) relative to their nonexistent (dead) tritium concentrations. 300

Figure 6.26: Subplot showing temporal comparisons of environmental tracers sampled at springs during March 2016 and March 2017. Regression (solid grey) and 1:1 lines (dashed black) are shown in each subplot. We observe large year to year discrepancies in $\delta^{13}\text{C}$ to compared to smaller variations in the other environmental tracers. 301

Figure 6.27: Variability matrix synthesizing the key physical, geochemical and isotopic variability metrics presented in this study. Temperature and major ions variability are separated out as columns because these factors are the most important ecologically. Springs with no color for a given variable do not exhibit significant variability. Springs shaded in yellow are moderately variable while springs shaded in red are highly variable for a given metric. Springs denoted by “N/A” were not included in the analysis for that particular variable. 303

Figure 6.28: Histogram showing the elevation distribution of springs within Death Valley National Park (DEVA). Data is from Don Sada (*personal communication*). There is a sharp cutoff in spring emerge above 2200 meters. The high histogram count for springs below sea level corresponds to a number of springs and seeps that emerge at similar elevations on the valley floor (e.g., the Cottonball Marsh and Badwater spring complexes). 306

Figure 6.29: Map of the study area showing known locations of springs (yellow circles) on different mountain blocks. There are relatively few high elevation (>2200m) springs in the study area (orange circles). 307

Figure 6.30: Google Earth photo showing IES-021 (Lubken Canyon Spring 1) and IES-054 (Lubken Canyon Spring 2). Photo annotations show that while these springs have similar geochemical profiles, the difference in emergence conditions between the two springs leads to differences in ecological community structure. 309

Figure 6.31: A tolerance matrix based on the presence/absence of intolerant and tolerant taxa in IES springs (i.e., the numbers in this figure are reflective of presence/absence and not population statistics of the sample). Springs on the left side of the matrix (dark blue) are dominated by intolerant taxa while springs on the right side of the matrix are dominated by tolerant taxa (dark red). Each spring sample is represented by a “box”. Springs can be identified by the spring ID in the upper left-hand portion of the box. In the lower portion of the box there are two numbers. The top number represents the % tolerant taxa as a decimal and the bottom number represents the % intolerant taxa in a sample as a decimal. Intolerant taxa have a TV < 3 and tolerant taxa have a TV > 7. The three colored rectangles in the upper right-hand portion of the box represent spring.. 313

Figure 6.32: A tolerance matrix based on the community population statistics in IES springs. Springs on the left-hand side of the matrix have a low community tolerance value. Community tolerance values increase moving to the right. Springs can be identified by the spring ID in the upper left-hand portion of the box. In the lower portion of the box there are three numbers. The large black number on the left represents the community tolerance value (0-1). The green number on the right represents the percentage of tolerant (TV>7) population of a sample expressed as a fraction. The blue number on the right represents the percentage of tolerant (TV<3) population of a sample expressed as a fraction. The three colored rectangles in the upper right-hand portion of the box represent spring geochemical characteristics as described in Figure 6.32. 314

Figure 6.33: Plots showing historical and recent stable isotope data for springs in the Spring Mountains. The red line on each plot marks the start of the 2011-2017 California drought. Our results show that Spring Mountain springs were highly depleted at the end of the drought but quickly shifted isotopically following drought amelioration back to historical baselines..... 316

Figure 6.34: Hydrograph from the USGS showing the gage height of the Amargosa River from 2011 to early 2020. 317

ABSTRACT

In arid regions, springs are important in many aspects of society due to the scarcity of surface water features. In the Great Basin of the United States, desert springs support the majority of regional biodiversity and are critical for supporting rare, threatened, and endangered organisms. Despite their importance, there are numerous threats to desert springs, with the most ubiquitous being climate change. In contrast to many studies examining potential metrics to describe the vulnerability of streams, wetlands and other surface water features to the effects of climate change, springs are often overlooked. Part of the knowledge gap stems from the complexity of springflow generation and the rarely field-tested connection between groundwater response time and groundwater residence time.

This dissertation tests, in a systematic way, different metrics that may help define criteria to evaluate whether a spring is likely to persist or desiccate with increasing regional hydrologic stress due to climate change. Field data was collected over a 4-year period from >80 springs across the topographically and geologically heterogeneous terrain of the southern Great Basin. Throughout this dissertation, I use a variety of different tools (e.g., remote sensing, environmental tracers, geospatial analysis) to “attack” this complicated problem from different angles. I begin by examining factors indicative of hydrogeologic resistance to major drought. After finding a connection between groundwater residence time and hydrogeologic resistance, I examine other factors (e.g., geochemical, topographic, ecological, variability) that are related to groundwater residence time and also identify where these relationships fail.

CHAPTER 1. INTRODUCTION

1.1 Spring systematics

Springs are defined as points where groundwater discharges to the Earth's surface (Springer and Stevens, 2009). As this is a relatively broad term and includes a range of hydrogeologic features from high discharge hanging gardens to diffuse seeps, classification systems have been developed to characterize and describe springs on the basis of geomorphic considerations (e.g., hydrostratigraphic unit, orifice geomorphology, etc.), flow conditions, water quality, habitat suitability, biota, and disturbance (Bryan, 1919; Springer et al., 2008; Springer and Stevens, 2009). Springs are unique and complex features for several reasons: 1) springs straddle the groundwater/surface water interface as surficial expressions of groundwater flow that frequently host rich ecological communities, 2) springs emerge at the land surface due to a variety of different factors (e.g., the intersection of the water table with the land surface, fracture networks, permeability barriers from faults or geologic contacts, etc.), 3) springs may integrate many different water sources and flowpaths (Manga, 2001; Springer and Stevens, 2009; Criss, 2010; Manning et al., 2012; Frisbee et al., 2013), and 4) these flowpaths have distinct physical, chemical and biological signatures (Springer and Stevens, 2009; Frisbee et al., 2013a,b). According to Tóth (1999), groundwater adjusts to changes in geology, topography, and climate. Springflow generation is predicated not only on the three primary factors but also on the mechanism causing spring emergence. Therefore, it is not uncommon for springs to integrate flowpath distributions, either in a topography-driven flow system (Tóth, 1963) consisting of local flowpaths (i.e., shallow circulation and short residence time) scaling to regional flowpaths (i.e., deeper circulation and longer residence time), or in a structurally or hydrostratigraphically controlled flow system.

Groundwater flow systems, and subsequently, spring flowpath distributions, change over both climatic (i.e., short-term) and tectonic (i.e., long-term) timescales due to changes in these principal forcings (i.e., geology, topography, and climate). Over longer timescales, regional tectonics alter topography, basin configuration, subsurface structural complexity and regional climatology. Over shorter timescales, changes in climate (e.g., glacial/interglacial cycles, megadroughts, etc.) alter groundwater recharge processes and these signals propagate through groundwater flow systems. Spring response to these changes is a function of the flowpath

distribution supporting springflow and the hydraulic diffusivity of the aquifer. A common, but relatively untested conceptual model is that deep groundwater flowpaths moderate or provide some buffering to the immediate effects of climate change (e.g., Sophocleous, 2012). Thus, springs with highly variable flowpath distributions, or flowpath distributions reliant on a substantial proportion of local flowpaths, may be more sensitive to the effects of climate change than springs with stable flowpath distributions (Rademacher et al., 2001; Singleton and Moran, 2010; Bredehoeft, 2011; Sophocleous, 2012; Manning et al., 2012). In the absence of aquifer data, it is extremely difficult to estimate or calculate groundwater response times. One way to assess potential spring response times is through the use of geochemistry and environmental tracers. Residence times offer a way to gain insight into the length of time that water stays in an aquifer and thus, provide a sense of how perturbations may propagate through the aquifer. However, response times are rarely equivalent to groundwater residence times.

Flowpaths of different scales and lengths have characteristic solute loads, heat fluxes, and mean residence times (Pinder and Jones, 1969). Local scale flowpaths may not circulate deeply and predominately interact with highly weathered minerals, leading to minimal geothermal heating and decreased solute fluxes. Intermediate and regional scale flowpaths may become geothermally heated and interact with more reactive minerals. Additionally, the longer residence times associated with these flowpath lengths allow more opportunity for rock-water interaction, leading to geochemically evolved groundwater (i.e., increased solute loads). Therefore, changes in flowpath distribution associated with climate change perturbations can manifest as changes in mean residence time, changes in solute concentrations, changes in heat flow, or changes in the variability of these components. Measurements of geochemistry and residence time, therefore, provide information about potential response times or spring vulnerability. While geochemistry is somewhat easier to assess (e.g., simple geochemical metrics like conductivity and pH, major ions, trace elements, etc.), different environmental tracers (e.g., ^3H , CFCs, ^3H - ^3He , ^4He , ^{14}C , $^{36}\text{Cl}/\text{Cl}$, etc.) “see” different parts of the residence time spectrum (Cartwright et al., 2017) (Figure 1.1). Therefore, multitracer approaches are often utilized to understand ranges or distributions of groundwater residence time at springs or in complex groundwater systems.

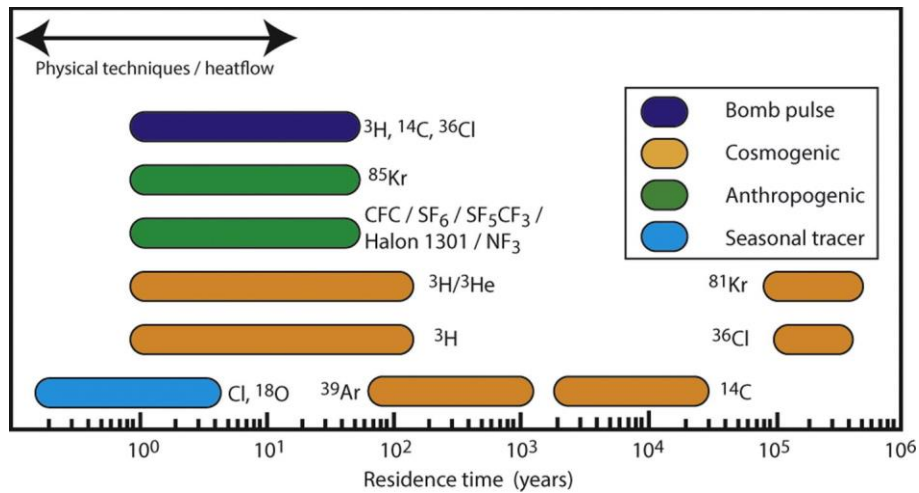


Figure 1.1. Chart showing residence time coverage of environmental tracers. Figure reproduced as published in Cartwright et al. (2017).

1.2 The importance of desert springs

In arid regions like the desert southwest of North America, surface water features are limited, nonexistent, or hypersaline. In these areas, the importance of springs is increased as they are often the only source of perennial fresh water and therefore hold a very important position in many aspects of human life (Frisbee, 2013c) (Figure 1.2). As oases in harsh environments and water-limited regions, desert springs have long held sacred cultural and religious importance to indigenous communities across the world (Stanley, 1912; Mills and Ferguson 1998; Jett, 1992; Idris, 1996, Box et al., 2008; Amiel, 2010; Jian, 2010; Santoro et al., 2012). Springs have also been important historically for human expansion/migration, the founding of permanent settlements, and the establishment of trade routes across inhospitable landscapes (Woo and Hughson, 2004; Box et al., 2008; Jiao, 2010; Frisbee et al., 2013). While groundwater extraction from deep aquifers has become the primary source of municipal water supplies in arid regions, desert springs continue to serve as sources of water for local communities (Idris, 1996; Cereceda et al., 1992) and are still relied upon for recreational uses (e.g., swimming, fishing, and camping) (Shepard, 1993; Sada et al., 2005; Jiao, 2010; Zekri et al., 2011). Furthermore, in the western United States, springs are frequently relied on as sources of water for commercial and agricultural uses such as livestock grazing operations (Sada et al., 2005; Kodric-Brown et al., 2007; Kodric-Brown and Brown, 2007) However, arguably the most important role of desert springs is ecological as they provide critical habitats for endemic, threatened, endangered, and migrating species.

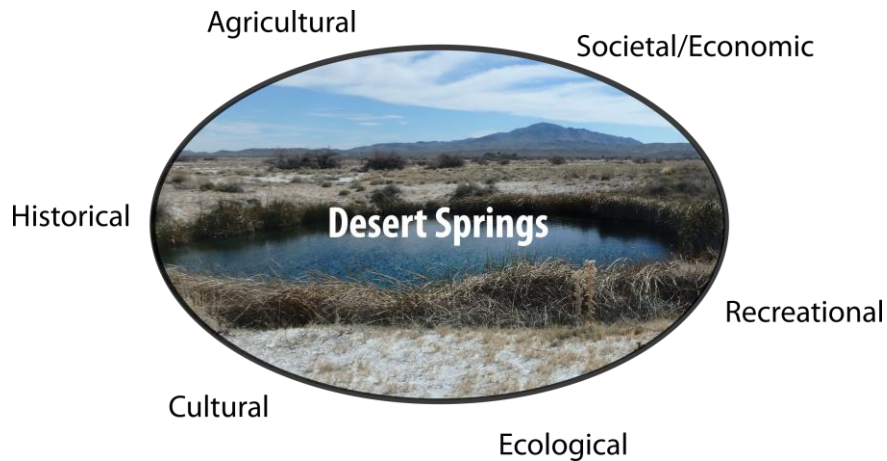


Figure 1.2. Conceptual diagram showing how desert springs are integral components to many aspects of human life and to ecological systems.

Desert springs have been referred to as “aquatic archipelagos” (Minckley and Deacon, 1968; Unmack and Minckley, 2008) and “keystone features” (Perla and Stevens, 2008; Freed et al., 2019) because of their disproportionate ecological worth relative to their size and spatial extent (Davis et al., 2017). For example, in the Great Basin of the United States, springs and riparian areas occupy 1 percent of the land surface yet support the majority of regional biodiversity (Sada, 2008). Desert springs provide a direct supply of water to local terrestrial flora and fauna for habitat and consumption (Wauer, 1962; Wauer, 1964; Jaeger et al. 2001, Bradford et al. 2003; Sada et al. 2005; Fleishman et al. 2006). In addition, desert springs also provide secondary, indirect ecological services including opportunities for pollination, herbivory, and predation based on the habitat they provide (Shepard, 1993). Desert springs are well established places of respite for migratory birds crossing large swaths of desert (Smyth and Coulombe, 1971; Sada et al., 2001). There are many examples of deserts spring providing critical habitats for threatened, endangered, and endemic aquatic species and these cases are particularly well documented in western North America and Australia (e.g., Hershler, 1989; Witt et al., 2006; Schroeder et al., 2015; Stanislawczyk et al., 2018). However, much of the ecology diversity of desert springs is poorly documented as they are often remote, inaccessible, or unknown/unmapped (Unmack and Minckley, 2008). Thus, the diversity and endemism supported by desert spring systems maybe far higher than what is currently known (Witt et al., 2006).

There are myriad reasons for the ecological richness and diversity of desert springs other than the fact that they are rare sources of water in regions that are parched. In the southern Great Basin, the high endemism of aquatic species (e.g., springsnails and pupfish) in desert springs is thought to result from the desiccation and isolation of a once interconnected hydrologic system over climatic and tectonic time scales (Hubbs and Miller, 1948; Smith et al., 2002; Echelle and Echelle, 2005; Echelle, 2008; Hershler and Liu, 2008). In times of rapid warming and drying, perennial desert springs likely provided hydrologic refugia, or areas where populations of organisms were able to survive unfavorable conditions. In contrast with other surface water features, springs can provide extremely stable physicochemical conditions (i.e., temperature, salinity, dissolved oxygen), especially close to the spring orifice, because of the constancy of the groundwater system. As the distance between desert springs is often great (e.g., 20-100 km) (Shepard, 1993) and many spring-dwelling or crenobiotic species are non-vagile, the continued permanence of springs in arid landscapes is essential to preventing the loss of endemic species, and the subsequent ecological collapse of these systems. Fragmented and isolated ecological communities like desert springs that host rare and endemic fauna have elevated extinction risk (Fagan et al., 2002).

1.3 Desert springs are in decline

While the importance of conserving small features like desert springs that have large ecological roles has been well established (e.g., Hunter, 2017), the demise and loss of desert springs has been reported across almost every continent over the last century (Miller, 1961; Brune, 1981; Keleher and Rader, 2008; Jiao, 2010; Powell et al., 2015; Powell and Fensham, 2016). This has occurred even in regional aquifers with residence times spanning millennia (Fairfax and Fensham, 2002; Powell et al., 2015; Powell and Fensham, 2016). Even in “environmentally conscious” countries such as the United States, there are few federal legal protections for small, isolated springs that are considered geographically isolated wetlands with no connections to major streams and rivers (Aldous and Bach, 2011; Rohde et al., 2017). To date, the largest threat to aridland springs has been large-scale groundwater extraction and overpumping (Unmack and Minckley, 2008). This has resulted in water table declines, spring desiccation, and thus irreversible loss of spring ecosystems (Miller, 1961; Brune, 1981; Kodric-Brown and Brown, 2007; Patten et al., 2008; Powell and Fensham, 2015). Low volume extractions, even over long timescales, e.g.

the Palmyra Oasis in Syria (Schutt, 1987), are less of a threat compared to rapid, industrial scale extractions. Besides groundwater pumping, other anthropogenic effects such as spring modification, the introduction of invasive species (Holmquist et al., 2011), and disturbances from grazing or livestock (Hershler, 1998; Sada et al., 2001; Sada and Vinyard, 2002) are major threats to desert springs and their ecological communities (e.g., Figure 1.3). While springs may be able to withstand diversion, alteration, and other disturbances, a spring subjected to drying will have its crenobiotic community decimated with little chance of recovery to a reference condition.

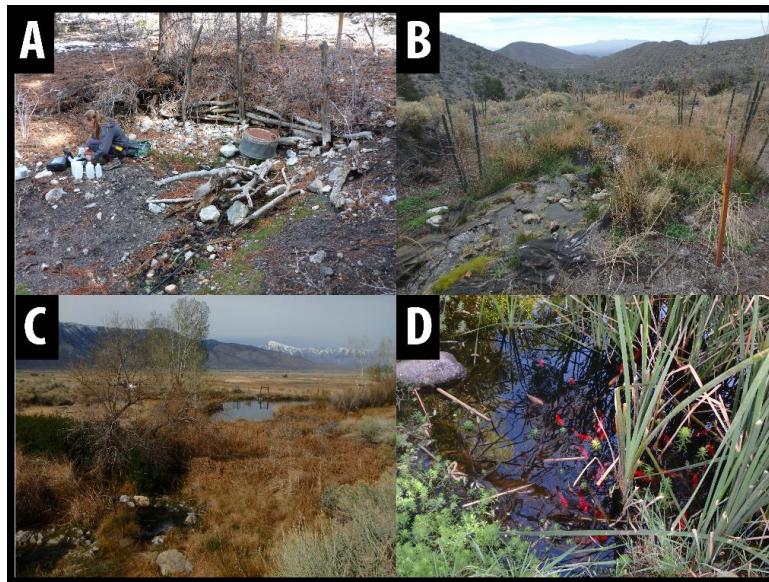


Figure 1.3. Examples of spring disturbance. A) Buck Spring (IES-006) altered by the construction of a spring box. B) Kiup Spring (IES-004) showing restoration efforts to increase native vegetation after disturbance. C) Warm Spring A (IES-031) disturbed by livestock grazing. D) China Garden Spring (IES-035) disturbed by introduction of non-native species.

Despite the myriad threats to desert springs that already exist, another major threat is on the horizon, and perhaps, has already arrived, the effects of anthropogenic climate change. While the effects of climate change in arid regions will be highly variable depending on the region, most areas are projected to see increases in temperature (Ragab and Prudhomme, 2002). For the desert Southwest of the United States, the focus of this study, increased aridity (i.e., increased temperature and decreased precipitation) is predicted (Seager et al., 2007; MacDonald, 2010) and is currently being observed (Figure 1.4). Mountainous regions of the western United States have already seen declining mountain snowpacks over the last century (Mote et al., 2005; Mote et al.,

2018). Increased rain-on-snow events, leading to more runoff and less groundwater recharge, have also been observed (Musselman et al., 2018). These trends are concerning since the majority of mountain-block groundwater systems in the western U.S. rely on slowly infiltrating snowmelt as the principal mechanism for aquifer recharge (Wilson and Guan, 2004). Ultimately, these trends are unsustainable for southwestern aquifers (Meixner et al., 2016) that support many groundwater-dependent ecosystems in the rain-shadow of the Sierra Nevada (Patten et al., 2008). In fact, climate change has already been linked to changes in the hydrological cycle (Snyder et al., 2019), changing discharge at springs (Weissinger et al., 2016) and the collapse of desert ecological communities (Iknayan and Beissinger, 2018) in the Great Basin and western U.S. However, there is still a high degree of uncertainty about how rapidly these changes will occur and which spring systems will be the most vulnerable to predicted changes. There are even studies which argue that some groundwater systems, (e.g., aquifers that underlie closed basin playas), may see enhanced recharge due to increased precipitation variability associated with climate change (McKenna and Osvaldo, 2018). From a paleohydrologic perspective, recent studies in the southern Great Basin have found that desert wetlands and associated flora responded rapidly to past climate change, with wetland expansion and contraction occurring at timescales ranging from millennial to possibly decadal (Springer et al., 2015; Pigati et al., 2019). However, this prior work only applies to springs that have left mounds or a paleohydrologic record on the land surface, which account for the minority of springs in the southern Great Basin (Quade et al., 1995). It is also important to understand not just which springs are vulnerable to desiccation, but how physicochemical changes (e.g., geochemistry, temperature) associated with changes in surface temperature, recharge, and subsequently flowpath distribution will propagate through the aquifer system and affect ecological communities. For example, recent work predicts that changes in groundwater temperature will lag surface temperatures by up to 20 years at higher elevations with slower responses (~60 years) occurring at lower elevations (Burns et al., 2017). While these types of physicochemical propagations may not change the hydrogeological functioning of a spring, these changes have serious implications from crenobiotic species that rely on stable conditions.

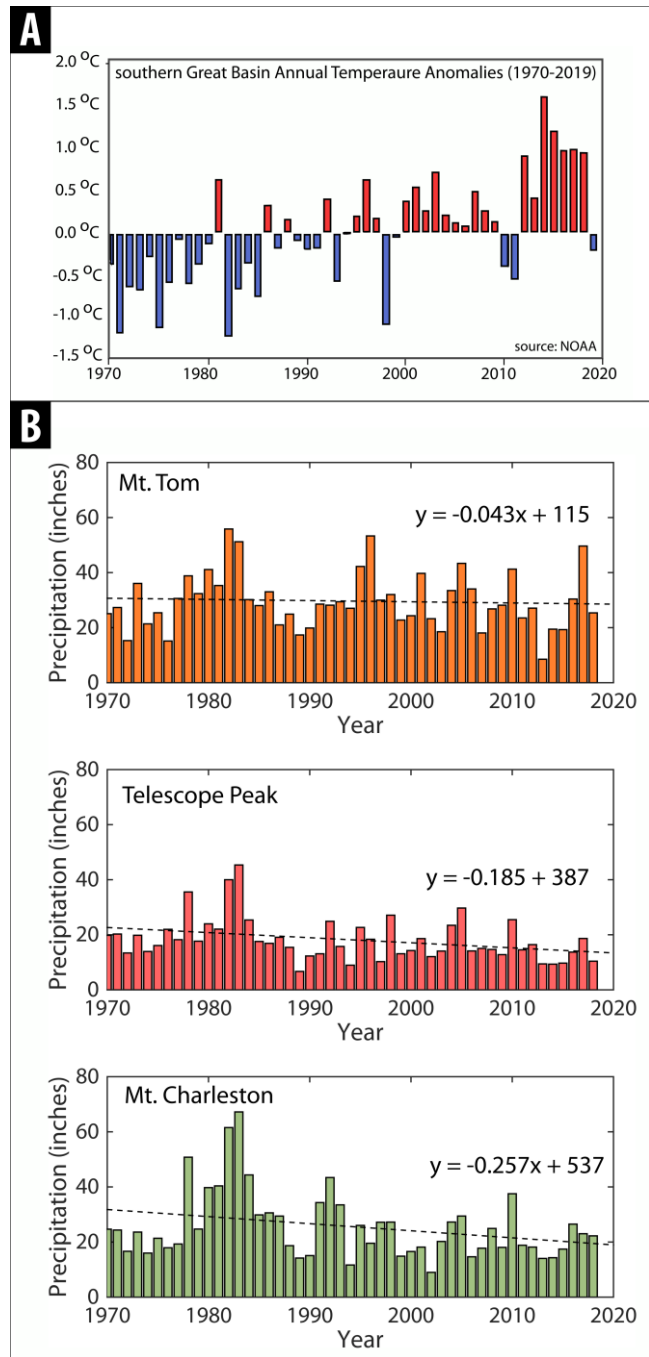


Figure 1.4. Figures showing the effects of climate change in the southern Great Basin since 1970. A) Temperature anomalies in the southern Great Basin since 1970 from NOAA (<https://www.ncdc.noaa.gov/cag/>) for 37.3° N, 118.7° W. B) Changes in annual precipitation since 1970 at three representative peaks in the southern Great Basin from PRISM (Parameter-elevation Regressions on Independent Slopes Model) data (<https://prism.oregonstate.edu/explorer/>): 1) Mt Tom (eastern Sierra Nevada), 2) Telescope Peak (Panamint Range), and 3) Mt Charleston (Spring Mountains) (PRISM Climate Group, Oregon State University, <http://prism.oregonstate.edu>, created 21 Feb 2020).

1.4 Motivation and overarching question

Sections 1.1-1.3 emphasize that desert springs: 1) have immense recreational, commercial, and cultural value in today's society, 2) are critically important to healthy ecosystem functioning in arid landscapes, 3) host numerous rare, endemic, threatened, and endangered flora and fauna, 4) are currently disturbed and threatened by numerous anthropogenic activities, and 5) are likely to experience increased stress over the next century as the effects of climate change propagate through groundwater systems.

Ultimately, this dissertation sets out to address one overarching question: What metrics (i.e., hydrogeologic, geochemical, and geomorphic, and ecological) best describe the *resistance, resilience, and/or vulnerability* of desert springs to climate change? In each chapter of this dissertation, a different metric or series of metrics is examined under the umbrella of the overarching question.

We define the terms resilience and resistance similarly to Lincoln (1998) and Cartwright et al. (2018). Resistance refers to the ability to weather and endure environmental change whereas resilience refers to the capacity to recover from perturbations such as drought or other disturbances. These qualities do not necessarily have to be mutually exclusive, however the ecological implications may be different from the hydrogeologic implications.

To answer these questions, a large, interdisciplinary research team has embarked on a multi-year, collaborative sampling campaign of ecologically undisturbed desert springs across a broad study area, the southern Great Basin (Figure 1.5). This is one of the best studied areas regarding the ecology, density, and distribution of spring ecosystems in the world (Junghans et al., 2016). The body of existing work allows us to leverage prior knowledge and combine it with insights gleaned from this study towards a better understanding the vulnerability of these spring systems. Within the southern Great Basin we have three focus areas; 1) Spring Mountains/Ash Meadows, 2) Death Valley, and 3) Owens Valley. Collaborative spring sampling (e.g., hydrochemistry, spring ecology, microbiology) occurred between March 2016 and June 2019 over 11 different sampling campaigns. A subset of springs (~30) have been designated for repeat sampling, and with these springs we aim to capture the variability of the study area in terms of elevation, temperature, spatial scale, chemistry, and residence time. Springs designated as one-time samples are in more remote/inaccessible locations (e.g., the Panamint Range) and aim to fill

critical gaps in the repeat sampling dataset with respect to the spatial and topographic distribution of springs across the study area. In total, over 80 springs have been sampled across the region.

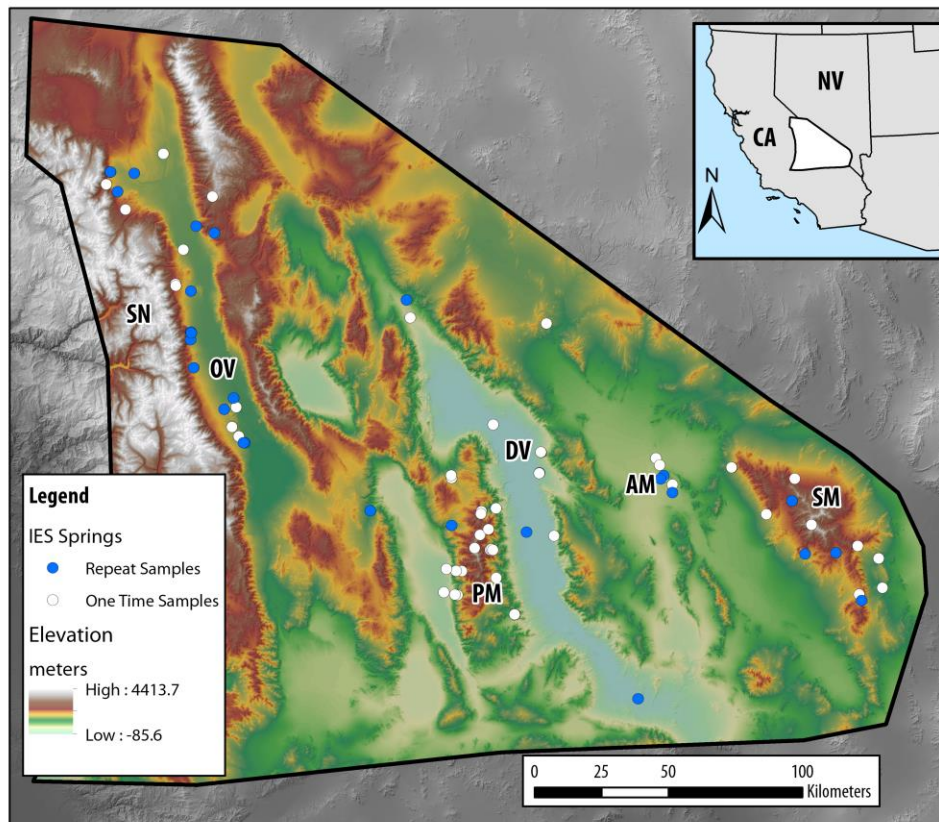
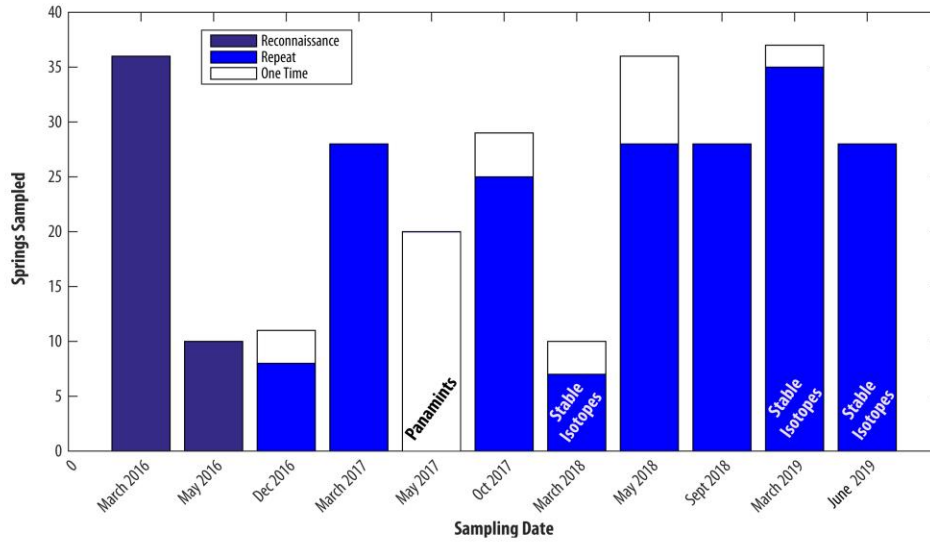


Figure 1.5. Bar graph (top) and regional map (bottom) showing the timing and distribution of spring sampling across the southern Great Basin.

1.5 Site Description

1.5.1 Study Area Extent and Regional Geography

The study area for this project is bounded to the west by the eastern crest of the Sierra Nevada (CA) and to the east by the northwest-southeast trending ridgeline of the Spring Mountains (NV). The southern boundary is defined by the Garlock-Stateline fault system and the northern boundary is defined by the northernmost extents of the Funeral-Grapevine Mountains and White-Inyo Range (Figure 1.5). The majority of this area is located in the southern Great Basin, a closed drainage basin that terminates in Death Valley, CA. This region is characterized by a series of northwest-southeast trending mountain ranges separated by relatively equidistantly spaced basins, usually about 20-30 kilometers in width. Mountain belts occupy roughly 25 percent of the landscape and are surrounded by low-lying basins. In the northern portion of the study area, mountains trend more in a north-south orientation, while transtensional influence from the Walker Lane changes basin orientation to more NNE near Death Valley (Jayko, 2012). Alluvial-filled basins can be intermontane or valley floor and are formed from extensional grabens that create a high amount of relief between the ranges and valley bottoms (Faunt, 1997). This extensional regime allows for fault-block ranges to form where slip is occurring along normal faults. Large interfingering alluvial fans (i.e., bajadas) are common on the east side of mountain ranges and smaller alluvial fans, associated with high-angle normal fault scarps, are common on the west side of ranges.

1.5.2 Geologic Overview

The regional geology within the study area is very complex (Figure 1.6). The crystalline basement underlying the majority of the region formed around 1.7 Ga (Wasserburg et al., 1959) and is exposed in several sections of the Black Mountains and Panamint Range. There is a major unconformity between the crystalline basement and the Pahrump Group, a thick succession of Proterozoic sedimentary rocks formed during the incipient stages of the Cordilleran miogeocline (Heaman and Grotzinger, 1992). Rocks of the Pahrump Group are well exposed in the Salt Spring Hills area near Saratoga Spring (i.e., sample number IES-020). Several carbonate formations (i.e., the Noonday Dolomite and the Ibex Formation) overlie the Pahrump Group and formed as a carbonate bank developed during the initial stages of continental rifting associated with the

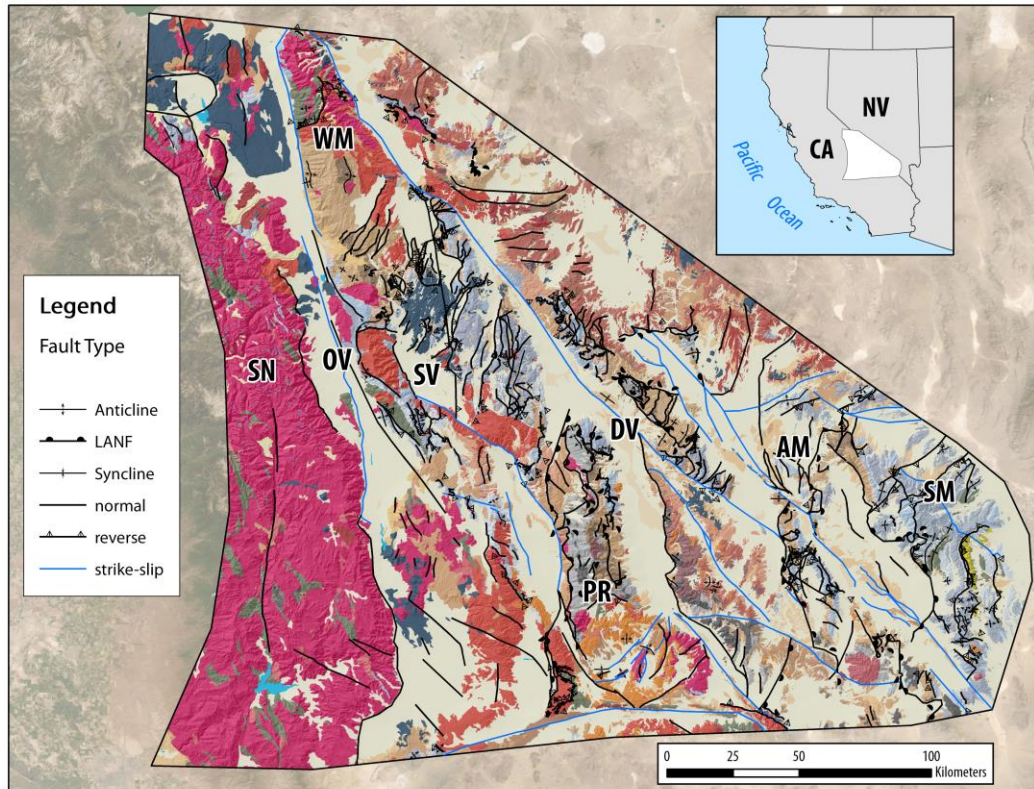
breakup of Rodinia and prior to passive margin formation. As a true passive margin formed during the Late Proterozoic and Early Paleozoic, a thick siliciclastic wedge (~1800m) was deposited. The units comprising the wedge, the Johnnie Formation, the Stirling Quartzite, and the Wood Canyon Formation, primarily consist of shales, sandstones and conglomerates deposited at the base of opposing continental shelves. Today, these units, along with the Pahrump Group, form the Lower Clastic-Confining Unit (LCCU) of the regional carbonate aquifer described by Sweetkind et al. (2004).

During the Paleozoic, a very thick (> 6000m) succession of limestones and dolomites was deposited above the siliciclastic wedge. This carbonate shelf and associated units (e.g., the Carrara Formation, the Bonanza King Formation, the Nopah Formation, the Pogonip Group, etc.) currently form the regional carbonate aquifer underlying much of the study region (i.e., the Lower Carbonate Aquifer [LCA]). In some areas, this sequence of carbonates is interrupted by a relatively thin Upper Clastic Confining Unit (UCCU) (Sweetkind et al., 2004) that primarily formed during the Ordovician. Carbonate deposition above the UCCU, i.e., the Upper Carbonate Aquifer (UCA) continued into the Triassic. UCA units are well exposed in the Spring Mountains (NV).

Passive margin sedimentation ended during the Mesozoic as the Farallon Plate subducted underneath the western continental margin of North America. This period is associated with large scale thrust faulting, the emplacement of the Sierra Nevada Batholith (i.e., the magmatic arc), and widespread plutonism throughout the Death Valley region. Large scale thrust faults created a significant amount of shortening in the present-day Spring Mountains and uplifted large portions of the LCA. Widespread volcanism and metamorphism largely abated during the late Mesozoic. During the late Cretaceous, the region is considered to have been a quiescent, high-elevation, westward or radial draining plateau, i.e., the “Nevadaplano” (Jayko et al., 2009; Snell et al., 2014). Starting around 12-14 Ma, the opening of a slab window underneath the southwestern United States initiated large-magnitude crustal extension (Atwater, 1970) This extension was largely accommodated by normal and strike-slip faulting throughout the region, with transtensional displacement initiating ~3.4 Ma (Phillips et al., 2011). This rapid Neogene extension is responsible for the present-day basin and range topography.

Over the last 500 ka, the influence of tectonics has been fairly minor, and the primary driver of hydrologic and geologic processes has been global glacial/interglacial cycles (Phillips, 2008). During glacial periods, basins functioned as axial fluvial drainage systems and pluvial lakes

formed at the lowest depositional centers in each basin. Flowing rivers between the paleolakes created an interconnected drainage system. During some periods, lake spillover was significant enough to hydrologically connect the Owens Valley to Amargosa Valley, as all axial rivers eventually flowed into Lake Manly (i.e., present-day Death Valley; Knott et al., 2008). Currently, most valley bottoms are playas containing extensive evaporite deposits from the evaporation of both surface runoff (i.e., flooding) following storm events and groundwater discharge in the valley floor. The riverine-lacustrine system became connected as glaciers advanced (i.e., an increase in runoff and lake spillover at low elevations) and disconnected as glaciers retreated during interglacial periods.



Geologic map units

Symbol: Definition (Epoch)

- Qlp: Lacustrine and playa deposits (Pleistocene-Holocene)
- Qa: Alluvium, undivided (Pleistocene-Holocene)
- Qg: Glacial deposits, undivided (Pleistocene-Holocene)
- QTP: Lacustrine and playa deposits (Pliocene-Pleistocene)
- QTSx: Rock avalanche breccias and landslide deposits (Pliocene-Pleistocene)
- QTS: Sediments and sedimentary rocks, undivided (Pliocene-Pleistocene)
- QTVB: Volcanic rocks of Badwater Assemblage (Pliocene-Pleistocene)
- QTB: Basalt (Pliocene-Pleistocene)
- Tb: Basalt (Middle Miocene-Pliocene)
- Tertiary volcanic rocks, undivided (Middle Miocene-Pliocene)
- TxF: Furnace Creek Assemblage: Fault rocks (Upper Miocene-Pliocene)
- TsxF: Furnace Creek Assemblage: Rock avalanche breccia (Upper Miocene-Pliocene)
- TsF: Furnace Creek Assemblage: Sedimentary rocks (Upper Miocene-Pliocene)
- TvF: Furnace Creek Assemblage: Volcanic rocks (Upper Miocene-Pliocene)
- TIF: Furnace Creek Assemblage: Intrusive rocks (Upper Miocene-Pliocene)
- TxN: Navadu Assemblage: Fault rocks (Middle-Upper Miocene)
- TsxN: Navadu Assemblage: Rock avalanche breccia (Middle-Upper Miocene)
- TsN: Navadu Assemblage: Sedimentary rocks (Middle-Upper Miocene)
- TvN: Navadu Assemblage: Volcanic rocks (Middle-Upper Miocene)
- TIN: Navadu Assemblage: Intrusive rocks (Middle-Upper Miocene)
- Tsxo: Owshead Assemblage: Rock avalanche breccia (Middle Miocene)
- Tso: Owshead Assemblage: Sedimentary rocks (Middle Miocene)
- Tvo: Owshead Assemblage: Volcanic rocks (Middle Miocene)
- Tio: Owshead Assemblage: Intrusive rocks (Middle Miocene)

- TsH: Hell's Gate Assemblage: Sedimentary rocks (Middle Miocene)
- TvH: Hell's Gate Assemblage: Volcanic rocks (Middle Miocene)
- TfXT: Titus Canyon Assemblage: Fault rocks (Eocene-Lower Miocene)
- TsxT: Titus Canyon Assemblage: Rock avalanche breccia (Eocene-Lower Miocene)
- TsT: Titus Canyon Assemblage: Sedimentary rocks (Eocene-Lower Miocene)
- TvT: Titus Canyon Assemblage: Volcanic rocks (Eocene-Lower Miocene)
- TKI: Dikes and subvolcanic intrusive rocks (Cretaceous-Oligocene)
- Klw: Lavinia Wash sequence (Cretaceous)
- Kis: Intrusive rocks, mostly silicic (Cretaceous)
- Ja: Aztec Sandstone (Jurassic)
- Jis: Intrusive rocks, mostly quartz monzonite (Jurassic)
- JTRIs: Intrusive rocks, silicic (Triassic-Jurassic)
- JTRsv: Non-intrusive rocks, undivided (Triassic-Jurassic)
- Mzim: Mafic intrusive rocks (Triassic-Cretaceous)
- PPu: Sedimentary rocks, undivided (Pennsylvanian-Permian)
- PPb: Bird Spring Formation (Pennsylvanian-Permian)
- OMu: Sedimentary rocks (Lower Ordovician- upper Mississippian)
- Cbn: Bonanza King, Nopah, and Emigrant formations (Middle- Upper Cambrian)
- Pzu: Metamorphic and sedimentary rocks, undivided (Paleozoic)
- Cc: Cararra, Mule Springs, and Monola formations (Lower Cambrian)
- ZCwsz: Eocambrian clastic wedge, undivided (Neoproterozoic- Lower Cambrian)
- Zj: Johnnie and Wynn formations (Neoproterozoic)
- Zyp: Pahump Group, undivided (Mesoproterozoic-Neoproterozoic)
- Yc: Crystal Springs formation (Mesoproterozoic)
- Xmi: Basement crystalline complex (Paleoproterozoic)

Figure 1.6. Map showing simplified geologic units and major structural features of the study region. Adapted from Lutz et al. (2017).

1.5.3 Climate and Hydrology

The southern Great Basin, including Death Valley National Park, is well known as the hottest and most arid area in North America. The emplacement of the Sierra Nevada batholith, the highest mountain range in the contiguous United States, changed local and regional climate patterns. One of the largest impacts was the creation of a pervasive rain shadow that becomes progressively more arid moving eastward towards Death Valley (the lowest point in North America). This is due to numerous Basin and Range fault-bounded mountain blocks that siphon off Pacific-derived moisture (Ingraham and Taylor, 1991). While the climate in the southern Great Basin can generally be described as hot and arid, there are large contrasts in average temperature and precipitation between basins and ranges. Generally, increases in elevation equate to decreases in temperature and more potential for precipitation (Hunt, 1960). For example, at Furnace Creek, CA (elevation = -59 meters), the average annual high temperature is 32.2 °C, the average annual low temperature is 16.9 °C and the average annual precipitation is 5.7 cm (<https://wrcc.dri.edu/cgi-bin/cliMAIN.pl?ca2319>). In contrast, at the Mount Charleston Fire Station, a high elevation weather station in the Spring Mountains (elevation = 2274 meters), the average annual high temperature is 15.4 °F, the average annual low temperature is 0.9 °F, and the average precipitation is 58.6 cm (<https://wrcc.dri.edu/cgi-bin/cliMAIN.pl?nv5400>).

The southern Great Basin is known for its extremes (e.g., relief, temperature, elevation, salinity, etc.). Despite this, springs number in the thousands across the study area, are ubiquitous across a variety of different landscape positions (e.g., mountains, hillslopes, bajadas, drainages, valley floors), and host fauna with an incredible amount of biodiversity. Other than two rivers, the Owens River and the Amargosa River, springs represent the only source of surficial water. King and Bredehoeft (1999), identified four different types of springs in the Death Valley area: 1) springs along steeply dipping faults, 2) mountain springs, 3) springs emerging at impermeable structural barriers, and 4) springs on the edge of alluvial fans. While many of these springs emerge from mountain block, alluvial, and basin-fill aquifers, the Death Valley region is unique for the regional carbonate aquifer that underlies many of the mountain ranges within the study area. High discharge warm springs found at Ash Meadows (NV) and Furnace Creek (CA) have been previously attributed to interbasin groundwater flow, i.e., groundwater flow occurring underneath surface water drainage divides, routed through regional carbonate aquifer (Hunt and Robinson,

1960; Miller, 1977; Winograd and Thordarson, 1975; Harrill et al., 1988; Steinkampf and Werrell, 2001; Belcher et al, 2009).

1.6 Organization of the Dissertation

This dissertation tests, in a systematic way, different metrics that may define whether a spring is likely to persist or desiccate with increasing regional hydrologic stress due to climate change. While this work is focused on the southern Great Basin (US) with its large diversity of spring ecosystems, geologic units, landscape gradients, and ecotones, the resulting metrics may have implications for the vulnerability of aridland springs globally.

Research into desert springs and their permanence on the landscape spans a variety of disciplines. As such, multiple tools are used in this dissertation including remote sensing, geospatial analysis, geochemistry and geochemical modeling, isotope hydrology and age-dating, physical hydrogeology, and collaborative work regarding field ecology (macroinvertebrate and microbial). Only when studied in unison can true metrics be derived. The work is more powerful and impactful when thinking about the crossover between disciplines.

Each chapter is structured as has its own Abstract, Introduction, Methods, Results, Discussion, Conclusions, and References sections and (with the exception of Chapter 2) is designed to test a different metric or combination of metrics. Moreover, each chapter and has its own science question(s) which fall(s) under the umbrella of the overarching questions. The concluding chapter synthesizes this body of work and addresses the overarching questions.

1.7 Chapter Descriptions

In Chapter 2 (An Alternative Data Preprocessing Method for Generating Geochemical Clusters from Major Ion Data), an alternative data preprocessing technique is presented as an attempt to mitigate current problems with the prevailing workflow utilized in studies employing geochemical clustering. Geochemical clustering methods (e.g., hierarchical clustering analysis, k-means clustering, fuzzy k-means clustering, etc.) are often performed as an initial step in groundwater characterization and are useful for identifying groundwater facies, grouping samples on the basis of geochemical similarity, and categorizing samples flowing through similar geologic units. In relation to the greater IES project, geochemical clustering results have significant

implications for the integration of geochemical data with ecological data. The current most utilized geochemical clustering workflow in the literature (i.e., “traditional methodology”) has been previously criticized for ignoring geochemical kinetics, overlooking geologic complexity, and showing a bias towards tracking changes in groundwater salinity rather than geochemical evolution through particular units. However, there are very few published alternatives to this workflow. Therefore, in this chapter, a new data preprocessing methodology was developed with the goal of taking the strengths from graphical diagnostic tools and applying them to multivariate analysis techniques. The alternative methodology was tested against the traditional methodology for two case studies of differing spatial scales and dataset sizes 1) a small dataset of springs emerging from the eastern Sierra Nevada in Owens Valley (CA) and 2) a larger dataset of springs emerging throughout the Spring Mountains (NV). Clustering results obtained using the alternative preprocessing methodology more closely matched hypothesized geochemical evolution pathways from the literature (e.g., Warix et al., 2020) and provide an alternative option depending on the goals of the analyst.

Chapter 3 (Old Groundwater Buffers the Effects of Climate Change in Groundwater-Dependent Ecosystems) directly addresses the short-term *resistance* of springs in response to a major drought by using a novel combination of remote sensing and groundwater residence time data. In desert landscapes, vibrant, green vegetation is an indicator of water availability and healthy ecosystem functioning. Perennial springflow plays a large role in sustaining groundwater-dependent ecosystems (GDEs) in harsh desert environments like the southern Great Basin, USA to such an extent that vegetation is a reliable indicator of groundwater emergence (i.e., springs). The vegetation surrounding these spring emergences only persists because of the water availability. Therefore, I hypothesize that the vegetation response in these zones to significant perturbations, such as a long-term drought, should be indicative of a spring’s hydrologic stability and that groundwater residence time, a proxy for hydrologic stability, can be used to predict spring vegetation response. I present an analysis of riparian vegetation surrounding snowmelt-recharge driven springs in Owens Valley, CA during the historic 2011-2017 California drought, the driest period since records began in 1895. This was accomplished by extracting time series of NDVI derived from Landsat 7 multispectral imagery from digitized polygons surrounding spring emergences. Vegetation stability metrics were computed from these time series, including the standard deviation of annual peak NDVI and the slope of the linear regression fitted to annual peak

NDVI for the 2011-2016 period after onset of the drought and prior to drought recovery in 2017. These metrics were coupled with residence time environmental tracer data, including tritium (^3H) and chlorine-36 (^{36}Cl), to establish criteria for young/old classification of spring waters. Our results indicate that groundwater dependent ecosystems discharging a large component of young water (post- 1950s/60s) were more susceptible to dying/drying during the drought than springs discharging a substantial component of submodern or ancient groundwater (pre- 1950s/60s to thousands of years). While the springs with a higher fraction of modern water displayed steady decreases in their yearly peak NDVI as the drought progressed, springs largely discharging older water displayed dampened or no vegetation response and were relatively unaffected by drought conditions as indicated by both NDVI metrics.

Chapter 4 (The Effect of Spatial Scale and Time on Geochemical Evolution Inferred from Springs in the Southeastern Sierra Nevada, USA: Revisiting Garrels and Mackenzie (1967)) examines the relationship between groundwater residence time and geochemical evolution at the mountain-block scale, i.e. intermediate flowpath length. This chapter builds on seminal work from Feth (1964) and Garrels and Mackenzie (1967). The motivating research question of this chapter is to understand at what spatial and temporal scales simple metrics like specific conductivity and temperature serve as proxies for residence time, i.e., can a simple metric like conductivity be used to infer groundwater residence time with increasing spatial scale and flowpath length? In this chapter I utilize a multitracer approach (e.g., stable isotopes, general chemistry, $^{87}\text{Sr}/^{86}\text{Sr}$, noble gases, ^3H , $^{36}\text{Cl}/\text{Cl}$, ^{14}C) and employ inverse geochemical modeling to understand the controls on geochemical evolution of springs emerging on the mountain front of the eastern Sierra Nevada. The results of this study show that while geologic heterogeneity exerts a dominant control on geochemical evolution, even in a relatively geologically homogeneous mountain block such as the Sierra Nevada batholithic, within geochemical groups sourcing plutons and/or geologic units of similar petrologic composition, a simple metric like conductivity can be used to infer residence time.

In Chapter 5 (Examining Spring Landscape Placement and Emergence Mechanism as Controls on Hydrochemical Characteristics and Ecological Community Structure), I seek to understand the significance of where and why a spring emerges and potential hydrochemical characteristics related to vulnerability. In this chapter I address the following research questions:

- 1) Are there systematic patterns with spring landscape placement and hydrochemical

characteristics that can be predicted by topographic metrics and/or landform analysis? and 2) If present, how do these patterns influence benthic macroinvertebrate community structure at the regional scale, where the effects of heterogeneity (e.g., Chapter 4) are significantly dampened by groundwater residence time and flowpath length? The southern Great Basin is the ideal place to answer these questions because springs are found across all topographic features, are generally isolated from one another, and host diverse benthic communities. The first question is answered by creating a regional hydrochemical dataset of springs in the southern Great Basin from government databases, consultant reports, and scientific journals. Spring hydrochemical characteristics (e.g., discharge temperature, specific conductance, radiocarbon activity, etc.) from the regional dataset are tested against qualitative landscape placement classifications and quantitative topographic indices (e.g., elevation, slope, Topographic Wetness Index, profile curvature, relative elevation). Springs from recent sampling efforts (i.e., the IES springs) are examined against the regional dataset to assess whether they are representative of regional trends prior to benthic macroinvertebrate (BMI) analysis. Finally, I use a combination of non-metric multidimensional scaling (NMDS) and ecological indices to examine landscape controls on BMI community structure at the regional scale. My results show that there are systematic relationships of increasing temperature, specific conductance, and groundwater residence time moving from high topographic positions (e.g., Nival, High Alpine) to lower topographic positions (e.g., Low Alpine, Valley Floor). These relationships fail moving from the “Valley Floor” to “Playa” topographic settings. These systematic trends create an environmental harshness gradient that structures BMI communities at the regional scale. From high topographic positions to low topographic positions, BMI community tolerance increase, richness decreases, and diversity decreases. The summation of results from this chapter led to the development of a coupled topographic/hydrochemical/ecological conceptual model of spring systems in the southern Great Basin.

In Chapter 6 (Is Temporal Variability an Indicator of Groundwater Residence Time? Tales from the Southern Great Basin), I seek to understand whether decreased temporal variability of spring hydrochemical characteristics is correlated with increased groundwater residence time. In other words, is dampened temporal variability indicative of long-term hydrogeological stability? This chapter focuses on 33 springs within the southern Great Basin that were sampled up to 8 times between 2016-2019 for a suite of geochemical measurements (e.g., temperature, major ions, trace

elements, $^{87}\text{Sr}/^{86}\text{Sr}$, $\delta^{18}\text{O}$, $\delta^2\text{H}$, etc.). This sampling interval is interesting as it captures the tail end of the historical 2011-2017 California drought as well as the subsequent drought recovery of the region. I utilize time series analysis and metrics of variability (e.g., standard deviation and variance) to understand which springs were the most variable and which springs were the most stable over the sampling interval. Overall, the results of this chapter are somewhat inconclusive. The majority of springs (26/33) show very minimal variability over the sampling interval and these springs span a wide range of groundwater residence time from bomb-pulse (i.e., 60-70 years) to ancient (10,000 years +). Springs that do show increased variability across a suite of geochemical metrics have this variability attributed to ecologically unfavorable surface conditions (e.g., low discharge, specific spheres of emergence, disturbance) or increased flowpath variability (e.g., injections of modern groundwater as substantial component of the flowpath distribution). The results of this chapter emphasize the need to decouple hydrogeological vulnerability from ecological variability,

In Chapter 7, I provide conclusions and recommendations for future work.

1.8 References

- Amiel, R. B., Grodek, T., & Frumkin, A. (2010). Characterization of the hydrogeology of the sacred Gihon Spring, Jerusalem: a deteriorating urban karst spring. *Hydrogeology Journal*, 18(6), 1465-1479.
- Atwater, T. (1970). Implications of plate tectonics for the Cenozoic tectonic evolution of western North America. *Geological Society of America Bulletin*, 81(12), 3513-3536.
- Belcher, W. R., Bedinger, M. S., Back, J. T., & Sweetkind, D. S. (2009). Interbasin flow in the Great Basin with special reference to the southern Funeral Mountains and the source of Furnace Creek springs, Death Valley, California, US. *Journal of Hydrology*, 369(1-2), 30-43.
- Box, J. B., Duguid, A., Read, R. E., Kimber, R. G., Knapton, A., Davis, J., & Bowland, A. E. (2008). Central Australian waterbodies: the importance of permanence in a desert landscape. *Journal of Arid Environments*, 72(8), 1395-1413.
- Bradford, D. F., Neale, A. C., Nash, M. S., Sada, D. W., & Jaeger, J. R. (2003). Habitat patch occupancy by toads (*Bufo punctatus*) in a naturally fragmented desert landscape. *Ecology*, 84(4), 1012-1023.
- Bredehoeft, J. D. (2011). Monitoring regional groundwater extraction: the problem. *Groundwater*, 49(6), 808-814.
- Brune, G. M. (2002). Springs of Texas (Vol. 1). Texas A&M University Press.
- Bryan, K. (1919). Classification of springs. *The Journal of Geology*, 27(7), 522-561.

- Burchfiel, B. C., Fleck, R. J., Secor, D. T., Vincelette, R. R., & Davis, G. A. (1974). Geology of the Spring Mountains, Nevada. *Geological Society of America Bulletin*, 85(7), 1013-1022.
- Burns, E. R., Zhu, Y., Zhan, H., Manga, M., Williams, C. F., Ingebritsen, S. E., & Dunham, J. B. (2017). Thermal effect of climate change on groundwater-fed ecosystems. *Water Resources Research*, 53(4), 3341-3351.
- Cartwright, I., Cendón, D., Currell, M., & Meredith, K. (2017). A review of radioactive isotopes and other residence time tracers in understanding groundwater recharge: Possibilities, challenges, and limitations. *Journal of Hydrology*, 555, 797-811.
- Cartwright, J., & Johnson, H. M. (2018). Springs as hydrologic refugia in a changing climate? A remote-sensing approach. *Ecosphere*, 9(3), e02155.
- Cereceda, P., Schemenauer, R. S., & Suit, M. (1992). An alternative water supply for Chilean coastal desert villages. *International Journal of Water Resources Development*, 8(1), 53-59.
- Criss, R. E. (2010). A Darcian Model for the Flow of Big Spring and the hydraulic head in the Ozark aquifer, Missouri, USA. *Acta Carsologica*, 39(2).
- Davis, J. A., Kerezszy, A., & Nicol, S. (2017). Springs: conserving perennial water is critical in arid landscapes. *Biological Conservation*, 211, 30-35.
- Döll, P., & Fiedler, K. (2007). Global-scale modeling of groundwater recharge. *Hydrology and Earth System Sciences Discussions*, 4(6), 4069–4124
- Echelle, A. A. (2008). The western North American pupfish clade (Cyprinodontidae: Cyprinodon): mitochondrial DNA divergence and drainage history. *Special Paper of the Geological Society of America*, 439, 27.
- Echelle, A. A., Carson, E. W., Echelle, A. F., Van Den Bussche, R. A., Dowling, T. E., & Meyer, A. (2005). Historical biogeography of the new-world pupfish genus *Cyprinodon* (Teleostei: Cyprinodontidae). *Copeia*, 2005(2), 320-339.
- Fagan, W. F., Aumann, C., Kennedy, C. M., & Unmack, P. J. (2005). Rarity, fragmentation, and the scale dependence of extinction risk in desert fishes. *Ecology*, 86(1), 34-41.
- Feth, J. H. F., Robertson, C. E., & Polzer, W. L. (1964). *Sources of mineral constituents in water from granitic rocks, Sierra Nevada, California and Nevada* (No. 1535-I). US Govt. Print. Off.,.
- Fleishman, E., Murphy, D. D., & Sada, D. W. (2006). Effects of environmental heterogeneity and disturbance on the native and non-native flora of desert springs. *Biological Invasions*, 8(5), 1091.
- Freed, Z., Aldous, A., & Gannett, M. W. (2019). Landscape controls on the distribution and ecohydrology of central Oregon springs. *Ecohydrology*, 12(2), e2065.
- Frisbee, M. D., Phillips, F. M., White, A. F., Campbell, A. R., & Liu, F. (2013). Effect of source integration on the geochemical fluxes from springs. *Applied Geochemistry*, 28, 32-54.

- Frisbee, M. D., Wilson, J. L., Gomez-Velez, J. D., Phillips, F. M., & Campbell, A. R. (2013). Are we missing the tail (and the tale) of residence time distributions in watersheds?. *Geophysical Research Letters*, 40(17), 4633-4637.
- Frisbee, M. D., Wilson, J. L., & Sada, D. W. (2013). Climate Change and the Fate of Desert Springs: Innovation Working Group on the Response of Springs to the Effects of Climate Change; Jemez Springs, New Mexico, 1–3 October 2102. *Eos, Transactions American Geophysical Union*, 94(15), 144-144.
- Faunt, C. C. (1997). *Effect of faulting on ground-water movement in the Death Valley region, Nevada and California* (No. USGS/WRIR-95-4132). Geological Survey, Denver, CO (United States).
- Garrels, R. M., & Mackenzie, F. T. (1967). Origin of the chemical compositions of some springs and lakes.
- Harrill, J. R., Gates, J. S., & Thomas, J. M. (1988). *Major ground-water flow systems in the Great Basin region of Nevada, Utah, and adjacent states* (No. 694-C). US Geological Survey.
- Heaman, L. M., & Grotzinger, J. P. (1992). 1.08 Ga diabase sills in the Pahrump Group, California: Implications for development of the Cordilleran miogeocline. *Geology*, 20(7), 637-640.
- Hershler, R. (1999). A systematic review of the hydrobiid snails (Gastropoda: Rissoidea) of the Great Basin, western United States. Part II. Genera *Colligyru*s, *Fluminicola*, *Pristinicola*, and *Tryonia*. *The Veliger*.
- Hershler, R., & Liu, H. (2008). Ancient vicariance and recent dispersal of springsnails (Hydrobiidae: Pyrgulopsis) in the Death Valley system, California-Nevada. *Special Papers-Geological Society of America*, 439, 91.
- Holmquist, J. G., Schmidt-Gengenbach, J., & Slaton, M. R. (2011). Influence of invasive palms on terrestrial arthropod assemblages in desert spring habitat. *Biological Conservation*, 144(1), 518-525.
- Hubbs, C. L., & Miller, R. R. (1948). *The Great Basin: With Emphasis on Glacial and Postglacial Times. The Zoological Evidence: Correlation Between Fish Distribution and Hydrographic History in the Desert Basins of Western United States. II*. University of Utah.
- Hunt, C. B., & Robinson, T. W. (1960). Possible interbasin circulation of ground water in the southern part of the Great Basin. *US Geological Survey Professional Paper*, B273-B274.
- Hunter Jr, M. L., Acuña, V., Bauer, D. M., Bell, K. P., Calhoun, A. J., Felipe-Lucia, M. R., ... & Lundquist, C. J. (2017). Conserving small natural features with large ecological roles: a synthetic overview. *Biological Conservation*, 211, 88-95.
- Idris, H. (1996). Springs in Egypt. *Environmental Geology*, 27(2), 99-104.

- Iknayan, K. J., & Beissinger, S. R. (2018). Collapse of a desert bird community over the past century driven by climate change. *Proceedings of the National Academy of Sciences*, 115(34), 8597-8602.
- Ingraham, N. L., & Taylor, B. E. (1991). Light stable isotope systematics of large-scale hydrologic regimes in California and Nevada. *Water Resources Research*, 27(1), 77-90.
- Jaeger, J. R., Riddle, B. R., Jennings, R. D., & Bradford, D. F. (2001). Rediscovering *Rana onca*: evidence for phylogenetically distinct leopard frogs from the border region of Nevada, Utah, and Arizona. *Copeia*, 2001(2), 339-354.
- Jayko, A. S., Oldow, J. S., & Cashman, P. H. (2009). Deformation of the late Miocene to Pliocene Inyo surface, eastern Sierra region, California. Late Cenozoic Structure and Evolution of the Great Basin–Sierra Nevada Transition: *Geological Society of America Special Paper*, 447, 313-350.
- Jayko, A. S., & Bursik, M. (2011). Active transtensional intracontinental basins: Walker Lane in the western Great Basin. *Tectonics of sedimentary basins: Recent advances*, 226-248.
- Jett, S. C. (1992). An introduction to Navajo sacred places. *Journal of Cultural Geography*, 13(1), 29-39.
- Jiao, J. J. (2010). Crescent Moon Spring: a disappearing natural wonder in the Gobi desert, China. *Groundwater*, 48(1), 159-163.
- Junghans, K., Springer, A. E., Stevens, L. E., & Ledbetter, J. D. (2016). Springs ecosystem distribution and density for improving stewardship. *Freshwater Science*, 35(4), 1330-1339.
- Keleher, M. J., & Rader, R. B. (2008). Bioassessment of artesian springs in the Bonneville Basin, Utah, USA. *Wetlands*, 28(4), 1048-1059.
- King, M. J., & Bredehoeft, J. D. (1998). Death Valley Springs Geochemical Investigation Yucca Mountain Nuclear Repository, Inyo County Oversight-1998. *Hydrodynamics Group*, Edmonds, Washington, USA.
- Knott, J. R., Machette, M. N., Klinger, R. E., Sarna-Wojcicki, A. M., Liddicoat, J. C., David, B. T., & Ebbs, V. M. (2008). Reconstructing late Pliocene to middle Pleistocene Death Valley lakes and river systems as a test of pupfish (Cyprinodontidae) dispersal hypotheses. *Late Cenozoic drainage history of the southwestern Great Basin and lower Colorado River region: geologic and biotic perspectives*, 439, 1.
- Kodric-Brown, A., & Brown, J. H. (2007). Native fishes, exotic mammals, and the conservation of desert springs. *Frontiers in Ecology and the Environment*, 5(10), 549-553.
- Kodric-Brown, A., Wilcox, C., Bragg, J. G., & Brown, J. H. (2007). Dynamics of fish in Australian desert springs: role of large-mammal disturbance. *Diversity and Distributions*, 13(6), 789-798.
- Lincoln, R. J. (1998). A dictionary of ecology, evolution and systematics (No. C/574.5 L5).

- Lutz, B. M., Axen, G. J., & Phillips, F. M. (2017). New Geologic Map and Structural Cross Sections of the Death Valley Extended Terrain (southern Sierra Nevada, California to Spring Mountains, Nevada): Toward 3D Kinematic Reconstructions. *AGUFM*, 2017, T41B-0625.
- MacDonald, G. M. (2010). Water, climate change, and sustainability in the southwest. *Proceedings of the National Academy of Sciences*, 107(50), 21256-21262.
- Mahon, R. C., Dehler, C. M., Link, P. K., Karlstrom, K. E., & Gehrels, G. E. (2014). Geochronologic and stratigraphic constraints on the Mesoproterozoic and Neoproterozoic Pahrump Group, Death Valley, California: A record of the assembly, stability, and breakup of Rodinia. *Geoscience Bulletin*, 126(5-6), 652-664.
- Manga, M. (1999). On the timescales characterizing groundwater discharge at springs. *Journal of Hydrology*, 219(1-2), 56-69.
- Manga, M. (2001). Using springs to study groundwater flow and active geologic processes. *Annual Review of Earth and Planetary Sciences*, 29(1), 201-228.
- Manning, A. H., Clark, J. F., Diaz, S. H., Rademacher, L. K., Earman, S., & Plummer, L. N. (2012). Evolution of groundwater age in a mountain watershed over a period of thirteen years. *Journal of Hydrology*, 460, 13-28.
- McKenna, O. P., & Sala, O. E. (2018). Groundwater recharge in desert playas: current rates and future effects of climate change. *Environmental Research Letters*, 13(1), 014025.
- Meixner, T., Manning, A. H., Stonestrom, D. A., Allen, D. M., Ajami, H., Blasch, K. W., ... & Flint, A. L. (2016). Implications of projected climate change for groundwater recharge in the western United States. *Journal of Hydrology*, 534, 124-138.
- Miller, R. R. (1961). Man and the Changing Fish Fauna of the American Southwest. *Papers of the Michigan Academy of Science, Arts, and Letters*, 46, 365-404.
- Miller, G. A. (1977). Appraisal of the water resources of Death Valley, California-Nevada (No. 77-728). US Geological Survey,.
- Mills, B. J., & Ferguson, T. J. (1998). Preservation and research of sacred sites by the Zuni Indian tribe of New Mexico. *Human Organization*, 30-42.
- Minckley, W. L., & Deacon, J. E. (1968). Southwestern Fishes and the Enigma of "Endangered Species". *Science*, 159(3822), 1424-1432.
- Mote, P. W., Hamlet, A. F., Clark, M. P., & Lettenmaier, D. P. (2005). Declining mountain snowpack in western North America. *Bulletin of the American Meteorological Society*, 86(1), 39-50.
- Mote, P. W., Rupp, D. E., Li, S., Sharp, D. J., Otto, F., Uhe, P. F., ... & Allen, M. R. (2016). Perspectives on the causes of exceptionally low 2015 snowpack in the western United States. *Geophysical Research Letters*, 43(20), 10-980.

- Mote, P. W., Li, S., Lettenmaier, D. P., Xiao, M., & Engel, R. (2018). Dramatic declines in snowpack in the western US. *Npj Climate and Atmospheric Science*, 1(1), 1-6.
- Musselman, K. N., Lehner, F., Ikeda, K., Clark, M. P., Prein, A. F., Liu, C., ... & Rasmussen, R. (2018). Projected increases and shifts in rain-on-snow flood risk over western North America. *Nature Climate Change*, 8(9), 808-812.
- Patten, D. T., Rouse, L., & Stromberg, J. C. (2008). Isolated spring wetlands in the Great Basin and Mojave Deserts, USA: potential response of vegetation to groundwater withdrawal. *Environmental Management*, 41(3), 398-413.
- Perla, B. S., & Stevens, L. E. (2008). Biodiversity and productivity at an undisturbed spring in comparison with adjacent grazed riparian and upland habitats. *Aridland springs in North America: Ecology and conservation*, 230-243.
- Phillips, F. M., Reheis, M. C., Hershler, R., & Miller, D. M. (2008). Geological and hydrological history of the paleo-Owens River drainage since the late Miocene. *Special Papers-Geological Society of America*, 439, 115.
- Phillips, F. M., McIntosh, W. C., & Dunbar, N. W. (2011). Chronology of late Cenozoic volcanic eruptions onto relict surfaces in the south-central Sierra Nevada, California. *GSA Bulletin*, 123(5-6), 890-910.
- Pigati, J. S., Springer, K. B., & Honke, J. S. (2019). Desert wetlands record hydrologic variability within the Younger Dryas chronozone, Mojave Desert, USA. *Quaternary Research*, 91(1), 51-62.
- Pinder, G. F., & Jones, J. F. (1969). Determination of the ground-water component of peak discharge from the chemistry of total runoff. *Water Resources Research*, 5(2), 438-445.
- Powell, O., & Fensham, R. (2016). The history and fate of the Nubian Sandstone Aquifer springs in the oasis depressions of the Western Desert, Egypt. *Hydrogeology Journal*, 24(2), 395-406.
- Powell, O., Silcock, J., & Fensham, R. (2015). Oases to oblivion: The rapid demise of springs in the south-eastern Great Artesian Basin, Australia. *Groundwater*, 53(1), 171-178.
- Quade, J., Mifflin, M. D., Pratt, W. L., McCoy, W., & Burckle, L. (1995). Fossil spring deposits in the southern Great Basin and their implications for changes in water-table levels near Yucca Mountain, Nevada, during Quaternary time. *Geological Society of America Bulletin*, 107(2), 213-230.
- Rademacher, L. K., Clark, J. F., Hudson, G. B., Erman, D. C., & Erman, N. A. (2001). Chemical evolution of shallow groundwater as recorded by springs, Sagehen basin; Nevada County, California. *Chemical Geology*, 179(1-4), 37-51.
- Rademacher, L. K., Clark, J. F., Clow, D. W., & Hudson, G. B. (2005). Old groundwater influence on stream hydrochemistry and catchment response times in a small Sierra Nevada catchment: Sagehen Creek, California. *Water Resources Research*, 41(2).

- Ragab, R., & Prudhomme, C. (2002). Sw—soil and Water: climate change and water resources management in arid and semi-arid regions: prospective and challenges for the 21st century. *Biosystems Engineering*, 81(1), 3-34.
- Rohde, M. M., Froend, R., & Howard, J. (2017). A global synthesis of managing groundwater dependent ecosystems under sustainable groundwater policy. *Groundwater*, 55(3), 293-301.
- Sada, D. W., & Herbst, D. B. (2001). Macroinvertebrates and environmental characteristics of Owens Valley springs, Inyo County, California. Bishop: City of Los Angeles Department of Water and Power.
- Sada, D. W., & Vinyard, G. L. (2002). Anthropogenic changes in biogeography of Great Basin aquatic biota. *Smithsonian Contributions to the Earth Sciences*, (33), 277-294.
- Sada, D. W., Fleishman, E., & Murphy, D. D. (2005). Associations among spring-dependent aquatic assemblages and environmental and land use gradients in a Mojave Desert mountain range. *Diversity and Distributions*, 11(1), 91-99.
- Sada, D. (2008). Great Basin riparian and aquatic ecosystems. In: Chambers, Jeanne C.; Devoe, Nora; Evenden, Angela, eds. Collaborative management and research in the Great Basin—examining the issues and developing a framework for action. Gen. Tech. Rep. RMRS-GTR-204. Fort Collins, CO: US Department of Agriculture, Forest Service, Rocky Mountain Research Station. p. 49-52, 204.
- Schroeder, R. A., Smith, G. A., Martin, P., Flint, A. L., Gallegos, E., & Fisher, R. N. (2015). The source, discharge, and chemical characteristics of selected springs, and the abundance and health of associated endemic anuran species in the Mojave network parks (No. 2015-5027). US Geological Survey.
- Schütt, H., & Şeşen, R. (1989). The freshwater molluscs of Ceylanpinar. *Zoology in the Middle East*, 3(1), 55-58.
- Seager, R., Ting, M., Held, I., Kushnir, Y., Lu, J., Vecchi, G., ... & Li, C. (2007). Model projections of an imminent transition to a more arid climate in southwestern North America. *Science*, 316(5828), 1181-1184.
- Shepard, W. D. (1993). Desert springs—both rare and endangered. *Aquatic Conservation: Marine and Freshwater Ecosystems*, 3(4), 351-359.
- Singleton, M. J., & Moran, J. E. (2010). Dissolved noble gas and isotopic tracers reveal vulnerability of groundwater in a small, high-elevation catchment to predicted climate changes. *Water Resources Research*, 46(10).
- Smith, G. R., Dowling, T. E., Gobalet, K. W., Lugaski, T. S. D. K., Shiozawa, D. K., & Evans, R. P. (2002). Biogeography and timing of evolutionary events among Great Basin fishes. *Great Basin aquatic systems history*, 33, 175-234.

- Smyth, M., & Coulombe, H. N. (1971). Notes on the use of desert springs by birds in California. *The Condor*, 73(2), 240-243.
- Snell, K. E., Koch, P. L., Druschke, P., Foreman, B. Z., & Eiler, J. M. (2014). High elevation of the 'Nevadaplano' during the Late Cretaceous. *Earth and Planetary Science Letters*, 386, 52-63.
- Snyder, K. A., Evers, L., Chambers, J. C., Dunham, J., Bradford, J. B., & Loik, M. E. (2019). Effects of changing climate on the hydrological cycle in cold desert ecosystems of the Great Basin and Columbia Plateau. *Rangeland Ecology & Management*, 72(1), 1-12.
- Sophocleous, M. (2014). On Understanding and Predicting Groundwater Response Time (Retraction of Ground Water, vol 50, pg 528-540, 2012). *Ground Water*, 52(2), 322-322.
- Springer, A. E., Stevens, L. E., Anderson, D. E., Parnell, R. A., Kreamer, D. K., Levin, L. A., & Flora, S. P. (2008). A comprehensive springs classification system. *Aridland springs in North America: ecology and conservation*. University of Arizona Press and Arizona–Sonora Desert Museum, Tucson, 49-75.
- Springer, A. E., & Stevens, L. E. (2009). Spheres of discharge of springs. *Hydrogeology Journal*, 17(1), 83.
- Stanley, C. V. B. (1912). The Oasis of Siwa. *Journal of the Royal African Society*, 11(43), 290-324.
- Steinkampf, W. C., & Werrell, W. L. (2001). *Ground-water flow to Death Valley, as inferred from the chemistry and geohydrology of selected springs in Death Valley National Park, California and Nevada* (Vol. 98, No. 4114). US Department of the Interior, US Geological Survey.
- Sweetkind, D. S., Belcher, W. R., Faunt, C. C., & Potter, C. J. (2004). Geology and hydrogeology. *Death Valley regional ground-water flow system, Nevada and California—Hydrogeologic framework and transient ground-water flow model*: US Geological Survey Scientific Investigations Report, 5205, 21-98.
- Toth, J. (1963). A theoretical analysis of groundwater flow in small drainage basins. *Journal of Geophysical Research*, 68(16), 4795-4812.
- Tóth, J. (1999). Groundwater as a geologic agent: an overview of the causes, processes, and manifestations. *Hydrogeology Journal*, 7(1), 1-14.
- Unmack, P. J., & Minckley, W. L. (2008). The demise of desert springs. *Aridland springs in North America: ecology and conservation*. University of Arizona Press, Tucson, 11-34.
- Wasserburg, G. J., Wetherill, G. W., & Wright, L. A. (1959). Ages in the precambrian terrane of Death Valley, California. *The Journal of Geology*, 67(6), 702-708.
- Wauer, R. H. (1962). A survey of the birds of Death Valley. *The Condor*, 64(3), 220-233.
- Wauer, R. H. (1964). Ecological distribution of the birds of the Panamint Mountains, California. *The Condor*, 66(4), 287-301.

- Weissinger, R., Philippi, T. E., & Thoma, D. (2016). Linking climate to changing discharge at springs in Arches National Park, Utah, USA. *Ecosphere*, 7(10), e01491.
- Wilson, J. L., & Guan, H. (2004). Mountain-block hydrology and mountain-front recharge. *Groundwater recharge in a desert environment: The Southwestern United States*, 9.
- Winograd, I. J., & Thordarson, W. (1975). Hydrogeologic and hydrochemical framework, south-central Great Basin, Nevada-California, with special reference to the Nevada Test Site.
- Wright, L. A., & Troxel, B. W. (1966). Strata of late Precambrian-Cambrian age, Death Valley region, California-Nevada. *AAPG Bulletin*, 50(5), 846-857.
- Woo, D., & Hughson, D. (2004). Zzyzx Mineral Springs—Cultural Treasure and Endangered Species Aquarium. In *Protecting Our Diverse Heritage: The Role of Parks, Protected Areas, and Cultural Sites*. Proceedings of the 2003 George Wright Society/National Park Service Joint Conference. Hancock, Michigan: The George Wright Society.
- Zekri, S., Mbaga, M., Fouzai, A., & Al-Shaqsi, S. (2011). Recreational value of an oasis in Oman. *Environmental Management*, 48(1), 81-88.

CHAPTER 2. AN ALTERNATIVE DATA PREPROCESSING METHOD FOR GENERATING GEOCHEMICAL CLUSTERS FROM MAJOR ION DATA

2.1 Abstract

Multivariate statistical methods are frequently applied to water chemistry data as a means of reducing the magnitude and complexity of a dataset into a series of principal components or geochemical clusters. Hierarchical clustering analysis (HCA) using Ward's linkage method and Euclidean distance is the most commonly used algorithm for generating geochemical clusters from major cation and anion data. Data treatment prior to HCA, termed "traditional data preprocessing" (TDP) in this paper, typically consists of log transformation and standardization of raw cation and anion concentrations. This data treatment has become standard and is a part of many sequential workflows where cluster centroids from HCA results are used as inputs for geochemical modeling and for conceptual model formation. However, there are concerns that preprocessing of this type can obscure potential geochemical relationships and result in bias during HCA.

Here I present an alternative data preprocessing (ADP) technique for major cation and ion data prior to HCA. This preprocessing technique takes the strengths from graphical diagnostic tools (e.g., piper and stiff diagrams) and numerically quantifies them while providing some degree of user customization. I test our technique by comparing HCA results obtained using TDP and ADP methods for two hydrochemical case studies in geologically distinct regions: 1) the eastern Sierra Nevada in Owens Valley, CA and 2) the Spring Mountains (NV). Our results show that TDP prior to HCA results in clusters that tend to track changes in overall salinity rather than specific geochemical "fingerprints". Geochemical clusters derived from ADP more closely track groundwater evolution through specific units and more consistently partition specific water facies. Depending on the goals of the user, both methods are viable, but provide the user with different information. In conclusion, we urge: 1) a **return** to basics (i.e., bivariate solute plots) prior to multivariate analysis, 2) **awareness** of the potential tendencies or biases of different clustering and data preprocessing methods, 3) **openness** in trying alternative preprocessing techniques that may better address the goals of the analyst, and 4) **caution** when exercising sequential or patterned workflows, as it is imperative to fully evaluate if clustering results are kinetically feasible or geologically sensible. This works seeks to inform others to use caution when exercising patterned

workflows for clustering/grouping of water chemistry data that may have inherent biases, not to criticize the utility and value of information gleaned from prior studies. Our methodology simply offers an alternative approach.

2.2 Introduction

2.2.1 What is useful about water chemistry data?

The chemical composition or geochemical “fingerprint” of natural waters (e.g., lakes, rivers, streams, wetlands, springs, groundwater, etc.) is a product of many factors (e.g., climate, geology, topography, aerosol deposition, mixing, etc.) and a direct reflection of interactions between terrestrial earth systems. As such, dissolved constituents have long been used as natural tracers (Back, 1966) to investigate processes that we cannot physically see or processes that occur at timescales or spatial scales that are difficult to measure. This point is especially valid for groundwater studies, where analytes such as major ions, trace elements, and rare earth elements are frequently used to provide indirect observations about source rock type, biogeochemical cycling, groundwater circulation and flowpath delineation, mixing of water sources, and water quality (Hem, 1985).

2.2.2 Why do people cluster or group water chemistry data?

There are myriad reasons why “clustering” or grouping of water chemistry data is performed. Clustering is a common, first-order, hydrogeological reconnaissance approach for groundwater characterization (Belkhir et al., 2010) and/or distinguishing hydrochemical facies (Güler et al., 2004; McNeil et al., 2005; Gabellone et al., 2008; Bushman et al., 2010). In instances where the hydrochemical framework is well understood, clustering has been used to examine temporal processes such as geochemical evolution (King et al., 2014), temporal dynamics (Zelazny et al., 2011), and temporal variability (Lin et al., 2012) of individual sites or study areas. When multivariate clustering results are projected into a Geographic Information System (GIS), they can be used to understand spatial groundwater evolution patterns at regional and local scales (Suk and Lee, 1997; Farnham et al., 2000; Kebede et al., 2005; Koonce et al., 2006; Cloutier et al., 2008; Monjerezi et al., 2011; Ghesquière et al., 2015) and to delineate probable groundwater flowpaths (Bushman et al., 2010; Al-Qudah et al., 2011).

Other specific uses of geochemical clustering include: 1) Assessing the influence of anthropogenic activities on natural water (Fitzpatrick et al., 2007; Güler et al., 2012) , 2) investigating the relationship between geochemical composition (including trace and rare earth elements) and aquifer mineralogy (Kreamer et al., 1996; Güler et al., 2004), 3) identifying previously unrecognized regional waters in well-sparse regions (Hershey et al., 2010), 4) distinguishing between “fast” and “slow” flowpaths (Elsenbeer et al., 1995), 5) understanding the interaction between groundwater and surface water (Woocay and Walton, 2008) or shallow and deep aquifers (Carucci et al., 2011), 6) constraining spring source waters (Swanson et al., 2001), and 7) exploration of hydrothermal groundwaters (Blake et al., 2016).

2.2.3 What are the different types of clustering and what are their strengths?

There are two overarching methodologies for clustering or classification of water chemistry data: 1) multivariate statistical analysis methods (MSMs) (Woocay and Walton, 2008) and 2) graphical methods. Results from both of these methodologies are often projected into a GIS to understand spatial patterns. These three pathways: multivariate, graphical, and geospatial, are the primary tools for hydrochemical reconnaissance (Figure 2.1). Multivariate techniques have been applied to water chemistry problems for over 35 years (e.g., Steinhorst and Williams, 1985) and include “hard” clustering methods (i.e., sample belongs to one group or cluster), “soft” clustering methods (i.e., sample can probabilistically belong to multiple groups), and factor analysis (e.g., principal component analysis). The two most common forms of hard clustering applied to water chemistry data are k-means clustering (k-means) and hierarchical clustering analysis (HCA). HCA can either be Q-mode (samples are clustered) or R-mode (parameters are clustered). Soft clustering techniques applied to water chemistry problems using fuzzy logic (e.g., fuzzy k-means clustering) have become more prevalent over the last 20 years (Chang et al., 2001; Güler et al., 2004; Grande et al., 2005; Sârbu et al., 2005; Güler et al., 2012). Factor analysis is generally used to examine the factors controlling the variance in a dataset and is seldom used for clustering, although sometimes factor scores generated for each observation are utilized in a clustering analysis (Suk and Lee, 1999).

Graphical methods for classification of water chemistry data involve the use of Piper diagrams (Piper, 1944), ternary diagrams, stiff diagrams (Stiff, 1951), Durov plots (Durov, 1948), etc. to visually partition groups of water or geochemical facies. A comprehensive review of various

multivariate and graphical methods for examining water chemistry data can be found in Güler et al. (2002).

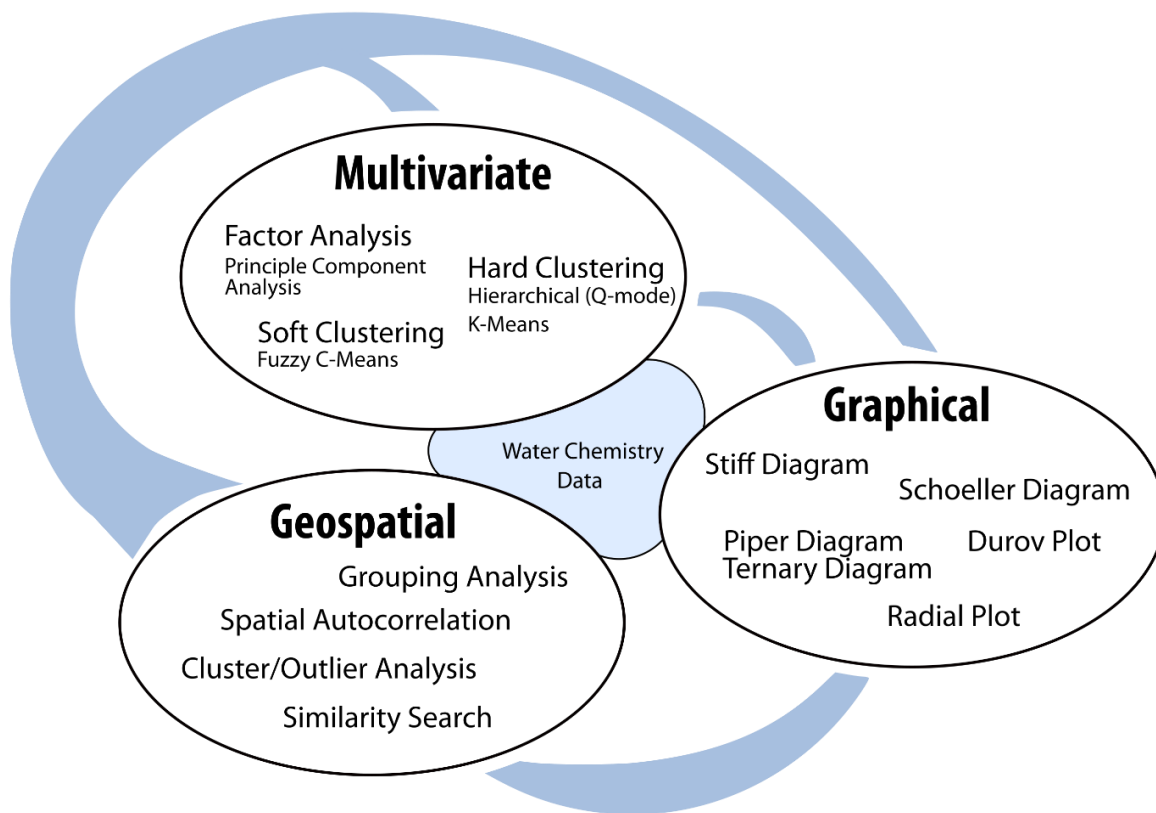


Figure 2.1. Conceptual diagram showing common analysis pathways when using water chemistry data for hydrological reconnaissance. Preliminary analysis of water chemistry data often falls under three categories; graphical, multivariate, and geospatial. Subcategory headings show specific plots, techniques, or algorithms associated with each category. Finding ways to combine multiple analysis pathways can be very powerful and elicit hidden information. For example, the program *Geostiff* (Boghici and Boghici, 2001) combines graphical and geospatial methods. In this paper we present an approach which combines graphical and multivariate methods (i.e., uses concepts of graphical tools in inform multivariate data preprocessing treatment). Results from this approach can then be imported into a geospatial platform to explore spatial relationships.

2.2.4 What are the problems with current clustering workflows and what will be gained by this study?

The various strengths, weaknesses, and potential biases of the aforementioned approaches are less frequently discussed and often ignored. While graphical methods are perhaps the most useful as a reconnaissance tool, there is an element of subjectivity to geochemical partitions created

from purely graphical means. Soft clustering overcomes some of the limitations of hard clustering (i.e., forcing group membership to one sample when it is more representative as a mixture of groups) and can generally be considered more robust when clusters appear to be overlapping or continuous (Güler et al., 2012). Still, this technique often requires large data sets and can have computational problems when a large number of variables are included (Templ et al., 2008). Hard clustering methods, with HCA being the most utilized method overall, have become the prevalent choice for geochemical partitioning throughout the literature in recent decades. However, these methods are not without flaws and have been previously criticized for ignoring kinetics and geochemical complexity as well as minimizing the chemical significance of the data through preprocessing (Dreher, 2003). Several papers have acknowledged that clustering results from HCA seem either biased (Belkhiri et al., 2010) or more attuned (Monjerezi et al., 2011) towards tracking changes in salinity or increasing total dissolved solid concentrations rather than geochemical composition or evolution. However, this has seldom been talked around moreso than directly stated. These critiques are important to consider, especially as the prevalence of the methodology increases and patterned workflows (i.e., Thyne et al., 2004) are developed that use the results from HCA or K-Means clustering as inputs for inverse geochemical modeling or geochemical reaction modeling (Meng and Maynard, 2001; Guler et al 2004; Kebede et al., 2005; Helstrup et al., 2007; Belkhiri et al., 2010; Figure 2.2). Modeling results and accompanying stability diagrams or saturation indices derived from clustering results are frequently used as statistical and geochemical proof to support conceptual models. This is a very precarious practice as cluster analysis is highly dependent on data preparation (Templ et al., 2008).

In this study, we evaluate the effects of data preprocessing on HCA of major cation and anion data. We compare HCA results from traditional data preprocessing methods (e.g. Güler et al., 2004) to those obtained using alternative data preprocessing methods (presented in this study) for two different study sites, the eastern Sierra Nevada (Owens Valley, NV) and the Spring Mountains (NV). For both study sites, we utilize water quality data at springs to understand groundwater flow processes, patterns, and evolutionary pathways inside complex mountain blocks. Both study sites have few to no bedrock wells, thus springs offer a glimpse into the complex groundwater dynamics within mountain blocks. We then examine the geochemical and spatial patterns of the HCA results and interpret how these results compare with existing hydrogeologic conceptual models.

patterned workflow for geochemical analysis

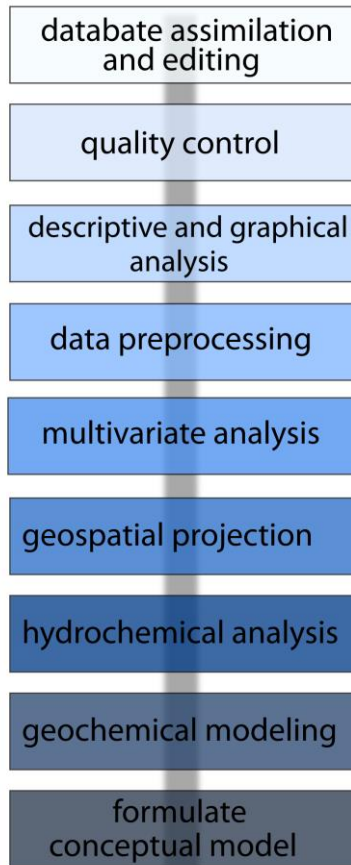


Figure 2.2. Conceptual diagram showing a generalized interpretation of a “patterned” or “sequential” workflow commonly used to evaluate water chemistry data. This workflow has a lot of steps to ensure quality control and robustness. One problem, however, is that changes in data preprocessing have a large effect on the results derived from multivariate analysis, thus affecting the rest of the workflow.

2.3 Methods

2.3.1 Workflow using traditional methodology

Traditional methods and a general patterned methodology for geochemical clustering using HCA are outlined in Güler et al. (2002) and Thyne et al. (2004). These methods are also presented

in a case study by the authors (Güler and Thyne, 2004). A simplified workflow of the sequential process presented in these papers is shown in Figure 2.2 and consists of the following steps: (1) database assimilation and editing, (2) data quality control, (3) descriptive statistics and graphical analysis, (4) data preprocessing, (5) multivariate statistical analysis, (6) geospatial projection of results, (7) hydrochemical analysis, (8) inverse geochemical modeling of cluster centroids, and finally, (9) conceptual model formulation. This approach has a number of built-in assumptions which can be found in Thyne et. al. (2004).

For the purposes of this paper we primarily focus on how alternative approaches in step 4 (data preprocessing) affect the chain of analysis starting with HCA. Prior to data preprocessing it is assumed that all samples with charge balance error (CBE) > 10% have been removed and all samples with data gaps have either been filled or omitted (Güler et al., 2002; Güler et al., 2004, Thyne et al., 2004). The traditional approach for data preprocessing is to log transform and then standardize (i.e., z-score) the matrix of data. Log transformation is performed to convert the data into resembling a normal distribution if the data are highly skewed, as is typical for natural systems. Standardization following log transformation converts 99.7% of the data to values between 3 and -3 centered around a mean of 0. This is done to prevent variables with large magnitudes from being over weighted during the Euclidean distance calculation of HCA (Judd, 1980; Güler et al., 2002).

The formula for z-score standardization is as follows:

$$z = \frac{(x - \mu)}{\sigma}$$

z = z-score

x = observed value

μ = sample mean

σ = same standard deviation

Following data preprocessing, the matrix of data to be used for HCA is generally imported into a statistical software package (e.g., MATLAB, R, Statistica, Minitab, etc.). For HCA, the user needs to specify a distance (i.e., similarity) measure and a linkage rule (i.e., algorithm for computing the distance between clusters). For geochemical studies, Euclidean distance is commonly used as the similarity measure. The prevalent linkage rule is Ward's method. The similarity measure is used to define the dissimilarity between samples while the linkage rule determines dissimilarity between clusters. Ward's method rule uses the inner squared distance or minimum variance algorithm and is thought to produce the most distinctive groups for

geochemical applications (Templ et al., 2008) A hierarchical cluster tree is produced from the levels of similarity which can then be visualized in the form of a dendrogram. The dendrogram can then be “cut” by a phenon line at an appropriate similarity index and the resulting branches form clusters of data. Different groups of clusters can be produced depending on where the phenon line is cut. While the choice for the exact similarity index location for the phenon line may be semi-subjective and there is no “wrong” place to cut the dendrogram, large gaps in the dendrogram or the emergence of many subclusters at a given linkage distance may suggest an appropriate location (Swan and Sandilands, 1995; Knodel et al., 2007). For details on the traditional post-clustering workflow (i.e., steps 6-9), please refer to Thyne et al. (2004).

2.3.2 Alternative data preprocessing methodology

The alternative data preprocessing technique presented in this paper is simple in concept and seeks to numerically quantify the descriptive strength of graphical methods, specifically Piper and Stiff diagrams. Both of these graphical approaches successfully capture the geochemical “fingerprint” of a water sample, however, clusters derived purely from graphical approaches are prone to subjectivity even though specific regions on these diagrams have geochemical significance (Piper, 1944). Data treatment using alternative preprocessing consists of the following steps:

1. Steps 1-3 from the traditional preprocessing approach.
2. Separate out complete, quality controlled major cation and anion data (e.g., Ca^{2+} , Mg^{2+} , Na^+ , K^+ , Cl^- , HCO_3^- , and SO_4^{2-} and convert to meq/L.
3. Calculate the % meq/L for each ion based on the sample composition. Each cation is divided by the meq/L sum of all cations in a sample and each anion is divided by the meq/L sum of all anions in a sample. For more alkaline pH ranges, CO_3^{2-} can also be included. These are essentially the same steps towards constructing a Piper diagram, however, we do not combine Na^+ and K^+ into one variable.
4. Vectors of each major ion and cation form the first 7 columns of the data matrix. Other geochemical constituents that are potentially important, such as Sr^{2+} , NO_3^- , or Si (as SiO_2), can be added as individual vectors. Because this methodology is primarily based on the proportions of the major ions with respect to one another, total dissolved solids (TDS) or specific conductance (SPC) can also be added as variables to give the overall

magnitude of dissolved constituents a small amount of weight. However, it is important not to add too many additional variables as the data dimensionality will reduce the significance of multivariate groupings (Bellman, 1961). Additional variables incorporated into the analysis should be log-transformed if they are not normally distributed. After that, each variable is normalized to scale between 0-1, the same range as the major cation and ion data. In this study, silicate weathering is an important contributor to geochemical evolution in both Owens Valley and the Spring Mountains. Therefore, we use TDS and Si (as SiO₂) as two additional variables for a total of 9 vectors in the data matrix.

5. Following data preprocessing and concatenation of the data matrix, the rest of the steps used in this study are identical to the traditional methodology (e.g., HCA in a statistical software package with Ward's linkage and Euclidean distance measure). However, this is simply a preprocessing method and the analyst can use any clustering method they choose (e.g., K-means, Fuzzy K-means). For the purposes of comparison with traditional preprocessing and because it is the most widely used method, we test with Q-mode HCA in both case studies.

2.3.3 Case Studies

Case studies have been previously used to evaluate the strengths and weaknesses of empirical methods for clustering water chemistry data (Steinhorst and Williams, 1985; Guler et al., 2002; Thyne et al., 2004; Templ et al., 2008; Woocay and Walton, 2008). The two study sites used in this paper were chosen based on contrasting hydrogeology and flow regimes, confidence in preexisting conceptual models, differences in dataset size, and availability of data. The Owens Valley dataset is relatively small ($n = 20$), while the Spring Mountains (SM) dataset is larger ($n = 153$). The difference in sample size between the two study sites allows us to examine clustering relationships at the individual sample scale (OV) and for spatial groups of samples (SM).

2.3.3.1 Owens Valley (CA)

Owens Valley is a deep extensional graben lying directly to the east of the southern Sierra Nevada and to the west of the White-Inyo Mountains. Ridgelines on both sides of the valley exceed

4250 meters (~14,000 ft) while the valley floor slopes southward from ~1200 meters to ~1000 meters at its southernmost extent. In this region, the Sierra Nevada is primarily comprised of Cretaceous plutonic rocks ranging in petrologic composition from alaskite to diorite, quartz diorite, and hornblende gabbro. The majority of plutons fall in the range of quartz monzonite to granodiorite (Figure 2.3). Penn-Permian metasedimentary roof pendants of country rock correlated with units in the White-Inyo ranges are laterally extensive at high elevations in several portions of the eastern Sierra Nevada (Figure 2.3). These roof pendants contain various facies including marble, calc-hornfels, micaceous quartzite, and biotite schist (Moore, 1963). Other notable geologic units include volcanic rocks of Jurassic and Triassic age found in the Mount Pinchot and Mount Whitney quadrangles, Quaternary flood basalts and cinder cones of the Big Pine Volcanic Field associated with Cenozoic extension, and the Volcanic Tableland area (i.e., Bishop Tuff) at the north end of Owens Valley associated with the eruption of the Long Valley Caldera.

The eastern Sierra Nevada is the site of two seminal studies in the field of water chemistry, Feth (1964) and Garrels and Mackenzie (1967), focusing on chemical weathering and geochemical evolution through plutonic rocks. There are several important tenants from these papers that are applicable to this study: 1) the origin and composition of springs in the Sierra Nevada can be directly related to the mineralogy of the rock materials and the composition of the chief weathering products (e.g., kaolinite and ca-montmorillonite) and 2) groundwater ion concentrations derived from rock-water interaction will scale with distance from recharge, and thus, residence time and circulation depth. We utilize the tenants from these papers and other like studies in the area (i.e., Pretti and Stewart, 2002) and leverage the vast amount of petrologic information available for plutonic rocks in Owens Valley (e.g., Moore, 1963; Bateman, 1965; Abbott, 1972; Moore, 1987).

For this case study, geochemical data is presented from 20 spring sites emerging on the mountain front of the western side of the valley (Figure 2.3) sampled during the spring of 2016. One additional site was sampled during October 2017. The majority of these springs emerge at mapped fault zones and source mountain block recharge from high elevation areas (*see* Chapter 4) (2800-3300 meters). Samples further away from the drainage divide (e.g., springs west of the Alabama Hills) likely source mountain system recharge from both the mountain block and basin fill aquifers.

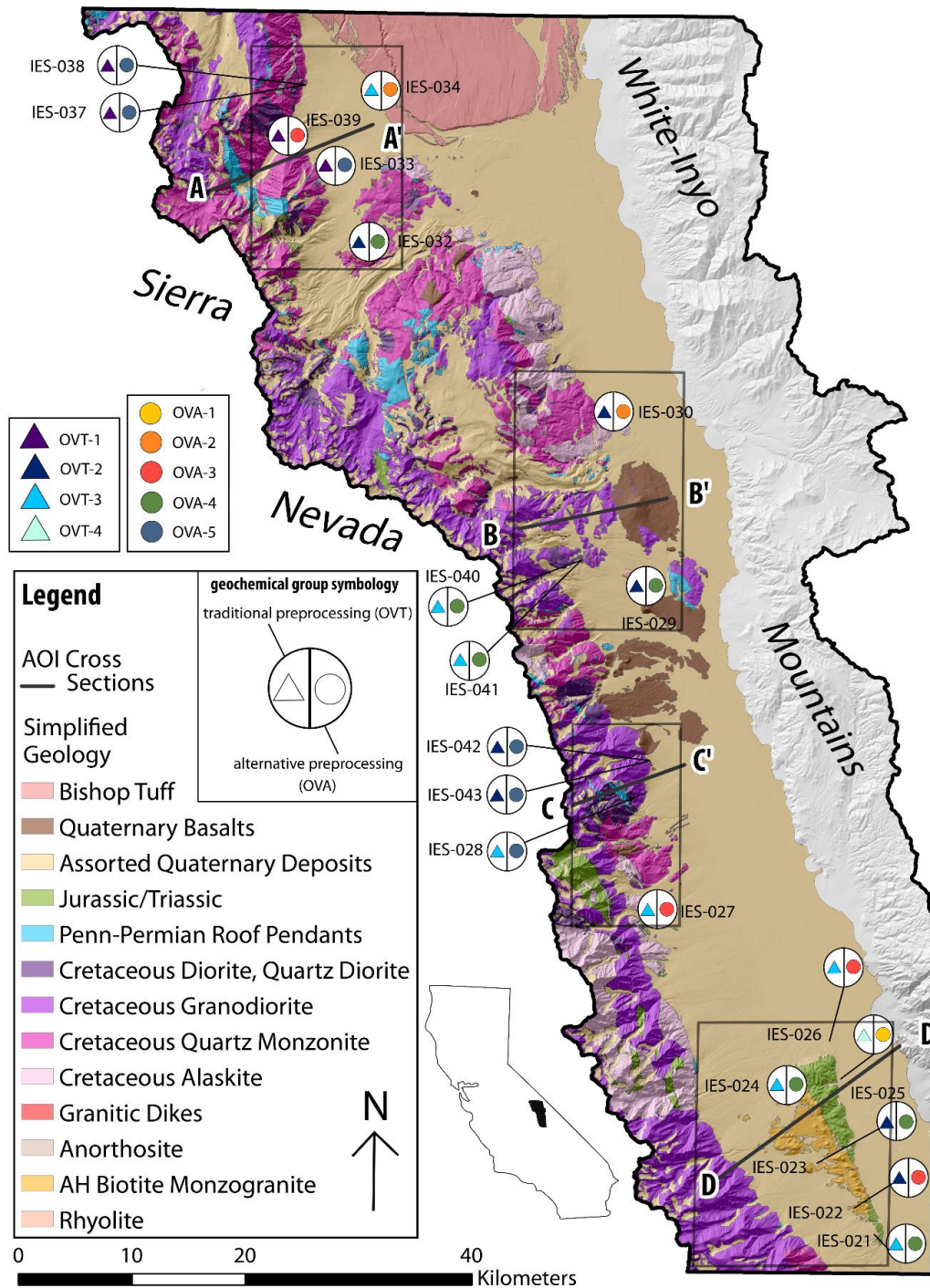


Figure 2.3. Simplified geologic map of the eastern Sierra Nevada in Owens Valley, CA. Spring sample locations are marked on the map. Springs are symbolized by shape to indicate data preprocessing technique and by color to indicate the geochemical group. Traditional preprocessing groups are show as triangles while alternative preprocessing groups are shown as circles. Lines on the map indicate geologic cross sections (see Chapter 4). Regional boxes on the map around the springs indicate areas where we present an additional figure to zoom in on the geologic connections to springs (Figure 2.5).

2.3.3.2 *The Spring Mountains (NV)*

The Spring Mountains are a northwest-southeast trending mountain range near the southern border of California and Nevada. The central crest of the mountain range rises over 3600 m and defines the division between the Great Basin physiographic province and the Las Vegas Valley watershed. Numerous hydrogeological studies and geochemical investigations have identified the Spring Mountains as an important recharge zone for the Death Valley Regional Groundwater Flow System (DVRGFS) and for the Las Vegas Valley aquifer system (Winograd and Pearson, 1976, Winograd et al., 1998; Belcher et al., 2009; Belcher and Sweetkind, 2010). More recently, the role of the central Spring Mountains as an important recharge zone and the importance of thrust faults as zones of mixing have been highlighted by Warix et al. (2020).

The Spring Mountains are primarily comprised of Paleozoic marine strata; predominately quartzite, limestone and dolostone; that formed from the development of a clastic wedge and an overlying carbonate shelf on the passive margin between the Cordilleran miogeocline and the North American craton (Page et al., 2005). Sandstones, siltstones, and conglomerates of Mesozoic origin are found in the southeastern portion of the range and are correlated with the Mojave Jurassic arc terrane (Marzolf, 1990; Page et al., 2005). Large thrust faults (e.g., the Keystone Thrust, the Lee Canyon Thrust, the Macks Canyon Thrust, the Deer Creek Thrust, and the Wheeler Pass Thrust) and regional folding associated with the Sevier Orogeny created complex topography and exposed large sections of the regional carbonate aquifer to the surface. Basin and Range extension created displacement between the Spring Mountains and adjacent ranges as well as incited normal faulting throughout the mountain range that cross-cuts thrust faults.

We combine the results of recent sampling efforts in the region (2016-2018) with data from Hershey (1989), Anderson (2002) and the USGS Water Quality Database (<https://waterdata.usgs.gov/nwis/qw>) to amass a dataset consisting of 153 samples with complete major cation and anion information. Where bicarbonate data was missing from these samples, HCO_3^- was calculated from pH and alkalinity. This larger dataset allows us to capture the spatial resolution and geological complexity of the mountain range. We leverage information from prior studies to evaluate how well HCA results obtained using different data preprocessing methods conform to prior conceptual models of inferred groundwater flowpaths and the effect of structure on groundwater flow (e.g., Warix et al., 2020). Regional scale flowpaths have been geochemically modeled from high elevation springs in the central Spring Mountains towards lower elevations in

Pahrump Valley and Las Vegas Valley (Hershey et al., 1989; Hershey et al., 2016). Strontium isotopes also support this conceptual model of recharge initiating in the central Spring Mountains (Warix et al., 2020). Large scale thrust faults cut the mountain range into geologically distinct sections that have been identified as places of groundwater mixing between flow regions (Warix et al., 2020).

2.4 Results

2.4.1 Owens Valley Case Study

HCA results using both traditional preprocessing and alternative preprocessing techniques are shown for the Owens Valley springs in Figure 2.4. For each technique we present a dendrogram showing the phenon line, or area where dendrogram is “cut”, with the resulting agglomerative clusters shaded in different colors. We also provide a graphical breakdown for each technique showing stiff diagrams for each sample and a piper diagram showing all samples. Samples clustered using the traditional preprocessing approach are represented by triangles while samples clustered using the alternative preprocessing approach are symbolized by circles. Detailed, zoomed-in, areas of the geologic map associated with the boxes in Figure 2.3 can be found in Figure 2.5.

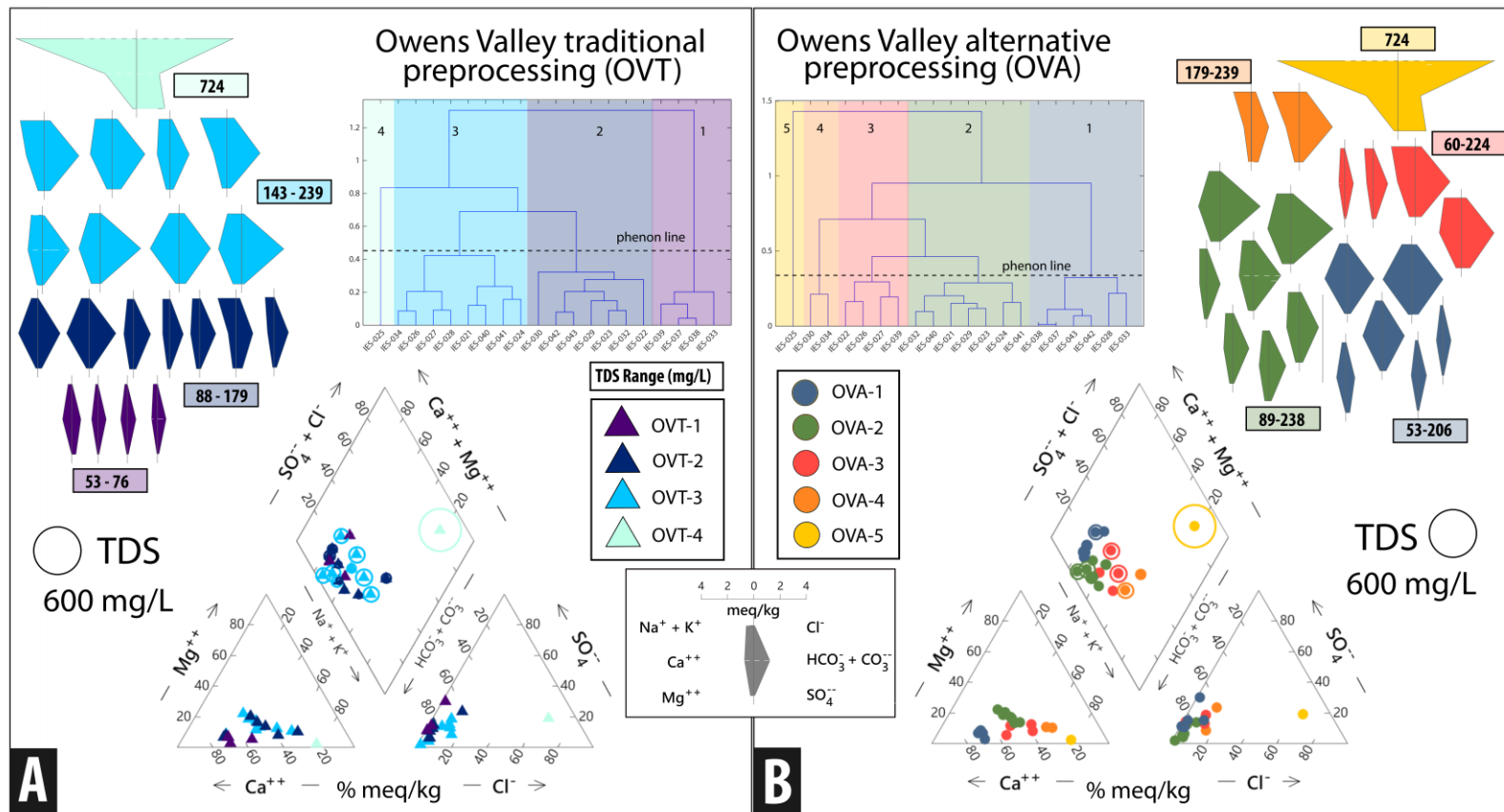


Figure 2.4. This figure summarizes the geochemical differences between the traditional (OVT) and alternative (OVA) preprocessing results for springs in Owens Valley. OVT results are presented in section A and OVA results are presented in section B. Each section contains a dendrogram with the agglomerative clusters shaded by color. The phenon lines depict where the dendrograms are cut. Every spring has an associated stiff diagram and a point in the Piper diagram. Boxes next to the stiff diagrams show TDS ranges for each group of springs.

2.4.1.1 Traditional Preprocessing Results

Using the traditional preprocessing approach (OVT = Owens Valley Traditional), the 20 spring samples are clustered into four groups (OVT-1, OVT-2, OVT-3, and OVT-4) (Figure 2.4A). As shown by the stiff diagrams, the clusters generated using the traditional approach show a propensity towards grouping based on total dissolved solid concentrations, showing a consistent increase in TDS from Group OVT-1 to OVT-4. Group OVT-1 contains four low TDS samples (53-76 mg/L) that have a Ca-HCO₃ water type. All four of these spring samples are located in the Round Valley area west of Bishop, CA. Group OVT-2 contains seven samples of slightly evolved water (TDS 88-179 mg/L) with mixed water types of Ca-HCO₃ and Na-HCO₃. Samples in Group OVT-2 are distributed across the southern, central, and northern portions of the western Owens Valley mountain front. Group OVT-3 contains 8 samples of moderately evolved water (TDS 143-239 mg/L) containing both Ca-HCO₃ and Na-HCO₃ water types. Group OVT-3 springs are found across many parts of Owens Valley, and include the two highest elevation samples (IES-040 and IES-041) and two samples located near the basin floor (IES-026 and IES-034). Group OVT-4 includes one spring, IES-025, a Na-Cl type seep emerging at the toe of the Alabama Hills with an elevated TDS (724 mg/L) relative to other springs in the area.

Graphical interpretations of HCA results obtained using the traditional preprocessing approach show clear distinctions in the stiff diagrams based on total dissolved solid concentrations. However, these groupings do not contain springs with similar geochemical fingerprints. Groups OVT-1, OVT-2, OVT-3 are all clustered over the same subspace in the Piper diagram with no clear distinctions between groups. Additionally, we also do not observe clear spatial patterns with upgradient geology and HCA cluster. I use the term upgradient geology to imply that springs are supported by recharge occurring upgradient of the spring and in the geology associated with the inferred recharge zone. Springs hypothesized as flowing through the same units or similar geology (i.e., sets of plutons) are not clustered together. For example, IES-034, which flows through the Bishop Tuff, is grouped together with springs that emerge from granodiorite plutons. The exception to this observation is with “twin” springs or springs emerging in a complex that are located less than 1 km apart (e.g., IES- 037 & IES-038, IES-040 & IES-041, and IES 042 & IES-043).

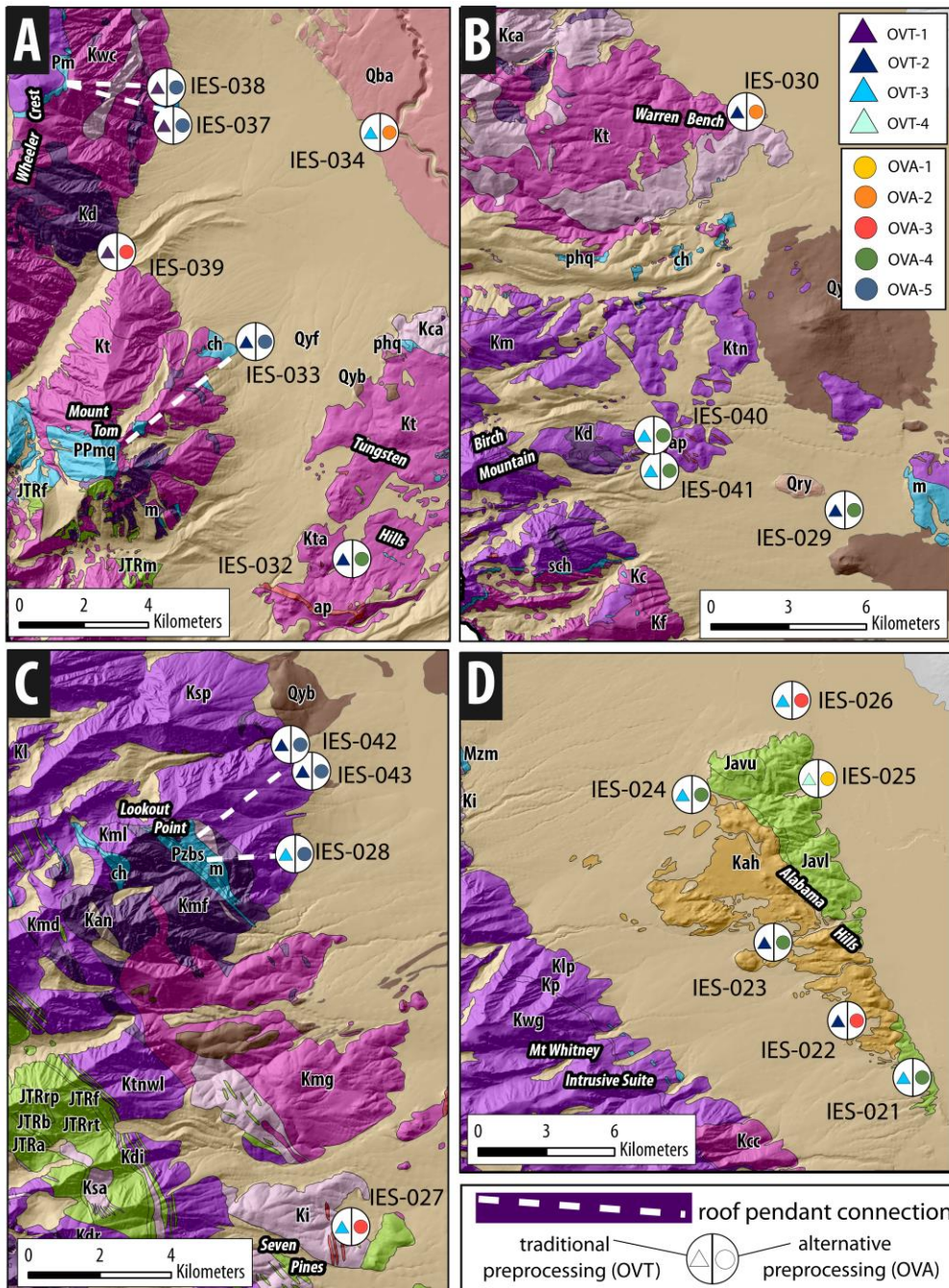


Figure 2.5. Zoomed-in geologic maps associated with the boxes in Figure 2.3. Spring locations are denoted and springs are symbolized by shape (preprocessing technique) and color (geochemical group). White dotted lines indicate connection of Group OVA-1 springs to Penn-Permian metasedimentary roof pendants directly upgradient.

2.4.1.1 *Alternative Preprocessing Results*

HCA using alternative preprocessing techniques (OVA) resulted in five clusters for the 20 Owens Valley springs. Compared to the OVT results, the OVA clusters have considerably larger intergroup ranges in TDS and are structured more distinctly based on geochemical facies (i.e., solute relationships and proportions) (Figure 2.4B). We also observe spatial relationships in sample groupings associated with local geology (Figure 2.5).

Group OVA-1 samples range from dilute to moderately evolved (TDS 53-206 mg/L) and are all strongly Ca-HCO₃ dominant waters. Geologically, all springs in Group OVA-1 are located downgradient from Penn-Permian metasedimentary roof pendants surrounded by quartz monzonite or granodiorite plutons (Figure 2.5). Group OVA-2 samples have a TDS range from 89-238 mg/L and are all Ca-HCO₃ type waters. This group has samples from three separate geologic areas, however the petrology upgradient and in the likely recharge zone of these spring waters is all similar. IES-021, IES-023, and IES-024 all emerge to the west of the Alabama Hills and downgradient from the Mount Whitney intrusive suite, a group of nested granodiorite plutons (Hirt, 2007). IES-029, IES-041 and IES-40 emerge from the Granodiorite of McMurray Meadows and undifferentiated mafic rocks in the Birch Mountain area. IES-029 may receive some flow through quaternary flood basalts associated with the Big Pine volcanic field (e.g., Red Mountain). IES-032 emerges out of the Tungsten Hills quartz monzonite west of Bishop, CA, however, local masses of diorite, quartz diorite, and hornblende gabbro are present.

Group OVA-3 consists of four springs (IES-022, IES-026, IES-027, and IES-039) and has the largest TDS range for any group (66-204 mg/L). This group has mixed facies representation, two springs are Na-HCO₃ type and the other two are Ca-HCO₃ type. However, the distinctive geochemical feature of this group is that both Ca²⁺ and Na⁺ are elevated (though either one may dominate) compared to a lower overall proportion of Mg²⁺. Springs in Group OVA-3 are geologically heterogeneous upgradient of the spring, often reflecting a mix of felsic plutonic rocks (e.g., alaskite and anorthosite) and granodiorite. Group OVA-4 is comprised of two moderately evolved springs that are strong Na-HCO₃ type waters with a distinctive geochemical fingerprint (Figure 2.4B). IES-034 sources water from flowing through the Volcanic Tableland while IES-030 flows through alaskite and felsic dikes and masses comprising the Warren Bench. Group OVA-5 is the same as Group OVT-4 and just consists of one spring, IES-025, an Na-Cl-type seep at the toe of the Alabama Hills with an elevated TDS concentration.

2.4.2 Spring Mountains Case Study

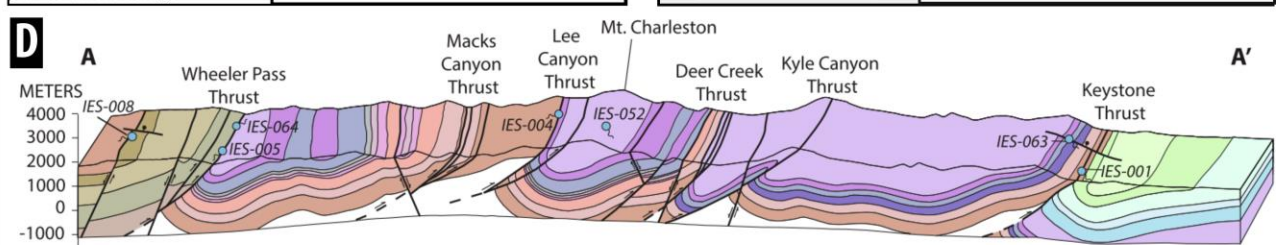
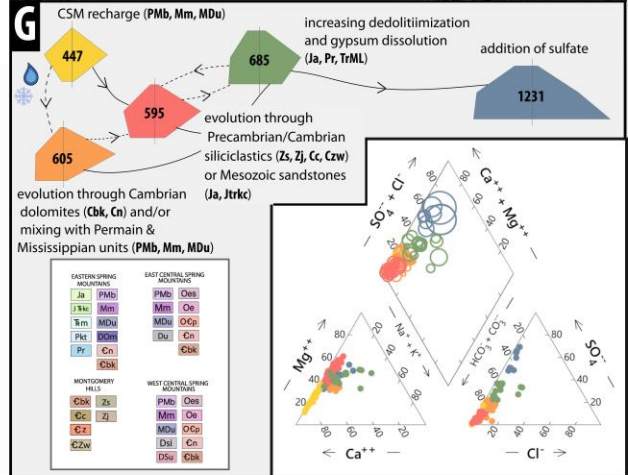
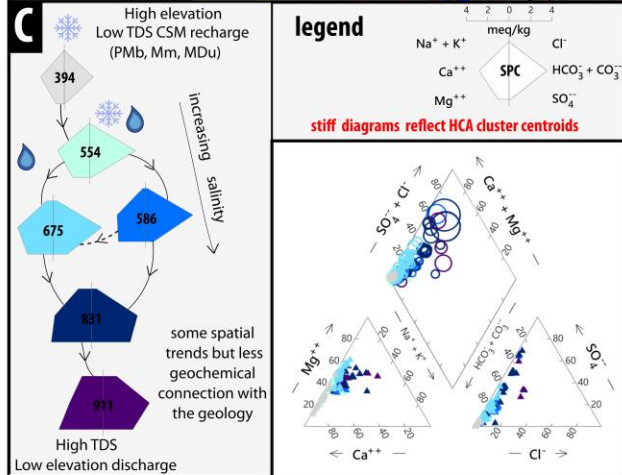
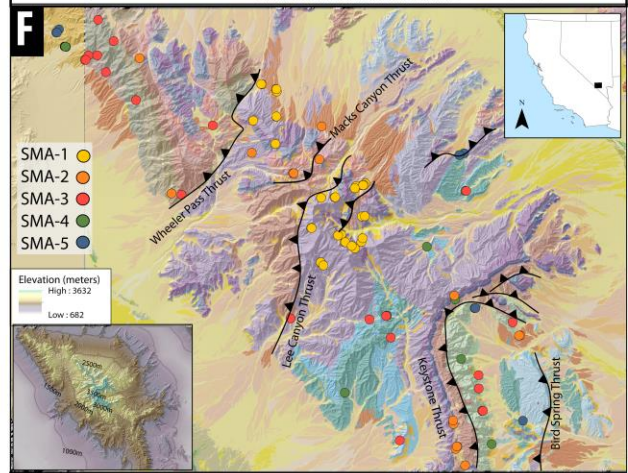
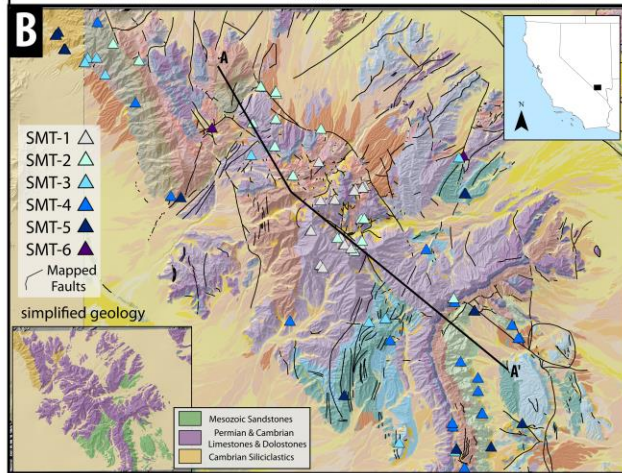
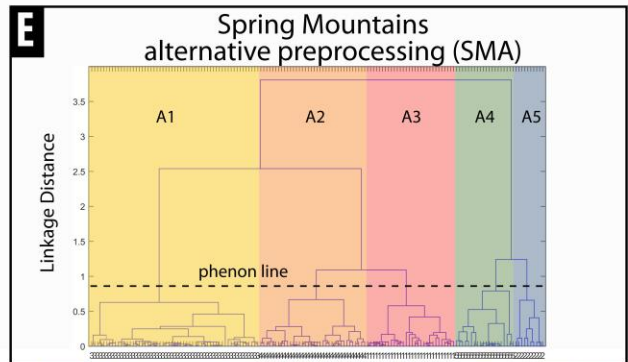
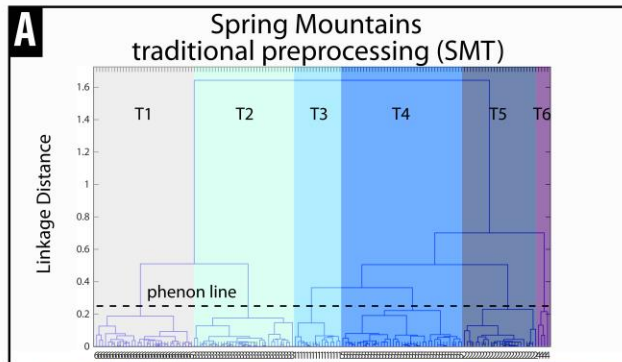
HCA results from traditional and alternative preprocessing techniques are summarized for the Spring Mountains case study in Figure 2.6. For each technique we present a dendrogram highlighting the agglomerative clusters created by the phenon lines. All dendrograms are plotted with the optimal leaf order to show the maximum distance (i.e., samples on the far left and right of the dendrogram have the greatest dissimilarity). All spring samples are symbolized by shape for preprocessing type and by color for cluster membership. We present regional geologic maps of the Spring Mountains adapted from Page et al. (2005) showing mapped faults (Figure 2.6B) and interpreted large-scale thrust faults (Figure 2.6E). Inset maps within the geologic map show simplified geology (Figure 2.6B) and local topography (Figure 2.6F) The included cross section is adapted from Page et al. (2005) and Warix et al. (2020) (Figure 2.6G). Total dissolved solid data was not available for all springs, therefore specific conductance (SPC $\mu\text{S}/\text{cm}$) was used as a measure of overall geochemical evolution.

Due to the large sample size, cluster centroids (i.e., the statistical average of a cluster) representing each group are depicted in the Stiff and Piper diagrams (2.6C and 2.6F). The number of samples and variability of the cluster centroid is based on how many samples are present in the geochemical cluster. Based on work from Guler et al. (2004) using a similar methodology, we examine the geochemical signature and spatial significance of the cluster centroids and then make interpretations about the regional flow system. Hypothetical geochemical evolution pathways are annotated for each technique based on the geochemical composition of the cluster centroids and spatial relationships observed with the regional geology and major structural features.

2.4.2.1 *Traditional Preprocessing Results*

HCA using traditional data preprocessing resulted in six geochemical groups (SMT) for the Spring Mountains case study. The cluster centroids representing each group show one overall geochemical evolution pattern from high and mid elevation recharge waters (SMT-1 & SMT-2) to low elevation discharge waters (SMT-5 & SMT-6). Groups SMT-3 and SMT-4 appear to represent intermediate/transitional waters between the central highlands and basin floor. This pattern of regional evolution is shown by a steadily increasing geochemical fingerprint and consistent increases in SPC from SMT-1 to SMT-6 (Figure 2.6C).

Figure 2.6. This plot is similar to Figure 2.4 and shows the geochemical clustering results for the Spring Mountain springs using traditional (SMT) and alternative (SMA) preprocessing methods. SMT results are depicted as triangles and shown in subplots A, B, and C. SMA results are depicted as circles and shown in subplots E, F, and G. Each preprocessing method depicts a dendrogram showing all springs, the pheneon line, and the resulting agglomerative clusters shaded by color. We also include geologic maps showing all samples symbolized by preprocessing type and geochemical group. The geologic map legend is shown in Subplot 2.6G. The geologic map in subplot 2.6B shows minor faults and a cross section line associated with the cross section in subplot 2.6D. The inset geologic map in subplot 2.6B shows a simplified geologic map. The geologic map in subplot 2.6F shows the major thrust faults. The inset map in subplot 2.6F shows a shaded DEM with 500m contour lines to show elevation (meters). Subplots 2.6C and 2.6G show stiff diagrams of the cluster centroids and Piper diagrams showing all samples shaded by geochemical group. We interpret the geochemical relationships among cluster centroids with annotations between stiff diagrams in Figure 2.6G. The cross section in Subplot 5D is adapted from Page et al., (2005) and Warix et al., (2020).



Groups SMT-1 and SMT-2 are highly dissimilar, based on the linkage distance, from Groups SMT 3-6. Based on the geospatial configuration of the clusters and information about the flow system from previous studies (e.g., Hershey et al., 1989; Winograd et al., 1998; Warix et al., 2020), groups SMT-1 & SMT-2 are indicative of shallow groundwater evolving primarily from snowmelt recharge. Springs in Group SMT-1 have an average specific conductance of 395 $\mu\text{S}/\text{cm}$ and primarily emerge from the Bird Spring Formation (Pmb) and the Pogonip Group around high elevation areas of the central Spring Mountains (CSM). Springs in Group SMT-2 have an average specific conductance of 554 $\mu\text{S}/\text{cm}$ and are predominately located within two areas of the mountain range: 1) at mid elevation locations in the central Spring Mountains and 2) in the Montgomery Hills area of the northwestern Spring Mountains. Group SMT-2 springs primarily emerge in Permian limestones and dolostones (Pmb and Mm) and Cambrian and Ordovician limestones and dolostones.

Group SMT-3 springs have an elevated SPC (675 $\mu\text{S}/\text{cm}$) and represent a spatial and geochemical evolution from Group SMT-2 waters in the absence of prevalent dolomite dissolution. These springs primarily emerge at mid to low elevation areas in siliciclastic geologic formations of Proterozoic, early Cambrian (e.g., Zj, Zs), and Mesozoic (Trml, Ja) age. Springs in Group SMT-4 cluster on the “evolved” side of the dendrogram despite having an average SPC of 586 $\mu\text{S}/\text{cm}$, only slightly elevated from Group SMT-2. We attribute this separation to decreased Ca/Mg ratios compared to Group SMT-1 and Group SMT-2 waters. Many SMT-4 springs either: 1) emerge in mid to low elevations out of limestones and dolostones of Cambrian (Cbk) and Mississippian (Mm & Mdu) age or 2) emerge downgradient from these units due to offset by large scale thrust faults (Figure 2.6B). Cluster centroids from Groups SMT-5 and SMT-6 represent an increase in overall salinity as well as magnesium and sulfate concentrations from Groups SMT-1 – SMT-4. The cluster centroid for Group SMT-5 reflects a Mg-HCO₃ type water with increases in all ion concentrations, specifically sulfate, magnesium, and sodium, from mid-elevation groundwaters (e.g., SMT-3 and SMT-4). Samples with membership to SMT-5 are found at low elevations, frequently at the toes of slopes, emerging from spatially and geologically heterogeneous locations throughout the mountain range (Figure 2.6B). Group SMT-6 consists of only four samples that are distinguished by having the highest mean specific conductance (911 $\mu\text{S}/\text{cm}$) and magnesium concentrations.

2.4.2.2 *Alternative Preprocessing Results*

Alternative preprocessing of geochemical data prior to HCA resulted in five geochemical groups (SMA) for the Spring Mountains: 1) one shallow groundwater (i.e., recharge) endmember (SMA-1), 2) three transitional endmembers (SMA-2, SMA-3, and SMA-4) representative of intermediate evolution from shallow groundwater by way of interaction with various lithologies (e.g., Precambrian/Cambrian siliciclastics, Cambrian dolomites, and Mesozoic sandstones), and 3) one endmember representing the most evolved waters at low-lying, basin locations (SMA-5).

Group SMA-1 is representative of Ca-HCO₃ type water evolving through the Bird Spring Formation, Pogonip Group, and undivided Mississippian and Devonian Limestones. Springs clustered in this group are found at high elevations in the central Spring Mountains (CSM) and high to mid elevations in the north-central Spring Mountains. Springs with membership to Group SMA-2 have a slightly higher mean specific conductance (605 $\mu\text{S}/\text{cm}$) than SMA-1 springs and are distinguished by increases in Mg²⁺ and HCO₃⁻ from the CSM recharge endmember. Based on the spatial locations of SMA-2 springs, we interpret this chemical evolution to be derived from interaction with Cambrian dolomites (Cn & Cbk), where large-scale thrust faulting places these units proximal to Permian limestones. Group SMA-2 springs are found along the Keystone Thrust, the Macks Canyon Thrust, and the Wheeler Pass Thrust (Figure 2.6F). Spring waters in Group SMA-3 have a cluster centroid with a mean specific conductance of 595 $\mu\text{S}/\text{cm}$ with increases in most major ions, particularly Na⁺, K⁺, SO₄²⁻, and Mg²⁺, from the CSM recharge endmember. Spring waters in Group SMA-3 represent a geochemical evolution pathway where CSM recharge interacts primarily with flow through siliciclastic rocks; either Precambrian and Cambrian quartzites (Zs, Zj, Cc, Czw) or Mesozoic sandstones and conglomerates (Ja, TRmu, TRml) (Figure 2.6G). Group SMA-4 has a cluster centroid with a mean specific conductance of 685 $\mu\text{S}/\text{cm}$ and exhibits distinct increases in Na⁺, K⁺, Mg²⁺ and SO₄²⁻ from the other three more dilute groups. Springs in this group emerge primarily from mid to lower elevation exposures of the Johnnie Formation and Mesozoic sandstones and conglomerates (Figure 2.6G). We attribute the increases in Na⁺, K⁺ to siliciclastic weathering and the increases in Mg²⁺ and SO₄²⁻ to dedolomitization and gypsum dissolution (Warix et al., 2020). Spring waters in Group SMA-5 have a Mg-SO₄ water type and show a substantial increase in salinity from the three intermediate groups (Figure 2.6G). These springs are exclusively found at low elevation portions of the mountain range emerging

from siliciclastic units (Zj, TRml, Ja) and are often found on major thrust or normal faults (Figure 2.6F).

2.5 Discussion

Past studies have shown that preprocessing of geochemical data can have a significant effect on multivariate clustering results (e.g., Dreher et al., 2003; Templ et al., 2008). However, one “traditional” preprocessing approach has emerged as the prevailing method despite its potential limitations. Here we provide an alternative data preprocessing technique and evaluate its performance against the traditional approach for two case studies: Owens Valley (CA) and the Spring Mountains (NV). The following sections will comment on the strengths and weaknesses of each approach for each case study and how the clustering results relate to the contrasting dataset types, hydrogeological settings, and existing conceptual models. We also discuss the implications of this work and potential paths forward.

2.5.1 Owens Valley Case Study

The Owens Valley (OV) case study was used to evaluate a small dataset ($n = 20$) of mountain front springs in a predominately silicate terrain. Prior work from Meyers et al., *in prep* (i.e., Chapter 3) provides the conceptual framework for interpreting the clustering results. Faults, mostly normal and strike-slip, are the primary mechanism driving groundwater flow to the surface for the OV springs. Stable isotopes ($\delta^2\text{H}$ and $\delta^{18}\text{O}$) and noble gas data indicate that these mountain front springs are predominately supported by cold, high elevation (2800-3300m) recharge that flows through fractured, plutonic mountain-block aquifers before interacting with alluvial fill on the mountain front. One of the main findings from Chapter 4 is that the geologic heterogeneity of the Sierra Nevada batholith exerts the primary control on spring geochemistry.

The OV dataset is distinguished by a relatively small range in TDS, e.g., 19 of the 20 samples are between 53-224 mg/L. These samples do not resemble a normal distribution in terms of SPC (2.7). HCA of OV springs produced two starkly different agglomerative clustering results. Results obtained using traditional data preprocessing (OVT) are strongly controlled by the salinity of the groundwater, i.e., dilute samples group together, moderately evolved samples group together, and the most evolved sample(s) group together. There is little overlap in total dissolved solid

concentrations between groups (Figure 2.4A). While there are some limited spatial relationships, the OVT clustering results do not show strong connections with aquifer geology/mineralogy or geochemical fingerprint (Figure 2.5). In contrast, clustering results derived from alternative preprocessing methods (OVA) show no bias toward overall salinity. Four out of the five geochemical groups have wide, overlapping ranges in TDS (Figure 2.4B). Instead, distinctions among OVA groups can be clearly identified on the basis of their geochemical fingerprint, i.e., relative proportions cations and anions in relation to each other. The stiff diagrams and clustering of samples on the Piper diagram show this clearly (Figure 2.4B). Geochemical fingerprints associated with each group can be tied back to slight differences in the aquifer mineralogy upgradient of the springs in their presumed recharge areas (Chapter 4). The OVA clusters from this study match the geochemical groupings from Chapter 4 that are based on solute biplots, geochemical modeling, and $^{87}\text{Sr}/^{86}\text{Sr}$. Only one spring, IES-026, falls into a different geochemical group based on the alternative clustering than the groups outlined by Meyers et al. (in prep) based on multiple hydrochemical indicators (i.e., geochemistry, $^{87}\text{Sr}/^{86}\text{Sr}$, stable isotopes, inverse geochemical modeling, etc.).

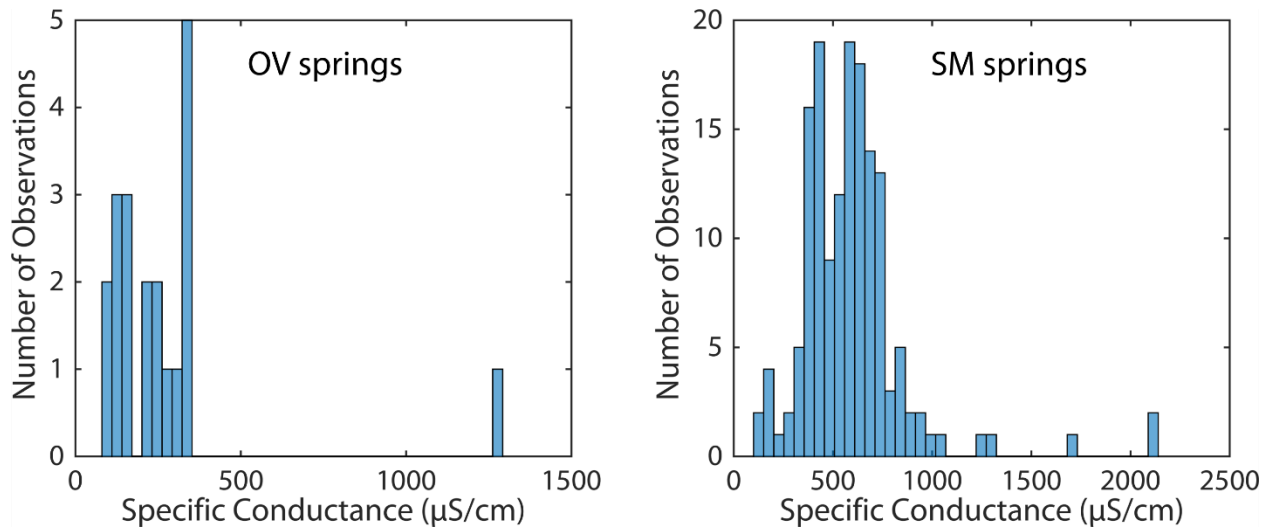


Figure 2.7. Histograms of specific conductance for Owens Valley springs (left) and Spring Mountain springs (right) used in the clustering analysis. The Spring Mountain springs more closely resemble a normal distribution.

2.5.2 Spring Mountains Case Study

The Spring Mountains case study provides an opportunity to compare and contrast traditional and alternative preprocessing methods for HCA at the mountain range scale. This case study includes a larger number of samples ($n = 153$) in a more structurally and geologically complex terrain. Prior studies of groundwater flow in the mountain range provide several conceptual foundations with which to evaluate the geochemical significance of the clusters: 1) groundwater recharge throughout the mountain range primarily occurs from snowmelt recharge at high elevations, specifically in the central Spring Mountains, however local contributions from rain are not insignificant (e.g., the Montgomery Hills and Wilson Cliffs), 2) major geochemical zones are defined by stratigraphic blocks separated by regional thrust faults, and 3) mixing of groundwater between geochemical regions occurs along zones of thrust faulting and cross-cutting normal faults (Hershey et al., 1989; Warix et al., 2020).

Compared to the OV dataset, the SM dataset has a larger range in TDS and water type (Figure 2.6). Statistically, SM spring TDS concentrations more closely resemble a normal distribution (Figure 2.7). Hierarchical clustering of the Spring Mountains dataset results in similar, yet distinctive, geochemical groupings when comparing the two different preprocessing methods. Hierarchical clustering using traditional preprocessing (SMT) results in six geochemical groups that are predominately, but not entirely, structured by increasing dissolved ion concentrations (Figure 2.6C). There is both spatial and geochemical overlap between SMT and SMA results because increases in dissolved ion concentrations are correlated with increases in specific ionic ratios (i.e., Mg/K) or ionic “fingerprints” in the Spring Mountain flow system. For example, both methods identify dilute, high elevation, CSM recharge as a geochemical endmember (e.g., Groups SMT-1 and SMA-1). However, this is due to the opposing strengths of each preprocessing method. SMT-1 identifies the most dilute waters (i.e., waters with low concentrations of most major ions) on the mountain block, which happen to be in the high elevation regions of the CSM. Group SMA-1 captures spring waters that are heavily dominated by Ca^{2+} as the primary dissolved cation and by HCO_3^- as the primary dissolved anion. This is a geochemical fingerprint of shallow groundwater flowing through Permian limestones (e.g., Pmb, Mm, Mdu) that are uplifted at high elevations in the CSM. While SMA-1 and SMT-1 do capture a similar subset of springs, differences between the clustering results are highlighted in the north-central Spring Mountains and in Kyle Canyon. Springs in these areas belong to SMA-1, even though they are slightly more evolved (500-600

$\mu\text{S}/\text{cm}$), because they flow through Permian limestones (e.g., Pmb, Mm, Mdu) and have the same geochemical fingerprint as more dilute springs. However, these same springs fall into group SMT-2, whereas Group SMA-2 almost exclusively includes springs located in areas of regional thrust faulting where Permian limestones intersect Cambrian dolomites. Similarly, Group SMA-3 almost exclusively reflects waters flowing through siliciclastic rocks (e.g., quartzite, sandstone) of Jurassic, Triassic or Cambrian age. While both methods have similar results overall, The SMA results more closely capture geochemical fingerprints of groundwater flowing through specific stratigraphic sections or mixing between geochemical flow regions. These relationships are clearly seen in the stacked histogram (Figure 2.8). Additionally, the SMA results capture unique geochemical mixtures that occur at regional thrust faults (Figure 2.6F).

The geologic make-up of the SMT clustering results is consistently more mixed (Figure 2.6). However, the SMT results clearly do an effective job of identifying areas of dilute water, geochemical evolution in local topography, and regional scale changes in geochemistry (Figure 2.6B). Another difference between the two methods is that the traditional approach identifies one evolutionary pathway (Figure 2.6C) instead of identifying multiple pathways that can be tied back to the underlying geology (e.g., Figure 2.6F). In a system that has as much structural complexity and juxtaposition of contrasting geologic units as the Spring Mountains (e.g., Figure 2.6D), we would expect more than one geochemical evolutionary pathway.

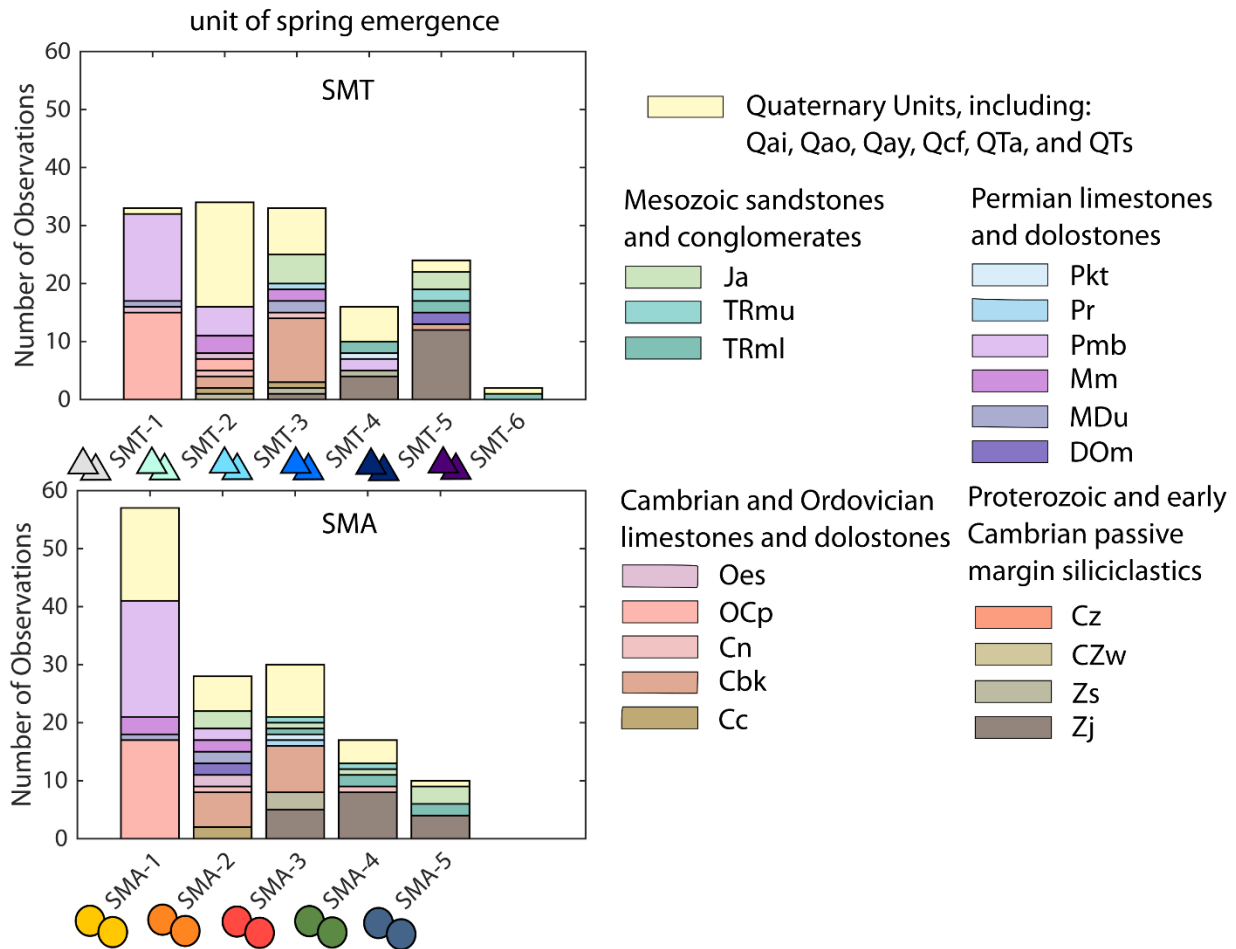


Figure 2.8. Stacked histograms of SMT springs (top) and SMA springs (bottom) showing the number of springs emerging from a geologic unit in each geochemical group. Colors on the stacked histograms are associated with the geologic units in the legend and in the Spring Mountains geologic map. Overall, SMA geochemical clusters are more closely associated to the emergence geology than the SMT geochemical clusters.

2.5.3 Commentary on both methods and case study results

HCA using traditional data preprocessing methods clearly shows a propensity towards grouping samples based on overall TDS concentration. This is true even if the imported data matrix does not directly include SpC (specific conductance) or TDS as a variable, and just includes the major cations and anions as individual vectors. The traditional data preprocessing approach is likely prone to biases because increases in major ions tend to be positively correlated with one another. High numbers of correlated vectors can increase their overall statistical “weight” in multivariate analyses. Although these vectors are log transformed and standardized, the fact that

increases in most major solutes tend to be correlated with overall TDS is not fixed by these preprocessing measures. These preprocessing measures mainly serve to stop one variable from being more highly weighted than another variable. This problem of high numbers of correlated vectors may be problematic if clustering is used to group samples in areas where molar ratios may be more indicative of geochemical processes than dissolved solute concentrations.

Conversely, alternative preprocessing of major ion data may also have a bias, albeit towards grouping samples with similar ionic ratios rather than similar TDS concentrations. While alternative preprocessing may underweight the importance of overall evolution (e.g., Owens Valley example) even when TDS or SPC is included as a variable during HCA, this method has proven useful for linking small changes in geochemical fingerprint or water facies type to aquifer mineralogy and structural configuration. The utility of this approach is seen in both case studies. OVA geochemical groups are specific to either flowing through granite/granodiorite, granite/granodiorite + roof pendant, volcanic rock/felsic plutonic rock, or interaction with basinal brines. These results are corroborated by inverse geochemical models and strontium isotopes (Meyers et al., in prep). SMA geochemical groups were successful in identifying specific geochemical fingerprints correlated to individual stratigraphic blocks and mixing of facies between stratigraphic blocks.

Both preprocessing methods highlight different geochemical groups and trends within the case study datasets. Depending on the end goal, there are many reasons why an analyst would want to utilize one or both of these methods, as each has strengths and potential biases. For example, traditional preprocessing may be favorable for understanding groundwater flow in areas with large ranges in TDS (e.g., alluvial aquifers, regional groundwater systems, or closed, saline basins), in areas where there is a chemically evolving system with uniform geology, or in water quality applications where TDS is the most important indicator. Alternative preprocessing is more useful if the goal is to identify groundwater facies. Specifically, groupings obtained using the alternative preprocessing method may be useful in systems with geologic complexity or heterogeneity or where multiple geochemical processes (e.g. sulphate reduction, cation exchange) are occurring that can shape the geochemical fingerprint.

2.6 Conclusions

Without careful consideration of likely aquifer units, the mineralogy of these units, and the most representative cations and anions driving separation among geochemical groups, common preprocessing workflows and statistical approaches to analyzing water chemistry data (k-means clustering, Q-mode hierarchical clustering analysis, etc.) can obscure potential geochemical relationships. While these approaches have been criticized for ignoring geochemical complexities (e.g., Dreher, 2003), data from this study offers an example of how statistical clustering methods, while useful, must be used cautiously and thoughtfully (i.e., taking potential biases into consideration) and how alternative preprocessing techniques can provide valuable information that is overlooked and obscured during traditional data preprocessing treatment.

The alternative data preprocessing technique presented in this study: 1) takes the strengths from graphical diagnostic tools and numerically quantifies them and 2) aims to circumvent some of the inherent biases that accompany HCA results derived from traditional data preprocessing. In our case study examples, groups derived from HCA using alternative data preprocessing (OVA & SMA) had stronger connections to geological and hydrogeological settings. HCA clusters derived from traditional data preprocessing ignored some of the geochemical complexity in the case study flow systems in favor of grouping water samples largely based on similarities in total dissolved solid concentrations. However, there are likely different geologic areas where each method would outperform the other and it is not disputed that there are instances where having each type of clustering information would be valuable. A workflow (e.g., Figure 2.9) where the user tried multiple clustering approaches and examined the relationship between the clustering results and the aquifer mineralogy and likely kinetic pathways would be the most preferable

This work seeks to inform others to use caution when exercising patterned workflows for clustering/grouping of water chemistry data that may have inherent biases. As the prevalence of using multivariate techniques for analyzing water chemistry data grows, the feasibility of quickly analyzing a dataset becomes easier with software packages (e.g., Minitab, Statistica, Matlab, R) that incorporate multiple clustering algorithms. However, despite the ease of analysis, it is important not to become complacent and fall into sequential or patterned workflows that utilize HCA results for inverse modeling or conceptual model formation without rigorously evaluating the dataset.

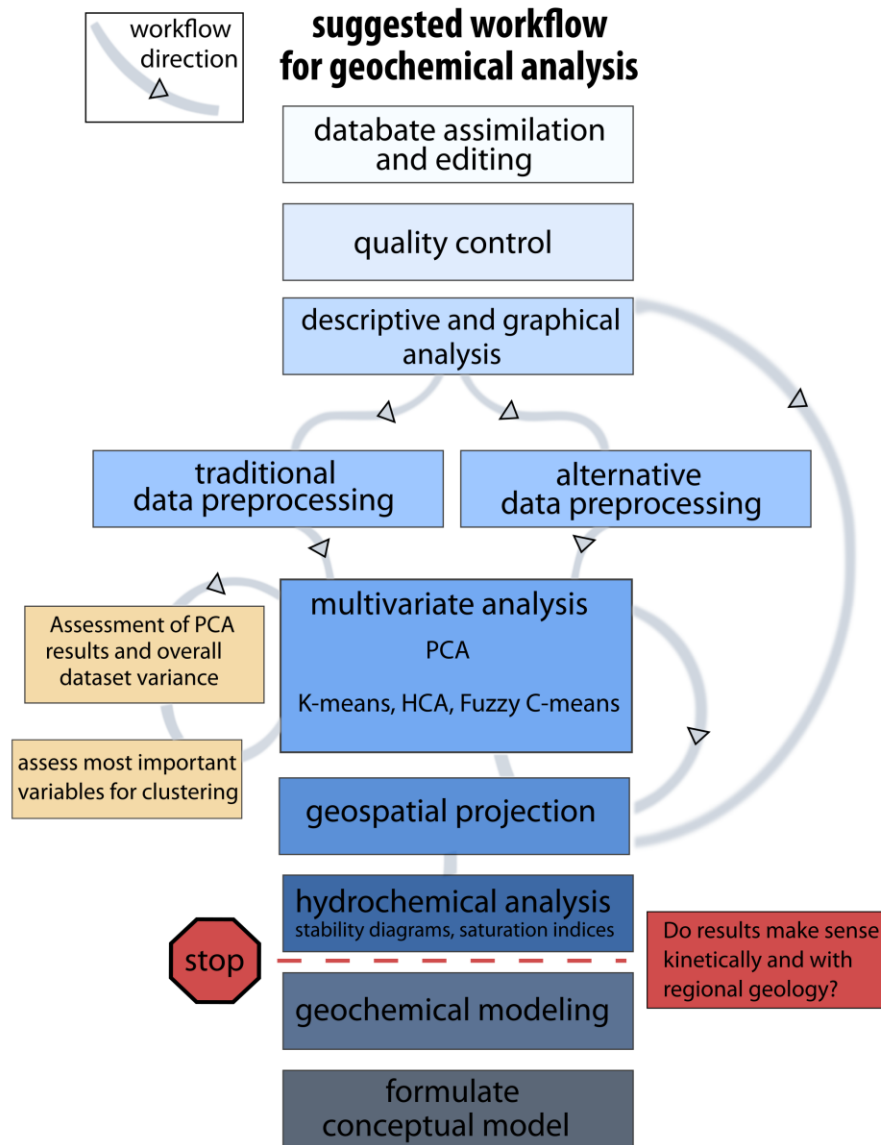


Figure 2.9. Conceptual figure showing a suggested workflow based on the findings from this study.

Our work suggests that users should: 1) be aware of potential biases in the traditional workflow, 2) be open to other data treatment options that might better suit the needs of the analyst, 3) use caution, i.e., check to make sure that clustering results make sense with the hydrogeological framework, and 4) revisit basic geochemical patterns (e.g., solute-solute plots) prior to clustering. It is important to start small and understand simple geochemical relationships before performing multivariate analysis (Siegel, 2008). Cluster analysis should not be used as “proof” of spatial or geochemical relationships (Templ et al., 2008), but rather as a hydrological reconnaissance tool.

2.7 References

- Al-Qudah, O., Woocay, A., & Walton, J. (2011). Identification of probable groundwater paths in the Amargosa Desert vicinity. *Applied Geochemistry*, 26(4), 565-574.
- Anderson, K. W. (2002). Contribution of local recharge to high flux springs in Death Valley National Park, California-Nevada (Doctoral dissertation, Brigham Young University. Department of Geology).
- Back, W. (1960). Hydrochemical facies and ground-water flow patterns in Northern Atlantic Coastal Plain. *AAPG Bulletin*, 44(7), 1244-1245.
- Bateman, P. C., Pakiser, L. C., & Kane, M. F. (1965). Geology and tungsten mineralization of the Bishop district, California, with a section on gravity study of Owens Valley and a section on seismic profile (No. 470). US Govt. Print. Off.
- Belcher, W. R., Bedinger, M. S., Back, J. T., & Sweetkind, D. S. (2009). Interbasin flow in the Great Basin with special reference to the southern Funeral Mountains and the source of Furnace Creek springs, Death Valley, California, US. *Journal of Hydrology*, 369(1-2), 30-43.
- Belcher, W. R., & Sweetkind, D. S. (2010). Death Valley regional groundwater flow system, Nevada and California—Hydrogeologic framework and transient groundwater flow model: US Geological Survey Professional Paper, 398.
- Belkhiri, L., Boudoukha, A., Mouni, L., & Baouz, T. (2010). Application of multivariate statistical methods and inverse geochemical modeling for characterization of groundwater—a case study: Ain Azel plain (Algeria). *Geoderma*, 159(3-4), 390-398.
- Bellman, R. (1961). Curse of dimensionality. Adaptive control processes: a guided tour. Princeton, NJ, 3, 2.
- Blake, S., Henry, T., Murray, J., Flood, R., Muller, M. R., Jones, A. G., & Rath, V. (2016). Compositional multivariate statistical analysis of thermal groundwater provenance: a hydrogeochemical case study from Ireland. *Applied Geochemistry*, 75, 171-188.
- Boghici, E.M., Boghici, R., (2001). GeoStiff-A program that produces Stiff diagrams as GIS ArcInfo polygon coverages. Texas Water Development Board Open File Report 01-001.
- Bushman, M., Nelson, S. T., Tingey, D., & Eggett, D. (2010). Regional groundwater flow in structurally-complex extended terranes: an evaluation of the sources of discharge at Ash Meadows, Nevada. *Journal of Hydrology*, 386(1-4), 118-129.
- Carucci, V., Petitta, M., & Aravena, R. (2012). Interaction between shallow and deep aquifers in the Tivoli Plain (Central Italy) enhanced by groundwater extraction: a multi-isotope approach and geochemical modeling. *Applied Geochemistry*, 27(1), 266-280.

- Chang, N. B., Chen, H. W., & Ning, S. K. (2001). Identification of river water quality using the fuzzy synthetic evaluation approach. *Journal of Environmental Management*, 63(3), 293-305.
- Cloutier, V., Lefebvre, R., Therrien, R., & Savard, M. M. (2008). Multivariate statistical analysis of geochemical data as indicative of the hydrogeochemical evolution of groundwater in a sedimentary rock aquifer system. *Journal of Hydrology*, 353(3-4), 294-313.
- Dreher, T. (2003). Comment on Güler C, Thyne GD, McCray JE, Turner AK (2002): Evaluation of graphical and multivariate statistical methods for classification of water chemistry data (Hydrogeology Journal 10: 455–474). *Hydrogeology Journal*, 11(5), 605-606.
- Durov, S. A. (1948). Natural waters and graphic representation of their composition. In *Dokl Akad Nauk SSSR* (Vol. 59, No. 3, pp. 87-90).
- Elsenbeer, H., Lack, A., & Cassel, K. (1995). Chemical fingerprints of hydrological compartments and flow paths at La Cuenca, western Amazonia. *Water Resources Research*, 31(12), 3051-3058.
- Farnham, I. M., Stetzenbach, K. J., Singh, A. K., & Johannesson, K. H. (2000). Deciphering groundwater flow systems in Oasis Valley, Nevada, using trace element chemistry, multivariate statistics, and geographical information system. *Mathematical Geology*, 32(8), 943-968.
- Feth, J. H. F., Robertson, C. E., & Polzer, W. L. (1964). Sources of mineral constituents in water from granitic rocks, Sierra Nevada, California and Nevada (No. 1535-I). US Govt. Print. Off.
- Fitzpatrick, M. L., Long, D. T., & Pijanowski, B. C. (2007). Exploring the effects of urban and agricultural land use on surface water chemistry, across a regional watershed, using multivariate statistics. *Applied Geochemistry*, 22(8), 1825-1840.
- Gabellone, N. A., Solari, L., Claps, M., & Neschuk, N. (2008). Chemical classification of the water in a lowland river basin (Salado River, Buenos Aires, Argentina) affected by hydraulic modifications. *Environmental Geology*, 53(6), 1353-1363.
- Garrels, R. M., & Mackenzie, F. T. (1967). Origin of the chemical compositions of some springs and lakes.
- Ghesquière, O., Walter, J., Chesnaux, R., & Rouleau, A. (2015). Scenarios of groundwater chemical evolution in a region of the Canadian Shield based on multivariate statistical analysis. *Journal of Hydrology: Regional Studies*, 4, 246-266.
- Grande, J. A., Andújar, J. M., Aroba, J., De La Torre, M. L., & Beltrán, R. (2005). Precipitation, pH and metal load in AMD river basins: an application of fuzzy clustering algorithms to the process characterization. *Journal of Environmental Monitoring*, 7(4), 325-334.

- Güler, C., Thyne, G. D., McCray, J. E., & Turner, K. A. (2002). Evaluation of graphical and multivariate statistical methods for classification of water chemistry data. *Hydrogeology Journal*, 10(4), 455-474.
- Güler, C., & Thyne, G. D. (2004). Delineation of hydrochemical facies distribution in a regional groundwater system by means of fuzzy c-means clustering. *Water Resources Research*, 40(12).
- Güler, C., & Thyne, G. D. (2004). Hydrologic and geologic factors controlling surface and groundwater chemistry in Indian Wells-Owens Valley area, southeastern California, USA. *Journal of Hydrology*, 285(1-4), 177-198.
- Güler, C., Kurt, M. A., Alpaslan, M., & Akbulut, C. (2012). Assessment of the impact of anthropogenic activities on the groundwater hydrology and chemistry in Tarsus coastal plain (Mersin, SE Turkey) using fuzzy clustering, multivariate statistics and GIS techniques. *Journal of Hydrology*, 414, 435-451.
- Hem, J. D. (1985). Study and interpretation of the chemical characteristics of natural water (Vol. 2254). Department of the Interior, US Geological Survey.
- Helstrup, T., Jørgensen, N. O., & Banoeng-Yakubo, B. (2007). Investigation of hydrochemical characteristics of groundwater from the Cretaceous-Eocene limestone aquifer in southern Ghana and southern Togo using hierarchical cluster analysis. *Hydrogeology Journal*, 15(5), 977-989.
- Hershey, R. L. (1989). Hydrogeology and hydrogeochemistry of the Spring Mountains. Clark County, Nevada [MS thesis]: Las Vegas, University of Nevada.
- Judd, A. G. (1980). The use of cluster analysis in the derivation of geotechnical classifications. *Bulletin of the Association of Engineering Geologists*, 17(4), 193-211.
- Kebede, S., Travi, Y., Alemayehu, T., & Ayenew, T. (2005). Groundwater recharge, circulation and geochemical evolution in the source region of the Blue Nile River, Ethiopia. *Applied Geochemistry*, 20(9), 1658-1676.
- King, A. C., Raiber, M., & Cox, M. E. (2014). Multivariate statistical analysis of hydrochemical data to assess alluvial aquifer–stream connectivity during drought and flood: Cressbrook Creek, southeast Queensland, Australia. *Hydrogeology Journal*, 22(2), 481-500.
- Knödel, K., Lange, G., & Voigt, H. J. (2007). Environmental geology: handbook of field methods and case studies. Springer Science & Business Media.
- Koonce, J. E., Yu, Z., Farnham, I. M., & Stetzenbach, K. J. (2006). Geochemical interpretation of groundwater flow in the southern Great Basin. *Geosphere*, 2(2), 88-101.
- Kreamer, D. K., Hodge, V. F., Rabinowitz, I., Johannesson, K. H., & Stetzenbach, K. J. (1996). Trace element geochemistry in water from selected springs in Death Valley National Park, California. *Groundwater*, 34(1), 95-103.

- Lin, C. Y., Abdullah, M. H., Praveena, S. M., Yahaya, A. H. B., & Musta, B. (2012). Delineation of temporal variability and governing factors influencing the spatial variability of shallow groundwater chemistry in a tropical sedimentary island. *Journal of Hydrology*, 432, 26-42.
- Marzolf, J. E. (1990). Reconstruction of extensionally dismembered early Mesozoic sedimentary basins; southwestern Colorado Plateau to the eastern Mojave Desert. Basin and range extensional tectonics near the latitude of Las Vegas, Nevada, 176, 477-500.
- McNeil, V. H., Cox, M. E., & Preda, M. (2005). Assessment of chemical water types and their spatial variation using multi-stage cluster analysis, Queensland, Australia. *Journal of Hydrology*, 310(1-4), 181-200.
- Meng, S. X., & Maynard, J. B. (2001). Use of statistical analysis to formulate conceptual models of geochemical behavior: water chemical data from the Botucatu aquifer in Sao Paulo state, Brazil. *Journal of Hydrology*, 250(1-4), 78-97.
- Monjerezi, M., Vogt, R. D., Aagaard, P., & Saka, J. D. (2011). Hydro-geochemical processes in an area with saline groundwater in lower Shire River valley, Malawi: an integrated application of hierarchical cluster and principal component analyses. *Applied Geochemistry*, 26(8), 1399-1413.
- Moore, J. G. (1963). Geology of the Mount Pinchot quadrangle, southern Sierra Nevada, California (Vol. 1130). US Government Printing Office.
- Moore, J. G. (1987). Mount Whitney Quadrangle, Inyo and Tulare Counties, California: Analytic Data (No. 1760). Department of the Interior, US Geological Survey.
- Page, W. R., Lundstrom, S. C., Harris, A. G., Langenheim, V. E., Workman, J. B., Mahan, S., ... & Bell, J. W. (2005). Geologic and geophysical maps of the Las Vegas 30'x 60'quadrangle, Clark and Nye counties, Nevada, and Inyo County, California (No. 2814).
- Piper, A. M. (1944). A graphic procedure in the geochemical interpretation of water-analyses. *Eos, Transactions American Geophysical Union*, 25(6), 914-928.
- Pretti, V. A., & Stewart, B. W. (2002). Solute sources and chemical weathering in the Owens Lake watershed, eastern California. *Water Resources Research*, 38(8), 2-1.
- Sarbu, C., & Pop, H. F. (2005). Principal component analysis versus fuzzy principal component analysis: a case study: the quality of Danube water (1985–1996). *Talanta*, 65(5), 1215-1220.
- Siegel, D. (2008). Reductionist hydrogeology: ten fundamental principles. *Hydrological Processes: An International Journal*, 22(25), 4967-4970.
- Suk, H., & Lee, K. K. (1999). Characterization of a ground water hydrochemical system through multivariate analysis: clustering into ground water zones. *Groundwater*, 37(3), 358-366.
- Woocay, A., & Walton, J. (2008). Multivariate analyses of water chemistry: surface and ground water interactions. *Groundwater*, 46(3), 437-449.

Steinhorst, R. K., & Williams, R. E. (1985). Discrimination of groundwater sources using cluster analysis, MANOVA, canonical analysis and discriminant analysis. *Water Resources Research*, 21(8), 1149-1156.

Stiff Jr, H. A. (1951). The interpretation of chemical water analysis by means of patterns. *Journal of Petroleum Technology*, 3(10), 15-3.

Swan, A. R., & Sandilands, M. (1995). Introduction to geological data analysis. In *International Journal of Rock Mechanics and Mining Sciences and Geomechanics Abstracts* (Vol. 8, No. 32, p. 387A).

Swanson, S. K., Bahr, J. M., Schwar, M. T., & Potter, K. W. (2001). Two-way cluster analysis of geochemical data to constrain spring source waters. *Chemical Geology*, 179(1-4), 73-91.

Templ, M., Filzmoser, P., & Reimann, C. (2008). Cluster analysis applied to regional geochemical data: problems and possibilities. *Applied Geochemistry*, 23(8), 2198-2213.

Thyne, G., Güler, C., & Poeter, E. (2004). Sequential analysis of hydrochemical data for watershed characterization. *Groundwater*, 42(5), 711-723.

Warix, S. R., Rademacher, L. K., Meyers, Z. P., & Frisbee, M. D. (2020). Groundwater geochemistry and flow in the Spring Mountains, NV: Implications for the Death Valley Regional Flow System. *Journal of Hydrology*, 580, 124313.

Winograd, I. J., & Pearson Jr, F. J. (1976). Major carbon 14 anomaly in a regional carbonate aquifer: Possible evidence for megascale channeling, south central Great Basin. *Water Resources Research*, 12(6), 1125-1143.

Winograd, I. J., Riggs, A. C., & Coplen, T. B. (1998). The relative contributions of summer and cool-season precipitation to groundwater recharge, Spring Mountains, Nevada, USA. *Hydrogeology Journal*, 6(1), 77-93.

Żelazny, M., Astel, A., Wolanin, A., & Małek, S. (2011). Spatiotemporal dynamics of spring and stream water chemistry in a high-mountain area. *Environmental Pollution*, 159(5), 1048-1057.

CHAPTER 3. OLD GROUNDWATER BUFFERS THE EFFECTS OF A MAJOR DROUGHT IN GROUNDWATER-DEPENDENT ECOSYSTEMS OF THE EASTERN SIERRA NEVADA (USA)

3.1 Abstract

Global groundwater resources are stressed and the effects of climate change are projected to further disrupt recharge processes. Therefore, we must identify the buffers to climate change in hydrogeologic systems in order to understand which groundwater resources will be disproportionately affected. Here, we utilize a novel combination of remote sensing (e.g., Landsat) and groundwater residence time data to quantify the hydrogeologic stability of aridland mountain-front springs in response to a major climate event, the 2011-2017 California drought. Desert springs within Owens Valley (CA) support unique ecosystems that are surrounded by lush, green vegetation sustained only by discharging groundwater and are not reliant on localized precipitation. Therefore, the health or ecological response of this vegetation is a direct reflection of the hydrogeologic stability of the mountain-block groundwater system since water is the limiting resource for riparian plant growth in arid regions. We compared spring water residence times to vegetation metrics computed from Landsat imagery leading up to and during the drought interval. We observe that the vegetation surrounding springs discharging a high fraction of modern and bomb-pulse groundwater (<100 years) showed evidence of increased drying and desiccation as the drought progressed. In comparison, springs discharging a higher fraction of old groundwater (>100 years) showed little response thereby supporting the conceptual model where old groundwater, i.e., a distribution of deep and stable groundwater flowpaths, buffers short-term climate perturbations and may provide hydrogeologic resistance to future effects from climate change.

3.2 Introduction

What are the buffers to climate change impacts on natural hydrologic systems? The answer to this question has global significance as water resources, particularly groundwater, continue to be stressed by global population growth, changes in annual recharge, and increasing reliance on groundwater pumping (Vörösmarty et al., 2000; Famiglietti 2014). Additionally, recent work suggests that we may be sitting on a ‘environmental time bomb’ where impacts to recharge caused

by climate change may take human timescales to propagate through groundwater systems (Cuthbert et al., 2019). While old groundwater (i.e., >100 yrs) is postulated as an important contributor to hydrogeologic resistance (e.g., Sophocleous, 2012), the influence of groundwater residence time on the responses of hydrologic systems to disturbance is an area of current research that remains poorly understood and rarely quantified. Here we define hydrogeologic resistance as the resistance of a hydrologic system to changes in forcing (e.g., recharge) that are induced by perturbations (e.g., droughts) (Cartwright et al., 2018). In contrast, we define hydrogeologic resilience as the ability of a system to recover and return to pre-disturbance equilibrium following a perturbation.

One of the primary conceptual models for how old groundwater influences hydrogeologic resistance to climate change is that old groundwater, commonly supplied by a substantial contribution from regional (or deep) flowpaths, provides a buffer (i.e., a dampening of the effects of a perturbation) to the hydrological response of a system (Rademacher et al., 2005; Singleton and Moran 2010; Frisbee et al., 2012). If true, then this conceptual model also suggests that if a groundwater flowpath distribution contains a substantial component of young groundwater, then the effects of a perturbation may propagate more rapidly through the groundwater system.

In our conceptual model, a groundwater distribution comprised of long/deep flowpaths increases the integrated response time of the aquifer and dampens the effects of disturbances. In this case, the response time of groundwater is directly proportional to the flowpath length and inversely proportional to hydraulic diffusivity, a measure of how changes in hydraulic pressure are propagated through an aquifer (Erksine and Papaioannou 1997; Markovich et al., 2016). A distribution comprised of short flowpaths (i.e., young groundwater) would therefore result in a rapid response time. Landscape perturbations such as forest fires, land-use/land-cover change, and droughts can impact recharge fluxes, alter groundwater flowpaths, and subsequently change residence time distributions. However, uncertainties remain when determining the hydrogeologic resistance or resilience of groundwater systems and quantifying their response to perturbations. Additionally, the time scales and severity of these responses remain poorly quantified.

The concepts of groundwater response times and hydrogeologic resistance or hydrogeologic resilience to disturbances are extremely important in semi-arid locations globally and perhaps most acutely so in the American Southwest. Increased aridity is predicted for the desert Southwest of the United States during the 21st century as a consequence of climate change

(MacDonald, 2010). Reductions in alpine snowpack for the western U.S are already observed (Mote et al., 2018). Snowpack reduction is a critical concern since snowmelt is the principal recharge source for mountain block groundwater systems (Wilson and Guan, 2004). The emerging trend of declining snowpack is unsustainable for southwestern aquifers (Meixner et al., 2016). Many of these aquifers support threatened or endangered groundwater-dependent ecosystems (GDEs) in the rain shadow of the Sierra Nevada (Patten et al., 2008). Desert springs in this region are important since they play a vital role in sustaining ecological niches (Sada et al., 2005) and are often relied upon for irrigation, human consumption, and economic uses (Frisbee et al., 2013). While these springs are often limited in spatial extent, they support the majority of regional biodiversity (Sada, 2008). Many of these springs have supported aquatic life for thousands of years, as evidenced by the presence of speciated fish (Echelle and Echelle 1993; Echelle et al., 2005; Knott et al., 2008) and benthic macroinvertebrate (e.g., springsnail) (Hershler 1989; Hershler et al., 1999) populations in isolated oases. However, there is concern about whether these keystone features will be able to sustain flow under a decreased recharge regime associated with the effects from climate change. The relationship between changes in springflow to changes in recharge is likely non-linear due to the presence of a distribution of flowpaths an inherent time lag between recharge and discharge.

The presence of perennial springs and focused groundwater discharge points in arid regions like the southern Great Basin (e.g., Independence, CA) with minimal precipitation (< 13 cm/yr) (<https://wrcc.dri.edu/cgi-bin/cliMAIN.pl?ca4232>) and high evapotranspiration (ET) allow for dense, green vegetation to exist outside of high elevation, sky-island ecotones. (Figure 3.1). In contrast to salt-tolerant vegetation at lower-lying basin locations and drought-tolerant vegetation on alluvial slopes (with rooting depths well above the water table) (Cormstock and Ehleringer, 1992; Elmore et al., 2003; Naumburg et al., 2005), the ample water availability and persistent surface discharge in spring riparian areas allows for drought-evasive vegetation to thrive in an otherwise inhospitable environment (Patten et al., 2008). Therefore, we interpret the health of the groundwater-dependent vegetation at springs to be a direct reflection of the stability of the groundwater flow system since water availability is the limiting resource for drought evasive vegetation (Kemp, 1983; Harrison, 2016). Based on these observations, the presence of green, healthy riparian vegetation during a multi-year drought would suggest that the spring flowpath distribution is stable and resistant to perturbations. If the aforementioned conceptual model is valid

then we would expect the groundwater flowpath distribution to contain a substantial component of long residence time groundwater. On the other hand, vegetation that dies/dries would suggest the flowpath distribution is not resistant to drought disturbance and likely contains a substantial component of young groundwater. Groundwater-dependent ecosystems, especially those in arid regions, are vulnerable to the effects of climate change (e.g., major droughts) that alter recharge processes (Morsy et al., 2017).

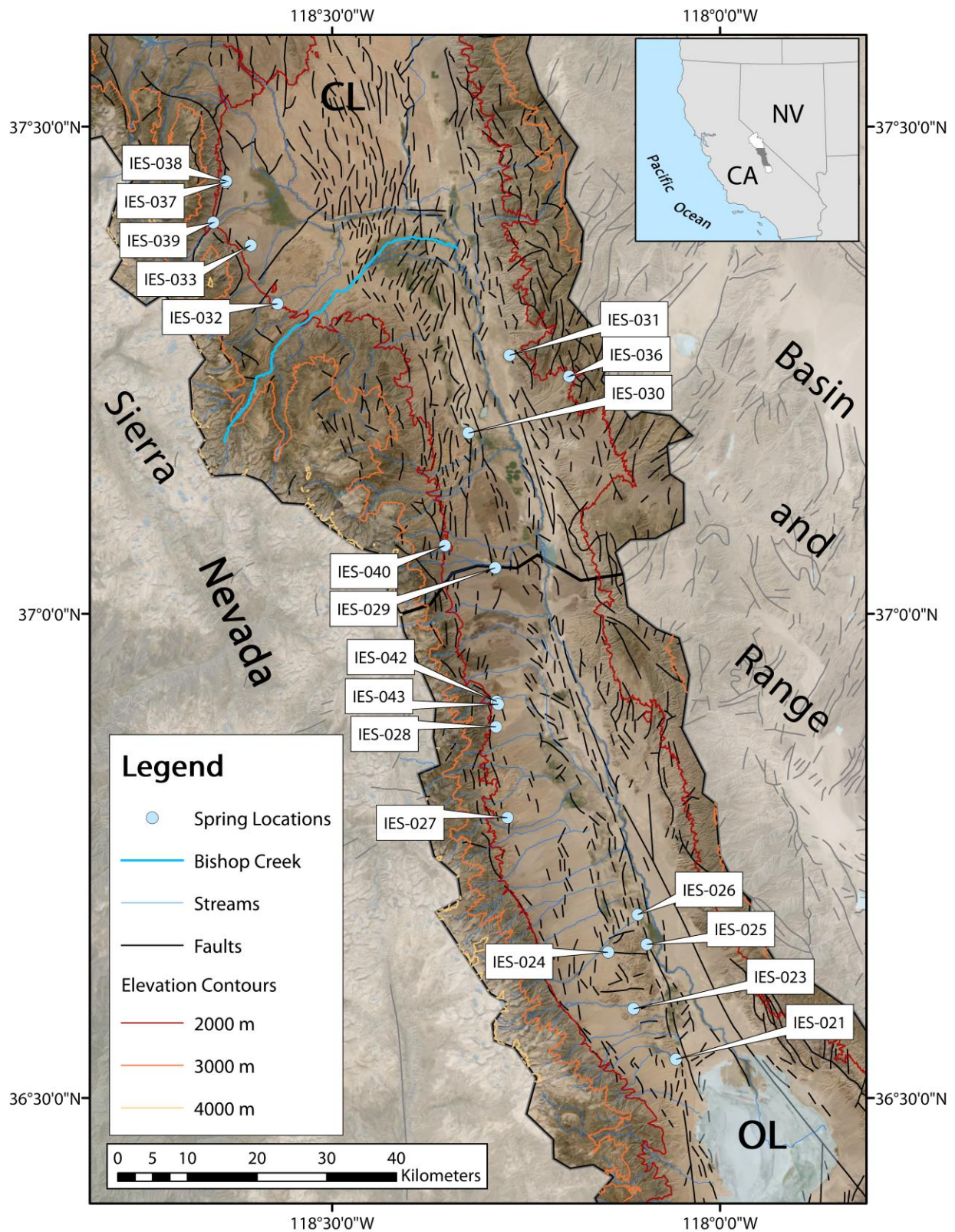


Figure 3.1. Birds-eye imagery (Google Earth, 2019) and complementary field photographs of spring-dependent vegetation along the eastern Sierra Nevada in Owens Valley (CA). Drought evasive vegetation, present around springs and the riparian areas surrounding streams, is green and lush in contrast to drought tolerant vegetation on alluvial slopes (Elmore et al., 2003). A & B correspond to IES-043, South Harry Birch Spring. C & D correspond to the confluence area of IES-037 & IES-038, Wells Meadow.

The 2011-2017 California drought was the driest 6-year period since records began in 1895. While this drought was notable for its record heat (Griffin and Anchukaitis, 2014), large areas of the western United States also experienced record low snowpack (Mote et al., 2016). Vegetation was noticeably affected as progressive canopy water loss was observed in 10.6 billion ha of California forests (Asner et al., 2016). Because of its severity and duration, this historic drought presents an excellent opportunity to evaluate the relative stability of perennial springs in Owens Valley, CA (Figure 3.2) using vegetation health metrics (e.g. Normalized Difference Vegetation Index [NDVI]) coupled with groundwater residence time data. While previous studies have demonstrated that groundwater residence time can be used to identify declining recharge and flowpath transience (Manning et al., 2012), to our knowledge residence time data has not been previously paired with vegetation metrics from remote sensing data to understand coupled ecologic/hydrologic system responses. In fact, recent work by Cartwright et al. (2018) argues that field data, including measurement of groundwater age, is an area of needed combination with remote sensing data in order to identify potential hydrologic refugia.

Here we evaluate whether the responses of spring-dependent vegetation to a historic drought: 1) can provide a proxy for the overall hydrogeologic resistance of a spring, and 2) can be predicted using spring residence times. We hypothesize that springs discharging a large fraction of old groundwater (> 100 yrs) will exhibit less extreme vegetation dying/drying and high hydrological resistance to extreme short-term drought conditions. In comparison, springs that discharge a large fraction of young groundwater (< 100 yrs) will have less hydrogeologic resistance and vegetation will respond more rapidly to extreme drought conditions. The most direct way to test this hypothesis is to monitor vegetation health over the drought interval through remote sensing techniques, derive vegetation stability metrics from this data, and then compare these metrics to spring residence time partitions. We accomplish this by extracting NDVI time series from Landsat imagery for spring riparian areas in Owens Valley (CA) during the historic drought. We then compute vegetation stability metrics from the NDVI time series. These metrics are then compared with age partitions derived from tritium (^3H) and chlorine-36 (^{36}Cl) data collected during the spring of 2016.

Figure 3.2. The inset map shows the study area, the Mono-Owens Lake watershed (HUC 180901), shaded in white in the regional context of CA and NV. The dark grey area within HUC 180901 represents the area depicted in the larger map. The larger map depicts orthoimagery of the Owens Valley region within the Mono-Owens Lake watershed (outlined in black) lying east of the Sierra Nevada and west of the southern extent of the Basin and Range. OL represents the Owens Lake subwatershed of HUC 180901 and CL represents the Crowley Lake subwatershed. Light blue circles represent spring sampling locations from a spring 2016 hydrological field campaign. Bishop Creek, a major stream draining the Sierra Nevada, is shown in cyan. A hydrograph for Bishop Creek spanning the duration of the drought is shown in Figure 3.4. Known faults are shown by the small black lines and streams are shown by the small blue lines. Contour lines representing 2000m, 3000m, and 4000m are shown in the red, orange, and yellow lines, respectively.



3.3 Methods

3.3.1 Study area and spring sampling

The Mono-Owens Lake Watershed is an internally draining watershed in eastern California (HUC 180901) comprised of the Mono Lake Watershed, the Crowley Lake Watershed, and the Owens Lake Watershed. This study focuses on the Crowley Lake and Owens Lake portions of HUC 180901, hereby referred to as Owens Valley (Figure 3.2). Owens Valley lies in a rain shadow on the leeward side of the Sierra Nevada and is bounded by the White-Inyo Mountains to the east. Structurally, Owens Valley is a rift basin with over 3,000 meters of basin fill lying just outside the Basin and Range physiographic province in what is known as the Walker Lane Transitional Zone (Jayko, 2011). This tectonic setting creates significant relief where Owens Valley (1000-1400 mamsl) is surrounded on both sides by north-south trending ranges with ridgelines and peaks exceeding 4000 mamsl. The eastern Sierra Nevada is primarily composed of plutonic rocks of Cretaceous age, while the White-Inyo Mountains are predominately Penn-Permian metasedimentary rocks.

Nineteen springs were sampled in Owens Valley during the spring of 2016. Seventeen emerge from the eastern slope of the Sierra Nevada and two emerge on the western front of the White-Inyo Mountains (Figure 3.2). The majority of these springs emerge at structural features, mostly small faults, associated with the Sierra Nevada Frontal Fault Zone, the Owens Valley Fault Zone, or the White Mountain Fault Zone. Few faults in the area have published depths, offset, or displacement data, however numerous conceptual models interpret these spring emergences as areas of mixing between deeper groundwater (e.g. mountain block recharge), alluvial groundwater, and local sources of recharge (e.g. losing streams) (Danskin, 1998; Harrison, 2016; Zdon et al., 2019).

Understanding the effects of the 2011-2017 California drought on water resources (including springs) in Owens Valley is of particular hydrologic significance as both groundwater and surface water support ecosystems which are home to endemic and threatened species (Miller and Pister, 1971; Chen et al., 2007; Conroy et al., 2017). This watershed also contributes to municipal water supply in Los Angeles, CA via the Los Angeles Aqueduct (LAA).

3.3.2 General chemistry collection and analysis

General chemistry samples were filtered in the field and collected in 250 ml high-density polyethylene (HDPE) bottles and refrigerated upon sampling until sent for analysis. Major cations and anions were measured at the New Mexico Bureau of Geology and Mineral Resources Chemistry Lab. Cations were measured using inductively coupled plasma optical emission spectrometric techniques (ICP-ES) according to EPA 200.7. Anions were measured using an ion chromatograph (IC) according to EPA 300.0. Duplicates were run on every 10th sample. Low bromide analysis was performed for samples under the bromide detection limit of 0.1 mg/L. All springs included in the analysis have change balance error (CBE) < 5%.

3.3.3 Tritium collection and analysis

One 1 L sample of water with minimal headspace was collected from each spring in HDPE bottles for tritium analysis. Springs were sampled as close as possible to the source or discharging seepage face by inserting platinum-cured silicone tubing into flowing fractures or into the spring orifice. Water samples were collected using a GeoTech peristaltic pump. Samples were then sent for gas proportional counting analysis at the University of Miami Tritium Laboratory (<https://tritium.rsmas.miami.edu/>). Electrolytic enrichment and low-level counting were performed for accuracy and precision of 0.1 TU.

3.3.4 Chlorine-36 collection and analysis

Sampling of spring waters for ³⁶Cl/Cl was completed in the same method as tritium except water was pumped through 0.22 μm polyethersulfone membrane Sterivex-GP pressure filters. AgCl was used for chemical preparation of the sample before AMS measurement. Samples were analyzed at the Purdue PRIME Lab (<http://www.physics.purdue.edu/primelab>) and results are reported as ³⁶Cl/Cl ratios x 10⁻¹⁵ along with standard deviations for individual samples.

³⁶Cl/Cl was also analyzed on fresh vegetation (e.g. pine and pinyon-juniper needles, n = 5) as well as duff (n=3) from across the southern Great Basin in order to investigate the effect of chloride recycling in vegetation on groundwater residence time interpretations. Chloride extraction methods were followed from Vogt and Herpers (1988) and Sharma et al. (1990). Chloride was extracted from pine and juniper needles by leaching in 4 N HNO₃ for three days in a hot water

bath. Chloride was precipitated from the leachate as AgCl and purified by washing in HNO₃. Sulfur was removed by precipitation as BaSO₄ and chloride further isolated from impurities by anion chromatography. The final AgCl product was centrifuged into a pellet, dried, and loaded into AgBr filled copper cathodes for measurement of ³⁶Cl/^{Total}Cl ratios by accelerator mass spectrometry at PRIME Lab, Purdue University.

3.3.5 Age partitioning

Tritium (³H) and chlorine-36 (³⁶Cl) were used to partition waters into “young” and “old”. While cosmogenically produced ³⁶Cl can be used for dating ancient groundwater ($t_{1/2} = 301,000$ years), the atmospheric concentrations of both ³⁶Cl and ³H ($t_{1/2} = 12.3$ years) were elevated in the 1950s and 1960s due to atmospheric and submarine nuclear weapons testing (Phillips, 2000). Thus, both tracers can be used to detect the presence of relatively young groundwater (<60 years) and, in turn, recent recharge. ³⁶Cl is particularly suited for identifying the presence of bomb-pulse groundwater due to its long half-life (Phillips, 2000). Groundwater velocities are high enough in the Owens Valley groundwater system (e.g. Danskin, 1998) such that atmospheric production of ³⁶Cl far exceeds subsurface production. Chloride concentrations and Cl-/Br- ratios of spring waters were used to aid in these interpretations by further constraining the origins of groundwater salinity (e.g., Davis et al., 1998; Davis, 2001).

We classify spring waters as “old” when we detect pre-anthropogenic ³⁶Cl/Cl ratios (< 600 x 10⁻¹⁵) and low ³H (< 0.2 TU), as these waters do not contain a significant fraction of recharge from the 1950s/60s to present. This tritium threshold is similar to one used by Visser et al. (2012) (<0.3 TU = “tritium dead”) in their California GAMA study of drinking water wells. In comparison, “young” spring waters have bomb-pulse ³⁶Cl/Cl ratios (> 600 x 10⁻¹⁵) and elevated ³H (> 0.2 TU). Additionally, springs with elevated tritium (TU > 2.0) that do not contain bomb pulse ³⁶Cl/Cl ratios are interpreted to be discharging water comparable to modern precipitation or post bomb-pulse recharge and are also classified as “young”. These young/old classification criteria are based on pre-anthropogenic ³⁶Cl/Cl ratios in groundwater from empirical data presented by Davis (2003). Preanthropogenic ³⁶Cl/Cl ratios for the region range from ~250-500 (Davis, 2003).

3.3.6 Vegetation indices for monitoring GDEs

Spectrally-derived vegetation indices have been previously used to map (Barron et al., 2012; Gou et al., 2014; Klausmeyer et al., 2018) and monitor (Petus et al., 2013; White et al., 2016) GDEs. However, past research has mainly focused on how GDEs or phreatophytic vegetation respond to anthropogenic activities such as groundwater pumping (Patten et al., 2008; Petus et al., 2013). Of these different vegetation indices, Normalized Difference Vegetation Index (NDVI) is a widely used and reliable metric for chlorophyll content, vegetation coverage, and density of “greenness”, a proxy for vegetation health (Carlson and Ripley, 1997). Computation of NDVI relies on both the visible and near-infrared portions of the electromagnetic spectrum and calculated NDVI values range from 1 to -1. Values 0.1 and below typically represent bare earth, snow, or rock lacking substantial vegetation cover. Values closer to 1 indicate dense vegetation cover. In arid and semiarid systems, plant density is correlated with water availability, which is growth limiting in these environments, as well as in places where vegetation is dependent on groundwater (Eamus et al, 2015; Harrison, 2016).

Numerous studies have observed systematic NDVI decreases when vegetation has reduced accessibility to groundwater (Wang et al., 2011; Aguilar et al., 2012). There is also a precedent using remotely sensed data to compare the greenness of vegetation over time to identify areas that remain green during seasonal or multi-year droughts (e.g., Lv et al., 2013). Our study builds on a robust body of work in Owens Valley linking changes in hydrology to changes in vegetation health or NDVI (Elmore et al., 2003; Elmore et al., 2006; Mata-González et al., 2012; Pritchett and Manning, 2012). However, the majority of these studies have focused on linking vegetation change to water table decline (i.e., groundwater pumping) and the effect of groundwater residence time in natural systems has not been considered. Peak NDVI, which represents the maximum NDVI value in an annual time series (relating to the time of peak photosynthetic activity), has been used as a key metric for understanding vegetation response to climate (Jia et al., 2003; Cleland et al., 2006) and interannual variability (Trujillo et al., 2012). Our study relies on the use of peak NDVI to understand how GDEs of varying residence time distributions respond to climate perturbations, such as major droughts, which are ongoing threats to GDEs (Klørve et al., 2014).

3.3.7 Extraction and smoothing of NDVI data and creation of NDVI metrics

Though drought conditions technically extended to the beginning of 2017, initial drought recovery began in mid-2016. Therefore, we limit our analysis range to the beginning of 2016 to avoid mixing a recovery vegetation signal when the drought had been continually worsening for 4 years. NDVI time series were calculated for each spring from 2012-2016 using Landsat 7 32-Day NDVI Composite scenes. These scenes were made from Level L1T orthorectified scenes using (TOA) reflectance after Chander et al. (2009) with Google Earth Engine (GEE), a recently developed cloud-computing geospatial analysis platform that has been used in numerous terrestrial and planetary studies (e.g., Johansen et al., 2015; Huang et al., 2017; Robinson et al., 2017). NDVI ranges in value from -1 to 1 and is calculated from the Near-IR and Red bands using the following equation:

$$NDVI = (NIR - Red)/(NIR + Red)$$

The entire riparian areas of springs were digitized in GEE and then reduced to one NDVI value for each 32-Day composite scene using a mean reducer. Reducers allow aggregation of multiple inputs over time or space to produce a single output (Gorelick et al., 2017). Some springs with viable tracer data were excluded from analysis because their riparian areas were too limited in extent (smaller than the size of one pixel); and thus, were not suitable for this type of analysis given the multispectral resolution. Time series for each spring were extracted from GEE and then processed in Matlab. Raw NDVI data often have a large amount of noise and are very susceptible to low value outliers. To smooth the data, we implemented a weighted, least-squares regression approach into a MATLAB code with a moving temporal window that is recommended for remote sensing phenology by the USGS/EROS (Swets et al., 1999) (https://phenology.cr.usgs.gov/methods_data.php). The two parameters in the code are the size of the moving window and the chi-squared value for outlier removal. Following smoothing, yearly peak NDVI values were extracted (Figure 3.3). The standard deviation of peak NDVI for the 2011-2016 period and the slope of the linear regression fitted to annual peak NDVI during this same period are the two primary metrics used to evaluate vegetation health. We interpret the standard deviation of peak NDVI as an indicator of interannual variability during the drought (i.e., vegetation stability) and the slope of the linear regression fitted to annual peak NDVI as an indicator of direction and magnitude of the vegetation response as a result of drought progression and duration (e.g., Figure 3.3).

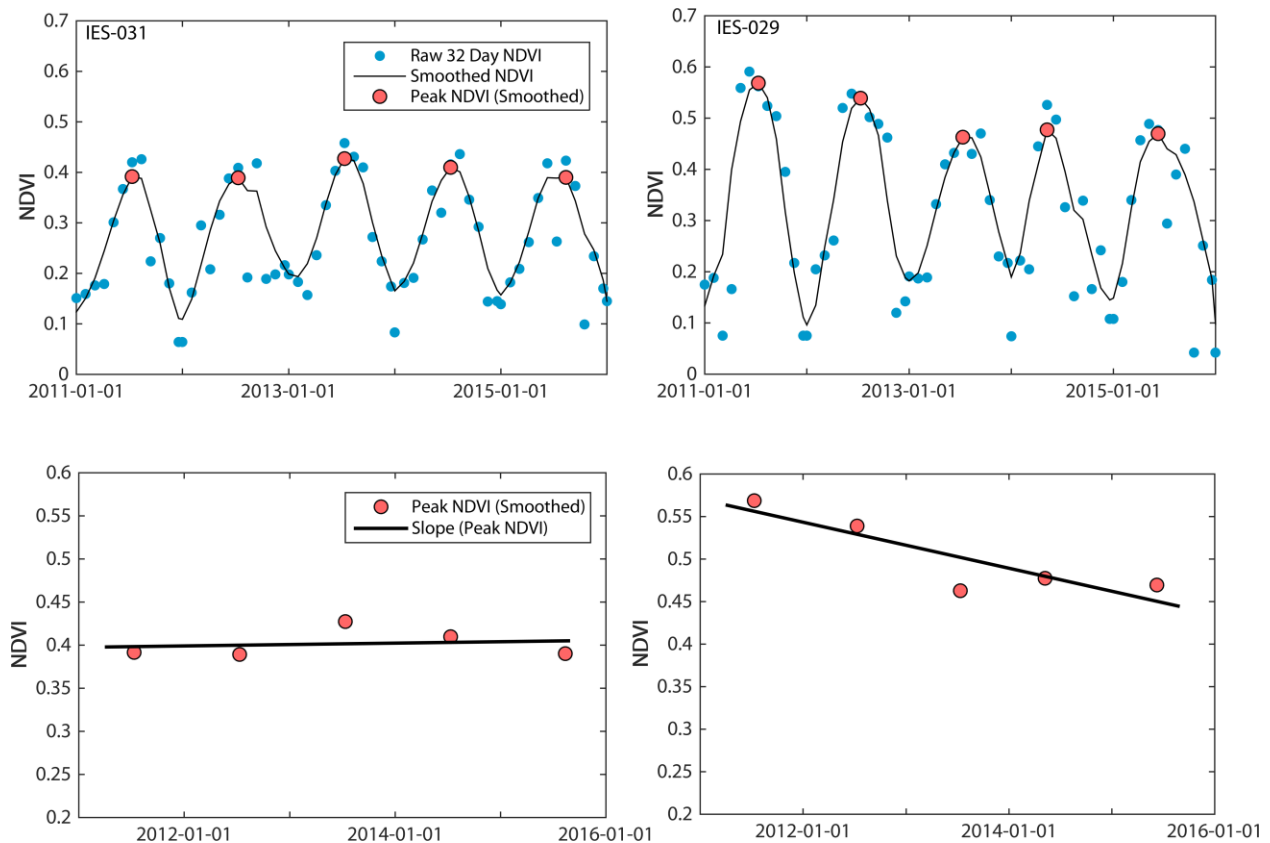


Figure 3.3. Example NDVI time series extracted from Landsat 7 multispectral imagery of an “old” (IES-031) and a “young” (IES-029) spring. The blue circles represent the Raw 32-Day Composite NDVI data prior to smoothing. The black line represents a smoothed fit of the data using a moving window, weighted, least-squares approach to temporal NDVI smoothing used by the USGS (Swets et al., 1999). Annual peak NDVI values are shown by the red circles. In the lower figures, a trendline is displayed showing the linear regression fitted to annual peak NDVI over the course of the drought. The slope of this line is one of our calculated metrics designed to measure spring groundwater-dependent vegetation response to drought duration.

3.4 Results and Discussion

3.4.1 Drought progression in Owens Valley and the effect on streamflow

While the Eastern Sierra was not experiencing drought at the end of 2011, continued lack of snowpack in the high Sierra caused the drought condition in this region to progressively worsen from 2012-2014 before peaking in mid to late 2015 (Figure 3.4) (U.S. Drought Monitor: <http://droughtmonitor.unl.edu/>). At the drought’s peak, over 80% of the Mono-Owens Lake

watershed was experiencing D4 conditions (i.e., exceptional drought) while the remaining area was experiencing D3 conditions (i.e., extreme drought) (Figure 3.4) Atmospheric river conditions during the winter of 2016-2017 brought a series of intense storms to the region, largely ameliorating surface water drought conditions and returning large portions of the eastern Sierra to a “No Drought” classification. The effects of this drought were observed in major surface waters draining the eastern Sierra Nevada, as confirmed by declining baseflow and seasonal snowmelt pulses in Bishop Creek (Figure 3.4).

3.4.2 The origin of salinity in Owens Valley spring waters

Excluding the basinal brine sample (IES-025, $[\text{Cl}^-] = 264 \text{ mg/L}$), Owens Valley spring waters have chloride concentrations ranging from 0.23 to 16.9 mg/L with an average concentration of 5.6 mg/L. The majority of Owens Valley spring waters ($n = 16$) have Cl^-/Br^- ratios in the range of dilute to moderately evolved groundwaters unaffected by halite dissolution or anthropogenic sources ($\text{Cl}^-/\text{Br}^- < 300$) (Davis 1998) (Figure 3.5). One spring, IES-028, is just above this threshold with a ratio of 334. Two other springs show clear contributions from non-conservative sources of chloride and have Cl^-/Br^- ratios > 900 . These springs, whose local names may be an indicator of their outlier status, are Boron Springs B (IES-025) and Boron Springs A (IES-027). The linear trend observed when Cl^-/Br^- is plotted against $[\text{Cl}^-]$ (Figure 3.5A) suggests that chloride is acquired conservatively for most spring waters and that chloride is primarily introduced to mountain-block groundwater systems from atmospheric deposition.

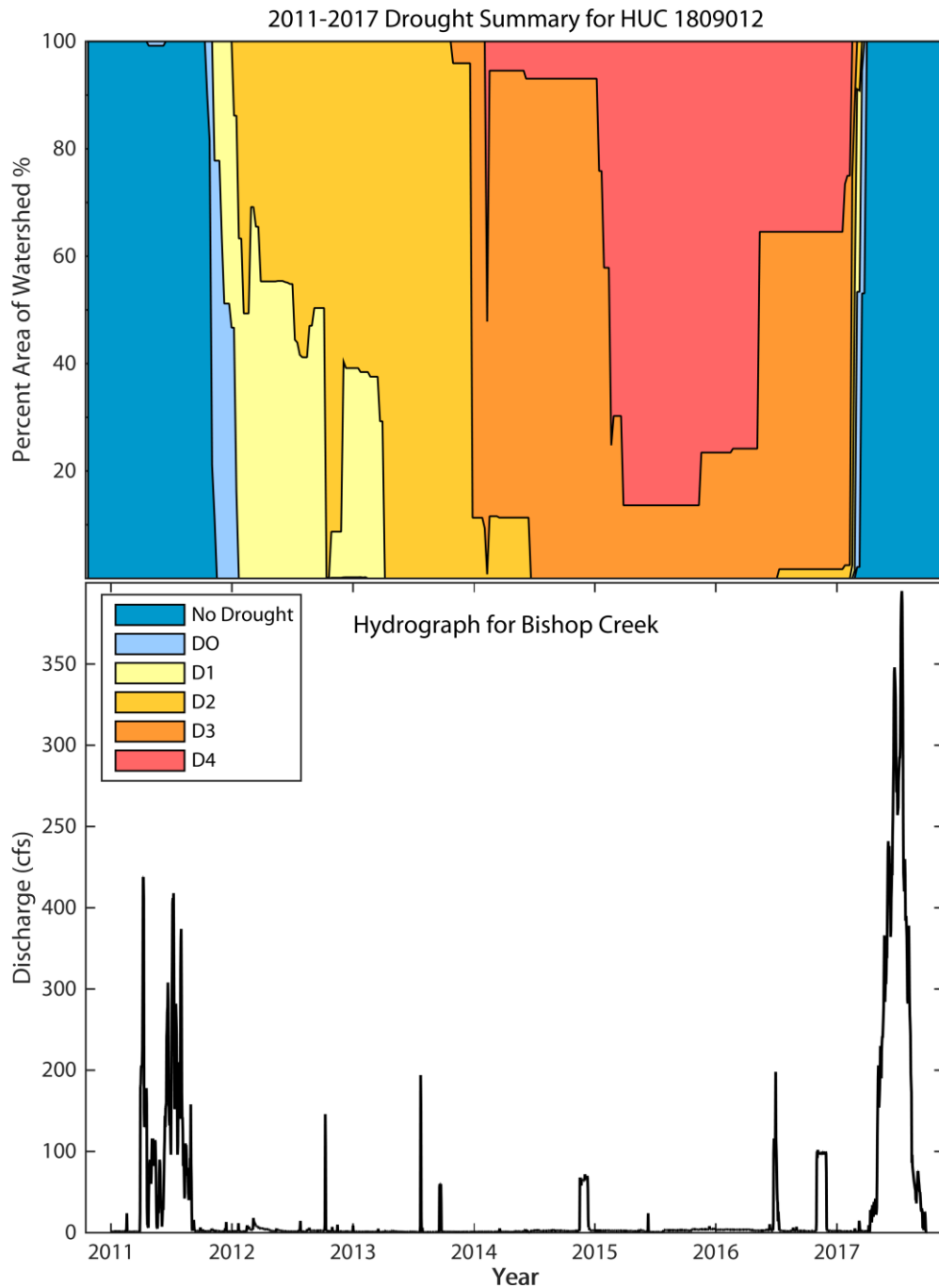


Figure 3.4. Combined watershed drought severity area plot and hydrograph (Bishop Creek) for the duration of the drought. Stacked area plot depicts the drought summary for HUC 180901 from 2011-2017. The drought summary shows the percent area of the watershed experiencing different levels of drought intensity as defined by the USDM (U.S. Drought Monitor: <http://droughtmonitor.unl.edu/>). D0, D1, D2, D3, and D4 stand for Abnormally Dry, Moderate Drought, Severe Drought, Extreme Drought, and Exceptional Drought, respectively. Below, a hydrograph for Bishop Creek, a major stream draining the Eastern Sierra crest, is shown during the same interval.

3.4.3 $^{36}\text{Cl}/\text{Cl}$ in spring waters and vegetation

Preanthropogenic $^{36}\text{Cl}/\text{Cl}$ ratios of groundwater in the southern Great Basin range from 300-500 (Davis, 2003). This range is similar to modern (i.e., post bomb pulse) $^{36}\text{Cl}/\text{Cl}$ ratios in precipitation for the same region (Moyley et al., 2003). A clear trend is observed between Cl^- concentration and $^{36}\text{Cl}/\text{Cl}$ ratios of spring waters. Springs with background or below background $^{36}\text{Cl}/\text{Cl}$ ratios have higher amounts of chloride, while dilute spring waters have elevated $^{36}\text{Cl}/\text{Cl}$ indicative of bomb-pulse recharge (Figure 3.5B). Examining the relationship between $^{36}\text{Cl}/\text{Cl}$ ratio and ^3H concentration allows for distinguishing between submodern, modern, and bomb-pulse spring waters. As shown in Figure 3.5C, ^3H alone can distinguish modern water and bomb-pulse groundwater from submodern groundwater, however it is not possible to distinguish modern recharge from bomb-pulse recharge without ^{36}Cl as the ^3H concentration is nonunique to both groups.

Fresh pine and juniper-pinyon needles from across the southern Great Basin have an average $^{36}\text{Cl}/\text{Cl}$ ratio of 384 (n=5). This is slightly lower than average $^{36}\text{Cl}/\text{Cl}$ ratios measured in duff and litterfall ($^{36}\text{Cl}/\text{Cl} = 412$, n =3). We interpret the fresh vegetation to be indicative of tracking $^{36}\text{Cl}/\text{Cl}$ ratios in modern precipitation. We attribute the elevated $^{36}\text{Cl}/\text{Cl}$ ratios in duff and litterfall to be an integration of fresh vegetation, and subsequently precipitation, from the past few decades. Our results do not support significant chloride cycling in vegetation, namely the recycling of bomb-pulse chloride, as a major contributor of potential bias in ^{36}Cl residence time interpretations as described in Milton et al. (2003). In comparison to groundwaters that would be significantly be influenced by vegetation recycling of ^{36}Cl , all but 1 of the “young” springs have $^{36}\text{Cl}/\text{Cl}$ in excess of 1400.

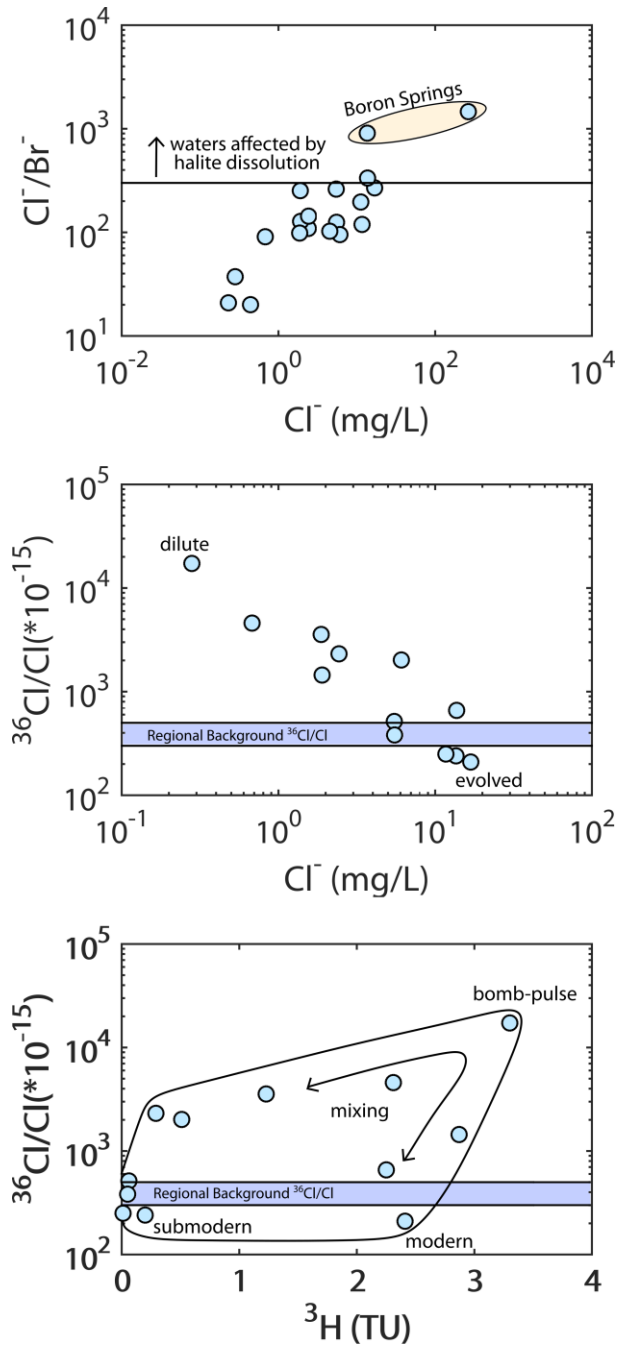


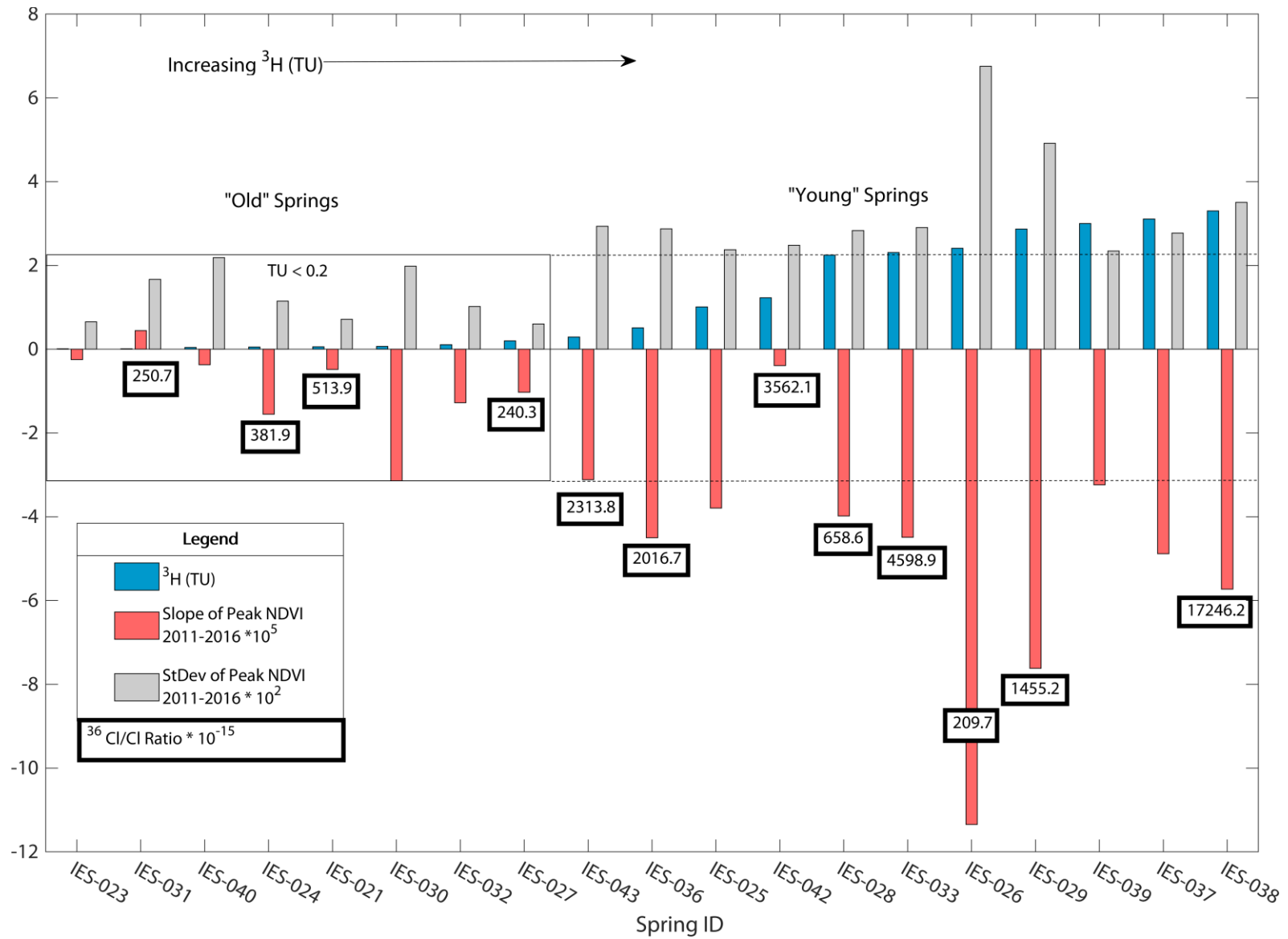
Figure 3.5. Spring samples are represented by the blue circles. A) Relationship between log Cl^- concentration and Cl^-/Br^- ratio for spring waters. Springs below the black line are indicative of natural waters unaffected by halite dissolution ($\text{Cl}^-/\text{Br}^- \leq \sim 300$). Two springs well above the line are Boron Spring A (IES-027) and Boron Spring B (IES-025). B) Relationship between log Cl^- concentration and log $^{36}\text{Cl}/\text{Cl}$. Preanthropogenic background $^{36}\text{Cl}/\text{Cl}$ ratios in groundwater from Davis et al. (2003) are shown in the blue bounding box. Springs dilute with respect to chloride have elevated, bomb-pulse $^{36}\text{Cl}/\text{Cl}$. C) Relationship between $^{36}\text{Cl}/\text{Cl}$ ratio and ^3H (TU). This plot shows separation and potential mixing lines between submodern, bomb-pulse, and modern spring waters based on $^{36}\text{Cl}/\text{Cl}$ ratios and ^3H concentration.

3.4.4 Comparison of vegetation metrics and age partitions

Eight springs are classified as “old”. A subset of these springs may have residence times upwards of 1000 years based on radiocarbon ages (IES-024 & IES-031). Overall, the riparian areas surrounding the “old” groundwater discharge points exhibited little to no interannual variability during the drought (average standard deviation of peak NDVI 2011-2016 = 0.012) in comparison to the “young” springs (Figure 3.6). In fact, these eight springs had the eight smallest standard deviations in annual peak NDVI of all springs. Furthermore, these springs also displayed increased ecohydrogeologic resistance as drought conditions progressed, having eight of the ten smallest slopes of the linear regression fitted to annual peak NDVI. One of these springs, IES-031, even had a slightly positive slope in response to the drought.

In comparison, “young” spring waters (n = 11) showed increased susceptibility to vegetation dying/drying as a result of the progressively worsening drought condition (Figure 3.6). These springs exhibited larger standard deviations in their annual peak NDVI (0.033) and more negative slopes of the fitted annual peak NDVI regression line when juxtaposed with the old groundwater springs. Three of the young springs did not exhibit as much variability or vegetation response as other springs in the group (IES-028, IES-042, and IES-043) and their response may be influenced by a forest fire that ravaged the central Owens Valley a few years prior to drought onset. While there is precedent to exclude areas affected by forest fires in vegetation/drought studies (e.g., Asner et al., 2016), these springs were included in this analysis for transparency and to validate the methodology used to infer vegetation responses. A summary of the results from Figure 3.6 showing the statistical differences in the vegetation responses and geochemical compositions between “old” and “young” spring waters is shown in Figure 3.7.

Figure 3.6. Bar plot combining residence time environmental tracer data with the results of metrics derived from NDVI time series analysis. Sampled springs are shown on the x-axis and are ordered from lowest tritium concentration on the left to highest tritium concentration on the right. Tritium values (in TU) are also displayed by the blue bars. The left to right trend approximately corresponds to increased amounts of young water. Springs within the solid black box have a TU < 0.2 and are binned as “old”. The coral bars represent the linear regression fitted to the slope of annual peak NDVI from 2011-2016 $\times 10^5$. The grey bars represent the standard deviation in annual peak NDVI from 2011-2016 $\times 10^2$. $^{36}\text{Cl}/\text{Cl}$ ratios $\times 10^{-15}$ are shown in the black boxes. IES-026, which is interpreted as receiving part of its flow from leakage along the LAA is more susceptible to reductions in surface water flow (Figure 3.4) and has the highest values for both metrics. Notice that while the other “young” springs have elevated $^{36}\text{Cl}/\text{Cl}$ ratios indicative of bomb pulse waters, IES-026 has a low value consistent with modern precipitation. Overall, the “young” springs with TU > 0.2 and bomb-pulse $^{36}\text{Cl}/\text{Cl}$ ratios exhibit greater interannual variability in their spring-related vegetation and persistent peak NDVI decline over the course of the drought than the springs with smaller amounts of modern water. The dotted lines intersecting the “young” springs represent the maximum metrics observed in the old springs and provide a means of comparison between the two groups.



3.4.5 Spring vegetation supplied by modern groundwater affected the most

One spring, IES-026 (known locally as Reinhackle Spring), serves as an important hypothesis test for our methodology. IES-026 was the only spring in the dataset where the environmental tracers indicated that it is being supported by modern, post-bomb recharge and the groundwater-dependent vegetation at this site suffered more than any other spring. A 2004 INYO/LA Geochemical Cooperative Study on groundwater resources and springs in the Owens Valley interpreted Reinhackle Spring as having a direct connection to the LAA based on geochemistry and isotopic signatures. Geographically, the LAA is less than a kilometer upgradient from the spring emergence. Surface flow suffered dramatically during the drought, reaching a critical low in 2015 (Figure 3.4). During this period of peak drought and minimal surface flow, the groundwater-dependent vegetation surrounding Reinhackle Spring reached its lowest annual peak NDVI. Thus, we conclude that the vegetation at Reinhackle Spring suffered more than at any other spring over the course of the drought due to the greatly reduced seepage from the LAA and the short groundwater residence time between the LAA and the spring.

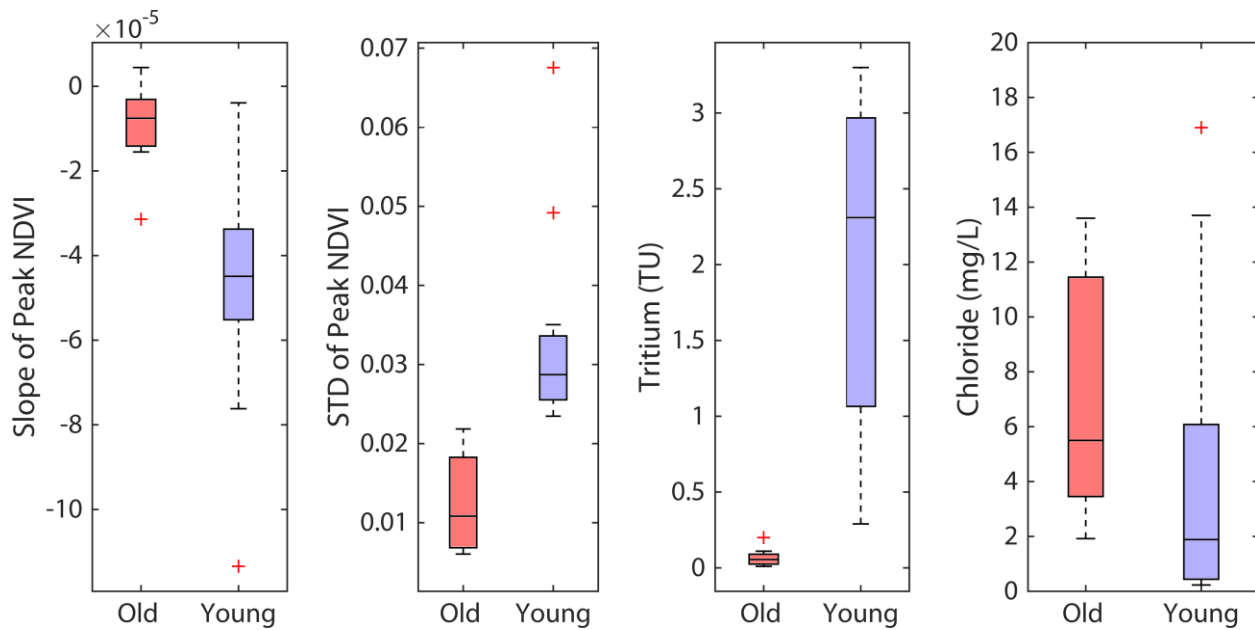


Figure 3.7. Boxplots summarizing the results for “old” and “young” spring water bins from Figure 3.6. The central mark in each box represents the median value. The bottom and top extent of each box represent the 25th and 75th percentiles, respectively. The whiskers extend to the maximum and minimum data points not considered outliers. Outliers are represented by the “+” symbols. As given in Figure 3.6 and summarized in this plot, springs classified as “old” had less negative slopes and smaller standard deviations of peak NDVI over the course of the drought when compared to the “young” springs. The chloride boxplot excludes IES-025, a basinal brine with 264 mg/L, from the “young” springs.

3.5 Conclusions

While recent efforts have focused on locating and mapping GDEs, these efforts have not answered fundamental questions about the stability of these systems. Our study demonstrates that old groundwater provides significant buffering to the effects of short-term perturbations such as severe droughts, thereby supporting the conceptual model that old groundwater can buffer hydrological responses. Riparian vegetation surrounding the discharge area of “old” groundwater springs were more resistant to the drought and exhibited dampened vegetation responses compared to the “young” groundwater springs. Springs discharging a large proportion of old groundwater, therefore, have greater hydrogeologic resistance because they likely have a substantial fraction of long flowpaths in the flowpath distribution that contributes flow to the spring. This contribution from old groundwater translates to stable hydrologic conditions in the discharge area, which is reflected in the vegetation response. Springs discharging a larger proportion of young groundwater show increased drying/desiccation of vegetation. We, therefore, interpret that these springs are not

resistant but instead likely having varying degrees of resilience. The observed connection between long groundwater residence time and dampened vegetation response to drought conditions is critically important because it provides direct evidence that residence time distributions, which are themselves a reflection of flowpath distributions, are first order controls on hydrogeologic stability. Future work examining the post-drought recovery of the groundwater-dependent vegetation surrounding the “young” springs may help to quantify the primary controls on hydrogeologic resilience, or the ability for these springs to recover and return to pre-drought conditions.

3.6 References

- Aguilar, C., Zinnert, J. C., Polo, M. J., & Young, D. R. (2012). NDVI as an indicator for changes in water availability to woody vegetation. *Ecological Indicators*, 23, 290-300.
- Asner, G. P., Brodrick, P. G., Anderson, C. B., Vaughn, N., Knapp, D. E., & Martin, R. E. (2016). Progressive forest canopy water loss during the 2012–2015 California drought. *Proceedings of the National Academy of Sciences*, 113(2), E249-E255.
- Barron, O. V., Emelyanova, I., Van Niel, T. G., Pollock, D., & Hodgson, G. (2014). Mapping groundwater-dependent ecosystems using remote sensing measures of vegetation and moisture dynamics. *Hydrological Processes*, 28(2), 372-385.
- Carlson, T. N., & Ripley, D. A. (1997). On the relation between NDVI, fractional vegetation cover, and leaf area index. *Remote Sensing of Environment*, 62(3), 241-252.
- Cartwright, J., & Johnson, H. M. (2018). Springs as hydrologic refugia in a changing climate? A remote-sensing approach. *Ecosphere*, 9(3), e02155.
- Chander, G., Markham, B. L., & Helder, D. L. (2009). Summary of current radiometric calibration coefficients for Landsat MSS, TM, ETM+, and EO-1 ALI sensors. *Remote Sensing of Environment*, 113(5), 893-903.
- Chen, Y., Parmenter, S., & May, B. (2007). Introgression between Lahontan and endangered Owens tui uhubs, and apparent discovery of a new tui chub in the Owens Valley, California. *Conservation Genetics*, 8(1), 221-238.
- Cleland, E. E., Chiariello, N. R., Loarie, S. R., Mooney, H. A., & Field, C. B. (2006). Diverse responses of phenology to global changes in a grassland ecosystem. *Proceedings of the National Academy of Sciences*, 103(37), 13740-13744.
- Comstock, J. P., & Ehleringer, J. R. (1992). Plant adaptation in the Great Basin and Colorado plateau. *The Great Basin Naturalist*, 195-215.
- Conroy, C. J., Patton, J. L., Lim, M. C., Phuong, M. A., Parmenter, B., & Höhna, S. (2016). Following the rivers: historical reconstruction of California voles *Microtus californicus*

- (Rodentia: Cricetidae) in the deserts of eastern California. *Biological Journal of the Linnean Society*, 119(1), 80-98.
- Cuthbert, M. O., Gleeson, T., Moosdorf, N., Befus, K. M., Schneider, A., Hartmann, J., & Lehner, B. (2019). Global patterns and dynamics of climate–groundwater interactions. *Nature Climate Change*, 9(2), 137-141.
- Danskin, W. R. (1998). Evaluation of the hydrologic system and selected water-management alternatives in the Owens Valley, California (Vol. 2370). US Geological Survey, Information Services.
- Davis, S. N., Whittemore, D. O., & Fabryka-Martin, J. (1998). Uses of chloride/bromide ratios in studies of potable water. *Groundwater*, 36(2), 338-350.
- Davis, S. N., Cecil, L. D., Zreda, M., & Moysey, S. (2001). Chlorine-36, bromide, and the origin of spring water. *Chemical Geology*, 179(1-4), 3-16.
- Echelle, A. A., & Echelle, A. F. (1993). Allozyme perspective on mitochondrial DNA variation and evolution of the Death Valley pupfishes (Cyprinodontidae: Cyprinodon). *Copeia*, 275-287.
- Echelle, A. A., Carson, E. W., Echelle, A. F., Van Den Bussche, R. A., Dowling, T. E., & Meyer, A. (2005). Historical biogeography of the new-world pupfish genus *Cyprinodon* (Teleostei: Cyprinodontidae). *Copeia*, 2005(2), 320-339.
- Elmore, A. J., Mustard, J. F., & Manning, S. J. (2003). Regional patterns of plant community response to changes in water: Owens Valley, California. *Ecological Applications*, 13(2), 443-460.
- Elmore, A. J., Manning, S. J., Mustard, J. F., & Craine, J. M. (2006). Decline in alkali meadow vegetation cover in California: the effects of groundwater extraction and drought. *Journal of Applied Ecology*, 43(4), 770-779.
- Erskine, A. D., & Papaioannou, A. (1997). The use of aquifer response rate in the assessment of groundwater resources. *Journal of Hydrology*, 202(1-4), 373-391.
- Famiglietti, J. S. (2014). The global groundwater crisis. *Nature Climate Change*, 4(11), 945-948.
- Frisbee, M. D., Phillips, F. M., Weissmann, G. S., Brooks, P. D., Wilson, J. L., Campbell, A. R., & Liu, F. (2012). Unraveling the mysteries of the large watershed black box: Implications for the streamflow response to climate and landscape perturbations. *Geophysical Research Letters*, 39(1).
- Frisbee, M. D., Wilson, J. L., & Sada, D. W. (2013). Climate Change and the Fate of Desert Springs: Innovation Working Group on the Response of Springs to the Effects of Climate Change; Jemez Springs, New Mexico, 1–3 October 2102. *Eos, Transactions American Geophysical Union*, 94(15), 144-144.

- Gorelick, N., Hancher, M., Dixon, M., Ilyushchenko, S., Thau, D., & Moore, R. (2017). Google Earth Engine: Planetary-scale geospatial analysis for everyone. *Remote Sensing of Environment*, 202, 18-27.
- Gou, S., Gonzales, S., & Miller, G. R. (2015). Mapping potential groundwater-dependent ecosystems for sustainable management. *Groundwater*, 53(1), 99-110.
- Griffin, D., & Anchukaitis, K. J. (2014). How unusual is the 2012–2014 California drought?. *Geophysical Research Letters*, 41(24), 9017-9023.
- Harrison, R. (2016). Hydrogeologic Conceptual Model for the Owens Valley Groundwater Basin (6-12), Inyo and Mono Counties, Report prepared by the Inyo County Water Department.
- Hershler, R. (1989). Springsnails (Gastropoda: Hydrobiidae) of Owens and Amargosa River (exclusive of Ash Meadows) drainages, Death Valley system, California-Nevada. *Proceedings of the Biological Society of Washington*.
- Hershler, R., Mulvey, M., & Liu, H. P. (1999). Biogeography in the Death Valley region: evidence from springsnails (Hydrobiidae: Tryonia). *Zoological Journal of the Linnean Society*, 126(3), 335-354.
- Huang, H., Chen, Y., Clinton, N., Wang, J., Wang, X., Liu, C., ... & Zhu, Z. (2017). Mapping major land cover dynamics in Beijing using all Landsat images in Google Earth Engine. *Remote Sensing of Environment*, 202, 166-176.
- Jayko, A. S., & Bursik, M. (2011). Active transtensional intracontinental basins: Walker Lane in the western Great Basin. *Tectonics of sedimentary basins: Recent advances*, 226-248.
- Jia, G. J., Epstein, H. E., & Walker, D. A. (2003). Greening of arctic Alaska, 1981–2001. *Geophysical Research Letters*, 30(20).
- Johansen, K., Phinn, S., & Taylor, M. (2015). Mapping woody vegetation clearing in Queensland, Australia from Landsat imagery using the Google Earth Engine. *Remote Sensing Applications: Society and Environment*, 1, 36-49.
- Kemp, P. R. (1983). Phenological patterns of Chihuahuan Desert plants in relation to the timing of water availability. *The Journal of Ecology*, 427-436.
- Klausmeyer, K., Howard, J., Keeler-Wolf, T., Davis-Fadtke, K., Hull, R., & Lyons, A. (2018). Mapping Indicators of Groundwater Dependent Ecosystems in California: Methods Report.
- Kløve, B., Ala-Aho, P., Bertrand, G., Gurdak, J. J., Kupfersberger, H., Kværner, J., ... & Uvo, C. B. (2014). Climate change impacts on groundwater and dependent ecosystems. *Journal of Hydrology*, 518, 250-266.

- Knott, J. R., Machette, M. N., Klinger, R. E., Sarna-Wojcicki, A. M., Liddicoat, J. C., David, B. T., & Ebbs, V. M. (2008). Reconstructing late Pliocene to middle Pleistocene Death Valley lakes and river systems as a test of pupfish (Cyprinodontidae) dispersal hypotheses. *Late Cenozoic drainage history of the southwestern Great Basin and lower Colorado River region: geologic and biotic perspectives*, 439, 1.
- Lv, J., Wang, X. S., Zhou, Y., Qian, K., Wan, L., Eamus, D., & Tao, Z. (2013). Groundwater-dependent distribution of vegetation in Hailiutu River catchment, a semi-arid region in China. *Ecohydrology*, 6(1), 142-149.
- MacDonald, G. M. (2010). Water, climate change, and sustainability in the southwest. *Proceedings of the National Academy of Sciences*, 107(50), 21256-21262.
- Manning, A. H., Clark, J. F., Diaz, S. H., Rademacher, L. K., Earman, S., & Plummer, L. N. (2012). Evolution of groundwater age in a mountain watershed over a period of thirteen years. *Journal of Hydrology*, 460, 13-28.
- Mata-González, R., McLendon, T., Martin, D. W., Trlica, M. J., & Pearce, R. A. (2012). Vegetation as affected by groundwater depth and microtopography in a shallow aquifer area of the Great Basin. *Ecohydrology*, 5(1), 54-63.
- Meixner, T., Manning, A. H., Stonestrom, D. A., Allen, D. M., Ajami, H., Blasch, K. W., ... & Flint, A. L. (2016). Implications of projected climate change for groundwater recharge in the western United States. *Journal of Hydrology*, 534, 124-138.
- Miller, R. R., & Pister, E. P. (1971). Management of the Owens Pupfish, *Cyprinodon radiosus*, in Mono County, California. *Transactions of the American Fisheries Society*, 100(3), 502-509.
- Milton, G. M., Milton, J. C. D., Schiff, S., Cook, P., Kotzer, T. G., & Cecil, L. D. (2003). Evidence for chlorine recycling—hydrosphere, biosphere, atmosphere—in a forested wet zone on the Canadian Shield. *Applied Geochemistry*, 18(7), 1027-1042.
- Morsy, K. M., Alenezi, A., & AlRukaibi, D. S. (2017). Groundwater and dependent ecosystems: revealing the impacts of climate change. *Int J Appl Eng Res*, 12(13), 3919-3926.
- Mote, P. W., Rupp, D. E., Li, S., Sharp, D. J., Otto, F., Uhe, P. F., ... & Allen, M. R. (2016). Perspectives on the causes of exceptionally low 2015 snowpack in the western United States. *Geophysical Research Letters*, 43(20), 10-980.
- Mote, P. W., Li, S., Lettenmaier, D. P., Xiao, M., & Engel, R. (2018). Dramatic declines in snowpack in the western US. *Npj Climate and Atmospheric Science*, 1(1), 1-6.
- Moysey, S., Davis, S. N., Zreda, M., & Cecil, L. D. (2003). The distribution of meteoric $^{36}\text{Cl}/\text{Cl}$ in the United States: a comparison of models. *Hydrogeology Journal*, 11(6), 615-627.
- Naumburg, E., Mata-Gonzalez, R., Hunter, R. G., McLendon, T., & Martin, D. W. (2005). Phreatophytic vegetation and groundwater fluctuations: a review of current research and application of ecosystem response modeling with an emphasis on Great Basin vegetation. *Environmental Management*, 35(6), 726-740.

- Patten, D. T., Rouse, L., & Stromberg, J. C. (2008). Isolated spring wetlands in the Great Basin and Mojave Deserts, USA: potential response of vegetation to groundwater withdrawal. *Environmental Management*, 41(3), 398-413.
- Petus, C., Lewis, M., & White, D. (2013). Monitoring temporal dynamics of Great Artesian Basin wetland vegetation, Australia, using MODIS NDVI. *Ecological Indicators*, 34, 41-52.
- Phillips, F. M. (2000). Chlorine-36. In *Environmental tracers in subsurface hydrology* (pp. 299-348). Springer, Boston, MA.
- Pritchett, D., & Manning, S. J. (2012). Response of an intermountain groundwater-dependent ecosystem to water table drawdown. *Western North American Naturalist*, 72(1), 48-59.
- Rademacher, L. K., Clark, J. F., Clow, D. W., & Hudson, G. B. (2005). Old groundwater influence on stream hydrochemistry and catchment response times in a small Sierra Nevada catchment: Sagehen Creek, California. *Water Resources Research*, 41(2).
- Robinson, N. P., Allred, B. W., Jones, M. O., Moreno, A., Kimball, J. S., Naugle, D. E., ... & Richardson, A. D. (2017). A dynamic Landsat derived normalized difference vegetation index (NDVI) product for the conterminous United States. *Remote Sensing*, 9(8), 863.
- Sada, D. W., Fleishman, E., & Murphy, D. D. (2005). Associations among spring-dependent aquatic assemblages and environmental and land use gradients in a Mojave Desert mountain range. *Diversity and Distributions*, 11(1), 91-99.
- Sada, D. (2008). Great Basin riparian and aquatic ecosystems. In: Chambers, Jeanne C.; Devoe, Nora; Evenden, Angela, eds. *Collaborative management and research in the Great Basin-examining the issues and developing a framework for action. Gen. Tech. Rep. RMRS-GTR-204. Fort Collins, CO: US Department of Agriculture, Forest Service, Rocky Mountain Research Station.* p. 49-52, 204.
- Sharma, P., Kubik, P. W., Fehn, U., Gove, H. E., Nishiizumi, K., & Elmore, D. (1990). Development of ³⁶Cl standards for AMS. *Nuclear Instruments and Methods in Physics Research Section B: Beam Interactions with Materials and Atoms*, 52(3-4), 410-415.
- Singleton, M. J., & Moran, J. E. (2010). Dissolved noble gas and isotopic tracers reveal vulnerability of groundwater in a small, high-elevation catchment to predicted climate changes. *Water Resources Research*, 46(10).
- Sophocleous, M. (2012). On Understanding and Predicting Groundwater Response Time. *Ground Water*.
- Swets, D., Reed, B. C., Rowland, J., & Marko, S. E. (1999). A weighted least-squares approach to temporal NDVI smoothing. In *From image to information: 1999 ASPRS Annual Conference*.
- Trujillo, E., Molotch, N. P., Goulden, M. L., Kelly, A. E., & Bales, R. C. (2012). Elevation-dependent influence of snow accumulation on forest greening. *Nature Geoscience*, 5(10), 705-709.

- Visser, A., Moran, J. E., Aql, R., Singleton, M. J., & Esser, B. K. (2012). Examination of Water Quality in " Tritium-Dead" Drinking Water Wells (No. LLNL-TR-558107). Lawrence Livermore National Lab.(LLNL), Livermore, CA (United States).
- Vogt, S., & Herpers, U. (1988). Radiochemical separation techniques for the determination of long-lived radionuclides in meteorites by means of accelerator-mass-spectrometry. *Fresenius' Zeitschrift für analytische Chemie*, 331(2), 186-188.
- Vörösmarty, C. J., Green, P., Salisbury, J., & Lammers, R. B. (2000). Global water resources: vulnerability from climate change and population growth. *Science*, 289(5477), 284-288.
- Wang, P., Zhang, Y., Yu, J., Fu, G., & Ao, F. (2011). Vegetation dynamics induced by groundwater fluctuations in the lower Heihe River Basin, northwestern China. *Journal of Plant Ecology*, 4(1-2), 77-90.
- White, D. C., Lewis, M. M., Green, G., & Gotch, T. B. (2016). A generalizable NDVI-based wetland delineation indicator for remote monitoring of groundwater flows in the Australian Great Artesian Basin. *Ecological Indicators*, 60, 1309-1320.
- Wilson, J. L., & Guan, H. (2004). Mountain-block hydrology and mountain-front recharge. *Groundwater recharge in a desert environment: The Southwestern United States*, 9.
- Zdon, A., Rainville, K., Buckmaster, N., Parmenter, S., & Love, A. H. (2019). Identification of Source Water Mixing in the Fish Slough Spring Complex, Mono County, California, USA. *Hydrology*, 6(1), 26.

CHAPTER 4. THE EFFECT OF SPATIAL SCALE AND TIME ON GEOCHEMICAL EVOLUTION INFERRED FROM SPRINGS IN THE SOUTHEASTERN SIERRA NEVADA, USA: REVISITING GARRELS AND MACKENZIE (1967)

4.1 Abstract

The seminal studies of Feth et al. (1964) and Garrels and Mackenzie (1967) describe the chemical weathering processes controlling the geochemistry of spring waters in the Sierra Nevada (CA) and provide a framework for understanding geochemical weathering processes at local groundwater scales (short distances between recharge and subsequent groundwater discharge). Local-scale flowpaths typically have short residence times and show the least geochemical weathering. While Garrels and Mackenzie (1967) studied local-scale flow, we infer these processes to scale with increasing spatial scale and time. However, studies have not tested this assumption

Here we extend these concepts to investigate the factors controlling geochemical evolution at intermediate, mountain block scales with increased flowpath length, circulation depth, and residence time. We accomplish this by using a multi-tracer approach to study mountain front springs emerging along the Sierra Nevada frontal fault zone in Owens Valley, CA. These springs emerge at a significantly lower elevation (1100-2000 mamsl) than the eastern Sierra crest (4000+ mamsl) and provide a window the hydrogeological and hydrochemical processes occurring from high-elevation mountain block recharge to low elevation mountain front discharge, a recognized knowledge gap in hydrogeology. We were able to approximately delineate spring contributing areas using stable isotopes of water and noble gases. We subsequently identified the likely geologic units sourcing springflow and used spring geochemistry to classify four major geochemical groups. Our results show that geologic heterogeneity (i.e., differences in plutonic compositions and the presence of Paleozoic metasedimentary roof pendants) exerts a dominant control on geochemical evolution with increased scale. Within geochemical groups and amongst all springs, geochemical evolution does show separation with residence time partitions and discharge temperature, however these relationships are not always linear or without outliers. When aquifer mineralogy is relatively homogenous with increased scale, ours results indicate that a simple metric like conductivity can

be used to infer residence time, thereby supporting relationships inferred from Garrels and Mackenzie (1967).

4.2 Introduction

Chemical evolution from ephemeral springs to perennial springs in the Sierra Nevada, CA, USA is the basis for two classic papers in the field of water chemistry; Feth et al. (1964) and Garrels and Mackenzie (1967). These seminal works provide a framework for groundwater geochemical evolution and weathering-derived aqueous geochemistry that is still held in high esteem today. The establishment of a conceptual model that groundwater chemistry can rigorously tested using aquifer mineralogy is a significant contribution of these papers. Additionally, there is an underlying tenet within Garrels and Mackenzie (1967) that groundwater ion concentrations derived from more rock-water interaction will scale with distance from recharge, and thus, residence time and possibly circulation depth. This point is critical as we seek to understand how weathering and geochemistry evolve with increasing flowpath length and residence time in a kinetically-limited flowpath continuum beyond local-scale shallow groundwater to intermediate and regional scales.

Just as Garrels and Mackenzie (1967) built upon the work by Feth et al. (1964) in improving our understanding of the controls on aqueous geochemistry in a well-studied granitic terrain, a number of other well-cited geochemical studies have followed in these footsteps and improved our understanding of the Sierra Nevada, making it one of the best studied mountain ranges, hydrologically and geochemically, in the United States. Studies in the Sierra Nevada have examined 1) chemical evolution in shallow groundwater (Feth et al., 1964; Garrels and Mackenzie, 1967; Rademacher et al., 2001), 2) small catchment-scale geochemical evolution (Williams and Melack, 1991; Holloway and Dahlgren, 2001; Rademacher et al., 2001; Rademacher et al., 2005) 3) sources of solutes in streamflow (Blum et al., 1993; Pretti and Stewart, 2002), and 4) regional evolution from the mountain block into alluvial basins (Guler and Thyne, 2004; Guler and Thyne, 2004; Guler and Thyne, 2006). Figure 4.1A illustrates the relationships known at local scales. However, there still exists a knowledge gap regarding geochemical evolution and chemical weathering at depth in the mountain block, i.e., groundwater flowing at intermediate scales prior to chemical overprinting by alluvial basin material (Figure 4.1B). While hillslope and small catchment-scale groundwater flow studies are useful in understanding hydrogeochemical

processes at shorter time scales following recharge, it can be difficult to apply the findings from these studies to areas where deeper/older groundwater may dominate baseflow or springflow (i.e., Frisbee et al., 2011). On the other hand, regional studies have shown a tendency to be overwhelmed by geochemical evolution derived from highly soluble evaporites and alluvial basin fill, overlooking the complexity of geochemical processes occurring between initial recharge and the mountain front (Dreher, 2003).

Mountain-block groundwater is identified as one of the least understood components of the hydrologic cycle (Gardner et al., 2018). Capturing this intermediate-scale, mountain block flow component is difficult as bedrock wells are expensive and few in number (Manning and Solomon, 2005). However, perennial springs emerging at the mountain front provide an alternate window into mountain block groundwater processes (Manning and Solomon, 2003; Wilson and Guan, 2004). Many of these springs are found in Owens Valley, CA at the Sierra Nevada frontal fault zone along the eastern escarpment of the Sierra Nevada. These springs are representative of intermediate scale groundwater flow as they emerge at a significantly lower elevation (1000-2000 mamsl) than their likely recharge areas (2600-4000+ mamsl) in talus and fractured bedrock above the tree line. Therefore, these springs provide a means to naturally extend the work of Feth et al. (1964) and Garrels and Mackenzie (1967) from local scale flowpaths to intermediate scale flowpaths (e.g., Figure 4.1).

Here we use multiple geochemical and isotopic diagnostic tools to delineate groundwater flowpaths and provide insight into the processes that control geochemical evolution at intermediate scales by examining mountain front springs in Owens Valley, CA (Figure 4.2). We seek to answer the following questions: 1) how does increasing spatial scale and groundwater residence influence spring geochemical composition and 2) what are the dominant controls on geochemical evolution with increasing scale? We infer from Garrels and Mackenzie (1967) that simple measurements such as electrical conductance and temperature are proxies for residence time and flowpath length. However, local-scale flowpath distributions capture a limited set of mineralogic variability present in the bedrock. We explicitly test the hypothesis that geochemical composition can be used to infer flowpath length at increased spatial scale and residence time and that there is a geochemical continuum (i.e., systematic geochemical evolution) from local-scale to intermediate-scale (i.e., inset “Local” and “Intermediate” graphs within 4.1).

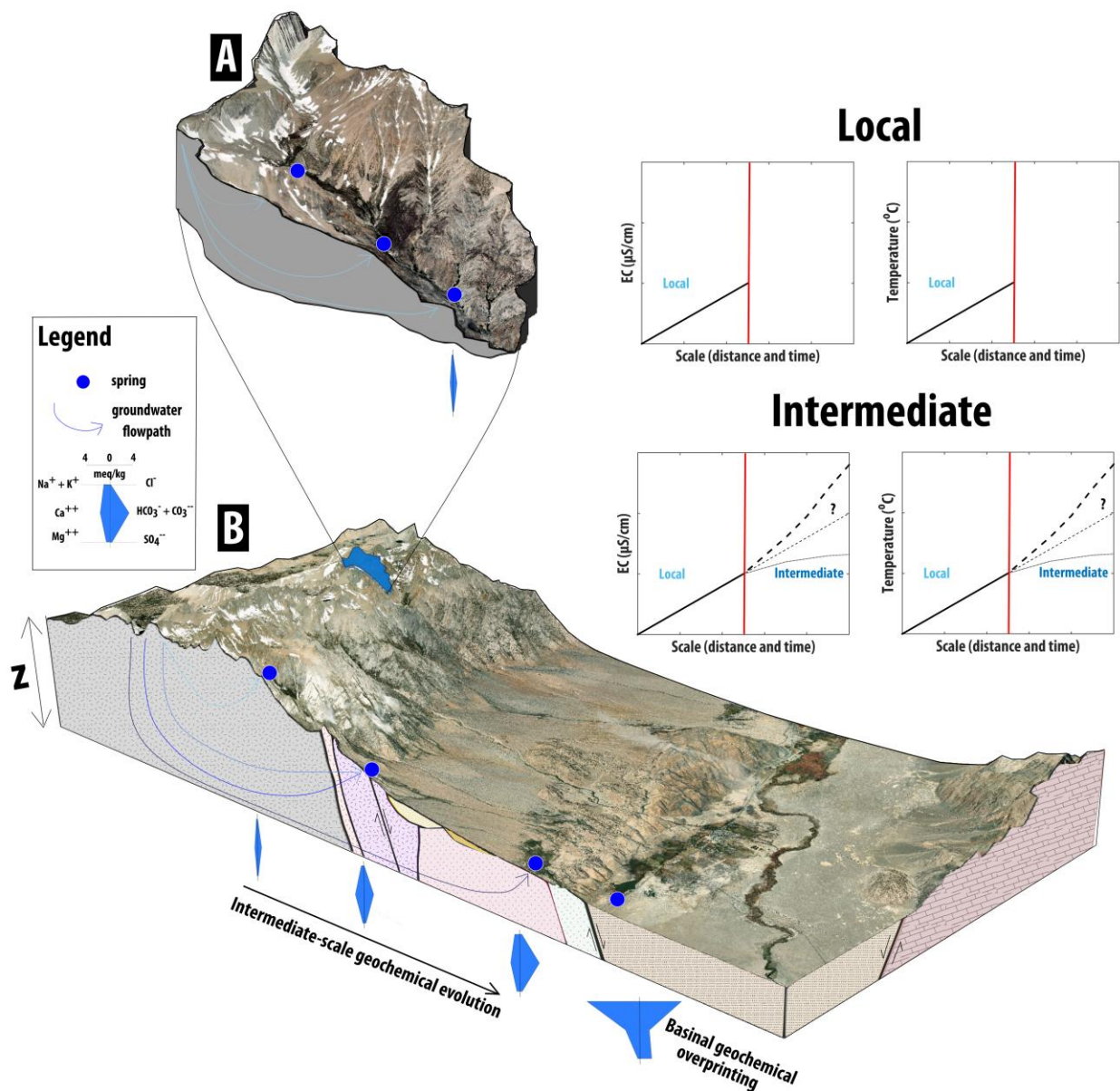


Figure 4.1: Conceptual model for geochemical evolution at intermediate scales as shown by mountain block and mountain front springs. Geochemical overprinting by basinal brines and alluvial material can obscure the relationship between flowpath length, residence time, and geochemical evolution. A) Feth (1964) and Garrels and Mackenzie (1967) provide a conceptual model at local scales describing the processes controlling chemical evolution from ephemeral to perennial springs in the Sierra Nevada (CA). Rademacher et al. (2001) and (2005) quantified the relationship between residence time and chemical evolution at local scales showing linear evolutionary trends with mineral weathering and residence time (inset “Local”). B) At intermediate, mountain block scales this relationship is hard to quantify and poorly understood (inset “Intermediate”).

4.3 Study Area

4.3.1 Regional geography

The Mono-Owens Lake Watershed is an internally draining watershed in eastern California (HUC 180901) comprised of the Mono Lake Watershed, the Crowley Lake Watershed, and the Owens Lake Watershed. This study focuses on the Crowley Lake and Owens Lake portions of HUC 180901 (Figure 4.2). These watersheds are bounded by the eastern Sierra Nevada to the west and the White-Inyo Mountains to the east. Moving southward across the Volcanic Tableland, elevation decreases significantly from Crowley Lake (2065 m) to Bishop, CA (1267 m) over a distance of 40 kilometers. From Bishop to the terminus of the Owens River south of Lone Pine, the elevation change is more gradual, with a net change of ~185 meters over 108 kilometers.

4.3.2 Climate and precipitation

Owens Valley lies in the rain shadow of the Sierra Nevada and averages 13.4 cm of precipitation annually, the majority of which falls as rain (NOAA Station: Bishop, CA, (<https://wrcc.dri.edu/cgi-bin/cliMAIN.pl?ca0822>)). At the northern end of the valley (i.e., Bishop, CA), the average high temperature is 23.6 °C and the average low temperature is 3.1 °C. At higher elevations in the eastern Sierra Nevada, precipitation usually falls as snow and annual amounts are highly variable due to the effects of local topography (Elder et al., 1989; Zheng et al., 2016). High elevation locations average over 250 cm of total snowfall annually. Alpine areas in the eastern Sierra alpine have average annual high temperatures of 10 to 13°C and average annual low temperatures of -2.5 to -3°C (NOAA Stations: South Lake, CA (<https://wrcc.dri.edu/cgi-bin/cliMAIN.pl?ca8406>) and Lake Sabrina, CA (<https://wrcc.dri.edu/cgi-bin/cliMAIN.pl?ca4705>)).

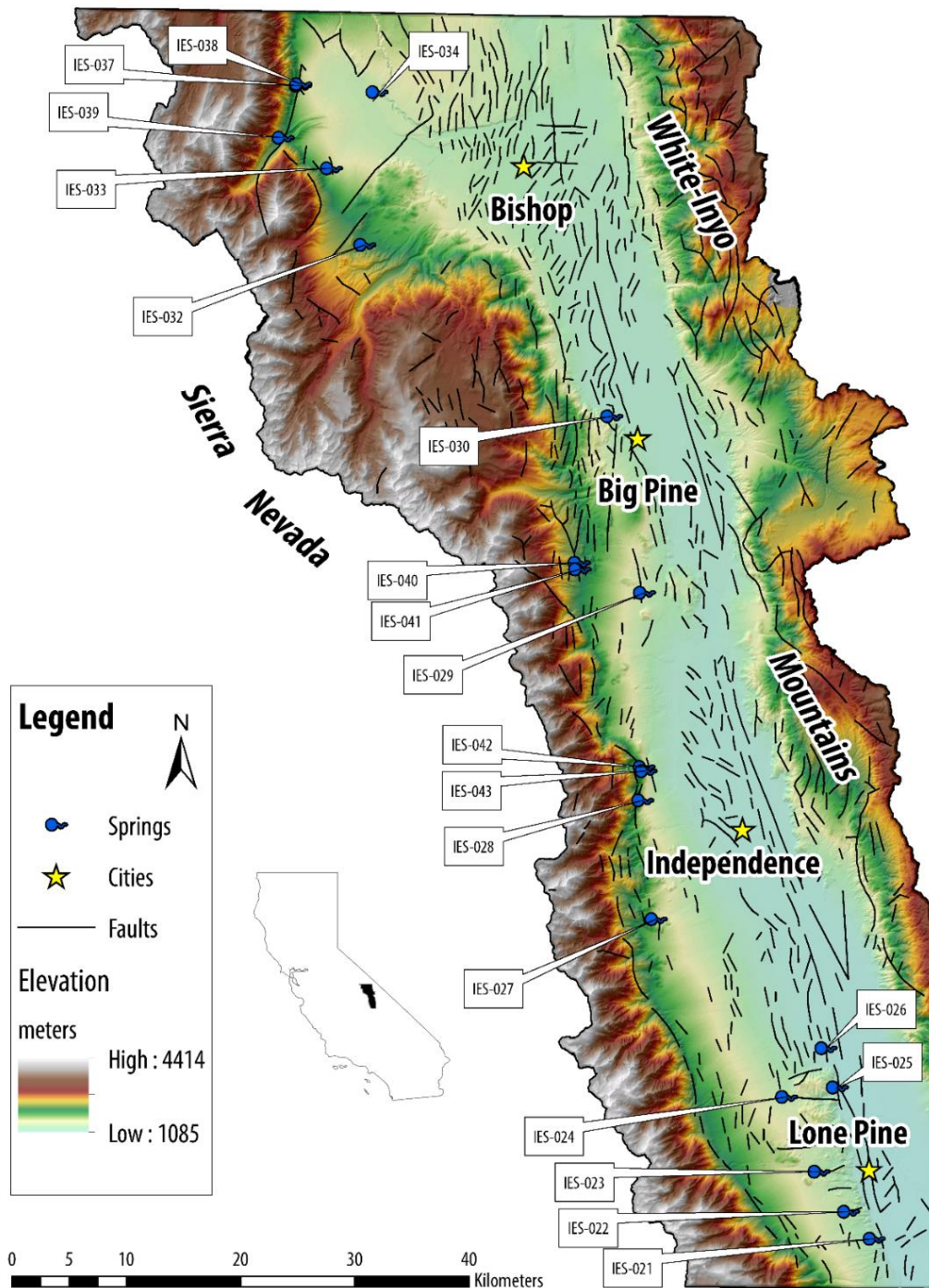


Figure 4.2.: Map showing locations and sample IDs (IES-###) of sampled springs in Owens Valley, CA within the Crowley Lake and Owens Lake watersheds. Eastern and western map boundaries correspond to watershed divides. Map outline location within California is highlighted on the inset map. Elevation data for the study area was acquired from The National Map (TNM), a part of the USGS National Geospatial Program

4.3.3 Hydrology

Snowmelt from the Sierra Nevada and White-Inyo Mountains drives surface water flow into Owens Valley and is the principal recharge mechanism for both the mountain block and basin fill aquifers (Danksin 1988; Danskin, 1998). In the basin, surface water flow initiates primarily from snowmelt runoff in the northern part of the watershed in Mono County before flowing southward via an axial drainage system (the Owens River) and terminating in the now dry Owens Lake. Perennial streams drain the ranges on both sides of the valley, however a far greater number of tributaries to the Owens River emerge from the western side of the valley as the White-Inyo Mountains are in a prevailing rain-shadow and receive significantly less precipitation. Both the surface water and groundwater systems in Owens Valley have been significantly altered by construction of the Los Angeles Aqueduct (LAA) by the Los Angeles Department of Water and Power (LADWP). A secondary aqueduct was added in 1970 (Kahrl, 1976). The LAA altered the hydrology and thus the economic development of Owens Valley by diverting water from the Owens River and supplementing these diversions with groundwater pumping from the basin aquifer during dry years (Kahrl, 1976). The development of the LAA ultimately led to the desiccation of Owens Lake, an endorheic basin lake just south of Lone Pine, CA. Groundwater recharge via precipitation at lower elevations in the basin is minimal (Danskin, 1998).

Numerous perennial springs emerge along the mountain front of the eastern Sierra Nevada and are often associated with zones of faulting (strike slip and normal) (Danksin 1988; Hollett et al., 1991; Danskin, 1998). We sampled a subset of these springs (Figure 4.2) during the spring of 2016 to capture: 1) a broad spatial distribution, 2) the geologic heterogeneity of the batholith, and 3) to address questions about geochemical evolution with increasing space and time from the mountain block to the mountain front. The majority of sampled springs are pristine rheocrenes (i.e., springs that form small streams) with spring brooks that eventually infiltrate into pluton-derived alluvial material.

4.4 Geology

4.4.1 General overview

Structurally, Owens Valley is a rift basin with over 3,000 meters of basin fill lying just outside the Basin and Range physiographic province in what is known as the Walker Lane

(Wesnousky, 2005; Jayko, 2011). This tectonic setting creates a significant amount of relief where Owens Valley (~1000-1400 meters above mean sea level [mamsl]) is surrounded on both sides by north-south trending ranges with ridgelines and peaks exceeding 4000 mamsl. Faulting in the area is pervasive due to the complex tectonic history. There are many small transform faults associated with strike-slip displacement from the Walker Lane, locally known as the Eastern California Shear Zone (ECSZ) (Wesnousky, 2005; Jayko, 2011), as well as numerous normal and detachment faults associated with Basin and Range extension (Taylor and Dewey, 2009). As shown in Figure 4.2, these faults are prevalent throughout the basin and are often related to areas of groundwater emergence in the form of springs and seeps due to the structural barriers and permeability contrasts they create (Forster and Evans, 1991; Bense et al., 2013).

Due to the lack of regional, detailed geologic maps, pluton-scale and simplified (i.e., geologic lumped by petrologic composition) geologic maps were created for the study area (Figure 4.3). These maps were created by digitizing geologic quadrangles from Moore (1963), Bateman and Moore (1965), Bateman et al., (1965), Ross (1965), Nelson (1966), Lockwood and Lydon (1975), Moore (1981), and Stone et al., (2000) (Figure 4.3). The following geologic description is summarized from the synthesis of these geologic maps. The geology of the eastern Sierra Nevada is predominately composed of Cretaceous plutonic rocks ranging from felsic alaskite to more mafic diorite, quartz diorite and hornblende gabbro (Figure 4.3). Most plutons are in the granitic petrologic range from quartz monzonite to granodiorite. In addition to Cretaceous plutonic rocks, areas of the eastern Sierra enclose pre-Cretaceous rocks of two different varieties; Paleozoic metasedimentary roof pendants and metavolcanic rocks of Mesozoic age. The lithology of the roof pendants varies significantly and includes facies of marble, calc hornfels, pelitic hornfels, micaceous quartzite, and biotite schist (Moore, 1963; Bateman et al., 1965). On the eastern side of the valley, the White and Inyo Mountains are primarily composed of Paleozoic carbonates and these units have limited to no influence on groundwater geochemistry on the eastern side of the valley.

There are a number of geologic units that are only found locally yet are easily weathered (e.g., glacial deposits and mafic rocks) and thus have the potential to significantly influence groundwater geochemistry, where present. For example, extensive glacial till deposits are found at high and mid elevations of the eastern Sierra Nevada; most notably the Tioga Till and the Tahoe Till. In the northern part of Owens Valley, the Bishop Tuff, a pyroclastic flow and ash fall deposit

related to the eruption of the Long Valley Caldera, outcrops over a large area with a thickness up to 200 meters. Lava flows and cinder cones are also present in the valley, most notably at the Big Pine Volcanic Field, a zone of alkali-olive basalts associated with Cenozoic extension (Ormerod et al., 1991)

The southeastern Sierra Nevada is geologically complex. To aid the reader we have included detailed geologic descriptions for four geographic areas of interest (AOIs) where sampled springs and host aquifers are located. Each AOI is outlined in Figure 4.3, shown with increased detail in Figure 4.4, and has an associated geologic cross section (Figure 4.5). Table 4.1 provides petrologic information for likely flowpath units that are described for each AOI.

4.4.2 Bishop AOI

Sampled springs within the Bishop AOI source water from three different subregions; Wheeler Crest (n = 3), Mount Tom and the Tungsten Hills (n = 2), and the Bishop Tuff (n = 1) (Figure 4.4A). Unit names and geologic descriptions are derived from Bateman et al. (1965).

4.4.2.1 Wheeler Crest

Wheeler Crest is a 13 km north-south trending ridge west of Round Valley, CA. It is bisected from Mount Tom by lateral moraines extending into Round Valley from Pine Creek Canyon. There are five geologic units that have the potential to affect the geochemistry of springs emerging along the mountain front of Wheeler Crest; the Round Valley Peak Granodiorite (Krv), the Wheeler Crest Quartz monzonite (Kwc), rocks similar to Cathedral Peak Granite (Kca), unnamed diorite, quartz diorite, and hornblende gabbro (Kd), and the Pine Creek Pendant (Pm & Ppmq). Two springs emerge at high angle faults downgradient of marble and micaceous quartzite facies of the Pine Creek Pendant at Wells Meadow (IES-037 & IES-038). One spring emerges from a lateral moraine within Pine Creek Canyon (IES-039) below a significant mass of Kd.

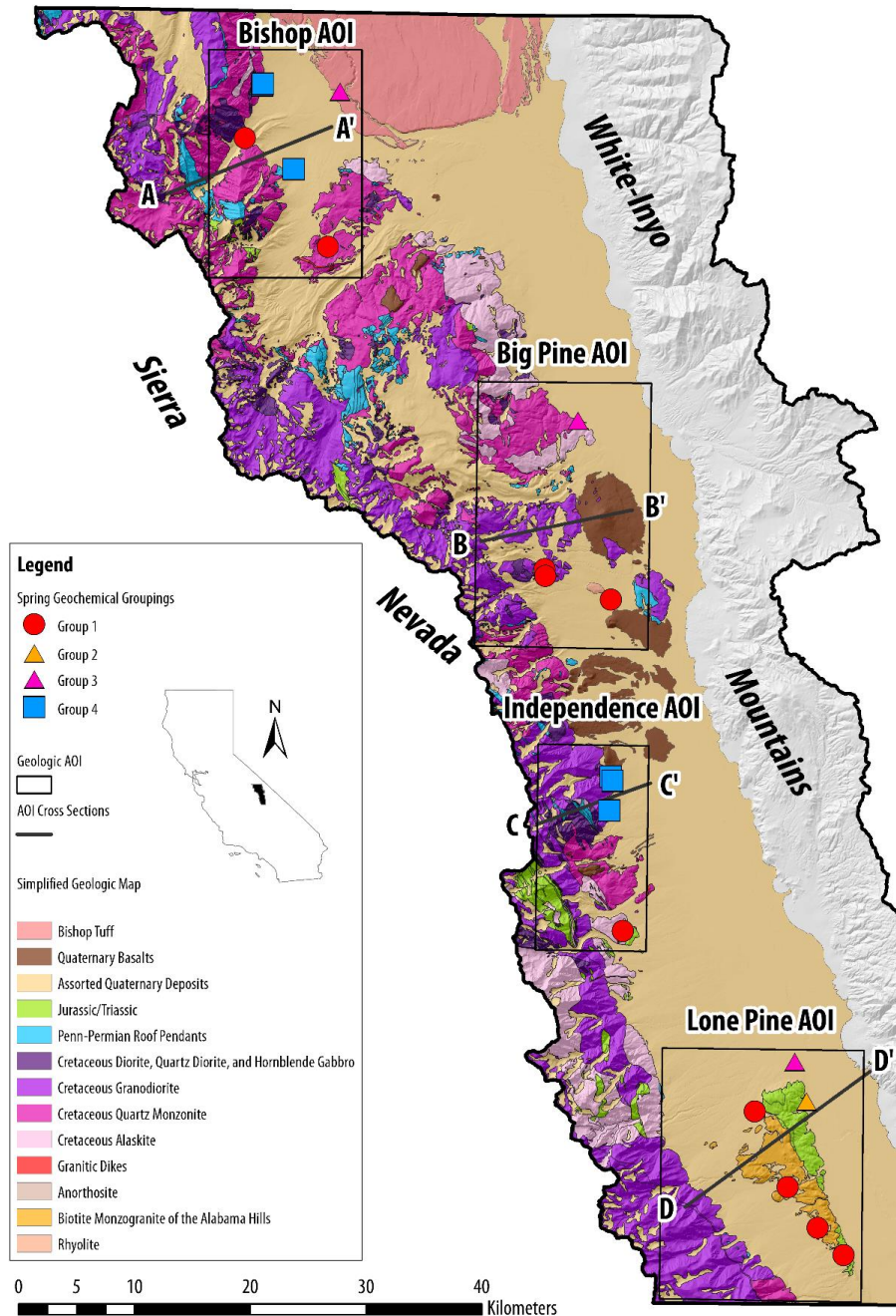


Figure 4.3.: Simplified geologic map of Owens Valley with major petrologic compositions and significant geologic units (e.g., the Bishop Tuff) grouped by color. This geologic map was created by simplifying units across 10 geologic quadrangles. For granitic plutons, color ranges from light pink (alaskite) to dark purple (mafic rocks like diorite, quartz diorite, and hornblende gabbro). This color scheme is adapted from Bateman (1964). Spring locations are symbolized by their spring geochemical groupings. Four geologic areas of interest (AOIs) are shown in the black rectangles. Cross section lines are shown in the black lines across each geologic AOI. These lines correspond to cross sections in Figure 4.5.

4.4.2.2 *Mount Tom and the Tungsten Hills*

Mount Tom is a prominent peak west of Bishop that rises over 4100 meters. Mount Tom shares similar units to Wheeler Crest including the Wheeler Crest Quartz Monzonite, unnamed diorite, quartz diorite, and hornblende gabbro, and the Pine Creek Pendant. The bulk of the mountain is composed of the Tungsten Hills Quartz Monzonite (Kt). Metamorphic rocks in smaller masses, namely calc-hornfels, are exposed at lower elevations of the mountain near Elderberry Canyon. One spring, IES-033, emerges in this area along a high angle normal fault at the base of Mt. Tom.

The Tungsten Hills are primarily comprised of the Tungsten Hills quartz monzonite (Kt), an albitized rock with local hydrothermally altered zones (Bateman et al., 1965). Northeastern portions of the Tungsten Hills contain small isolated masses of metamorphosed sedimentary material, however most of these zones are downgradient from IES-032, a spring which emerges southwest of Grouse Mountain. Aplite, pegmatite and alaskite felsic dikes and masses are laterally extensive across the southwestern Tungsten Hills into Buttermilk Country.

4.4.2.3 *Bishop Tuff*

The Bishop Tuff is a ~150-200-meter-thick welded tuff that was emplaced as a result of a rhyolitic pyroclastic flow during the collapse of the Long Valley caldera (760 ka) (Bailey et al., 1976). This eruption is thought to be one of the largest of the Quaternary period. Within the Mount Tom Quadrangle there are three mapped subunits of the Bishop Tuff; a hard agglutinated tuff, a soft tuff with rounded pumice fragments, and a basal layer of white angular pumice (Bateman et al., 1965). The predominant mineralogy of the tuff is a biotite-plagioclase-quartz-sanidine high-silica rhyolite (Hildreth and Wilson, 2007). One spring, IES-034, emerges directly from the Bishop Tuff in Birchim Canyon less than a kilometer west of the Owens River Gorge.

4.4.3 *Big Pine AOI*

There are two geologic subregions within the Big Pine AOI that contain sampled springs; the Warren Bench (n =1) and Birch Mountain (n = 3) (Figure 4.4B). Unit names and geologic descriptions are derived from Bateman et al. (1965).

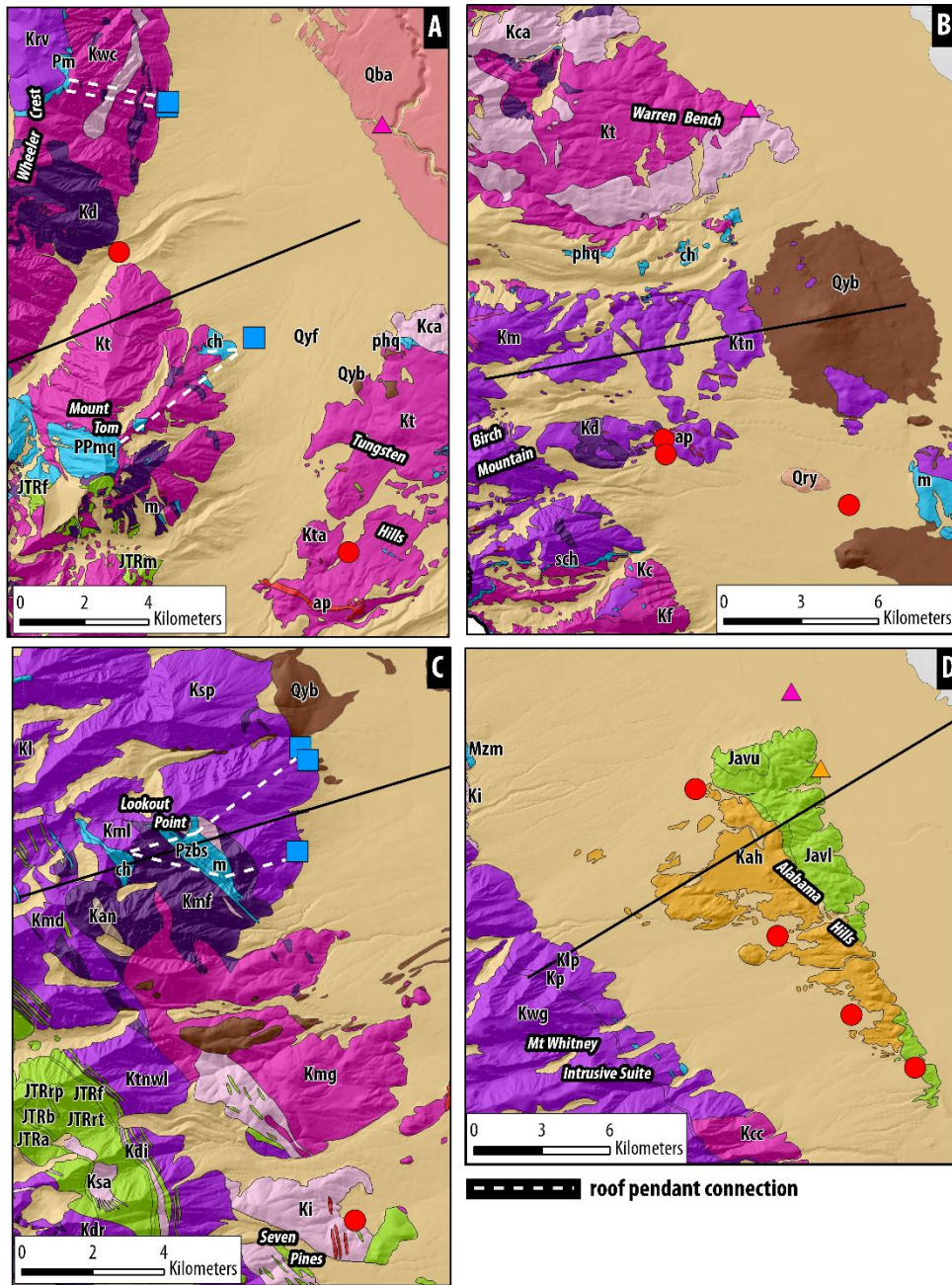


Figure 4.4.: Zoomed-in geologic maps showing geologic AOIs, springs symbolized by geochemical grouping, and hypothesized connections (white dashed lines) to Group 4 springs (blue squares) from Paleozoic metasedimentary roof pendants (blue geologic units). A) Bishop AOI with Wheeler Crest, Mount Tom, Tungsten Hills subregions shown, B) Big Pine AOI with Warren Bench and Birch Mountain subregions shown C) Independence AOI with Lookout Point and Seven Pines subregions shown, and C) Lone Pine AOI with Mt Whitney Intrusive Suite and Alabama Hills subregions shown.

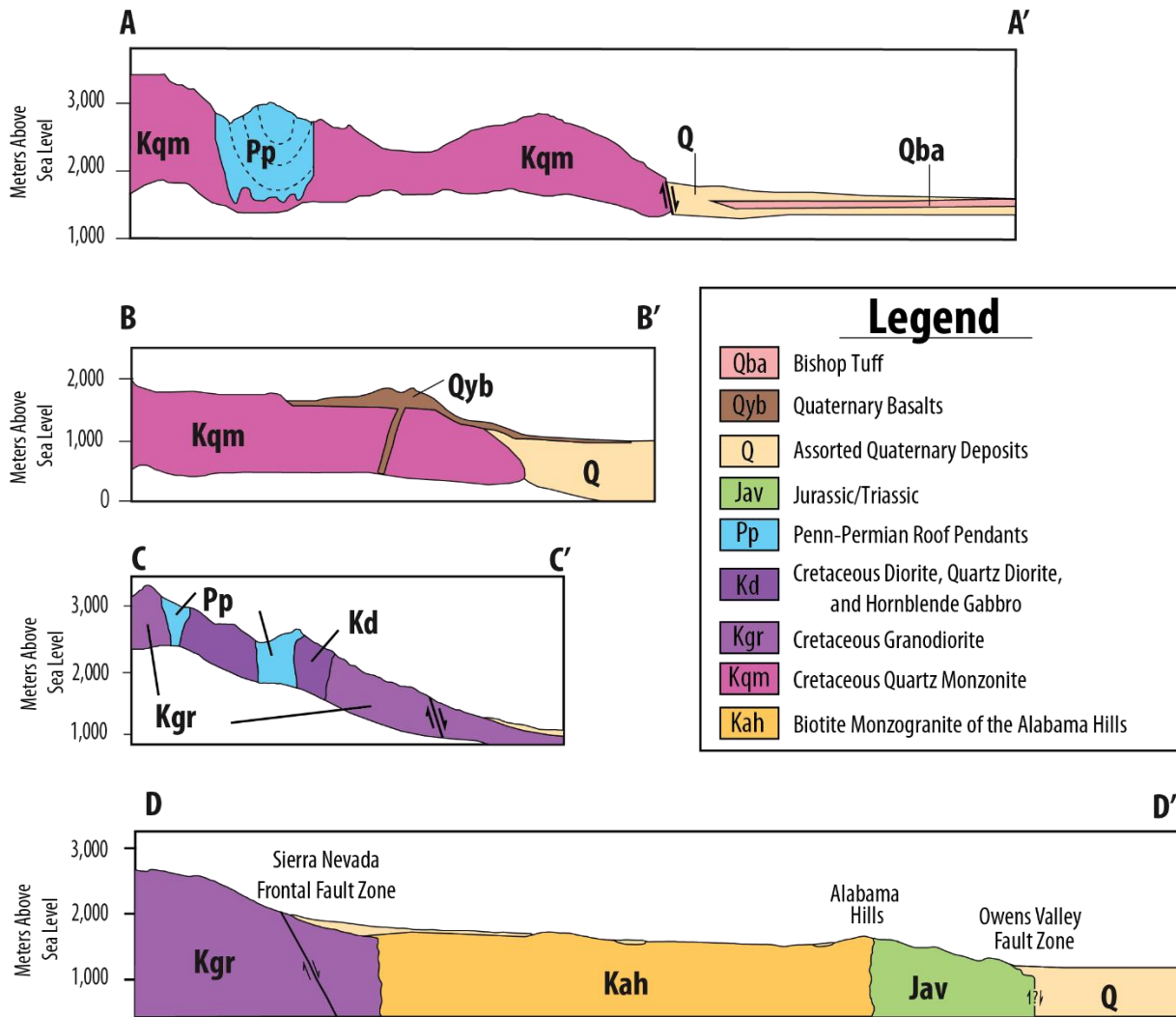


Figure 4.5.: Simplified geologic cross sections across transects outlined in Figure 3. The cross sections are described as follows: A) A transect across the Pine Creek Pendant into Round Valley, CA. Cross section adapted from Bateman et al. (1963), B) A transect through the Big Pine AOI from north of Birch Mountain to Crater Mountain. Cross section adapted from Bateman et al. (1963), C) Simplified cross section through metasedimentary roof septa and Spook Pluton near Independence, CA. IES-028, IES-042, and IES-043 likely source units featured in this cross section. Cross section adapted from Moore et al. (1963), D) Simplified cross section of the geologic AOI near Lone Pine, CA. Springs IES-021, IES-022, IES-023, IES-024 are likely influenced by the Mount Whitney Intrusive Suite and Alabama Hills biotite monzogranite. Cross section adapted from Stone et al. (2000).

4.4.3.1 Warren Bench

The Warren Bench is a small sloping plateau that extends from the Sierra Nevada escarpment into Big Pine, CA. There are two large masses of plutonic rocks in this region; rocks similar to the Cathedral Peak granite (Kca) and the Tungsten Hills Quartz Monzonite (Kt). Small exposures of diorite, quartz diorite, and hornblende gabbro are exposed at higher elevations below Round Mountain. The Warren Bench and areas upgradient have a high concentration of high angle normal faults with downthrown sides predominately to the west. IES-030 emerges from a concealed high angle fault which offsets an aplite felsic dike.

4.4.3.2 Birch Mountain

Three plutonic masses in the Birch Mountain subregion cover the bulk of the surface area and likely have the most influence on groundwater flow to springs in the area. The Tinemaha Granodiorite (Ktn) is exposed at the highest elevations including Birch Mountain and Mt Tinemaha and is distinguished by an abundance of hornblende compared to other granodiorites in the area (Bateman, 1965). The Tinemaha granodiorite is bisected downgradient from Birch Mountain by the Granodiorite of McMurray Meadows, notable for having the highest range of petrologic modal analyses in the region. Unnamed rocks of diorite, quartz diorite, and hornblende gabbro (Kd) are exposed on Mt Tinemaha as well as in the center of the Granodiorite of McMurray Meadows (Km). IES-40 and IES-041 emerge near high angle normal faults in an area with a mixture of these three units as well as numerous felsic dikes. IES-029 emerges 8 km west of Birch Mountain at a long, laterally continuous, high angle normal fault between two of the major cindercones of the Big Pine Volcanic Field; Crater Mountain and Red Mountain. Quaternary basalt flows (Qyb) in this region may impact the geochemistry at IES-029.

4.4.4 Independence AOI

The Independence AOI lies within the Mount Pinchot Quadrangle. This area is geologically complex and contains Cretaceous plutonic masses, Paleozoic roof pendant septa, Jurassic and Triassic metavolcanic rocks, and the Independence dike swarm (Moore, 1963). Unit names and geologic descriptions are derived from Moore (1963). Four springs were sampled in this region, three in the Lookout Point subregion and one in the Seven Pines subregion (Figure 4.4C).

4.4.4.1 Lookout Point

Lookout Point is a 3100 m peak 15 km to the northwest of Independence, CA. The largest and most laterally extensive pluton in the area is the Spook Pluton (Ksp), a zoned silicic granodiorite with an inner silicic facies and an outer, more mafic facies. Other small plutonic exposures within the AOI include the McDoogie Pluton (Kmd), the Mule Lake Pluton (Kml), the Independence Pluton (Ki), unnamed mafic plutonic rock (Kmf), and unnamed anorthosite (Kan). Mixed Paleozoic metasedimentary rocks are dispersed throughout the AOI and include facies of marble (m), calc-hornfels (ch), biotite schist (Pzbs), and pelitic hornfels and quartzite (Pzch) (Moore, 1961). Two septa containing three of these facies are found southeast and southwest of Lookout Point. The mineralogy of these pendant rocks is highly variable even within mapped units of the same facies (Moore, 1963). Fine grained diorite and granodiorite porphyry dikes of the Independence dike swarm are numerous and trend northwest-southeast across roof pendant septa, Ki, Kmf, and Kml. Three springs (IES-028, IES-042, and IES-043) were sampled in the Lookout Point area at the contact of the Spook Pluton and the alluvial fan.

4.4.4.2 Seven Pines

The Seven Pines subregion is directly west of Independence and contains large exposures of the alaskitic Independence Pluton and two other plutons not present in the Lookout Point subregion; the Dragon Pluton (Kdr) and the Woods Lake mass of the Tinemaha Granodiorite (Ktnwl). Jurassic and Triassic metavolcanic rocks are exposed at high elevations west of the Seven Pines area. These rocks include metarhyolite (Jtrt, Jtrf, Jtrp) meta-andesite and metadacite (Jtra, Jtraw), and metabasalt and meta-andesite (Jtrb). The southern extent of the Independence dike swarm terminates just south of Seven Pines. Paleozoic roof pendant rocks are not present in this region.

4.4.5 Lone Pine AOI

The Lone Pine AOI contains two major geologic features likely to contribute flow to springs; the Mount Whitney Intrusive Suite and the Alabama Hills (Figure 4.4D). Unit names and geologic descriptions are derived from Stone et al. (2000).

4.4.5.1 The Mount Whitney Intrusive Suite

The Mount Whitney Intrusive Suite is a nested intrusion comprised of three granitic plutons of a similar age (88-83 ma) that are exposed from oldest to youngest moving westward and upgradient (Hirt, 2007). Numerous peaks in the Mount Whitney Intrusive Suite reach over 4000 m, including Mount Whitney, the highest point in the contiguous 48 states. The oldest of these units, the Granodiorite of Lone Pine Creek (Klp), is classified as a biotite hornblende granodiorite. This unit is the most mafic of the suite, containing abundant mafic inclusions, and has a higher plagioclase anorthite content. Moving upgradient, the Paradise Grandodiorite (Kp) is a biotite hornblende granodiorite only exposed surficially within the AOI at a small zone between the Grandiorite of Lone Pine Creek and the Whitney Granodiorite (Kwg). Compositionally, the Paradise Grandiorite is slightly less mafic than the Granodiorite of Lone Pine Creek and distinguished by 1-3 cm long phenocrysts of potassium feldspar. The Whitney Granodiorite is the most felsic unit of the suite and is classified as a hornblende biotite granodiorite and granite. This unit is distinguished by 4-8 cm phenocrysts of potassium feldspar, a lower average An content in plagioclase crystals, and higher Mg and Mn contents of biotites. $^{87}\text{Sr}/^{86}\text{Sr}$ ratios for the Mount Whitney Intrusive Suite range from 0.7068-0.7076 (Hirt et al., 2007). Springs in this area primarily emerge downgradient of the Mount Whitney Intrusive Suite and upgradient of the Alabama Hills along mapped faults (Figure 4.2).

4.4.5.2 The Alabama Hills

Five kilometers of alluvium separate the mountain front, marked by the Sierra Nevada Frontal Fault Zone, from the Alabama Hills. The Alabama Hills are composed of the Alabama Hills Granite and the Volcanic complex of the Alabama Hills. The placement of the Alabama Hills basement block is perplexing considering its age is similar to the Mount Whitney Intrusive Suite (1.5-3 km higher in elevation). Recent work suggests the Alabama Hills is a dropped-down normal fault block as opposed to a transpressional uplift or massive landslide (Ali et al., 2009). Petrologically, the Alabama Hills granite (Kah) is a highly weathered, medium-grained biotite monzogranite containing abundant aplite and few pegmatite dikes (Stone et al., 2000). The volcanic complex of the Alabama Hills is divided into upper and lower subunits. The upper unit (Javu) is a massive, slightly welded tuff principally composed of quartz and potassium feldspar

with small percentages of plagioclase and biotite. The lower unit (Jav1) contains volcanogenic conglomerates, siltstones, and sandstones as well as a lower subunit of rhyolite tuff.

4.5 Methods

4.5.1 Field sampling procedures

Samples from 20 springs emerging on the west side of Owens Valley were collected during the spring of 2016. Springs on LADWP land were sampled in March while the remainder of the springs, located inside the Inyo National Forest (INF) boundary, were sampled during May. The majority of the sampled springs are classified as rheocrenes (Springer and Stevens, 2008). However, among all springs there is diversity in the emergence style (i.e., subaerial, subaqueous, or seepy/diffuse). The quality of the emergence has implications for tracer collection, especially with gaseous tracers. In all cases, springs were sampled as close to the spring emergence as possible. A Masterflex platinum-cured silicone tubing was placed at the spring source and sometimes positioned with a rock or zip tie if the discharge was too turbulent or fast. Samples were collected using a GeoTech peristaltic pump and filtered, depending on the tracer, using .22 μm polyethersulfone membrane Sterivex-GP pressure filter units.

Parameters measured in the field yield information about groundwater conditions at the time of emergence. Field geochemical data were measured with a YSI Professional Plus multi-parameter probe including: temperature ($^{\circ}\text{C}$), pressure (mm/Hg), pH, conductivity ($\mu\text{S}/\text{cm}$), and dissolved oxygen (mg/L and % of saturation). Specific conductance ($\mu\text{S}/\text{cm}$) and total dissolved solids (mg/L) are reported by the YSI and are calculated from conductivity. All equipment and tubing were sanitized with quaternary ammonia and ethanol to prevent transmission of invasive species and endangering spring ecology between sampling sites.

Table 4.1. Petrologic data for likely plutons supporting flow to springs in Owens Valley (CA).

Table 4.1: Petrologic data for plutons affecting sourcing springflow in Owens Valley, CA

Geologic Unit	Petrologic Source	Unit Abbreviation	Volume Percent						Accessory and Secondary Minerals			Springs Influenced (IES #)
			Quartz	K-Feldspar	Plagioclase	Biotite	Hornblende	Pyroxene	Mafic Minerals	Plag (An)		
Whitney Granodiorite	Moore 1987	Kw	24.9	23.5	44.9	-	-	-	-	6.7	25-27*	21,22,23,24,25,26
Paradise Granodiorite	Moore 1987	Kp	23	20.9	46.2	-	-	-	-	9.9	29-31*	21,22,23,24,25,26
Granodiorite of Sugarloaf	Moore 1987	Ksl	21.6	20	44.6	-	-	-	-	13.9	36*	21,22,23,24,25,26
Lone Pine Creek Granodiorite	Moore 1987	Klp	21.6	10.7	47	-	-	-	-	20.7	N/A	21,22,23,24,25,26
Dikes and Sills	Moore 1987	Kgd	38.1	29.8	30.7	-	-	-	-	1.4	16-26*	27
Dragon Pluton	Moore 1987	Kd	8.3	28	54.6	-	-	-	-	9	19*	26?,27
Dragon Pluton	Moore 1963	Kd	12.7	24.5	51.5	7.3	1.9	Tr	2	-	23	26?,27
Independence Pluton	Moore 1987	Ki	28.9	35.6	32.8	-	-	-	-	2.7	16*	28,42,43
Independence Pluton	Moore 1963	Ki	30	42.7	24.7	1.8	-	-	0.9	-	14	27,28,42,43
Tinemaha Granodiorite (Woods Lake Mass)	Moore 1963	Ktnwl	23.6	21.8	41.8	8.2	2.8	-	1.9	-	30	27
Alabama Hills Granite (Kah)	Abbott 1972	Kah	-	-	-	-	-	-	-	-	-	21,22,23,24,25,26
Spook Pluton (Outer)	Moore 1963	Ksp	24.5	18.3	46.7	6.9	2.4	-	1.3	-	32	28,42,43
Spook Pluton (Inner)	Moore 1963	Ksp	24.4	20.4	49.2	4.7	0.1	-	1.2	-	26	28,42,43
Bullfrog Pluton	Moore 1983	Kb	24.9	39.6	33	-	-	-	-	2.5	14*	24,25,26,27
Bullfrog Pluton	Moore 1963	Kb	25	37.3	34.7	1.8	0.2	-	1	-	10	24,25,26,28
Rocks Similar to Cathedral Peak Granite (Alaskite)	Bateman 1965	Kca	33	38.6	25.8	1.8	0.2	-	2.2	2.9	~15	37,38,30
Tungsten Hills quartz monzonite (Pine Creek)	Bateman 1965	Kt	31.9	29.1	32.5	4.8	3.9	-	1.4	6.5	28-30	30,33
Tungsten Hills quartz monzonite (Bishop Creek)	Bateman 1965	Kt	29.8	31	33.2	5.5	0.2	-	2.1	6.2	28-31	32
Tungsten Hills quartz monzonite (Shannon Canyon)	Bateman 1965	Kt	27.7	33.5	32.9	4	0.1	-	2.9	5.9	~15	30
Round Valley Peak granodiorite	Bateman 1965	Krv	26.8	18.7	44.4	7.2	3.6	-	1.9	10.1	33-38	37,38
Wheeler Crest Quartz Monzonite (kwc)	Bateman 1965	Kwc	29.3	25.3	35.3	5.8	1.6	-	1.6	10.1	28-36	37,38,33,39
Granodiorite of McMurray Meadows	Bateman 1965	Kmm	20.5	26.4	40.1	8	3.1	-	1.6	12.7	37	40,41
Tinemaha Granodiorite	Bateman 1965	Ktn	21.3	23.6	39	4.6	6	-	3.4	16.1	38	40,41,29
Mafic plutonic masses	Moore 1963	Km	8	8.625	54.975	11.2	8.5	5.75	-	-	30-70	28,42,43
Diorite, quartz diorite, hornblende gabbro	-	Kd	-	-	-	-	-	-	-	-	-	37,38,33,39,40,41
Felsic Dikes	-	ap	-	-	-	-	-	-	-	-	-	32,40,41

Table 4.2. Additional units supporting springflow that do not have petrologic data.

Table 4.2: Additional units affecting spring hydrochemistry

Unit	Springs Influenced (IES #)
Qyb (young basalts)	29
Bishop Tuff	34
ch (Calc-hornfels)	28,33,42,43
phq (Pelitic hornfels)	29,32
Pm,m (marble)	37,38,33,28,42,43
PPmq (micaceous quartzite)	37,38
Pzbs (biotite schist)	28,42,43
JTrt (metarhyolite)	27
Volcanic Complex of the Alabama Hills (upper part)	21,25,26
Volcanic Complex of the Alabama Hills (lower part)	21,25,26

4.5.2 Stable isotopes of water ($\delta^2\text{H}$ and $\delta^{18}\text{O}$)

Stable isotopes of oxygen and hydrogen have a multitude of uses in hydrologic studies, especially at the hillslope scale. At larger spatial scales $\delta^2\text{H}$ and $\delta^{18}\text{O}$ are valuable tools for identifying sources of groundwater recharge (Blasch and Bryson, 2007; Liu and Yanamaka, 2012; Gleason et al., 2020) and for calculating apparent recharge elevations of spring waters (James et al., 2000).

Stable isotopes of oxygen of hydrogen were collected unfiltered in 2 ml vials and kept on ice or refrigerated until being sent for analysis. Analysis was performed at the University of California, Davis Stable Isotope Facility (SIF). Isotope ratios ($\delta^2\text{H}$ and $\delta^{18}\text{O}$) of spring water samples were analyzed simultaneously using a Laser Water Isotope Analyzer V2 (Los Gatos Research, Inc., Mountain View, CA, USA). The samples were injected six times and only the last four injections were used to calculate the average stable isotopic composition. All stable isotope measurements are standardized relative to VSMOW. The reported uncertainty for this analysis is 0.83‰ for $\delta^2\text{H}$ and 0.08‰ for $\delta^{18}\text{O}$.

Additionally, Groundwater $\delta^2\text{H}$ and $\delta^{18}\text{O}$ data from a geographic bounding box surrounding Owens Valley were extracted from the USGS Water Quality Portal (<https://waterdata.usgs.gov/nwis/qw/>). These data were used to create a Local Ground Water Line

(LGWL) and to supplement data collected in this study to examine regional patterns in groundwater stable isotope composition.

4.5.3 General chemistry

Major anion and cation concentrations for natural waters provide information about source rock type, biogeochemical cycling, and groundwater circulation (Hem, 1985). General chemistry analysis serves as the backbone for many groundwater studies seeking to identify flowpaths and can be thought of as a geochemical fingerprint.

General chemistry samples were filtered and collected in 250 ml high-density polyethylene (HDPE) bottles and refrigerated upon sampling until sent for analysis. Major cations and anions were measured at the New Mexico Bureau of Geology and Mineral Resources Chemistry Lab. Cations were measured using inductively coupled plasma optical emission spectrometric techniques (ICP-ES) according to EPA 200.7. Anions were measured using an ion chromatograph (IC) according to EPA 300.0. Duplicates were run on every 10th sample. Low bromide analysis was performed for water samples under the bromide detection limit of 0.1 mg/L. Charge balance errors (CBE) for all springs were under 5%.

4.5.4 $^{87}\text{Sr}/^{86}\text{Sr}$ analyses and rock leaching of $^{87}\text{Sr}/^{86}\text{Sr}$

Strontium often behaves conservatively in natural waters and thus $^{87}\text{Sr}/^{86}\text{Sr}$ ratios inherited from weatherable Sr^{2+} can be ideal tracers of mineral weathering processes and groundwater mixing. Strontium isotopes have been used at local (Blum et al., 1993; Clow et al., 1997; Pretti and Stewart, 2000) and regional (Johnson et al., 2000; Stewart-Maddox et al., 2018) scales for flowpath delineation via identification of likely endmember sources of weatherable strontium.

Samples for strontium isotope analysis of spring waters were field filtered and collected in 125 ml HDPE bottles. Strontium isotopes were prepped and analyzed in the Johnson Lab at the University of Illinois Urbana-Champaign (UIUC). Column chemistry was performed to adhere the strontium to a resin while a series of washes were performed to remove other cations and anions. Strontium was eluted from each sample before a concentration check was performed using inductively coupled plasma mass spectrometry (ICPMS) to achieve a goal concentration of 100 ppb. Samples with concentrations greater than 100 ppb were diluted. A Nu Plasma HR

multicollector inductively-coupled-plasma mass-spectrometer (MC-ICPMS) was used for strontium isotope analysis. Samples with low concentrations and thus lower voltages were specified for longer analytical runs. Reported analytical uncertainty for $^{87}\text{Sr}/^{86}\text{Sr}$ ratios is 10^{-5} .

Differential or preferred weathering of certain minerals may contribute to observable differences in whole rock versus groundwater $^{87}\text{Sr}/^{86}\text{Sr}$ ratios (Blum et al., 1993; Blum et al., 1998; Bataille and Bowen, 2012). To address these differences, rock samples were collected from different geologic units in the study area for a leaching experiment. Whole rock samples were leached using deionized water to supplement existing whole-rock literature values. Samples were collected from plutonic rocks and metasedimentary roof pendants that represent likely flowthrough aquifers supplying groundwater to sampled springs. Rock preparation and leaching was conducted at Purdue University. Rock samples were crushed and sieved. For each geologic unit, 200 mg of crushed rock was added to 1 L HDPE bottles filled with deionized water. The bottles were capped tightly, sealed with electrical tape, and stored for two months in the laboratory. After the allotted time, leachate samples were decanted and filtered. Chemical preparation and MC-ICPMS analysis was performed at UIUC in the same manner as the spring water samples.

4.5.5 Tritium (^3H)

Tritium is a naturally occurring radioisotope ($t_{1/2} = 12.43$ years) formed in the atmosphere (bombardment of ^{14}N by secondary neutron cosmic rays) and subsurface (fission of ^6Li). High levels of anthropogenic tritium were produced in the atmosphere during the 1950s and 1960s, peaking in 1963, as a result of thermonuclear weapons testing. Tritium becomes directly incorporated into the water molecule and thus can be thought of as an ideal tracer in hydrologic systems. Because the tritium input function is nonunique and subject to mixing and decay in the recharge area, tritium is generally not used for determining absolute groundwater residence times. Instead, tritium functions as a powerful relative indicator of the presence of bomb-pulse or modern recharge (<100 years) (Rose, 1992).

Samples for tritium analysis were not filtered and were collected in 1L HDPE bottles. Tritium concentrations of spring waters were analyzed using gas proportion analysis at the University of Miami Tritium Laboratory (<https://tritium.rsmas.miami.edu/>). Samples were subjected to electrolytic enrichment and low-level counting for increased accuracy and precision.

Tritium concentrations are expressed in tritium units (TU). Reported errors range from 0.09-0.11 TU and represent one standard deviation.

4.5.6 Chlorine-36 (^{36}Cl)

Chlorine-36 is a radioisotope with a long half-life ($t_{1/2} = 300,000$ years) typically used for dating ancient groundwaters. Chlorine-36 is naturally produced in the atmosphere and in the subsurface. The relative influence of these two production pathways on ^{36}Cl concentrations in groundwater is dependent on whether the groundwater is circulating rapidly (atmospheric production dominant) or is static (subsurface production dominant) (Phillips, 2000). Variations in background atmospheric ^{36}Cl can be attributed to distance inland from the coastline and atmospheric circulation patterns. Empirical data have been used to map $^{36}\text{Cl}/\text{Cl}$ isopleths across the United States in preanthropogenic groundwater (Davis et al., 2003) and for modeling isopleths in modern precipitation (Moysey et al., 2003). Similar to tritium, ^{36}Cl concentrations in the atmosphere became orders of magnitude higher during the 1950s and 1960s as a result of thermonuclear weapons testing. However, the ^{36}Cl peak was roughly ten years earlier and the production of anthropogenic ^{36}Cl was mainly due to submarine irradiation of seawater (Phillips, 2000). The long half-life of ^{36}Cl in comparison to ^3H allows the use of ^{36}Cl as a diagnostic tool to distinguish bomb-pulse recharge from modern recharge. Additionally, when paired with chloride concentrations and chloride to bromide ratios (Cl^-/Br^-), ^{36}Cl can be used to understand the origins of spring water (Davis et al., 2001).

Samples for ^{36}Cl analysis were filtered in the field and collected in 1L HDPE bottles. Samples were prepared with AgCl prior to accelerator mass spectrometry measurement at the Purdue Rare Isotope Measurement Laboratory (PRIME Lab). Results are reported as $^{36}\text{Cl}/\text{Cl}$ ratios $\times 10^{-15}$. Analytical uncertainty is reported for each individual sample.

4.5.7 Noble Gases

Dissolved noble gases in groundwater have a wide range of utility as forensic tools in hydrogeology. Noble gases can provide information about recharge conditions (e.g., recharge temperature and elevation), interaction with deeply circulating groundwater (i.e., mantle and crustal reservoirs of helium via the $^3\text{He}/^4\text{He}$ ratio), and residence time (e.g., $^3\text{H}/^3\text{He}$ dating and ^4He

accumulation) (Stute and Schlosser, 2000). Concentrations of noble gases in groundwater are dependent on five main factors: 1) recharge temperature, 2) atmospheric pressure at the time of recharge (recharge elevation), 3) recharge salinity, 4) excess air, and 5) fractionation of the excess air component. The first three factors affect the dissolution of atmospheric air according to solubility equilibrium (Stute and Schlosser, 2000).

Noble gas samples were collected in copper tubes only at springs with clear emergences lacking turbulent flow and excessive bubbles. Samples were analyzed for Ar, Kr, Xe, Ne, ^4He , $^3\text{He}/^4\text{He}$ ratio at the University of Utah Noble Gas Lab (<https://noblegaslab.utah.edu/>). The measurement error for helium is $\pm 1\%$ of the reported value. For all other gases the measurement error is between 1% and 5% of the reported value. $^3\text{He}/^4\text{He}$ ratios (R) are reported normalized to the atmospheric $^3\text{He}/^4\text{He}$ ratio (R_a) ($1.38 * 10^{-6}$) as R/R_a . Typically, R/R_a ratios far exceeding 1 are indicative of an excess ^3He component, usually mantle or primordial helium. R/R_a ratios ~ 1 are typical of surface waters and shallow groundwaters. R/R_a ratios < 1 can indicate radiogenic helium accumulation from crustal fluxes (Clark and Fritz, 1997). R/R_a values have been previously shown to scale with residence time and flowpath distance (Kulongoski et al., 2003).

Raw noble gas measurements were corrected with Noble90, a non-linear, error weighted least squares inversion MATLAB program that allows for noble gas concentrations to be corrected by solving for recharge temperature, recharge pressure (elevation), recharge salinity, excess air, and fractionation (Aeshbach-Hertig et al., 1999; Aeshbach-Hertig et al., 2000; Kipfer et al., 2002; Peeters et al., 2002). Noble90 allows for a variety of fitting options and has a built in Monte Carlo simulation component to estimate reasonable errors. In our case we used the ta-1 fit (closed equilibration model) with 100 Monte Carlo simulations per sample. A ta-2 fit (partial reequilibration model) was used if the ta-1 fit yielded nonrealistic results. We utilized four solving parameters; Ne, Ar, Kr, and Xe. Helium was not used as a solving parameter because there are both geogenic and terrigenous sources of helium within the study area. Recharge salinity was assumed to be zero for Owens Valley spring waters. Because recharge pressure (elevation) is unknown, two approaches were taken. The first approach was to solve for recharge temperature across a suite of elevations from the spring emergence to the regional peak. The intersection of this family of solutions with the local environmental lapse rate (ELR) can be thought of as an approximate recharge elevation (Zuber et al., 1995; Manning and Solomon, 2003; Doyle et al., 2015; Peters et al., 2018). ELRs are typically constructed from local weather station data at varying

elevations. However, in this study area there are few weather stations across a relatively wide range of elevation (1300m – 4000+m). Therefore, a synthetic lapse rate was constructed by extracting values of elevation and mean annual temperature (O'Donnell and Ignizio, 2012) from randomly distributed points (~6,000) within a bounding region of the study area (Figure 4.6). A linear regression was fit to these points in order to derive a local annual ELR (Figure 4.7). An alternate approach for deriving a recharge elevation necessary to solve for the other parameters is the use of the median elevation of the watershed or contributing area (Thomas et al., 2003; Paukert, 2014). For this approach we used an elevation of 2600 m, the approximate median elevation from the Owens Valley basin floor to the Sierra Nevada crest east of Owens Valley. Both approaches were both used for calculating recharge temperatures and deriving excess helium concentrations necessary for performing a helium mass balance to calculate terrigenic ^4He and tritogenic ^3He . Terrigenic ^4He can be used as an accumulation tracer while tritogenic ^3He is used for ^3H - ^3He dating. ^3H - ^3He ages were calculated for springs with tritium > 0.2 TU as low ^3H concentrations are unreliable for ^3H - ^3He dating.

4.5.8 Radiocarbon (^{14}C)

Radiocarbon is one of the few environmental tracers that can “see” in the 1,000-50,000-year residence time window (Clark and Fritz, 1997). However, derived ages in the younger and older portion of this spectrum are more uncertain. Other tracers that can potentially date waters in this range have high uncertainties (^4He) or require large volumes of water that makes field sampling inconvenient (Clark and Fritz, 1997).

As meteoric water recharges into the groundwater table through the soil zone, it incorporates soil CO_2 in the form of dissolved inorganic carbon (DIC). The soil zone sets the initial radiocarbon activity, which is assumed to be the activity of the atmospheric CO_2 or 100 percent modern carbon (pmc) (Plummer and Glynn, 2013). Once recharged through the soil zone into the aquifer, $^{14}\text{CO}_2$ becomes incorporated into the groundwater system and its decay along some groundwater flowpath, from recharge to discharge, becomes a proxy for residence time (Clark and Fritz, 1997). The incorporation of dead carbon into groundwater DIC can skew the radiocarbon activity resulting in an old age bias. Fortunately, $\delta^{13}\text{C}$ values can be used to track the evolution and incorporation of dead carbon when endmembers such as the $\delta^{13}\text{C}$ of initial recharge are well constrained (Clark and Fritz, 1997). The $\delta^{13}\text{C}$ value of initial recharge can be assumed based on

the presence of C3 or C4 plant respiration in the soil zone, however in regions with mixed vegetation or when recharge occurs in talus above treeline, this value is more uncertain.

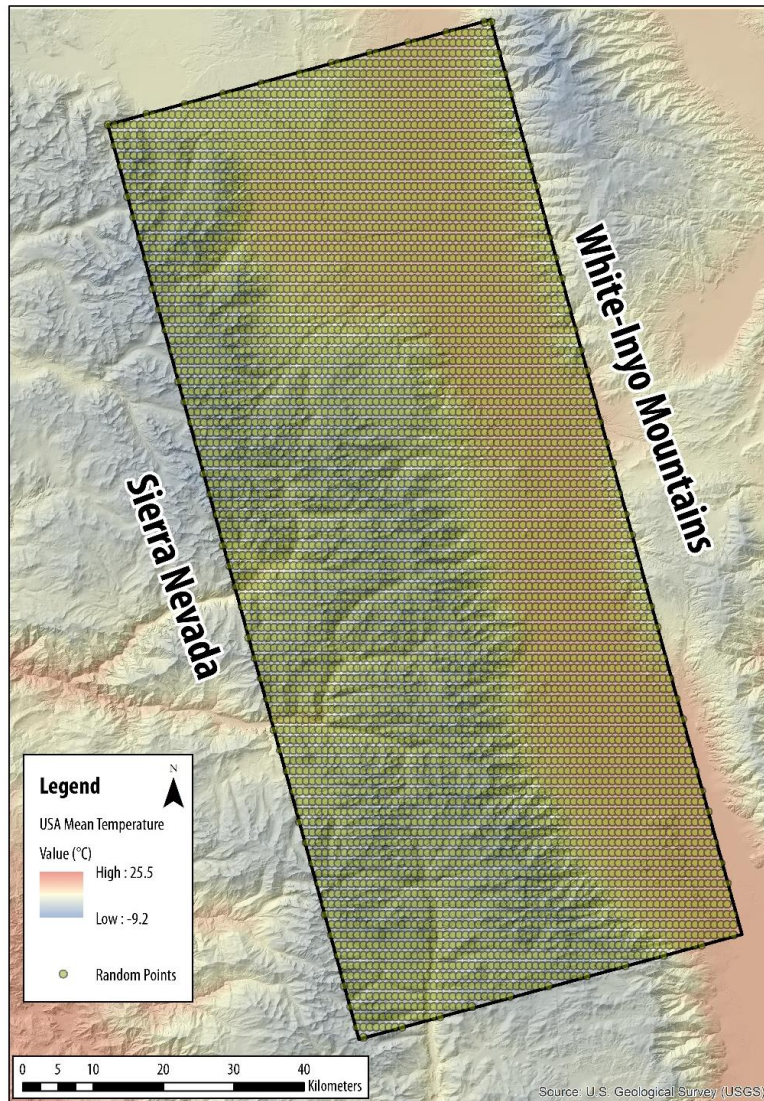


Figure 4.6: Map showing the study area, Owens Valley, CA, bounded by the Sierra Nevada to the west and the White-Inyo Mountains to the east. A USA mean temperature raster developed by the USGS (O'Donnell and Ignizio, 2012) is draped over a hillshade constructed from a digital elevation model. Values of mean annual temperature and surface elevation were extracted from random points within the bounding region (black box) to create a synthetic environmental lapse rate (ELR).

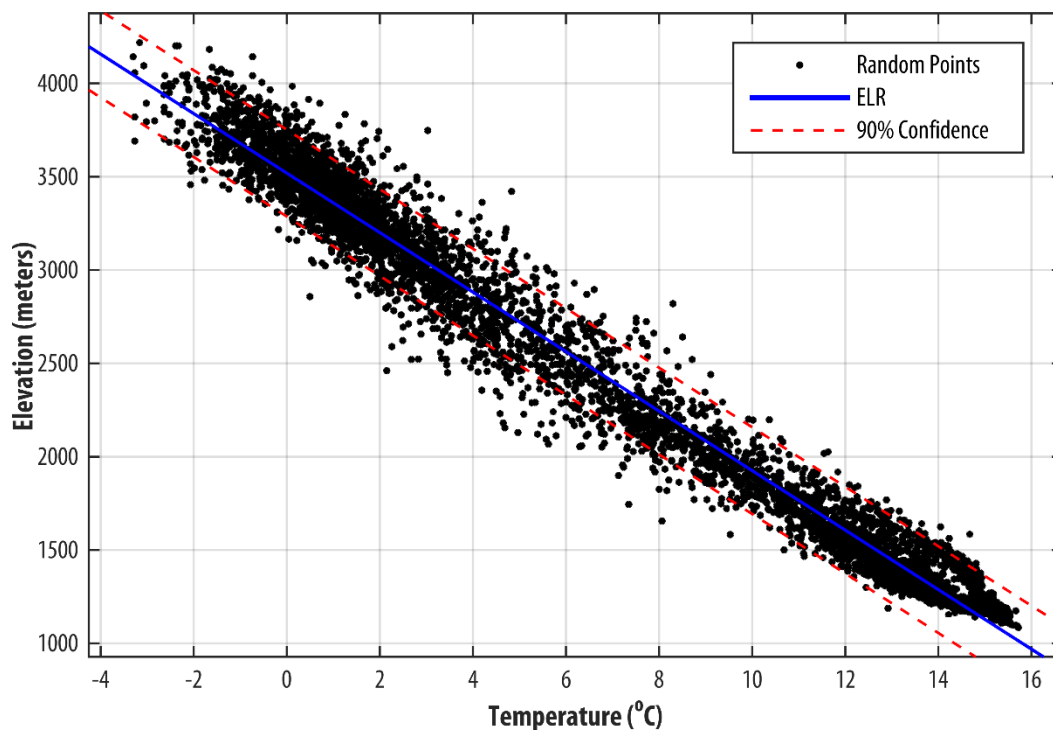


Figure 4.7: Annual environmental lapse rate (ELR) (blue line) for the study area created from random points (black circles) shown in Figure 4.6. A linear regression was fitted to the ~6,000 points to create the ELR. Lines of 90% confidence for the regression are shown by the red dotted line.

Radiocarbon samples were not filtered and collected, where appropriate, in two 500 ml HDPE bottles. Samples were collected with minimal headspace and then caps were sealed with electrical tape to minimize atmospheric exchange. Samples were analyzed at the University of Arizona Accelerator Mass Spectrometry Lab. Radiocarbon activity reported as percent modern carbon (pmc) and $\delta^{13}\text{C}$ relative to Pee Dee Belemnite (PDB) were reported for groundwater DIC. Percent modern carbon was calculated as a weighted average from multiple machine runs. Radiocarbon residence times were calculated in NethpathXL (Parkhurst and Charlton, 2008) using traditional radiocarbon adjustment models. To our knowledge, radiocarbon dating on groundwaters in the Owens Valley region has been extremely limited and there is not data on the $\delta^{13}\text{C}$ for soil gas or groundwater recharge within the study area. Therefore, wells and springs in the Owens Lake and Crowley Lake watersheds with both $\delta^{13}\text{C}$ (‰) and ^{14}C (pmc) values reported were extracted from the USGS NWIS database (<https://waterdata.usgs.gov/nwis/qw>). A linear regression was fitted to a plot of $\delta^{13}\text{C}$ versus ^{14}C activity for 94. These samples were collected

between 2006-2013. The intersection of this regression with a horizontal reference line of 100 pmc was used as a plausible endmember for $\delta^{13}\text{C}$ of soil gas. The value found at this intersection was $\sim 15\text{‰}$ (Figure 4.8A). This value is not anomalous for groundwaters in arid/semiarid regions where there is a large range of soil gas $\delta^{13}\text{C}_{\text{PDB}}$ from (-6 to -25%) and a suitable initial approximation is -16 to -18‰ (Faure, 1986; Pearson and Handshaw 1970; Anderson, 2002). The regional USGS carbon isotope data also shows a clear relationship with ^3H , i.e., high concentrations of ^3H (TU) are associated with elevated radiocarbon activity (pmc) (Figure 4.8B).

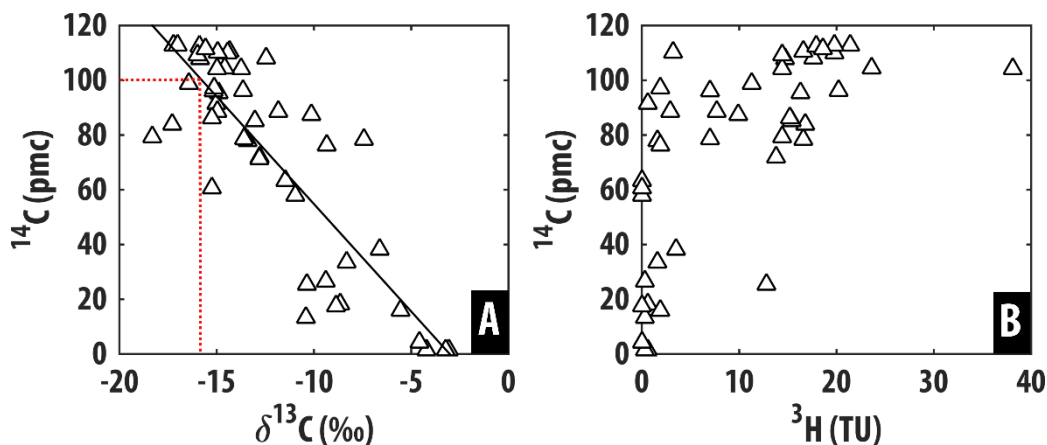


Figure 4.8: Environmental tracer plots from USGS NWIS groundwater samples (wells and springs) in the Crowley Lake and Owens Lake watersheds. A) Linear regression fitted to a plot of $\delta^{13}\text{C}$ versus ^{14}C activity for 94 samples. The intersection of this regression with a horizontal reference line of 100 pmc was used as a plausible endmember for $\delta^{13}\text{C}$ of soil gas. The value found at this intersection was $\sim 15\text{‰}$. B) Relationship between ^3H and ^{14}C activity for USGS NWIS groundwater samples.

4.5.9 Geochemical modeling

Inverse modeling of general chemistry data is commonly employed to reconstruct the chemical composition of water into a series of weatherable minerals and precipitable clays that have reacted or formed to create the resulting chemistry. Increases in major cations and anions, and therefore dissolved minerals, often scale with distance (Guler and Thyne, 2004; Rissmann et al., 2015) and residence time (Rademacher et al., 2001; Rademacher et al., 2005).

We used Netpath-XL (Parkhurst and Charlton, 2008) to identify suitable and mass-balanced inverse geochemical models describing the amount and suite of weathered minerals

necessary to form an observed final water composition from an initial starting water. Netpath-XL was also used for radiocarbon correction.

Many of the springs in this study emerge at fault zones along the eastern Sierra Nevada mountain front and there are not springs or wells upgradient that have been sampled or are plausible candidates for an initial starting water. Therefore, precipitation was used as the pre-weathering chemical composition of spring waters and the geochemical composition of springs was modeled using the known mineralogy of geologic units in the study area as model constraints. While there is precipitation chemistry data available through the National Atmospheric Deposition Program (NADP) for one station inside HUC 180901, NTN Site CA34 (Bishop, CA), this data is problematic for several reasons: 1) data are only available for a small period between 1980-1982, 2) the standard deviation in many of the reported analytes over that three year period is very high (in some cases the Cl^- and SO_4^{2-} values in precipitation are higher than spring water values), 3) Bishop, CA lies in the basin of Owens Valley and thus doesn't provide a good endmember for high elevation recharge, and 4) Bishop precipitation chemistry data might be influenced by aeolian deposition from Owens (Dry) Lake. Rather than use data from CA34, NADP data was averaged from three high elevation sites in the southern Sierra Nevada: CA99 (Yosemite National Park- Hogdon Meadow, elev. 1393 mamsl), CA28 (Kings River Experimental Watershed, elev. 2000 mamsl), and CA75 (Sequoia National Park- Giant Forest, elev. 1921mamsl) to calculate an initial precipitation endmember to model from. Alkalinity and bicarbonate are not reported for NADP data; however, bicarbonate was added to averaged precipitation chemistry to rectify the charge imbalance. Chloride, a conservative ion, is often used for calculating geochemical enrichment in the subsurface as increases in the subsurface can be attributed to the effects of evaporation and transpiration. In this case, many springs had chloride values close to the detection limit (0.1 mg/L). For our purposes, we chose to consider the effects of evapotranspiration negligible and attributed all chloride enrichment to the dissolution of halite, a plausible alternative due to the proximity of the study area to multiple playas and Owens (Dry) Lake.

In NETPATH, the user is required to specify both elemental constraints and mineral phases to calculate possible geochemical models. This requires detailed assessment of the aquifer mineralogy, including the stoichiometry of these minerals. For example, small differences in plagioclase composition, like choosing An_{30} versus An_{40} , can substantially alter model results and number of possible solutions. While NETPATH has its own mineral database, it is sometimes

necessary to add in minerals or alter existing mineral stoichiometry to effectively model the likely aquifer dissolution reactions.

Due to the nonunique nature of NETPATH, models can often yield multiple solutions. Knowledge from calculated saturation indices and/or stability diagrams can be used to help inform and critique model results. For this study, stability diagrams were created using Geochemist Workbench Student Edition 11.0 (GWB) and saturation indices for a suite of mineral phases were calculated with PHREEQC. If certain phases are likely to be present, they can be forced into the model solution. Similarly, phases can be restricted to only dissolve or only precipitate. Including these constraints often reduces the number of potential models.

The main phases used for Netpath-XL of modeling the chemical compositions of Owens Valley spring waters include CO₂ gas, quartz (SiO₂), gypsum, halite, calcite, plagioclase (An₁₅-An₄₅ depending on the candidate aquifers), potassium feldspar, biotite (phlogopite), hornblende, augite, kaolinite, and Ca-montmorillonite. Published geologic quadrangles (e.g., Moore, 1963; Bateman, 1964; Stone et al., 2000) and associated cross sections (Figure 4.5) helped to constrain the likely aquifer units for individual springs. Petrologic data such as modal analyses of minerals from thin section analysis and CIPW norms helped to inform model phases and forcing constraints. CIPW norms were only used to inform plagioclase stoichiometry when thin section modal analysis data was not available. Mineralogic data was compiled from multiple studies (Moore, 1963; Bateman, 1965; Michael, 1983; Moore, 1987; and Hirt, 2007) and is summarized in Table 4.1. Additional units influencing flow without petrologic data are summarized in Table 4.2.

4.5.10 Partitioning young and old groundwater with ³H, ³⁶Cl, and ¹⁴C

Prior studies have shown that age partitioning is an effective way to classify groundwater age without a priori knowledge of age distributions and numerous assumptions (Jasechko, 2016). Tritium (³H), chlorine-36 (³⁶Cl), and ¹⁴C were used to classify spring waters as “young”, “old”, or “mixed” in order to evaluate the effect of residence time and, potentially, deeper groundwater circulation on geochemical weathering. Both ³H and ³⁶Cl can be used to detect the presence of young water (<60 years). Due to its relatively short half-life, bomb pulse ³H that has undergone aquifer mixing and decay can be difficult to distinguish from present-day ³H concentrations in precipitation. However, by combining ³H with long lived ³⁶Cl (t_{1/2} = 301,000 yrs.), it is possible to

not just partition waters into “old” and “young” but distinguish between springs with a large proportion of bomb pulse or modern/post-bomb recharge.

We classify spring waters as “old” when we detect pre-anthropogenic $^{36}\text{Cl}/\text{Cl}$ ratios ($< 600 \times 10^{-15}$) and low ^3H (< 0.2 TU), as these waters do not contain a significant fraction of recharge from the 1950s/60s or later. For context, Visser et al. (2012) classified California waters with TU < 0.3 as tritium dead, and the majority of their samples were collected prior to 2011. In comparison, we classify “young” spring waters as having bomb-pulse $^{36}\text{Cl}/\text{Cl}$ ratios ($> 600 \times 10^{-15}$) and elevated ^3H (> 0.2 TU). Additionally, springs with elevated tritium (TU > 2.0) and modern $^{36}\text{Cl}/\text{Cl}$ ratios (e.g., Moysey et al., 2003) are interpreted to be discharging water comparable to modern precipitation or post bomb-pulse recharge and are also classified as “young”. These young/old classifications are based on pre-anthropogenic $^{36}\text{Cl}/\text{Cl}$ ratios in groundwater from empirical data presented by Davis (2003).

Radiocarbon ages calculated in Netpath-XL for two correction models, Vogel (1970) and Tamers, (1975) in NETPATH were used to supplement these partitions and/or provide information on samples that may be a mixed origin of young and old groundwater. If samples are radiocarbon “modern” as indicated by the correction models, radiocarbon activity can still be used as a relative indicator of residence time. Blumhagen and Clark (2008) found a strong relationship between ^{14}C (pmc) and CFC apparent age in Sagehen Basin even though the majority of samples were likely well below the threshold for radiocarbon dating. Part of this relationship was attributed to bomb pulse ^{14}C flushing through the shallow groundwater system. For springs that meet sampling criteria and have sufficient tritium, ^3H - ^3He ages are also reported.

4.6 Results

4.6.1 Field observations

Twelve springs emerge directly along the mountain front near the Sierra Nevada Frontal Fault Zone (1258- 1989 mamsl). Four springs emerge at smaller faults on the west side of the Alabama Hills, slightly lower into the basin (1240-1393 mamsl). Two springs emerge near the basin center (1128-1145 mamsl) and one spring emerges directly out of the Bishop Tuff (1482 mamsl) (Figure 4.2).

All sampled springs (n= 20) are cold springs with discharge temperatures ranging from 11.1 to 21.7°C (mean discharge temperature = 14.9°C). There is a positive correlation ($R^2 = 0.47$, $p < 0.05$) between spring water temperature and elevation (Figure 4.9A). Spring elevation is moderately correlated ($R^2 = 0.33$, $p < 0.05$) with distance from the regional divide (Figure 4.9B). Most springs fall above the local annual ELR (Figure 4.9A), which can be interpreted to be indicative of some potential geothermal heating as a result of groundwater circulation. All spring waters are neutral to slightly alkaline with pH values falling in the range of 6.8-8.0 (Table 4.3). Eighteen of the 20 springs are oxidizing, however three springs (IES-039, IES-041, and IES-043) exhibit reducing conditions based on field dissolved oxygen measurements. While IES-043 likely experiences reducing conditions due to its emergence as a low-discharge seep, IES-039 is heavily altered and affected by barrel modification at its source. Field data is summarized in Table 4.3.

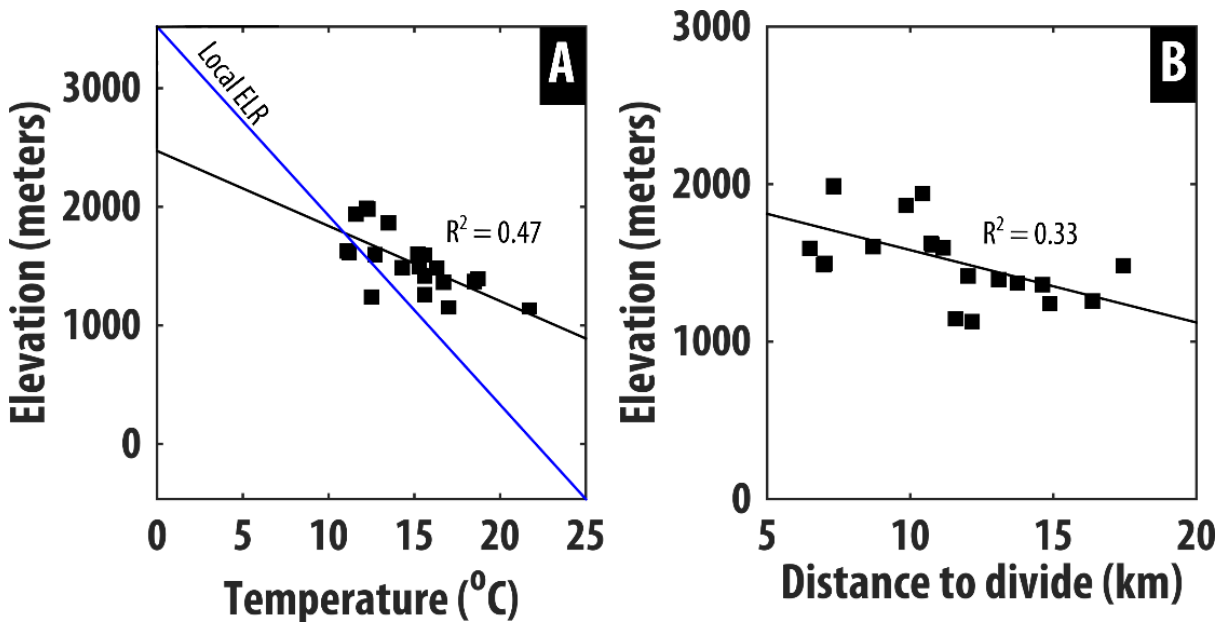


Figure 4.9: Spring discharge temperature versus spring elevation. Springs are symbolized by the black squares. The local environmental lapse rate (ELR) based on average annual temperature is shown as the blue reference line. The majority of springs fall above the local ELR which can be interpreted as indicative of some geothermal heating from groundwater circulation. B) Spring elevation is plotted against distance to the eastern regional divide, the crest of the Sierra Nevada. Distance to divide is used since spring flowpaths cannot be delineated similar to streams/surface water

Table 4.3. Locations and field geochemical data for springs in Owens Valley (CA).

Table 4.3: Spring location, elevation, and field parameters

Sample ID	Spring Name	Date	UTM 11 S		Elevation (m)	Temp. °C	Specific		TDS (ppm)	ORP (mV)	DO (mg/L)	DO (%)	AOI
			E	N			Conductance (mS/cm)	pH					
IES-021	Lubkin Canyon Spring 1	3/19/2016	405405	4044353	1240.623	12.5	479	7.85	311.35	124.3	56.1	5.98	Lone Pine
IES-022	Indian Spring	3/19/2016	403165	4046717	1362.247	16.7	191.8	7.36	124.8	143.7	52.1	5.07	Lone Pine
IES-023	Lone Pine Ck. Complex Spring along Hogback Ck. A	3/19/2016	400577	4050223	1370.655	18.5	239.7	7.42	156	112.5	65.1	6.08	Lone Pine
IES-024	Boron Springs B	3/19/2016	397732	4056750	1393.323	18.7	397.4	6.95	260	174.2	72.9	6.79	Lone Pine
IES-025	Reinhackle Spring	3/19/2016	402195	4057591	1127.741	21.7	2670	7.81	1729	185.1	64.9	5.65	Lone Pine
IES-026	Boron Springs A	3/19/2016	401193	4061012	1144.635	17	515.1	7.75	334.1	195.5	69.8	6.73	Lone Pine
IES-027	Grover Anton Spring	3/20/2016	386328	4072314	1601.774	15.2	470.7	7.88	317.8	186.6	63	6.31	Independence
IES-028	Unnamed spring north of Red Mountain	3/20/2016	385165	4082719	1593.781	15.6	480	7.63	312	235.6	72.3	7.21	Independence
IES-029	Unnamed spring north of Big Pine	3/20/2016	385305	4100901	1417.509	15.6	273.5	7.75	154.05	206.4	58.8	5.84	Big Pine
IES-030	Sharps Meadow	3/20/2016	382448	4116323	1258.998	15.6	428.2	7.68	279.5	204.8	79.2	7.85	Big Pine
IES-032	Elderberry Canyon Spring	3/21/2016	360840	4131349	1939.347	11.6	179.9	8.14	117	183.7	72.8	7.92	Bishop
IES-033	Birchim Cyn. Spring B	3/21/2016	357900	4138046	1596.346	12.7	164.8	7.73	107.25	249.7	81.8	8.65	Bishop
IES-034	Wells Meadow A	5/17/2016	364114	4144865	1482.941	16.3	427	7.53	276.9	201.6	70	6.59	Bishop
IES-037	Wells Meadow B	5/17/2016	355178	4145270	1625.426	11.1	67.3	7.11	43.55	99.1	67.6	7.37	Bishop
IES-038	Unnamed spring along Pine Ck.	5/17/2016	355222	4145412	1614.472	11.2	66.1	7.87	41.5	52.5	69.6	7.59	Bishop
IES-039	McMurray Mdw.Spring A	5/17/2016	353679	4140727	1863.984	13.5	83.2	7.17	53.95	47.7	33.8	3.45	Bishop
IES-040	North Fuller Mdw. Spring	5/17/2016	379576	4103521	1989.348	12.2	216.2	7.5	140.4	107.2	58.3	6.25	Big Pine
IES-041	North Harry Birch Spring	5/18/2016	379636	4102941	1981.63	12.3	292.4	6.63	189.8	112.7	25.4	2.7	Big Pine
IES-042	South Harry Birch Spring	5/18/2016	385273	4085645	1486.732	14.3	191.9	7.61	124.8	-2.1	53	5.43	Independence
IES-043		5/18/2016	385440	4085284	1497.738	15.3	243.5	6.94	158.6	77.7	29.5	2.94	Independence

4.6.2 Stable isotope observations

Owens Valley spring waters have a $\delta^2\text{H}$ range from -134.2 to -116.8‰ (n = 20). Spring water $\delta^{18}\text{O}$ values range from -18.0 to 15.2‰. A line was fitted to the IES spring data to create a Local Spring Water Line (LSWL; $\delta^2\text{H} = 6.38 * \delta^{18}\text{O} - 17.39$). This line is nearly parallel to, yet offset from, the Local Meteoric Water Line (LMWL) defined by Friedman (2002) ($\delta^2\text{H} = 7.12 * \delta^{18}\text{O} - 3.6$). Both the LSWL and the Local Groundwater Water Line (LGWL) ($\delta^2\text{H} = 7.326 * \delta^{18}\text{O} - 2.7$; created from USGS well and spring data) have lower slopes than the Global Meteoric Water Line (GMWL) from Craig (1961) (Figure 4.10A). Calculated deuterium excess values ($\delta^2\text{H} - 8 * \delta^{18}\text{O}$) span from 13.0 to 4.7‰, though the majority of samples (14/20) have values between 9.0 and 12.0‰, indicative of a similar vapor source region. Springs further away from the mountain front emerging near the basin center have deuterium excess values ranging from 7.1- 4.7 ‰.

IES and USGS (NWIS) $\delta^2\text{H}$ and $\delta^{18}\text{O}$ values for Owens Valley groundwaters cluster spatially by geographic region (Figure 4.10B). Samples in the Bishop geographic region, furthest north, are the most isotopically depleted. Samples in the Lone Pine region, furthest south, are the

most isotopically enriched. For both IES and USGS samples, elevation is a poor indicator of isotopic composition (Figure 4.11), even when broken out by geographic area.

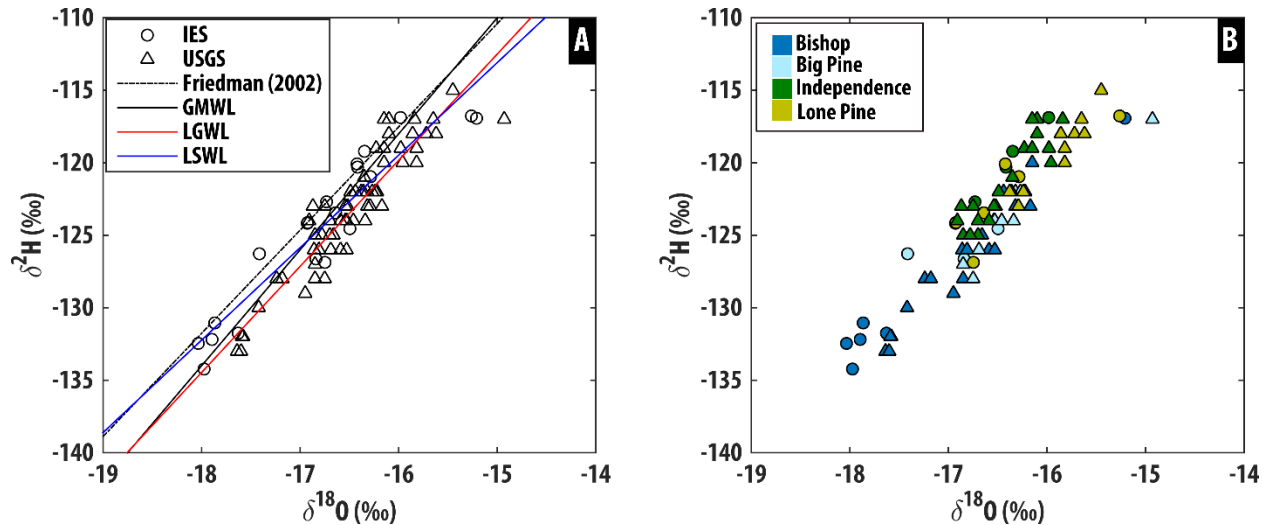


Figure 4.10: Dual isotope plots showing $\delta^{18}\text{O}$ versus $\delta^2\text{H}$ for spring waters from this study (IES) and Owens Valley spring and well waters from the USGS Water Quality Portal (USGS). IES springs are shown in the circles and USGS waters are shown in the triangles. A) Waters from both datasets are plotted with four different reference lines; 1) a local meteoric water line from Friedman (2002) (dashed black line), 2) the global meteoric water line (GMWL) from Craig (1961), 2) a local groundwater line (LGWL) fitted to USGS samples, and 4) a local spring water line fitted to IES samples. B) Dual isotope plot ($\delta^{18}\text{O}$ versus $\delta^2\text{H}$) with USGS and IES samples colored by geographic region within Owens Valley. Samples in the north near Bishop are isotopically depleted while samples in the south near Lone Pine are more isotopically enriched.

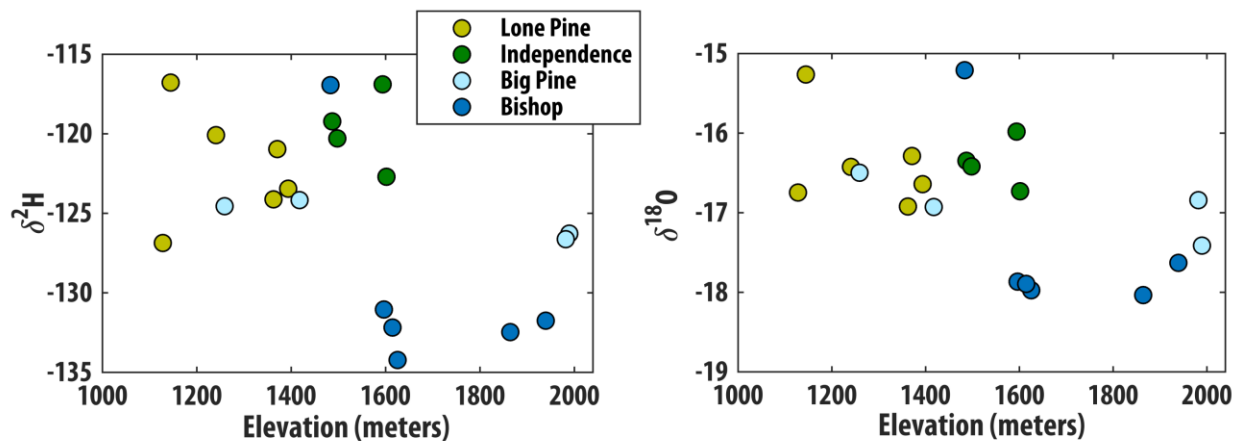


Figure 4.11: Poor relationships exist between water stable isotopes ($\delta^2\text{H}$ and $\delta^{18}\text{O}$) and elevation, even when separated by geographic area, precluding the use of $\delta^2\text{H}$ and $\delta^{18}\text{O}$ as recharge elevation tracers. Springs are symbolized by geographic region within Owens Valley.

4.6.3 General Chemistry

Geochemically, Owens Valley springs are either Ca-HCO₃ (n = 15) or Na-HCO₃ (n = 4) type waters with the exception of one spring, IES-025, which is classified as an Na-Cl type water (Figure 4.12). Despite the possibility that these springs are sourcing intermediate and/or regional scale flowpaths from their recharge zone to the spring emergence, they are relatively dilute (with the exception of IES-025) and have TDS concentrations < 250 mg/L. Moderate to strong positive correlations ($R^2 > 0.55$; $p < 0.05$) exist between all major ions and specific conductance with the exception of sulfate and silica (Figure 4.13). Calcium and bicarbonate are the strongest predictors of specific conductance with R^2 values of 0.73 and 0.88, respectively. Geochemistry data is shown in Table 4.

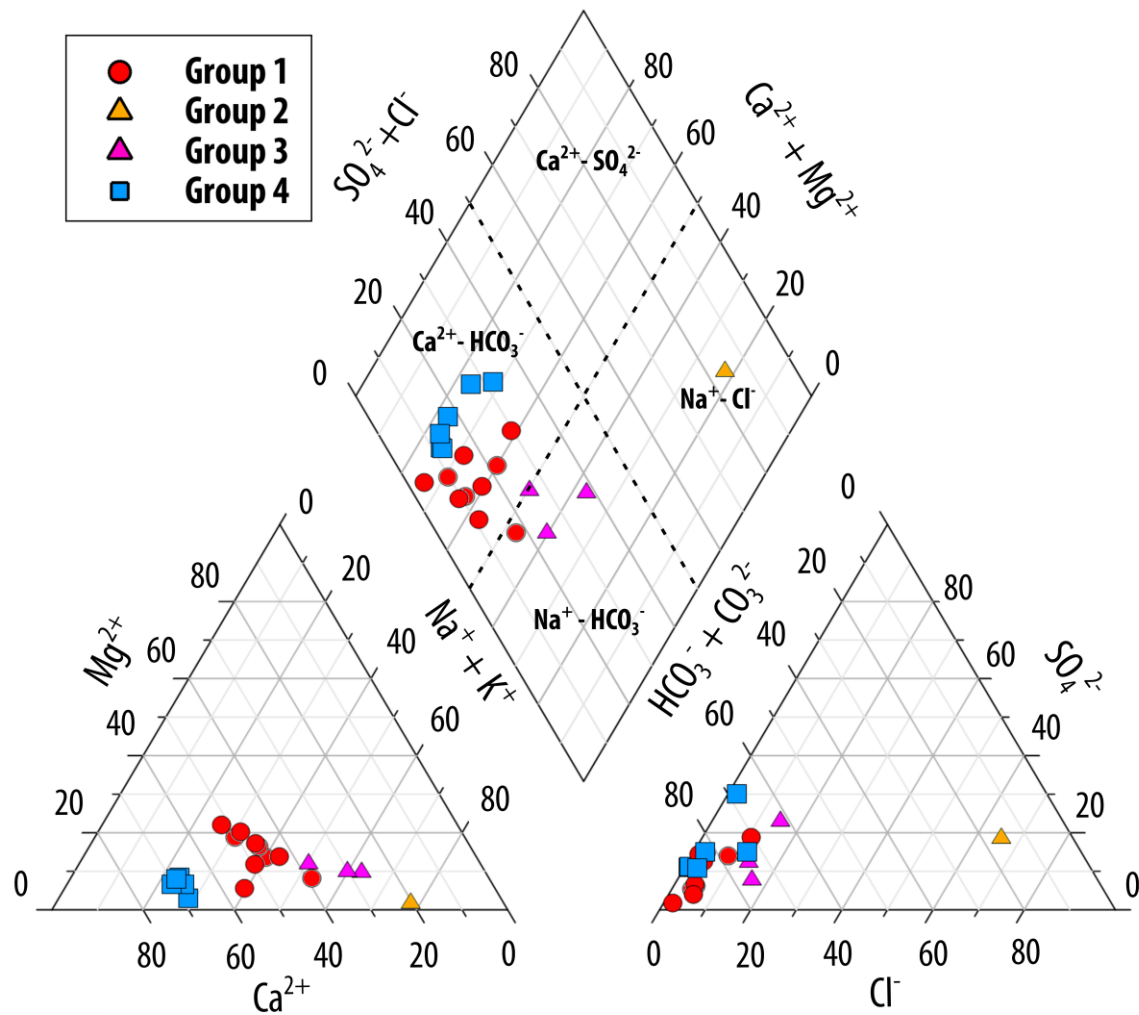


Figure 4.12: Piper diagram showing geochemical compositions of spring waters. Springs are symbolized by geochemical grouping

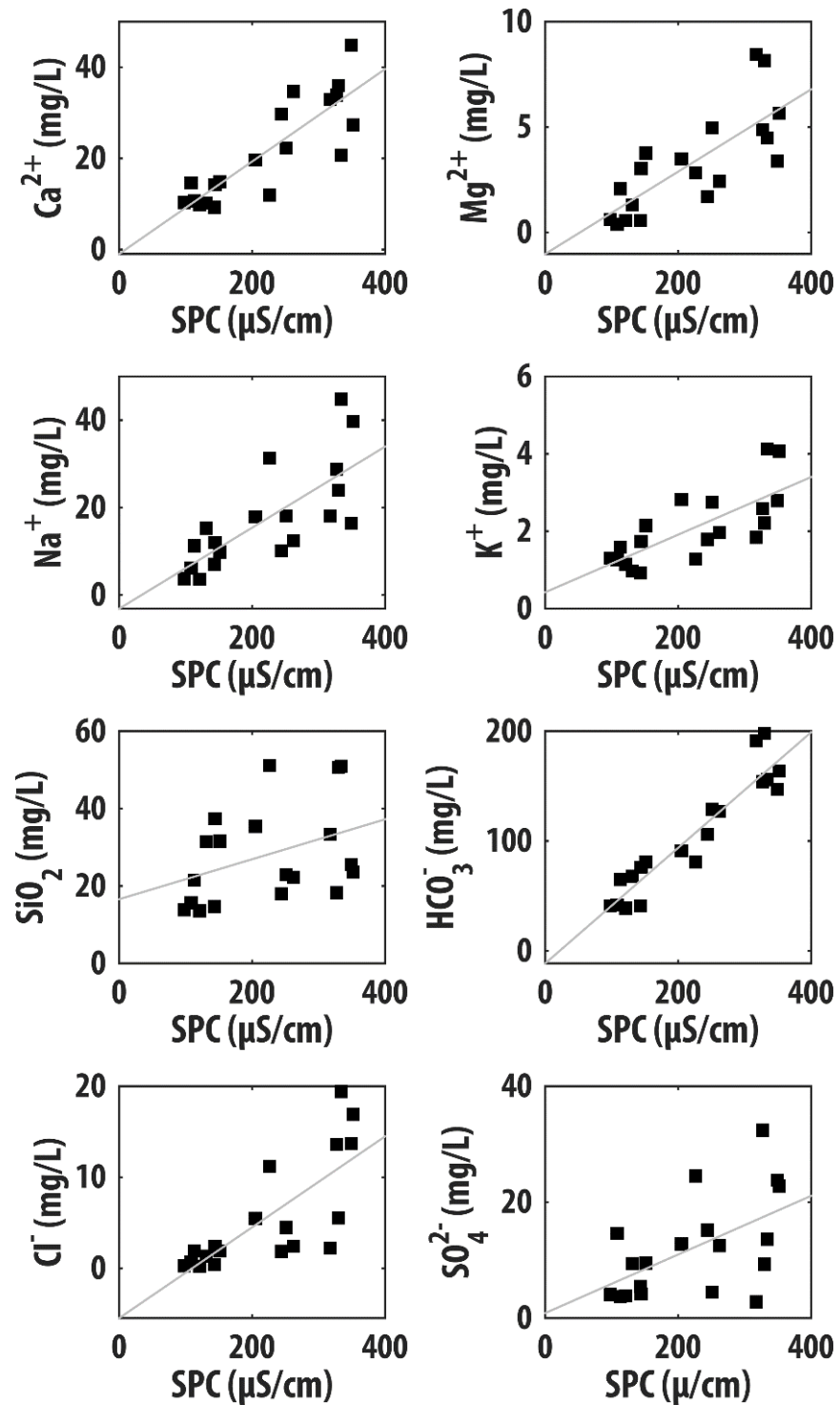


Figure 4.13: Relationships between specific conductance and solute concentrations for major cations and anions for Owens Valley spring waters. Ca^{2+} and HCO_3^- have the highest coefficients of determinate for predicting specific conductance (R^2 of 0.73 and 0.88, respectively). These trends are indicative of plagioclase weathering as a major control on solute compositions.

Owens Valley spring waters can be classified into four geochemical groups based on solute-solute plots, ionic ratios, and likely flowpath geology inferred from geologic maps and associated cross sections (Figure 4.14). These geochemical groupings are independent of the geographic AOIs (Figure 4.4) and reflect geochemical evolution via the petrology of the spring contributing areas (with the exception of Group 3). Group 1 consists of springs with a granitic (alaskite-quartz monzonite-granodiorite) weathering signature typical interaction with Sierra Nevada plutonic rocks. This group is the largest ($n = 10$) and exhibits the greatest intragroup variation in weathering trends (Figure 4.14). Group 2 consists of one spring, IES-025, a basinal brine emerging on the eastern side of the Alabama Hills with high a TDS concentration (724 mg/L). Group 3 is comprised of three springs (IES-026, IES-030, and IES-034) that are Na-HCO₃ type waters with elevated sodium, potassium, and silica concentrations. The geochemical compositions of these springs are interpreted to be influenced by volcanic weathering from ash flows or tuffs, felsic dikes and masses, or contributions from surface water features (e.g. the LAA or the Owens River). Birchim Cyn. Spring B (IES-034) and Reinhackle Spring (IES-026) are both located near the Owens River or LAA, have enriched $\delta^2\text{H}$ and $\delta^{18}\text{O}$ values compared to other spring waters, and cluster with surface water samples (Figure 4.12). Other studies have also attributed some portion of flow at Reinhackle Spring to aqueduct leakage (Bassett et al., 2008). Springs in Group 4 have Paleozoic metasedimentary roof pendants enclosed within granitic rocks upgradient in their likely recharge areas. These springs have chemical signatures (i.e., significantly excess calcium) reflecting a mixture of carbonate (e.g., marble, micaceous quartzite, calc-hornfels) and granitoid dissolution.

The geochemical differences among these four groups can be seen on the Piper diagram (Figure 4.12) and in the geochemical plots (Figure 4.14). While trends showing geochemical evolution exist between major ions like Ca²⁺ vs Mg²⁺ and Ca²⁺ vs HCO₃⁻ when considering all springs, these evolution pathways are stronger after springs are broken out into their respective geochemical groupings, as shown in Figure 4.14A and 4.14B. Figure 4.14C shows intergroup separation when magnesium/potassium molar ratios are plotted against calcium/sodium molar ratios. A reference line for the Mg²⁺/K⁺ ratio expected from biotite weathering (~3) is plotted horizontally in addition to a vertical bounding area of expected Ca²⁺/Na⁺ ratios for Owens Valley granitoids based on an average range of plagioclase compositions from An₂₈ to An₃₆ (Table 1). The majority of springs ($n = 17$) have Mg²⁺/K⁺ ratios at or below the reference line and likely do

not receive significant amounts of magnesium from pyroxenes or amphiboles like hornblende. In areas like Sagehen, CA where amphiboles like hornblende are well-documented as a major contributor to solute weathering fluxes, Mg^{2+}/K^+ molar ratios typically exceed > 3 (calculated from data in Rademacher et al., 2001). IES-024 and IES-041 plot well above the reference line and have sources of hornblende in their likely recharge area. Ca^{2+}/Na^+ molar ratios for spring waters in Group 2 and Group 3 fall below or at the minimum extent of the bounded region. Group 1, which is interpreted to consist of springs weathering granitic plutonic rocks, is predominately in excess of the bounded region, having an average Ca^{2+}/Na^+ molar ratio of 0.72 and a range from 0.38-1.05. Ca^{2+}/Na^+ molar ratios for Group 4 range from 1.35-1.69 with an average of 1.57 and are far in excess of Ca^{2+}/Na^+ ratios predicted solely by the weathering of granitic plutonic rocks.

The relationship between milliequivalents for dominant anions (HCO_3^- and SO_4^{2-}) and cations (Ca^{2+} and Mg^{2+}) is shown in Figure 4.14D. All samples fall below the equiline interpreted to indicate a 1:1 balance between carbonate weathering (above the line) and silicate weathering (below the line). Group 4 spring waters plot closest to the equiline while Group 3 spring waters plot furthest away. Figures 4.14E and 4.14F are adapted from Pretti and Stewart (2002) and show mol % for dissolved SiO_2 and Na^+ relative to Ca^{2+} . Predicted ratios based on the weathering of plagioclase to kaolinite, plagioclase to smectite, and calcite dissolution in equilibrium with plagioclase to smectite weathering are shown as three reference lines in Figure 4.14E. Figure 4.14F elaborates on the point illustrated with Figure 4.14C: 1) The majority of Group 1 waters would need to weather plagioclase with An above the average range for Owens Valley granitoids (An₂₈-An₃₆) to create the observed Ca^{2+}/Na^+ ratios and 2) the majority of Group 4 waters would need to weather An $>$ An₅₀ to create the observed Ca^{2+}/Na^+ ratios, indicative of additional source of calcium in addition to disseminated calcite. Modal analyses (Table 1) indicate that plutons with average plagioclase compositions of An₅₀ or greater are not present in Owens Valley with the exception of mafic plutonic masses (An₃₀-An₇₀) which are not found in the recharge area of Group 4 waters.

Figure 4.14: Geochemical relationships among weathering derived solutes for Owens Valley spring waters. Springs are symbolized by geochemical grouping A) Relationship between calcium and magnesium ion concentrations in sampled spring waters. Springs are well below the 1:1 Mg^{2+} : Ca^{2+} line representative of hornblende weathering. B) Relationship between calcium and bicarbonate ion concentrations C) Relationship between magnesium/potassium ion ratios and calcium/sodium ion ratios in sampled spring waters. The trend line expected for biotite weathering for Mg^{2+}/K^+ (~3) is shown by the blue line. The expected Ca^{2+}/Na^+ weathering ratio for granitic plutons in Owens Valley (Table 4.1) (An_{28} - An_{36}) is bounded for reference in the grey box. D) Relationship between dominant anions (HCO_3^- and SO_4^{2-} meq/L) and cations (Ca^{2+} and Mg^{2+} meq/L). All samples fall below the 1:1 reference line indicative of equal contributions from carbonate and silicate weathering. Group 4 springs lie the closest to the 1:1 line. E) Relationship between mol % SiO_2 and mol % Ca. Reference lines for predicted weathering trends are shown for 1) calcite dissolution and plagioclase to smectite weathering in a 1:1 ratio, 2) plagioclase to smectite weathering, and 3) plagioclase to kaolinite weathering. F) Relationship between mol % Ca and mol % Na. Predicted weathering trends for An_{25} and An_{45} plagioclase are shown. Plots E & F adapted from Pretti and Stewart (2002).

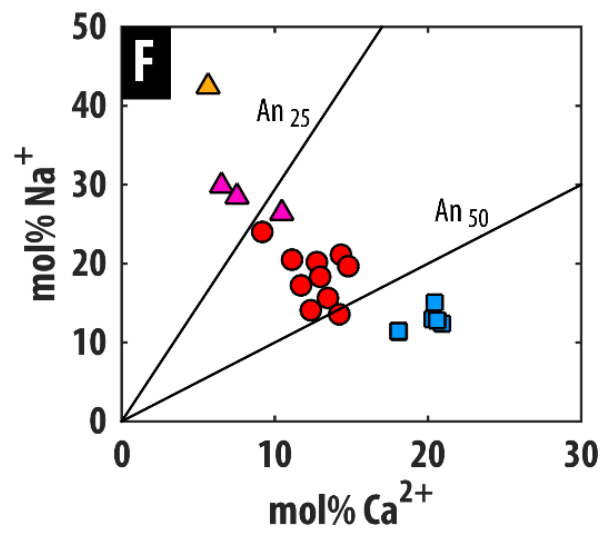
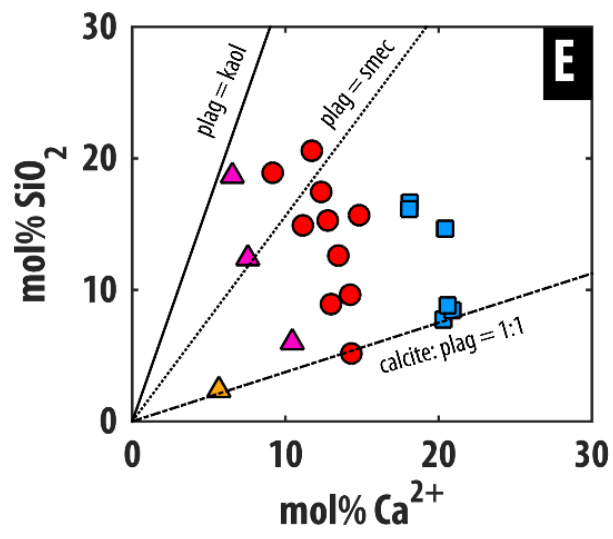
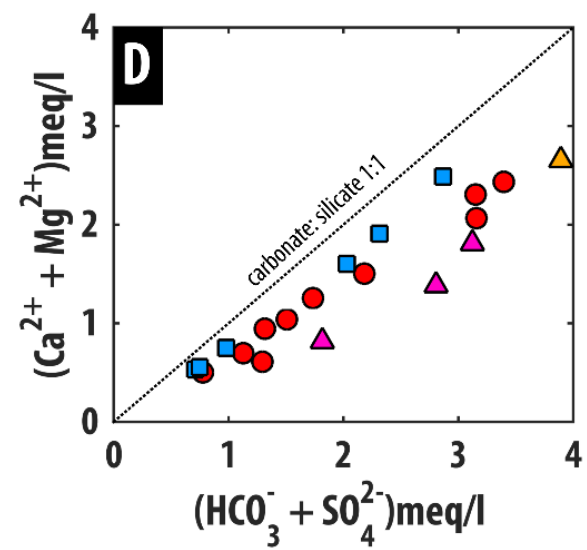
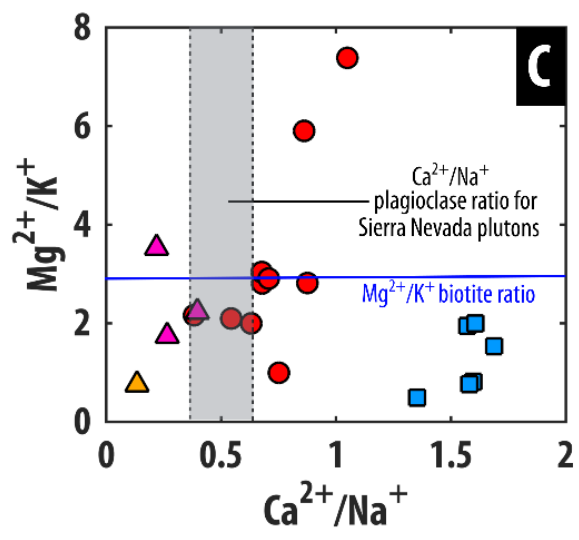
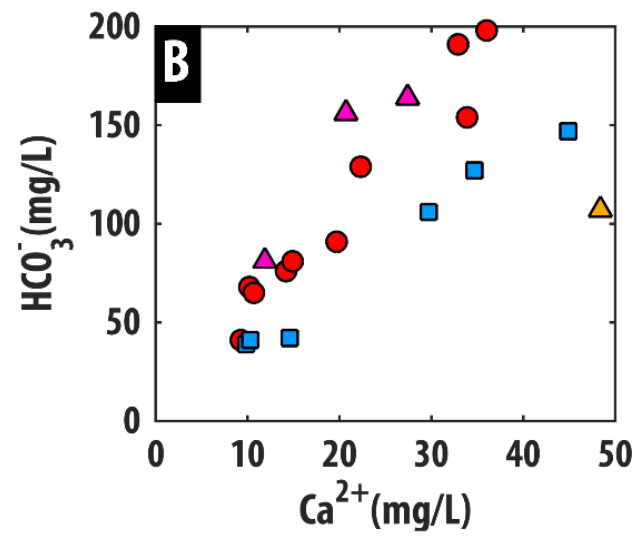
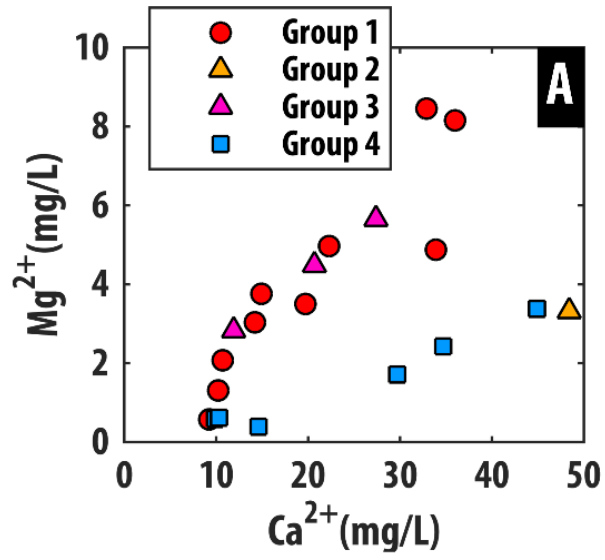


Table 4.4. General chemistry data and geochemical groupings for Owens Valley springs.

Table 4.4

Sample ID	Ca ²⁺ (mg/L)	Mg ²⁺ (mg/L)	Na ⁺ (mg/L)	K ⁺ (mg/L)	Sr ²⁺ (mg/L)	Br ⁻ (mg/L)	Cl ⁻ (mg/L)	Cl/Br	F ⁻ (mg/L)	SO ₄ ²⁻ (mg/L)	HCO ₃ ⁻ (mg/L)	Si as SiO ₂ (mg/L)	TDS (mg/L)	Charge Balance (%)	pH	Lithium (ppb)	Boron (ppb)	Geo- chemical Group
IES-021	19.7	3.5	17.9	2.82	0.284	0.021	5.48	261	0.13	12.8	91	35.4	143	4.9	6.8	10	101	1
IES-022	10.2	1.31	15.3	0.975	0.119	-	1.36	181*	0.45	9.45	68	31.5	105	-2.28	6.9	14	92	1
IES-023	14.2	3.04	12	1.74	0.162	0.022	2.4	109	-	4.15	76	37.4	113	4.38	6.8	7	36	1
IES-024	36	8.15	24	2.22	0.411	0.044	5.52	125	-	9.33	198	50.6	238	-1.06	7.1	50	101	1
IES-025	48.4	3.31	209	7.01	1.59	0.18	264	1467	3.16	105	107	30.7	724	1.72	7.2	441	3584	2
IES-026	27.4	5.65	39.7	4.07	0.195	0.063	16.9	268	0.51	22.8	164	23.6	224	-0.24	7.5	74	572	3
IES-027	33.9	4.88	28.7	2.58	0.174	0.015	13.6	907	-	32.4	154	18.3	213	-2.93	8	8	373	1
IES-028	44.9	3.38	16.4	2.79	0.188	0.041	13.7	334	0.23	23.8	147	25.6	206	-0.45	7.2	33	298	4
IES-029	14.9	3.76	9.77	2.15	0.098	-	1.9	253*	0.15	9.51	81	31.6	115	-2.08	7.8	1	16	1
IES-030	11.9	2.83	31.3	1.29	0.08	0.057	11.2	196	0.63	24.5	81	51.1	179	-0.41	7.4	17	91	3
IES-032	10.7	2.07	11.3	1.59	0.076	0.015	1.92	128	0.33	3.73	65	21.5	89	-1.18	7.9	9	12	1
IES-033	14.6	0.388	6.19	1.27	0.053	-	0.68	91*	0.34	14.6	42	15.7	76	0.55	7.8	4	8	4
IES-034	20.7	4.48	44.8	4.13	0.108	0.063	19.4	308	0.72	13.6	156	51	239	-0.17	7.7	178	1000	3
IES-037	9.86	0.58	3.54	1.15	0.027	0.011	0.23	21	0.23	3.85	39	13.6	53	-1.85	7.7	2	8	4
IES-038	10.3	0.617	3.74	1.3	0.031	-	0.28	37*	-	4.1	41	13.8	56	-2.75	7.8	2	14	4
IES-039	9.25	0.574	7.06	0.925	0.026	0.022	0.44	20	0.25	5.49	41	14.7	60	0.46	7.3	3	10	1
IES-040	22.3	4.97	18.1	2.75	0.114	0.044	4.51	103	0.98	4.48	129	23	146	-0.42	7.2	2	23	1
IES-041	32.9	8.45	18	1.84	0.204	-	2.25	300*	0.1	2.82	191	33.4	196	-1.65	7.1	2	26	1
IES-042	29.7	1.71	10.1	1.79	0.129	0.019	1.87	98	0.51	15.2	106	18	133	-0.99	7.7	16	76	4
IES-043	34.7	2.43	12.4	1.96	0.164	0.017	2.43	143	0.44	12.5	127	22.3	153	1.68	7.4	14	114	4

* 0.075 or 75% of the detection limit was used for calculating Cl/Br with Br-concentrations below the detection limit (0.1 mg/L).

4.6.4 Saturation indices, stability diagrams, and inverse geochemical models

Theoretical mineral saturation indices were calculated for Owens Valley spring waters in PHREEQC. All spring waters are undersaturated with respect to anhydrite, gypsum, halite, and sepiolite while saturated with respect to quartz. Only the most dilute samples are undersaturated with respect to chalcedony. IES-025, a Group 2 water, is modeled as saturated with respect to aragonite and dolomite.

Stability diagrams were constructed to identify the most kinetically favorable clays to precipitate out of solution. Garrels and Mackenzie (1967) considered kaolinite the primary weathering product when modeling the evolution from precipitation to ephemeral springs based on aluminosilicate residue compositions. They also considered the evolution of ephemeral springs to perennial springs to yield weathering products of kaolinite and ca-montmorillonite. However, the majority of Owens Valley spring waters lie in the kaolinite stability field rather than in the ca-montmorillonite (shown as beidellite-ca) stability field (Figure 4.15). Spring with lower $\text{Ca}^{2+}/\text{Na}^{+}$ molar ratios, including two Group 3 waters, are more kinetically favorable to precipitate out ca-montmorillonite.

Inverse geochemical models were constructed to discern the suite and amount of mineral weathering necessary to create spring water compositions evolving from NADP-derived precipitation chemistry. Model phases and phase stoichiometries were based on field petrologic data (Table 1). Model inputs including mineral forcing constraints and favorable precipitating clays were determined from saturation indices and stability diagrams. Hydrochemically realistic models with a minimal number of solutions were created for 18 of the 20 springs. Two of the springs, IES-026 and IES-030 were not able to be modeled successfully. IES-26 likely inherits some part of its geochemical composition from the Owens River or leakage along the LAA. IES-030 has an anomalously high $^{87}\text{Sr}/^{86}\text{Sr}$ ratio compared to Sierra Nevada plutonic rocks and its general chemistry composition cannot be explained by weathering through the surrounding geology.

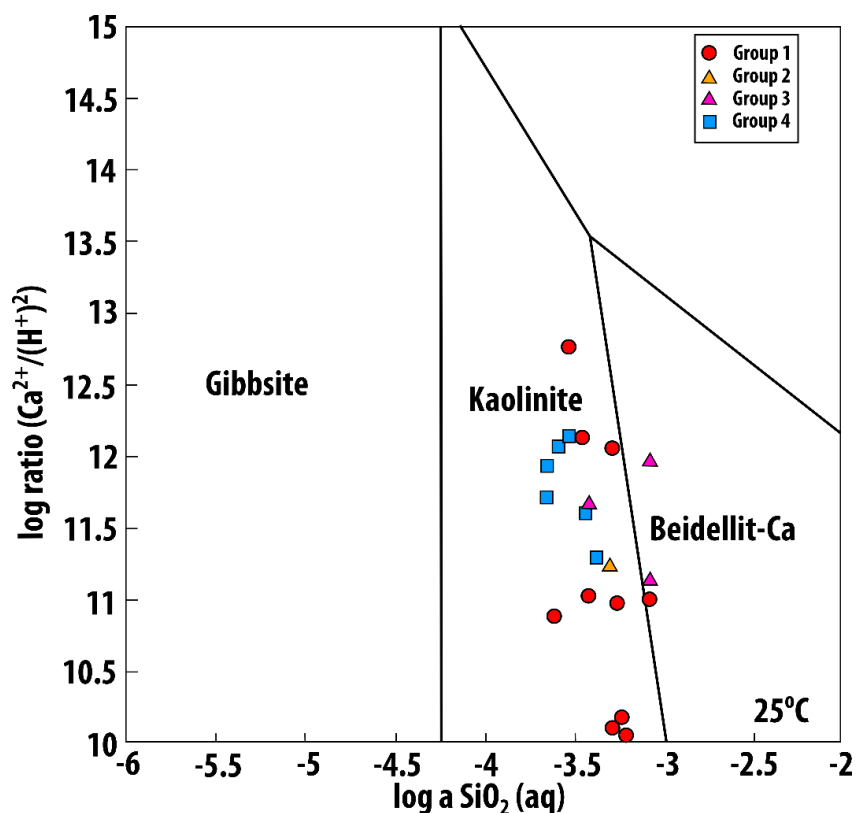


Figure 4.15: Diagram showing the log activity of SiO_2 vs log ratio $\text{Ca}^{2+}/(\text{H}^+)^2$ for Owens Valley spring water samples. Springs are symbolized by geochemical grouping. Mineral stability fields are bounded by the black lines. The majority of springs reside in the kaolinite stability field.

For the successfully modeled springs, CO_2 , gypsum, halite, calcite, K-spar, plagioclase, and biotite or hornblende are required to dissolve for every model. Either SiO_2 and kaolinite or montmorillonite are also required to precipitate in every model (Figure 4.16). Model results are highly influenced by the An composition of plagioclase. In some cases where the An value could not be well constrained from the petrologic data, multiple model results were considered across a suite of plagioclase compositions. Average model mol transfers are shown in Figure 4.16. The majority of spring waters only have one viable model. In contrast with Rademacher et al. (2001) and Blumhagen and Clark (2008), viable models for all springs require calcite as a phase, however mol transfer amounts are often small, except for Group 4 waters. Group 4 waters require large mol transfers of calcite, in terms of percent composition, to successfully model their geochemical compositions (Figure 4.16).

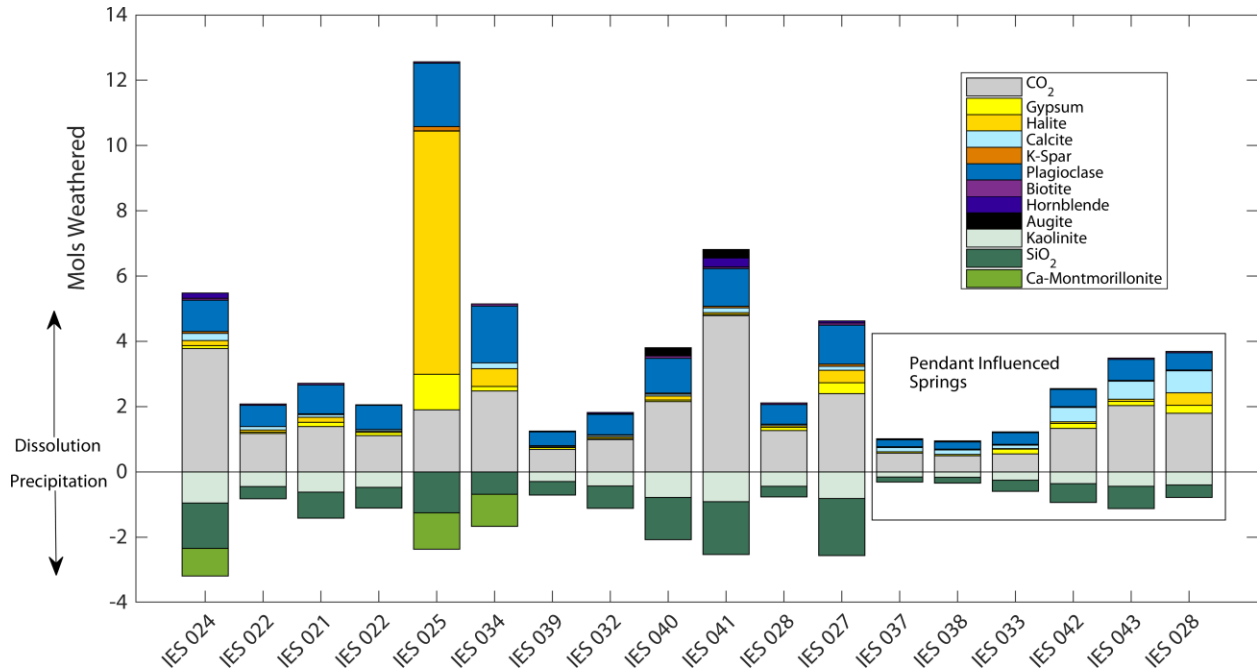


Figure 4.16: Results from NETPATH inverse geochemical modeling from NADP precipitation to spring geochemical compositions. Positive mol transfers indicate dissolution and negative mol transfers indicate precipitation. In instances where multiple models were found, the average of mol transfers is shown. Successful model solutions do not exist without including calcite in these models. Group 4 springs are indicated by the rectangular bounding box. These springs require large mol transfers (% wise) of calcite to successfully model their geochemical compositions.

4.6.5 Chloride, Chloride/Bromide, and Chlorine-36

The majority of Owens Valley spring waters ($n = 16$) have Cl^-/Br^- ratios ranging from (37-300) and are in the range of dilute to moderately evolved groundwaters ($\text{Cl}^-/\text{Br}^- \leq 300$) (Davis, 1998). Two springs, IES-028 and IES-034, are just above this threshold with ratios of 334 and 308, respectively. Two other springs show clear contributions from non-conservative sources of chloride and have Cl^-/Br^- ratios > 900 . These springs, whose local names may be an indicator of their outlier status, are Boron Springs A (IES-025) and Boron Springs B (IES-027). The linear trend observed when Cl^-/Br^- is plotted against $[\text{Cl}^-]$ suggests that chloride is being acquired conservatively for most spring waters (Figure 4.17A).

Preanthropogenic $^{36}\text{Cl}/\text{Cl}$ ratios of groundwater southern Great Basin range from 300-500 (Davis, 2003). This range is similar to modern (post bomb pulse) $^{36}\text{Cl}/\text{Cl}$ ratios in precipitation for the same area (Moysey et al., 2003). A clear trend is observed between Cl^- concentration and $^{36}\text{Cl}/\text{Cl}$ ratios of spring waters (Figure 4.17B). Springs with background or below background

$^{36}\text{Cl}/\text{Cl}$ ratios have higher amounts of chloride. Examining the relationship between $^{36}\text{Cl}/\text{Cl}$ ratio and ^3H concentration allows for distinguishing between submodern, modern, and bomb-pulse spring waters. As shown in Figure 4.17C, ^3H alone can distinguish modern water and bomb-pulse groundwater from submodern groundwater, however it is not possible to distinguish modern recharge from bomb-pulse recharge without ^{36}Cl as the tritium concentration is nonunique to both groups.

4.6.6 Strontium and $^{87}\text{Sr}/^{86}\text{Sr}$

Sr^{2+} concentrations show a strong linear relationship with Ca^{2+} , especially when separated out by geochemical grouping (Figure 4.18A). Group 1 waters sourcing flow from the Mount Whitney intrusive suite in the Lone Pine AOI show a diverging geochemical trend and acquire more Sr^{2+} per mol of Ca^{2+} compared to other Group 1 waters (Figure 4.18A).

For 19 out of the 20 springs, $^{87}\text{Sr}/^{86}\text{Sr}$ ratios fall in a range from 0.70729 to 0.71000. Most values are slightly above the expected window for eastern Sierra Mesozoic granitoids (0.70600-0.70800) (Chen and Tilton, 1991; Hirt, 2007; Chapman et al., 2015). One spring, IES-030, has an anomalously high $^{87}\text{Sr}/^{86}\text{Sr}$ ratio (0.71234) (not shown in Figure 4.18) in comparison to other spring waters that cannot be reconciled based on whole rock strontium ratios of the surrounding geology in the Warren Bench area. It is possible that this elevated ratio could be a result of weathering felsic dikes and masses in the area, chiefly aplite, pegmatite, and alaskite. Not considering the outlier value, average $^{87}\text{Sr}/^{86}\text{Sr}$ ratio for the geochemical groups are 0.70835, 0.70856, 0.70912, and 0.70927 for Groups 1-4, respectively. The average $^{87}\text{Sr}/^{86}\text{Sr}$ ratio for Group 4 waters plots closest to the expected range for Penn-Permian roof pendants (>0.710) based on whole rock values (Kistler and Petermann, 1973; Goff, 1991) and surface waters sourcing areas with roof pendants (Pretti and Stewart, 2002). This $^{87}\text{Sr}/^{86}\text{Sr}$ range is wide and highly variable even among different facies within the same roof pendant septa.

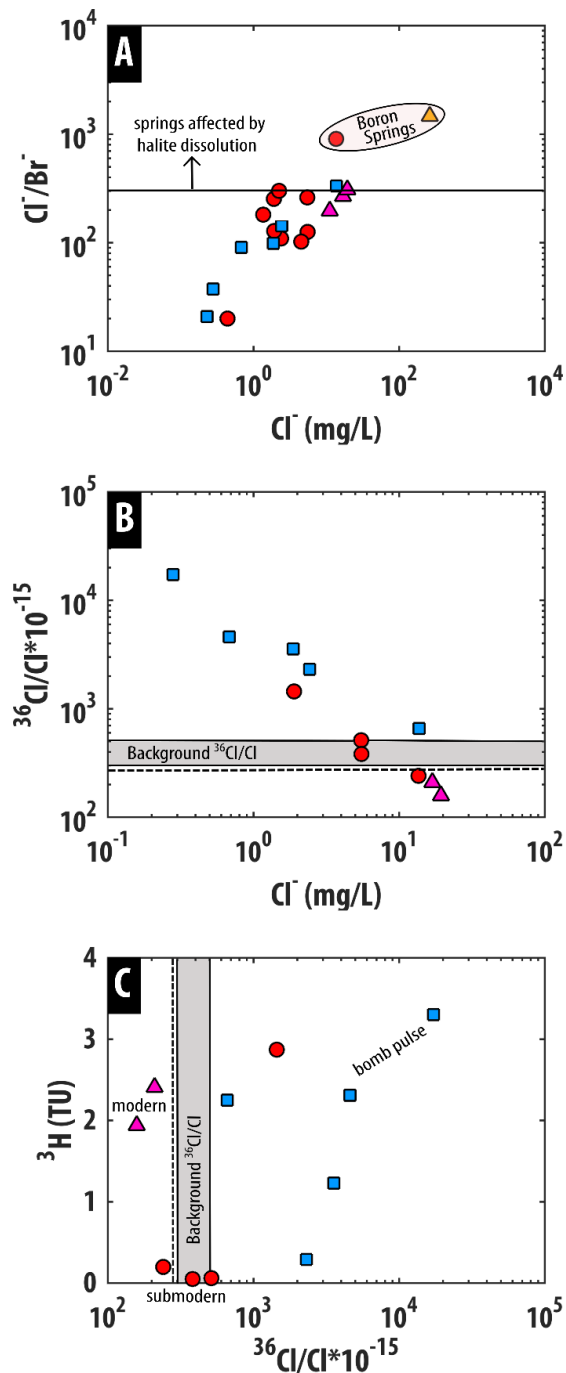


Figure 4.17: A) Relationship between $\log \text{Cl}^-$ concentration and Cl^-/Br^- ratios in spring waters. Springs below the black line are indicative of natural waters unaffected by halite dissolution. Two springs well above the line are Boron Spring A (IES-027) and Boron Spring B (IES-025). B) Relationship between $\log \text{Cl}^-$ concentration and $\log ^{36}\text{Cl}/\text{Cl}$. Preanthropogenic background $^{36}\text{Cl}/\text{Cl}$ ratios in groundwater from Davis et al. (2003) shown in the grey bounding box. Springs dilute with respect to chloride have elevated, bomb-pulse $^{36}\text{Cl}/\text{Cl}$. C) Relationship between $^{36}\text{Cl}/\text{Cl}$ ratio and ^3H (TU). This plot shows separation and mixing between submodern, bomb-pulse, and modern spring waters based on $^{36}\text{Cl}/\text{Cl}$ ratio and ^3H .

Mesozoic granitoid leachates have a narrow range of $^{87}\text{Sr}/^{86}\text{Sr}$ ratios (0.708462 - 708879) with an average isotopic value of 0.708598. These values are also elevated when compared to expected whole rock $^{87}\text{Sr}/^{86}\text{Sr}$ ratios for Mesozoic granitoids, however more closely match the ratios for spring waters. One sample was leached from the Bishop Tuff and this yielded a slightly higher $^{87}\text{Sr}/^{86}\text{Sr}$ ratio of 0.70948. This value closely matches the $^{87}\text{Sr}/^{86}\text{Sr}$ ratio of Birchim Cyn. Spring B (IES-034), which emerges directly out of the Bishop Tuff.

Results from general chemistry and inverse geochemical modeling were combined with $^{87}\text{Sr}/^{86}\text{Sr}$ ratios for leachates and spring waters. With the exception of IES-30, Owens Valley spring waters show a systematic trend of decreasing $\text{Ca}^{2+}/\text{Sr}^{2+}$ (Figure 4.18B) as a function of decreasing $^{87}\text{Sr}/^{86}\text{Sr}$. Blum et al. (1998) utilized Ca/Sr ratios to differentiate carbonate versus silicate weathering in a watershed with Ca sources from silicates, marble, and vein calcite. Group 4 waters, interpreted to be weathering a combination of Sierra Nevada granitoids and Penn-Permian roof pendants, fall within the $\text{Ca}^{2+}/\text{Sr}^{2+}$ range of 200-400 and have 6 of the 7 highest ratios. While Groups 1,2, and 3 do not show strontium isotope evolution as carbonate weathering increases as a function of overall weathering (carbonate/ (plagioclase + carbonate)), Group 4 waters show a linear decrease in $^{87}\text{Sr}/^{86}\text{Sr}$ (Figure 4.18C).

A simple metric like the amount of dissolved silica in solution has been found to increase with decreasing elevation in silicate watersheds (Drever and Zobrist, 1990) and thus can be inferred to represent residence time. Similarly, inverse model results like the amount of plagioclase weathered or kaolinite precipitated are informative in understanding how mineral weathering affects $^{87}\text{Sr}/^{86}\text{Sr}$. Spring waters in all geochemical groups show a systematic decrease in $^{87}\text{Sr}/^{86}\text{Sr}$ as a function of plagioclase weathering (Figure 4.18D), amount of clay mineral formation (Figure 4.18E), and silicate dissolution (Figure 4.18F). As each of these metrics increase, Owens Valley spring waters converge towards the whole rock $^{87}\text{Sr}/^{86}\text{Sr}$ range for Mesozoic Granitoids in Owens Valley and away from rock leaching values.

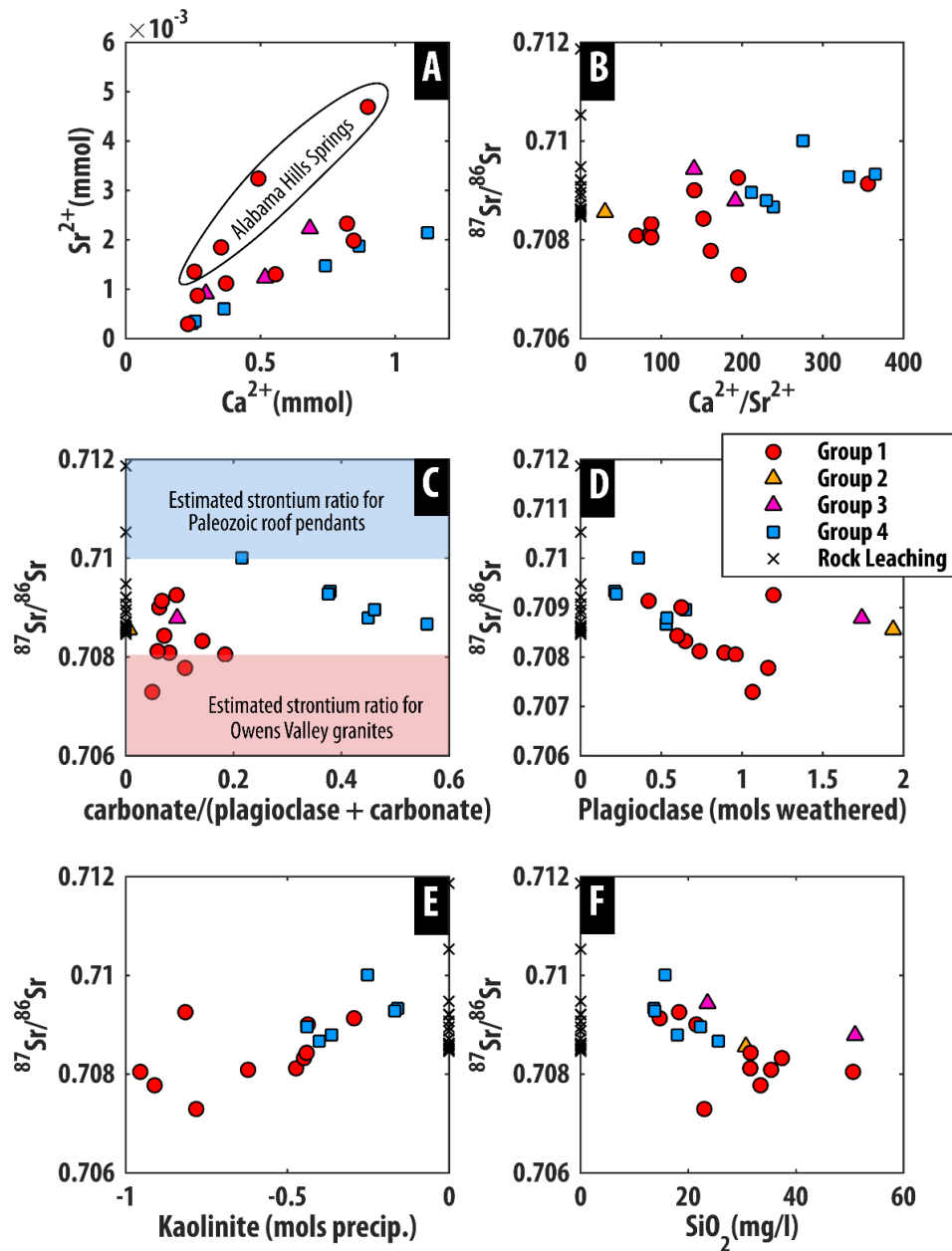


Figure 4.18: Relationships with $^{87}\text{Sr}/^{86}\text{Sr}$, geochemistry, and inverse modeling results for sampled spring waters. Springs are symbolized by geochemical grouping. For plots B-F rock leachate values for Sierra Nevada granitoids are symbolized by the black Xs. A) Relationship between strontium and calcium ion concentrations in sampled spring waters. Springs emerging on the western flank of the Alabama Hills are geochemically distinct from other Group 1 waters. B) Relationship between $^{87}\text{Sr}/^{86}\text{Sr}$ and $\text{Ca}^{2+}/\text{Sr}^{2+}$ ionic ratios in spring waters. C) Mols transfers of carbonate/(plagioclase + carbonate) from inverse geochemical models versus $^{87}\text{Sr}/^{86}\text{Sr}$. The expected strontium ratio for Owens Valley granites (0.706-0.708) is shown in the pink shaded area. The estimated strontium ratio for Paleozoic roof pendants is shown in the blue shaded area. D) Average plagioclase mol transfer from inverse geochemical models versus $^{87}\text{Sr}/^{86}\text{Sr}$. E) Average kaolinite mol transfer (negative for precipitation) from inverse geochemical models versus $^{87}\text{Sr}/^{86}\text{Sr}$. F) Relationship between silica (as SiO_2) and $^{87}\text{Sr}/^{86}\text{Sr}$.

Table 4.5. Raw isotope data, corrected radiocarbon ages, and age partition distinctions for Owens Valley springs.

Table 4.5

Sample ID	$\delta^2\text{H}$ ± 0.83	$\delta^{18}\text{O}$ ± 0.08	d_{excess} (‰)	$^{87}\text{Sr}/^{86}\text{Sr}$ ± 0.00005	^3H (TU) ± 0.1	$^{36}\text{Cl}/\text{Cl}$ Ratio (* 10^{-15})	$^{36}\text{Cl}/\text{Cl}$ Std. Dev. (* 10^{-15})	$\delta^{13}\text{C}$ (‰)	^{14}C (pmc)	^{14}C Age		Age
										Vogel	Tamers	Partition
IES-021	-120.1	-16.42	11.3	0.70809	0.06	513.9	13.1	-12.4	95.4 ^a	modern	modern	Old
IES-022	-124.1	-16.92	11.3	0.70812	0.11	-	-	-9.7	98.28 ^a	modern	modern	Old
IES-023	-121.0	-16.29	9.3	0.70832	0.01	-	-	-7.4	95.54 ^a	modern	modern	Old
IES-024	-123.5	-16.64	9.7	0.70805	0.05	381.9	11.4	-4.2	53.81	3779	919	Old
IES-025	-126.9	-16.75	7.1	0.70856	1.01	-	-	-	-	-	-	Young ^b
IES-026	-116.8	-15.26	5.3	0.70943	2.41	209.7	5.7	-6.7	92.19	modern	modern	Young ^c
IES-027	-122.7	-16.73	11.2	0.70924	0.2	240.3	6.3	-4.6	82.32	265	modern	Old
IES-028	-116.9	-15.98	11.0	0.70867	2.25	658.6	11.5	-7.4	73.85	1162	modern	Young
IES-029	-124.2	-16.93	11.3	0.70843	2.87	1445.2	66	-9.5	93.28	modern	modern	Young
IES-030	-124.5	-16.50	7.4	0.71234	0.07	-	-	-	-	-	-	Old
IES-032	-131.8	-17.63	9.3	0.70901	0.11	-	-	-	-	-	-	Old
IES-033	-131.0	-17.87	11.9	0.71001	2.31	4599.0	766	-6.7	91.05	modern	modern	Young
IES-034	-116.9	-15.21	4.7	0.70882	1.94	157.9	5.1	-7.3	81.07	391	modern	Young ^c
IES-037	-134.2	-17.97	9.6	0.70933	3.11	-	-	-8.9	88.9	-	-	Young
IES-038	-132.2	-17.90	11.0	0.70928	3.3	17246.2	678	-15	79.06	598	modern	Young
IES-039	-132.5	-18.03	11.8	0.70913	3	-	-	-	-	-	-	Young
IES-040	-126.3	-17.41	13.0	0.70729	0.04	-	-	-10	86.39	modern	modern	Old
IES-041	-126.6	-16.84	8.1	0.70778	0.83	-	-	-10.2	98.89	modern	modern	Young
IES-042	-119.2	-16.35	11.6	0.70879	1.23	3562.1	88.0	-7.6	91.46	modern	modern	Young
IES-043	-120.3	-16.42	11.0	0.70896	0.29	2313.8	29.3	-12.5	86.6	modern	modern	Young

^a Samples likely affected by atmospheric contamination

^b Samples omitted from age partitioning related to geochemical trends based on influence from brines

^c Samples omitted from age partitioning related to geochemical trends based on influence from surface water

4.6.7 Noble gas and radiocarbon trends among all springs

Raw carbon isotope data and corrected radiocarbon ages are shown in Table 4.5. Corrected radiocarbon ages are shown using two correction models, Vogel (1970) and Tamers (1975), are shown in Table 4.5. Using the Vogel correction model, five springs (IES-024, IES-027, IES-028, IES-034, and IES-038) have non-modern radiocarbon ages ranging from 265 years (IES-027) to 3779 years (IES-024). Using the Tamers correction model, only one spring, IES-024, has a non-modern radiocarbon age (919 years). Because only a minimal number of springs have non-modern radiocarbon ages, radiocarbon activity is used to examine trends with radiocarbon data and other hydrochemical analytes

There is a poor relationship between $\delta^{13}\text{C}$ (‰) and ^{14}C activity (pmc) for Owens Valley spring waters (Figure 4.19A). Evolutionary trends are not discernable among geochemical groups, let alone when considering all spring waters. This result is similar to poor $\delta^{13}\text{C}$ vs ^{14}C activity relationships in Owens Valley groundwaters by the USGS (Figure 4.8) and in other Sierra Nevada groundwaters (e.g., Blumhagen and Clark, 2008). Repeat sampling for Owens Valley spring waters has found that $\delta^{13}\text{C}$ is highly variable temporally while ^{14}C activity does not change significantly. These results suggest that ^{13}C evolution in Owens Valley groundwaters, at least at large scales, is a poor indicator of ^{14}C dilution. Thus, calculating dilution factors and radiocarbon ages with various correction models using ^{13}C might be highly suspect especially when the $\delta^{13}\text{C}$ of recharging groundwater is also highly uncertain. However, the fact that ^{14}C activities are stable temporally and that there is a relationship between ^{14}C activity and HCO_3^- among geochemical groupings (Figure 4.19B) is conducive to using ^{14}C as a relative indicator of residence time.

Raw noble gas data and calculated parameters are shown in Table 4.6. The relationship between ^{14}C activity and $^3\text{He}/^4\text{He}$ ratios of spring waters normalized to the $^3\text{He}/^4\text{He}$ ratio of atmospheric air (R/R_a) is shown in Figure 4.19C. Springs with lower ^{14}C activities correspond to springs with lower R/R_a . All springs with the exception IES-029 have $R/R_a < 1$. IES-029 emerges in the vicinity of the Big Pine Volcanic Field near Red Mountain, one of the major volcanic cones in the area. When Group 3 waters are not considered, there are positive correlations between lithium concentration and R/R_a ($R^2 = 0.88$, $p < 0.05$) (Figure 4.19D) and spring discharge temperature and R/R_a ($R^2 = 0.54$, $p < 0.05$) (Figure 4.19E). Lithium concentrations in groundwater are often correlated with geothermal heating (Coolbaugh et al., 2002) These relationships suggest that R/R_a is an indicator of both residence time (^{14}C) and groundwater circulation (Li & spring temperature) for Owens Valley spring waters.

Figure 4.20A shows the Ne/He elemental ratio versus R/R_a for Owens Valley spring waters. Similar to the result found by Aeschbach-Hertig et al. (2000), Owens Valley spring waters define a mixing line between radiogenic and atmospheric endmembers for spring water samples. IES-029 is well above this mixing line. The relationship between ^{14}C activity and terrigenous ^4He is shown in Figure 4.20B. Petrologic differences in granitic rocks, and subsequent differences in uranium and thorium contents in the rock matrix, likely lead to differences between accumulated ^4He and ^{14}C activity and preclude the use of ^4He as an accumulation tracer of groundwater residence time.

Noble gas recharge parameters are shown in Table 4.6. Noble gas recharge elevations derived from the ELR method (Zuber et al., 1995; Manning and Solomon, 2003; Doyle et al., 2015; Peters et al., 2018) range from 1900-3400 mamsl with an average recharge elevation of 2820 mamsl (Figure 4.22). Springs further away from the mountain front (i.e., springs near the Alabama Hills) have lower calculated recharge elevations. Recharge temperatures using the median elevation between the Owens Valley basin floor and the Sierra Nevada crest (2600 m) as a solving parameter range from 1.6°C to 7.7°C with an average recharge temperature of 4.3°C. Recharge temperatures derived using the ELR method are within a range of $\pm 3.5^\circ\text{C}$ of the recharge temperatures calculated using a median elevation (Table 4.6). The amount of offset depends on if the calculated recharge elevation using the ELR method is above the median elevation (cooler) or below the median elevation (warmer).

Table 4.6. Raw noble gas data and derived parameters from Noble90 for the Owens Valley springs.

Table 6

Sample ID	Raw Data						Calculated parameters			
	Ar total (ccSTP/g)	Ne total (ccSTP/g)	Kr total (ccSTP/g)	Xe total (ccSTP/g)	⁴ He (ccSTP/g)	R/R _a	Recharge Elevation ^a (meters)	Recharge Temp ^b (°C)	³ H/ ³ He Age ^c (yrs)	⁴ He _{terr} ^b (ccSTP/g)
IES-021	3.17E-04	1.65E-07	7.51E-08	1.11E-08	4.71E-08	0.807	2500	6.1	-	9.07E-09
IES-022	-	-	-	-	-	-	-	-	-	-
IES-023	-	-	-	-	-	-	-	-	-	-
IES-024	3.13E-04	1.67E-07	7.17E-08	1.04E-08	1.89E-07	0.308	1900	7.7	-	1.50E-07
IES-025	-	-	-	-	-	-	-	-	-	-
IES-026	3.38E-04	1.56E-07	8.23E-08	1.21E-08	3.69E-08	0.978	3400	3.2	7.2	1.86E-09
IES-027	3.16E-04	1.50E-07	7.21E-08	1.02E-08	5.51E-08	0.691	1900	7.4	-	2.06E-08
IES-028	3.14E-04	1.44E-07	7.64E-08	1.18E-08	2.63E-07	0.469	3000	5.0	56.4	2.28E-07
IES-029	3.70E-04	1.92E-07	8.86E-08	1.25E-08	1.46E-07	1.036	2500 ^c	2.3	54.7	1.01E-07
IES-030	-	-	-	-	-	-	-	-	-	-
IES-032	-	-	-	-	-	-	-	-	-	-
IES-033*	-	-	-	-	-	-	-	-	-	-
IES-034	1.42E-04	1.17E-07	2.59E-08	3.36E-09	7.90E-08	0.595	-	48.8 ^d	30.2	4.73E-08
IES-037	3.35E-04	1.58E-07	8.19E-08	1.21E-08	3.68E-08	0.986	3400	3.4	4.9	1.54E-09
IES-038	-	-	-	-	-	-	-	-	-	-
IES-039	-	-	-	-	-	-	-	-	-	-
IES-040	3.35E-04	1.73E-07	7.99E-08	1.26E-08	4.10E-08	0.984	3300	3.5	-	1.70E-09
IES-041	3.53E-04	1.70E-07	8.86E-08	1.29E-08	4.09E-08	0.972	3000 ^c	1.6	17.6	2.74E-09
IES-042	3.38E-04	1.66E-07	8.13E-08	1.21E-08	5.17E-08	0.879	3300	3.6	28.2	1.41E-08
IES-043	3.33E-04	1.74E-07	8.16E-08	1.21E-08	5.09E-08	0.878	3200	3.9	44.0	1.11E-08

*Noble gas sampled collected but stripped

^aCalculated with the ELR intersection method

^bCalculated assuming a median recharge elevation of 2600 meters

^cCalculated using partial re-equilibration (PR) rather than closed system equilibration

^dRecharge temperature elevated, however sample does not appear to be stripped

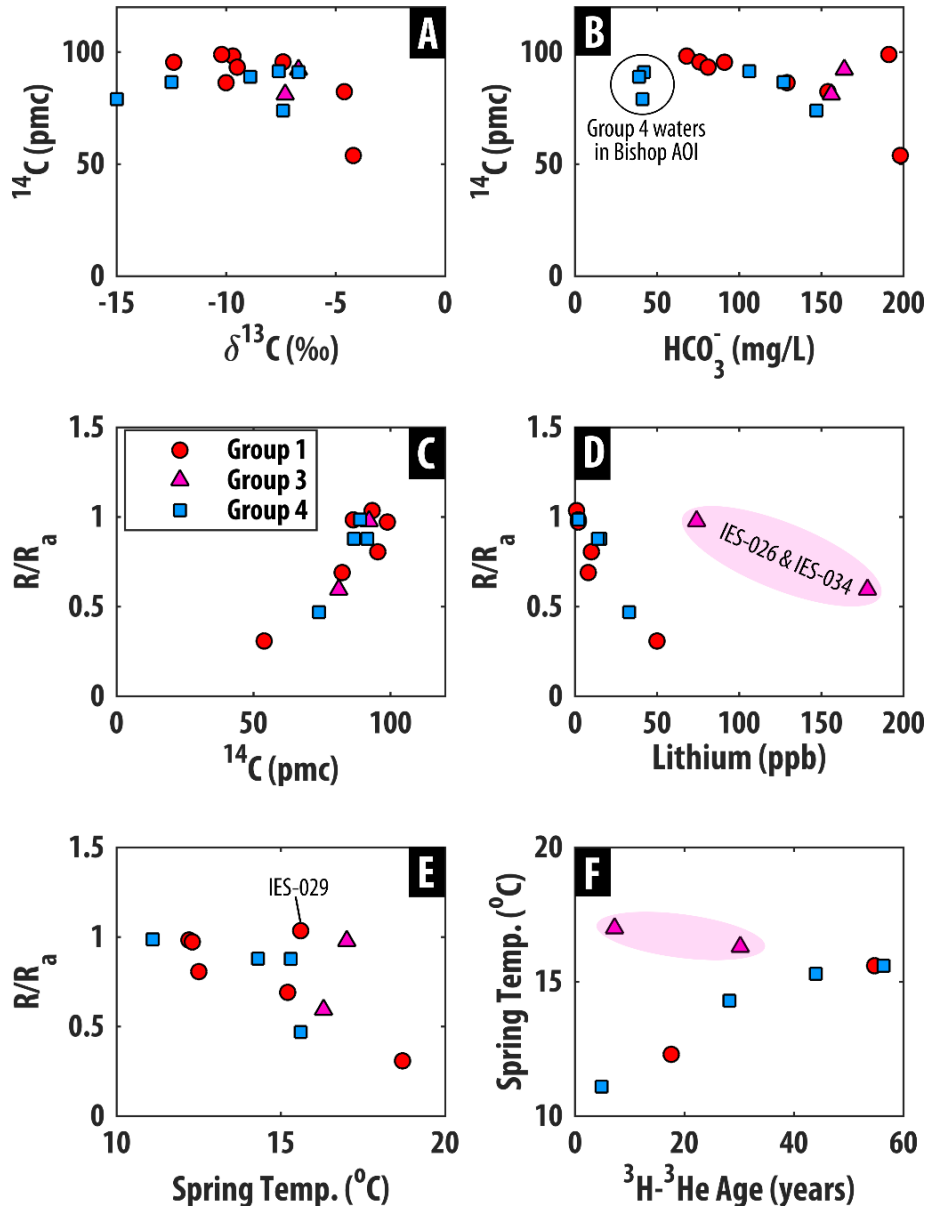


Figure 4.19: Trends with radiocarbon, noble gas, and temperature data. A) Shows poor trend between $\delta^{13}\text{C}$ (‰) versus ^{14}C activity (pmc) for Owens Valley spring waters. B) Relationship between bicarbonate concentration and ^{14}C activity (pmc) for Owens Valley spring waters. C) Relationship between ^{14}C activity and $^3\text{He}/^4\text{He}$ ratio normalized to the $^3\text{He}/^4\text{He}$ ratio of air (R/R_a). Springs with lower R/R_a ratios have lower ^{14}C activities. D) Relationship between lithium concentration (ppb) and R/R_a . There is a strong correlation with the exception of Group 3 waters. E) Relationship between spring discharge temperature and R/R_a . Spring waters with lower R/R_a ratios, interpreted to be circulating deeper and at increased flowpath lengths in order to accumulate excess ^4He , have increased discharge temperatures. F) ^3H - ^3He age versus spring temperature. As apparent age increases, spring temperature increases. Group 3 waters fall off the trendline.

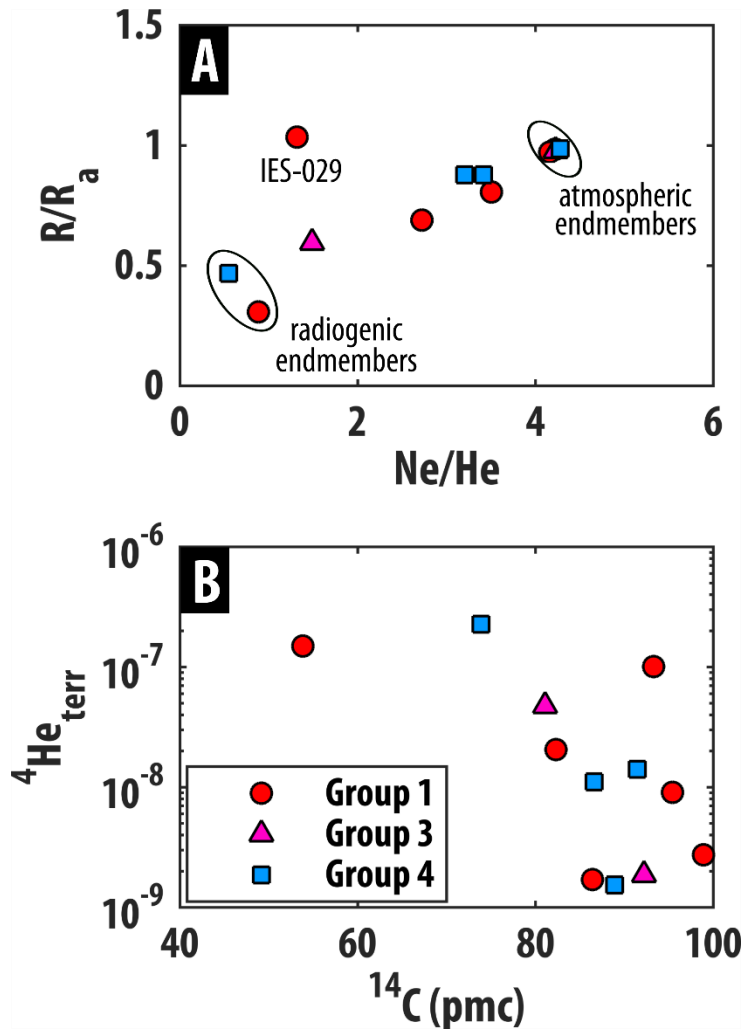


Figure 4.20: A) Ne/He elemental ratio vs R/R_a . These data define a mixing line between radiogenic and atmospheric endmembers for spring water samples. IES-029, which emerges near Red Mountain in the vicinity of the Big Pine Volcanic Field, is well above this mixing line. B) Relationship between ^{14}C activity and terrigenic ^4He . Petrologic differences in granitic rocks, and subsequent differences in uranium and thorium contents in the rock matrix, likely lead to differences between accumulated $^4\text{He}_{\text{terr}}$ and ^{14}C activity.

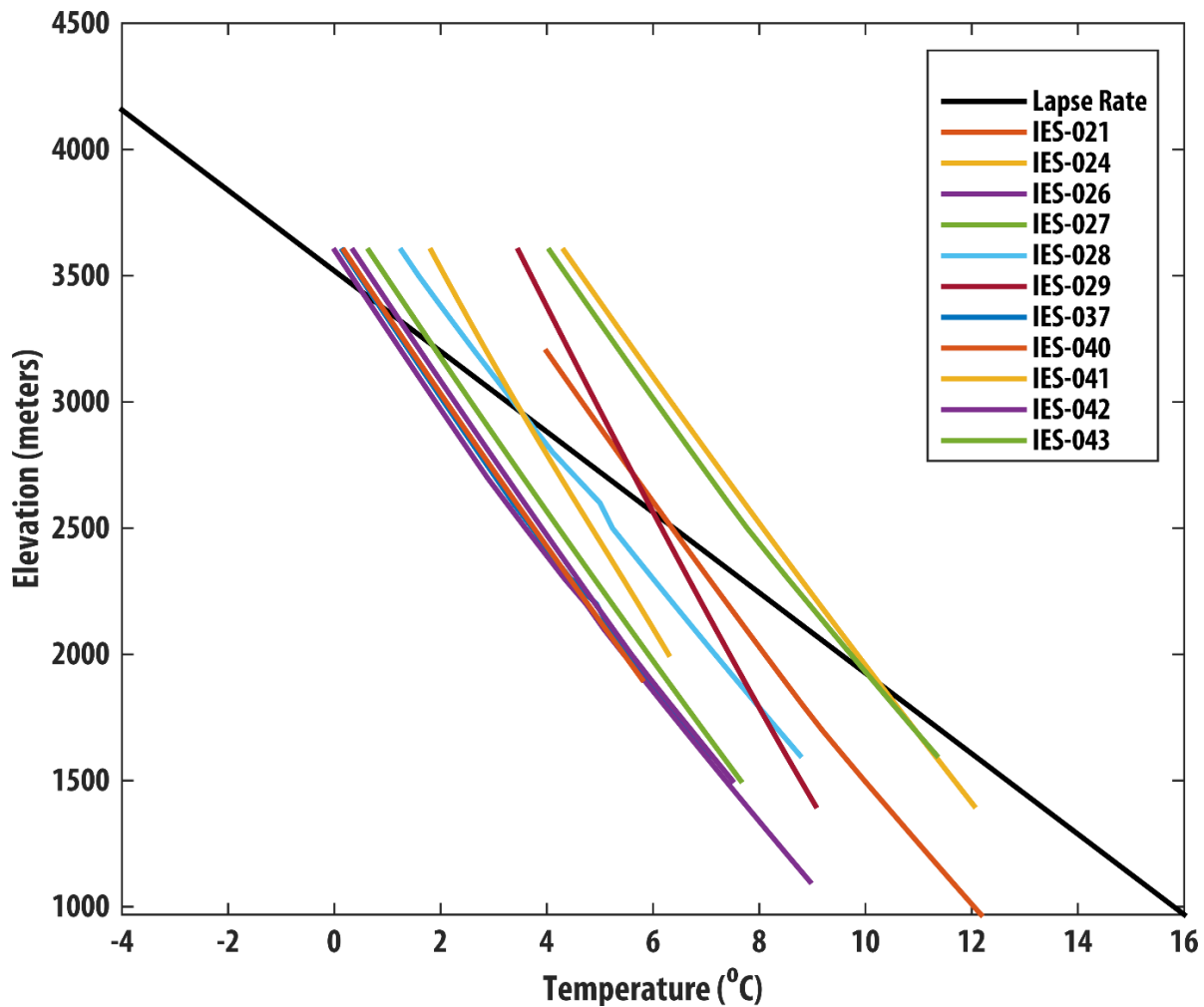


Figure 4.21: Shows recharge temperature solved at 100m increments from the elevation of the spring emergence to the local high elevation point. Intersection with the environmental lapse rate can be used to estimate recharge elevation (H) and calculate recharge temperature when H is unknown as shown by Zuber et al. (1995), Aeschbach-Hertig et al. (1999), Doyle et al. (2015), and Peters et al. (2018).

4.6.8 Age partitioning and spring residence times

Age partitioning resulted in 12 springs classified as “young” or having a large proportion of their discharge attributed to water recharging during the last 70 years. Ten of these springs exhibited ^3H concentrations greater than 0.2 TU and had $^{36}\text{Cl}/\text{Cl}$ well above historical background ratios ($659\text{-}17,246 \cdot 10^{-15}$). These springs are interpreted to be discharging a large proportion of water recharged during the 1950s-1960s bomb pulse. Two of these springs (IES-026 & IES-034) exhibited ^3H concentrations greater than 0.2 TU yet had $^{36}\text{Cl}/\text{Cl}$ well below background ($158\text{-}210 \cdot 10^{-15}$). These springs are interpreted to be discharging modern, post-bomb pulse water. This

interpretation agrees with geochemical separations, $^{87}\text{Sr}/^{86}\text{Sr}$, and spatial contextualization where these two springs are receiving a substantial proportion of water from Owens River losing conditions or LAA leakage.

With the exception of one spring, IES-028, all “young” springs have ^{14}C activities greater than 79 percent modern carbon (pmc) with a mean activity of 88 pmc. Radiocarbon corrections for springs activities yield negative ages, designated as modern waters, using all correction methods other than the empirical Vogel method (Table 4.5). Unfortunately, not all 12 “young” springs were suitable for noble gas collection and one sample was determined to be stripped, so ^3H - ^3He ages are only reported for 8 springs (Table 4.6). ^3H - ^3He ages for these spring waters range from 5-56 years, with a mean apparent age of 30 years. There is a very strong trend between ^3H - ^3He age and discharge temperature for “young” springs with the exception of Group 3 waters interpreted to be influenced by surface water (Figure 4.19F). Springs with older ^3H - ^3He ages are warmer while springs with younger ^3H - ^3He ages are cooler. These apparent ages are in agreement with the interpretation that the majority of these springs are discharging a large proportion of groundwater that was recharged since the bomb-pulse.

Age partitioning resulted in 8 springs being classified as “old”. These springs are interpreted as having a minimal proportion of recharge since the bomb-pulse based on ^3H concentrations (< 0.2 TU) and $^{36}\text{Cl}/\text{Cl}$ ratios in the range of preanthropogenic waters. ^3H - ^3He ages are not reported for these springs because waters with ^3H values as low as 0.2 TU are not appropriate for ^3H - ^3He age dating. Radiocarbon ages for these springs range from modern to several thousand years with corresponding ^{14}C activities from 86.4-53.8 with a mean activity of 74 pmc. Three springs in the Alabama Hills region have ^3H ranging from 0.06- 0.11 TU, however, ^{14}C activities between 98-95 pmc. These springs are extremely low discharge and were noted in the field as questionable for radiocarbon dating based on seepy, diffuse conditions (Figure 4.22). It is likely that these three samples have equilibrated with atmospheric CO_2 and that these ^{14}C activities are not representative of ^3H dead waters.



Figure 4.22: Field photos (March 2016) showing spring emergence conditions for IES-021, IES-022, and IES-023. Samples for ^{14}C analysis were collected from these springs despite seepy, diffuse, and low discharge emergence conditions. While ^3H results for all three springs were all ≤ 0.11 TU, ^{14}C activities were all measured as > 95 pmc. While ^3H is not susceptible to atmospheric contamination or equilibration, we interpret the ^{14}C activities to be contaminated and thus not representative of the actual residence times of these spring waters.

4.6.9 Age partitioning trends

There are substantial physical, geochemical, and isotopic differences between “young” and “old” waters as indicated by Figure 4.23. Waters interpreted to be interacting with surface waters and/or basinal brines were excluded from age partitioning analysis. These geochemical and

isotopic differences are supported by prior work (Chapter 2), that found that riparian, groundwater-dependent vegetation surrounding Owens Valley springs discharging a large proportion of old groundwater were better able to tolerate the 2011-2017 California drought than springs discharging a large proportion of bomb pulse or modern recharge.

“Old” springs are warmer on average (Figure 4.23A) and have a warmer range of temperature values in comparison to the average and range for “young” springs (value). Chloride is being inherited conservatively for most spring waters ($n = 18$) (Figure 4.23A) and “old” springs have higher average chloride concentrations (Figure 4.23B) in comparison to “young” spring waters. “Old” springs also have an elevated range of TDS concentrations (Figure 4.23C) when compared to the range for “young” springs. Additionally, the results of inverse geochemical modeling suggest that geochemical fluxes from “old” springs are substantially higher than from “young” springs as evidenced by the weathering of plagioclase, a ubiquitous mineral found in Mesozoic granitoids and volcanics across the study area (Figure 4.23D)

There is also geochemical separation between “old” and “young” springs based on strontium isotopes and strontium ionic ratios. “Old” spring waters have a lower average $^{87}\text{Sr}/^{86}\text{Sr}$ ratio closer to the expected range for whole rock values for Sierra Nevada granitoids (0.706-0.708). In comparison, “young” springs have a higher average $^{87}\text{Sr}/^{86}\text{Sr}$ composition (value) that is closer to Sierra Nevada granitoid leachate from this study (value) than the expected range for whole rocks (Figure 4.23E). This same separation between “young” and “old” spring waters is even more distinct when comparing $\text{Ca}^{2+}/\text{Sr}^{2+}$ ratios (Figure 4.23F).

$^3\text{He}/^4\text{He}$ ratios normalized to the $^3\text{He}/^4\text{He}$ ratio of atmospheric air (R/R_a) are lower on average for “old” springs than for “young” springs. This observation is consistent with warmer discharge temperatures (Figure 4.23E) and increased solute loads in older and deeper circulating groundwaters. Finally, noble gas recharge temperatures (NGRT) are also warmer for “old” spring waters than for “young” spring waters (Figure 4.23H). While this may seem counterintuitive, “old” spring waters are generally further away from the regional divide (e.g., springs emerging upgradient of the Alabama Hills) and likely source larger aquifer volumes from a broader spatial area.

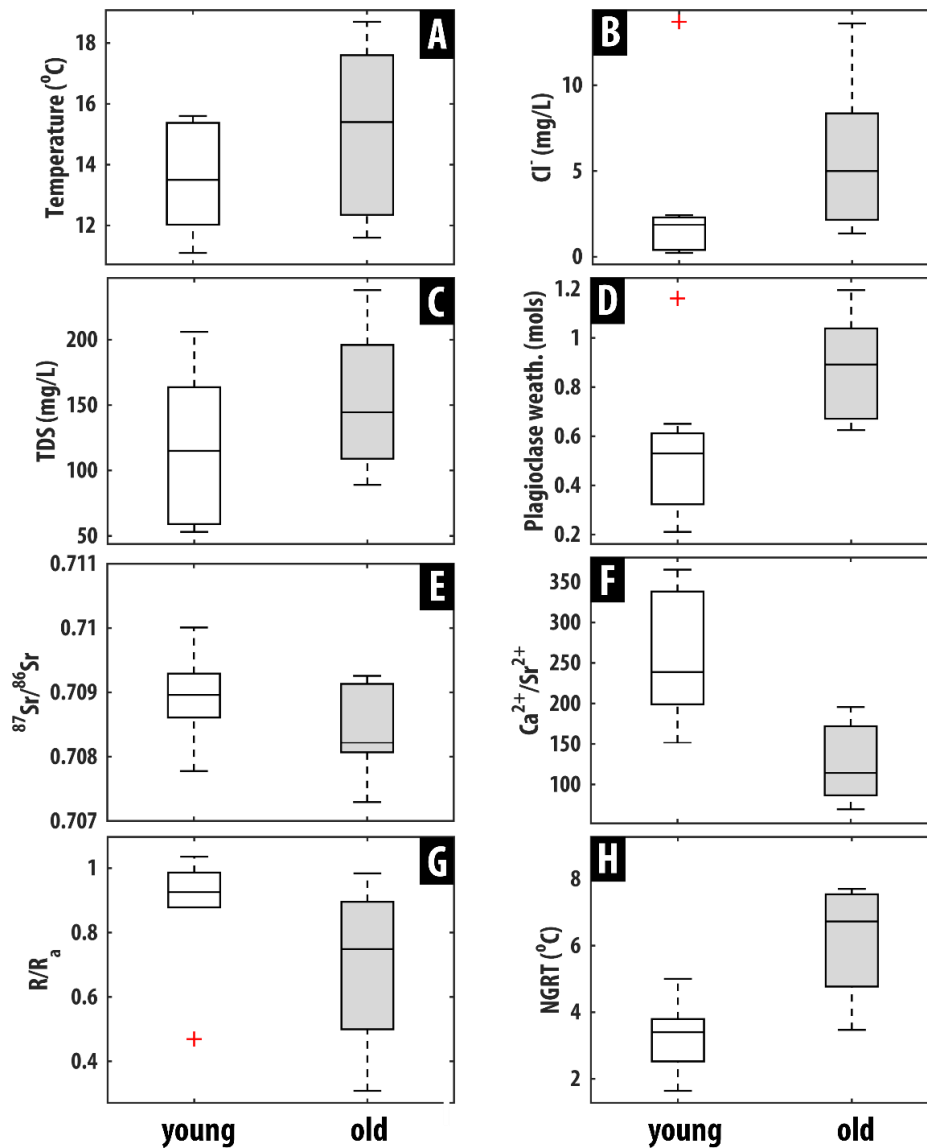


Figure 4.23: Boxplots showing geochemical and isotopic differences between “young” and “old” spring waters. The central mark on each box plot represents the median value while the bottom and top of each box represent the 25th and 75th percentiles, respectively. Whiskers extend to minimum and maximum values not considered to be outliers. Outliers, if applicable, are shown by the red crosses. Differences between young and old waters are shown for spring discharge temperature (A), chloride concentration (B), total dissolved solids (C), plagioclase weathered from NETPATH inverse geochemical models (D), $^{87}\text{Sr}/^{86}\text{Sr}$ (E), $\text{Ca}^{2+}/\text{Sr}^{2+}$ (F), $^3\text{He}/^4\text{He}$ ratio normalized to the $^3\text{He}/^4\text{He}$ ratio of air (R/R_a) (G), and noble gas recharge temperature computed using the median elevation method (H).

4.7 Discussion

4.7.1 Spring sourcing and contributing areas

Delineating contributing areas to springs is an acknowledged problem in hydrogeology because groundwater divides are inherently different than topographic surface waters divides (Frisbee et al., 2013). In order to understand the dominant controls on geochemical evolution with increased spatial scale and residence time, it is first necessary to determine some conceptual bounds on the extent of spring contributing areas in order to identify likely host aquifers. The Sierra Nevada batholith is both long and wide and it is unknown how fracture porosity and interconnectivity change with depth in the bedrock. Therefore, it is unknown how fracture networks route groundwater flow to intermediate and regional-scale springs. However, spring discharge temperatures, stable isotopes, and noble gas recharge elevations and temperatures can inform conceptual models for contributing areas to mountain front emergences emerging at the base of the eastern Sierra Nevada.

4.7.1.1 Spring temperature

The positive correlation between spring discharge temperature and elevation (Figure 4.9A) suggests that higher elevation springs are sourcing shorter, more local scale flowpaths and lower elevation springs are sourcing longer, deeper flowpaths. Elevation is a rough proxy for distance to drainage divide, and therefore, increasing flowpath length (Figure 4.9B). The majority of springs fall above the calculated local annual ELR and thus can be interpreted to potentially indicate geothermal heating as a result of groundwater circulation in the mountain block. However, none of these springs have elevated enough temperatures to be classified as warm or hot springs indicative of geothermal heating as a result of deep circulation.

4.7.1.2 Stable isotopes of spring waters as indicators of the geographic extent of recharge

$\delta^2\text{H}$ and $\delta^{18}\text{O}$ values from the USGS (NWIS) and from this study display a dependence on geographic location within Owens Valley (Figure 4.10B). Isotopically light samples are found in the Round Valley area west of Bishop, CA and near Big Pine, CA in the northern part of Owens Valley. These samples correspond to isotopically depleted areas in the eastern Sierra identified by

Friedman and Smith (1972). Isotopically enriched samples are found in southern portions of the valley (near Independence, CA and Lone Pine, CA) and at lower-lying basin locations (IES-026 and IES-034). High resolution deuterium contours of eastern Sierra Nevada winter precipitation from Friedman and Smith (1972) support an interpretation that mountain front Owens Valley spring waters are sourcing the majority of their recharge from east of the Sierra Nevada drainage divide, otherwise deuterium contents would likely be more depleted. These results combine to provide support an interpretation that recharge to springs is locally sourced (east of the Sierra Nevada drainage divide) and geographically isolated by region within Owens Valley.

The strong influence of geography makes it challenging for stable isotopes to serve as recharge elevation tracers at a regional scale. Although $\delta^2\text{H}$ and $\delta^{18}\text{O}$ are weakly correlated with elevation (Figure 4.11), these relationships are not strong enough to derive potential recharge elevations as illustrated by James et al. (2000). However, $\delta^2\text{H}$ and $\delta^{18}\text{O}$ still have utility in distinguishing sources and geographic location of recharge. $\delta^2\text{H}$ and $\delta^{18}\text{O}$ values from 18 springs, including the basinal brine (IES-025), are consistent with snowmelt-derived recharge from the eastern Sierra Nevada. Dual isotope and d_{excess} values suggest that IES-026 and IES-034, both of which lie towards the geographic center of the basin, are not primarily sourcing snowmelt derived recharge and thus are probably not indicative of flowpaths with increased scale from high elevation areas. These springs are likely discharging recharge from lower elevations or recharge with a higher percentage derived from rainfall as opposed to snowmelt.

4.7.1.3 Noble gas recharge parameters

Noble gas recharge elevations derived from the ELR method indicate that the majority of recharge is occurring below the Sierra Nevada crest at elevations between 1900 and 3400 mamsl. This range of elevations is found directly upgradient for most of the springs. Noble gas recharge temperatures, both from the ELR method (avg. 4.0°C) and the median elevation method (avg. 4.3°C) indicate that mountain front springs in Owens Valley source cold recharge, likely snowmelt. Springs further away from the drainage divide like those in the Alabama Hills (IES-021 & IES-024) or near Red Mountain (IES-029) may have greater recharge accumulation zones and thus decreased recharge elevations and increased recharge temperatures. These metrics serve as an important baseline for evaluating how these springs will respond to changes in recharge due to climate change if the snowline increases. The coupling of these results with interpretations from

$\delta^2\text{H}$ and $\delta^{18}\text{O}$ (i.e., recharge is supporting springs is geographically limited) and spring discharge temperatures leads us to infer that the plutons and geologic units upgradient of springs are the primary aquifers supplying springflow and that spring contributing areas are spatially limited in extent. While some springs may have long groundwater residence times, this does not necessarily imply large aquifer volumes.

4.7.2 The influence of local geology on geochemistry

Local-scale flowpath distributions capture a limited set of geological variability present in bedrock. However, geologic heterogeneity increases with increasing spatial scale and becomes the primary driver of geochemical evolution. This relationship is clearly shown by the geochemical patterns exhibited in Owens Valley spring waters where four dominant geochemical groups were identified. These groups can be attributed to petrologic differences in probable spring contributing areas based on information gleaned from stable isotopes (spatial extent of recharge) and noble gases (recharge elevation and recharge temperature).

Group 1 spring waters are the most abundant and represent groundwater evolving as a result of rock-water interaction with Sierra Nevada plutonic rocks (i.e., alaskite, quartz monzonite, granodiorite, and diorite, quartz diorite, and hornblende gabbro). Group 1 has the most intragroup geochemical variation and this can be attributed to the widely varying petrologic compositions of the plutons supplying flow to springs (Table 1). Subgroups can be identified from within this group that are controlled by local geology. For example, springs downgradient of the Mount Whitney Intrusive Suite emerging from the biotite monzogranite of the Alabama Hills have a separate Sr^{2+} vs Ca^{2+} evolutionary line when compared to other Group 1 waters (Figure 4.18A). Springs with $\text{Mg}^{2+}/\text{K}^+ \geq 3$ (Figure 4.14C) can be explained by upgradient presence of the either granodiorites or diorite/quartz diorite/hornblende gabbro.

Groups 2 and 3 are both outlier groups and do not conform to the inferred conceptual model where solute concentrations increase with increasing spatial scale. Group 2 consists of one spring, IES-025, an Na-Cl type seep emerging on the eastern side of the Alabama Hills. This spring is incredibly saline and geochemically evolved compared to other spring waters. Both its geochemistry and landscape placement are indicative of interaction with alluvial material and/or basinal evaporite deposits. However, its stable isotopic signature is depleted compared to other springs emerging at low elevations (i.e., IES-026 and IES-034), perhaps indicating that basinal

brines similar to IES-025 may be sourced from snowmelt recharge at higher elevations. There are numerous lines of evidence supporting a connection between surface water features (Owens River and LAA) and at least two of the three Group 3 waters (IES-026 and IES-034). This evidence includes: 1) enrichment in stable isotope ($\delta^2\text{H}$ and $\delta^{18}\text{O}$) and deuterium excess values, 2) geochemical similarity to surface water features (Figure 4.12), 3) and enrichment in lithium concentration (Figure 4.19D), 4) modern, post-bomb residence times despite their landscape placement far away from where recharge predominately occurs, and 5) spatial proximity to surface water features. The chemical compositions at IES-026 and IES-030 cannot be explained by the surrounding geology resulting in no viable inverse model solutions from NETPATH. In fact, many geochemical trends would be better without including these springs (e.g., Figure 4.19D, Figure 4.19F, Figure 17, etc.)

Springs in Group 4 have a distinctive geochemical evolutionary pathway that we interpret to represent a mixture of roof pendant (e.g., marble, micaceous quartzite, calc-hornfels, and biotite schist) and granitoid dissolution. This evidence is based on; 1) spatial proximity to Paleozoic metasedimentary roof pendants that are directly upgradient (Figures 4.4A & 4.4C), 2) geochemical separation from springs that are spatially close and in a similar geologic AOIs without roof pendants upgradient in their likely recharge areas (IES-032 & IES-039), 3) $\text{Ca}^{2+}/\text{Na}^+$ well in excess of 0.4-0.6, and 4) strontium isotope evolution with increasing carbonate influence (Figure 4.19C). It is unclear if these roof pendants are areas of enhanced recharge or, as is more likely the case, these are areas of preferential weathering and therefore increased solute fluxes. An alternative hypothesis for the excess calcium in Group 4 spring waters is that they are influenced by excess calcium stemming from the weathering of freshly exposed glacial rock (e.g., Blum et al., 1998). IES-32 and IES-39 (Group 4) are both springs located proximally to recently glaciated areas, however these springs do not have roof pendants and have Ca/Na ratios less than 1.0. The source of excess calcite is likely from roof pendant limestones and hornfels but can also weather from other facies present in roof pendant metamorphic septa like schists.

Our results show that geologic heterogeneity is a dominant control on geochemical evolution pathways with increased scale in contrast with local-scale flowpath distributions in a geologically homogenous area. Differences in Group 1 waters, all sourcing flow through Mesozoic granitoids, can be attributed to subtle variations in plutonic composition (i.e., increased abundance of mafics like pyroxene, hornblende percent composition over 5%, etc.). Roof pendant septa, such

as the Pine Creek and Bishop Creek roof pendants, exert a control on the geochemistry of springs downgradient (Group 4 waters), even though they are limited in spatial extent in surface area and at depth. Distinct geochemical compositions of aridland springs, which serve as keystone ecological features due to the limited presence of surface waters, have implications for the structure and diversity of ecological communities such as benthic macroinvertebrates.

4.7.3 Excess calcium in intermediate scale groundwaters

As previous studies examining silicate weathering have observed, waters flowing in granitic terranes have been documented having higher $\text{Ca}^{2+}/\text{Na}^+$ molar ratios than what would be expected solely from the dissolution of plagioclase (White et al., 1998). Plagioclase weathering is the primary source of calcium in granitic watersheds, however calcium fluxes can be augmented by selective anorthite leaching or dissolution of other silicate phases like hornblende. Excess calcium in the form of calcite was first postulated by Garrels and Mackenzie (1967) as a solution to unaccounted weathering products in their inverse geochemical model, White et al. (1998) primarily attributed calcium excesses in granitic watershed to disseminated calcite and further determined that trace amounts of calcite are ubiquitous in Sierra Nevada granitoids. Trace amounts of calcite in granite massifs can present as disseminated grains in the silicate matrix, calcite replacement of plagioclase, or vein calcite filling fractures (White et al., 1998). While calcite has been shown to be a significant source of solutes in granitic watersheds in multiple surface water studies, especially in glaciated catchments where fresh bedrock is readily exposed (Blum et al., 1994; Blum et al., 1998; Pretti and Stewart, 2002), there have been a dearth of studies examining the sources responsible for excess calcium in groundwaters.

Mesozoic granitoids (not including diorites) supplying flow to springs in Owens Valley have anorthite compositions ranging from An_{10} to An_{38} with the majority ranging from An_{28} to An_{36} . Therefore, expected $\text{Ca}^{2+}/\text{Na}^+$ fluxes, assuming no other sources of calcite, should range between 0.4-0.6. Group 1 and Group 4 waters identified as sourcing intermediate scale groundwater flowpaths have excess calcium ($\text{Ca}^{2+}/\text{Na}^+ > 0.6$) than what would be predicted by An_{28} to An_{36} . In particular, Group 4 waters interpreted to be receiving some portion of flow through metasedimentary roof pendants have an “excess of excess” calcium ($\text{Ca}^{2+}/\text{Na}^+ > 1.5$) probably reflecting a combination of contributions from disseminated calcite within the granitoids and

calcite associated with schists, marble, and hornfels from the Pine Creek, Bishop Creek, and Mount Pinchot roof pendants.

The results from inverse modeling support the presence and influence of disseminated calcite as a component of the geochemical compositions of all Group 1 and Group 4 spring waters. All springs require calcite as a dissolving phase or else the models will not converge to a solution. Other studies have pointed to weathering of silicate phases like hornblende as potential sources of excess Ca^{2+} (Clow et al., 1993; White et al., 1998). In our case hornblende is included as a phase in all models where it has a documented presence in the modal analyses of the likely flowthrough plutonics, however it is not critical (like calcite) to establishing model solutions and is rarely selected by NETPATH as a phase in viable solutions.

The presence of both disseminated calcite and excess calcite from metasedimentary roof pendants has implications for $\delta^{13}\text{C}$ values in groundwater and subsequent radiocarbon correction models (i.e., Pearson and Handshaw, 1970 and Fontes and Garnier, 1979). In Sagehen Basin, a high elevation watershed with granodiorite bedrock in the eastern Sierra Nevada, Blumhagen and Clark (2008) found little, if any, contributions from disseminated calcite to ΣCO_2 in shallow groundwaters. The majority of their $\delta^{13}\text{C}$ values ranged from -17.6 to -19‰, with one outlier sample measured at -16.2‰. In contrast, waters in our study area receive contributions from disseminated calcite that are not insignificant. We also find anomalous $\delta^{13}\text{C}$ values for a crystalline watershed, with a sample range from -4.6 to -15‰ with a mean $\delta^{13}\text{C}$ of -8.7‰. Helium isotopes do not support a contribution of mantle or geogenic CO_2 to Owens Valley spring waters, with the potential exception of IES-029. Other possible additions of carbonate, such as the deposition of aerosols like trona from Owens Lake are not supported by inverse geochemical modeling. Sampling error could offer another potential explanation for the anomalous $\delta^{13}\text{C}$ values in this study; however, we have seen similar results over multiple sampling campaigns (see Chapter 6) and our results are consistent with elevated $\delta^{13}\text{C}$ values from wells and springs sampled by the USGS in Owens Valley (Figure 4.8). Our results indicate that disseminated calcite may be a source of enriched $\delta^{13}\text{C}$ values in Owens Valley groundwaters.

4.7.4 The influence of groundwater residence time

Our results show that there are substantial physical, geochemical, and isotopic differences between “young” and “old” waters (Figure 4.23). Older waters tend to be: 1) warmer, 2) more

geochemically evolved (higher average amounts of dissolved TDS and Cl^- , inferred to be behaving conservatively for these waters based on Cl^-/Br^-), and 3) sourcing longer and deeper flowpaths (inferred from R/R_a relationships). However, the geological heterogeneity of the eastern Sierra Nevada exerts a strong control on geochemical evolution, evidenced by the four separate geochemical groups, and this partially precludes the use of a simple metric like conductivity as a proxy for groundwater residence time at larger spatial scales.

Several other factors prevented this study from exploring the effects of residence time on geochemical evolution in more depth: 1) not all springs were candidates, based on emergence conditions, for noble gas collection, 2) only a subset of springs collected for noble gas analysis had ^3H concentrations suitable for ^3H - ^3He age dating, and 3) residence times derived from radiocarbon were primarily modern and, furthermore, anomalous $\delta^{13}\text{C}$ values made radiocarbon correction with more robust techniques (e.g., Fontes and Garnier (1979) and Pearson and Handshaw (1970)) problematic. While the use of ^3H and ^{36}Cl proved to be a powerful combination for distinguishing springs with large proportions of modern, bomb-pulse, and submodern (preanthropogenic) groundwater (4.17C), this age partitioning process cannot directly quantify residence time and can potentially be problematic for deciphering groundwaters with bimodal, mixed, or complicated age distributions. Nevertheless, we were still able to draw several meaningful conclusions from our analysis of groundwater residence time and geochemical evolution.

1. Inferred residence time does scale with geochemical evolution in areas where there are multiple springs emerging from similar plutons or lithologies, e.g., Group 4 waters primarily weathering quartz monzonite granitic plutons and metasedimentary roof pendants (Figure 4.24), Group 1 waters in the Lone Pine AOI weathering the Mount Whitney Intrusive suite (Figure 4.25), and Group 1 waters in the Bishop AOI (Figure 4.25).
2. Mol transfers of minerals that are ubiquitous across a study area (i.e., plagioclase and biotite) calculated from inverse geochemical models may provide a more robust metric indicative of geochemical evolution as opposed to TDS or an ion with multiple sources. Rademacher et al. (2001) showed strong relationships between residence time and biotite and hornblende weathering in shallow groundwater. In Owens Valley, plagioclase is present in almost all plutons and plagioclase composition can be altered for individual

inverse geochemical models to account for plagioclase An differences among plutons. The geochemical difference between “old” and “young” waters is more substantial for plagioclase weathered (Figure 4.23D) than for TDS (Figure 4.23C). We also see strong trends with plagioclase weathered vs biotite weathered for Group 1 and Group 4 waters symbolized by tritium concentration (Figure 4.26).

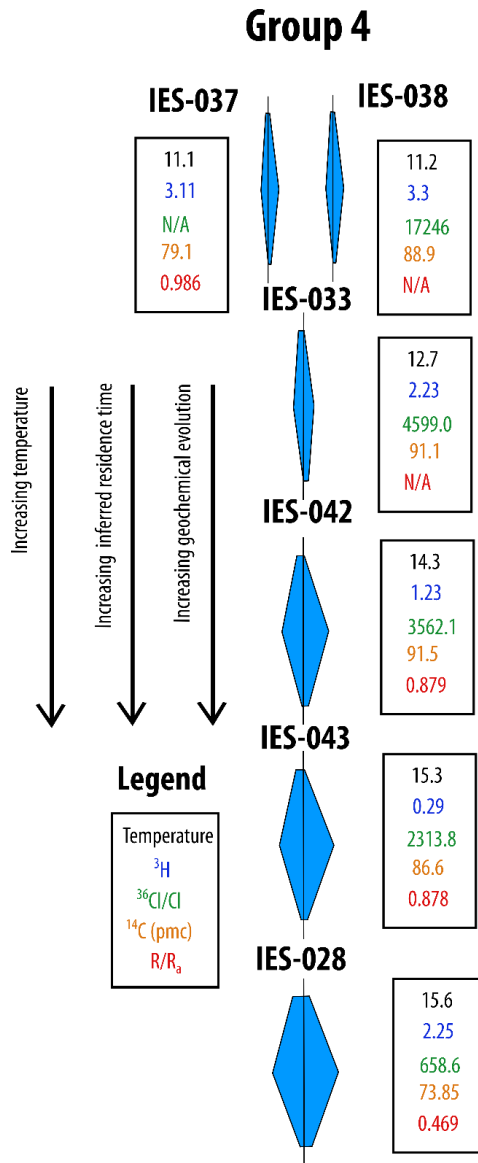


Figure 4.24: Geochemical evolution among Group 4 waters scales with inferred residence time and temperature. Spring temperature, ³⁶Cl/Cl, and R/R_a show linear trends with geochemical evolution. ³H and ¹⁴C activity have more convoluted relationships with geochemical evolution. ³H is nonunique and there are a variety of factors that can affect radiocarbon activities outside other than the decay of the parent radionuclide.

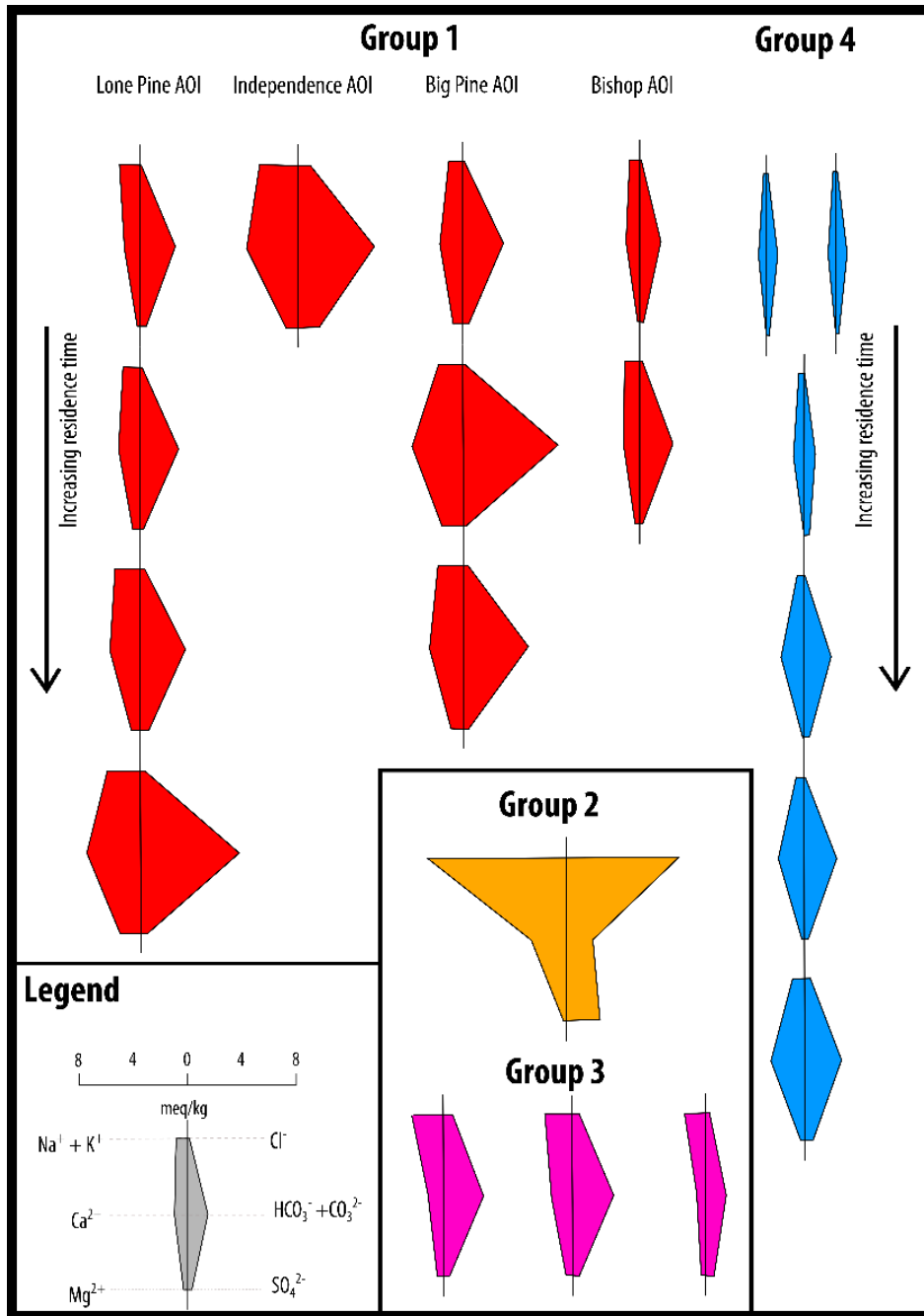


Figure 4.25: Complementary figure to Figure 4.24. Figure shows geochemical evolution with increasing groundwater residence time for Group 1 spring waters in the Lone Pine AOI and the Bishop AOI as well as Group 4 spring waters.

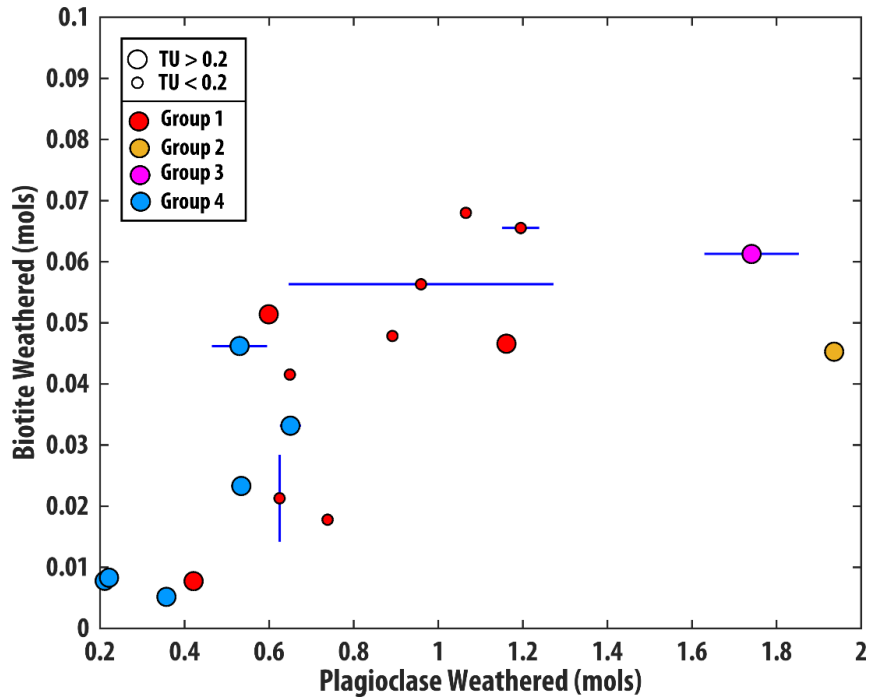


Figure 4.26: Results from inverse geochemical models showing mol transfers of plagioclase vs mol transfers of biotite for Owens Valley spring waters. In cases where more than one geochemical model, error bars represent minimum and maximum mol transfers of plagioclase and biotite from inverse geochemical models. Springs without error bars only have one viable model. Springs are symbolized by color for geochemical grouping and symbolized by size based on ^3H concentrations. “Old” waters have more plagioclase and biotite weathered compared to “young” spring waters. Group 2 and Group 3 spring waters fall off the general trendline for mineral weathering, perhaps indicative that these springs are not weathering Mesozoic granitoids like Group 1 and Group 4 waters.

3. Spring discharge temperature is not as susceptible to influence from geologic heterogeneity and serves as a complementary metric to geochemistry as an indicator of residence time at intermediate scales. This inference is supported by trends with ^3H - ^3He age (Figure 4.19F) and discharge temperature as well as R/R_a (Figure 4.19E) and discharge temperature. Within different geochemical groups (i.e., Group 4), there are strong relationships between inferred residence time and spring discharge temperature (Figure 4.23A).
4. Differences in $^{87}\text{Sr}/^{86}\text{Sr}$ between “young” and “old” waters are attributed to differential mineral weathering. Dilute, “young” waters have strontium isotopes that are elevated in comparison to whole rock values due to the preferential weathering of calcite, elevating

the $\text{Ca}^{2+}/\text{Sr}^{2+}$ ratio, and other easily weatherable minerals. For more evolved water in silicate watersheds, as shown by increases in silica (Figure 4.18F), plagioclase dissolution (Figure 4.18D), and kaolinite precipitation (Figure 4.18F), strontium isotopes converge towards the range for whole rock values. This indicates that young waters are obtaining Sr^{2+} from more readily weathered minerals while old waters are obtaining Sr^{2+} from a wider suite of minerals (both high and low solubilities).

4.8 Conclusions

In this study we set out to address two overarching questions based on prior work from Garrels and Mackenzie (1967): 1) how does increasing spatial scale and groundwater residence influence spring geochemical composition and 2) what are the dominant controls on geochemical evolution with increasing scale? Our results show that with increased scale (i.e., distance, flowpath length, and residence time) the principal factor driving geochemical evolution is geologic heterogeneity. This point is emphasized by the effect of Paleozoic metasedimentary roof pendants, when present in inferred recharge areas, on spring geochemical compositions. Distinct geochemical compositions at aridland springs have implications for ecological community structure and diversity in groundwater-dependent ecosystems. Additionally, our results show that disseminated calcite within granitic plutons is a major component of solute fluxes out of granitic watersheds, not just in shallow groundwater, surface water, and glaciated catchments, but in intermediate and regional scale groundwater. This result has implications for modeling solute fluxes out of watersheds and potential implications for $\delta^{13}\text{C}$ values that are used for radiocarbon correction in granitic terranes. Finally, our results show that geochemical evolution can serve as a relative indicator of residence time. However, this relationship may not hold up at intermediate to regional scales where geologic heterogeneity becomes a major factor. Instead of TDS or a particular solute, it may be useful to look at inverse geochemical mol transfers of a mineral that is ubiquitous across a watershed (i.e., plagioclase) as an indicator of geochemical weathering, and subsequently, groundwater residence time.

4.9 References

Aeschbach-Hertig, W., Peeters, F., Beyerle, U., & Kipfer, R. (1999). Interpretation of dissolved atmospheric noble gases in natural waters. *Water Resources Research*, 35(9), 2779-2792.

- Aeschbach-Hertig, W., Peeters, F., Beyerle, U., & Kipfer, R. (2000). Palaeotemperature reconstruction from noble gases in ground water taking into account equilibration with entrapped air. *Nature*, 405(6790), 1040-1044.
- Ali, G. A., Reiners, P. W., & Ducea, M. N. (2009). Unroofing history of Alabama and Poverty Hills basement blocks, Owens Valley, California, from apatite (U–Th)/He thermochronology. *International Geology Review*, 51(9-11), 1034-1050.
- Anderson, K. W. (2002). Contribution of local recharge to high flux springs in Death Valley National Park. California-Nevada: Master's thesis, Brigham Young University.
- Bailey, R. A., Dalrymple, G. B., & Lanphere, M. A. (1976). Volcanism, structure, and geochronology of long valley caldera, Mono County, California. *Journal of Geophysical Research*, 81(5), 725-744.
- Bassett, R. L., Steinwand, A., Jorat, S., Petersen, C., & Jackson, R. (2008). Forensic isotope analysis to refine a hydrologic conceptual model. *Groundwater*, 46(3), 372-383.
- Bataille, C. P., & Bowen, G. J. (2012). Mapping $^{87}\text{Sr}/^{86}\text{Sr}$ variations in bedrock and water for large scale provenance studies. *Chemical Geology*, 304, 39-52.
- Bateman, P. C., & Moore, J. G. (1965). Geologic map of the Mount Goddard quadrangle. Fresno and Inyo counties, California: US Geological Survey Map GQ-429, scale, 1(62,500).
- Bateman, P. C., Pakiser, L. C., & Kane, M. F. (1965). Geology and tungsten mineralization of the Bishop district, California, with a section on gravity study of Owens Valley and a section on seismic profile (No. 470). US Govt. Print. Off.,.
- Bense, V. F., Gleeson, T., Loveless, S. E., Bour, O., & Scibek, J. (2013). Fault zone hydrogeology. *Earth-Science Reviews*, 127, 171-192.
- Blasch, K. W., & Bryson, J. R. (2007). Distinguishing sources of ground water recharge by using $\delta^2\text{H}$ and $\delta^{18}\text{O}$. *Groundwater*, 45(3), 294-308.
- Blum, J. D., Erel, Y., & Brown, K. (1993). $^{87}\text{Sr}/^{86}\text{Sr}$ ratios of Sierra Nevada stream waters: Implications for relative mineral weathering rates. *Geochimica et Cosmochimica Acta*, 57(21-22), 5019-5025.
- Blum, J. D., Gazis, C. A., Jacobson, A. D., & Page Chamberlain, C. (1998). Carbonate versus silicate weathering in the Raikhot watershed within the High Himalayan Crystalline Series. *Geology*, 26(5), 411-414.
- Blumhagen, E. D., & Clark, J. F. (2008). Carbon sources and signals through time in an Alpine groundwater Basin, Sagehen California. *Applied Geochemistry*, 23(8), 2284-2291.
- Chapman, J. B., Ducea, M. N., DeCelles, P. G., & Profeta, L. (2015). Tracking changes in crustal thickness during orogenic evolution with Sr/Y: An example from the North American Cordillera. *Geology*, 43(10), 919-922.

- Chen, J. H., & Tilton, G. R. (1991). Applications of lead and strontium isotopic relationships to the petrogenesis of granitoid rocks, central Sierra Nevada batholith, California. *Geological Society of America Bulletin*, 103(4), 439-447.
- Clark, I. D., & Fritz, P. (1997). Environmental isotopes in hydrogeology. CRC press.
- Clow, D. W., Mast, M. A., Bullen, T. D., & Turk, J. T. (1997). Strontium 87/strontium 86 as a tracer of mineral weathering reactions and calcium sources in an alpine/subalpine watershed, Loch Vale, Colorado. *Water Resources Research*, 33(6), 1335-1351.
- Coolbaugh, M. F., Taranik, J. V., Rains, G. L., Shevenell, L. A., Sawatzky, D. L., Bedell, R., & Minor, T. B. (2002). A geothermal GIS for Nevada: defining regional controls and favorable exploration terrains for extensional geothermal systems. *Transactions-Geothermal Resources Council*, 485-490.
- Craig, H. (1961). Isotopic variations in meteoric waters. *Science*, 133(3465), 1702-1703.
- Danskin, W. R. (1998). Evaluation of the hydrologic system and selected water-management alternatives in the Owens Valley, California (Vol. 2370). US Geological Survey, Information Services.
- Davis, S. N., Cecil, L. D., Zreda, M., & Moysey, S. (2001). Chlorine-36, bromide, and the origin of spring water. *Chemical Geology*, 179(1-4), 3-16.
- Davis, S. N., Moysey, S., Cecil, D. L., & Zreda, M. (2003). Chlorine-36 in groundwater of the United States: empirical data. *Hydrogeology Journal*, 11(2), 217-227.
- Doyle, J. M., Gleeson, T., Manning, A. H., & Mayer, K. U. (2015). Using noble gas tracers to constrain a groundwater flow model with recharge elevations: A novel approach for mountainous terrain. *Water Resources Research*, 51(10), 8094-8113.
- Dreher, T. (2003). Comment on Güler C, Thyne GD, McCray JE, Turner AK (2002): Evaluation of graphical and multivariate statistical methods for classification of water chemistry data (Hydrogeology Journal 10: 455-474). *Hydrogeology Journal*, 11(5), 605-606.
- Drever, J. I., & Zobrist, J. (1992). Chemical weathering of silicate rocks as a function of elevation in the southern Swiss Alps. *Geochimica et Cosmochimica Acta*, 56(8), 3209-3216.
- Elder, K., Dozier, J., & Michaelsen, J. (1989). Spatial and temporal variation of net snow accumulation in a small alpine watershed, Emerald Lake basin, Sierra Nevada, California, USA. *Annals of Glaciology*, 13, 56-63.
- Faure, G. (1986). Principles of isotope geology. John Willey and Sons Inc. New York.
- Feth, J. H. F., Robertson, C. E., & Polzer, W. L. (1964). *Sources of mineral constituents in water from granitic rocks, Sierra Nevada, California and Nevada* (No. 1535-I). US Govt. Print. Off.,.
- Fontes, J. C., & Garnier, J. M. (1979). Determination of the initial ^{14}C activity of the total dissolved carbon: A review of the existing models and a new approach. *Water Resources Research*, 15(2), 399-413.

- Forster, C. B., & Evans, J. P. (1991). Hydrogeology of thrust faults and crystalline thrust sheets: Results of combined field and modeling studies. *Geophysical Research Letters*, 18(5), 979-982.
- Friedman, I., Smith, G. I., Johnson, C. A., & Moscati, R. J. (2002). Stable isotope compositions of waters in the Great Basin, United States 2. Modern precipitation. *Journal of Geophysical Research: Atmospheres*, 107(D19), ACL-15.
- Frisbee, M. D., Phillips, F. M., Campbell, A. R., Liu, F., & Sanchez, S. A. (2011). Streamflow generation in a large, alpine watershed in the southern Rocky Mountains of Colorado: Is streamflow generation simply the aggregation of hillslope runoff responses?. *Water Resources Research*, 47(6).
- Gardner, W. P., Jencso, K., Hoylman, Z. H., & Thiros, N. E. (2018, December). Mountain Water-The Role of Deep Groundwater in Mountain Watersheds. In AGU Fall Meeting Abstracts.
- Garrels, R. M., & Mackenzie, F. T. (1967). Origin of the chemical compositions of some springs and lakes.
- Gleason, C. L., Frisbee, M. D., Rademacher, L. K., Sada, D. W., & Meyers, Z. P. (2020). Hydrogeology of desert springs in the Panamint Range, California, USA: Identifying the sources and amount of recharge that support spring flow. *Hydrological Processes*, 34(3), 730-748.
- Goff, F., Wollenberg, H. A., Brookins, D. C., & Kistler, R. W. (1991). A Sr-isotopic comparison between thermal waters, rocks, and hydrothermal calcites, Long Valley caldera, California. *Journal of Volcanology and Geothermal Research*, 48(3-4), 265-281.
- Güler, C., & Thyne, G. D. (2004). Delineation of hydrochemical facies distribution in a regional groundwater system by means of fuzzy c-means clustering. *Water Resources Research*, 40(12).
- Güler, C., & Thyne, G. D. (2004). Hydrologic and geologic factors controlling surface and groundwater chemistry in Indian Wells-Owens Valley area, southeastern California, USA. *Journal of Hydrology*, 285(1-4), 177-198.
- Guler, C., & Thyne, G. D. (2006). Statistical clustering of major solutes: use as a tracer for evaluating interbasin groundwater flow into Indian Wells Valley, California. *Environmental & Engineering Geoscience*, 12(1), 53-65.
- Hem, J. D. (1985). Study and interpretation of the chemical characteristics of natural water (Vol. 2254). Department of the Interior, US Geological Survey.
- Hirt, W. H. (2007). Petrology of the Mount Whitney Intrusive Suite, eastern Sierra Nevada, California: Implications for the emplacement and differentiation of composite felsic intrusions. *Geological Society of America Bulletin*, 119(9-10), 1185-1200.
- Hollett, K. J., Danskin, W. R., McCaffrey, W. F., & Walti, C. L. (1991). Geology and water resources of Owens Valley, California (No. 2370-B). USGPO.
- Holloway, J. M., & Dahlgren, R. A. (2001). Seasonal and event-scale variations in solute chemistry for four Sierra Nevada catchments. *Journal of Hydrology*, 250(1-4), 106-121.

- James, E. R., Manga, M., Rose, T. P., & Hudson, G. B. (2000). The use of temperature and the isotopes of O, H, C, and noble gases to determine the pattern and spatial extent of groundwater flow. *Journal of Hydrology*, 237(1-2), 100-112.
- Jasechko, S. (2016). Partitioning young and old groundwater with geochemical tracers. *Chemical Geology*, 427, 35-42.
- Jayko, A. S., & Bursik, M. (2011). Active transtensional intracontinental basins: Walker Lane in the western Great Basin. *Tectonics of sedimentary basins: Recent advances*, 226-248.
- Johnson, T. M., Roback, R. C., McLing, T. L., Bullen, T. D., DePaolo, D. J., Doughty, C., ... & Murrell, M. T. (2000). Groundwater “fast paths” in the Snake River Plain aquifer: Radiogenic isotope ratios as natural groundwater tracers. *Geology*, 28(10), 871-874.
- Kahrl, W. L. (1976). The Politics of California Water: Owens Valley and the Los Angeles Aqueduct, 1900-1927. *California Historical Quarterly*, 55(1), 2-25.
- Kipfer, R., Aeschbach-Hertig, W., Peeters, F., & Stute, M. (2002). Noble gases in lakes and ground waters. *Reviews in Mineralogy and Geochemistry*, 47(1), 615-700.
- Kistler, R. W., & Peterman, Z. E. (1973). Variations in Sr, Rb, K, Na, and initial Sr⁸⁷/Sr⁸⁶ in Mesozoic granitic rocks and intruded wall rocks in central California. *Geological Society of America Bulletin*, 84(11), 3489-3512.
- Kulongoski, J. T., Hilton, D. R., & Izbicki, J. A. (2003). Helium isotope studies in the Mojave Desert, California: implications for groundwater chronology and regional seismicity. *Chemical Geology*, 202(1-2), 95-113.
- Liu, Y., & Yamanaka, T. (2012). Tracing groundwater recharge sources in a mountain–plain transitional area using stable isotopes and hydrochemistry. *Journal of Hydrology*, 464, 116-126.
- Lockwood, J. P., & Lydon, P. A. (1975). Geologic Map of the Mount Abbot Quadrangle, Central Sierra Nevada, California. US Geological Survey.
- Manning, A. H., & Solomon, D. K. (2003). Using noble gases to investigate mountain-front recharge. *Journal of Hydrology*, 275(3-4), 194-207.
- Manning, A. H., & Solomon, D. K. (2005). An integrated environmental tracer approach to characterizing groundwater circulation in a mountain block. *Water Resources Research*, 41(12).
- Michael, P. J. (1983). Chemical differentiation of the Bishop Tuff and other high-silica magmas through crystallization processes. *Geology*, 11(1), 31-34.
- Moore, J. G. (1963). Geology of the mount Pinchot quadrangle, southern Sierra Nevada, California (Vol. 1130). US Government Printing Office.
- Moore, J. G. (1981). Geologic map of the Mount Whitney quadrangle. Inyo and Tulare Counties, California: US Geological Survey Geologic Quadrangle Map GQ-1545, scale, 1(62,500).

- Moore, J. G. (1987). Mount Whitney Quadrangle, Inyo and Tulare Counties, California: Analytic Data (No. 1760). Department of the Interior, US Geological Survey.
- Moysey, S., Davis, S. N., Zreda, M., & Cecil, L. D. (2003). The distribution of meteoric $^{36}\text{Cl}/\text{Cl}$ in the United States: a comparison of models. *Hydrogeology Journal*, 11(6), 615-627.
- Nelson, C. A. (1966). Geologic map of the Waucoba Mountain quadrangle. Inyo County, California: US Geological Survey Geologic Quadrangle Map GQ-528, scale, 1(62), 500.
- O'Donnell, M. S., & Ignizio, D. A. (2012). Bioclimatic predictors for supporting ecological applications in the conterminous United States. US Geological Survey Data Series, 691(10).
- Ormerod, D. S., Rogers, N. W., & Hawkesworth, C. J. (1991). Melting in the lithospheric mantle: Inverse modelling of alkali-olivine basalts from the Big Pine Volcanic Field, California. *Contributions to Mineralogy and Petrology*, 108(3), 305-317.
- Paukert, A. N. (2014). Mineral Carbonation in Mantle Peridotite of the Samail Ophiolite, Oman: Implications for permanent geological carbon dioxide capture and storage (Doctoral dissertation, Columbia University).
- Parkhurst, D. L. (1995). User's guide to PHREEQC: A computer program for speciation, reaction-path, advective-transport, and inverse geochemical calculations (Vol. 95, No. 4227). US Department of the Interior, US Geological Survey.
- Parkhurst, D. L., & Charlton, S. R. (2008). NetpathXL, an Excel Interface to the Program NETPATH (p. 11). US Department of the Interior, US Geological Survey.
- Pearson, F. J., & Hanshaw, B. B. (1970). Sources of dissolved carbonate species in groundwater and their effects on carbon-14 dating. *Isotope Hydrology*, 1970, 271-285.
- Peeters, F., Beyerle, U., Aeschbach-Hertig, W., Holocher, J., Brennwald, M. S., & Kipfer, R. (2003). Improving noble gas based paleoclimate reconstruction and groundwater dating using $^{20}\text{Ne}/^{22}\text{Ne}$ ratios. *Geochimica et Cosmochimica Acta*, 67(4), 587-600.
- Peters, E., Visser, A., Esser, B. K., & Moran, J. E. (2018). Tracers Reveal Recharge Elevations, Groundwater Flow Paths and Travel Times on Mount Shasta, California. *Water*, 10(2), 97.
- Phillips, F. M. (2000). Chlorine-36. In *Environmental tracers in subsurface hydrology* (pp. 299-348). Springer, Boston, MA.
- Plummer, L. N., Prestemon, E. C., & Parkhurst, D. L. (1994). An interactive code (NETPATH) for modeling net geochemical reactions along a flow path, version 2.0. *Water-Resources Investigations Report*, 94, 4169.
- Plummer, L. N., & Glynn, P. D. (2013). Radiocarbon Dating in groundwater systems. Chapter 4. Isotope methods for dating old groundwater: Vienna. International Atomic.
- Pretti, V. A., & Stewart, B. W. (2002). Solute sources and chemical weathering in the Owens Lake watershed, eastern California. *Water Resources Research*, 38(8), 2-1.

- Rademacher, L. K., Clark, J. F., Hudson, G. B., Erman, D. C., & Erman, N. A. (2001). Chemical evolution of shallow groundwater as recorded by springs, Sagehen basin; Nevada County, California. *Chemical Geology*, 179(1-4), 37-51.
- Rademacher, L. K., Clark, J. F., Clow, D. W., & Hudson, G. B. (2005). Old groundwater influence on stream hydrochemistry and catchment response times in a small Sierra Nevada catchment: Sagehen Creek, California. *Water Resources Research*, 41(2).
- Rissmann, C., Leybourne, M., Benn, C., & Christenson, B. (2015). The origin of solutes within the groundwaters of a high Andean aquifer. *Chemical Geology*, 396, 164-181.
- Rose, S. (1992). Tritium in ground water of the Georgia piedmont: Implications for recharge and flow paths. *Hydrological Processes*, 6(1), 67-78.
- Ross, D. C. (1965). Geology of the Independence quadrangle, Inyo County, California (No. 1181-O). US Govt. Print. Off.,.
- Springer, A. E., & Stevens, L. E. (2009). Spheres of discharge of springs. *Hydrogeology Journal*, 17(1), 83.
- Stewart-Maddox, N. S., Frisbee, M. D., Andronicos, C. L., Genereux, D. P., & Meyers, Z. P. (2018). Identifying the regional extent and geochemical evolution of interbasin groundwater flow using geochemical inverse modeling and $^{87}\text{Sr}/^{86}\text{Sr}$ ratios in a complex conglomeratic aquifer. *Chemical Geology*, 500, 20-29.
- Stone, P., Dunne, G. C., Moore, J. G., & Smith, G. I. (2000). Geologic Map of the Lone Pine 15' Quadrangle, Inyo County, California. The Survey.
- Stute, M., & Schlosser, P. (2000). Atmospheric noble gases. In *Environmental tracers in subsurface hydrology* (pp. 349-377). Springer, Boston, MA.
- Tamers, M. A. (1975). Validity of radiocarbon dates on ground water. *Geophysical Surveys*, 2(2), 217-239.
- Taylor, T. R., & Dewey, J. F. (2009). Transtensional analyses of fault patterns and strain provinces of the Eastern California shear zone–Walker Lane on the eastern margin of the Sierra Nevada microplate, California and Nevada. *International Geology Review*, 51(9-11), 843-872.
- Thomas, J. M., Hudson, B. G., Stute, M., & Clark, J. F. (2003). Noble gas loss may indicate groundwater flow across flow barriers in southern Nevada. *Environmental Geology*, 43(5), 568-579.
- Vogel, J. C. (1970). Carbon-14 dating of groundwater. *Isotope Hydrology*, 1970, 235-237.
- Wesnousky, S. G. (2005). The San Andreas and Walker Lane fault systems, western North America: Transpression, transtension, cumulative slip and the structural evolution of a major transform plate boundary. *Journal of Structural Geology*, 27(8), 1505-1512.
- Williams, M. W., & Melack, J. M. (1991). Solute chemistry of snowmelt and runoff in an alpine basin, Sierra Nevada. *Water Resources Research*, 27(7), 1575-1588.

Wilson, J. L., & Guan, H. (2004). Mountain-block hydrology and mountain-front recharge. Groundwater recharge in a desert environment: The Southwestern United States, 9.

Zheng, Z., Kirchner, P. B., & Bales, R. C. (2016). Topographic and vegetation effects on snow accumulation in the southern Sierra Nevada: a statistical summary from lidar data. *The Cryosphere*, 10(1), 257-269.

Zuber, A., Weise, S. M., Osenbrück, K., Grabczak, J., & Ciężkowski, W. (1995). Age and recharge area of thermal waters in Ladek Spa (Sudeten, Poland) deduced from environmental isotope and noble gas data. *Journal of Hydrology*, 167(1-4), 327-349.

CHAPTER 5. EXAMINING LANDSCAPE PLACEMENT AND EMERGENCE MECHANISM AS CONTROLS ON SPRING HYDROCHEMICAL CHARACTERISTICS AND ECOLOGICAL COMMUNITY STRUCTURE

5.1 Abstract

Topographic metrics have been shown to be predictive of hydrogeological and hydrochemical characteristics (e.g., baseflow presence, temperature, salinity, permanence) in headwater networks, streams, lakes, and wetlands. Unfortunately, springs have largely been omitted from these types of topographic analysis and there are only a handful of studies that have examined the relationship between where (landscape placement) and why (mechanism) a spring emerges and hydrogeochemical characteristics. Examination of landscape controls on these characteristics, especially at regional scales, can provide insight into a knowledge gap that has long been debated; the factors controlling benthic macroinvertebrate (BMI) community structure in isolated desert springs. The southern Great Basin, extending from the Spring Mountains (NV) to the crest of the eastern Sierra Nevada, is the ideal place to test the role of landscape placement in the structure of spring hydrochemical characteristics and ecologic community for several reasons: 1) the regionally extended terrain creates an abundant diversity in topographic settings, structural features, and landform types, 2) springs are found across all topographic features, and 3) there is a wealth of pre-existing data from past studies that can be mined and combined with new data from the IES project that funded this research.

In this study, we leverage the plethora of existing work on springs in the southern Great Basin to amass a regional hydrochemical dataset. In this chapter I test the following question: Can qualitative landscape placement classifications, quantitative topographic indices (e.g., elevation, slope, Topographic Wetness Index, profile curvature, and relative elevation), and classified emergence mechanisms be used to predict spring hydrochemical characteristics across a geologically and topographically complex gradient? To evaluate the effect of spring emergence mechanism, springs are classified as “fault-controlled” or “non-fault controlled” using proximity analysis to major structural features. Finally, we use a combination of non-metric multidimensional scaling (NMDS) and ecological indices to examine landscape controls on ecological community structure at the regional scale.

Our results show that there are systematic relationships of increasing temperature, specific conductance, and groundwater residence time moving from high topographic positions (e.g., Nival, High Mountain) to lower topographic positions (e.g., Low Mountain-Bajada, Valley Floor). These relationships fail moving from the “Valley Floor” to “Playa” topographic settings. While, elevation and slope exhibit some linear predictive power, topographic indices like Topographic Wetness Index (TWI), curvature, and relative elevation do not. However, areas of high concavity, positive relative elevation, and extremely negative relative elevation (-1000 meters) tend to be areas associated with colder, more dilute, and younger spring waters. NMDS results show that BMI community structure at regional scales can be partially explained by spring landscape placement and groundwater residence time. Moving from high topographic positions to low topographic positions, BMI community stress tolerance increases while ecological richness and Shannon diversity decrease. As a culmination of this work, we synthesize the major topographic and ecological patterns to formulate a conceptual model of spring systems in the southern Great Basin.

5.2 Introduction

In conjunction with geology and climate, surface topography exerts one of the primary controls on groundwater flow and spatial patterns of saturated areas (Tóth, 1999). Topography may be the most important factor driving groundwater flow in arid, mountainous settings because topography creates the energy gradient necessary to generate nested flow systems, i.e., local, intermediate, and regional-scale flowpaths (Tóth, 1963; Tóth, 1995). However, it is difficult to decouple these controls from one another. For example, the effect of topography on groundwater flow and water table depth is dependent on climate (i.e., humid or arid, type and accumulation of precipitation), the hydraulic conductivity of the subsurface, and the magnitude of the topography (Toth, 1963; Marklund and Worman, 2007; Schaller and Fan, 2009; Gleeson et al., 2011; Condon and Maxwell, 2015). Topography also enhances processes like snow-sheltering, snow basins, and can be a factor on the routing of atmospheric moisture. While concepts such as “hydrologic landscapes” (e.g., Winter, 2000; Winter, 2001) have been created to synthesize multiple variables controlling groundwater flow properties under different qualitative umbrellas, an identified knowledge gap that persists, both at the catchment and regional scales, is the identification of relationships between groundwater conditions (e.g., temperature, salinity, residence time,

permanence etc.) and topographic properties (Buttle et al., 2002). Attempts to explain spatial variations in groundwater conditions in small basins using topographic metrics have been met with mixed success (Moore and Thompson, 1996; Munoz et al., 2016) and regional scale relationships with topography have been somewhat ignored altogether.

While groundwater divides are inherently different than surface water divides, there has been some promise, particularly at the catchment scale, linking topographic metrics to characteristics of groundwater-supported surface hydrologic features (e.g., groundwater-supported streams and wetlands). Topographic metrics have been most commonly applied to identify the presence or potential of groundwater discharge zones in surface water features. The TOPMODEL approach (i.e., Beven and Kirkby, 1979; Beven et al., 1995; Seibert et al., 2003), or related algorithms like TWI (Topographic Wetness Index) or TCI (Topographic Convergence Index), use a combination of upslope accumulated area (UAA) and slope derived from digital elevation models (DEMs). Occasionally, other metrics such as downslope index are incorporated into these algorithms (Hjerdt et al., 2004). These types of approaches have seen limited success predicting areas of saturation (Western et al., 1999; Grabs et al., 2009), subsurface rainfall-runoff response (Jencso and McGlynn, 2011), the extension and contraction of headwater networks (Prancevic and Kirchner, 2019), and wetland distribution across climate gradients (Rodhe and Siebert, 1999; Merot et al., 2003; Hjerdt et al., 2004; Infascelli et al., 2013). Other watershed indices such as profile curvature (Vivoni et al., 2008), basin hypsometry (Woods et al., 1997) and stream order (Sreedevi et al., 2005) have also been linked to exerting control on subsurface runoff generation processes and groundwater potential. Besides simply predicting the presence or potential of groundwater flow, topographic and basin metrics have also used to predict the temperature of discharging groundwater (Štulc, 1998; Jankowski and Schindler, 2019), patterns in groundwater salinity or geochemistry (Duffy and Al-Hassan, 1988; Welsch et al., 2001; Dowling et al., 2003; Peralta-Tapia et al., 2015), and even potential vulnerability or permanence (Gleeson and Manning, 2008; Fritz et al., 2008; Prancevic and Kirchner, 2019). Other quantitative topographic metrics (e.g., relative elevation, topographic wetness index, etc.) have been related to groundwater temperature and geochemistry (Thobaden and Hamilton, 2014; Naus et al., 2019) and qualitative topographic metrics (e.g., landform type) have been related to hydrogeologic flow potential (Anderson and Kneale, 1982), hydrologic resilience (Tooth, 2018), and hydrologic vulnerability (Winter, 2000). Unfortunately, all of these metrics have been predominately applied to

understanding groundwater-surface water interaction in surface-water bodies and are relatively untested at predicting the potential or hydrochemical characteristics associated with features such as springs or seeps that, while sometimes emerge at the surface as a reflection of the intersection of local topography with the water table, often emerge due to geologic configuration (i.e., contacts, permeability contrasts) or structural features.

In comparison to wetlands, shallow groundwater, and groundwater-supported streams, there is a dearth of studies examining topographic and landscape-scale controls on spring distribution and environmental characteristics (Perla and Stevens, 2008; Freed et al., 2011). Much of the geomorphological research surrounding springs has revolved around the influence of springs on geomorphology (e.g., Lamb et al., 2006) or the different spheres of discharge they create (e.g., Springer and Stevens, 2009), rather than on the influence of geomorphology or landscape position on spring characteristics (Williams and Vondracek, 2010). While it has long been recognized that where and why springs emerge have implications for hydrochemical characteristics and permanence (e.g., Bryan, 1919), springs are notoriously difficult to study and characterize because they integrate distributions of flowpaths (Manga, 1999; Manga, 2001), and in some cases, their emergence appears to have little correlation with surficial geology. Additionally, recharge areas supporting springs are not always neatly defined by surface water delineations (e.g., Stewart-Maddox et al., 2018). While there has been some headway in understanding spring watersheds or “springsheds” (e.g., Pacheco and Van der Weijed, 2012) via topographic or geochemical methods, approaches for calculating spring contributing areas are often site-specific (e.g., Aislin and McNamara, 2011; Frisbee et al., 2013; Setiawan et al., 2019) and are not necessarily applicable everywhere. Identifying the contributing area for springs remains an elusive target

The body of existing knowledge that does exist surrounding springs and their relationship to the landscape is varied. A significant amount of work is limited to karstic landscapes (e.g., Mugal et al., 2009; Williams and Vondracek, 2010) where hydrogeologic flow conditions are different due to the majority of flow routing through secondary porosity. Many studies have been focused on spring hydrologic potential (i.e., for drinking water) mapping/modeling for societal purposes (Ozdemir, 2011a; Ozdemir, 2011b; Khsravi et al., 2018; Rahmati et al., 2018). Spring density has been correlated with bedrock permeability, precipitation, and watershed age. (Jefferson et al. 2010). Modeling results in structurally complex terrain (e.g., fold and fault belts) imply that springs in valley aquifers are more likely to be insensitive to changing mountain water tables (Ball

et al., 2014). Connections between landscape metrics and spring hydrochemical characteristics show some degree of correlation at very local scales (e.g., Zapata-Rios et al., 2015; Gil-Marquez et al., 2017; Freed et al., 2019). While these studies provide clues into potential overarching patterns with springs, there are currently not well-detailed criteria or metrics, outside of local-scale case studies or certain types of landscapes (e.g., karst), that can be used to predict spring permeance or other hydrochemical characteristics. This fact is disconcerting considering the ecological importance and numerous threats to springs, particularly those in aridlands such as the western United States. Additionally, understanding if systematic relationships exist with springs landscape position and hydrochemical variables at the regional scale may shed insight into a major knowledge gap in aquatic ecology- the dominant controls on the community composition of spring dwelling benthic macroinvertebrates (BMI).

Benthic macroinvertebrates (BMI) are powerful biomonitoring tools in aquatic environments because they are found everywhere, consist of a multitude of species that have varying stress tolerance thresholds, are often sedentary or non-vagile, and are relatively long lived (Mandaville, 2002). In particular, the longevity of BMI is important because their existence and response provide integrated knowledge of conditions over longer timescales (Mandaville, 2002). In springs, where constant groundwater discharge provides a relative stable environment, spring BMI community structure can provide clues about spring permanence, hydrologic and geochemical stability, and overall environmental harshness (McCabe, 1998). However, throughout the literature, there is considerable disagreement and conflicting evidence regarding the factors most responsible for controlling BMI community structure in springs.

The effect of disturbance on BMI community structure, whether natural (e.g. avalanche, forest fire, flood scouring, etc.) or anthropogenically caused (e.g., livestock grazing, introduction of non-native species, spring alteration, groundwater pumping, etc.), is undeniable (e.g., Williams et al., 1997; Sada and Nachlinger, 1996; Sada et al., 2005; Fleishman et al., 2006; Keheher and Rader, 2008a; Mehler et al., 2015; Sada and Lutz, 2016). In instances where the effect of disturbance is minimal, i.e., reference or undisturbed settings with permanent flow, BMI community composition has been correlated with land use (Sada et al., 2005; Mehler et al., 2013), physical factors like discharge (Gathmann and Williams, 2006), wetted channel width, and substrate composition (Sada and Herbst, 2001; Mehler et al., 2015), elevation (Hogle et al., 2015), aquatic dispersal history (Rader et al., 2012), and environmental variables (e.g., temperature and

salinity) related to hydrogeology and aquifer provenance (Myers and Resh, 2002; Gathmann et al., 2009; Sada et al., 2015; Sada and Thomas, 2015; Stanislawczyk et al., 2018; Sada and Thomas, in review). Studies at local scales, i.e., minimal ranges in key environmental tolerance variables like temperature and specific conductance, have linked BMI community composition to variations in ion concentrations (Erman and Erman, 1995; Erman, 2002) and specific geochemical “fingerprints” (Pordel et al., in prep). Though it is known that there is a connection between BMI ecology and hydrogeology, the extent of this connection and how it changes with increasing spatial scale is unclear and an area of necessary investigation (Van der Kamp, 1995) due to a plethora of mixed results (e.g., Sada et al., 2015; Fattorini et al., 2016). Springs, nature’s “biological laboratories”, are an ideal place to test these relationships (Van der Kamp, 1995).

The structurally extended terrain and presence of springs across all topographic features (Figure 5.1) makes the southern Great Basin an ideal place to examine spring hydrochemical patterns with landscape setting at the regional scale. Within this study area there are numerous basins and ranges of differing elevations that lie in different positions relative to the Sierra Nevada rain shadow. In this study we address the following research questions: 1) Are there systematic patterns with spring landscape placement and hydrochemical characteristics (e.g., water temperature, specific conductance, groundwater residence time) that can be predicted by topographic metrics and/or landform analysis? and 2) If present, how do these patterns influence benthic macroinvertebrate community structure at the regional scale, where the effects of heterogeneity (e.g., Chapter 3) are significantly dampened by time and flowpath length? We answer these questions by first cultivating a regional hydrochemical database of springs within the study area. This database is used to examine regional patterns of spring hydrochemical characteristics with qualitative landform classification, topographic indices, and spring emergence mechanism. Following regional analysis and determination of whether springs from recent hydrochemical/ecological sampling efforts are representative of the regional trends within the study area, we analyze the effect of spring landscape placement and related hydrochemical characteristics on BMI community structure. This is achieved using a combination of nonmetric multidimensional scaling (NMDS) analysis and ecological indices computed from BMI data. The culmination of this work results in a synthesis used to formulate a regional conceptual model of spring systems in the southern Great Basin.

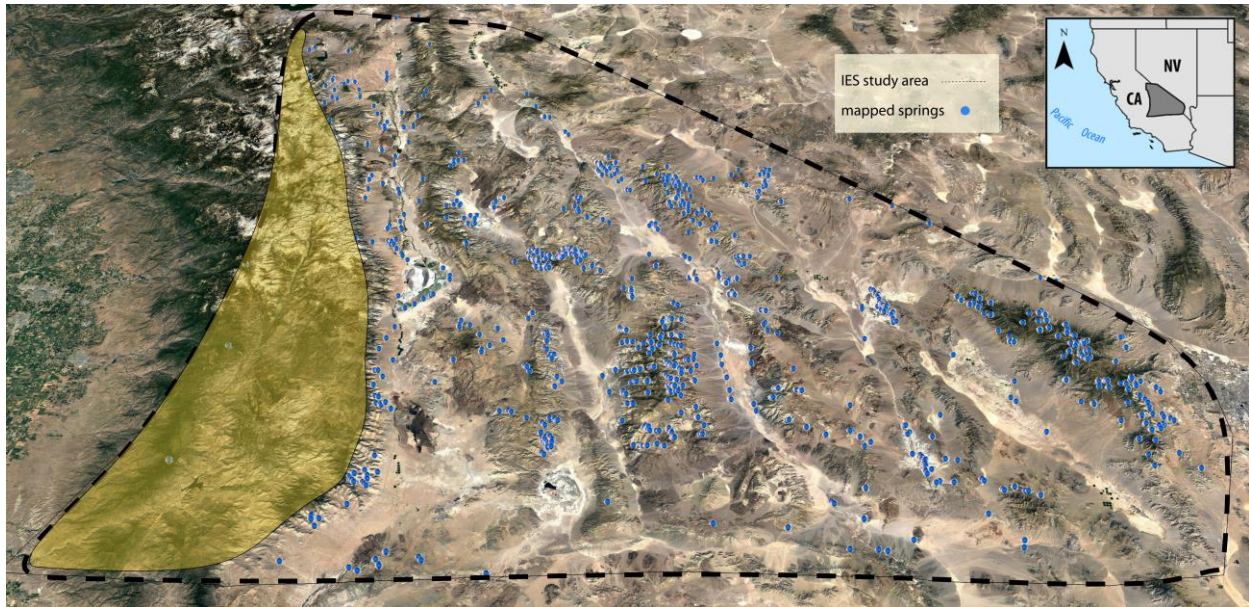


Figure 5.1. Map showing the study area for this paper, the structurally extended terrain of the southern Great Basin of the United States. The study area is bounded by the dotted line in the Google Earth orthoimagery capture (Google Earth, 2020) and by the shaded grey area within the inset map. The blue circles show locations of mapped springs, which are distributed across all landscape positions and landform types (e.g., mountains, bajadas, playas, etc.) throughout the study area. The Sierra Nevada, other than the eastern slope, is shaded in yellow and excluded from analysis in this paper as it is not part of the southern Great Basin.

5.3 Methods

The following sections describe the methods and workflow used in this study to answer the primary research questions. There are three fundamental steps to this process: 1) dataset creation, 2) topographic and emergence analysis, and 3) ecological analysis. A flowchart displaying the steps and relative chronological order of this workflow is shown in Figure 5.2.

5.3.1 Defining the regional study area

The regional study area boundary is shown in Figure 5.1 and is delineated by critical boundaries for a coupled tectonic-hydrogeological-landscape evolution model related to the goals of this dissertation. The eastern extent of the study region is defined by the northwest-southeast trending ridgeline of the Spring Mountains that separates the Las Vegas Valley drainage basin from the Death Valley Regional Flow System, the southernmost subwatershed of the Great Basin. The Garlock-Stateline fault system roughly defines the southern boundary of the study area. The

northern boundary of the study area is defined by the northernmost extents of the Funeral-Grapevine Mountains and White-Inyo Mountains. The western boundary of the region is within the fixed tectonic block of the Sierra Nevada Batholith. This study area is remarkable for the regionally extended terrain, the variety of landforms and ecological zones, and the significant relief. The absence of perennial surface water features, other than the Owens River and the Amargosa River, makes springs critically important, as they are the only permanent source of water and are found across all landscape features.

5.3.2 Creation of a regional geochemical spring dataset

Due to the substantial topographic and structural complexity of the southern Great Basin, it is imperative to use a large, regionally representative dataset in order to examine large-scale patterns of spring hydrochemical characteristics and topographic metrics. The goal of this step in the workflow was to gather as many springs as possible within the study area that contain hydrochemical data (e.g., temperature, geochemistry, residence time indicators). Past studies and dissertations have concatenated spring geochemical data from multiple studies in the Spring Mountains (Hershey, 1989) and in the greater Death Valley area (Anderson, 2002). To create the dataset used in this study, the large datasets from Anderson (2002) and Hershey (1989) are leveraged and combined with data from other journal publications, consultancy reports, institutional databases (e.g., Desert Research Institute), municipal/county geochemical cooperative studies, and federal databases (e.g., the USGS National Water Information System) (Figure 5.2). Quality control procedures were performed to eliminate well data, to convert hydrochemical data to consistent units, and to convert geospatial coordinates to consistent units. Spring location data was converted from geographic coordinates (i.e., latitude and longitude) to a Universal Transverse Mercator (UTM) projection using a NAD 83 datum. Fortunately, the entire study region lies within UTM Zone 11 N. Following database quality control procedures, the database was projected into ArcMap 10.3, a geographic information system (GIS).

For this study, three hydrochemical analytes are the most suitable, based on data availability and the information they provide about hydrogeologic processes for integrating with topographic and ecological indices: 1) spring discharge temperature, 2) specific conductance, and 3) radiocarbon activity. $^{13}\text{C}/^{12}\text{C}$ ratios, i.e., $\delta^{13}\text{C}$, are included for interpretation of regional radiocarbon activity trends. Discharge temperature and specific conductance (i.e., salinity) are two

of the primary environmental variables important for benthic macroinvertebrate community functioning (e.g., growth, food sources; Piscart et al., 2005). For example, water temperature is important for length-mass growth rates in spring aquatic gastropods (Mehler et al., 2015). Radiocarbon activity and tritium concentration are important indicators of groundwater residence time and have been used in global studies (e.g., Jasechko, 2016) to partition waters into old and young and in regional studies for understanding spring “regionalness” (Hershey et al., 2010). Groundwater residence time is strongly related to flowpath distribution and hydrogeological permanence. Radiocarbon (^{14}C) is one of the best environmental tracers for identifying ancient groundwater and calculating groundwater residence times in regional groundwater systems. In this region, past studies (e.g., Davisson et al., 1999) have examined large-scale patterns using radiocarbon activity rather than a calculated radiocarbon age for several reasons: 1) extensive interaction with Paleozoic carbonates (e.g., the regional carbonate aquifer) with a wide range of $\delta^{13}\text{C}$ makes accounting for this interaction extremely difficult using correction models, 2) aeolian carbonate dust deposition as well as interaction with pedogenic carbonates in the unsaturated zone can impact the early isotopic and carbon exchange and are difficult to quantify in the field (Spencer, 1990; Naiman et al., 2000), 3) there are large disagreements on the appropriate endmember value for $\delta^{13}\text{C}$ of recharge and soil carbon (e.g., -12 ‰ to -24 ‰) (Quade et al., 1989; Spencer, 1990; Anderson, 2002) and these parameters have a large influence on multiple radiocarbon correction models, and 4) in some areas, there are large amounts of nonlinear mixing (Davisson et al., 1999), especially at points of spring discharge.

Despite the utility of tritium (^3H) in parsing out distinctions between “young” and “old” groundwater, tritium (^3H) measurements were not included in regional analysis because there have been substantial improvements in analytical measurement uncertainty (i.e., many historical measurements simply reported ^3H concentration as <5 TU) as well as significant changes in the atmospheric concentration of low ^3H over the historical range of the dataset. Furthermore, the short half-life of ^3H (12.3 years) makes comparing historical data over several decades difficult. While this is also somewhat the case with bomb-pulse derived ^{14}C , the overall effects on the dataset are less pronounced due to its longer half-life and more precise historical measurement.

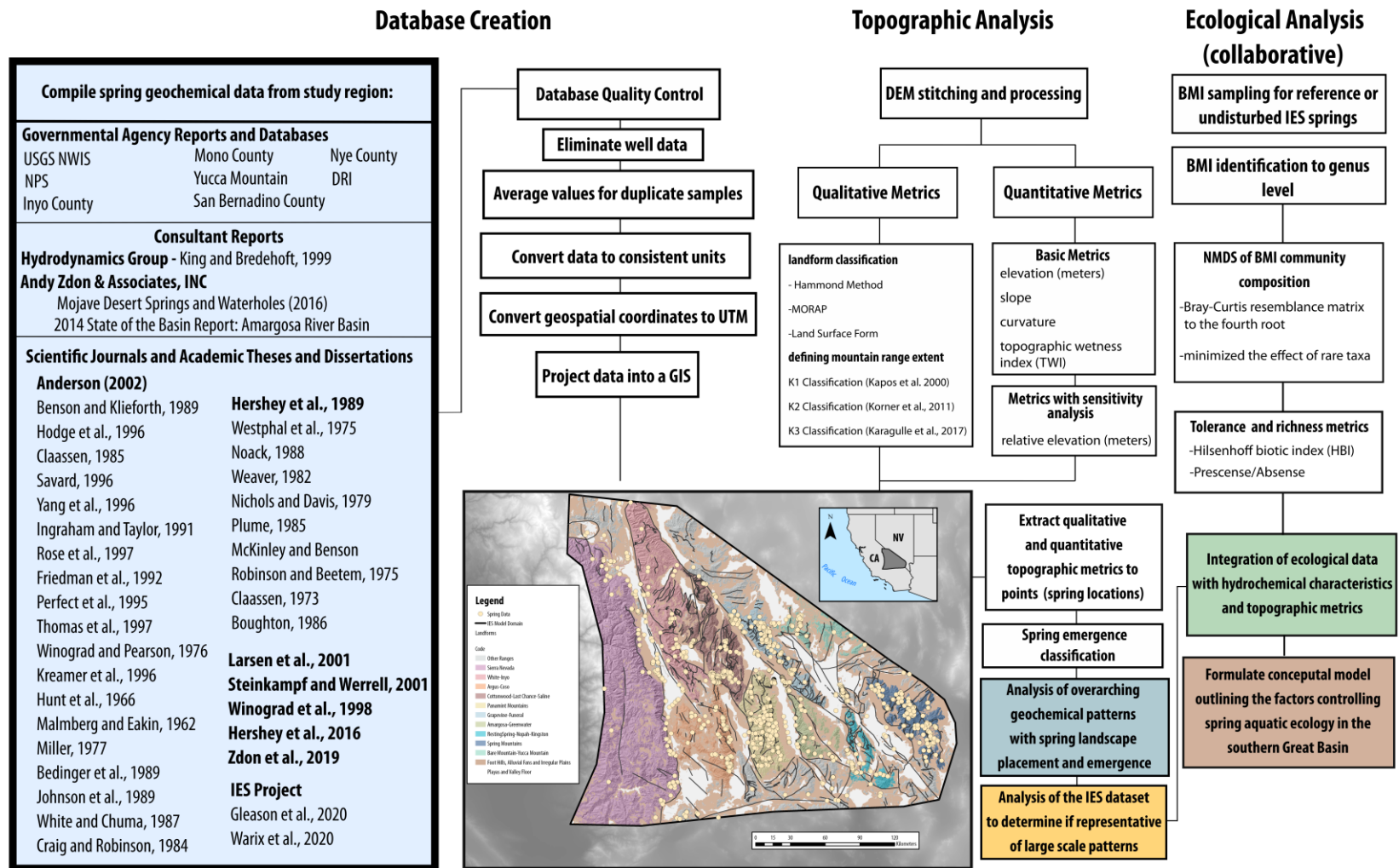


Figure 5.2. Flowchart showing the methodological workflow described in the paper. There are three main sections of the analysis: 1) database creation, 2) topographic analysis consisting of both qualitative and quantitative classification and metrics, and 3) ecological analysis.

5.3.3 Recent sampling efforts

The regional geochemical database, compiled from multiple agencies, reports, and literature (e.g., Figure 5.2) is used to examine regional connections between topographic metrics and hydrochemical characteristics. The IES dataset, a product of recent sampling efforts, is used to examine connections between hydrochemical characteristics, landscape placement, and BMI community composition. Recent collaborative sampling in the region from 2016-2019 (i.e., the IES dataset) have focused on undisturbed or reference (i.e., rehabilitated from past disturbance) springs in order to eliminate the effect of disturbance on BMI community composition. Prior work indicates that the effects of spring disturbance overprint the inherent environmental factors controlling aquatic ecological community structure (Williams et al., 1997; Sada and Nachlinger, 1996; Sada et al., 2005; Fleishman et al., 2006; Keheher and Rader, 2008a; Mehler et al., 2015; Sada and Lutz, 2016). In addition to spring condition, the distribution of springs was also chosen to capture the spatial and geomorphic heterogeneity of the study region. In total, 85 springs were sampled for a suite of hydrochemical analytes and 57 of these springs have a complete set of measurements (i.e., no missing samples across a suite of tracers) (Figure 5.3). Historical data from the USGS NWIS (<https://waterdata.usgs.gov/nwis>) was incorporated into the IES dataset for Peak Spring, IES-052 (missing discharge temperature), and Red Spring, IES-065 (pending ^{14}C activity analysis).

Ecological sampling was conducted in the summer months of 2017 and 2018 on 32 hydrologically persistent springs suitable for BMI collection (Figure 5.3). Springs were only sampled one time due to the harmful impact of BMI sampling on the aquatic community. Five subsamples were collected from each spring no more than 15 meters downstream from the spring orifice. The orifice of the springbrook typically has stable hydrochemical conditions suitable for BMI taxa (Glazier, 1991; McCabe, 1998). Samples were collected from 120 cm² quadrats using a 500 μm mesh net to capture suspended BMI in the water column following gentle roiling of the benthic substrate. After collection, samples were persevered in 70% ethyl alcohol before being sent for analysis at Rhithron Analytical Laboratory for taxonomic identification. Following the procedures of Vinson and Hawkins (1996), a minimum of 300 randomly selected individuals were chosen from each spring and identified to the genus level.

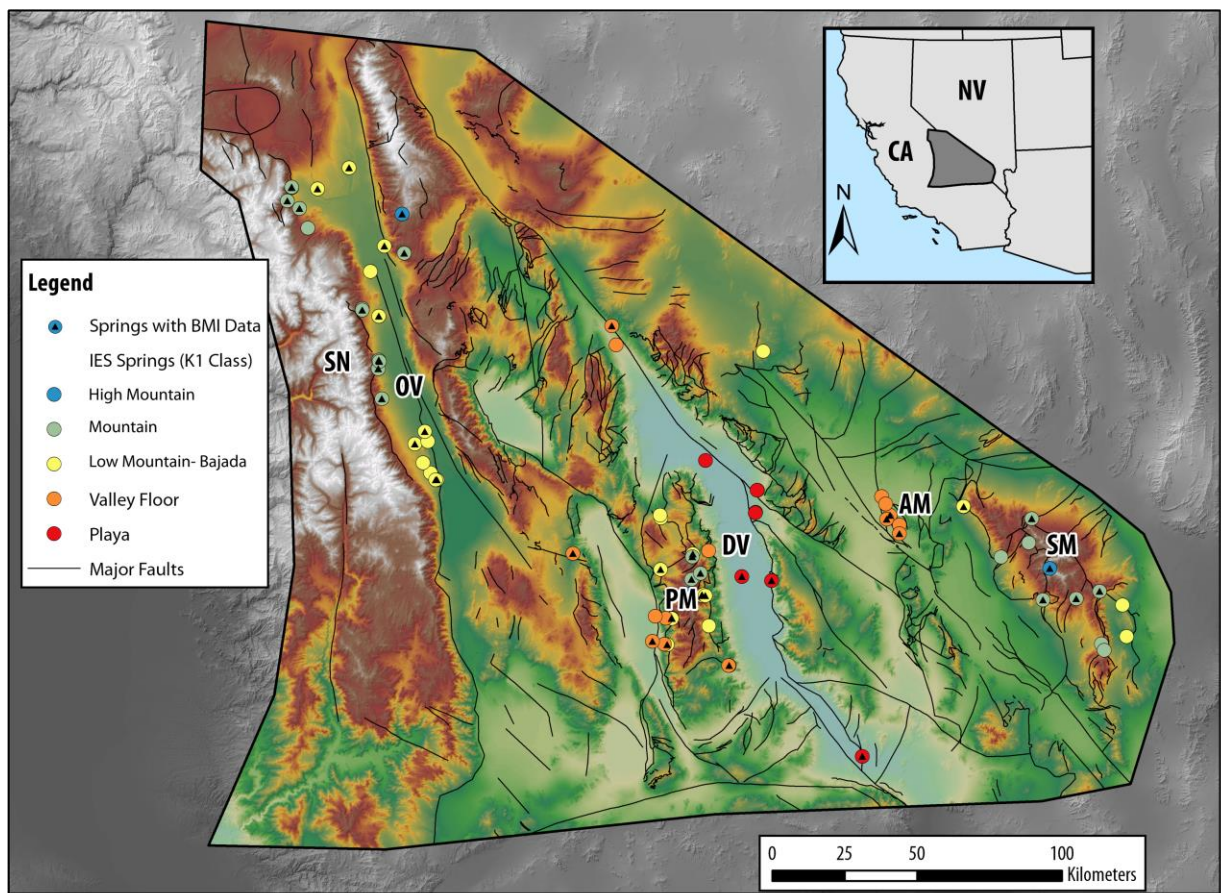


Figure 5.3. Map of the study area showing the IES springs (circles) symbolized by landscape position classification. Springs with associated BMI data are indicated by the inset black triangles within the circles.

5.3.4 Topographic analysis and indices

5.3.4.1 Elevation data acquisition and processing

Elevation data for the study area was acquired from The National Map (TNM), a part of the USGS National Geospatial Program. While small sections of the study area have 3DEP (3-D Elevation Program) elevation products available as 1-meter Digital Elevation Models (DEM), these high-resolution data are not available for the majority of the region. Therefore, 1/3 arc-second DEMs, the highest available resolution available for coverage over the entire study area, were downloaded as 1 X 1 degree GeoTIFFs from the TNM download manager (<https://viewer.nationalmap.gov/basic/>). A single 1/3 arc-second DEM of the entire study region was stitched together in ArcMap and clipped to the study area boundary. A secondary,

depressionless DEM was created using the Fill tool for the purpose of calculating error-free flow direction and flow accumulation rasters. These rasters are important inputs for calculating topographic metrics such as the Topographic Wetness Index (TWI).

5.3.4.2 Creating a topographic classification

Prior work from Sada and Thomas (2015) and Sada and Thomas (in review) found that qualitative classes indicative of different landscape placement positions and aquifer provenance for Great Basin springs (e.g., mountain, bajada, valley floor, playa, regional, and geothermal) were successful in predicting BMI community structure (i.e., springs at similar landscape placement were more similar to each other in terms of BMI taxa presence and abundance). However, these classifications were only partially based on topographic and morphometric indices and included the use of environmental characteristics (e.g., EC and temperature) to create partitions. For this study, we wanted to create a landscape placement classification for the southern Great Basin solely based on topographic and geomorphological criteria to assess the effect of topographic position on environmental characteristics. Therefore, the classification criteria from Sada and Thomas (2015) were not suitable for this analysis. However, the landscape placement positions utilized by Sada and Thomas (2015) were seemingly predicative, and therefore we wanted to find a way to mimic these classifications purely by using topographic indices. Before creating a new classification system, we wanted to examine if any existing topographic or landform classification systems would be suitable for this analysis.

The USGS, along with several partners (i.e., Esri, the University of Bern, the Global Mountain Biodiversity Assessment, and the Mountain Research Initiative) created the Global Mountain Explorer (GME; <https://rmgsc.cr.usgs.gov/gme/>) to create concrete topographic and/or bioclimatic criteria to quantitatively describe the boundaries of mountain ranges as well as separate different environments within mountains. The GME currently recommends three different mountain (and submountain) classification methods; K1, K2, and K3, named after the first letter of the authors' last names (i.e., Kapos et al., 2000; Körner et al., 2011; Karagulle et al., 2017). For the purposes of this study, the K1 class definition (Kapos et al., 2000) proved most appropriate because it incorporates elevation, slope, and terrain ruggedness and allows for discernment between intramontane classes within the study region. The K2 class definition is rather coarse (i.e., relies on a 1 km DEM resolution) and is perhaps most appropriate for continental or global

mountain/landform definition rather than for the extended and high-relief terrain of the southern Great Basin. The K3 class definition is somewhat similar to the K1 class output. However, it relies heavily on landform definitions as described by Hammond (1964) and has fewer intermontane classes to parse out differences between high mountains, mid-elevation mountains, and low mountains. In the K3 class definition, much of the western portion of the study area is under the same classification despite vast differences in relief and landform type.

Additional terrain definition is needed in the areas not characterized as mountains or bajadas by the K1 class criteria (i.e., there are areas within the study area that are not mountainous and thus were not classified by the K1 criteria). For these flatter, low lying areas, landforms (i.e., “land surface form”) were classified using methodology from the Missouri Resource Assessment Partnership (MoRAP) (True, 2002), a world leader in landform classification that built upon early work from Hammond (1964). The MoRAP method was not used to characterize landscape position at higher elevations because it has a limited power to characterize mountain classes at higher elevations due to a reliance on relief as a defining parameter. Due to this factor, the MoRAP method cannot distinguish between high mountains and deep canyons. Landscape position classes, based on a combination of elevation, slope, ruggedness, and relief criteria, were created for the study area by combining K1 class definition results for mountain areas with MORAP landform results for low-lying areas. The final result and associated class definitions are shown in Figure 5.4 and contain six classes: 1) Nival (i.e., treeless alpine), 2) High Mountain, 3) Mountain, 4) Low Mountain-Bajada, 5) Valley Floor, and 6) Playa.

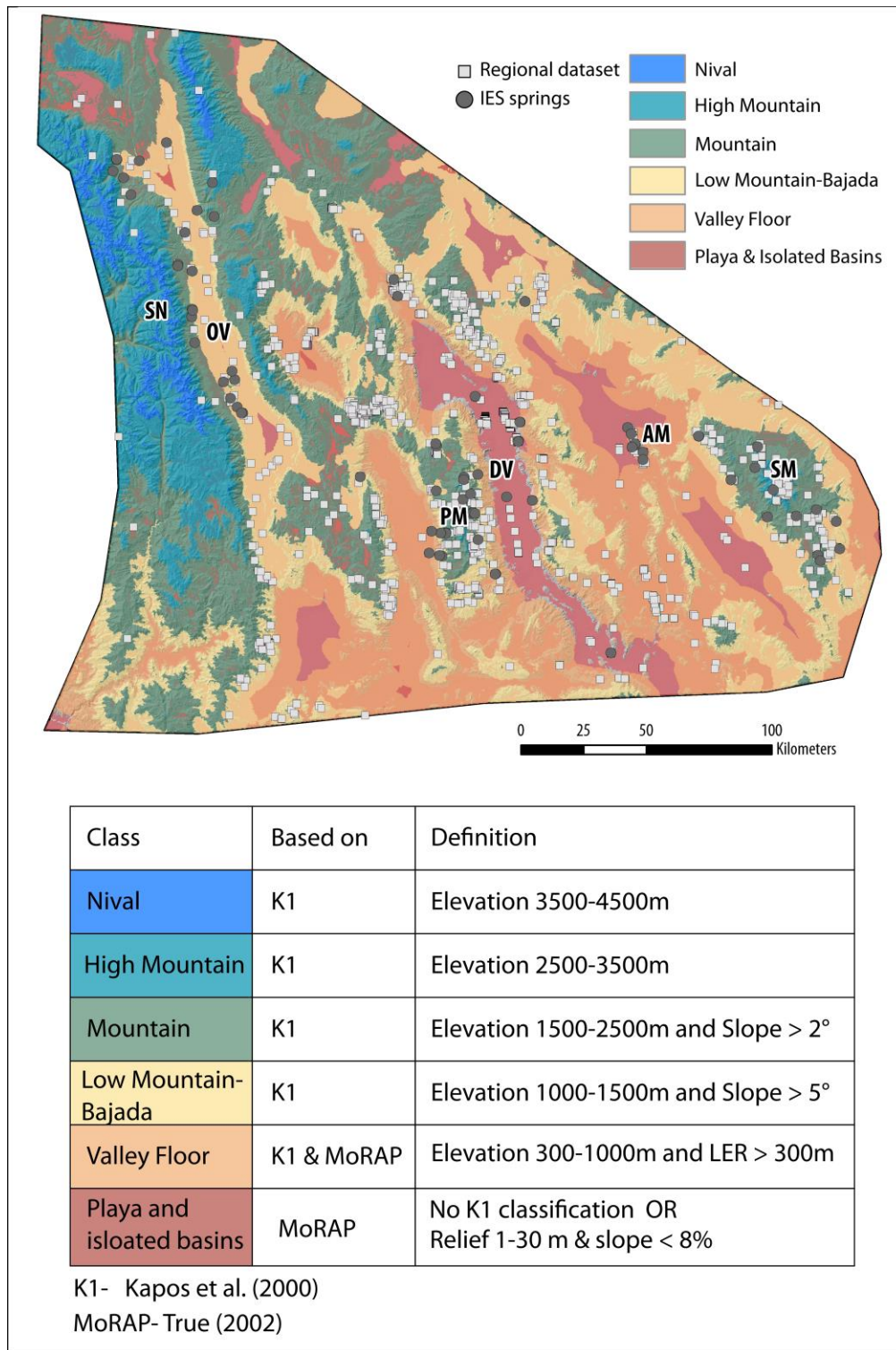


Figure 5.4. Map and associated table showing qualitative topographic classification of the study area derived by combining K1 classification (Kapos et al., 2000) with MoRAP classification (True, 2002). Class names (e.g., Nival, High Mountain, Mountain, Low Mountain-Bajada, Valley Floor, and Playa and isolated basins) were renamed to better characterize the study area and conform to prior classifications from Sada and Thomas (2015).

5.3.4.3 Quantitative analysis and indices

Methods for calculating topographic indices are described below. Associated maps and graphical descriptions are shown in Figure 5.5.

5.3.4.3.1 Elevation and slope

An elevation value for each point (i.e., spring) in the regional geochemical dataset was extracted from the stitched, non-filled, DEM based on the corresponding cell within the raster that the spring falls within. The slope, or gradient of maximum change in elevation value (i.e., first derivative of an elevation surface), was also calculated for each cell in the raster surface. Slope was calculated both in terms of degree (i.e., inclination) and percent rise.

5.3.4.3.2 Topographic Wetness Index (TWI)

Topographic Wetness Index (TWI), first developed by Beven and Kirby (1979), is a topographic index based on surface water metrics (i.e., upslope accumulated area) and slope. It is commonly used to evaluate the effects of topography on the characteristics (e.g., shallow groundwater level, chemistry, residence time) of hydrologic features supported by groundwater such as wetlands and streams (Western et al., 1999; Grabs et al., 2009; Welsch et al., 2001; Dowling et al., 2003; Peralta-Tapia et al., 2015). Rinderer et al. (2014) found that topographic indices such as TWI are best applied to groundwater problems in areas where groundwater levels change slowly.

Calculation of TWI is as follows:

$$TWI = \ln \left(\frac{a}{\tan(b)} \right)$$

a = upslope accumulation area (UAA), where UAA can be calculated by multiplying the flow accumulation raster output by the raster cell area size. Flow accumulation sums the number of cells that flow into any given cell and is calculated from the flow direction raster. Flow direction is calculated from a depressionless DEM and indicates the direction of flow from any given cell to the steepest downgradient neighbor.

b = slope (in radians)

5.3.4.3.3 Relative elevation

Relative elevation and Topographic Position Index (TPI) (Weiss, 2001) are both metrics that describe whether a given cell is at a higher or lower topographic position in comparison to surrounding cells (i.e., the neighborhood). Calculation of relative elevation or TPI generally requires some sensitivity analysis at the discretion of the analyst because the output is completely dependent on the size (i.e., distance) and shape (e.g., annulus, circle, square, etc.) of the neighborhood. A small neighborhood is used to examine topographic position at local scales, while larger neighborhoods are used to examine regional patterns. Compared with relative elevation, TPI is less used as a quantitative metric and more often used as an input into qualitative classification schemes such as Hillslope Position (Miller, 2014), Slope Position (Jenness, 2006), or Landform Class (Jenness, 2006). In this study we use relative elevation to examine regional trends in topographic position. A sensitivity analysis was performed to examine relative elevation results at varying neighborhood sizes and shapes in order to find an optimal neighborhood. After sensitivity analysis, it was determined that a 400-cell neighborhood was most appropriate for in a 30m DEM was appropriate for examining regional trends of topographic position in a high-relief setting such as the southern Great Basin. A precise methodology for calculating relative elevation is detailed in Miller (2014). Relative elevation is calculated by subtracting the inverse elevation from the base elevation within the analysis neighborhood. An inverse elevation grid is calculated by subtracting the highest and lowest elevation values within a neighborhood window.

5.3.4.3.4 Curvature

Landscape curvature is a measure of the shape (i.e., concavity or convexity) of an elevation surface and is calculated by finding the second derivative of a surface elevation raster. The importance of curvature in hydrologic applications has been documented by numerous studies (e.g., Woods et al., 1997 Hjerdt et al., 2004; Hoover and Wolman, 2005; Vivoni et al., 2008; Prancevic and Kirchner, 2019) and is attributed to the fact that concavity causes augmentation of local drainage, both on the surface and in the subsurface.

Curvature can either be calculated in the profile (i.e., parallel to the direction of slope) or planform (i.e., perpendicular to the direction of slope) directions. An “overall” curvature can be

calculated by summing profile and planform results for each cell. In hydrologic studies, profile curvature is the more commonly used metric as an indicator of the presence or environmental characteristics of subsurface flow. Therefore, in this study, profile curvature was used. Negative profile curvature values indicate upward convexity while positive curvature values indicate downward concavity. There are no limits or bounds of what these values can be, however, high relief, mountain settings tend to have profile curvature values between -4 (highly convex) and +4 (highly concave).

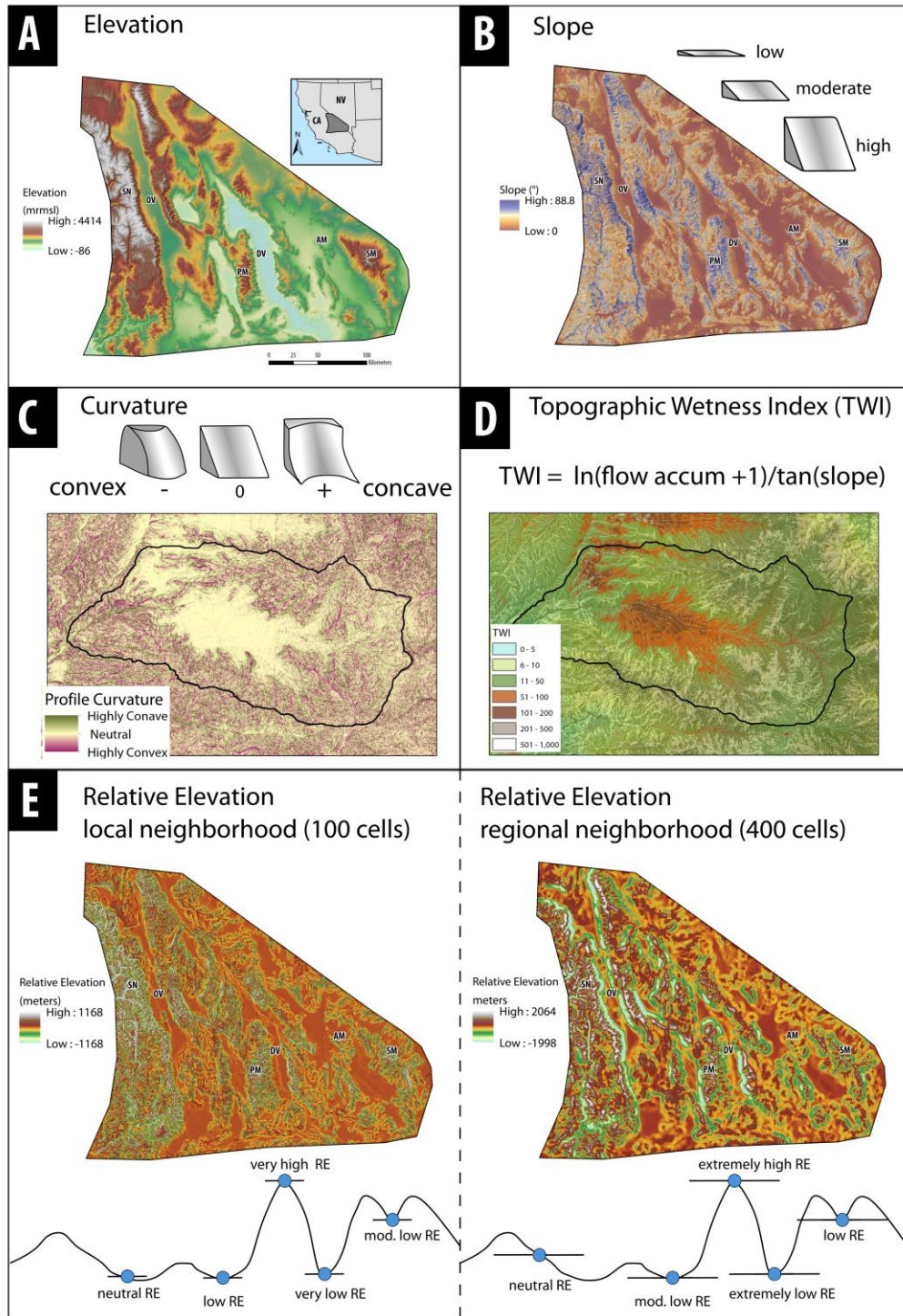


Figure 5.5. Diagram showing the following topographic metrics used in this study: A) Surface elevation, B) Slope, C) Curvature, D) Topographic Wetness Index (TWI), and E) Relative Elevation. For the purposes of clarity, curvature and TWI are both shown at the watershed scale for a catchment draining the western Panamint Range. Relative elevation is shown at both the local neighborhood (100 cell radius) and regional neighborhood (400 cell radius) scales.

5.3.5 Identifying springs emerging at fault zones

The original intention of this section was to provide an emergence classification for each spring in the regional dataset. Springs were to be designated as emerging due to structural features (i.e., faults), contacts, or topographic/unknown based on proximity analysis. Unfortunately, due to the extreme geologic and structural complexity of the study region, it is almost impossible to automate this process at a “big data” scale without individual spring emergence characterization and possible field confirmation. Major geologic contacts are numerous (Figure 5.6A) The number of minor faults in the area, obtained from combining geospatial data from the California Division of Mines and Geology (Jennings et al., 1977) and the Nevada Bureau of Mines and Geology (Stewart and Carlson, 1978), number the thousands (Figure 5.6B). Initial proximity analysis with minor faults and contacts resulted in significant overlap. Therefore, only major faults in the study region, as designated and classified by Lutz (2020) as critical areas of tectonic displacement or major hydrogeologic boundaries, were considered (Figure 5.6C).

Prior work on spring resource prospection and groundwater potential (e.g., Al-Hanbali and Kondoh, 2008; Odezmir, 2011; Pourtaghi and Pourghasemi, 2014; Khosravi et al., 2018) indicates that distance from fault can be used as a quantitative metric or classification criteria for determining the hydrochemical characteristics of groundwater. In this study we use two distance measurements, 100 meters and 1000 meters, as classification criteria to designate springs as “fault controlled” or “non-fault controlled” based on proximity to major structural features from Lutz et al. (2017).

5.3.6 BMI analysis and indices

The following sections describe various methods used in this paper for analyzing BMI data. Due to the qualitative nature of BMI data, multivariate statistical methods are commonly employed as a way to examine clustering or dissimilarity between samples. An alternative approach is to use ecological metrics such as stress tolerance values (e.g., Mandaville, 2002) to “score” different taxa and then compare results between sites or samples. In this paper we use both multivariate statistical methods and ecological indices to compare spring BMI results with topographic and geochemical metrics.

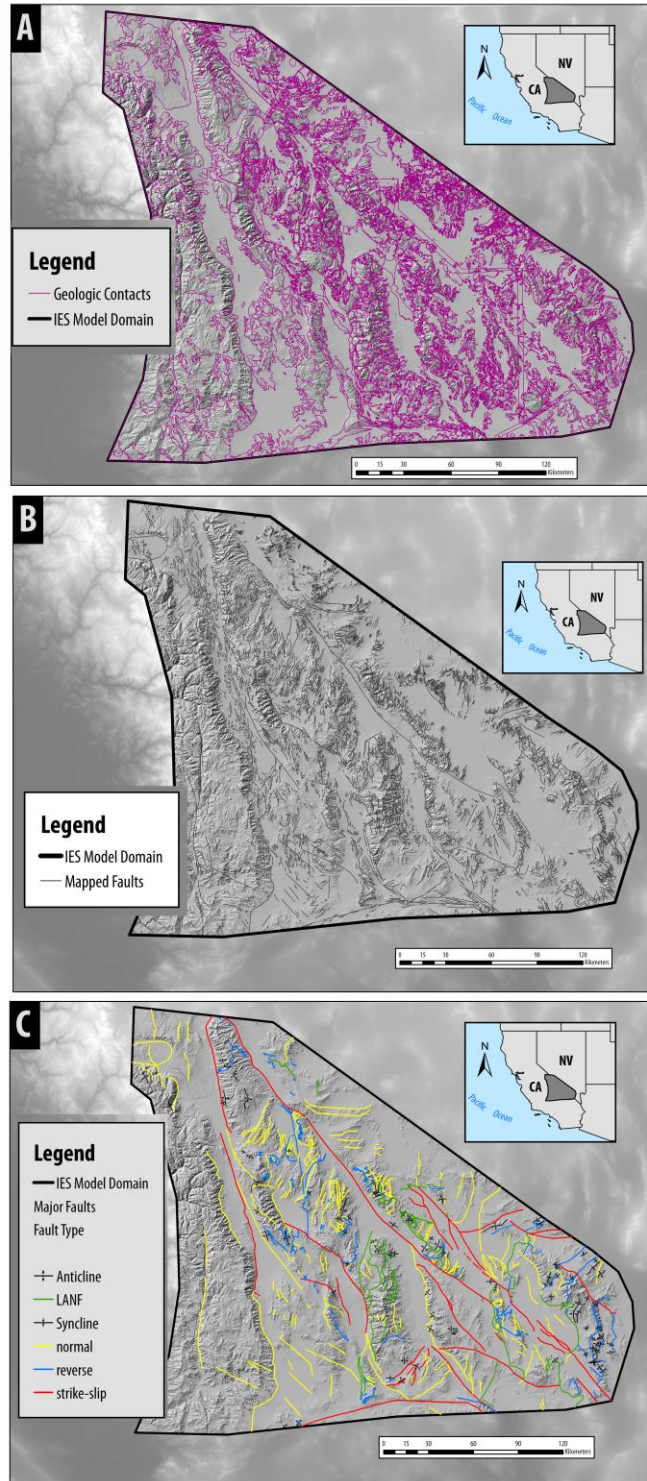


Figure 5.6. A) Map of the study area showing major geologic contacts. B) Map of the study area showing synthesized mapped fault locations in California (Jennings et al., 1977) and Nevada (Stewart and Carlson, 1978). C) Map of the study area showing major faults. There are six types of major faults identified in the study area: 1) anticlines, 2) low-angle normal faults (LANF), 3) syncline, 4) normal, 5) reverse, and 6) strike-slip.

5.3.6.1 Non-metric multidimensional scaling (NMDS) analysis

Non-metric multidimensional scaling or NMDS is a common analysis tool used in ecological studies for determining similarity, or alternatively, dissimilarity, between samples or sites. A successful NMDS results in a final ordination plot where there is fidelity between rank order of dissimilarities among pairs of samples and distances between these same samples in the NMDS plot (Clarke and Gorley, 2006). In other words, samples close together within the NMDS ordination indicate high community similarity while samples far apart imply high community dissimilarity. The “fit” of the NMDS ordination, i.e., whether the results are significant or arbitrary, is determined by the stress value. Stress values above 0.2 are not ideal and stress values above 0.3 indicate that the ordination is arbitrary. An example BMI plot is shown in Figure 5.

NMDS requires a definition of resemblance between pairs of samples. In this study I use Bray-Curtis resemblance matrix of the fourth root transformed BMI data, the most commonly used similarity coefficient in ecological studies, to calculate dissimilarity between samples. Previous studies have found that the presence of rare taxa can exert a large influence over bioassessment results (e.g., Cao et al., 2001; Shade et al., 2014). Therefore, the effect of rare taxa was minimized by limiting the analysis to genera present in 90% of samples. NMDS analysis in this study was performed using Primer v6 (Clark and Gorley, 2006).

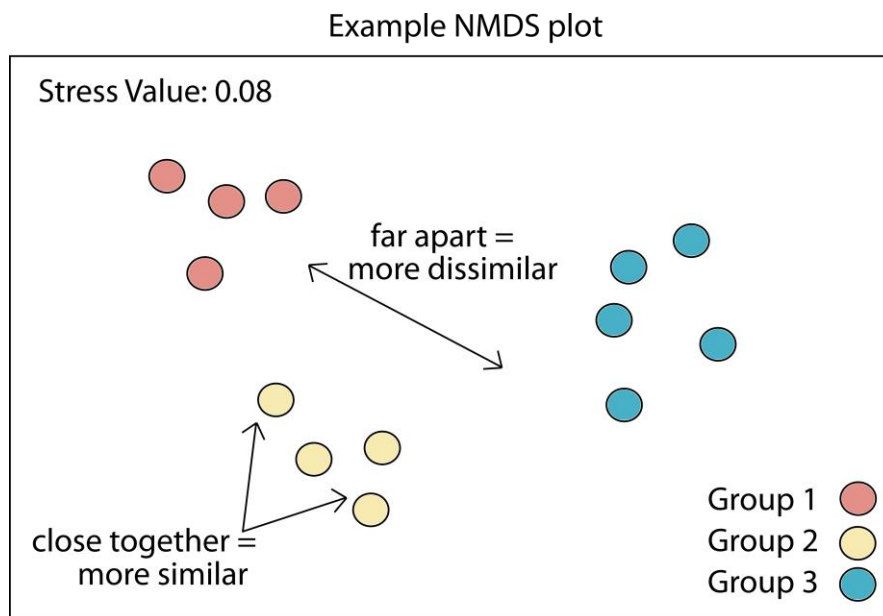


Figure 5.7. Example BMI plot showing relationship between NMDS distance and similarity.

5.3.6.2 Ecological metrics and indices

BMI function as bioindicators of water quality because they are sensitive to environmental factors, e.g., water temperature, salinity, dissolved oxygen concentration, oxidation-reduction potential, etc. Due to the relatively constant hydrochemical conditions created by discharging groundwater, spring-dwelling BMI are uniquely suited to their environment (McCabe, 1998). Therefore, the presence of individual BMI taxa or a community composition of BMI taxa in springs are considered indicative of environmental characteristics (Mandaville, 2002). In this study, we utilize several ecological metrics to understand spring BMI community composition. These metrics are powerful evaluation criteria and include total richness, Shannon diversity, the Hilsenhoff Biotic Index (HBI), percent tolerant taxa (presence/absence), and percent intolerant taxa (presence/absence).

In this study, total richness simply refers to the number of taxa present in each spring. Shannon diversity index, a biodiversity metric that is one of the most commonly used diversity indices, is calculated from the following equation and highly dependent on the number of total individuals in a sample:

$$SDI = -\sum \left[\left(\frac{n_i}{N} \right) * \ln \left(\frac{n_i}{N} \right) \right]$$

SDI = Shannon Diversity Index

n_i = number of individuals belonging to a particular taxon

N = total number of individuals in the sample

Calculation of HBI, percent tolerant taxa, and percent intolerant taxa are based upon a BMI tolerance rating system, Mandaville (2002), that has been extensively used for a variety of biomonitoring applications. Mandaville (2002) assigns a tolerance value (TV) from 1-10 to each taxa based on resistance of the organism to pollution or environmental harshness. Taxa with $TV < 3$ are considered intolerant while taxa with $TV > 7$ are considered tolerant.

The Hilsenhoff Biotic Index (HBI) shows the overall tolerance of the aquatic BMI community. HBI is calculated as follows:

$$HBI = \frac{\sum n_i \times a_i}{N}$$

n = total number of specimens in taxa

a = taxa tolerance value from Mandaville (2008)

N = total number of specimens in sample

As shown in the above equation, HBI is relatively sensitive to total number of specimens, both in the sample and for individual taxa. Numerous studies have indicated that simply the presence or absence of taxa within a sample can be indicative of water quality or stable physical/chemical conditions (Resh and Rosenberg, 1993; Hynes, 1998). Percent tolerant taxa (presence/absence) is simply calculated by dividing the number of tolerant taxa present in a sample by the total number of taxa present in a sample. Percent intolerant taxa (presence/absence) is simply calculated by dividing the number of intolerant taxa present in a sample by the total number of taxa present in a sample.

5.4 Results

5.4.1 Relationship between qualitative spring landscape placement classification and hydrochemical characteristics

Statistical boxplots showing the distribution of results for spring discharge temperature ($^{\circ}\text{C}$), specific conductance ($\mu\text{S}/\text{cm}$), radiocarbon activity (pMC), and $\delta^{13}\text{C}$ (‰ relative to VPDB) are shown for the regional dataset in Figure 5.8. Results are partitioned by the qualitative landscape placement classes described in Figure 5.5, however, there are no springs with historical hydrochemical data within the study region that fall into the “Nival” group. Our results show consistent increases in median values and quartile distributions with spring discharge temperature, specific conductance, and $\delta^{13}\text{C}$ from high topographic positions (i.e, High Mountain and Mountain) to lower topographic positions (i.e., Low Mountain and Valley Floor). Conversely, our results show relatively consistent decreases in radiocarbon activity with decreasing topographic position. However, springs that fall within the “Playa” class show a significant statistical increase in specific conductance and a decrease in spring discharge temperature from the “Valley Floor” springs. Little to no change is observed from “Playa” to “Valley Floor” springs with regards to radiocarbon activity and $\delta^{13}\text{C}$.

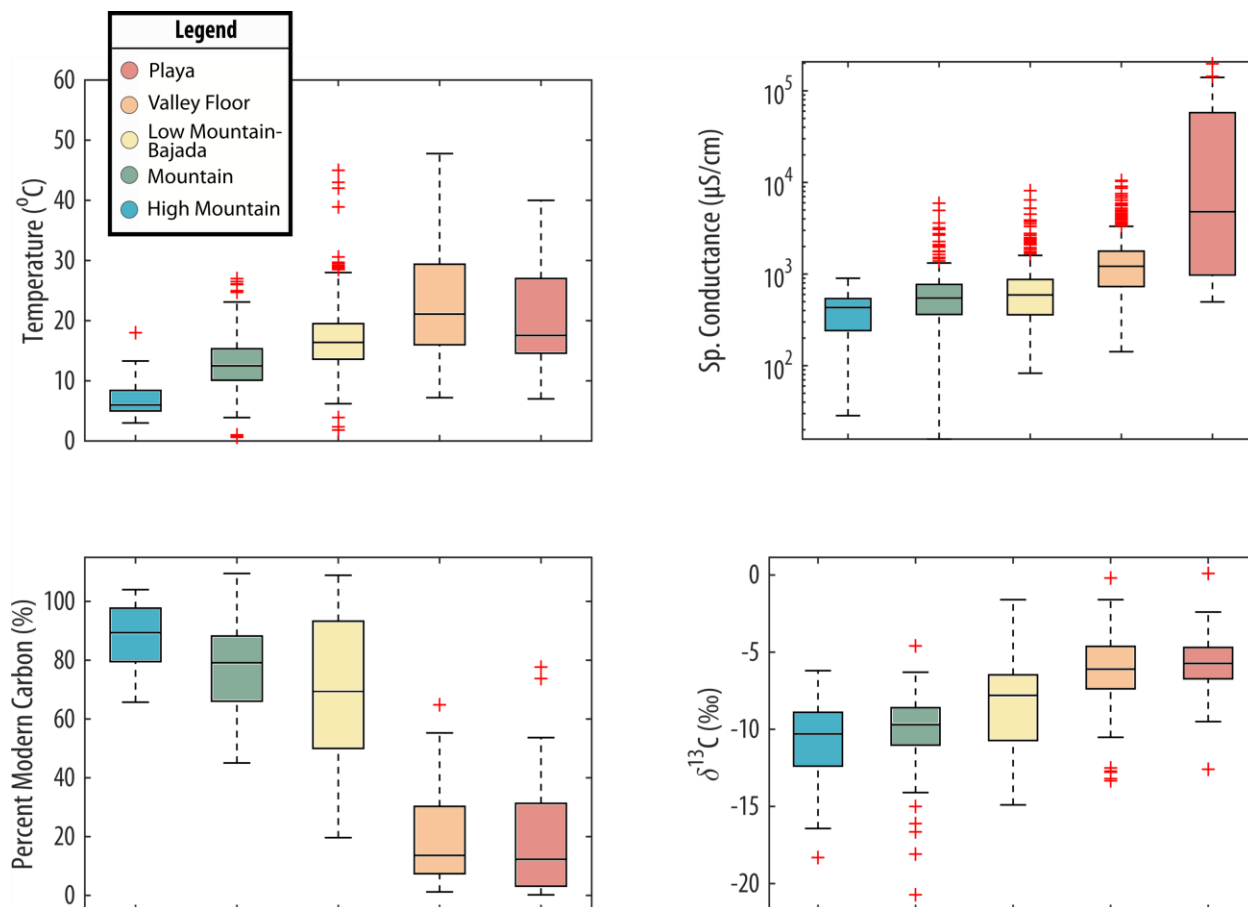


Figure 5.8 Boxplots showing systematic trends in spring temperature, specific conductance, radiocarbon activity (percent modern carbon), and delta carbon 13 with landscape placement classifications. The central mark in each box represents the median value. The bottom and top extent of each box represent the 25th and 75th percentiles, respectively. The whiskers extend to the maximum and minimum data points not considered outliers. Outliers are represented by the “+” symbols.

5.4.2 Relationship between quantitative topographic metrics and hydrochemical characteristics

Relationships with topographic metrics and spring discharge temperature, specific conductance, and radiocarbon activity are shown in Figure 5.9, Figure 5.10, and Figure 5.11, respectively. Each hydrochemical characteristic is plotted against elevation (meters), slope (degrees), TWI (unitless), curvature (unitless), and relative elevation (meters; 400 cell neighborhood) and symbolized by qualitative landscape placement class. On each plot, springs from the regional dataset are plotted as squares and springs from recent sampling efforts, the IES

dataset, are plotted as circles. The IES springs are included as a visual way to show how, as a smaller sample distribution, they are representative of regional trends.

In terms of spring temperature (Figure 5.9), both surface elevation ($R^2 = 0.23$, $P < 0.001$) and slope ($R^2 = 0.11$, $P < 0.001$) show relatively robust prediction potential. In contrast, TWI, a metric frequently used as a part of surface water studies and often applied to groundwater problems, shows relatively no predicative potential ($R^2 = 0.00$, $P = 0.72$). Profile curvature and relative elevation do not create trends that can be used as linear predication models; however, they are still informative. While areas of neutral and negative profile curvature produce results that are nonunique (i.e., similar profile curvature values are associated with a wide range of discharge temperatures), areas of elevated profile curvature have discharge temperature values predominately below 20°C. Similarly, springs with relative elevation values from -1000 meters to 0 meters are associated with a wide range of discharge temperatures. Springs emerging at positive (>0 meters) and highly negative (< -1000 meters) relative elevations have discharge temperature values predominately below 20°C.

Regional trends with topographic indices and spring specific conductance (Figure 5.10) and radiocarbon activity (Figure 5.11) are similar to those observed with discharge temperature. Surface elevation is a moderate, but robust, predictor of spring specific conductance ($R^2 = 0.2$, $P < 0.001$) and a strong predictor of radiocarbon activity ($R^2 = 0.49$, $P < 0.001$). Weaker correlations are observed with slope and spring specific conductance ($R^2 = 0.08$, $P < 0.001$) and radiocarbon activity ($R^2 = 0.19$, $P < 0.001$). TWI has no apparent prediction potential. The majority of springs emerging in areas of elevated profile curvature (i.e., very concave) tend to neither be extremely dilute (<100 $\mu\text{S}/\text{cm}$) nor evolved (>1000 $\mu\text{S}/\text{cm}$). Springs emerging in areas of positive relative elevation (>0 meters) or very negative relative elevation (< -1000 meters) predominately have specific conductance values <1000 $\mu\text{S}/\text{cm}$. Due to the limited number of samples and high degree of nonuniqueness, it is difficult to elucidate patterns with radiocarbon activity and profile curvature. Areas of positive relative elevation (>0) of highly negative elevation (< -1000 meters) primary have radiocarbon activity values > 60 pMC.

Scatter plots featuring springs emerging in two representative mountain blocks, the Funeral-Grapevine Mountains (hyperarid) and the Spring Mountains (more humid) are shown with the topographic metric most predictive of hydrochemical characteristics, surface elevation (Figure 5.12). These scatter plots show that the immense variability of the regional dataset contains buried,

more linear trends in individual mountain ranges. Correlations with surface elevation and temperature are stronger in individual mountain blocks, i.e., the Funeral-Grapevine Mountains ($R^2 = 0.31$, $P < 0.001$) and the Spring Mountains ($R^2 = 0.63$, $P < 0.001$) compared with the regional dataset. Stronger trends are also observed with radiocarbon activity for the Funeral-Grapevine Mountains ($R^2 = 0.80$, $P < 0.001$) and the Spring Mountains ($R^2 = 0.62$, $P < 0.001$) compared with the regional dataset. However, our results shown that for specific conductance, correlations area weaker for individual mountain blocks in comparison with the study area ($R^2 = 0.20$, $P < 0.001$).

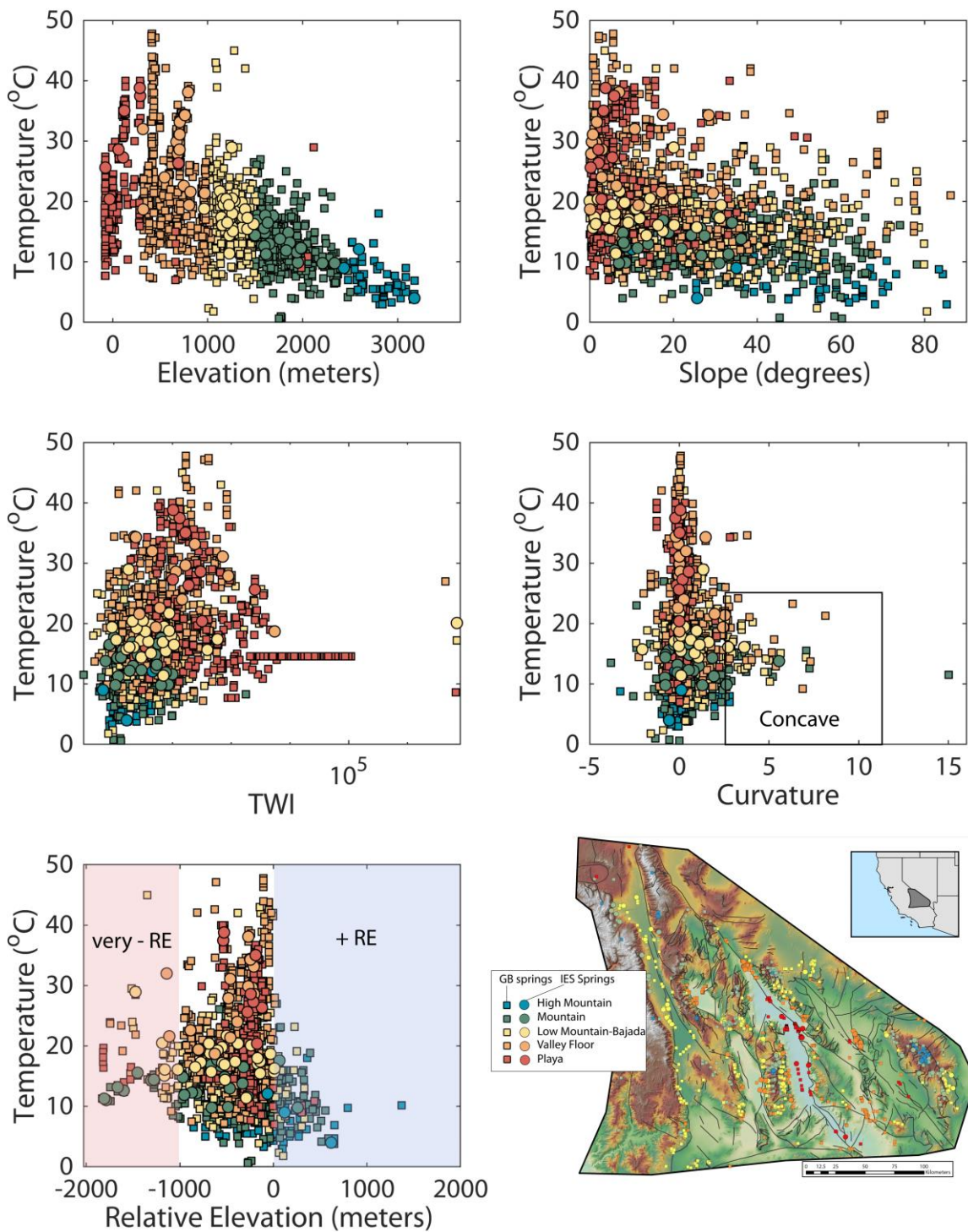


Figure 5.9. Spring discharge temperature is plotted against elevation (meters), slope (degrees), TWI (unitless), curvature (unitless), and relative elevation (meters; 400 cell neighborhood) and symbolized by qualitative landscape placement class. On each plot, springs from the regional dataset are plotted as squares and springs from recent sampling efforts, the IES dataset, are plotted as circles.

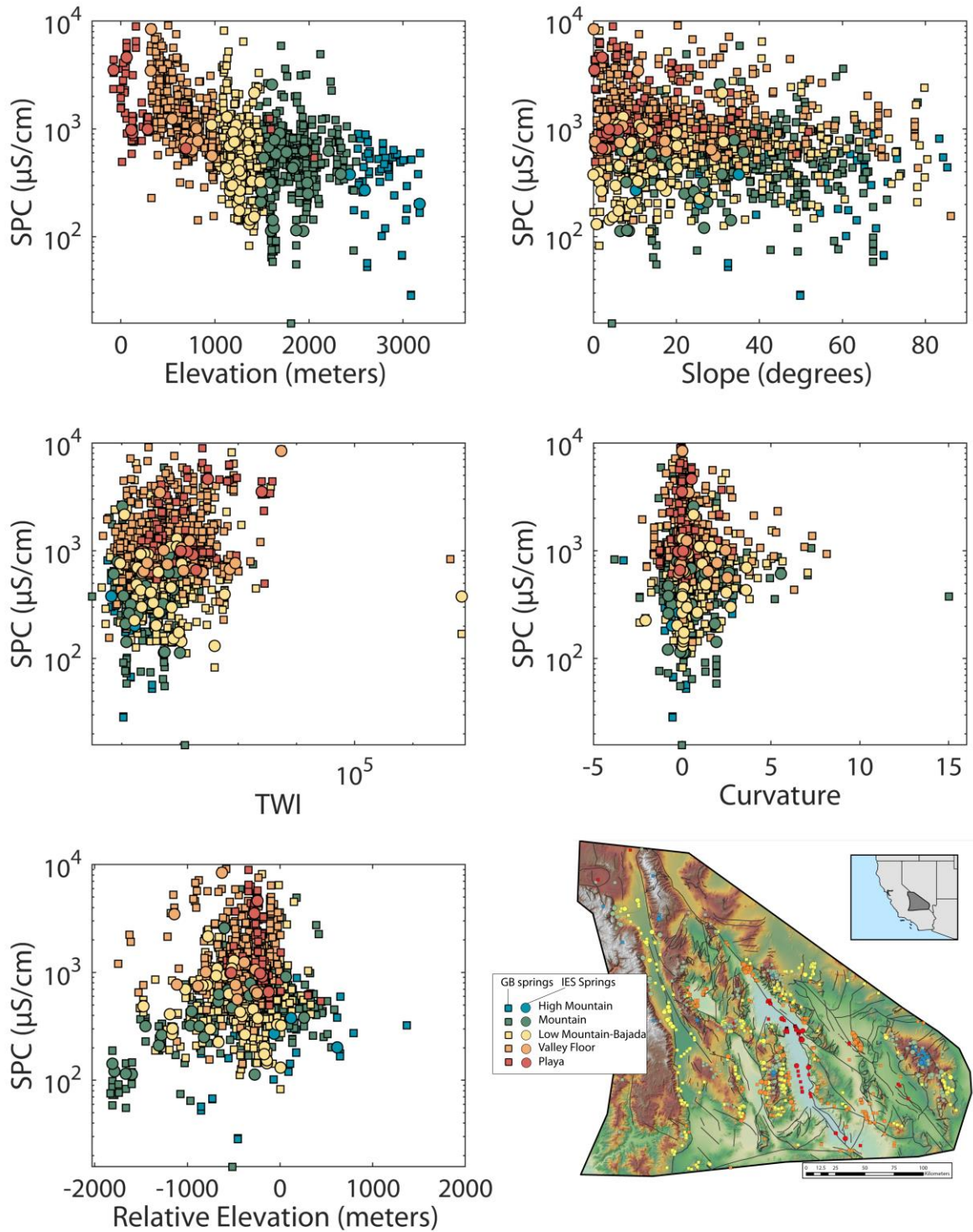


Figure 5.10 Spring specific conductance is plotted against elevation (meters), slope (degrees), TWI (unitless), curvature (unitless), and relative elevation (meters; 400 cell neighborhood) and symbolized by qualitative landscape placement class. On each plot, springs from the regional dataset are plotted as squares and springs from recent sampling efforts, the IES dataset, are plotted as circles.

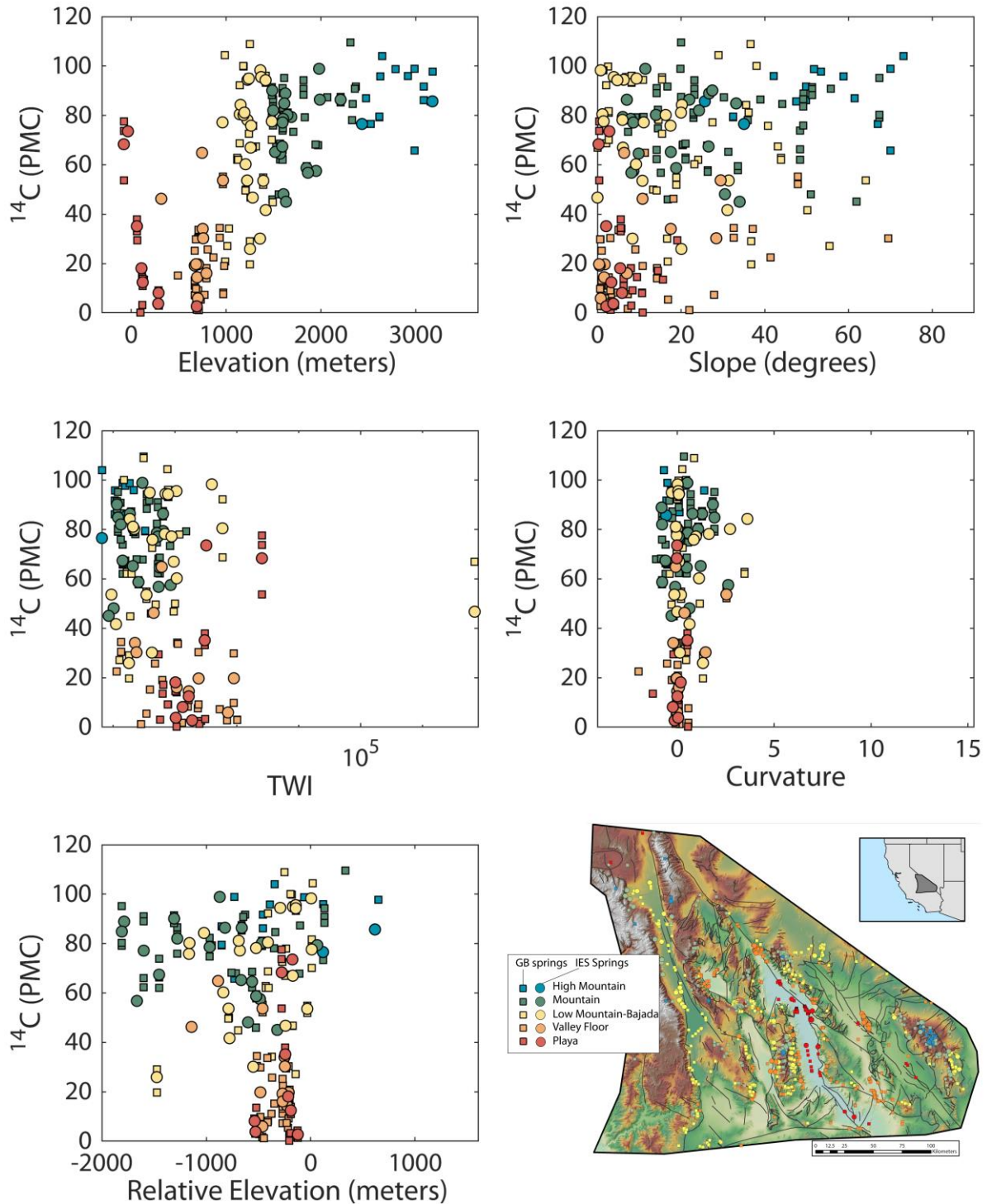


Figure 5.11. Spring radiocarbon activity is plotted against elevation (meters), slope (degrees), TWI (unitless), curvature (unitless), and relative elevation (meters; 400 cell neighborhood) and symbolized by qualitative landscape placement class. On each plot, springs from the regional dataset are plotted as squares and springs from recent sampling efforts, the IES dataset, are plotted as circles.

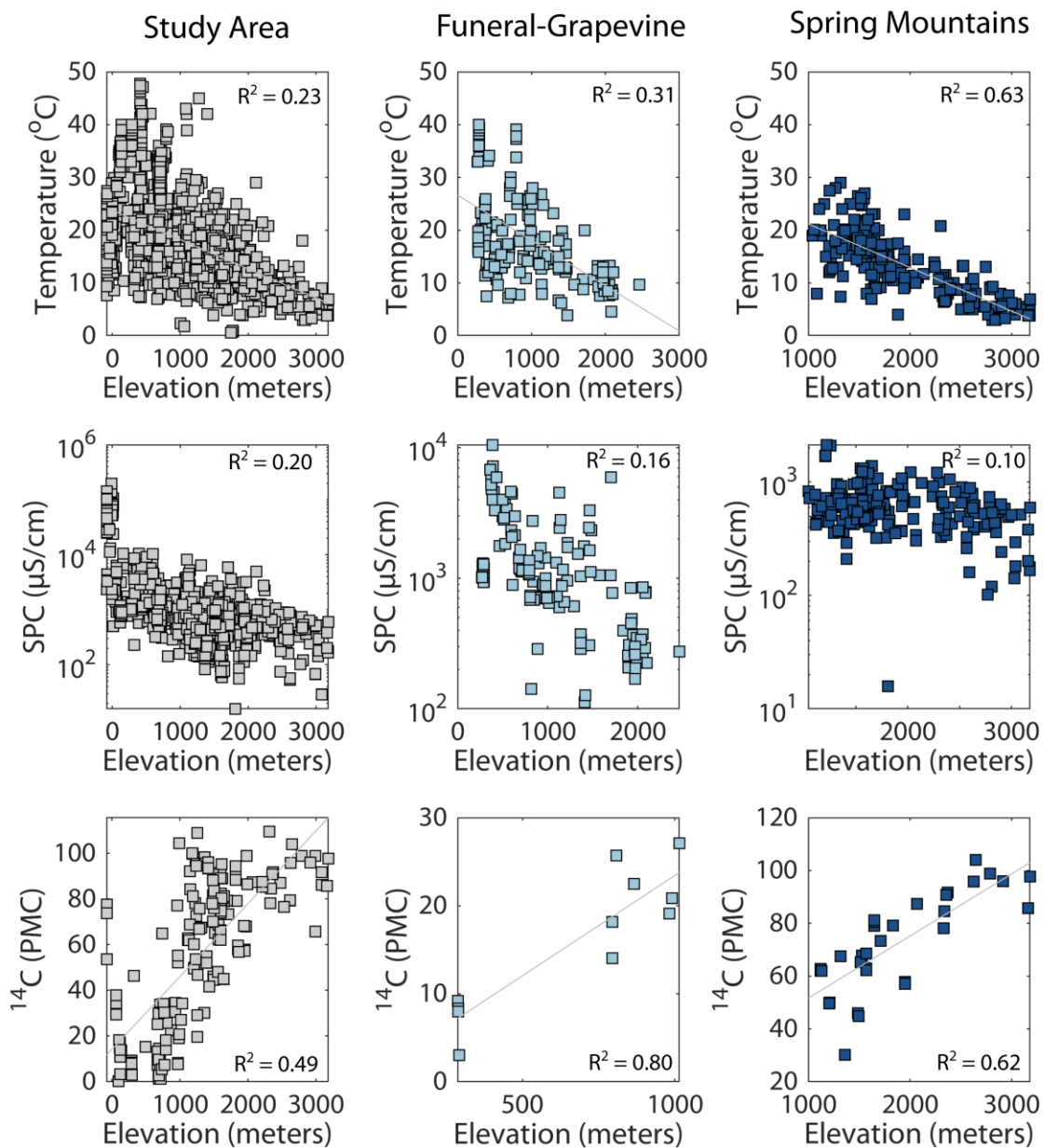


Figure 5.12. Plots of elevation versus radiocarbon activity, specific conductance, and spring discharge temperature for springs in the entire study area and two representative mountain blocks, the Funeral-Grapevine Mountains (light blue squares) and the Spring Mountains (dark blue squares).

5.4.3 Relationship between emergence mechanism and hydrochemical characteristics

Statistical boxplots showing the distribution of discharge temperature and radiocarbon activity for springs classified as either “fault-controlled” or “not fault-controlled” are shown in Figure 5.13. Springs are classified as either “fault-controlled” or “not fault-controlled” based on whether they emerge within 100 meters of a major structure feature (top) or within 1000 meters of a major structure feature (bottom). At the 100-meter proximity range, “fault-controlled” springs have a lower median value and quartile distribution of radiocarbon activity and discharge temperature compared with the “not fault-controlled” springs. However, there is a relatively narrow range of values for radiocarbon activity for “fault-controlled” springs, likely indicating that a 100-meter proximity is small of a distinction for classification purposes.

When fault proximity classification is extended to 1000 meters, “fault-controlled” springs have a lower median value and quartile distribution of radiocarbon activity compared with “not fault-controlled” springs. Similarly, “fault-controlled” springs are on average warmer, having a higher median value and quartile distribution of spring discharge temperature compared with “not fault-controlled” springs.

Springs classified as “fault-controlled” based on the 1000-meter proximity analysis are assigned the fault attribute characteristics (i.e., structural feature classification) of the nearest proximity fault. Boxplots showing the distribution of spring discharge temperature and radiocarbon activity for different structural feature types are shown in Figure 5.14.

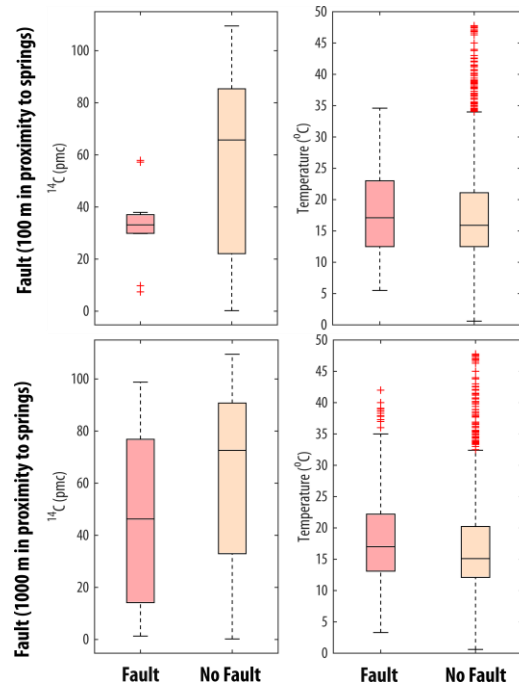


Figure 5.13. Boxplots comparing radiocarbon activity and spring temperature at “fault-controlled” and “non fault-controlled” springs.

Springs emerging at normal and strike-slip faults tend to have elevated median values and quartile distributions of discharge temperature compared with springs emerging at anticlines, low-angle normal faults (LANF), reverse faults (i.e., thrust), and synclines. Springs emerging at normal faults and strike-slip faults also have lower median values and quartile distributions of radiocarbon activity compared with springs emerging at LANF, reverse faults, and synclines. There are no springs within the regional dataset classified as emerging at mapped anticlines with applicable radiocarbon activity data.

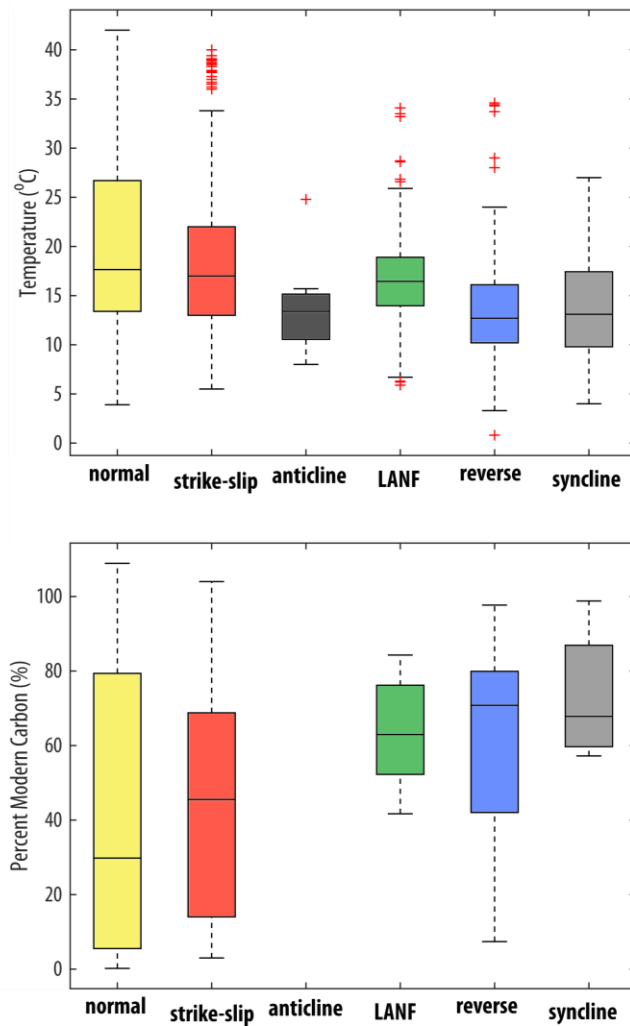


Figure 5.14. Boxplots showing comparison of spring temperature and percent modern carbon for springs emerging at different types of major faults (e.g., Figure 5.6C)

5.4.4 NMDS results

Ordination plots showing NMDS results of BMI community composition are shown in Figure 5.15 and Figure 5.16. Both ordination plots show the same NMDS results but have different symbologic definitions for the spring samples. The 2D stress value for the NMDS plots is 0.166, indicating that the ordination is relatively well fit and not suspect (> 0.2) or arbitrary (> 0.3).

In Figure 5.15, the NMDS results show that at least some aspect of BMI community structure dissimilarity can be described by qualitative classes of spring landscape position. While

there are not concrete distinctions between groups, the “High Mountain” and the majority of “Mountain” springs are clearly distinguished from the “Valley Floor” and “Playa Springs”. The BMI community structure of “Low Mountain-Bajada” springs exhibits the most intragroup spread. The complementary statistical boxplots for the IES springs (Figure 5.15) show the same systematic trends as the regional data (i.e., Figure 5.8), indicating that the springs sampled in this study are representative of regional patterns. Tritium (^3H) is included in these boxplots as another indicator of groundwater residence time because these springs were all sampled over a similar period (2016-2019) and analyzed with the same degree of precision.

In Figure 5.16, the NMDS results are symbolized by residence time partitions. The complementary 3D scatter plot within Figure 5.16 shows a graphical representation of how ^{14}C , ^3H , and $^{36}\text{Cl}/\text{Cl}$ ($\times 10^{-15}$) are used to partition samples. Groundwater residence times determined via the Tamers radiocarbon correction model quantitatively describe the differences between graphical partitions. The NMDS results in Figure 5.16 show subtle, but informative, distinctions from the landscape placement symbology (i.e., Figure 5.15). While the “Bomb-pulse” and “Submodern” springs largely overlap with the “High Mountain” and “Mountain” samples, springs classified as “Modern” (i.e., contain elevated tritium, background $^{36}\text{Cl}/\text{Cl}$ and a modern radiocarbon age) are more similar to 500-4000-year-old waters. In addition, other than one sample, the “4000+ year” springs show a clear clustering and are the most dissimilar from the majority of “Bomb-pulse” and “Submodern” samples.

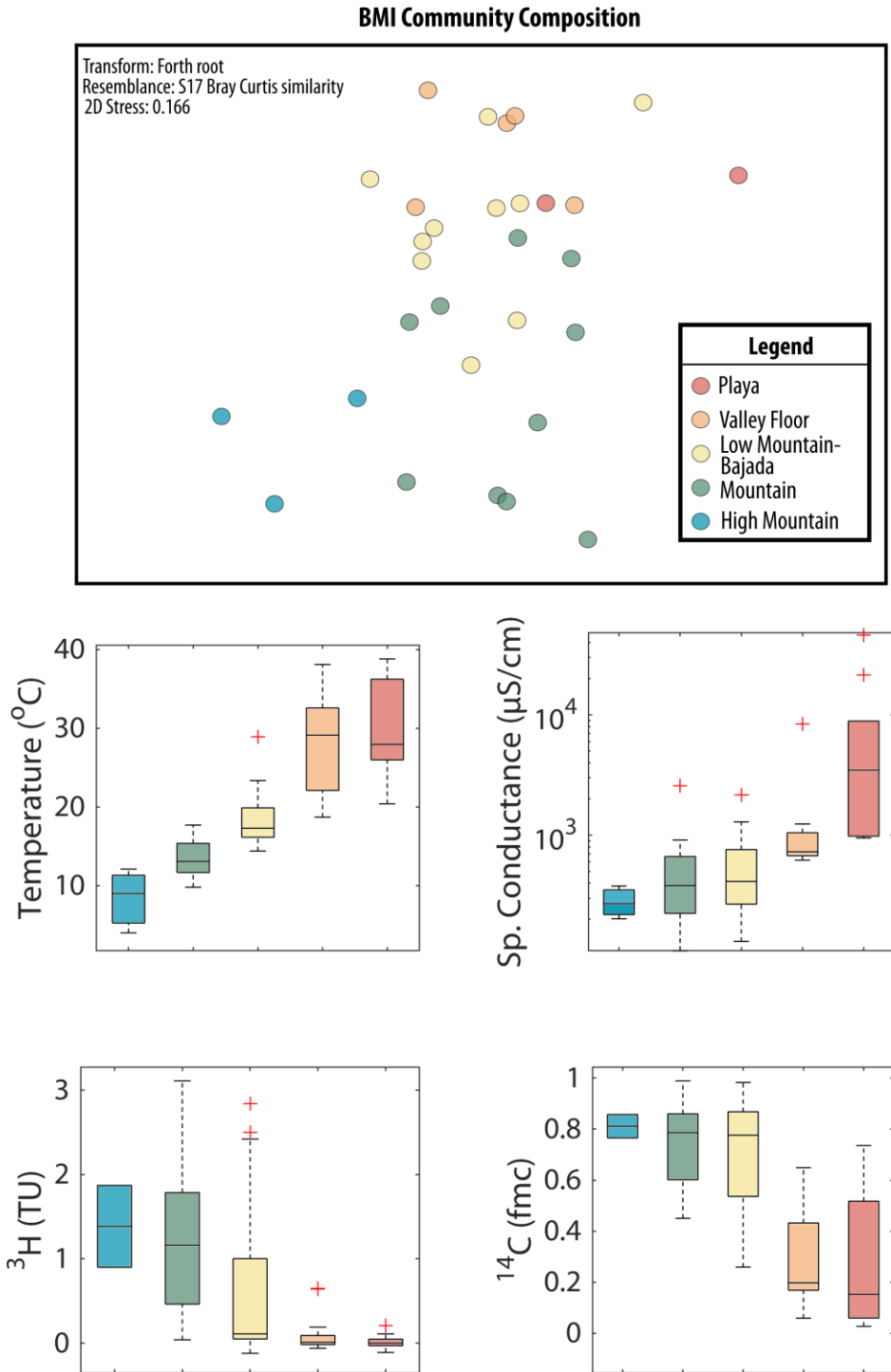


Figure 5.15. NMDS plot of BMI community structure with springs symbolized by landscape placement classification (Top). Boxplots symbolized by landscape placement classification showing systematic trends in temperature, specific conductance, tritium concentration, and radiocarbon activity for the IES springs (Bottom). These trends correspond to similar trends shown in the regional dataset (e.g., Figure 5.8).

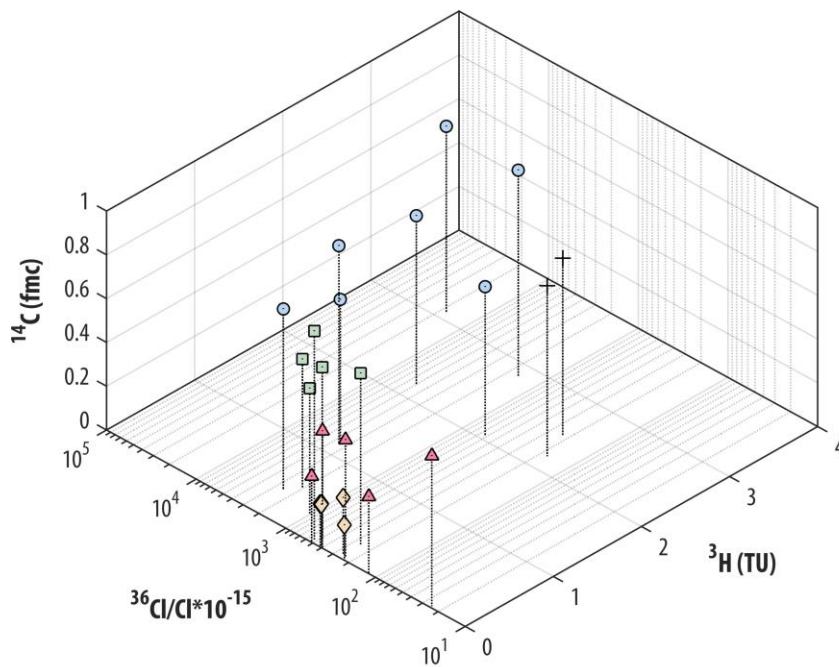
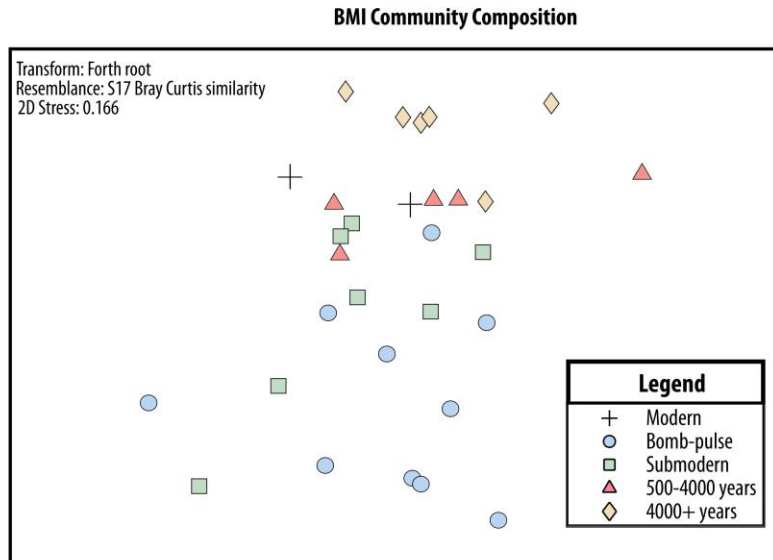


Figure 5.16. (Top) NMDS plot of BMI community structure with springs symbolized by groundwater residence time grouping. (Bottom) 3-D scatter plot showing spring concentrations of ^3H , $^{36}\text{Cl}/\text{Cl} (*10^{-15})$, and ^{14}C (fmc) symbolized by spring residence time grouping.

5.4.5 Relationships with hydrochemical characteristics and ecological indices

Trends of hydrochemical characteristics (e.g., discharge temperature, specific conductance, and radiocarbon activity) related to spring landscape position versus total richness and Shannon diversity are shown in Figure 5.17. Total BMI richness decreases with increasing temperature, increasing specific conductance (with the exclusion of two outliers, IES-019 and IES-020), and decreasing radiocarbon activity. Similarly, Shannon diversity decreases with increasing temperature, increasing specific conductance (exclusion of same outliers, IES-019 and IES-020), and decreasing radiocarbon activity.

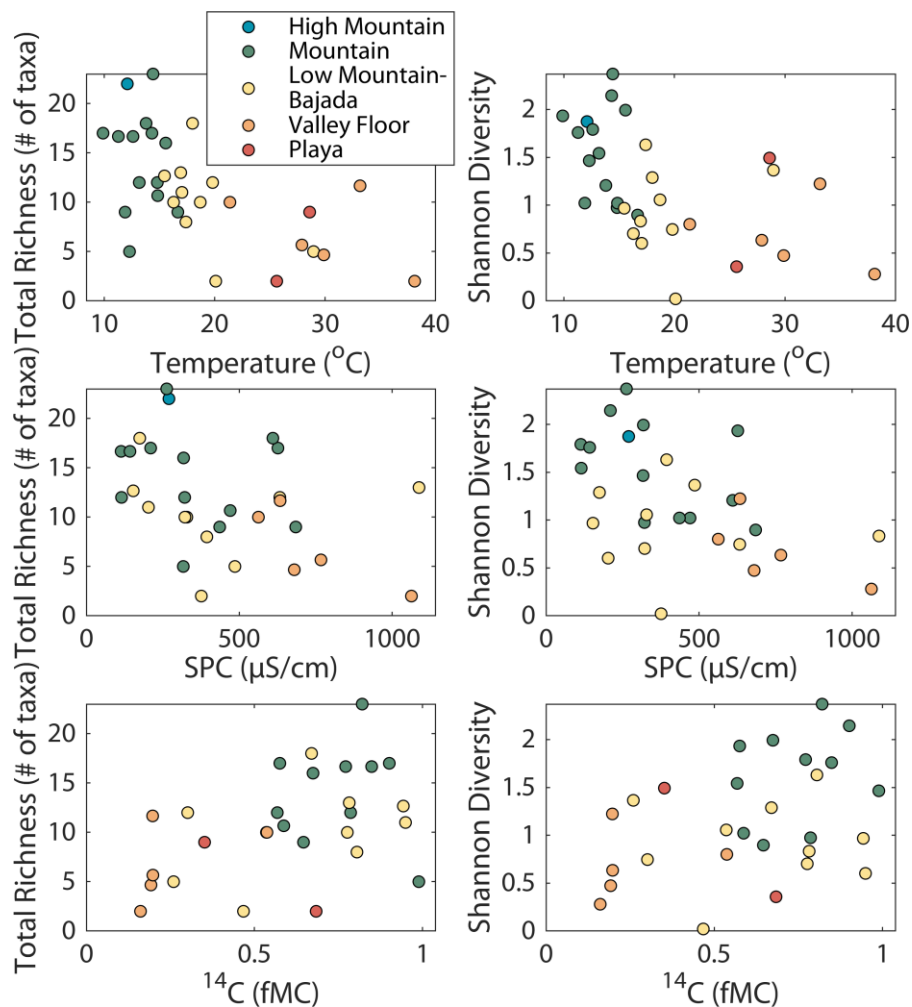


Figure 5.17. Plots showing linear relationships of hydrochemical characteristics (e.g., temperature and specific conductance) and elevation with total BMI richness (# of taxa) and Shannon Diversity. Two outliers, IES-019 & IES-020, are excluded from the SPC plots.

Scatter plots showing the relationship of tolerance indices (e.g., percent intolerant taxa, percent tolerant taxa, and HBI) and hydrochemical characteristics are shown in Figure 5.18. While there are not clear linear relationships with percent intolerant taxa (presence/absence), it is evident that springs above or below certain thresholds (e.g., temperature > 20°C; SPC > 1000 $\mu\text{S}/\text{cm}$; $\text{fMC} < 0.5$) do not contain any intolerant taxa. The percentage of tolerant taxa increases with increasing temperature and increasing specific conductance and decreases with increasing radiocarbon activity (when IES-019, an outlier, is excluded). HBI, a measure of community tolerance that incorporates sample population statistics, is poorly predicted by temperature and radiocarbon activity. There is a weak trend with HBI and specific conductance.

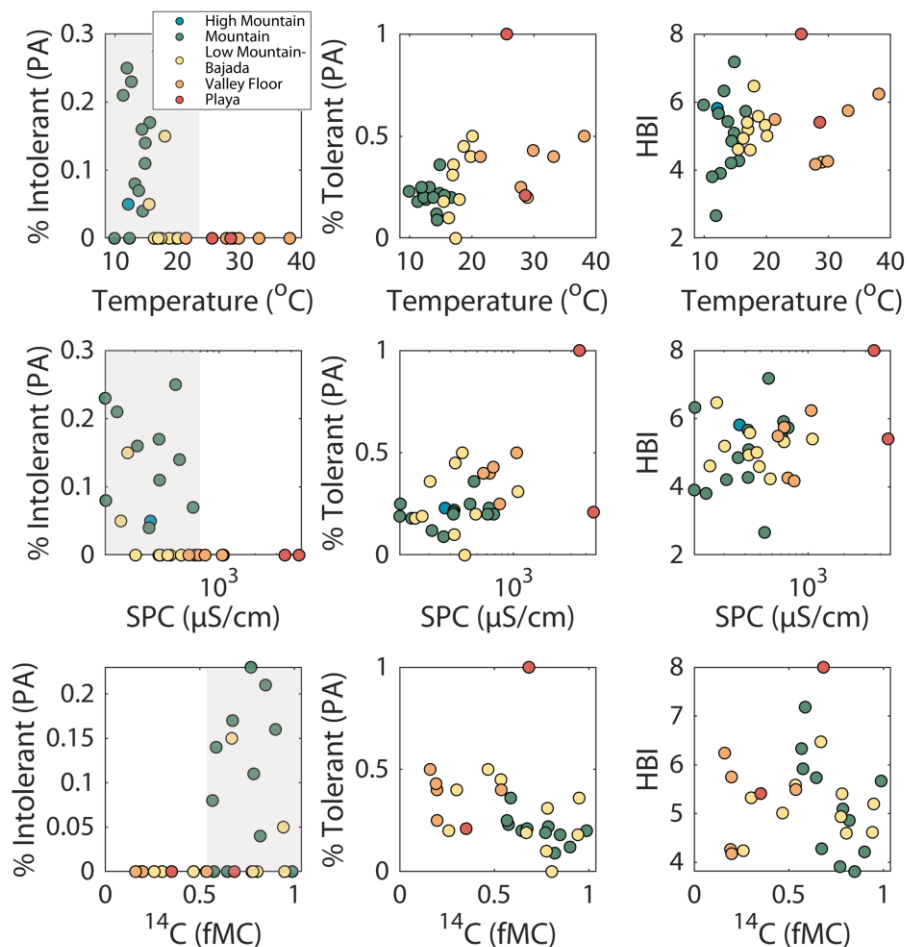


Figure 5.18. Plots showing trends with tolerance indices (e.g., % intolerant taxa, % tolerant taxa, and HBI) and hydrochemical characteristics. Springs are symbolized by landscape placement classifications.

5.5 Discussion

5.5.1 Systematic trends with landscape placement and hydrochemical characteristics

This work represents one of the first regional-scale studies examining the relationship among spring hydrochemical characteristics and landscape placement. Our results show that there are systematic trends with *where* and *why* a spring emerges in a landscape and hydrochemical characteristics. While these trends fail when extended to certain topographic settings (e.g., playa springs), the qualitative landscape placement classification and several of the quantitative topographic indices show predictive power to encapsulate complicated subsurface processes (e.g., rock-water interaction, geothermal heating, etc.) at regional scales and in individual mountain blocks. Elevation, followed by slope, are the most predictive topographic indices for determining linear relationships with hydrochemical characteristics. Other metrics, specifically profile curvature and relative elevation, do not necessarily exhibit linear relationships but still provide some extrapolative power. Metrics generally applied to catchment-scale studies of shallow groundwater (e.g., TWI), while used successfully in the past to predict the hydrochemical characteristics of groundwater-supported features such as wetlands, show little to no prediction power. These results are significant considering the true lack of understanding that currently exists surrounding delineating spring contributing areas. Additionally, these results potentially suggest that at least one key to solving the problem, other than the application of geophysics, lies in the simplest topographic metrics and an understanding of spring emergence mechanism.

Faults have the potential to increase spring contributing volumes by bringing up deeper groundwater flowpaths than topographic or contact-driven emergences. In this study, springs driven to the surface by faults tend to discharge warmer and older groundwater. Within the southern Great Basin, specific types of structural features (e.g., strike-slip faults and high angle normal faults) create increased displacement and larger impermeability barriers. These types of structural features tend to define the boundaries of mountain ranges and result in “Valley Floor” or “Low Mountain-Bajada” topographic classification rather than “Playa”.

At the study area scale, we find that linear relationships with surface elevation are weaker for radiocarbon and temperature compared with individual mountain blocks (e.g., the Funeral-Grapevine Mountains and the Spring Mountains). However, linear relationships are stronger with

specific conductance at the study area scale. We attribute this to increased dampening of the effects of geological heterogeneity and rock-water interaction at regional scales.

5.5.2 Scaling relationships and factors controlling BMI community structure

The results of this study address a major knowledge gap in studies of spring benthic macroinvertebrates: the factors controlling BMI community structure at regional scales in isolated desert springs. By only studying reference or undisturbed desert springs to minimize the effects of disturbance, our results indicate that hydrochemical and hydrogeological (e.g., permanence, hydrological stability, etc.) characteristics, which are encapsulated by landscape placement classification and select topographic indices, do exert a substantial control on BMI community composition. The NMDS analysis results show a clear gradation in community composition with the “High Mountain” and “Mountain” springs being the most dissimilar from “Valley Floor and “Playa” springs. This same pattern is mimicked in the NMDS analysis symbolized by groundwater residence time, with one significant exception, the “Modern” springs being more similar to springs discharging old groundwater (>500 years) as compared to “Bomb-pulse” or “Submodern” springs. We attribute this gradation to an increasing environmental harshness gradient associated with the hydrochemical and hydrogeologic characteristics. In other words, as landscape position decreases from Nival/High Mountain to Valley Floor/Playa, water temperature and salinity increase, and increases in these characteristics result in an increasing environmental harshness gradient. Springs discharging modern water may be subjected to increased flow and geochemical variability. The “Modern” springs in this study, IES-026 and IES-034, have been associated with increased susceptibility to drought conditions (see Chapter 3). Additionally, isotopic evidence at IES-026 and IES-034 (see Chapter 4) in the form of heavier water stable isotopes points to spring sourcing from diffuse and/or focused mountain system recharge, occurring closer to the valley floor, rather than mountain block recharge.

These interpretations are supported by ecological indices of richness, diversity, and tolerance. From a regional perspective, we observe clear trends of decreasing species richness, decreasing Shannon diversity, and an increase in spring community tolerance moving from areas of high topographic position to areas of low topographic position. Overarching trends with hydrochemical characteristics and tolerance indices indicate that presence/absence metrics may be more informative than indices incorporating population statistics (e.g., HBI). Both percent tolerant

and percent intolerant statistics show much higher potential to describe relationships with hydrochemical characteristics than the HBI. These results may indicate that population-based indices may be highly susceptible to the number of individuals present in a sample and that results may be highly dependent on the size of the spring and individual sampling protocol (e.g., number of grabs, amount of substrate roiling, etc.).

The results of this study corroborate novel work by Sada and Thomas (2015) and Sada and Thomas (in review), highlighting the importance of hydrogeology and related environmental characteristics in structuring BMI communities. Our results, however, are contrary to many studies conducted at smaller spatial scales. For example, at local scales (e.g., Erman and Erman, 1995; Erman, 2002), spring BMI community structure is highly dependent on spring permanence and increasing species richness and diversity are positively correlated with area and negatively correlated with elevation (Fattorini et al., 2016). Recent work at the intermediate scale, e.g., mountain front springs in Owens Valley (CA), found that “geochemical fingerprints” associated with chemical weathering of specific geologic units structure BMI communities rather than other variables such as spring discharge temperature or specific conductance (Pordel et al., *in prep.*). This culmination of work indicates that the factors controlling BMI community composition likely change with increasing scale. At local scales, under a minimal range of environmental conditions, spring community composition is controlled by a number of factors (e.g., geochemical ratios, solute availability for organisms, spring permanence, etc.). At these local scales, indices like diversity and richness may increase with spatial scale and related hydrochemical characteristics. At regional scales, especially in high relief settings supporting large regional flow systems, the opposite is true. In these settings there exists a significant gradient of environmental harshness (e.g., elevated temperature and conductivity) that precludes habitation of certain BMI taxa in permanent and hydrologically stable springs emerging at low topographic positions. However, the permanence of these springs does permit endemics and the support of speciation or species that can tolerate harsh conditions.

5.5.3 Conceptual model of spring systems in the southern Great Basin

The results of this study, combined with recent work conducted within the study area (e.g., Pordel et al., *in prep.*), provide an excellent framework for developing a conceptual model of spring systems in the southern Great Basin. Shown by the cartoon illustration in Figure 5.19, the

conceptual model shows qualitative ranges of discharge temperature, conductivity, and groundwater residence time for springs emerging at local-mountain, intermediate, valley floor-playa and regional settings. For each spring, several indicator species are shown that are representative of the aquatic habitat or benthic community composition. At local scales (i.e., a limited range in temperature and conductivity), benthic community structure is controlled by spring permeance, sometimes indicated by solute concentration, and spring geochemical composition (i.e., the geochemical fingerprint). When examining springs at a regional scale, both richness and diversity decrease from high topographic positions to lower topographic positions, while community tolerance increases.

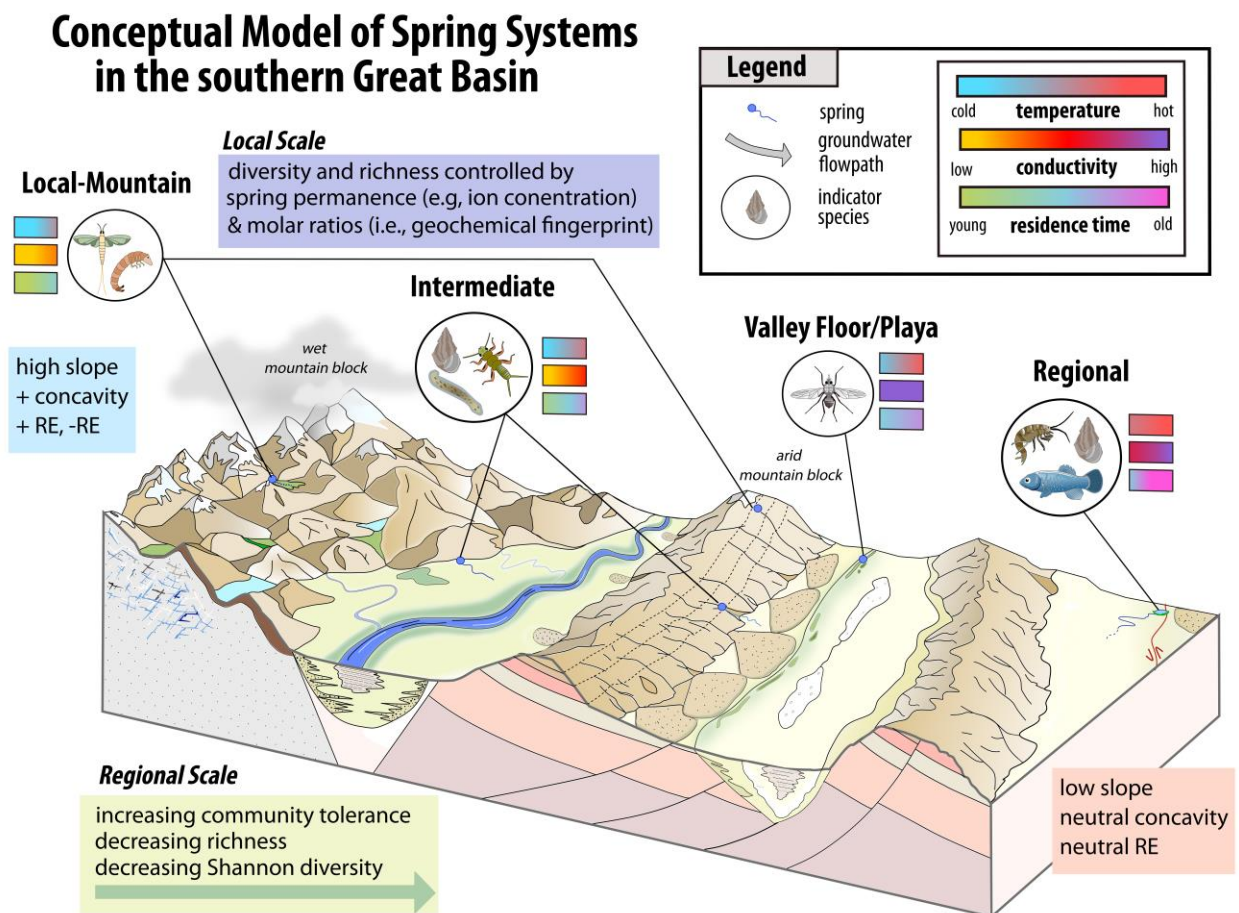


Figure 5.19. Conceptual model of the organization of spring systems in the southern Great Basin. Springs emerging at different landscape positions are given representative ranges in temperature, specific conductance, and residence time based on the results of this study. Indicator species for each spring are depicted based on interpretations about the landscape and hydrochemical controls on tolerance, richness, and community structure.

Local springs are found at mid to-high elevations in humid mountain blocks (e.g., the Sierra Nevada & the Spring Mountains) and at high elevations in arid mountain blocks (e.g., the Panamint Range & the Funeral-Grapevine Mountains). Local springs tend to emerge at high absolute elevation, high relative positions, very negative relative positions, and areas of high concavity (i.e., positive profile curvature). Local springs tend to discharge cold, dilute, and “young” groundwater. Springs at intermediate and regional scales show systematic increases moving downgradient in temperature, conductivity, and groundwater residence time. Intermediate springs tend to emerge along the mountain fronts of humid mountain blocks or at mid to high elevations in more arid mountain blocks. Within the southern Great Basin, regional springs (e.g. springs at Ash Meadows) frequently emerge at high angle normal faults or major strike-slip faults that create permeability barriers within the regional carbonate aquifer. Springs emerging on the valley floor or basin playa can have vary wide ranges in temperature, salinity and residence time based on the aquifer provenance and the flowpath distribution they source. These springs tend to host only very tolerant taxa (e.g., *Diptera*) due to the harsh environmental conditions.

5.6 Conclusions

In this study we set out to address the following research questions: 1) Are there systematic patterns with spring landscape placement and hydrochemical characteristics that can be predicted by topographic metrics and/or landform analysis? and 2) If present, how do these patterns influence benthic macroinvertebrate community (BMI) structure at the regional scale. We addressed the first question by cultivating a regional spring hydrochemical dataset from past studies in the southern Great Basin and testing both qualitative landscape placement classifications and quantitative topographic indices. We addressed the second question by sampling benthic macroinvertebrates in a subset of undisturbed or reference desert springs that capture the topographic and hydrochemical variance of the study region.

Our results show that there **are** systematic patterns with spring hydrochemical characteristics (e.g., spring discharge temperature, specific conductance, and radiocarbon activity) that can be predicted by landscape placement classes (i.e., a combination of Kapos et al. (2000) and True (2002)) and show correlations with some topographic indices (e.g., surface elevation and slope). TWI, a surface water metric, poorly predicts spring hydrochemical characteristics. Profile curvature and relative elevation cannot be used as linear prediction models; however, these metrics

still provide information regarding areas likely sourcing local to intermediate scale flowpaths (i.e., areas of high concavity, areas of positive relative elevation, and areas of very negative relative elevation). BMI community structure similarity, as shown by NMDS analysis of a subset of regionally representative springs, can be largely attributed to spring landscape placement and related hydrochemical characteristics. Ecological indices show that richness and Shannon diversity decrease with increasing scale while community tolerance tends to increase. These results differ from work on BMI community composition conducted at local (Erman and Erman, 1995; Erman, 2002) and intermediate (Pordel et al., *in prep.*) scales, however complement work by Sada and Thomas (1995) and Sada and Thomas (in review) and strong, independent support for the conceptual model that hydrogeology exerts an important control on BMI community composition. Additionally, the results of this study provide a topographic, hydrochemical, and ecological framework to develop a conceptual model of spring systems in the southern Great Basin.

Other than the development of a conceptual model for the region, there are several broader implications of this work that are novel and expand the knowledge base regarding springs. This work represents one of the first regional syntheses of spring hydrochemical data to examine systematic hydrochemical patterns with spring landscape position. This work clearly identifies that both where and why springs emerge have implications for hydrochemical characteristics and implies that both are important factors in understanding knowledge gaps such as spring contributing areas and spring permanence. While the results of our study are significant, there are several potential avenues for future work. One such avenue is an increased examination of spring emergence mechanism and hydrochemical characteristics beyond the scope of this study. Additionally, the topographic and landscape placement indices could be extended to include metrics focused on climate (e.g., annual precipitation or recharge) and regional ecotones (e.g., treeline or areas of juniper-pinyon vegetation). Remote sensing methods or related data products (e.g., PRISM) could be applied to compensate for the lack field weather stations or SNOTEL sites in the study region. In terms of future ecological work, while the focus of this study is on benthic community relationships at the macroinvertebrate scale, potential research on microbiological community composition still remains a major knowledge gap, especially if focused on undisturbed, isolated desert springs.

5.7 References

- Aishlin, P., & McNamara, J. P. (2011). Bedrock infiltration and mountain block recharge accounting using chloride mass balance. *Hydrological Processes*, 25(12), 1934-1948.
- Al-Hanbali, A., & Kondoh, A. (2008). Groundwater vulnerability assessment and evaluation of human activity impact (HAI) within the Dead Sea groundwater basin, Jordan. *Hydrogeology Journal*, 16(3), 499-510.
- Anderson, M. G., & Kneale, P. E. (1982). The influence of low-angled topography on hillslope soil-water convergence and stream discharge. *Journal of Hydrology*, 57(1-2), 65-80.
- Anderson, K. W. (2002). Contribution of local recharge to high flux springs in Death Valley National Park. California-Nevada: Master's thesis, Brigham Young University.
- Ball, L. B., Caine, J. S., & Ge, S. (2014). Controls on groundwater flow in a semiarid folded and faulted intermountain basin. *Water Resources Research*, 50(8), 6788-6809.
- Beven, K. J., & Kirkby, M. J. (1979). A physically based, variable contributing area model of basin hydrology/Un modèle à base physique de zone d'appel variable de l'hydrologie du bassin versant. *Hydrological Sciences Journal*, 24(1), 43-69.
- Beven, K. J., Lamb, R., Quinn, P., Romanowicz, R., & Freer, J. (1995). TOPMODEL. Computer models of watershed hydrology. VP Singh, 627-668.
- Bryan, K. (1919). Classification of springs. *The Journal of Geology*, 27(7), 522-561.
- Buttle, J. M., Hazlett, P. W., Murray, C. D., Creed, I. F., Jeffries, D. S., & Semkin, R. (2001). Prediction of groundwater characteristics in forested and harvested basins during spring snowmelt using a topographic index. *Hydrological Processes*, 15(18), 3389-3407.
- Cao, Y., Larsen, D. P., & Thorne, R. S. J. (2001). Rare species in multivariate analysis for bioassessment: some considerations. *Journal of the North American Benthological Society*, 20(1), 144-153.
- Clarke, K., and R. Gorley. "Primer v6." user manual/tutorial, plymouth routine in multivariate ecological research." (2006).
- Condon, L. E., & Maxwell, R. M. (2015). Evaluating the relationship between topography and groundwater using outputs from a continental-scale integrated hydrology model. *Water Resources Research*, 51(8), 6602-6621.
- Davisson, M. L., Smith, D. K., Kenneally, J., & Rose, T. P. (1999). Isotope hydrology of southern Nevada groundwater: stable isotopes and radiocarbon. *Water Resources Research*, 35(1), 279-294.
- Dowling, C. B., Poreda, R. J., & Basu, A. R. (2003). The groundwater geochemistry of the Bengal Basin: Weathering, chemisorption, and trace metal flux to the oceans. *Geochimica et Cosmochimica Acta*, 67(12), 2117-2136.

- Duffy, C. J., & Al-Hassan, S. (1988). Groundwater circulation in a closed desert basin: topographic scaling and climatic forcing. *Water Resources Research*, 24(10), 1675-1688.
- Erman, N. A., & Erman, D. C. (1995). Spring permanence, Trichoptera species richness, and the role of drought. *Journal of the Kansas Entomological Society*, 50-64.
- Erman, N. A. (2002). Lessons from a long-term study of springs and spring invertebrates (Sierra Nevada, California, USA) and implications for conservation and management. In *Conference proceedings. Springfed Wetlands: Important Scientific and Cultural Resources of the Intermountain Region*, Las Vegas, NV.
- Fattorini, S., Borges, P. A., Fiasca, B., & Galassi, D. M. (2016). Trapped in the web of water: Groundwater-fed springs are island-like ecosystems for the meiofauna. *Ecology and Evolution*, 6(23), 8389-8401.
- Fleishman, E., Murphy, D. D., & Sada, D. W. (2006). Effects of environmental heterogeneity and disturbance on the native and non-native flora of desert springs. *Biological Invasions*, 8(5), 1091.
- Freed, Z., Aldous, A., & Gannett, M. W. (2019). Landscape controls on the distribution and ecohydrology of central Oregon springs. *Ecohydrology*, 12(2), e2065.
- Frisbee, M. D., Phillips, F. M., White, A. F., Campbell, A. R., & Liu, F. (2013). Effect of source integration on the geochemical fluxes from springs. *Applied Geochemistry*, 28, 32-54.
- Fritz, K. M., Johnson, B. R., & Walters, D. M. (2008). Physical indicators of hydrologic permanence in forested headwater streams. *Journal of the North American Benthological Society*, 27(3), 690-704.
- Gathmann, F. O., & Williams, D. D. (2006, September). Insect emergence in Canadian coldwater springs: spatial and temporal patterns, and species-environment relationships. In *Annales de Limnologie-International Journal of Limnology* (Vol. 42, No. 3, pp. 143-156). EDP Sciences.
- Gathmann, F. O., Manne, L. L., & Williams, D. D. (2009). Spatial patterns in insect community composition in coldwater springs. *Aquatic Ecology*, 43(2), 501-512.
- Gil-Márquez, J. M., Barberá, J. A., Andreo, B., & Mudarra, M. (2017). Hydrological and geochemical processes constraining groundwater salinity in wetland areas related to evaporitic (karst) systems. A case study from Southern Spain. *Journal of Hydrology*, 544, 538-554.
- Glazier, D. S. (1991). The fauna of North American temperate cold springs: patterns and hypotheses. *Freshwater Biology*, 26(3), 527-542.
- Gleeson, T., & Manning, A. H. (2008). Regional groundwater flow in mountainous terrain: Three-dimensional simulations of topographic and hydrogeologic controls. *Water Resources Research*, 44(10).
- Gleeson, T., Marklund, L., Smith, L., & Manning, A. H. (2011). Classifying the water table at regional to continental scales. *Geophysical Research Letters*, 38(5).

- Grabs, T., Seibert, J., Bishop, K., & Laudon, H. (2009). Modeling spatial patterns of saturated areas: A comparison of the topographic wetness index and a dynamic distributed model. *Journal of Hydrology*, 373(1-2), 15-23.
- Hershey, R. L., Mizell, S. A., & Earman, S. (2010). Chemical and physical characteristics of springs discharging from regional flow systems of the carbonate-rock province of the Great Basin, western United States. *Hydrogeology Journal*, 18(4), 1007-1026.
- Hjerdt, K. N., McDonnell, J. J., Seibert, J., & Rodhe, A. (2004). A new topographic index to quantify downslope controls on local drainage. *Water Resources Research*, 40(5).
- Hogle, C., Sada, D., & Rosamond, C. (2015). Using benthic indicator species and community gradients to optimize restoration in the Arid, Endorheic Walker River Watershed, Western USA. *River Research and Applications*, 31(6), 712-727.
- Hoover, K. A., & Wolman, M. G. (2005). Beyond the semivariogram: Patterns, scale, and hydrology in a semi-arid landscape. *Advances in Water Resources*, 28(9), 885-898.
- Hynes, K. E. (1998). Benthic Macroinvertebrate Diversity and Biotic Indices for Monitoring of 5 Urban and Urbanizing Lakes Within the Halifax Regional Municipality (HRM), Nova Scotia, Canada:(Lakes Kearney [Halifax], McGrath [Brookside], Morris [Dartmouth], Springfield [Sackville] and Wrights [Hubley]. Soil & Water Conservation Society of Metro Halifax.
- Infascelli, R., Faugno, S., Pindozi, S., Boccia, L., & Merot, P. (2013). Testing different topographic indexes to predict wetlands distribution. *Procedia Environmental Sciences*, 19(0), 733-746.
- Jankowski, K. J., & Schindler, D. E. (2019). Watershed geomorphology modifies the sensitivity of aquatic ecosystem metabolism to temperature. *Scientific Reports*, 9(1), 1-10.
- Jasechko, S. (2016). Partitioning young and old groundwater with geochemical tracers. *Chemical Geology*, 427, 35-42.
- Jefferson, A., Grant, G. E., Lewis, S. L., & Lancaster, S. T. (2010). Coevolution of hydrology and topography on a basalt landscape in the Oregon Cascade Range, USA. *Earth Surface Processes and Landforms: The Journal of the British Geomorphological Research Group*, 35(7), 803-816.
- Jencso, K. G., & McGlynn, B. L. (2011). Hierarchical controls on runoff generation: Topographically driven hydrologic connectivity, geology, and vegetation. *Water Resources Research*, 47(11).
- Jenness, J. (2006). Topographic Position Index (tpi_jen. avx) extension for ArcView 3. x, v. 1.3 a. Jenness Enterprises.
- Jennings, C.W., Strand, R.G., & Rogers, T.H. (1977). Geologic map of California: California Division of Mines and Geology, scale 1:750,000.

- Kapos, V., Rhind, J., Edwards, M., Price, M. F., & Ravilious, C. (2000). Developing a map of the world's mountain forests. Forests in sustainable mountain development: a state of knowledge report for 2000. *Task Force on Forests in Sustainable Mountain Development.*, 4-19.
- Karagulle, D., Frye, C., Sayre, R., Breyer, S., Aniello, P., Vaughan, R., & Wright, D. (2017). Modeling global Hammond landform regions from 250-m elevation data. *Transactions in GIS*, 21(5), 1040-1060.
- Keleher, M. J., & Rader, R. B. (2008). Bioassessment of artesian springs in the Bonneville Basin, Utah, USA. *Wetlands*, 28(4), 1048-1059.
- Khosravi, K., Panahi, M., & Tien Bui, D. (2018). Spatial prediction of groundwater spring potential mapping based on an adaptive neuro-fuzzy inference system and metaheuristic optimization. *Hydrology & Earth System Sciences*, 22(9).
- Körner, C., Paulsen, J., & Spehn, E. M. (2011). A definition of mountains and their bioclimatic belts for global comparisons of biodiversity data. *Alpine Botany*, 121(2), 73.
- Lamb, M. P., Howard, A. D., Johnson, J., Whipple, K. X., Dietrich, W. E., & Perron, J. T. (2006). Can springs cut canyons into rock?. *Journal of Geophysical Research: Planets*, 111(E7).
- Lutz, B. M., Axen, G. J., & Phillips, F. M. (2017). New Geologic Map and Structural Cross Sections of the Death Valley Extended Terrain (southern Sierra Nevada, California to Spring Mountains, Nevada): Toward 3D Kinematic Reconstructions. AGUFM, 2017, T41B-0625.
- Mandaville, S. M. (2002). Benthic macroinvertebrates in freshwaters: Taxa tolerance values, metrics, and protocols (p. 128). Nova Scotia: Soil & Water Conservation Society of Metro Halifax.
- Manga, M. (1999). On the timescales characterizing groundwater discharge at springs. *Journal of Hydrology*, 219(1-2), 56-69.
- Manga, M. (2001). Using springs to study groundwater flow and active geologic processes. *Annual Review of Earth and Planetary Sciences*, 29(1), 201-228.
- Marklund, L., & Wörman, A. (2007). The impact of hydraulic conductivity on topography driven groundwater flow. *Publications of the Institute of Geophysics, Polish Academy of Sciences E-7* p, 159-167.
- McCabe, D. J. (1998). Biological communities in springbrooks. Studies in crenobiology. The biology of springs and springbrooks. Backhuys Publishers, Leiden, The Netherlands, 221-228.
- Mehler, K., Acharya, K., Sada, D., & Yu, Z. (2013). Elemental stoichiometry of basal resources and benthic macroinvertebrates along a land use gradient in a Great Basin watershed. *Hydrobiologia*, 716(1), 115-129.
- Mehler, K., Acharya, K., Sada, D., & Yu, Z. (2015). Factors affecting spatiotemporal benthic macroinvertebrate diversity and secondary production in a semi-arid watershed. *Journal of Freshwater Ecology*, 30(2), 197-214.

- Merot, P., Squidadant, H., Aurousseau, P., Hefting, M., Burt, T., Maitre, V., ... & Viaud, V. (2003). Testing a climato-topographic index for predicting wetlands distribution along an European climate gradient. *Ecological Modelling*, 163(1-2), 51-71.
- Miller, B. A. (2014). Semantic calibration of digital terrain analysis scale. *Cartography and Geographic Information Science*, 41(2), 166-176.
- Moore, R. D., & Thompson, J. C. (1996). Are water table variations in a shallow forest soil consistent with the TOPMODEL concept?. *Water Resources Research*, 32(3), 663-669.
- Mugel, D. N., Richards, J. M., & Schumacher, J. G. (2009). Geohydrologic investigations and landscape characteristics of areas contributing water to springs, the Current River, and Jacks Fork, Ozark National Scenic Riverways, Missouri (p. 80). US Geological Survey.
- Muñoz, E., Arumí, J. L., Wagener, T., Oyarzún, R., & Parra, V. (2016). Unraveling complex hydrogeological processes in Andean basins in south-central Chile: An integrated assessment to understand hydrological dissimilarity. *Hydrological Processes*, 30(26), 4934-4943.
- Myers, M. J., & Resh, V. H. (2002). Trichoptera and other macroinvertebrates in springs of the Great Basin: species composition, richness, and distribution. *Western North American Naturalist*, 1-13.
- Naiman, Z., Quade, J., & Patchett, P. J. (2000). Isotopic evidence for eolian recycling of pedogenic carbonate and variations in carbonate dust sources throughout the southwest United States. *Geochimica et Cosmochimica Acta*, 64(18), 3099-3109.
- Naus, F. L., Schot, P. P., Ahmed, K., & Griffioen, J. (2019). Groundwater salinity variation in Upazila Assasuni (southwestern Bangladesh), as steered by surface clay layer thickness, relative elevation and present-day land use. *Hydrology and Earth System Sciences*, 23(3), 1431-1451.
- Ozdemir, A. (2011). GIS-based groundwater spring potential mapping in the Sultan Mountains (Konya, Turkey) using frequency ratio, weights of evidence and logistic regression methods and their comparison. *Journal of Hydrology*, 411(3-4), 290-308.
- Ozdemir, A. (2011). Using a binary logistic regression method and GIS for evaluating and mapping the groundwater spring potential in the Sultan Mountains (Aksehir, Turkey). *Journal of Hydrology*, 405(1-2), 123-136.
- Pacheco, F. A., & Van der Weijden, C. H. (2012). Integrating topography, hydrology and rock structure in weathering rate models of spring watersheds. *Journal of Hydrology*, 428, 32-50.
- Peralta-Tapia, A., Sponseller, R. A., Ågren, A., Tetzlaff, D., Soulsby, C., & Laudon, H. (2015). Scale-dependent groundwater contributions influence patterns of winter baseflow stream chemistry in boreal catchments. *Journal of Geophysical Research: Biogeosciences*, 120(5), 847-858.
- Perla, B. S., & Stevens, L. E. (2008). Biodiversity and productivity at an undisturbed spring in comparison with adjacent grazed riparian and upland habitats. *Aridland springs in North America: Ecology and conservation*, 230-243.

- Piscart, C., Moreteau, J. C., & Beisel, J. N. (2005). Biodiversity and structure of macroinvertebrate communities along a small permanent salinity gradient (Meurthe River, France). *Hydrobiologia*, 551(1), 227-236.
- Pourtaghi, Z. S., & Pourghasemi, H. R. (2014). GIS-based groundwater spring potential assessment and mapping in the Birjand Township, southern Khorasan Province, Iran. *Hydrogeology Journal*, 22(3), 643-662.
- Prancevic, J. P., & Kirchner, J. W. (2019). Topographic controls on the extension and retraction of flowing streams. *Geophysical Research Letters*, 46(4), 2084-2092.
- Quade, J., Cerling, T. E., & Bowman, J. R. (1989). Systematic variations in the carbon and oxygen isotopic composition of pedogenic carbonate along elevation transects in the southern Great Basin, United States. *Geological Society of America Bulletin*, 101(4), 464-475.
- Rader, R. B., Keleher, M. J., Billman, E., & Larsen, R. (2012). History, rather than contemporary processes, determines variation in macroinvertebrate diversity in artesian springs: the expansion hypothesis. *Freshwater Biology*, 57(12), 2475-2486.
- Rahmati, O., Naghibi, S. A., Shahabi, H., Bui, D. T., Pradhan, B., Azareh, A., ... & Melesse, A. M. (2018). Groundwater spring potential modelling: Comprising the capability and robustness of three different modeling approaches. *Journal of Hydrology*, 565, 248-261.
- Resh, V. H., & Rosenberg, D. M. (Eds.). (1993). *Freshwater biomonitoring and benthic macroinvertebrates* (No. 504.4 FRE). New York, NY, USA: Chapman & Hall.
- Rinderer, M., van Meerveld, I., Stähli, M., & Seibert, J. (2016). Is groundwater response timing in a pre-alpine catchment controlled more by topography or by rainfall?. *Hydrological Processes*, 30(7), 1036-1051.
- Rodhe, A., & Seibert, J. (1999). Wetland occurrence in relation to topography: a test of topographic indices as moisture indicators. *Agricultural and Forest Meteorology*, 98, 325-340.
- Sada, D. W., & Nachlinger, J. L. (1996). *Spring Mountains Ecosystem: Vulnerability of spring-fed aquatic and riparian systems to biodiversity loss*. Nature Conservancy of Nevada.
- Sada, D. W., & Herbst, D. B. (2001). *Macroinvertebrates and environmental characteristics of Owens Valley springs, Inyo County, California*. Bishop: City of Los Angeles Department of Water and Power.
- Sada, D. W., Fleishman, E., & Murphy, D. D. (2005). Associations among spring-dependent aquatic assemblages and environmental and land use gradients in a Mojave Desert mountain range. *Diversity and Distributions*, 11(1), 91-99.
- Sada, D. W., Thomas, J. M. (2015). *Aquifer provenance, flow pathways, landscape setting and BMI community relationships in Great Basin and Mojave Desert springs*, Nevada Water Resources Association Conference: Reno, NV, December 9, 2015-December 11, 2015

- Schaller, M. F., & Fan, Y. (2009). River basins as groundwater exporters and importers: Implications for water cycle and climate modeling. *Journal of Geophysical Research: Atmospheres*, 114(D4).
- Seibert, J., Bishop, K., Rodhe, A., & McDonnell, J. J. (2003). Groundwater dynamics along a hillslope: A test of the steady state hypothesis. *Water Resources Research*, 39(1).
- Setiawan, O., Sartohadi, J., Hadi, M. P., & Mardiatno, D. (2019). Delineating spring recharge areas inferred from morphological, lithological, and hydrological datasets on Quaternary volcanic landscapes at the southern flank of Rinjani Volcano, Lombok Island, Indonesia. *Acta Geophysica*, 67(1), 177-190.
- Shade, A., Jones, S. E., Caporaso, J. G., Handelsman, J., Knight, R., Fierer, N., & Gilbert, J. A. (2014). Conditionally rare taxa disproportionately contribute to temporal changes in microbial diversity. *MBio*, 5(4), e01371-14.
- Spencer, E. B. (1990). A radiocarbon study of groundwater in the western Nevada Test Site and vicinity (Doctoral dissertation, University of Nevada, Reno).
- Springer, A. E., & Stevens, L. E. (2009). Spheres of discharge of springs. *Hydrogeology Journal*, 17(1), 83.
- Sreedevi, P. D., Subrahmanyam, K., & Ahmed, S. (2005). The significance of morphometric analysis for obtaining groundwater potential zones in a structurally controlled terrain. *Environmental Geology*, 47(3), 412-420.
- Stanislawczyk, K., Walters, A. D., Haan, T. J., Sei, M., Lang, B. K., & Berg, D. J. (2018). Variation among macroinvertebrate communities suggests the importance of conserving desert springs. *Aquatic Conservation: Marine and Freshwater Ecosystems*, 28(4), 944-953.
- Stewart, J. H., & Carlson, J. E. (1978). Geologic map of Nevada. US Geological Survey.
- Stewart-Maddox, N. S., Frisbee, M. D., Andronicos, C. L., Genereux, D. P., & Meyers, Z. P. (2018). Identifying the regional extent and geochemical evolution of interbasin groundwater flow using geochemical inverse modeling and $^{87}\text{Sr}/^{86}\text{Sr}$ ratios in a complex conglomeratic aquifer. *Chemical Geology*, 500, 20-29.
- Štulc, P. (1998). Combined effect of topography and hydrogeology on subsurface temperature—implications for aquifer permeability and heat flow. A study from the Bohemian Cretaceous basin. *Tectonophysics*, 284(1-2), 161-174.
- Thobaben, E. T., & Hamilton, S. K. (2014). The relative importance of groundwater and its ecological implications in diverse glacial wetlands. *The American Midland Naturalist*, 172(2), 205-218.
- Tooth, S. (2018). The geomorphology of wetlands in drylands: Resilience, nonresilience, or...?. *Geomorphology*, 305, 33-48.

- Toth, J. (1963). A theoretical analysis of groundwater flow in small drainage basins. *Journal of Geophysical Research*, 68(16), 4795-4812.
- Toth, J. (1995). Hydraulic continuity in large sedimentary basins. *Hydrogeology Journal*, 3(4), 4-16.
- Tóth, J. (1999). Groundwater as a geologic agent: an overview of the causes, processes, and manifestations. *Hydrogeology Journal*, 7(1), 1-14.
- True, D. (2002). Landforms of the lower Mid-west. Missouri Resource Assessment Partnership. MoRAP Map Series MS-2003-001 (1: 1,500,000). Available online at <http://morap.missouri.edu/Posters.aspx>.
- Van der Kamp, G. (1995). The hydrogeology of springs in relation to the biodiversity of spring fauna: a review. *Journal of the Kansas Entomological Society*, 4-17.
- Vinson, M. R., & Hawkins, C. P. (1996). Effects of sampling area and subsampling procedure on comparisons of taxa richness among streams. *Journal of the North American Benthological Society*, 15(3), 392-399.
- Vivoni, E. R., Di Benedetto, F., Grimaldi, S., & Eltahir, E. A. (2008). Hypsometric control on surface and subsurface runoff. *Water Resources Research*, 44(12).
- Weiss, A. (2001). Topographic Position and Landforms Analysis. Poster presentation, ESRI User Conference, San Diego, CA. Topographic Position Index (tpi_jen. avx) extension for ArcView 3. x, v. 1.3 a.
- Welsch, D. L., Kroll, C. N., McDonnell, J. J., & Burns, D. A. (2001). Topographic controls on the chemistry of subsurface stormflow. *Hydrological Processes*, 15(10), 1925-1938.
- Western, A. W., Grayson, R. B., Blöschl, G., Willgoose, G. R., & McMahon, T. A. (1999). Observed spatial organization of soil moisture and its relation to terrain indices. *Water Resources Research*, 35(3), 797-810.
- Williams, J. E., Bowman, D. B., Brooks, J. E., Echelle, A. A., Edwards, R. J., Hendrickson, D. A., & Landye, J. J. (1985). Endangered aquatic ecosystems in North American deserts with a list of vanishing fishes of the region. *Journal of the Arizona-Nevada Academy of Science*, 1-61.
- Williams, M. A., & Vondracek, B. (2010). Spring distributions and relationships with land cover and hydrogeologic strata in a karst landscape in Winona County, Minnesota, USA. *Carbonates and Evaporites*, 25(4), 333-347.
- Winter, T. C. (2000). The vulnerability of wetlands to climate change: a hydrologic landscape perspective 1. *JAWRA Journal of the American Water Resources Association*, 36(2), 305-311.
- Winter, T. C. (2001). The concept of hydrologic landscapes 1. *JAWRA Journal of the American Water Resources Association*, 37(2), 335-349.
- Woods, R. A., Sivapalan, M., & Robinson, J. S. (1997). Modeling the spatial variability of subsurface runoff using a topographic index. *Water Resources Research*, 33(5), 1061-1073.

Zapata-Rios, X., McIntosh, J., Rademacher, L., Troch, P. A., Brooks, P. D., Rasmussen, C., & Chorover, J. (2015). Climatic and landscape controls on water transit times and silicate mineral weathering in the critical zone. *Water Resources Research*, 51(8), 6036-6051.

CHAPTER 6. IS TEMPORAL VARIABILITY AN INDICATOR OF GROUNDWATER RESIDENCE TIME? TALES FROM THE SOUTHERN GREAT BASIN

6.1 Abstract

Temporal variations within the water cycle, whether physical, chemical, or isotopic, are usually the most substantial in precipitation. These signals are dampened in hydrologic reservoirs such as surface water features, soil water, shallow groundwater, and deep groundwater that integrate hydrologic signals over timescales ranging from hours to millennia. In streams and shallow groundwater there are well-established relationships that link temporal or seasonal variability to source integration patterns or groundwater residence time. However, the current body of research is remarkably vague about a “dampening continuum” at longer timescales where bomb-pulse groundwater (i.e., 60-70 years) could potentially be distinguished from ancient groundwater (i.e., 10,000 years +) on the basis of geochemical variability. In this study, I seek to understand if decreased temporal geochemical variability in springs is correlated with increased groundwater residence time. In extension, is dampened temporal variability indicative of long-term hydrogeological stability? Furthermore, we seek to understand how increased temporal variability relates to our conceptual framework of ecological community structure.

This study focuses on 33 springs within the southern Great Basin that were sampled up to 8 times between 2016-2019 for a suite of geochemical analytes (e.g., temperature, major ions, trace elements, $^{87}\text{Sr}/^{86}\text{Sr}$, $\delta^{18}\text{O}$, $\delta^2\text{H}$, etc.). The sampling interval captures the tail end and subsequent recovery of the historic 2011-2016 California drought. The spring distribution reflects the heterogeneity of the study area and captures a wide range of topographic and geological settings and geochemical characteristics. Over this four-year period, the vast majority of springs do not exhibit significant variability (e.g., coefficient of variation < 5%) across multiple geochemical analytes, leading to the interpretation that a 60-70 year mean groundwater residence time (i.e., a minimum range for the majority of springs in this study) may be enough to provide temporary buffering to the geochemical effects of major droughts. The time scale of the lagged hydrogeologic response to the drought, however, are still unknown. A small subset of springs (~7) exhibit increased variability across multiple geochemical analytes that can be attributed to low discharge, specific spheres of emergence, disturbance, or increased flowpath variability (e.g., ecologically

unfavorable surface conditions). These springs with increased variability host fewer intolerant taxa than what we would expect based on their geochemical profiles. The coupling of variability results and BMI tolerance results for southern Great Basin springs leads us to revise our hydrogeological/ecological framework from Chapter 5 to incorporate temporal variability as a secondary control on spring ecological community structure. In response to our initial research question, our results indicate that either: 1) there is not a dampening continuum with increasing groundwater residence time 2) the springs in this study do not capture the tail end of the spring topographic distribution (i.e., very high elevation, local-scale springs >2200m) and these springs would show increased variability in comparison to springs discharging primarily bomb-pulse or Pleistocene recharge, or 3) the lagged response is longer than our period of observation

6.2 Introduction

6.2.1 Temporal variability in hydrologic studies

Components of the terrestrial hydrosphere that more closely interact with precipitation and the atmosphere (e.g., headwater stream networks, lakes, shallow groundwaters) are typically assumed to exhibit increased hydrochemical temporal variability (e.g., temperature, conductivity, water isotopes, etc.) compared to deeper groundwater (e.g., a bedrock aquifer well, perennial spring discharge, etc.) that is shielded and has a longer lag time from the surface. Studies of temporal variability in hydrology have largely focused on surface waters where changes in flow (e.g., Unland et al., 2013), temperature (e.g., Keery et al., 2007), hydrochemistry (Ahearn et al., 2004; Bishop et al., 2004; Nagorski et al., 2003), and isotopic composition (Pinder and Jones, 1969; O'Driscoll et al., 2005; Jeelani et al., 2010; Penna et al., 2014; Engel et al., 2019) have been attributed to catchment stimuli or changes in streamflow source contribution. Physical and hydrochemical variability in surface waters have been linked to biologic activity, (Johnson et al., 1969), weather (e.g. solar radiation; Engel et al., 2019), seasonal precipitation and snowmelt (Engel et al., 2019), variations in groundwater or water table connection contribution (Pham et al., 2009; Luo et al., 2016), and even hydrological paradoxes (e.g., Kirchner et al., 2003; Bishop et al., 2004). The timescales of these studies cover a wide range from examining hourly, diel changes (Nagorski et al., 2003) to seasonal, interannual, or decadal patterns. A large proportion of these studies focus on quantifying temporal groundwater contribution patterns to rivers, streams, lakes

or wetlands and assume a stable groundwater endmember over time. However, the literature examining the hydrochemical temporal variability of springflow is remarkably thin.

6.2.2 A lack of temporal variability studies of groundwater

Perennial spring discharge is typically assumed to be a more stable, invariable component of the hydrologic cycle and therefore temporal studies examining patterns in variability are less frequently conducted and limited to: 1) studies of karst aquifers, 2) monitoring of groundwater level or water quality changes in response to groundwater withdrawal, 3) and shallow groundwater. Karst aquifers and springs are frequently analyzed temporally (e.g., Kattan et al., 1997; Mayer et al., 1999; Barbieri et al., 2005; Ozyurt, 2008; Liñán Baena et al., 2009; Al-Charideh, 2010; Muskgrove et al., 2010; Jeelani et al., 2015) due to fast aquifer transit times and the ability to identify event-scale responses in karst systems. Progressive monitoring of groundwater chemistry or isotopes (e.g., $^{87}\text{Sr}/^{86}\text{Sr}$) is often performed to identify contamination such as nitrate (Iqbal et al., 1997; Pauwels et al., 2001) or pesticides (Morvan et al., 2006). In situations of public health, analytes like fluoride (Davraz et al., 2008), arsenic, sulfate (Tichomirowa et al., 2010), and chloride/TDS (Lin et al., 2012) are continuously monitored as important indicators of water quality. Groundwater level, and to a lesser extent, geochemistry, are temporally monitored in regions of intense water consumption (Suursoo et al., 2017). Shallow groundwater frequently interacts with the vadose zone and therefore has the potential to be affected seasonally by precipitation, evaporation, and water table fluctuations (Eltahir and Yeh, 1999). Variations in temperature, geochemistry, and isotopic composition of shallow groundwater have been attributed to connections with seasonal recharge (Tan et al., 2016), dilution effects from more variable sources (e.g., Majumdar et al., 2005), bedrock weathering rates (Soulsby et al., 1998), extreme events (e.g., flooding) (Blake et al., 2016), and even seawater intrusion (Lin et al., 2012). Frequent connections have been made linking the geochemical variability in shallow groundwater to circulation depth (Van der Hoven et al., 2005) and/or groundwater residence time (Plummer et al., 2001; Swanson et al., 2001; Wright and Novakowski, 2019). In these cases, it is typical for temporal variability to be highest in the unsaturated zone and in shallow groundwater, but to attenuate rapidly with depth (Van der Hoven et al., 2005; Wright and Novakowski, 2019).

Outside of shallow groundwater, karst hydrogeology, and temporal water quality monitoring, there is a relatively small body of work examining the temporal hydrochemical and

isotopic variability in groundwater at longer timescales and deeper spatial scales, such as in mountain-block or regional aquifer systems. Mountain groundwater is recently recognized as an integral component of baseflow generation and buffering to climate change in mountainous bedrock catchments (Wilson and Guan, 2004; Singleton and Moran, 2010; Frisbee et al., 2011; Gardner et al., 2018), and it is this same groundwater that primarily supports mountain-block springs within the southern Great Basin (Gleason et al., 2020). Groundwater flow systems in mountainous terrains are controlled by many factors that can affect the water table elevation and subsequently affect groundwater discharge and geochemical fluxes (Forster and Smith, 1988). Additionally, recent work has unveiled the potential of groundwater recharge and flow in fractured crystalline and sedimentary rocks within mountain blocks (Wright and Novakowski, 2009; Gardner et al., 2018). Thus, even though residence times in mountain blocks can be long, changes to flowpath distributions may become readily apparent in the geochemical and isotopic fluxes of springs as the forcing changes (i.e., changes in recharge).

Understanding how changes in flowpath distribution manifest as changes in physical, chemical, or isotopic metrics is crucial for understanding the relationship between groundwater stability and vulnerability. While groundwater is typically slow moving and has a long “memory” (e.g., Cutbert et al., 2019), some studies have shown that groundwater can exhibit strong seasonal variations and can “feel” major events like droughts or floods for many years (Li et al., 2015). Evidence of groundwater residence time exerting a control on hydrochemical variability in shallow groundwater implies that there might be a continuum where deep, stable groundwater exhibits even less variability in comparison (e.g., Crowther and Pitty, 1982). This relationship implies that variability can serve as an indicator of relative groundwater residence time, flowpath distribution stability, or can be indicative of groundwater systems prone to dilution from shallow groundwater, fast flowpaths, and/or transient flowpaths (e.g., Majumdar et al., 2005). However, this hypothesis is untested, as the majority of studies finding correlations with decreased temporal variability associated with increased residence time are in groundwater systems with apparent ages younger than 60 years (e.g., Kattan, 1997; Swanson et al., 2001; Jeelani et al., 2010). Therefore, it is relatively unknown if and how this variability attenuates at longer timescales and how intermediate and regional flow systems would react to a significant climate perturbation (e.g., a major drought). In other words, do springs which discharge a large proportion of old groundwater show dampened variability in isotopic and geochemical signals? The driving question in this study is to understand

if geochemical and isotopic signals are continually attenuated at longer timescales and increased spatial scales (i.e. larger aquifer volume) and whether geochemical variability attenuation is correlated with groundwater residence time (Figure 6.1). This study hopes to shed light on this knowledge gap by examining temporal patterns in springs that capture a wide range of topographic positions and groundwater residence times.

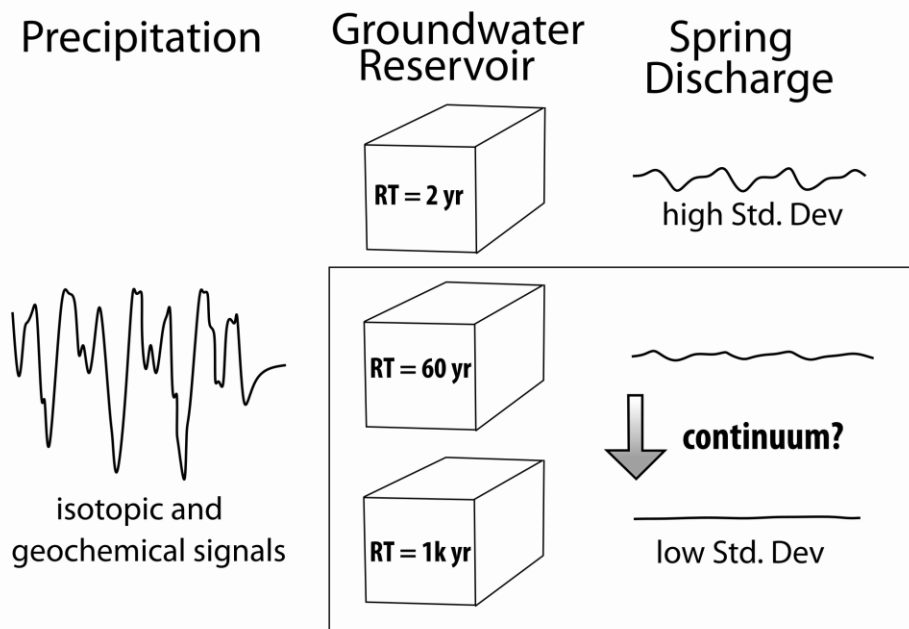


Figure 6.1: Conceptual figure adapted from Plummer et al. (2001) showing the primary research question driving this study; is there a continuum where geochemical and isotopic signals are continually attenuated at longer timescales and increased spatial scales (i.e. larger aquifer volume)?

6.2.3 Why study temporal variability in spring?

Springs differ from typical groundwater samples (i.e., wells) for two main reasons: 1) springs may represent integrations of groundwater flowpaths (Manga, 1999; Manga, 2001; Frisbee et al., 2013) rather than being samples from a discrete point in an aquifer (e.g., a well) where the flowpath distribution may be extremely limited and 2) springs are expressed at the land surface and support aquatic ecosystems. Groundwater flowpaths are primarily controlled by three factors; geology, topography, and climate (Toth, 1999). Springflow generation is complicated and dependent upon these processes as well as the processes driving flowpath convergence to the surface (e.g., structural features, local geological heterogeneity). This complexity results in

integrated physical, chemical, and biologic signatures at springs (Springer and Stevens, 2009; Frisbee et al., 2013). Because springs offer a rare glimpse into integrated groundwater processes within mountain blocks and in complex topography, temporal variations in spring hydrochemical properties may provide information about the stability or response timescales of these groundwater systems (Manga, 1999; Manga 2001). Additionally, temporal variations at springs are critically important because springs, especially in arid regions, host keystone aquatic ecosystems that often support endemic or threatened species.

Spring ecological environments tend to be more stable and support larger macroinvertebrate communities than streams because they exhibit less seasonal variability in temperature, chemistry, and discharge (McCabe, 1998). It is common in streams for there to be interhourly, short-term dynamics (Nagorski et al., 2003). Springs in arid regions are projected to be vulnerable due to climate change which may threaten these aquatic ecosystems (Frisbee et al., 2013b). Increases in mean annual springbrook temperature, an expected consequence of climate change, have been linked to decreases in animal density, biomass, and taxonomic richness in benthic organisms (Hogg and Williams, 1996). Hydrochemical stability in the source regions of springs is particularly important. Studies have found that as distance from spring source increases, species diversity decreases likely due to increased temperature and geochemical variations downstream (Resh, 1983). Increased variability in springs has been linked to decreased species richness (Erman and Erman, 1995; Erman, 2002) and increased crenobiotic mortality (Rossini et al., 2017).

6.2.4 Goals of the study and overarching research question

In this introduction I have identified several knowledge gaps regarding the controls on geochemical temporal variability in groundwater systems at increased timescales and spatial scales. With this study I aim to address these knowledge gaps by analyzing temporal hydrochemical and isotopic data collected from springs in the southern Great Basin from 2016-2019. The springs in this study are representative of the regional variance (e.g., Chapter 5) and capture a wide range of hydrochemical conditions, residence times, and topographic and geologic settings. The sampling interval (2016-2019) is particularly interesting as the first sampling event, March/May 2016, captures the end of a historic drought that devastated the region from 2011-2017

and progressively put over 58% of CA into “exceptional drought” status (<https://droughtmonitor.unl.edu/>). This climate perturbation was significant both in terms of record heat (Griffin and Anchukaitis, 2014) and diminished snowpack (Mote et al., 2016). Our three subsequent sampling campaigns (Dec. 2016, March 2017, and Oct. 2017) capture the deposition and melt of a historic snowpack during the winter of 2017 and subsequent drought recovery throughout the region (2017-2019) (Figure 6.2). This timing of events coupled with the temporal data presented in this study provides an opportunity to understand if events of significant magnitude like the 2011-2017 California drought can propagate quickly through groundwater systems and affect springs with complex flowpath distributions of intermediate to regional flowpath length.

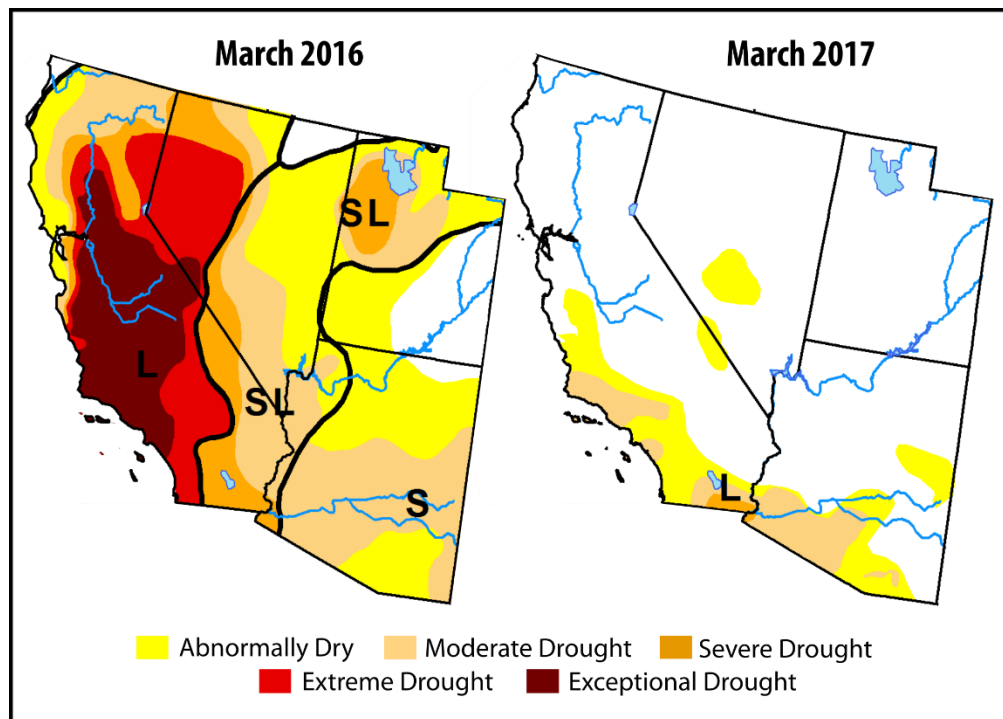


Figure 6.2: Historical drought index comparison between March 2016 and March 2017 for the desert southwest region of the United States (<https://droughtmonitor.unl.edu/>). In March 2016, large portions of the study area were classified under “Exceptional” or “Extreme” drought condition. A year later, the majority of the region changed to a “No Drought” classification. Sampling for this study started during March 2016 and continued through the summer of 2019.

Within this study, I aim to answer two research questions: 1) What are the primary controls on spring temporal geochemical variability? and 2) What is the effect of increased geochemical variability on ecological community structure? I hypothesize that increased temporal variability in both hydrochemical and isotopic analytes will inversely correlate with groundwater residence time (i.e., springs with elevated temporal variability in geochemical analytes and environmental tracers will have shorter residence times and correspond to higher topographic positions within the study region [Figure 6.3]). I expect these springs to be more influenced by climate perturbations such as droughts that affect more local scale flowpath distributions (Figure 6.3). This hypothesis will be tested by comparing variability metrics of spring discharge temperature, major ions, trace elements, $^{87}\text{Sr}/^{86}\text{Sr}$, stable isotopes of water ($\delta^2\text{H}$ and $\delta^{18}\text{O}$), and other environmental tracers indicative of groundwater residence time (^3H , ^{14}C , ^{36}Cl). Lastly, I assess how temporal geochemical variability in springs relates to our conceptual model of spring ecological community structure.

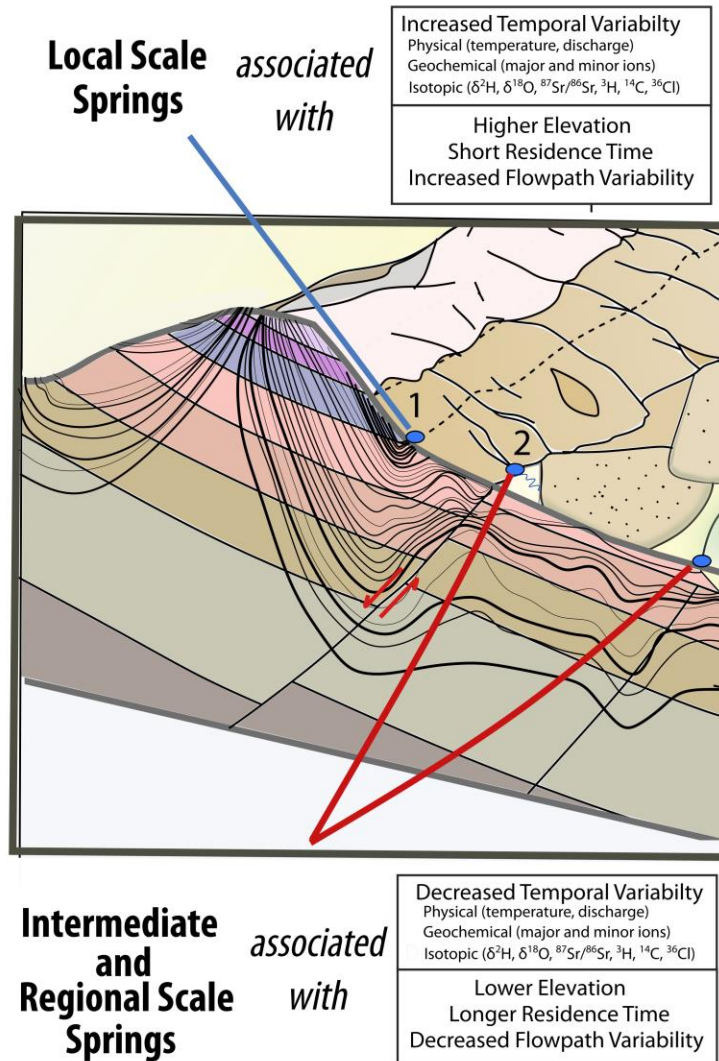


Figure 6.3: Conceptual model showing the hypothesis of the relationship among topographic position, flowpath transience, and temporal variability in physical, geochemical, and isotopic analytes. Illustrated flowlines are conceptual. I hypothesize that increased temporal variability in both hydrochemical and isotopic analytes will inversely correlate with groundwater residence time (i.e., springs with elevated temporal variability will have shorter residence times and correspond to higher topographic positions within the study region). Major climate events such as significant drought or a historic snowpack year will cause increased variability in local-scale, high elevation flowpath distributions that will be dampened at increasing spatial scales.

6.3 Methods

6.3.1 Site description

The study area for this paper is defined to the east by the drainage divide of the Spring Mountain (NV) and to the west by the crest of the eastern Sierra Nevada (CA) (Figure 6.4). The southern boundary of the region is defined by the Garlock-Stateline fault system while the northern boundary is defined by the northern extents of the Las Vegas Valley, Funeral-Grapevine Mountains, and White-Inyo Mountains. This region is defined by Miocene Basin and Range extension and contains rugged topography and significant relief between ranges and basins. In fact, both the highest (Mt. Whitney) and lowest (Badwater Basin) points in the contiguous 48 United States are found within the study area. The long, high crest of the Sierra Nevada places the entire region in a rain shadow that becomes progressively worse moving eastward as moisture is continuously siphoned off by successive fault-block mountain ranges (Ingraham and Taylor, 1991). The regional climate is extremely arid and both temperature and precipitation are highly elevation-dependent (Hunt, 1960). For example, within Death Valley annual temperatures range from -10 °C during winter at high elevations to 52 °C on the floor of Death Valley during the summer. Annual precipitation rarely exceeds 100 cm in mountains and is less than 6 cm on the floor of Death Valley. High elevation mountain ranges either further west (i.e., less in the rain shadow; e.g., the White-Inyo Mountains) or with an additional moisture source (e.g., the Spring Mountains, NV), typically receive additional snowfall. Similarly, basins with a valley floor at a higher elevation than Death Valley (e.g., Panamint Valley or Amargosa Valley) are slightly cooler.

Due to the aridity of the climate, perennial surface water features are rare and are mostly found in the form of isolated desert springs. Springs number in the thousands throughout the study region and are found across all landscape features (i.e., mountains, bajadas, playas, etc.). The extremes of the study area (e.g., relief, temperature, precipitation) are mimicked in the hydrochemical characteristics of the springs. Large ranges in spring discharge temperature (3-50°C) and electrical conductance (<100 μS/cm to > 10,000 μS/cm) have been observed in many regional spring surveys (Sada and Herbst, 2001; Sada and Pohlmann, 2007). While some springs at high elevations in the region are supported by short, local flowpaths and have apparent ages of 10 years or less (e.g., Winograd et al., 1998), other springs have been identified as discharging

water that was recharged during the last glacial period with residence times over 10,000 years (Belcher et al., 2009).

The springs used in this analysis capture large spatial and topographic distributions from different focus areas within the southern Great Basin (Figure 6.4). Spring head elevations range from -77 mrmsl (IES-019) to 2209 mrmsl (IES-006). Springs at the “oldest” end of the spectrum have groundwater residence times exceeding 10,000 years (e.g., IES-010, IES-011, IES-014, IESS-016, IEs-018, IES-049). Other than two springs that incorporate large mixtures of modern surface water into their flowpath distributions (IES-026 and IES-034), the youngest springs in our analysis are roughly 60-70 years old and contain a substantial proportion of recharge from the 1950s and 1960s (e.g., IES-038). The springs analyzed for temporal variability in this paper are categorized into five focus areas; 1) Spring Mountains, 2) Ash Meadows, 3) Death Valley, 4) White Mountains-Argus Range, and 5) Owens Valley (Figure 6.4). These focus areas represent individual geographic, geologic, and topographic provinces within the greater study area.

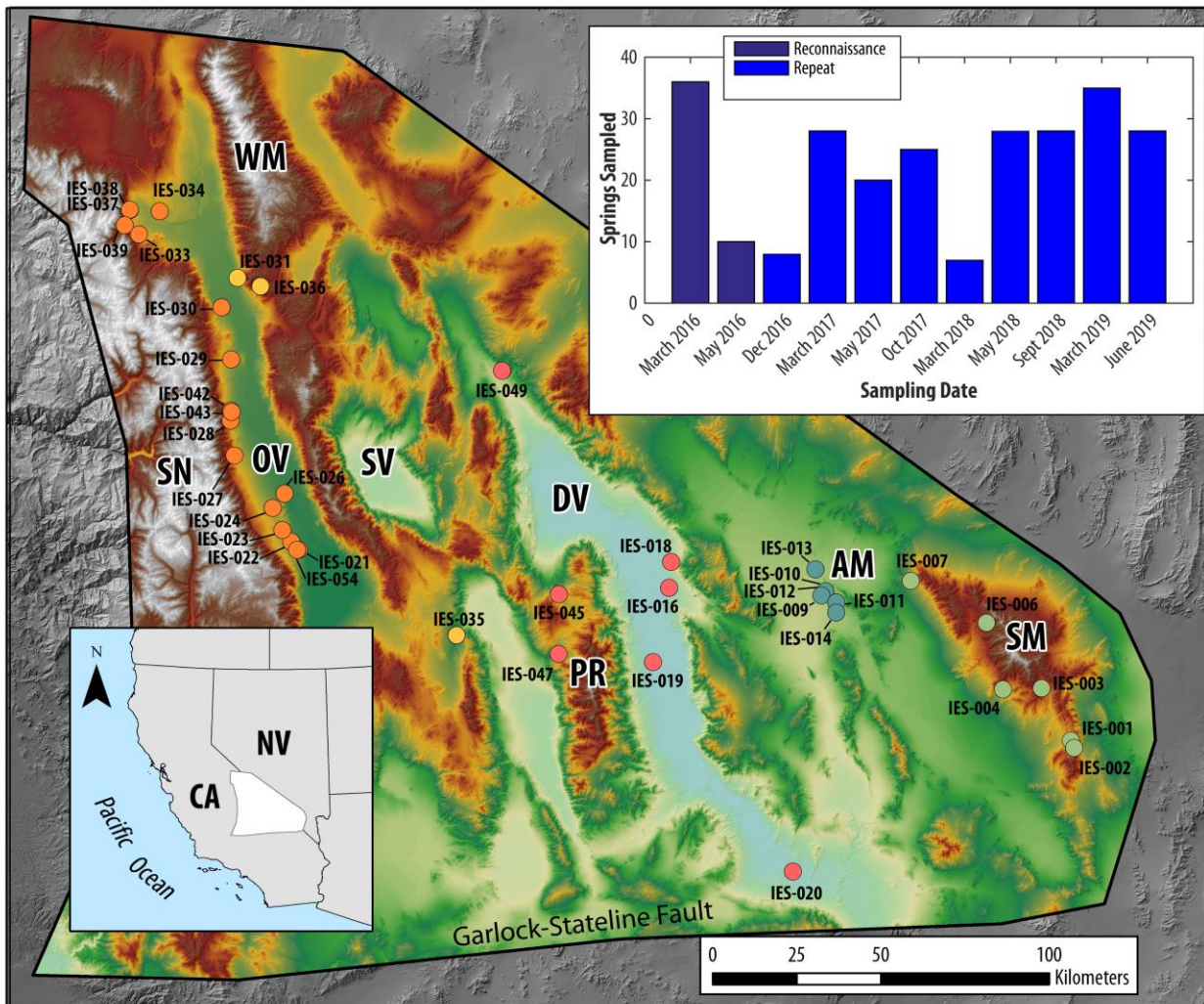


Figure 6.4: Map showing the study area boundary and springs selected for repeat sampling. Springs are annotated by their Integrated Earth Systems (IES) number (e.g. IES-001). Green, teal, coral, yellow, and orange circles represent springs in the Spring Mountains, Ash Meadows, Death Valley, WMAR, and Owens Valley focus areas, respectively. The inset map shows the location of the study area within the context of the western United States. The inset bar chart shows the number of springs sampled as a part of each repeat sampling event. Abbreviations on the map are as follows; SN – Sierra Nevada, OV- Owens Valley, WM- White Mountains, SV- Saline Valley, DV- Death Valley, PR-Panamint Range, AM- Ash Meadows, SM- Spring Mountains.

6.3.2 Sampling

Repeat field measurements and hydrochemical samples were taken from 35 springs over the course of eleven sampling campaigns between 2016 and 2019 (Figure 6.4): 1) March 2016, 2) May 2016, 3) Dec. 2016, 4) March 2017, 5) Oct. 2017, 6) March 2018, 7) May 2018, 8) Sept. 2018, 9) March 2019, 10) June 2019, and 11) August 2019. The research team conducted initial sampling for hydrogeological reconnaissance. Repeat sampling was conducted to identify springs with a significant modern component that may be susceptible to mixing or short-term climate variability. Unless otherwise stated, hydrochemical samples were collected directly from the groundwater emergence point or spring “source” using a GeoTech peristaltic pump and Masterflex platinum-cured silicone tubing. If needed, samples were filtered using .22 μm polyethersulfone membrane Sterivex-GP pressure filter units. Road closures, inclement weather conditions, and vehicular complications occasionally prevented each repeat sample from being collected during every sampling campaign. Weighing the significant cost of analysis, repeat environmental tracer, general chemistry, trace metal, and strontium isotope samples were stopped following the third or fourth sampling event because of a lack of significant variation. Measurements of temperature and water stable isotopes continued to be collected because these analytes exhibited more variations and were more cost effective for the analytical budget. The following sections provide information regarding sampling rationale, field protocol, and analytical methods.

6.3.2.1 Discharge temperature

Field parameters measured at the spring orifice provide information about the physical and chemical characteristics of groundwater at the time of emergence. Groundwater temperature variability has previously been correlated with groundwater circulation depth (Crowther and Pitty, 1982) and is inferred to be associated with groundwater residence time (Brumm et al., 2009).

Temperature ($^{\circ}\text{C}$) was measured with a YSI Professional Plus multi-parameter probe. Whenever possible, the probe was inserted directly into the orifice of the spring, submersed underwater, and allowed to equilibrate before the measurement was recorded. For seeps, diffuse emergences, and shallow pools, a FLIR camera was used to identify the exact area of groundwater emergence, frequently identifiable by a temperature anomaly. The YSI measurement uncertainty for temperature, the sole field analyte used in this chapter, is $\pm 0.1^{\circ}\text{C}$.

6.3.2.2 Major ions

Major ion temporal variability has been previously correlated with groundwater residence time (Swanson et al., 2001) and variations in groundwater recharge (Arndt and Richardson, 1993; Scheyt, 2012). Temporal variability in major ion data from springs has also been used to distinguish between aquifer source type (Blake et al., 2016).

General chemistry samples were filtered in field and collected in 250 ml high-density polyethylene (HDPE) bottles. Samples were refrigerated upon collection. Major cations and anions were measured at the New Mexico Bureau of Geology and Mineral Resources Chemistry Lab. Cations were measured using inductively coupled plasma optical emission spectrometric techniques (ICP-ES) according to EPA 200.7. Anions were measured using an ion chromatograph (IC) according to EPA 300.0. Duplicates were run on every 10th sample.

6.2.2.3 Trace elements

Trace elements function as indicators of chemical weathering, biologic processes, and flow conditions. While some trace element concentrations in groundwater are strongly related to rock-water interaction (e.g., boron, lithium, vanadium), others are more informative about redox conditions at the surface (e.g., iron, manganese, etc.; Hem, 1985). Trace element variability has been previously used to identify water source contributions in streams and groundwater (Musgrove et al., 2010; Engel et al., 2019) and influence from perturbations like saltwater intrusion (Lin et al., 2012). A common practice for analyzing trace metal, trace element, or rare earth element data in groundwater systems is to employ multivariate statistical analysis techniques like principal component analysis (PCA) that help to discern patterns that provide insight into aquifer processes and potential groundwater flowpaths (Kreamer et al., 1996; Johannesson et al., 1997; Stetzenbach et al., 1999; Farnham et al., 2003; Lin et al., 2012). In this study, PCA was utilized to discern patterns of temporal variation in major ions and trace elements for the IES springs.

Trace element samples were collected unfiltered in 60 ml HDPE bottles laced with 400 μ L of ultra-pure nitric acid and stored at room temperature. Trace element analysis was performed at the MM Lab in Las Vegas, NV. Samples were analyzed using inductively coupled plasma mass spectrometry (ICPMS). Trace element concentrations are reported by the MM lab as parts per billion (ppb).

6.2.2.4 Strontium isotopes

$^{87}\text{Sr}/^{86}\text{Sr}$ is an effective tracer for understanding mineral weathering and groundwater mixing processes at local (Blum et al., 1993; Clow et al., 1997; Pretti and Stewart, 2002) and regional (Johnson et al., 2000; Stewart-Maddox et al., 2018) spatial scales. Examining temporal changes in $^{87}\text{Sr}/^{86}\text{Sr}$ is one way of identifying potential changes to flowpath distributions, especially when paired with temporal major ion data (e.g., Sr^{2+}). Studies examining the temporal variation of $^{87}\text{Sr}/^{86}\text{Sr}$ in groundwater have found correlations with changes in climatic and hydrologic conditions even though variations are generally not large (Musgrove et al., 2004; Musgrove et al., 2010). Groundwater with variable $^{87}\text{Sr}/^{86}\text{Sr}$ is more common at the hillslope scale (e.g., Walker et al., 2003), in shallow groundwater that interacts with the vadose zone (Tichomirowa et al., 2010), or in alpine settings with localized groundwater flow. For example, Barbieri et al. (2005) observed non-negligible temporal $^{87}\text{Sr}/^{86}\text{Sr}$ variations in high elevation springs that they attributed to local flowpaths more susceptible to water table fluctuations. In our study we compare temporal variability in $^{87}\text{Sr}/^{86}\text{Sr}$ to Sr^{2+} variance and groundwater residence time to understand if high elevation, local-scale springs have more variable flowpath distributions than regional-scale springs.

$^{87}\text{Sr}/^{86}\text{Sr}$ samples were filtered in the field and collected in 125 ml HDPE bottles. Samples were analyzed at the Johnson Lab the University of Illinois Urbana-Champaign (UIUC). A Nu Plasma HR multicollector inductively-coupled-plasma mass-spectrometer (MC-ICPMS) was used for strontium isotope analysis. Samples with low concentrations and thus lower voltages were specified for longer instrument runs. Reported analytical uncertainty from the UIUC lab for $^{87}\text{Sr}/^{86}\text{Sr}$ is ± 0.00005 .

6.2.2.5 Stable isotopes

It is well established that $\delta^2\text{H}$ and $\delta^{18}\text{O}$ are highly variable in precipitation and less variable with increasing depth. Shallow groundwater often exhibits a seasonal amplitude in stable isotopic composition that is a dampened signal of precipitation (Plummer et al., 2001; Jeelani et al., 2010). Increased temporal variability of $\delta^2\text{H}$ and $\delta^{18}\text{O}$, whether related to seasonal signals or not, has been inversely correlated with groundwater residence time (Davis et al., 1970; Abbott et al., 2000; Plummer et al., 2001; Majumdar et al., 2005), water table shifts (Davisson and Criss, 1993), and

increased mixing with variable sources (Liu et al., 2011). Separate from seasonal fluctuations, temporal *shifts* in stable isotope composition have also been related to year-to-year variations in weather patterns that encapsulate decadal-scale climate change (Rademacher et al., 2002). Examining temporal variations of water stable isotopes is particularly interesting in snowfall-dominated areas where snowfall can become significantly depleted relative to rainfall (Maule et al., 1994; O'Driscoll et al., 2005; Gleason et al., 2020), causing large spatial variations in $\delta^2\text{H}$ and $\delta^{18}\text{O}$. This is true for the southern Great Basin, however the large spatial variation of $\delta^2\text{H}$ and $\delta^{18}\text{O}$ in groundwater can also be attributed to high evaporation rates, varying moisture sources (e.g., winter precipitation, summer precipitation and monsoon) (Winograd et al., 1998; Moreo et al., 2014) and the influence of paleorecharge from different climatic conditions (e.g., Pleistocene recharge). The southern Great Basin has a relatively thorough body of work characterizing the isotopic composition of precipitation and groundwater (Smith et al., 1979; Ingraham and Taylor, 1991; Winograd et al., 1998; Friedman et al., 2002a; Friedman et al., 2002b; Smith et al., 2002). The IES project has filled in spatial gaps of groundwater isotopic composition by sampling springs in Owens Valley (Chapter 3) and in the Panamint Range (Gleason et al., 2020).

One 2 ml vial of unfiltered water was collected in the field for analysis of $\delta^2\text{H}$ and $\delta^{18}\text{O}$. Samples were analyzed at the University of California, Davis Stable Isotope Facility (SIF) using a Laser Water Isotope Analyzer V2 (Los Gatos Research, Inc., Mountain View, CA, USA). All stable isotope measurements are reported relative to Vienna Standard Mean Ocean Water (VSMOW). The reported uncertainty for this analysis is 0.83‰ for $\delta^2\text{H}$ and 0.08‰ for $\delta^{18}\text{O}$.

6.2.2.6 Age-dating environmental tracers (^3H , ^{14}C , ^{36}Cl)

Age-dating environmental tracers are less frequently sampled multiple times compared to other hydrochemical reconnaissance tools like major ions or water stable isotopes often because repeat sampling can be cost prohibitive. However, temporal environmental data can be extremely informative for two reasons: 1) changes in groundwater residence time can indicate changes in groundwater flowpath distribution and 2) a groundwater sample from one point in time may not be representative of long-term environmental conditions. Recent work has shown that temporal analysis of age-dating environmental tracers can provide significant insight into flow system stability. Manning et al. (2012) related temporal changes in groundwater age to declines in snowpack and groundwater recharge. Other studies have found that a lack of interannual variations in tracer data is indicative of systems with longer groundwater residence time (e.g., Al-Charideh, 2011; Cendón et al., 2014) or a way to discern well-mixed systems from groundwater interacting with superficial systems (Davis et al., 1970; Majumdar et al., 2005). In the case of bomb-pulse tracers like tritium, identifying small versus large temporal changes in may be more meaningful now that bomb-pulse tritium has decayed enough to where a “tritium-dead” classification has significant meaning.

Tritium (^3H) samples were unfiltered in the field and collected in 1L HDPE bottles. Samples were analyzed at the University of Miami Tritium Laboratory (<https://tritium.rsmas.miami.edu/>) using gas proportion analysis with low-level counting and electrolytic enrichment for the highest possible accuracy and precision. Tritium concentrations are expressed in tritium units (TU) and analytical uncertainty (1 standard deviation) ranged from 0.09-0.11 TU for all springs included in this analysis.

Chlorine-36 (^{36}Cl) samples were filtered in the field and collected in 1L HDPE bottles. Samples were prepared with AgCl-precipitation techniques at Purdue University (IN) and analyzed with accelerator mass spectrometry (AMS) at the Purdue Rare Isotope Measurement Laboratory (PRIME Lab). Results are reported as $^{36}\text{Cl}/\text{Cl}$ ratios $\times 10^{-15}$. Standard deviations are also reported for individual samples.

Samples for radiocarbon (^{14}C) and carbon-13 ($\delta^{13}\text{C}$) were unfiltered and collected in two 500 ml HDPE bottles. Samples were analyzed at the University of Arizona Accelerator Mass Spectrometry Lab. Radiocarbon activity was reported as fraction of modern carbon and $\delta^{13}\text{C}$ was reported relative to Pee Dee Belemnite (PDB) for groundwater dissolved inorganic carbon (DIC).

Fraction of modern carbon (fmc) was calculated as a weighted average from multiple machine runs.

6.3.3 Examining variability

6.3.3.1 Standard deviation and coefficient of variation

Simple summary statistics (e.g., range, standard deviation, coefficient of variance) have proven to be effective tools for understanding temporal variability in hydrologic studies (Shuster and White, 1971; Plummer et al., 2001; Swanson et al., 2001; Brumm et al., 2009; Liñán Baena et al., 2009; Jeelani et al., 2010; Jiang, 2011; Tallini et al., 2013), especially when dealing with a limited number of samples. Standard deviation is a measure of spread and is an appropriate measurement of variation when comparing samples of similar magnitude. We use standard deviation to compare temporal variations in analytes like stable isotopes ($\delta^2\text{H}$, $\delta^{18}\text{O}$, $^{87}\text{Sr}/^{86}\text{Sr}$). The formula for standard deviation is as follows:

$$\sigma = \sqrt{\frac{\sum(x_i - \mu)^2}{N}}$$

σ = population standard deviation

N = the size of the population

x_i = each value from the populations

μ = the population mean

Coefficient of variance (CV) is a more appropriate measure of variance when comparing samples of differing magnitudes or comparing changes between analytes. CV is a measure of relative change or percent deviation. For example, assume two springs have a temporal standard deviation in chloride of 0.2 mg/L. One spring has a mean chloride concentration of 0.5 mg/L and another spring has a mean chloride concentration of 100 mg/L. While both springs have the same standard deviation, their percent deviation or variation in relation to the sample mean is quite different. Biplots of CV have previously been used to investigate if variations between different variables are correlated (Liñán Baena et al., 2009)

The formula for coefficient of variation is as follows:

$$CV = \frac{\sigma}{\mu}$$

$$\text{to express as a percentage: } CV = \frac{\sigma}{\mu} * 100\%$$

CV = the coefficient of variance (%)

σ = population standard deviation

μ = the population mean

6.3.3.2 Principal Component Analysis (PCA) and Hierarchical Clustering Analysis (HCA)

Multivariate statistical methods (MSMs) such as principal component analysis (PCA) and hierarchical clustering analysis (HCA) are used in this study to discern temporal patterns of geochemical variation in major ions and trace metal data. However, rather than examining “clustering” or variance by chemical composition (i.e., vectors are solutes) for multiple samples, we examine clustering by chemical variation (i.e., vectors are solute coefficients of variance for individual samples). This method creates a multivariate subspace where geochemically variable springs can be distinguished from geochemically invariable springs. Vectors for different solutes on the PCA biplots allow us to associate sample locations in PCA space with the direction and magnitude of the solute variability vectors. Ten variables (Ca^{2+} , Na^+ , Mg^{2+} , K^+ , Cl^- , SO_4^{2-} , HCO_3^- , Sr^{2+} , Si, and TDS) are used in PCA analysis to investigate temporal variability trends in major ion data. Only six variables were used to investigate trace metal variability over time (As, B, Fe, Li, Mo, and V) because other analytes were either already incorporated in a prior analysis (e.g., Mg^{2+} & Si) or had large number of samples with concentrations below analytical detection limits (>50%) impeding statistical analysis. In both PCA analyses, we use the CV of each analyte rather than standard deviation as our metric of temporal variability. This is done for two reasons: 1) large differences in trace element concentration among springs implies that the percent deviation is more informative than standard deviation for the purposes of comparison and 2) examining differences in CV minimizes potential data transformations needed for MSMs. Transformation of water

chemistry data can result in obscuring geochemical relationships (Dreher et al., 2003; Templ et al., 2008).

Hierarchical clustering analysis (HCA) was used to investigate temporal clustering trends in major ion data by examining if samples from the same spring always cluster on the same “branch” and are distinct relative to other springs. In theory, springs with increased variability might cluster on multiple branches with other springs and exhibit reduced “geochemical endemism”. HCA was run using two different preprocessing techniques (see Chapter 2) to assess chemical similarity over time. One technique emphasizes similarity as it relates to solute magnitude or overall salinity (traditional preprocessing) while the other preprocessing technique emphasizes the relative proportions of individual cations and anions in solution (i.e., the “geochemical fingerprint”).

6.4 Results

The following sections discuss the temporal variability results for the IES repeat springs. Each section (e.g., temperature, major ions, etc.) contains a slightly different number of springs utilized in the analysis based on the data availability. A complete list of the springs used for each analysis is shown in Table 6.1.

6.4.1 Discharge temperature

The temporal variability of discharge temperature was examined in 34 springs within the study area. Time series plots of discharge temperature for all springs, separated out by focus area, are shown in Figure 6.5 (*note that y-axis limits vary for each plot*). Owens Valley (OV) springs are separated into southern OV (6.5E; light orange) and northern OV (6.5F; dark orange) due to the high number of springs in OV compared to other focus areas. Mean daily temperature time series for local weather stations within specific focus areas (e.g., Lovell Summit (NV), Hunter Mtn (CA), Stovepipe Wells (CA), Deep Springs (CA), and South Lake (CA)) are included in the plots for comparison (Figure 6.5). In the Death Valley (DV) subplot (Figure 6.5C), Hunter Mtn. is representative of a high elevation weather station while Stovepipe Wells represents a low elevation weather station. The majority of springs included in this analysis (85%) have 5 or more measurements of discharge temperature from March 2016 - July 2019.

Table 6.1: Table showing springs included in temporal analyses. An “X” denotes whether a spring was sampled enough for a particular metric to be included in temporal analysis. The total number of springs analyzed for a particular metric is shown in the last row.

ID	E (UTM 11N)	N (UTM 11N)	Temp.	Gen. Chem	Tr. Elements	⁸⁷ Sr/ ⁸⁶ Sr	δ ² H & δ ¹⁸ O	¹⁴ C	³ H
IES-001	634808	3987716	X				X		
IES-002	635816	3985472	X	X	X	X	X	X	X
IES-003	626122	4003263	X	X	X	X	X	X	X
IES-004	614662	4002847	X	X	X	X	X	X	X
IES-006	609764	4022636	X	X	X	X	X	X	X
IES-007	587257	4035099	X	X	X		X		X
IES-010	561869	4032055	X	X	X		X	X	X
IES-011	560685	4030775	X	X	X		X	X	X
IES-014	565104	4025717	X	X	X		X	X	X
IES-016	515430	4033086	X	X	X		X	X	X
IES-018	516050	4040749	X	X	X		X	X	X
IES-019	510652	4010962	X	X	X	X	X	X	X
IES-020	552270	3948765	X	X	X	X	X	X	X
IES-021	405405	4044353	X	X	X	X	X	X	X
IES-023	400577	4050223	X				X		
IES-024	397732	4056750	X	X	X	X	X	X	X
IES-026	401193	4061012	X	X	X	X	X	X	X
IES-027	386328	4072314	X	X	X	X	X	X	X
IES-028	385165	4082719	X	X	X	X	X	X	X
IES-029	385305	4100901	X	X	X	X	X	X	X
IES-030	382448	4116323	X				X		
IES-031	387270	4125103	X	X	X	X	X	X	X
IES-033	357900	4138046	X	X	X	X	X	X	X
IES-034	364114	4144865	X	X	X	X	X	X	X
IES-035	452327	4018935	X	X	X		X	X	X
IES-036	394055	4122601	X	X	X	X	X	X	X
IES-037	355178	4145270	X				X		
IES-038	355222	4145412	X	X	X	X	X	X	X
IES-039	353679	4140727	X	X		X	X		
IES-042	385273	4085645	X	X	X	X	X	X	X
IES-043	385440	4085284	X	X	X	X	X	X	X
IES-045	482674	4031167					X		
IES-047	482637	4013420	X	X		X	X		X
IES-049	465797	4097533	X	X			X	X	X
IES-054	404916	4044329	X				X		
			34	29	26	21	35	26	28

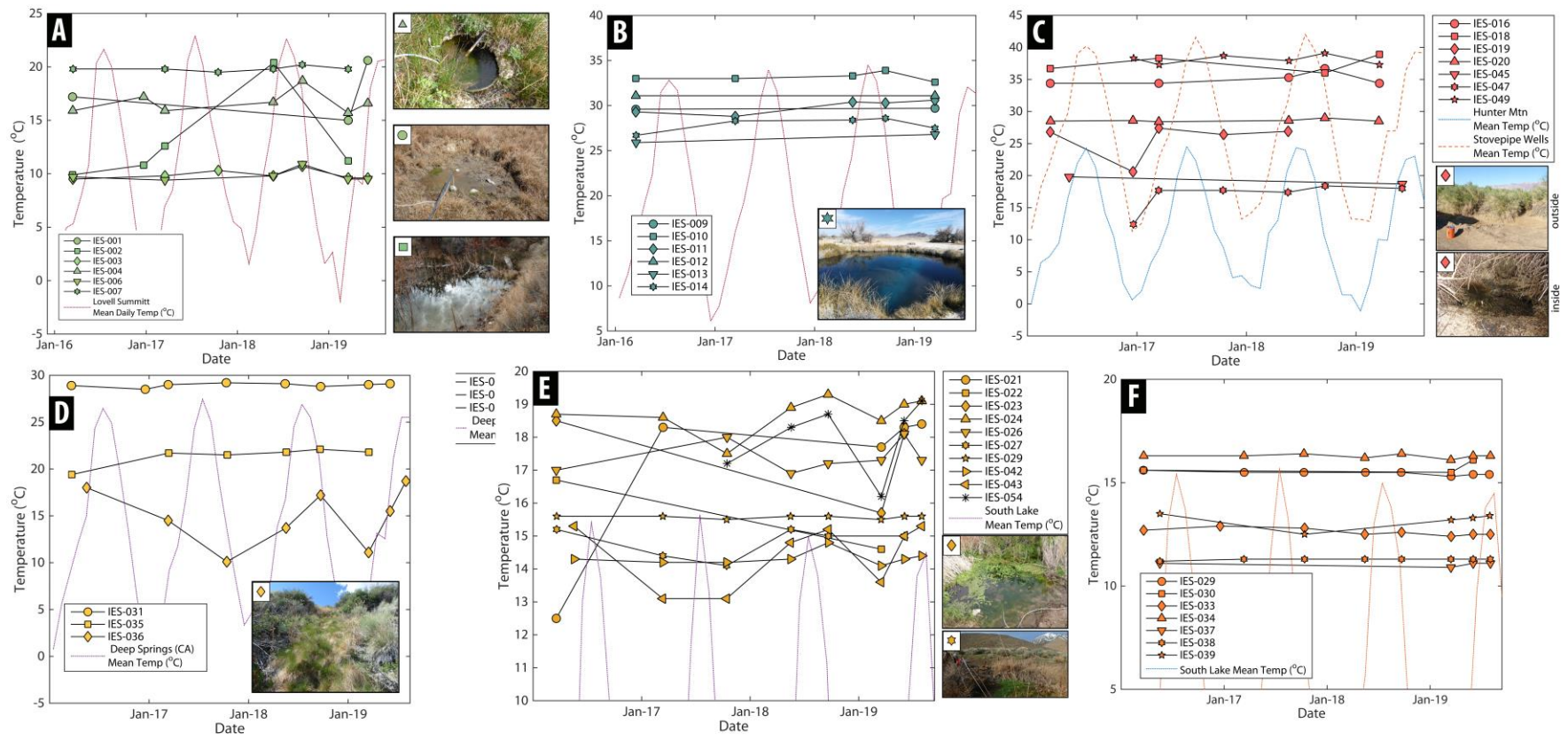


Figure 6.5: Time-series plots of discharge temperature at repeat springs separated out by focus area (A-F): A) Spring Mountains, B) Ash Meadows, C) Death Valley, D) WMAR, E) southern Owens Valley, F) northern Owens Valley. The majority of springs (21/34) have very stable discharge temperatures (i.e., $SD < 1.0^{\circ}C$). Moving temporal averages of mean daily temperature for local weather stations are included in each plot. Photos of selected springs are included for the purposes of discussion and can be identified by associating the symbol in the upper left-hand corner of the photo to the symbol in the subplot legend. Springs that are highly variable (e.g., IES-002, IES-019, IES-036, etc.) tend to mimic changes in mean annual air temperature.

Temporal standard deviations in spring source discharge temperature range from 0.04 to 4.26°C (Figure 6.6). The majority of springs (21/34) have standard deviations in the range of 0.0-1.0 °C. Out of the 13 springs with standard deviations greater than 1.0°C, 9 of these exhibit one or more of the following criteria: 1) low spring discharge (<0.1 L/s) (e.g., IES-001, IES-019), 2) artificial or disturbed emergence conditions, or 3) spheres of discharge (i.e., Springer and Stevens, 2009) that are more susceptible to surface environmental conditions. Artificial or disturbed emergence conditions include open-barrel spring box installation (e.g., IES-004) or spring geomorphic modification due to livestock (IES-021). In our study, spheres of discharge that are more susceptible to surface environmental conditions include shallow limnocrenes (e.g., IES-002 & IES-023) or diffuse helocrenes. These springs tend not to have point source emergences but are diffuse over a broad region or substantially gain over a long reach (e.g., IES-036).

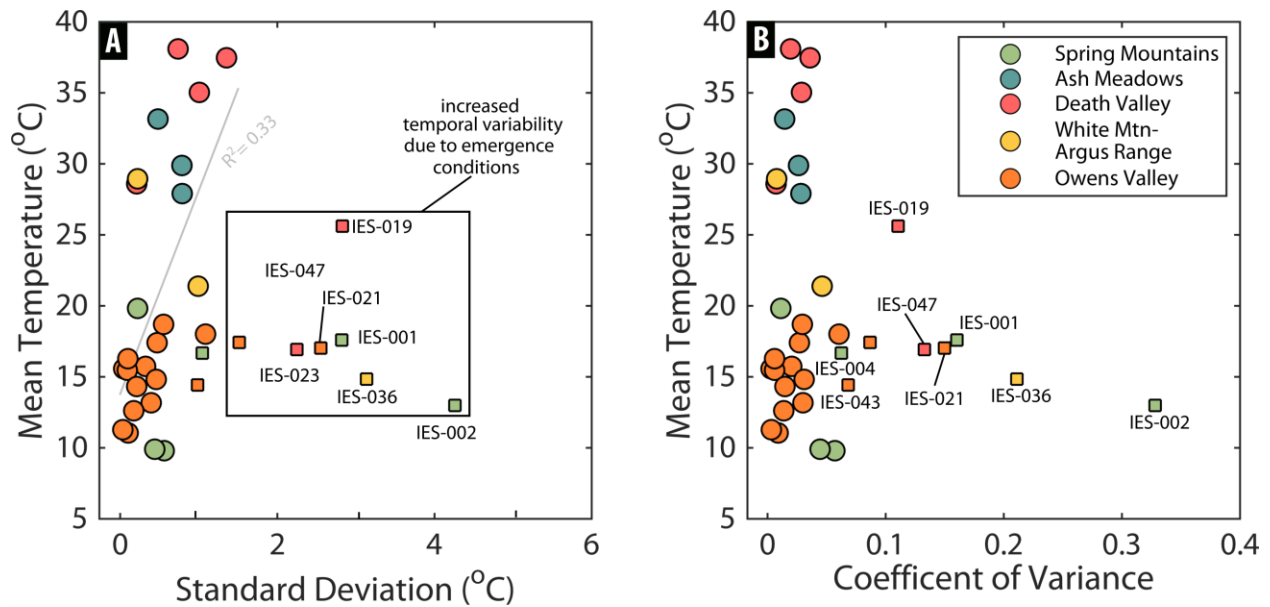


Figure 6.6: Subplots showing metrics of temperature temporal variability (i.e., standard deviation and the coefficient of variance) versus mean spring discharge temperature. Springs are symbolized by color according to focus area and symbolized by shape according to emergence condition. Springs symbolized as squares meet one of three conditions, either they are very low discharge springs, seeps with shallow pools, or springs with modifications that promote diel/seasonal fluctuations due to ambient air temperature or sunlight (e.g., open barrel modification). Springs that show significant deviations are annotated and many of these springs have inset photos in Figure 6.5. Springs symbolized as circles are either unmodified, have high discharge, or have modifications (e.g., a downstream weir) that do not promote diel/seasonal temperature changes.

These three criteria promote increased temperature variability that can be directly attributed to daily/seasonal changes in solar radiation and ambient air temperature based on discharge temperature variations that mimic the mean annual temperature trends of the local weather stations (Figure 6.5). These are the same types of diel/seasonal variations that are found in headwater streams that are strongly influenced by evapotranspiration (Irons et al., 1992; Bond et al., 2002; Graham et al., 2012). Therefore, these nine springs are excluded from further analysis because they exhibit discharge temperature variability that is primarily controlled by environmental surface conditions as opposed to groundwater flowpath changes. These springs are indicated by smaller squares instead of circles on Figure 6.6 and are not included in regression analysis between source temperature variability and metrics of groundwaters stability (i.e., temperature, conductivity, residence time). Our results show that springs with low discharge but with closed barrels in shaded regions, (e.g., IES-006, Buck Spring), do not appear to be as influenced by changes in solar radiation/mean air temperature as springs in open barrels or springs emerging in shallow pools.

For the 21 springs that do not fit the above criteria, we do not find any significant trends with discharge temperature standard deviation or coefficient of variance and any indicators of groundwater stability. The springs with the six lowest standard deviations (0-0.2°C) are all cold springs found in Owens Valley that have elevated ranges of ³H (2.1-3.1 TU) indicative of modern or bomb-pulse recharge. In contrast, the six springs in our study that have, historically and in recent sampling efforts, consistently yielded radiocarbon dates over 10,000 years, (IES-010, IES-011, IES-014, IES-016, IES-018, and IES-049) have a much larger range in standard deviations from (0.5-1.4°C). There is a slight correlation with discharge temperature standard deviation and discharge temperature ($R^2 = 0.33$) among the nonaffected springs (Figure 6.6A). However, this correlation does not exist when considering the discharge temperature coefficient of variance rather than standard deviation (Figure 6.6B), implying that, at certain flowpath lengths (i.e., intermediate and regional), springs with higher temperatures may source aquifers with larger natural temperature variations.

6.4.2 Major ions

Twenty-nine springs are included in temporal analysis of major ion variability. In general, temporal variations of major dissolved ions are very minor for IES springs. The majority of springs have variations so small that graphical distinctions are difficult to make between temporal samples.

A comparison of Stiff diagrams for the March/May 2016, March 2017, and Oct 2017 sampling campaigns is shown in Figure 6.7. Samples from a May 2018 sampling campaign were originally slated to be included in this analysis; however, these samples were subjected to microbial contamination and degradation during sample storage or transport.

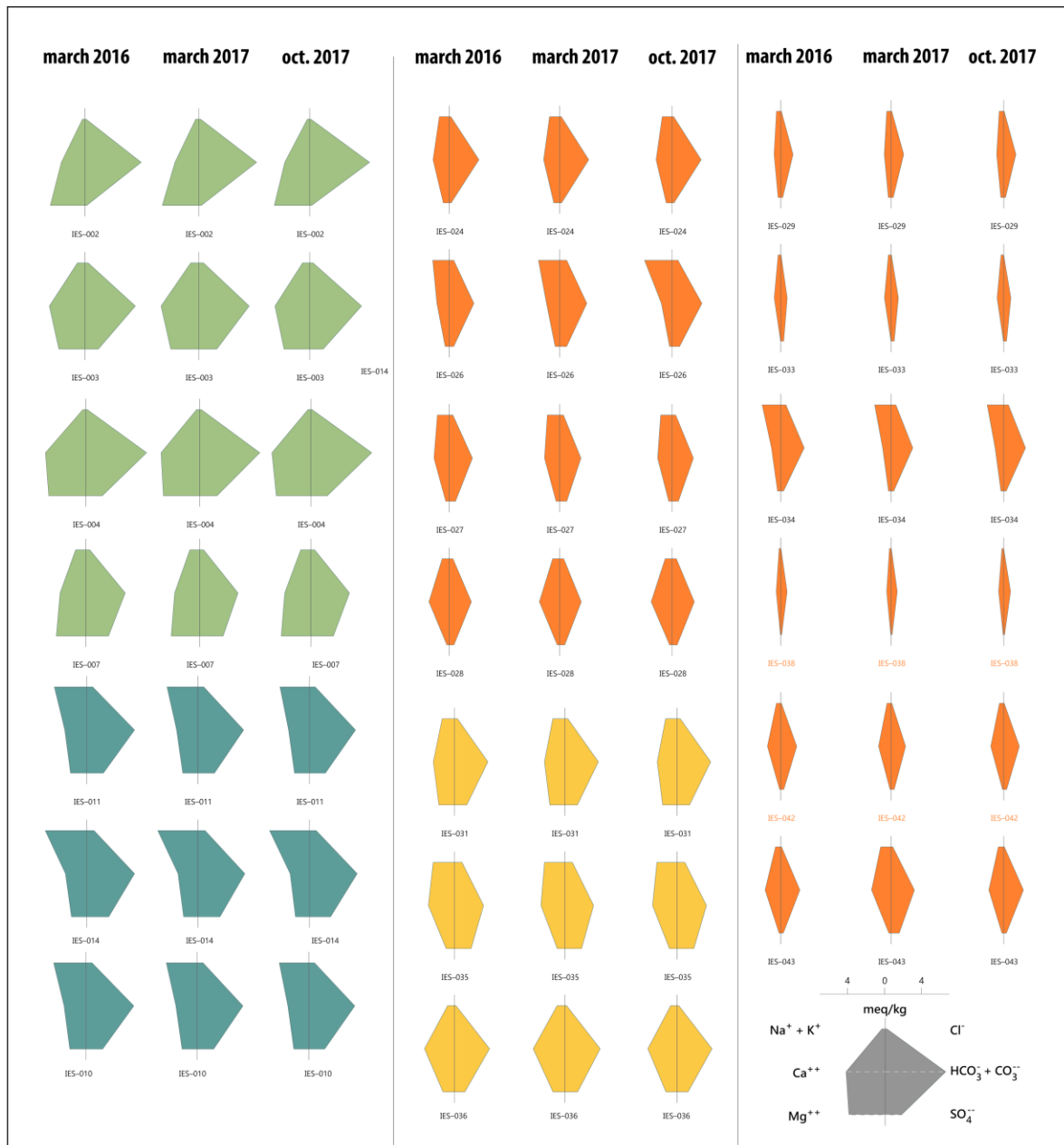


Figure 6.7: Figure showing Stiff diagrams for IES springs over three consecutive sampling events to illustrate the geochemical similarity in repeat spring samples over time. Overall, changes in spring geochemical compositions are very slight.

Similar to the temporal discharge temperature results, we do not observe significant rebounds, shifts, lags, or fluctuations in major ions coming out of the 2011-2017 drought into an extremely wet period. This lack of variation is clearly expressed in the HCA results (Figures 6.8 & 6.9) that includes both repeat and one-time samples from the IES dataset. Traditional HCA from major ions is displayed in Figure 6.8, while alternative HCA (e.g., Chapter 2) using major ions is displayed in Figure 6.9. HCA results show that temporal samples from individual springs almost always cluster together on the same branch rather than being more similar in chemical composition to other springs. This “geochemical endemism” exhibited by springs is persistent whether clustering is performed to enhance differences in solute magnitude (Figure 6.8) or differences in the proportion of solutes relative to total cations or anions in solution (Figure 6.9).

Our results show that, in all but a few cases, each spring has a unique geochemical fingerprint that is consistently distinctive over the sampling interval. The only exceptions are: 1) one sample from IES-011, Crystal Pool, that clusters with three other one-time samples from AM (Figure 6.9), 2) IES-026, Reinhackle Spring (Figure 6.9), and 3) IES-043, South Harry Birch Spring (Figures 6.8 & 6.9). We observe this “geochemical endemism” even amongst highly similar springs sourcing the same aquifer in very close proximity (e.g., Ash Meadows) and even in springs from the same spring complex (e.g., IES-021 & IES-054; IES-037 & IES-038). Temporal variations in major ions for the IES springs are slight enough that MSMs such as PCA are necessary to discern overarching variability patterns. A PCA analysis of geochemical variance for the IES springs is presented in Figure 6.10. This PCA was calculated using spring coefficients of variance of 10 major analytes as matrix vectors. An inset biplot shows the direction and magnitude (length) of each variable (Figure 6.10). Only two components, PCA 1 (72.7%) and PCA 2 (12.1%) control more than 10 percent of the overall variance. Scores for individual springs are plotted on these components and are symbolized by focus area. Springs with high PCA 1 scores are correlated with increased variability amongst all variables, however, most significantly with Cl^- and SO_4^{2-} . The fact that PCA 1 is representative of the vast majority of variance (72.7%) and all the solutes are positively correlated on PCA 1 implies that variability in one solute is generally indicative of increased variability amongst all solutes. Springs with high PCA 1 scores are annotated on Figure 6.10 and include IES-043, IES-006, IES-019, IES-026, and IES-039. Springs with high PCA 2 scores are correlated with increased variability in Cl^- and K^+ , and this variability is not related to variability in other ions (Figure 6.10). Springs with high PCA 2 scores include

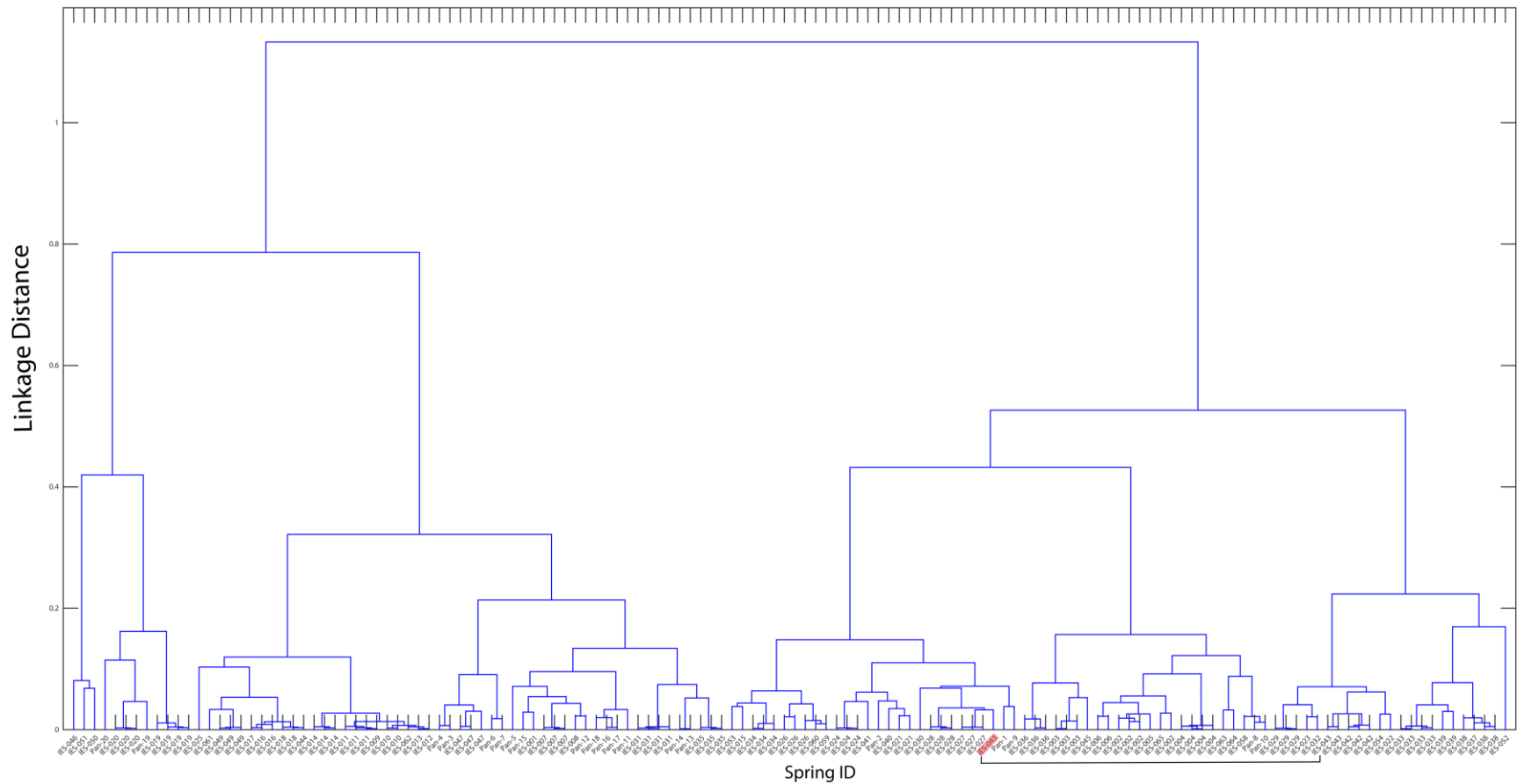


Figure 6.8: Hierarchical clustering analysis emphasizing solute magnitude (i.e., traditional preprocessing). Only one spring, IES-043, contains one geochemical sample that clusters with samples from another spring and is shaded in red.

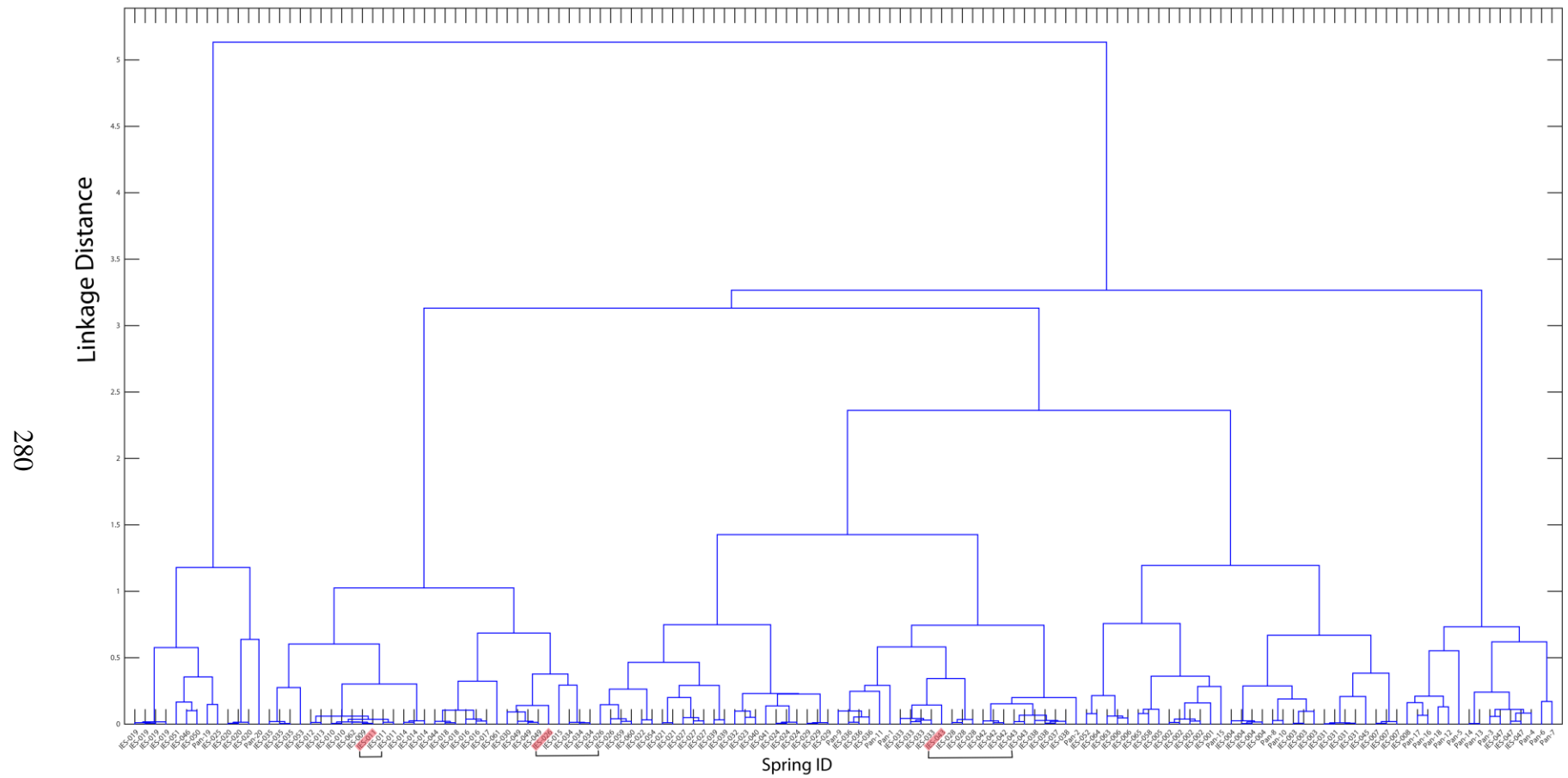


Figure 6.9: Hierarchical clustering analysis emphasizing solute proportion (i.e., alternative preprocessing). Only three springs, IES-011, IES-026, and IES-043 have samples that cluster on a branch with another spring over time and are shaded in red.

IES-039, IES-002, and IES-021. The majority of springs fall within a small bubble associated with low scores on PCA 1 and PCA 2, indicating a negative correlation with increased major ion variability. Stiff diagrams depicting the highest variance spring (i.e., highest PCA 1 score = IES-043) and a spring from the minimal variance bubble (IES-011) are shown in the righthand panel of Figure 6.10. It is clear from the graphical differences between these springs that this PCA analysis captures small, but potentially significant, geochemical variations. Tight clustering of PCA results can suggest minimal variability (e.g., Blake et al., 2016).

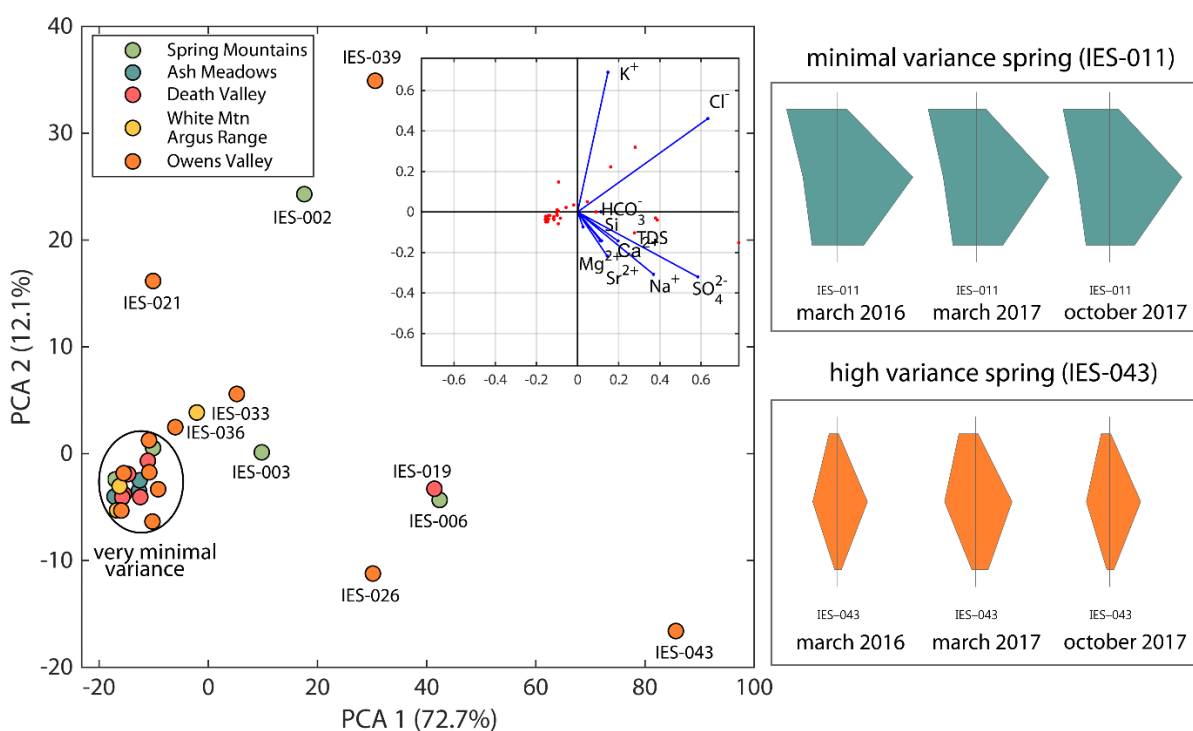


Figure 6.10: Principal Component Analysis (PCA) plot of geochemical variance of 10 major solutes for springs over the study interval. The 10 major solutes and their corresponding vector magnitudes are symbolized in the inset biplot. PCA 1 and PCA 2 control 84.8% of the overall temporal variance. The majority of springs, symbolized by the annotated cluster, exhibit very limited geochemical temporal variability (i.e., the chemical compositions of the major cations and anions are very stable over time). One major takeaway from this figure is that even though there are some springs that exhibit more variability than others over time, even the most variable springs do not change considerably. This point is illustrated by the Stiff diagrams included for IES-014 (which falls within the very minimal variance bubble) and IES-043, which has a very positive score on PCA 1. While IES-043 clearly exhibits more temporal variability in chemical composition from March 2016-October 2017, the degree of change is still fairly minimal considering it is the most variable spring in the dataset.

Statistical distributions (i.e., boxplots) of CV data for individual solutes are separated out by focus area in Figure 6.11. Amongst all springs, K^+ , Cl^- , and SO_4^{2-} are the most variable major ions. Owens Valley has the most springs with temporal geochemical data ($n=12$), while all other focus areas have smaller sample sizes ($n \geq 6$). The inset table within Figure 6.11 highlights the differences in mean spring temperature and environmental tracer concentrations amongst focus areas and gives a general sense of the dominant aquifer system in each focus area. The mean environmental tracer values within the inset plot (e.g., Figure 6.11) show that the Spring Mountains and Owens Valley host springs with a younger mean groundwater residence time. Springs included in this analysis from Death Valley and Ash Meadows have no discernable proportion of young water and many have been radiocarbon dated to well over 10,000 years (Anderson et al., 2006; Belcher et al., 2009; Bushman et al., 2011). Springs in the WMAR do not have a large proportion of young water but are colder and have younger apparent radiocarbon ages compared to springs in DV and AM. From a regional context, we observe that springs in the Spring Mountains and Owens Valley have larger CV distributions for individual solutes than other focus areas. The Spring Mountains is the only focus area where CV medians exceed 10% for solute boxplots (e.g., Cl^- and SO_4^{2-}). Other than one outlier (IES-019), springs in Ash Meadows and Death Valley show dampened temporal geochemical variability across all solutes ($CV < 5\%$) compared to springs in the younger focus areas.

6.4.3 Trace elements

Six trace elements (As, B, Fe, Li, Mo, and V) were originally planned to be used for PCA analysis of trace element temporal variability in twenty-six springs. However, after a preliminary PCA analysis it was found that very small temporal changes in vanadium (V) concentration were controlling a large amount of PCA variance on the first few principal components. In other words, temporal changes in vanadium are very small for all sampled springs (< 3 ppb) and therefore springs that exhibit changes at the higher end of this range (2-3 ppb) exerted a significant weight in the PCA. Furthermore, vanadium variability over time did not appear to be correlated with variability in any other trace metals. Therefore, the analysis was run again without vanadium (Figure 6.12).

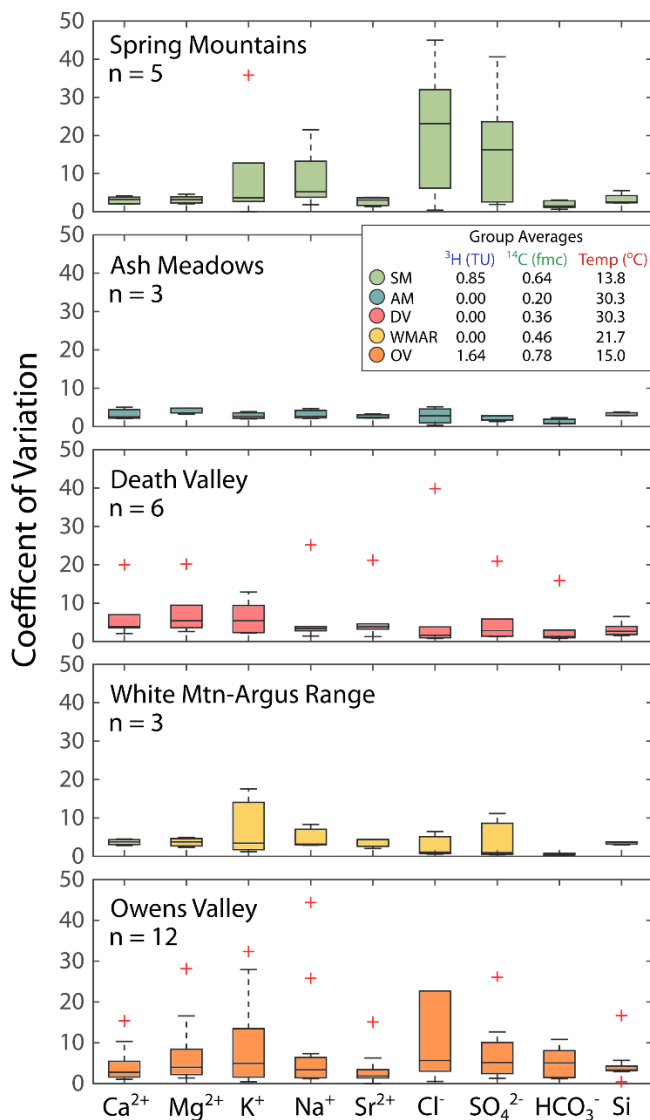


Figure 6.11: Boxplots showing statistical distributions of coefficient of variation for different solutes by study area. For each boxplot, the central line of the box represents the median. The upper and lower extents of the box represent the 75th and 25th percentiles, respectively. Whiskers extending from the upper and lower portions of the box indicate the spread of all data not considered outliers. Outlier samples are shown by the red crosses. The solutes shown on the x-axis are the same variables that were used in the PCA analysis of major ion geochemical variation. The study area and number of samples are described for each boxplot. The inset table shows focus area (group) averages in ³H, ¹⁴C and spring discharge temperature to allow comparison between these key metrics and boxplot spread. Broadly speaking, the most variable regional boxplots correspond to the focus areas with colder waters, shorter residence times, and more local flowpath distributions (i.e., Owens Valley and the Spring Mountains). Major outliers are IES-019 in Death Valley and IES-043 in Owens Valley.

PCA 1 explains 52% of the variance and is largely controlled by B variability. PCA 2 explains 24% of the variance and is largely controlled by Fe variability. Li variability is weakly correlated with PCA 1 and PCA 2, while As and Mo variability are weakly correlated with PCA 1 and weakly anticorrelated with PCA 2. PCA results show that the vast majority of springs (20/26) fall into a zone of minimal variation (i.e., scores less than ± 0.2 on both PCA 1 and PCA 2) that is associated with nominal trace element concentration variability for all included analytes. This zone is similar to, yet slightly larger than, the “minimal variation zone” observed in the major ion PCA analysis. If it were possible to include the trace elements that primarily returned non-detect results in the analysis of trace element variability, the minimal variation zone would likely be even smaller. IES-038 and IES-043, two springs falling outside the zone of minimal variation, have high PCA 1 and PCA 2 scores, respectively. IES-016, IES-019, IES-026, and IES-033 are primarily associated with low (< -0.2) PCA 2 scores, however, IES-033 has a high PCA 1 score that is mainly associated with increased boron variability.

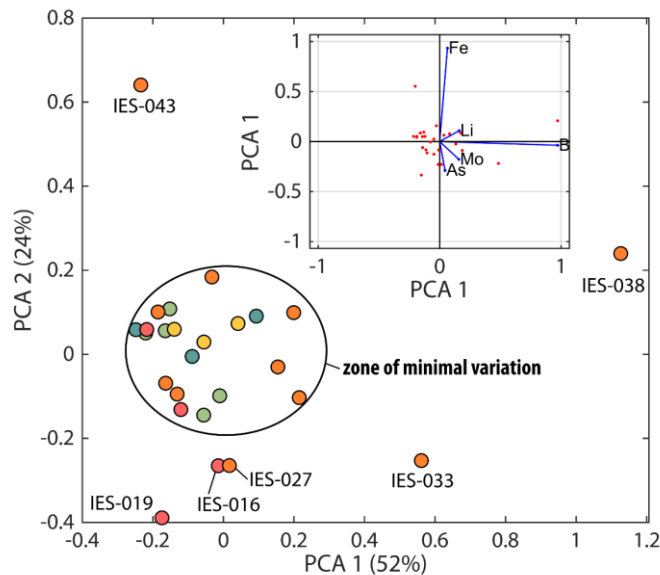


Figure 6.12: Similar to Figure 6.10, this figure is a PCA plot of trace element variability. Springs are symbolized as circles and colored by focus area. An inset biplot shows the vector magnitude of each variable and how PCA space relates to trace metal temporal variation. Because trace element concentrations were below the detection limit for most analytes, only 5 variables (As, B, Fe, Li, Mo) were used to understand which springs exhibit minimal variation, which springs display the most temporal variability, and how changes in trace metal concentration over time are related.

6.4.4 $^{87}\text{Sr}/^{86}\text{Sr}$ variability

6.4.4.1 $^{87}\text{Sr}/^{86}\text{Sr}$ regional framework

In order to understand controls on variability, it is first necessary to provide a regional $^{87}\text{Sr}/^{86}\text{Sr}$ framework. $^{87}\text{Sr}/^{86}\text{Sr}$ compositions of springs are wide ranging (0.70729-0.73373) and cluster by focus area, a reflection of the spatial complexity of the geologic units that are weathered to provide the primary input of strontium into groundwater (Figure 6.13). For the most part, IES springs in the Spring Mountains (e.g., Warix et al., 2020) and Owens Valley (Chapter 4) have $^{87}\text{Sr}/^{86}\text{Sr}$ compositions that reflect the whole rock $^{87}\text{Sr}/^{86}\text{Sr}$ of the host lithology. IES Springs throughout Death Valley, Ash Meadows, the Panamint Range, and in the northwest section of the Spring Mountains tend to have elevated $^{87}\text{Sr}/^{86}\text{Sr}$ relative to expected seawater values. This is attributed to post-depositional addition of radiogenic strontium from fluid circulation through rubidium-rich sections of the regional carbonate aquifer and the underlying passive margin sequence (Paces et al., 2005; Warix et al., 2020) or, in the rare case, interaction with igneous intrusive rocks and metamorphosed plutonic basement rock with elevated $^{87}\text{Sr}/^{86}\text{Sr}$ (Wasserburg et al., 1964; Gleason et al., 2020).

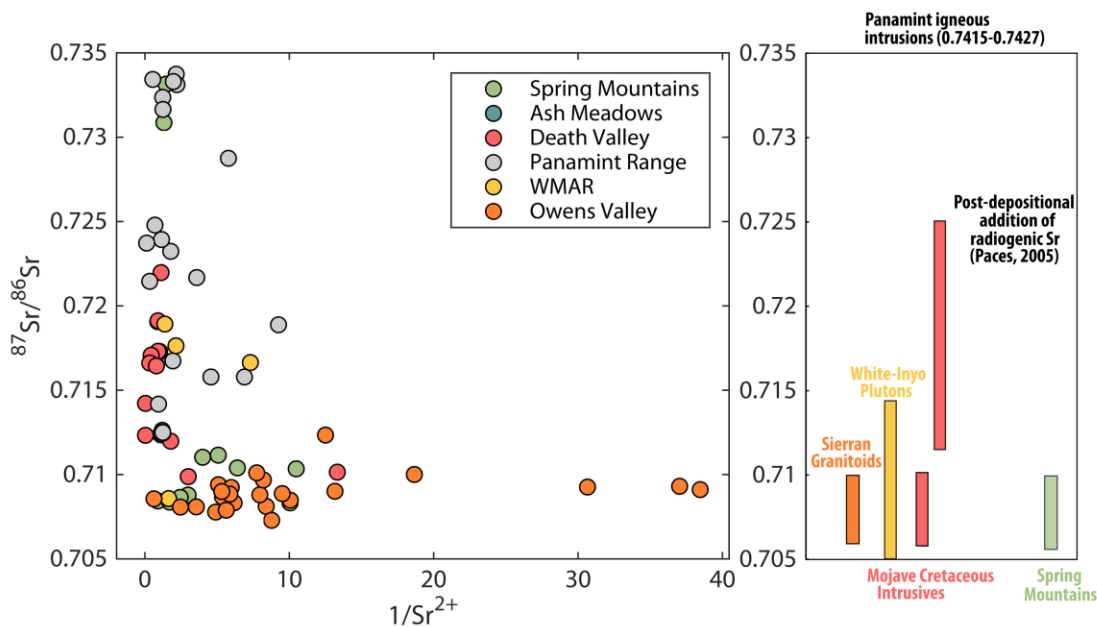


Figure 6.13: Plot showing $^{87}\text{Sr}/^{86}\text{Sr}$ as a function of $1/\text{Sr}^{2+}$. Springs are shaded by focus area. The associated bar chart on the right shows whole-rock ranges for focus areas and geologic units in the region from Wasserburg et al. (1964), Pretti and Stewart (2003), Paces et al., (2007), Hirt (2007), and Chapman (2015).

6.4.4.3 $^{87}\text{Sr}/^{86}\text{Sr}$ variability

Twenty-one springs were analyzed for temporal variations in $^{87}\text{Sr}/^{86}\text{Sr}$. Time series plots of $^{87}\text{Sr}/^{86}\text{Sr}$ composition over the sampling interval are shown in Figure 6.14. Y-axis errors bars show the analytical uncertainty for $^{87}\text{Sr}/^{86}\text{Sr}$ (± 0.00005). Death Valley and WMAR springs are presented in subplot “A”, while Spring Mountain and Owens Valley springs are shown in subplots “B” and “C”. Overall, spring $^{87}\text{Sr}/^{86}\text{Sr}$ compositions are very stable over the sampling period. Similar to the temperature and major ion results, we do not observe systematic changes in $^{87}\text{Sr}/^{86}\text{Sr}$ from drought to post-drought conditions (Figure 6.14).

Only five springs (IES-004, IES-019, IES-026, IES-034, and IES-043) have $^{87}\text{Sr}/^{86}\text{Sr}$ standard deviations greater than the analytical uncertainty of the $^{87}\text{Sr}/^{86}\text{Sr}$ measurement (± 0.00005) (Figure 6.15). Only one spring, IES-043, exhibits deviations in $^{87}\text{Sr}/^{86}\text{Sr}$ that are contemporaneous with increased Sr^{2+} variability. The four other springs with elevated $^{87}\text{Sr}/^{86}\text{Sr}$ variability not associated with increased Sr^{2+} standard deviations may potentially be indicative of changes in flowpath distribution. We do not observe relationships with the $^{87}\text{Sr}/^{86}\text{Sr}$ variability and any other physical, isotopic, or geochemical metrics. Connections between increased $^{87}\text{Sr}/^{86}\text{Sr}$ variability and flowpath distribution variability are further explored in the discussion.

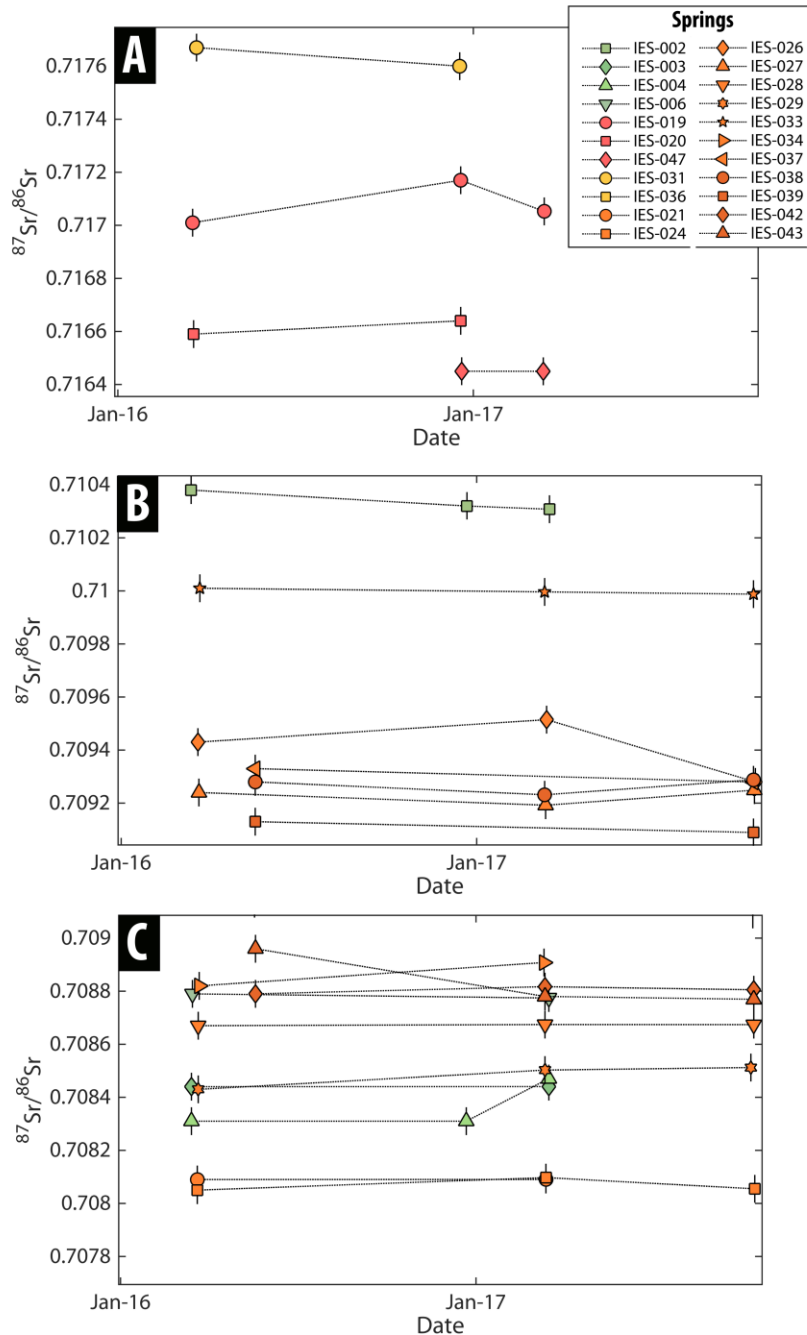


Figure 6.14: Time series plots of $^{87}\text{Sr}/^{86}\text{Sr}$ in spring waters. The results are separated into three panels to maximize the y-axis limits. The measurement uncertainty for $^{87}\text{Sr}/^{86}\text{Sr}$ is 0.00005 and is shown by the y-axis error bars. WMAR and Death Valley springs are shown in subplot “A” while Spring Mountains and Owens Valley springs are shown in subplots “B” and “C”. Overall there is very little temporal variation, however because the measurement uncertainty is minimal, small changes in $^{87}\text{Sr}/^{86}\text{Sr}$ (e.g., IES-004) can provide insight into changes in flowpath distribution.

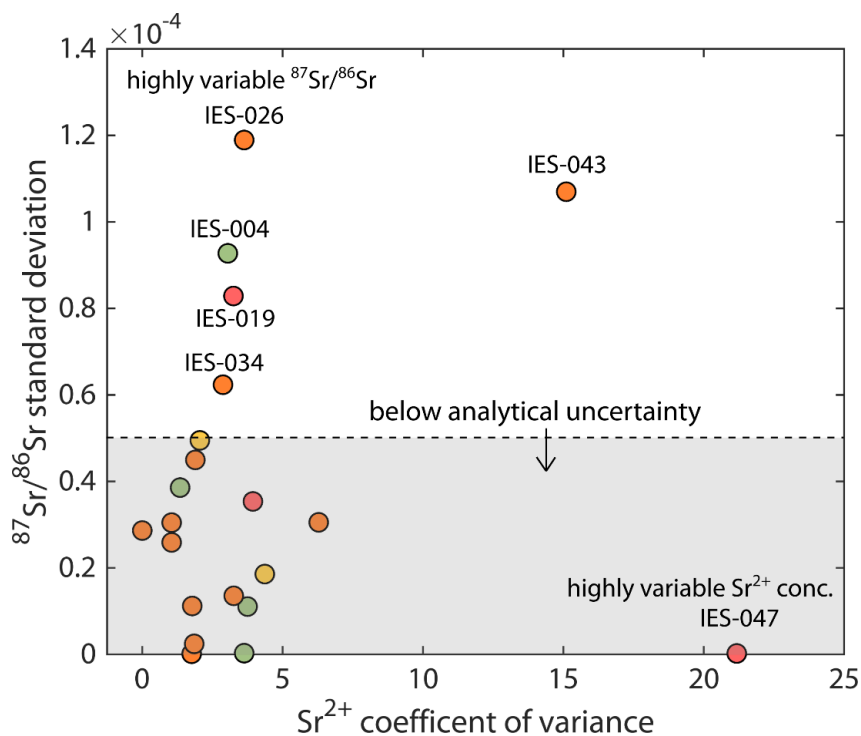


Figure 6.15: Plot showing Sr^{2+} coefficient of variation (%) versus $^{87}\text{Sr}/^{86}\text{Sr}$ standard deviation for spring waters. The majority of spring have $^{87}\text{Sr}/^{86}\text{Sr}$ standard deviations below the analytical uncertainty (grey box). Five springs have $^{87}\text{Sr}/^{86}\text{Sr}$ standard deviations greater than the analytical uncertainty. IES-043 appears to be the only spring where changes in spring $^{87}\text{Sr}/^{86}\text{Sr}$ can potentially be attributed to temporal variations in Sr^{2+} .

6.4.5 Stable isotopes of water ($\delta^2\text{H}$ and $\delta^{18}\text{O}$)

6.4.5.1 Regional framework

A regional dual isotope plot of IES samples is shown in Figure 6.16. One-time IES samples from the Panamint Range and other focus areas are included to assist in establishing the regional framework. Stable isotope samples of spring waters from the southern Great Basin show wide ranges in $\delta^2\text{H}$ and $\delta^{18}\text{O}$ and generally follow the global meteoric water line (Craig, 1961). The dominant regional trend is a general pattern of isotopic enrichment moving eastward from Owens Valley further into the rain shadow of the Sierra Nevada. However, the spread of $\delta^2\text{H}$ and $\delta^{18}\text{O}$ compositions within and amongst the different focus areas can be attributed to a variety of factors. In Chapter 4, we link $\delta^2\text{H}$ and $\delta^{18}\text{O}$ compositions in Owens Valley to spatial location along the mountain front (i.e., easting and northing) (Figure 6.16) and do not find consistent patterns with spring elevation, temperature, or groundwater residence time and isotopic composition. In the

Death Valley and Ash Meadows focus areas, springs at major fault zones discharge groundwater from the regional carbonate aquifer. Our results support prior interpretations that these groundwaters have a distinct isotopic signature ($\sim -15\text{‰} < \delta^{18}\text{O} < -13\text{‰}$) indicative of pluvial recharge from the Pleistocene (Winograd and Friedman, 1972; Winograd and Thordarson, 1976; Davisson et al., 1999; Smith et al., 2002; Belcher et al., 2009) (Figure 6.16B). Our results also support prior assertions that individual mountain ranges throughout the study area (e.g., the Panamint Range and the Spring Mountains) have spatial stable isotopic variations in mountain-block groundwater systems due to elevation-dependent fractionation, recharge type (e.g., snow vs rain), and seasonality in precipitation (e.g., monsoon vs winter precipitation) (Winograd et al., 1998; Gleason et al., 2020; Warix et al; 2020) (Figure 6.16C).

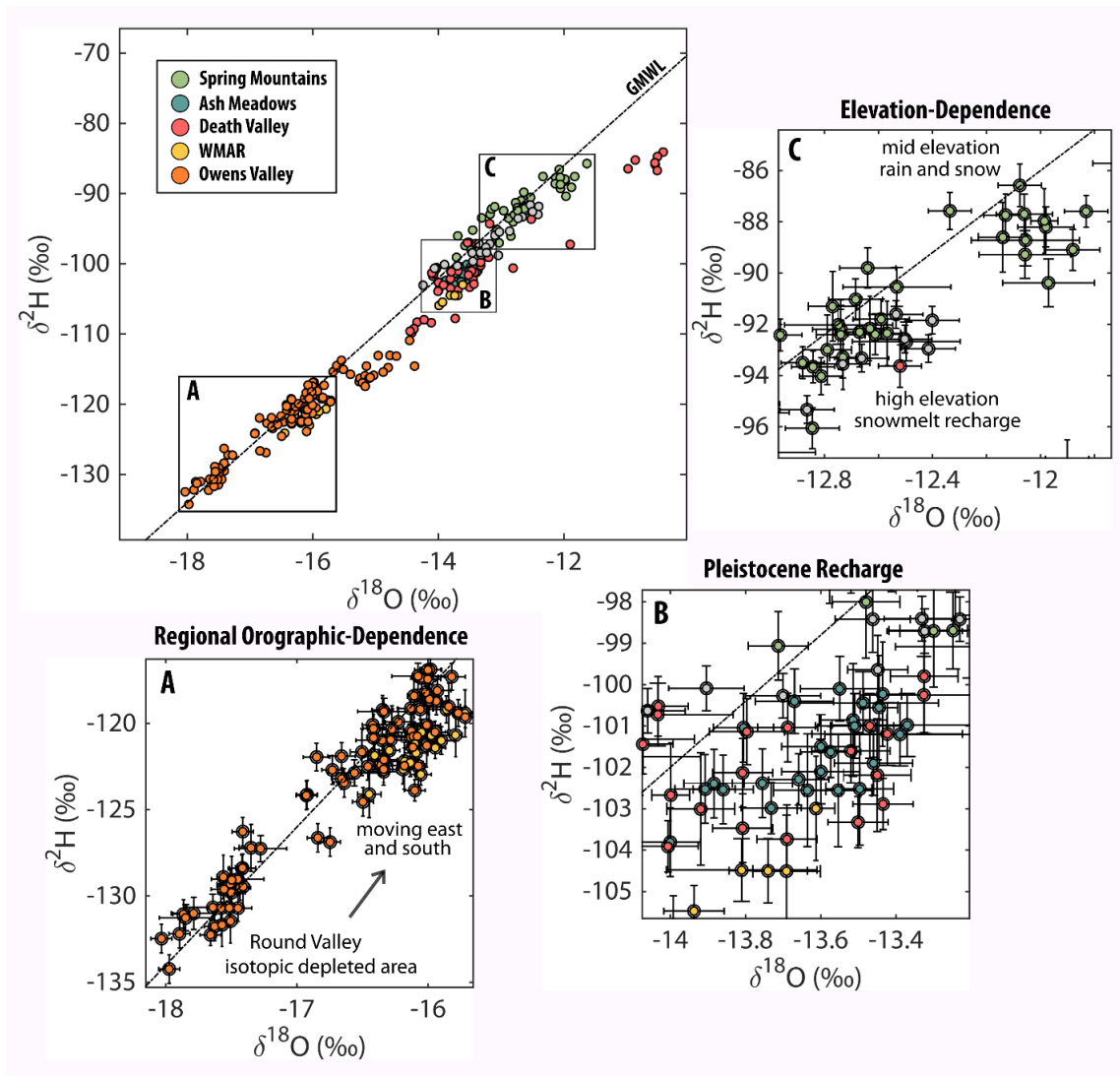


Figure 6.16: A general understanding of the spatial distribution of $\delta^{18}\text{O}$ and $\delta^2\text{H}$ in groundwater and the mechanisms driving $\delta^{18}\text{O}$ and $\delta^2\text{H}$ variation throughout the region is first needed prior to understanding the possible mechanisms for temporal variation. Geographic, climatic, and topographic factors all contribute to variations in $\delta^{18}\text{O}$ and $\delta^2\text{H}$ in groundwater throughout the study area, Geographic factors are seen in subplot “A” where isotopic composition of springs waters in Owens Valley is more closely related to geographic position within the valley (easting or northing) rather than elevation. Specifically, isotopes are highly depleted in the Round Valley area west of Bishop. Moving south and eastward toward the Alabama Hills region, spring water isotopes are more enriched (Chapter 4). Climatic factors driving isotopic variation are shown in subplot “B”. Waters discharging currently at Ash Meadows, Furnace Creek, and the Grapevine Springs complex have a unique isotopic signature reflective of Pleistocene recharge. An example of isotopic fractionation driven by topography and recharge type is shown in subplot “C”. In the Spring Mountains, groundwater that is locally isotopically light or depleted is interpreted to be sourced from cold, snowmelt recharge while springs discharging isotopically heavier water are dependent on lower elevation recharge, more rain, or a monsoonal moisture source.

6.4.5.2 Overall variability and (lack of) correlations

Standard deviation is utilized as a metric to assess stable isotope temporal variability. The standard deviations of $\delta^2\text{H}$ and $\delta^{18}\text{O}$ are examined in 35 IES springs over the sampling interval. Out of the 35 springs incorporated into this analysis, 29 springs were sampled between 5 and 8 times. A $\delta^{18}\text{O}$ - $\delta^2\text{H}$ variability plot with an accompanying correlation matrix is presented in Figure 6.17. When examining all springs, there is a slight correlation between the standard deviation of $\delta^{18}\text{O}$ and the standard deviation of $\delta^2\text{H}$ ($R^2 = 0.17$) (Figure 6.17). All springs but one, IES-054, display $\delta^2\text{H}$ and $\delta^{18}\text{O}$ standard deviations in exceedance of their respective analytical uncertainties (dark grey box). There are 16 springs that fall outside of the zone symbolizing 2x the analytical uncertainty (Light grey box). As shown by the inset correlation matrix, we do not observe any significant correlations with spring standard deviations of $\delta^2\text{H}$ and $\delta^{18}\text{O}$ and physical, geochemical, or isotopic metrics indicative of groundwater flow system stability (i.e., springhead elevation, discharge temperature, or groundwater residence time indicators) (Figure 6.17). There are no discernable patterns with $\delta^2\text{H}$ and $\delta^{18}\text{O}$ and focus area (Figure 6.18).

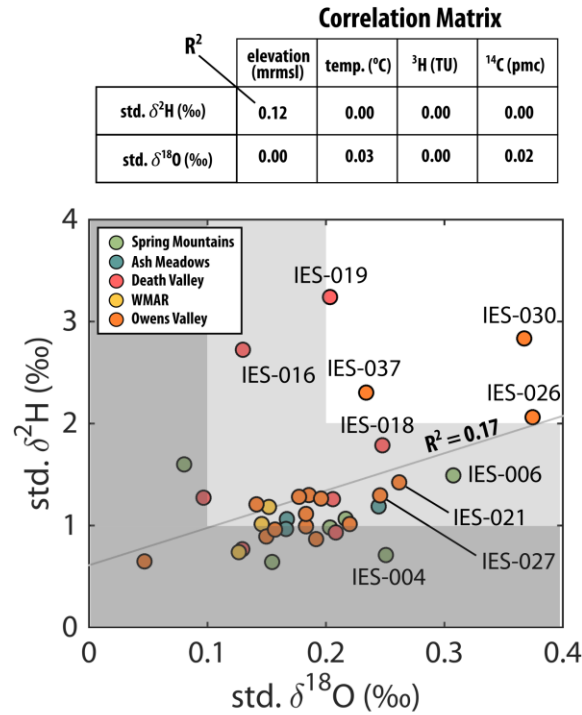


Figure 6.17: Plot and associated correlation matrix showing water isotope variability results. The plot shows the standard deviation of $\delta^{18}\text{O}$ versus the standard deviation of $\delta^2\text{H}$ ($R^2 = 0.17$) for springs sampled more than four times during the sampling period. The darker shaded region represents the average analytical uncertainty for $\delta^{18}\text{O}$ and $\delta^2\text{H}$ from while the lighter shaded region represents 2X the analytical uncertainty. The correlation matrix results show that we do not observe any significant correlations with spring standard deviations of $\delta^2\text{H}$ and $\delta^{18}\text{O}$ and physical, geochemical, or isotopic metrics indicative of groundwater flow system stability (i.e., springhead elevation, discharge temperature, or groundwater residence time indicators).

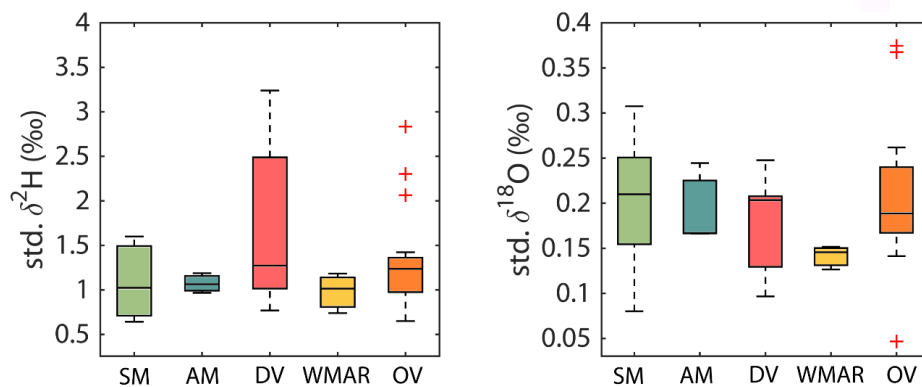


Figure 6.18: Boxplots showing statistical distributions of $\delta^{18}\text{O}$ and $\delta^2\text{H}$ standard deviation separated out by focus area. For each boxplot, the central line of the box represents the median. The upper and lower extents of the box represent the 75th and 25th percentiles, respectively. Whiskers extending from the upper and lower portions of the box indicate the spread of all data not considered outliers. Outlier samples are shown by the red crosses.

6.4.5.3 Temporal water stable isotope variability within Ash Meadows

Almost all the springs in Ash Meadows emerge on an interconnected network of north-striking, high-angle normal faults known as the Gravity Fault system (Figure 6.19; Bushman et al., 2010). Measurements of groundwater discharge temperature and radiocarbon activity from this study support prior hydrogeologic conceptual models that these springs are discharging water from the regional carbonate aquifer. While each spring does have its own unique geochemical signature (e.g., Figures 6.8 & 6.9), the geochemical and strontium isotopic compositions of all but the southernmost springs fall into a relatively narrow range (0.7123-0.7127) (Figure 6.19). The southernmost springs, including Big Spring (IES-014) and Bole Spring have an elevated $^{87}\text{Sr}/^{86}\text{Sr}$ range (0.7170-0.7191) and distinctive geochemical fingerprints compared to the other springs. These springs have previously been interpreted as receiving some proportion of their groundwater flowpath distribution from an alternative source (Thomas et al., 2013), perhaps from the present-day Nevada National Security Site (NNSS). However, the interconnection and compartmentalization of the flow system remains relatively unstudied.

While the Ash Meadows springs exhibit a high degree of geochemical similarity (e.g., Figures 6.8 & 6.9), stable isotope compositions are not unique among springs. The stable isotope results show that over time, the Ash Meadows springs tend to cluster by sampling event rather than by individual spring (Figure 6.20). These results are interesting considering the distance between springs within Ash Meadows (e.g., the distance between the southernmost and northernmost springs in our study is over eight miles). IES-014, which has a distinctive geochemical signature and $^{87}\text{Sr}/^{86}\text{Sr}$ composition, appears to shift in unison with the other Ash Meadows springs (Figure 6.20).

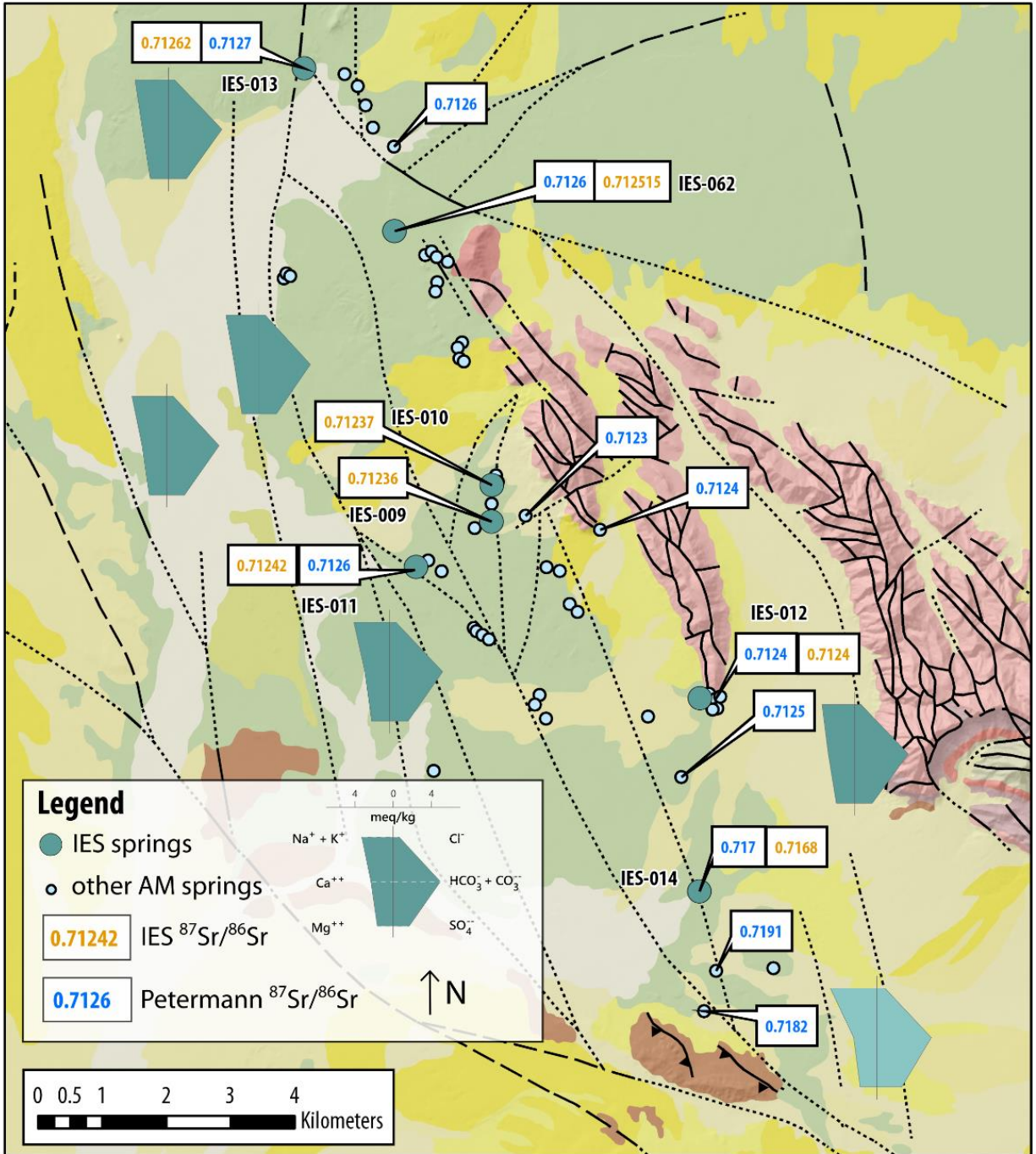


Figure 6.19: Map of the Ash Meadow region showing all known springs in Ash Meadows (small blue circles) and springs sampled as a part of IES sampling efforts (large teal circles). Strontium values from this study and Peterman et al. (1992) are shown in gold and blue callouts, respectively. Fault lines are shown throughout the area, with dotted lines indicating approximate fault location. Stiff diagrams are shown for the IES springs with a corresponding key in the legend. Note the difference in strontium and chemistry between the southernmost three springs, including IES-014, and the rest of the springs.

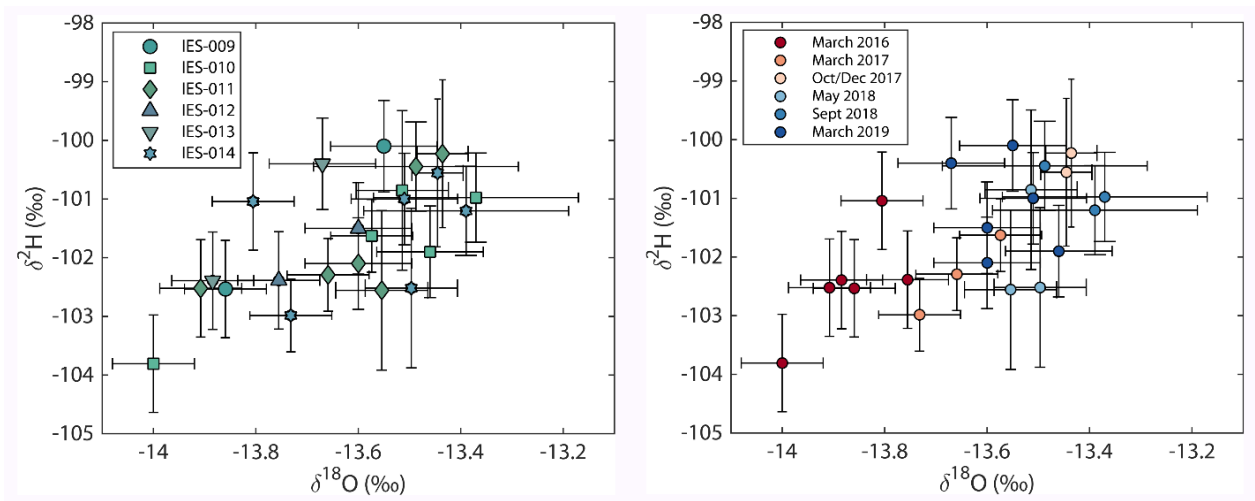


Figure 6.20: Subplots showing temporal stable isotope variation in springs at Ash Meadows National Wildlife Refuge. The figure on the left shows water stable isotope values over time symbolized by shape for each IES spring in Ash Meadows. Error bars represent the analytical uncertainty for each sample. The figure on the right shows water stable isotope values at Ash Meadows over time symbolized by color for each sampling campaign. Rather than cluster by spring (left), stable isotope values in the Ash Meadows flow system appear to cluster by sampling event (right). This finding has potential implications for groundwater movement and connectivity between springs in the Ash Meadows flow system despite the fact that the springs emerge at different faults and there are areas within the flow system that appear to receive flow from varying aquifer sources.

6.4.5.4 Isotopic shifting over time

In contrast to the other physical, geochemical, and isotopic analytes, temporal changes in water stable isotopes far exceed measurement analytical uncertainties. Therefore, we wanted to further examine: 1) whether there are systematic patterns (i.e., seasonal amplitudes or temporal shifts) over the sampling interval and 2) whether these patterns related to drought impacts or stability metrics.

Beginning in March 2016, we observe systematic increases (i.e., isotopic enrichment) in $\delta^2\text{H}$ and $\delta^{18}\text{O}$ for many springs throughout the study area. Examples of this increase are shown in time series plots for springs in the Spring Mountains (left) and northern Owens Valley (right) (Figure 6.21). To quantify this increase, we fit linear regressions to each spring and compare the rates of increase (i.e., slope). Slope is expressed as $\Delta\delta^2\text{H}/\text{day}$ and $\Delta\delta^{18}\text{O}/\text{day}$. The results for this analysis are presented in two stacked histograms, one for both $\delta^2\text{H}$ and $\delta^{18}\text{O}$ (Figure 6.22). The vast majority of springs have positive or nearly neutral slopes. Only three springs, IES-001, IES-

002, and IES-049, display negative $\Delta\delta^2\text{H}/\text{day}$ slopes over the 2016-2019 sampling interval. Both IES-001 and IES-002 have highly variable discharge temperatures and are likely prone to evaporation-related fractionation. The only spring with a negative $\Delta\delta^{18}\text{O}/\text{day}$ slope is IES-049, Mound Spring, an unmodified regional warm spring (38°C) emerging on the Northern Death Valley Fault Zone with a low mean radiocarbon activity (16 PMC). The largest shifts in $\Delta\delta^2\text{H}/\text{day}$ are predominately in Owens Valley springs while the largest shifts in $\Delta\delta^{18}\text{O}/\text{day}$ are found in Spring Mountains springs.

Out of the 35 springs included in temporal analysis of water stable isotopes, 13 springs have been sampled 7 times consistently. A dual isotope plot symbolized by sampling campaign is shown for these springs in Figure 6.23. Associated $\delta^2\text{H}$ and $\delta^{18}\text{O}$ boxplots show statistical changes in these springs over time. The patterns in the plot and corresponding boxplots reflect the same trends seen in the slope histograms; an overall increasing pattern in $\delta^2\text{H}$ and $\delta^{18}\text{O}$ starting in March/May 2016. These patterns are especially apparent in the Spring Mountains and Owens Valley. $\delta^2\text{H}$ compositions show a gradual enrichment over time while $\delta^{18}\text{O}$ compositions show a large shift following the March/May 2016 sampling event followed by minimal increase (Figure 6.23)

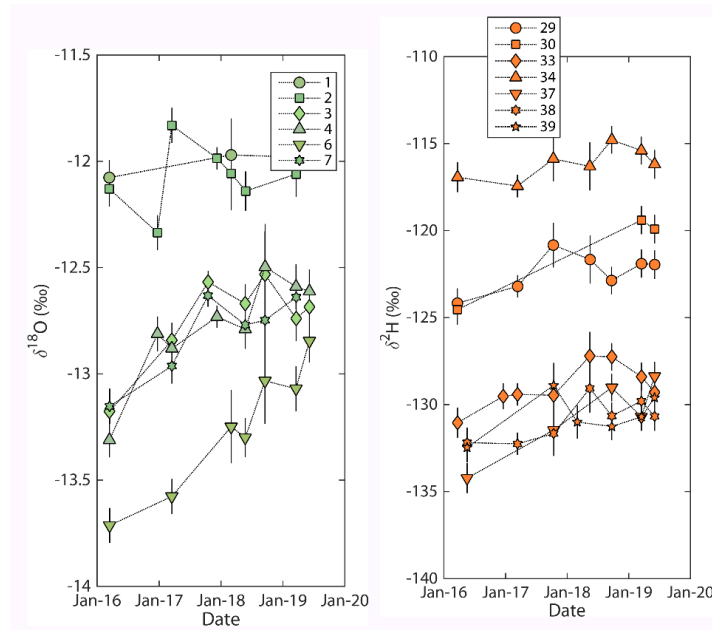


Figure 6.21: Plots showing temporal increases in $\delta^{18}\text{O}$ and $\delta^2\text{H}$ in the study area over the sampling interval (March 2016- June 2019). Springs are symbolized by IES number. Y-axis error bars represent the analytical uncertainty of each sample.

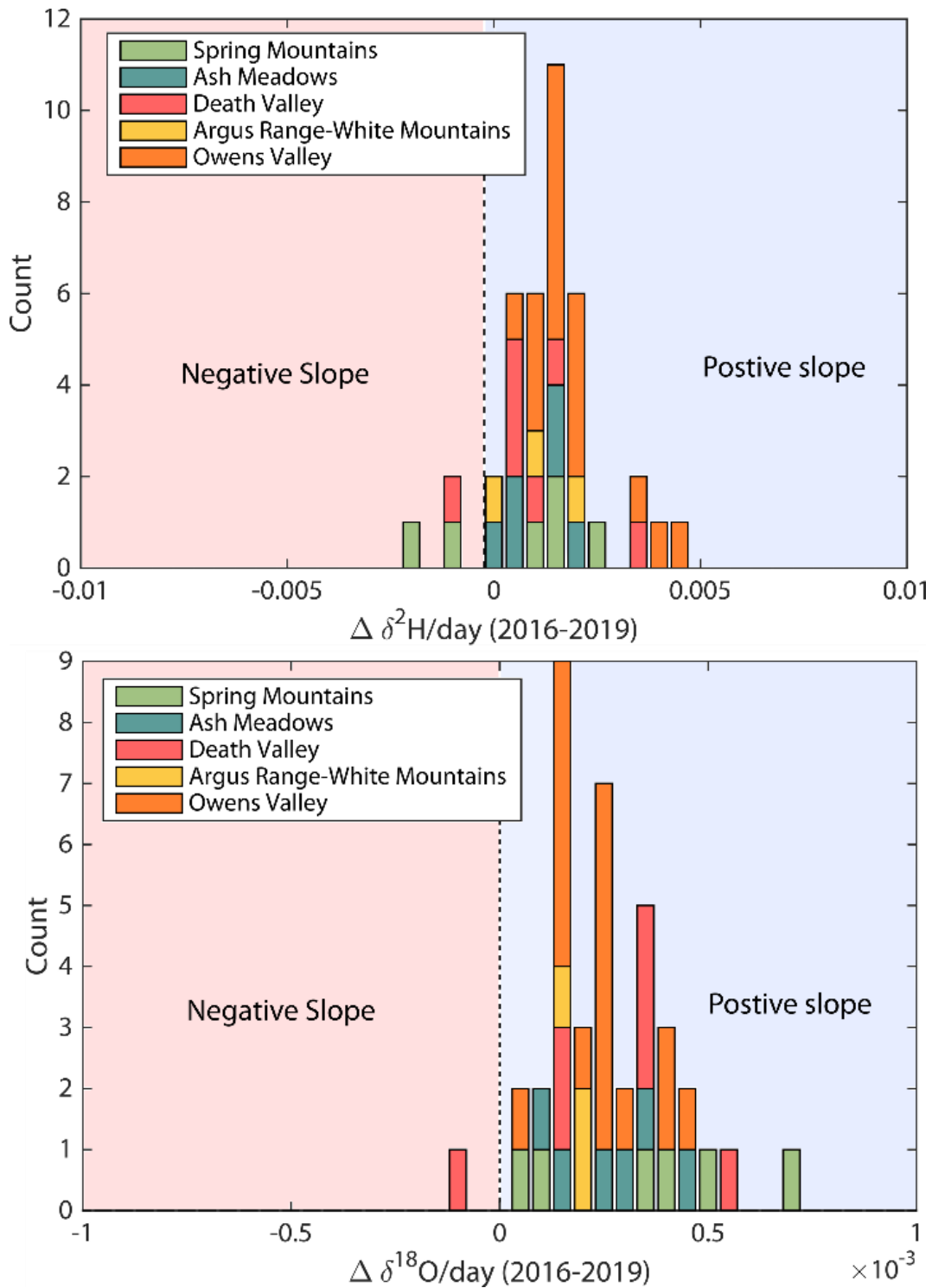


Figure 6.22: Histogram subplots showing counts of the direction and magnitude of the slope fitted to the linear regression of $\delta^{18}\text{O}$ and $\delta^2\text{H}$ over the sampling period. All but three springs had positive $\Delta\delta^2\text{H/day}$ slope over the sampling period (upper plot). All but one spring had a positive $\Delta\delta^{18}\text{O/day}$ slope over the sampling period (lower plot).

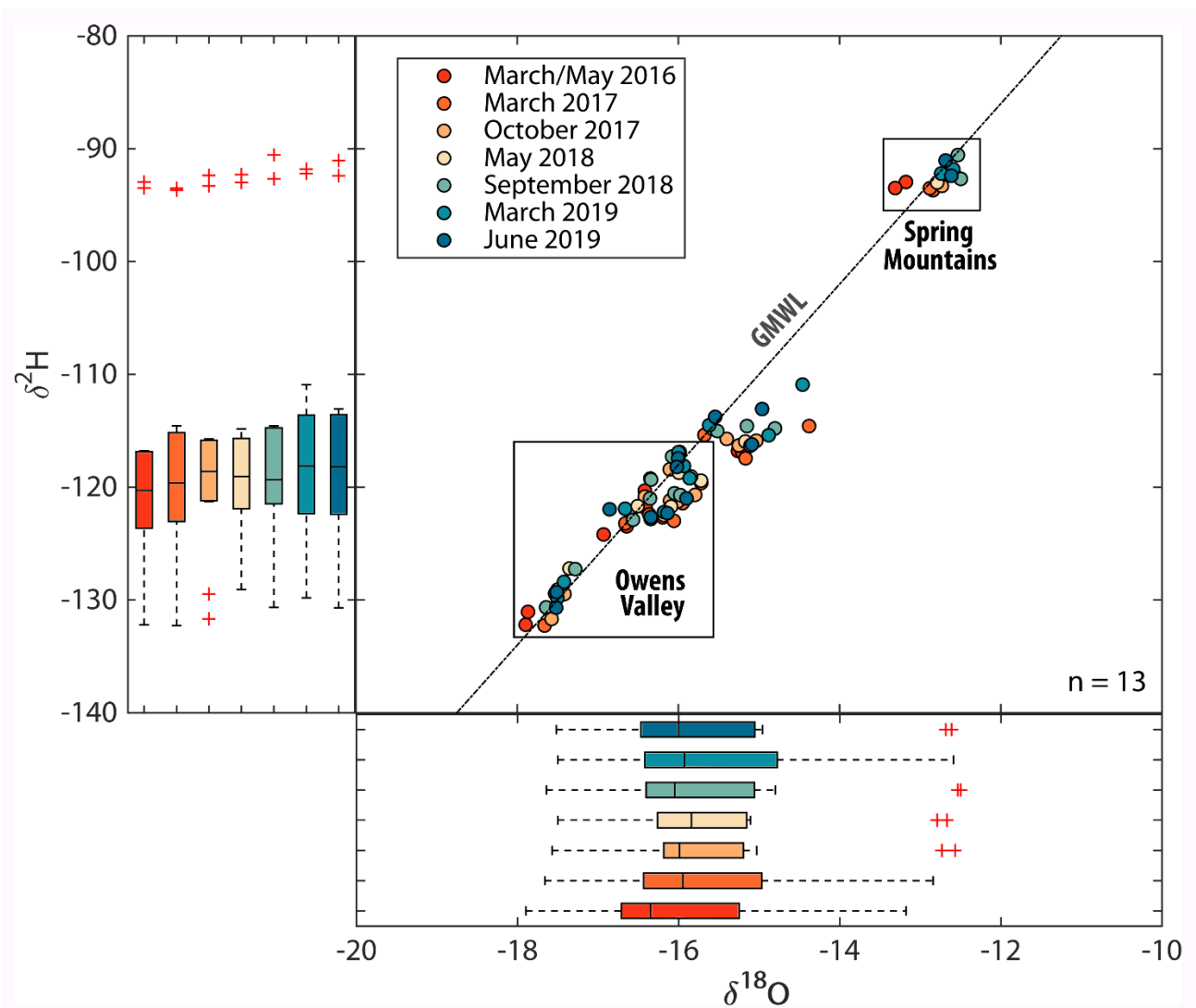


Figure 6.23: Plot of $\delta^{18}\text{O}$ versus $\delta^2\text{H}$ of springs ($n = 13$) that were never missed sampling during seven of the larger field campaigns. Springs are shaded by sampling event. Boxplots on each axis provide a statistical summary of change from the initial March/May 2016 sampling trip until June 2019. Areas of significant change in Owens Valley and the Spring Mountains are annotated on the plot.

6.4.6 Age-dating environmental tracers

In the following sections we compare temporal variability results for different age-dating environmental tracers (^3H , ^{14}C , $^{36}\text{Cl}/\text{Cl}$) for springs sampled up to 4 times. We include temporal $\delta^{13}\text{C}$ results to aid in interpretations of temporal changes in ^{14}C activity. One additional section compares environmental tracer results sampled during drought conditions (March/May 2016) to results sampled during post-drought recovery March 2017.

Variability results for ^3H are presented in Figure 6.24. Overall, temporal variations in ^3H are very low. The average spring ^3H standard deviation is 0.1 TU which is roughly equivalent to the analytical uncertainty range for the samples (0.09-0.11 TU). One spring, IES-034, is a clear outlier sample in the dataset and has a ^3H standard deviation of 0.43 TU. We observe a positive correlation ($R^2 = 0.55$) between average spring ^3H concentration (TU) and ^3H standard deviation (TU) (Figure 6.24A). A similar positive correlation is observed with ^3H standard deviation and ^{14}C activity ($R^2 = 0.23$) (Figure 6.24B). Springs with elevated tritium concentrations ($\text{TU} \geq 2.0$) have an elevated mean ^3H standard deviation (0.23 TU). This is substantially higher than springs that are tritium dead springs ($\text{TU} \leq 0.1$) which have a mean ^3H standard deviation of (0.05 TU). However, several tritium dead springs (e.g., IES-019 & IES-031) have ^3H variations ≥ 0.1 TU during the sampling period, suggesting that fluxes of young water can affect springs that are predominately tritium dead.

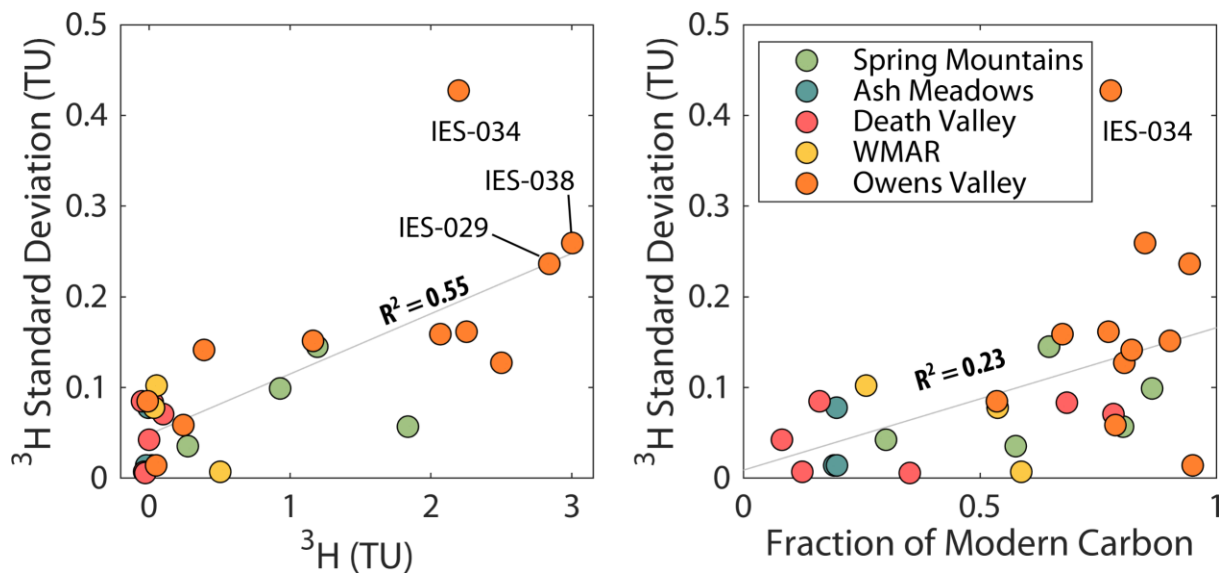


Figure 6.24: Plots showing ^3H standard deviation (TU) versus ^3H (left) and ^{14}C activity (fmc) right. Springs with elevated ^3H and more modern ^{14}C activities have larger ^3H standard deviations even though the analytical uncertainty is within the same range (0.09-0.11 TU) for all samples. One sample, IES-034, is an outlier relative to the rest.

The radiocarbon variability results are presented in Figure 6.25 and are similar to the ^3H variability results. Overall, a large proportion of springs (15/26) have ^{14}C standard deviations that are relatively small (<5% modern carbon). However, springs with high radiocarbon activities and elevated ^3H concentrations tend to have elevated ^{14}C standard deviations (Figure 6.25B). The majority of these springs are in the Owens Valley focus area. Exceptions include three springs in Ash Meadows (IES-010, IES-011, and IES-014) and IES-019, Tule Spring. These springs exhibit relatively large temporal variations in ^{14}C despite having no detectable ^3H .

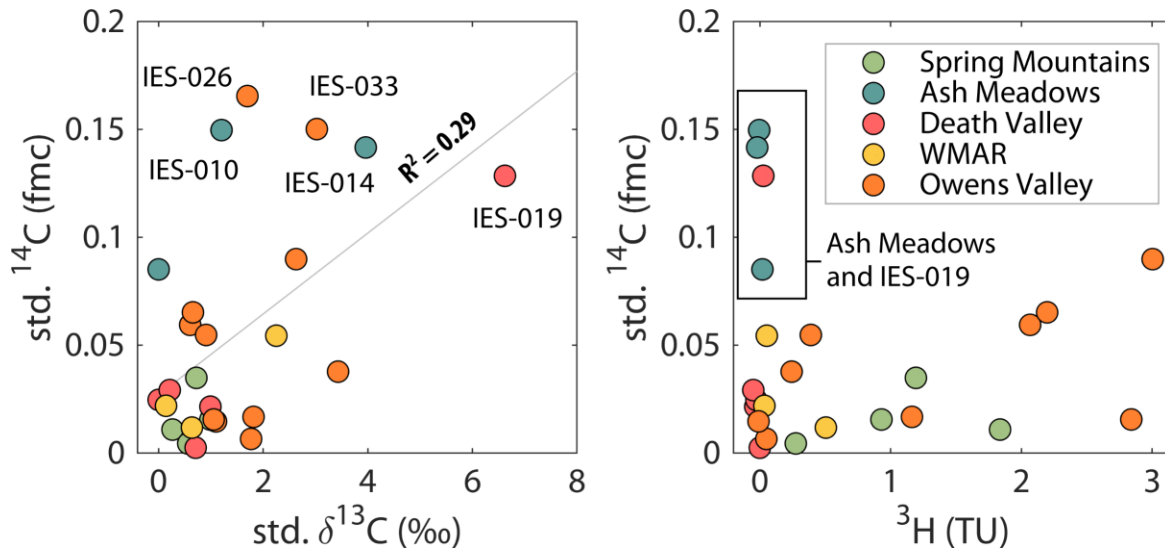


Figure 6.25: Plots showing standard deviation of ^{14}C (fmc) versus standard deviation of $\delta^{13}\text{C}$ (left) and mean tritium concentration (right). Both factors appear to exhibit some control on ^{14}C variability. However, IES-019, IES-010, IES-011, and IES-014 have relatively large standard deviations in ^{14}C (fmc) relative to their nonexistent (dead) tritium concentrations.

Environmental tracer results showing the stability of springs from drought to post-drought conditions are displayed in Figure 6.26. There are very minimal changes in ^3H ($R^2 = 0.98$) and $^{36}\text{Cl}/\text{Cl}$ ($R^2 = 0.99$) from the March/May 2016 to March 2017. The majority of springs fall on 1:1 lines. The correlation coefficient is not as strong when comparing drought and post-drought radiocarbon activities ($R^2 = 0.90$) where a number of springs are significantly shifted from the 1:1 line. The correlation between March 2016 samples and March 2017 samples for $\delta^{13}\text{C}$ is poor ($R^2 = 0.30$) compared to the other environmental tracers.

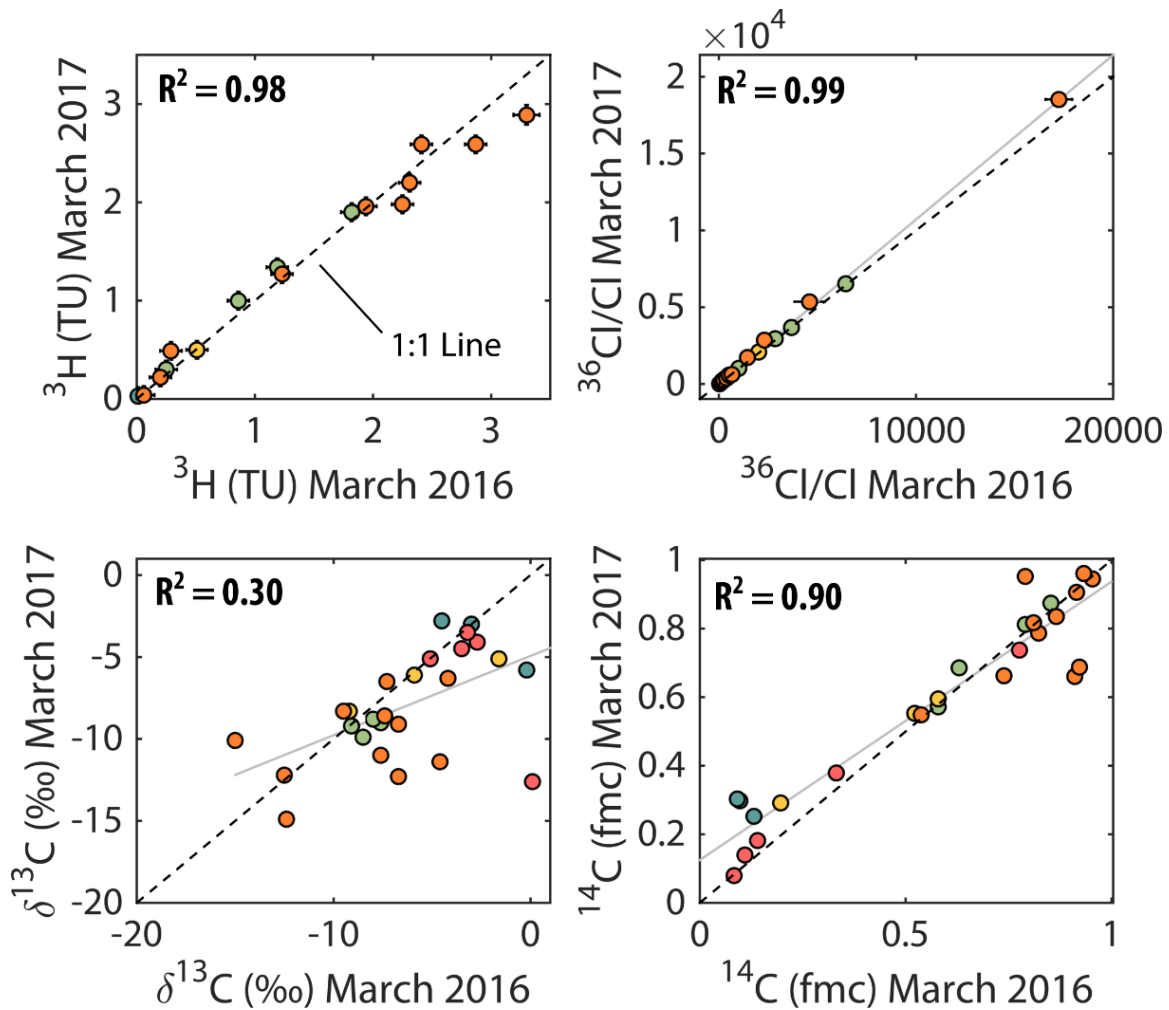


Figure 6.26: Subplot showing temporal comparisons of environmental tracers sampled at springs during March 2016 and March 2017. Regression (solid grey) and 1:1 lines (dashed black) are shown in each subplot. We observe large year to year discrepancies in $\delta^{13}\text{C}$ to compared to smaller variations in the other environmental tracers.

6.4.7 Variability matrix: synthesis of results

A synthesis of the temporal variability metrics examined in this study is presented in Figure 6.27. Springs marked in red for a particular metric are classified as “highly variable” while springs marked in yellow are classified as “moderately variable”. These distinctions are specific to each analyte because we do not observe significant variability in the majority of analytes overall. Springs classified as “highly variable” are typically outliers or exhibit temporal variability far in excess of the analytical uncertainty. Springs marked as “N/A” do not have enough data to meet

eligibility requirements for analysis. Stable isotope results are not included in this variability matrix because almost all samples are either “highly variable” or “moderately variable”. The metrics that we have prioritized as indicators of flowpath variability are shaded in red in Figure 6.27 and include temporal variations in discharge temperature, major ions, and $^{87}\text{Sr}/^{86}\text{Sr}$. The first two columns denote the temporal variability of spring discharge temperature and major ion concentrations. These columns are separate because these two metrics have importance ecologically (Mehler, et al., 2014). Springs associated with highly variable discharge temperatures tend to have either low discharge, specific spheres of emergence, or anthropogenic modifications that promote seasonal and diurnal fluctuations in source temperature (Figure 6.5). Our analysis of major ion variability indicates that focus areas that primarily consist of springs that are tritium dead have much smaller variations in major ion data (Figure 6.10). Except for IES-019, Tule Spring, all springs with increased variability in major ions have ^3H concentrations and $^{36}\text{Cl}/\text{Cl}$ ratios indicative of a substantial proportion of modern or bomb-pulse recharge. Increased major ion variability is the only major connection we find between groundwater residence time and any geochemical variability metric. The trace element variability results reveal a similar conclusion that the majority of springs are stable and exhibit minimal geochemical variations over the sampling interval. However, our results show that trace element variability is largely controlled by small variations in few variables. Therefore, trace element variability is not a reliable indicator of flowpath variability in this study. Variability results from two of the environmental tracers (^3H and ^{14}C) are also shown on the matrix. These results are included for the purposes of explanation but are not prioritized as indicators of flowpath variability because they only exhibit weak correlations across a relatively narrow range of variability (Figure 6.24 and Figure 6.25). Overall, the majority of springs do not exhibit significant variability across multiple metrics. There are several springs (e.g., IES-002, IES-019, IES-021, IES-026, IES-034, IES-036, IES-043) that have many “hits” and exhibit anomalous variability across a suite of metrics. The factors controlling increased variability in these seven springs and the potential implications on spring ecological community structure are discussed at length in the discussion.

Variability Synthesis

Spring	Temp.	Gen. Chem.	$^{87}\text{Sr}/^{86}\text{Sr}$	^3H	^{14}C
IES-001		N/A	N/A	N/A	N/A
IES-002					
IES-003					
IES-004					
IES-006					
IES-007			N/A		N/A
IES-010			N/A		
IES-011			N/A		
IES-014			N/A		
IES-016			N/A		
IES-018			N/A		
IES-019					
IES-020					
IES-021					
IES-024					
IES-026					
IES-027					
IES-028					
IES-029					
IES-030			N/A	N/A	N/A
IES-031					
IES-033					
IES-034					
IES-035			N/A		
IES-036					
IES-038					
IES-039					
IES-042					
IES-043					
IES-045			N/A	N/A	N/A
IES-047					
IES-049			N/A		
IES-054		N/A	N/A	N/A	N/A

 highly variable	 moderately variable
 N/A	not applicable

Figure 6.27: Variability matrix synthesizing the key physical, geochemical and isotopic variability metrics presented in this study. Temperature and major ions variability are separated out as columns because these factors are the most important ecologically. Springs with no color for a given variable do not exhibit significant variability. Springs shaded in yellow are moderately variable while springs shaded in red are highly variable for a given metric. Springs denoted by “N/A” were not included in the analysis for that particular variable.

6.5 Discussion

Temporal variability results from different physical, geochemical, and isotopic metrics illustrate two overarching themes: 1) the vast majority of springs are very stable and exhibit minimal variability across multiple metrics over the sampling interval (Figure 6.27) and 2) the relationship between temporal variability and groundwater residence time is complicated and nonlinear. The temporal variability results for spring discharge temperature, major ions, trace elements, $^{87}\text{Sr}/^{86}\text{Sr}$, and environmental tracer data are best characterized by the few springs that do exhibit changes rather than by the mass of springs showing insignificant changes. The anomalous results from this study, including the stable isotope results and the highly variable springs, are addressed following a discussion of the overall stability.

6.5.1 Overall springs are very stable

The discharge temperature, trace element, $^{87}\text{Sr}/^{86}\text{Sr}$, and environmental tracer temporal variability results indicate that majority of repeat springs in the IES dataset were very stable over the sampling interval. Other than the stable isotopes (*discussed in section 6.5.4*), large differences in variability between springs of different focus areas were only observed in the major ion data. The temporal stability exhibited by the IES dataset is particularly impressive for two reasons: 1) the 2011-2016 California drought was a significant hydrologic perturbation and the driest 6-year period since records began in 1895 and 2) the springs included in this analysis encompass a wide range of topographic positions, geochemical compositions, and groundwater residence times. For these reasons, we expected to see a spread in the variability results between ancient groundwaters (e.g., Ash Meadows) and higher elevation mountain-front springs (e.g., Owens Valley). For the most part, we do not observe a continuum (e.g., Figure 6.1) where increased temporal variability in different physical, geochemical, and isotopic metrics is associated with springs located at higher positions in the landscape with shorter groundwater residence times (e.g., IES-033, IES-038). Conversely, we also do not find that decreased or minimal temporal variability is exclusive to springs that have longer inferred residence times and emerge at lower topographic positions in the landscape (e.g., IES-014, IES-018, IES-049). Apart from the stable isotope results, we do not observe changes, rebounds, or systematic shifts associated with drought conditions or subsequent

drought amelioration. For these reasons we must reject our initial hypothesis, however, we can offer several potential explanations for the results.

Despite the fact that the springs in this study cover substantial ranges in topographic position and groundwater residence time, our temporal analysis does not capture the high elevation “tail” of the spring topographic distribution within the southern Great Basin; springs that emerge at elevations over 2280m (7500 ft). A survey of springs from numerous mountain ranges within Death Valley National Park (DEVA) found a substantial cutoff in the number of perennial springs emerging above the ~2200 m elevation line (Don Sada, *personal communication*) (Figure 6.28). This threshold roughly corresponds to the ecological transition zone between the pinyon-woodland and the alpine-boreal ecotones (Wauer, 1964). Apart from the eastern Sierra, there are few extant perennial extant springs within the southern Great Basin and Owens Valley physiographic provinces that emerge above 2200 m (Figure 6.29). These springs are predominately found in highly incised canyons below major ridgelines in the Spring Mountains, Panamint Range, and White-Inyo Mountains (Figure 6.29). A number of these springs such as Black Canyon Spring (IES-058), Jail Spring (PAN-1), and Peak Spring (IES-052) are included in the broader spring topographic characterization of the study area (Chapter 5), however these springs could not be included in repeat sampling efforts and subsequent temporal analysis because of limited accessibility. Historical time series data for high elevation springs within the study area is limited but suggests that these springs have the potential to be highly variable over short timescales (e.g., Winograd et al., 1998; Shelton et al., 2010). These springs tend to be significantly colder and discharge a much larger proportion of modern recharge. We can infer that these springs are supported by more local flowpath distributions and are more likely to interact with shallow groundwater from seasonal snowmelt. Recent IES sampling efforts discovered that perennial springs at high elevation locations in the Spring Mountains, White Mountains, and Panamint Range that were flowing over 20 years ago are now dry.

One possible interpretation of our results is that a 60-70 year mean residence time is long enough to dampen the immediate geochemical effects of a significant perturbation at intermediate scales (i.e., our “youngest” mountain block springs with a high proportion of bomb-pulse recharge). While these results are somewhat contradictory to the findings of Chapter 3, changes in pressure head travel substantially faster through aquifer systems than changes in geochemistry. Another possible explanation for the relative stability of many physical, geochemical, and isotopic metrics

in response to a major drought is that there is a hydrologic lag associated with the drought that has not been observed during the time span of the study. A lagged response may appear in the coming years and offers a unique opportunity to advocate for the continued monitoring of springs in the region (especially high elevation springs > 2200m).

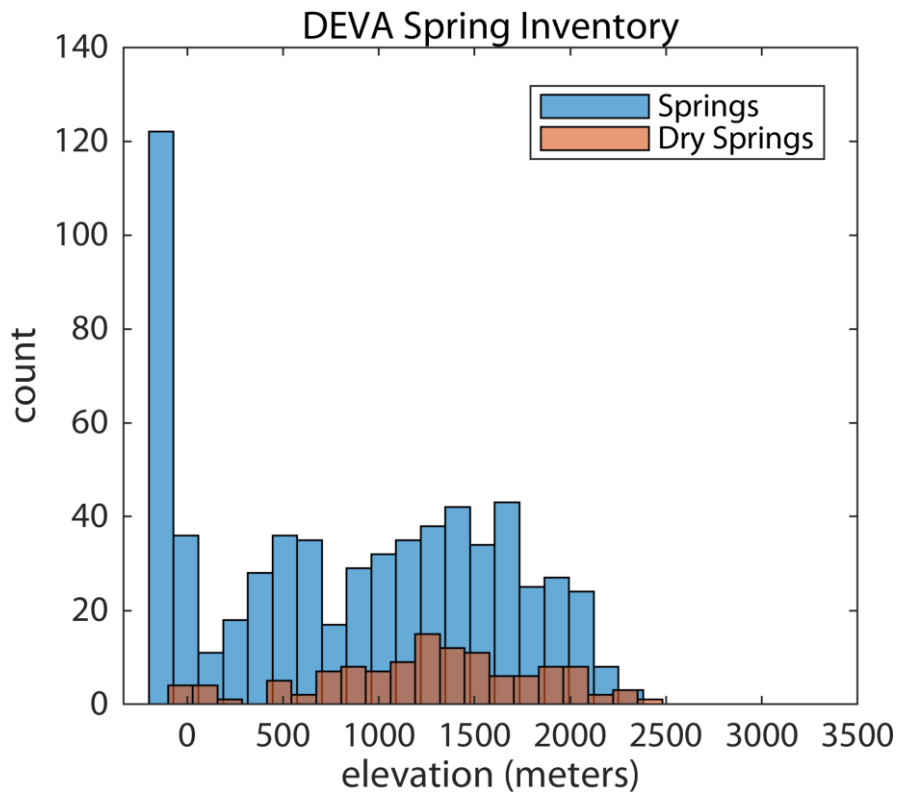


Figure 6.28: Histogram showing the elevation distribution of springs within Death Valley National Park (DEVA). Data is from Don Sada (*personal communication*). There is a sharp cutoff in spring emerge above 2200 meters. The high histogram count for springs below sea level corresponds to a number of springs and seeps that emerge at similar elevations on the valley floor (e.g., the Cottonball Marsh and Badwater spring complexes).

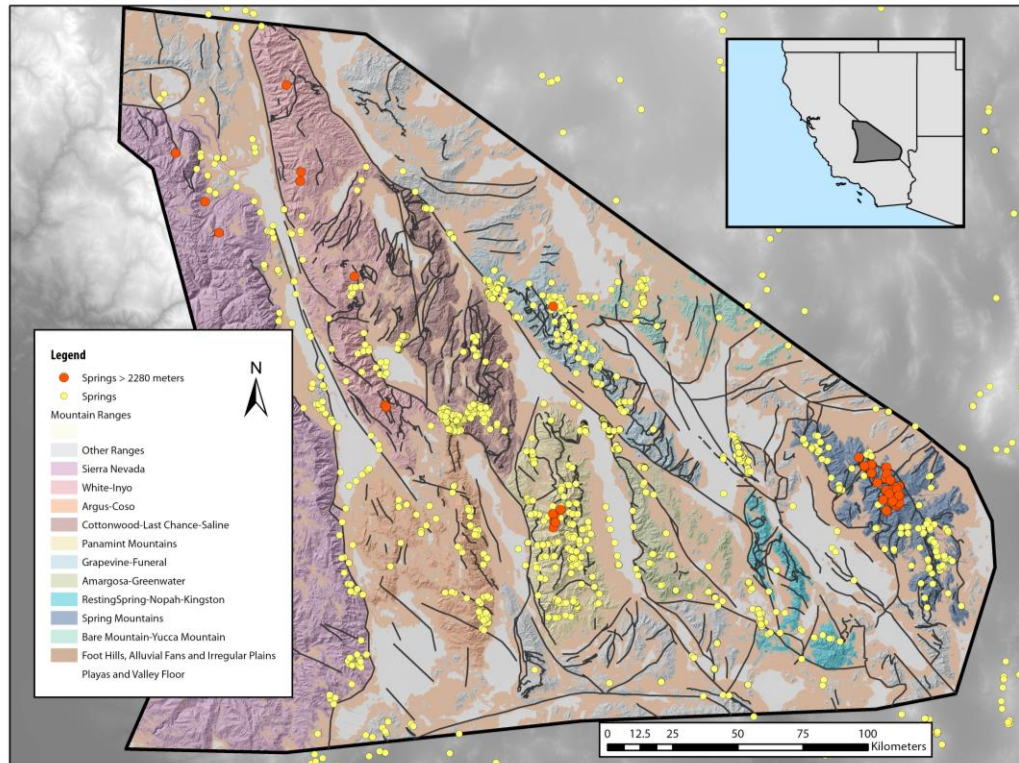


Figure 6.29: Map of the study area showing known locations of springs (yellow circles) on different mountain blocks. There are relatively few high elevation (>2200m) springs in the study area (orange circles).

6.5.2 Springs that show changes across multiple variables

Our results indicate that while the majority of springs are stable and exhibit minimal temporal variations. Springs that are variability outliers tend to be outliers across multiple metrics. There are 7 springs that either have multiple “highly variable” or “moderately variable” marks within the first three columns **or** more than one “highly variable” mark overall (Figure 6.27). These springs include IES-002, IES-004, IES-019, IES-021, IES-026, IES-034, IES-036, and IES-043. While there is not one consistent geochemical thread linking these springs (e.g., short groundwater residence time), increased temporal variability can be linked to two main factors: (1) ecologically unfavorable emergence conditions or (2) variable flowpath distributions.

Ecologically unfavorable surface conditions include low discharge, specific spheres of emergence that promote diurnal fluctuations (e.g. shallow limnocrenes or helocrenes that are diffuse and channelize later), and spring disturbance (e.g., open-barrel spring modification). In a low-discharge state where all other geomorphologic, geologic, climatic, and flow inputs remain

the same, ET is the main driver behind changes in water availability (Warix et al., 2020). ET can affect surface geochemical characteristics (e.g., temperature and chemistry) of normally stable groundwater discharge. IES-002, IES-021, and IES-036 are all examples of springs that have ecologically unfavorable surface conditions that promote increased variability. IES-002, Potosi Spring, is a low discharge seep that channelizes into a large pool with a small outflow channel in southern Spring Mountains (Figure 6.5A). While the primary source of water supporting Potosi Spring may largely consist of bomb pulse recharge based on elevated $^{36}\text{Cl}/\text{Cl}$ (6486) and ^3H (1.83 TU), the spring emerges within a drainage channel and is susceptible to modern contamination from runoff and infiltration within the drainage channel. The low discharge at the spring (~ 1 L/min) makes the spring more vulnerable to evapotranspiration and thus, temporal changes in temperature and major ions. IES-021, Lubken Canyon Spring 1, is a diffuse helocrene emerging on the southern edge of the Alabama Hills in Owens Valley.

The entire Lubken Canyon area is a spring complex that contributes perennial flow to nearby Lubken Creek. IES-021 emerges as a bowl-shaped wetland at the base of a steeply-eroded headcut. This spring has clear evidence of disturbance (i.e., trampling) by local livestock before channelizing downstream. IES-054 a sister spring to IES-021 with a similar geochemical profile, emerges just ~ 0.5 km to the west. However, IES-054 emerges as a rheocrene with a localized, high-quality source that is protected from livestock by *Mimulus* and parsnip. Both springs are tritium dead (0 TU), relatively cold and dilute, and have a similar total outflow (Figure 6.30). Geomorphological differences between the two springs affect the stability of geochemical characteristics at the source region. Similar to IES-002 and IES-021, we attribute the increased variability in geochemical metrics at IES-036, Batchelder Spring, to geomorphic emergence conditions. IES-036 is a gaining rheocrene that emerges over a steep gradient in a canyon separating the White Mountains and Inyo Mountains. IES-036 does not have a discernable spring orifice, but steadily gains over a steep reach.

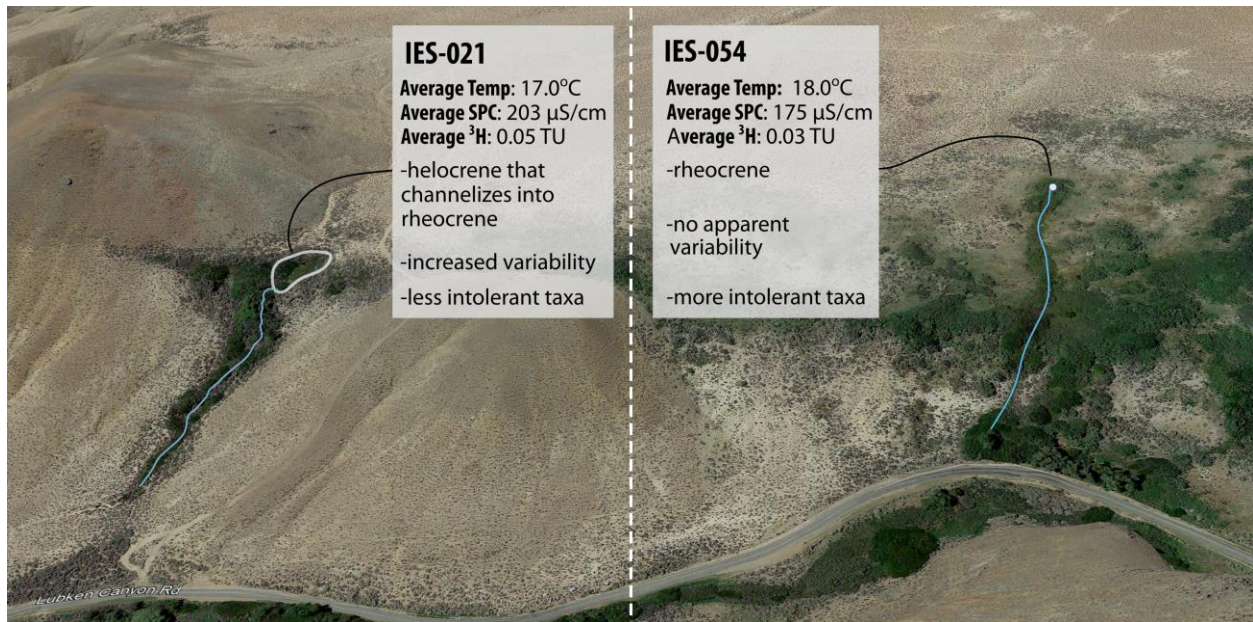


Figure 6.30: Google Earth photo showing IES-021 (Lubken Canyon Spring 1) and IES-054 (Lubken Canyon Spring 2). Photo annotations show that while these springs have similar geochemical profiles, the difference in emergence conditions between the two springs leads to differences in ecological community structure.

The rest of the springs that exhibit increased temporal variability across multiple hydrochemical analytes have this variability attributed to changes in flowpath distributions as opposed to solely geomorphic/surficial conditions. IES-004 and IES-043 both exhibit signs of variable flowpath distributions in addition to unfavorable ecological emergence conditions. Both springs show some of the largest changes in ⁸⁷Sr/⁸⁶Sr. There are several ephemeral springs within close proximity to IES-004 (Ford Spring, Hughes, 1966; West of Kiup Spring; Don Sada, personal communication) that activate during periods of snowmelt. The activation of snowmelt-driven ephemeral springs is indicative of shallow groundwater mobilization. While the increased variability in spring discharge temperature at the source of IES-004 can be attributed to the open barrel spring modification (Figure 6.5A), the increased geochemical variability (⁸⁷Sr/⁸⁶Sr and ³H) can be potentially attributed to shallow groundwater flowpath activation.

Other than IES-019, IES-043, South Harry Birch Spring, is the most geochemically variable spring in terms of exhibiting “flagged” variability across every metric. Along with nearby North Harry Birch Spring (IES-042), IES-043 emerges at a small fault along the Sierra Nevada

Frontal Fault zone. The discharge from IES-043 is not substantial (~0.5 L/s), however the riparian area supported by the springs is significant in extent (~3700 m²). The increased discharge temperature variability can potentially be related to low flow coupled with high ET resulting in decreased discharge and a higher influence of the ambient air temperature on spring reach temperature. However, IES-043 is one of the only springs that exhibited significant changes between drought conditions and post drought amelioration (March 2017) in terms of decreasing ⁸⁷Sr/⁸⁶Sr and increases in most major ions. These changes can potentially be attributed to influxes of recent recharge that mobilized water in storage that was more geochemically evolved. This results in a lower ⁸⁷Sr/⁸⁶Sr associated with increased rock-water interaction (e.g., Chapter 4). The geochemical behavior exhibited by IES-043 starkly contrasts with the geochemical behavior of stable IES-042 over the same time interval.

In Chapter 4, an investigation of the geochemical compositions of Owens Valley springs, our results corroborate the conclusions of prior work that links springflow at IES-026, Reinhackle Spring, to leakage from the Los Angeles Aqueduct. Our work also shows a similar link between IES-034 in Birchim Canyon and subsurface flow through fractured tuff due to losses from the Owens River in the Volcanic Tableland. Both IES-026 and IES-034 incorporate some component of modern surface flow into their flowpath distribution. Evidence for this connection is based on geochemistry, environmental tracers (³H, ³⁶Cl/Cl, $\delta^2\text{H}$ and $\delta^{18}\text{O}$), and physical proximity (Chapter 4). The results of this study indicate that both of these springs exhibit increased variability across multiple geochemical analytes over the sampling interval. We attribute this increased variability to these springs having a large proportion of “modern” recharge as a part of their flowpath distribution and integration of water that recharged from surface-water bodies and then re-emerged at the spring.

IES-019, Tule Spring, emerges at the transition zone between the Hanaupah Canyon alluvial fan and the fine-grained playa sediment of Badwater Basin. Tule Spring represents a mixture of two groundwater sources: 1) mountain front recharge from Hanaupah Canyon and 2) basin brines from Badwater Basin that are mobilized during Amargosa River flooding or mountain-system hydrologic interaction (Gleason et al., 2020). The variable groundwater sources comprising Tule Spring manifest as large variations in mean residence time (< 150 years to 1369 years) (Gleason et al., 2020) and elevated variability across every geochemical metric (Figure 6.27).

The summation of our results suggests that changes in flowpath distributions may manifest as temporal variations in hydrogeological features like springs and seeps that integrate multiple groundwater flowpaths. However, based on the results of this study, changes in flowpath distribution are not necessarily linked to groundwater residence time and are closely tied to groundwater systems susceptible to injections of modern water. Furthermore, our work suggests that springs emerging in certain geomorphic settings (e.g., low discharge, shallow limnocrene, diffuse helocrene) are also more prone to exhibiting temporal variations. Both of these results have implications for conceptual models of spring ecological community structure throughout the southern Great Basin (e.g., Chapter 5).

6.5.3 Ecological significance of highly variable springs

In Chapter 5 we present a conceptual model describing how spring systems are organized, both hydrogeologically and ecologically, within the southern Great Basin. To summarize, the Basin and Range tectonic setting creates a topographic configuration that contains local flow systems, intermediate flow systems (i.e., mountain block and mountain systems), and regional flow systems (e.g., the regional Paleozoic carbonate aquifer). Groundwater residence time, which is partially a function of flowpath length, exerts a primary control on spring geochemical composition (i.e., longer timescales for rock-water interactions to occur) and discharge temperature (i.e., groundwater circulation depth). Springs at higher topographic positions tend to be colder, geochemically dilute, and have shorter groundwater residence times. Springs at lower topographic positions tend to be warmer, geochemically evolved, and have longer groundwater residence times. However, at lower topographic positions there can be large variations in geochemical characteristics based on aquifer type or spring emergence mechanism. Intolerant BMI taxa are more abundant, both from a presence/absence perspective and a population perspective (i.e., abundance), in springs at higher topographic positions associated with less harsh hydrochemical conditions (e.g., elevated temperature and salinity). The inverse is true for tolerant BMI taxa. This coupled hydrogeologic/ecologic framework is the main criteria responsible for structuring spring aquatic communities in the southern Great Basin.

The results of our analysis indicate that two types of springs within our study are potentially the most susceptible to exhibiting increased temporal geochemical variability: 1) springs that have low discharge or a sphere of discharge that is susceptible to surface conditions or 2) springs that

have variable flowpath distributions. In our study, variable flowpath distributions are primarily caused by additions of modern water that either have a dilution effect or mobilize “older” water that is geochemically more evolved due to a longer contact time with mineral surfaces. In Figures 6.31 and 6.32 we present two organized matrices showing the link between geochemical data, BMI community structure, and the variability results from this study. Many springs mentioned in this study are not included in the ecological matrices (e.g., IES-002), because they do not meet the conditions required for BMI sampling. Each spring is represented as a box and is assigned to a position in the matrices based on taxonomic presence/absence metrics (Figure 6.31) or community tolerance composition metrics (Figure 6.32). The geochemical profile of each spring (i.e., temperature, specific conductance, residence time) is designated by the three colored panels in the upper right-hand corner. In line with the conceptual framework that is summarized above, BMI community structure, both in terms of taxonomic presence/absence and abundance, is primarily a function of spring discharge temperature and groundwater salinity. Intolerant taxa are predominantly associated with cold, dilute springs found at mid to high elevations in Owens Valley and the Spring Mountains. Tolerant taxa are associated with regional springs (e.g., springs in Ash Meadows and those that emerge on the Death Valley Fault Zone) and springs emerging from basinal alluvial aquifers. In these two matrices, springs that are classified as “highly variable” based on the results from this study (i.e., Figure 6.27) are labeled in red instead of black. For the most part, these flagged springs have a smaller proportion of intolerant taxa, or alternatively, a larger proportion of tolerant taxa, than what would be predicted by the geochemical profile of a spring alone. The pairs of twin springs (e.g., IES-042 & IES-043 and IES-021 & IES-054) are good examples of springs that have similar geochemical profiles but disparate ecological tolerance metrics. This “shift” towards a larger proportion of tolerant taxa or an increased community tolerance value can be explained by the increased harsh conditions that increased geochemical variability creates for spring ecological communities. For example, IES-019 has large temperature and geochemical fluctuations on top of already having harsh conditions (mid to high temperature and high salinity). This variability potentially exacerbates the already intolerant conditions at IES-019.

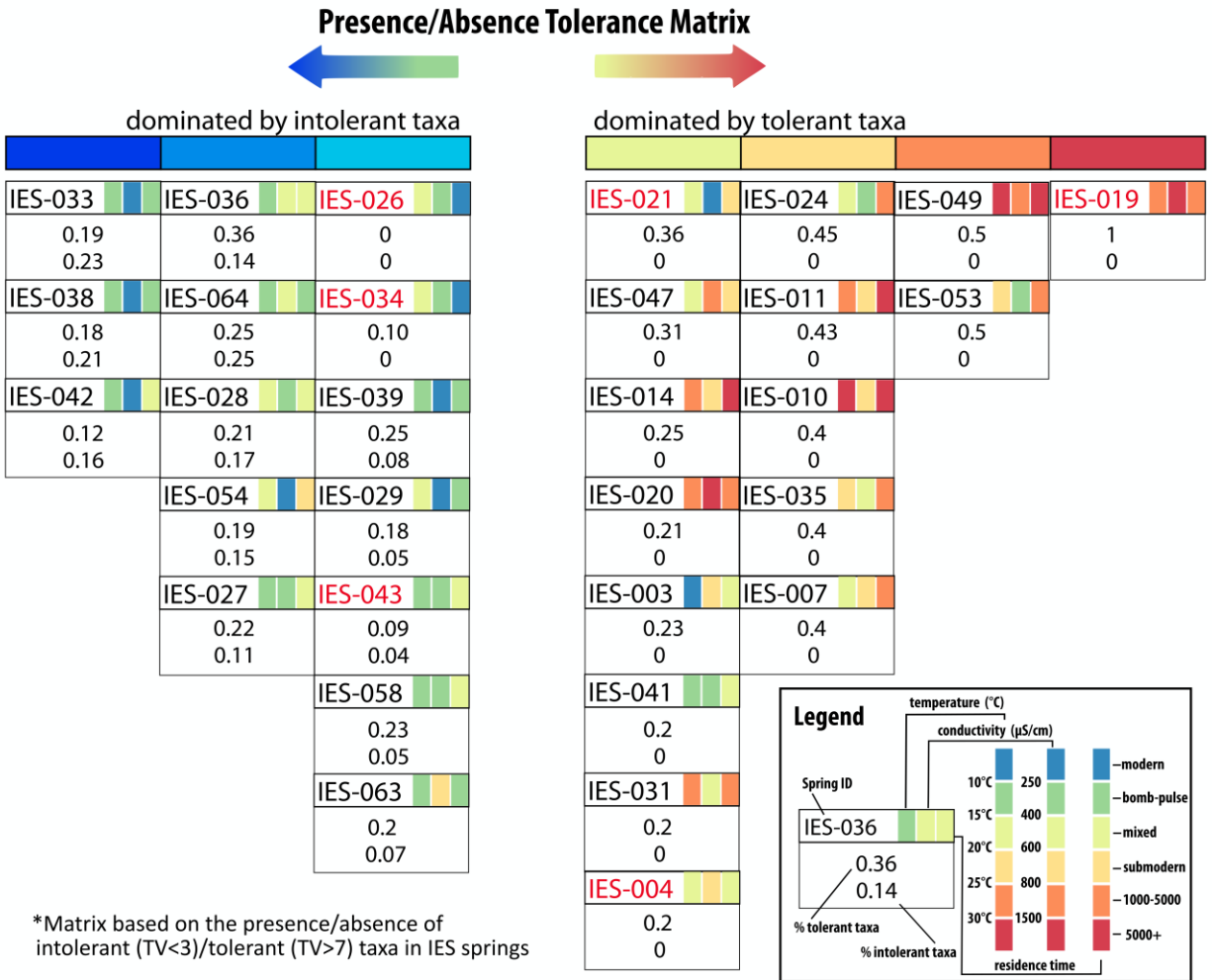


Figure 6.31: A tolerance matrix based on the presence/absence of intolerant and tolerant taxa in IES springs (i.e., the numbers in this figure are reflective of presence/absence and not population statistics of the sample). Springs on the left side of the matrix (dark blue) are dominated by intolerant taxa while springs on the right side of the matrix are dominated by tolerant taxa (dark red). Each spring sample is represented by a “box”. Springs can be identified by the spring ID in the upper left-hand portion of the box. In the lower portion of the box there are two numbers. The top number represents the % tolerant taxa as a decimal and the bottom number represents the % intolerant taxa in a sample as a decimal. Intolerant taxa have a TV < 3 and tolerant taxa have a TV > 7. The three colored rectangles in the upper right-hand portion of the box represent spring

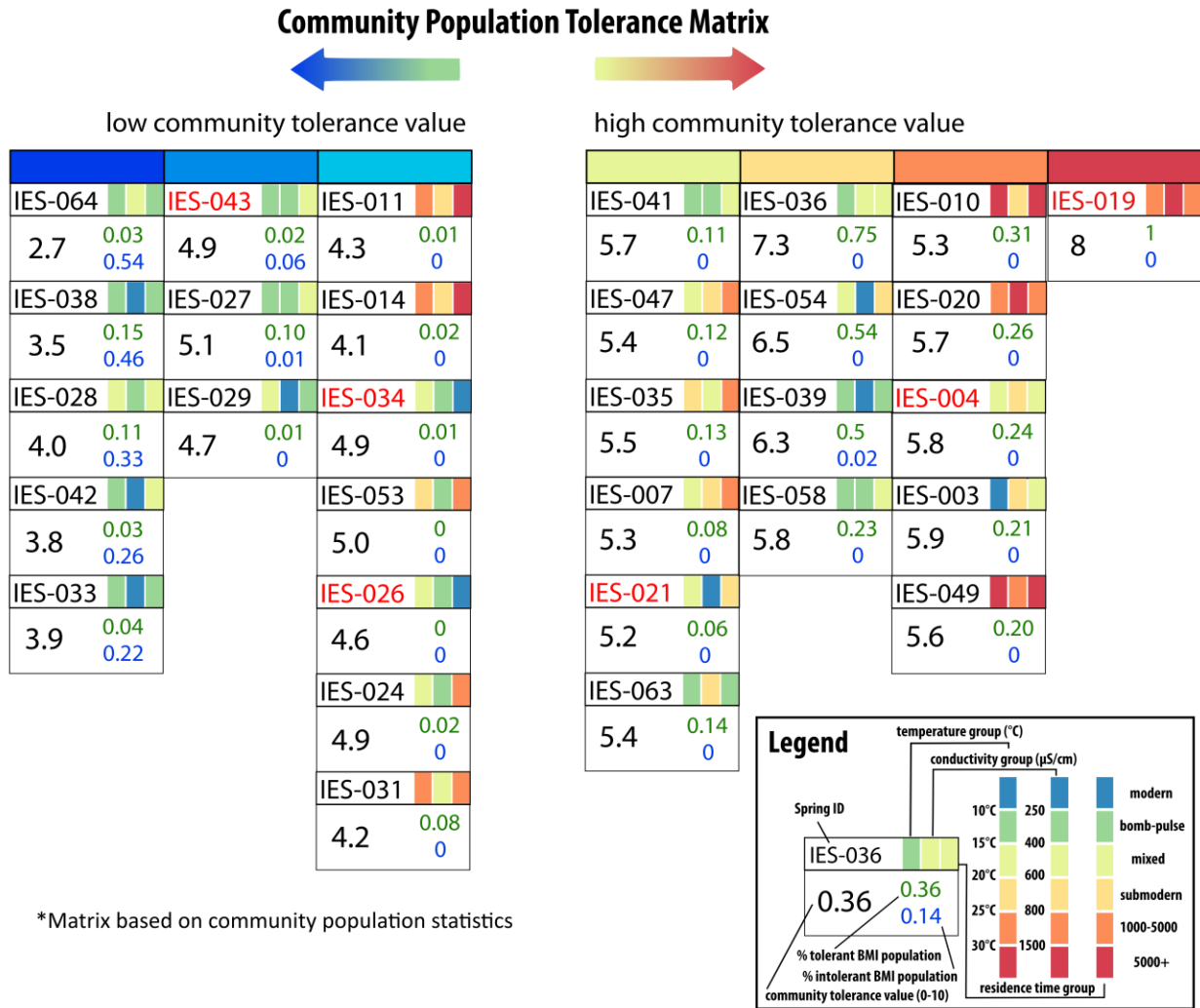


Figure 6.32: A tolerance matrix based on the community population statistics in IES springs. Springs on the left-hand side of the matrix have a low community tolerance value. Community tolerance values increase moving to the right. Springs can be identified by the spring ID in the upper left-hand portion of the box. In the lower portion of the box there are three numbers. The large black number on the left represents the community tolerance value (0-1). The green number on the right represents the percentage of tolerant (TV>7) population of a sample expressed as a fraction. The blue number on the right represents the percentage of tolerant (TV<3) population of a sample expressed as a fraction. The three colored rectangles in the upper right-hand portion of the box represent spring geochemical characteristics as described in Figure 6.32.

Our results provide support that geochemical variability exerts a secondary control on BMI ecological community structure. While at shorter timescales geochemical variability is correlated to groundwater residence time, our results show that at longer timescales, this variability can be attributed to geomorphological surface conditions or variable flowpath distributions. The influence

of surface conditions (i.e., spring geomorphology) in addition to variable flowpath distributions on ecological community structure emphasizes an important point; ecological resistance is related to but separate from hydrogeological resistance.

6.5.4 Stable isotope variability: response to a drought, long-term shifting, or other?

The stable isotope results from this study exhibit the most temporal variability compared to all other metrics. For the majority of springs, the temporal variability of both $\delta^2\text{H}$ and $\delta^{18}\text{O}$ is well in excess of the analytical uncertainty. Most springs also exhibit systematic shifting in the form of increasing (less negative) $\delta^2\text{H}$ and $\delta^{18}\text{O}$ over the sampling interval. However, stable isotope variability (i.e., standard deviation) and the magnitude of shift (i.e., slope) do not have strong correlations with any geochemical metrics that relate to our conceptual model of how spring systems in the southern Great Basin are structured (e.g., elevation, temperature, specific conductance, groundwater residence time, etc.).

Apart from IES-001 and IES-002, Spring Mountain springs show dramatic shifts in both isotopes, specifically $\delta^2\text{H}$, over the sampling interval (Figure 6.21 & Figure 6.22). When comparing these shifts to historical data from Don Sada (*personal communication*), Anderson (2002), Hershey (1989), and the USGS National Water Information System (NWIS) (<https://waterdata.usgs.gov/nwis/qw>), we find that SM isotopic compositions were significantly enriched at the beginning of the sampling interval. The enrichment that we have captured during recent sampling efforts appears to show the spring isotopic compositions moving back towards, rather than away from, historical norms (Figure 6.33).

Similar to the Spring Mountain springs, springs in Owens Valley also experience increased variability and dramatic shifts in both isotopes over the sampling interval. Unfortunately, historical data for springs in Owens Valley is very limited and only three springs can be compared to historical baselines. IES-026, IES-027, and IES-028, were sampled in 2002 as part of an Inyo/LA Geochemical Cooperative Study. Temporal comparisons with these results are presented in Figure 6.34 and indicate that there have been dramatic shifts over the last 15 years in two of the three springs. The limited data that we have indicates that several of these springs are showing potential long-term shifts related to climate change.

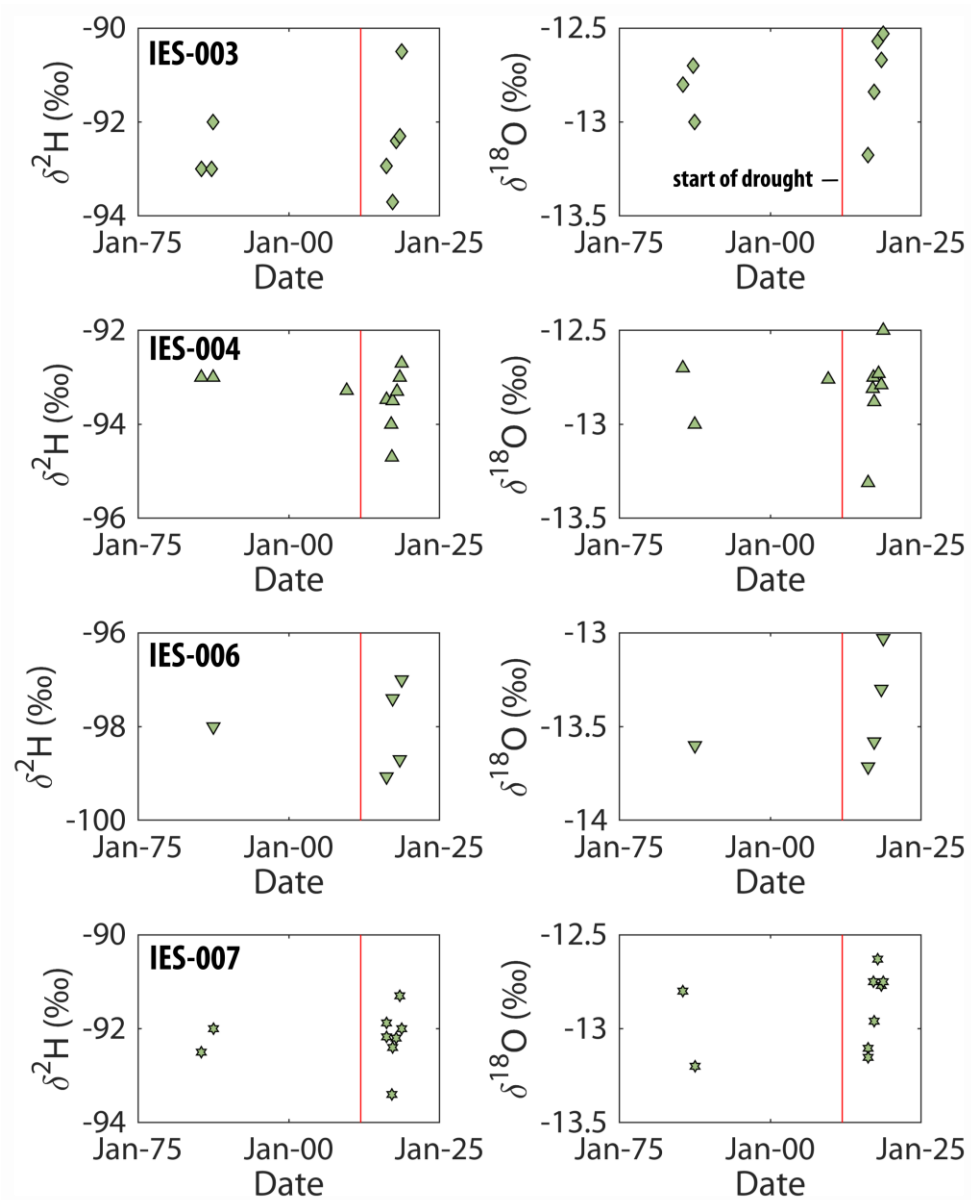


Figure 6.33: Plots showing historical and recent stable isotope data for springs in the Spring Mountains. The red line on each plot marks the start of the 2011-2017 California drought. Our results show that Spring Mountain springs were highly depleted at the end of the drought but quickly shifted isotopically following drought amelioration back to historical baselines.

Examining water isotope variability in the Death Valley and Ash Meadows focus areas is very complicated. Groundwater pumping in the central Amargosa Desert and Pahrump Valley has lead to significant changes in the Ash Meadows and Alkali-Flat-Furnace Creek Ranch groundwater basins. If not for groundwater extraction, groundwater levels would have naturally risen about 1 foot between 1972-2018 instead of declining by 2.4ft (Halford and Jackson, 2020).

Therefore, because of external influences, it is hard to quantify the factors leading to the increased isotopic variability and systematic shifting within Ash Meadows (i.e., Figure 6.20) even though our results may be a novel finding. The two springs in our analysis from Furnace Creek, IES-016 (Travertine Spring) and IES-018 (Nevares Spring), both exhibit large isotopic fluctuations (i.e. Figure 6.20). However, these springs are highly modified and emerge from large collection galleries, potentially exacerbating isotopic fluctuations from ET. IES-020, Saratoga Spring, also exhibited isotopic shifts over the sampling interval. Saratoga Spring, based on electric resistivity and magnetic surveys, is believed to integrate water from the regional Paleozoic aquifer with nearby transmission losses from the Amargosa River (Wamalwa et al., 2011). A hydrograph from the USGS for the Amargosa River at Tecopa, CA shows a significant increase in gage height since mid-2015, just before the start of IES sampling.

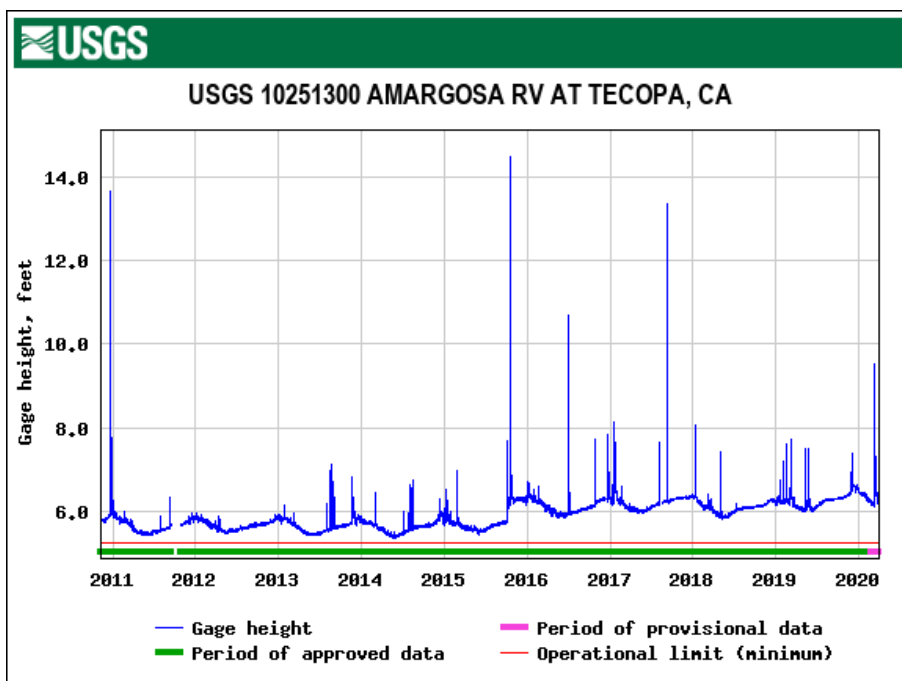


Figure 6.34: Hydrograph from the USGS showing the gage height of the Amargosa River from 2011 to early 2020.

In summary, even though we observe systematic isotopic shifts throughout the study region, these shifts are likely due to a variety of sources and cannot be solely attributed to any one factor (i.e., climate change). Isotopic variations in Owens Valley and in the Spring Mountains appear most likely to reflect changes in aquifer recharge or flowpath distributions.

6.6 Conclusions

The motivation for this study was to understand if there is a variability continuum where geochemical signals at springs are dampened in proportion to groundwater residence time. This work is novel as it focuses on 33 springs across a broad topographic and residence time gradient within the southern Great Basin that were repeatedly sampled from 2016-2019 for a suite of geochemical and isotopic tracers. This sampling interval encompassed the end and subsequent rapid surface water recovery of a historic regional drought, a potential golden interval to witness geochemical variations in vulnerable springs.

The primary finding of this study is that the majority of springs (26/33), which capture a wide range in mean groundwater residence time from 60 years to 20k years, are very stable and do not exhibit significant variations over the sampling interval across a variety of geochemical metrics (e.g., temperature, major ions, trace elements, $^{87}\text{Sr}/^{86}\text{Sr}$, etc.). This result is significant and suggests that these springs are well-buffered to the immediate effects of climate change. One possible interpretation of this result is that a 60-70 year mean residence time may provide sufficient buffering from geochemical impacts caused by a significant climate perturbation. An alternative interpretation is that the hydrologic signal from this major drought is lagged and is still propagating through intermediate and regional scale flowpath systems. Based on the majority of results and lack of significant correlations in this study relating variability metrics to groundwater residence time, I can neither reject nor accept the hypothesis that there is a continuum past shallow groundwater where decreased temporal variability of groundwater metrics is correlated with increased groundwater residence time.

While the majority of springs are stable, the springs that exhibit increased temporal variability in two or more key factors are either associated with either (1) spring emergence conditions where geochemical conditions are affected by evapotranspiration or (2) variable flowpath distributions. Ecologically unfavorable surface conditions include low discharge, specific spheres of discharge, and spring disturbance. In our study, springs with variable flowpath distributions are primarily related to injections of modern water that either has a dilution or mobilizing effect. Increased temporal variability, whether caused by surficial conditions or changes in flowpath distribution, has an impact on ecological community composition. Springs that have increased geochemical variability tend to have more tolerant ecological communities than what we would expect based solely on the spring geochemical profile. The springs that exhibit

increased geochemical variability due to conditions at the surface that are not directly connected to the hydrogeology are a clear example of where potential spring hydrogeological resistance is decoupled from spring ecological resistance.

Historical observations paired with the results from recent sampling efforts suggest one potential path forward- a focus on high elevation (>2200 m), local-scale springs that are not well represented in this study. A focus on these springs would help to determine at what flowpath length geochemical variability attenuates past the point of correlation with groundwater residence time. High elevation springs have the potential to be the “canaries in the coal mine” (Springer, 2015) of elevation-dependent hydrologic systems being further aridified by climate change. These are the springs that are likely to be affected (i.e., desiccate or exhibit geochemical changes) first and may function as the “alarm bells” of a mountain-block or physiographic region signaling hydrologic stress. However, alarm bells have already started going off as dry springs have been reported at high elevations in the Spring Mountains, Panamint Range, and White Mountains during recent sampling efforts.

While the results of this study are significant, another major contribution of this work is the creation of a high-resolution temporal baseline that can be used to evaluate changes in these springs in the future. Furthermore, these results also provide a framework to examine links between temporal changes in hydrochemistry and temporal changes microbial community composition.

6.7 References

- Abbott, M. D., Lini, A., & Bierman, P. R. (2000). $\delta^{18}\text{O}$, δD and ^3H measurements constrain groundwater recharge patterns in an upland fractured bedrock aquifer, Vermont, USA. *Journal of Hydrology*, 228(1-2), 101-112.
- Ahearn, D. S., Sheibley, R. W., Dahlgren, R. A., & Keller, K. E. (2004). Temporal dynamics of stream water chemistry in the last free-flowing river draining the western Sierra Nevada, California. *Journal of Hydrology*, 295(1-4), 47-63.
- Al-Charideh, A. (2011). Environmental isotope study of groundwater discharge from the large karst springs in West Syria: a case study of Figeih and Al-sin springs. *Environmental Earth Sciences*, 63(1), 1-10.

- Arndt, J. L., & Richardson, J. L. (1993). Temporal variations in the salinity of shallow groundwater from the periphery of some North Dakota wetlands (USA). *Journal of Hydrology*, 141(1-4), 75-105.
- Barbieri, M., Boschetti, T., Petitta, M., & Tallini, M. (2005). Stable isotope (^2H , ^{18}O and $^{87}\text{Sr}/^{86}\text{Sr}$) and hydrochemistry monitoring for groundwater hydrodynamics analysis in a karst aquifer (Gran Sasso, Central Italy). *Applied Geochemistry*, 20(11), 2063-2081.
- Belcher, W. R., Bedinger, M. S., Back, J. T., & Sweetkind, D. S. (2009). Interbasin flow in the Great Basin with special reference to the southern Funeral Mountains and the source of Furnace Creek springs, Death Valley, California, US. *Journal of Hydrology*, 369(1-2), 30-43.
- Bishop, K., Seibert, J., Köhler, S., & Laudon, H. (2004). Resolving the double paradox of rapidly mobilized old water with highly variable responses in runoff chemistry. *Hydrological Processes*, 18(1), 185-189.
- Blake, S., Henry, T., Murray, J., Flood, R., Muller, M. R., Jones, A. G., & Rath, V. (2016). Compositional multivariate statistical analysis of thermal groundwater provenance: a hydrogeochemical case study from Ireland. *Applied Geochemistry*, 75, 171-188.
- Blum, J. D., Erel, Y., & Brown, K. (1993). $^{87}\text{Sr}/^{86}\text{Sr}$ ratios of Sierra Nevada stream waters: Implications for relative mineral weathering rates. *Geochimica et Cosmochimica Acta*, 57(21-22), 5019-5025.
- Bond, B. J., Jones, J. A., Moore, G., Phillips, N., Post, D., & McDonnell, J. J. (2002). The zone of vegetation influence on baseflow revealed by diel patterns of streamflow and vegetation water use in a headwater basin. *Hydrological Processes*, 16(8), 1671-1677.
- Brumm, M., Wang, C. Y., & Manga, M. (2009). Spring temperatures in the Sagehen Basin, Sierra Nevada, CA: implications for heat flow and groundwater circulation. *Geofluids*, 9(3), 195-207.
- Bushman, M., Nelson, S. T., Tingey, D., & Eggett, D. (2010). Regional groundwater flow in structurally-complex extended terranes: an evaluation of the sources of discharge at Ash Meadows, Nevada. *Journal of Hydrology*, 386(1-4), 118-129.
- Cendón, D. I., Hankin, S. I., Williams, J. P., Van der Ley, M., Peterson, M., Hughes, C. E., ... & Chisari, R. (2014). Groundwater residence time in a dissected and weathered sandstone plateau: Kulnura–Mangrove Mountain aquifer, NSW, Australia. *Australian Journal of Earth Sciences*, 61(3), 475-499.
- Chapman, J. B., Ducea, M. N., DeCelles, P. G., & Profeta, L. (2015). Tracking changes in crustal thickness during orogenic evolution with Sr/Y: An example from the North American Cordillera. *Geology*, 43(10), 919-922.
- Clow, D. W., Mast, M. A., Bullen, T. D., & Turk, J. T. (1997). Strontium 87 /strontium 86 as a tracer of mineral weathering reactions and calcium sources in an alpine/subalpine watershed, Loch Vale, Colorado. *Water Resources Research*, 33(6), 1335-1351.

- Craig, H. (1961). Isotopic variations in meteoric waters. *Science*, 133(3465), 1702-1703.
- Crowther, J., & Pitty, A. F. (1982). Water temperature variability as an indicator of shallow-depth groundwater behaviour in limestone areas in West Malaysia. *Journal of Hydrology*, 57(1-2), 137-146.
- Cuthbert, M. O., Gleeson, T., Moosdorf, N., Befus, K. M., Schneider, A., Hartmann, J., & Lehner, B. (2019). Global patterns and dynamics of climate-groundwater interactions. *Nature Climate Change*, 9(2), 137-141.
- Davis, G. H., Lee, C. K., Bradley, E., & Payne, B. R. (1970). Geohydrologic interpretations of a volcanic island from environmental isotopes. *Water Resources Research*, 6(1), 99-109.
- Davisson, M. L., & Criss, R. E. (1993). Stable isotope imaging of a dynamic groundwater system in the southwestern Sacramento Valley, California, USA. *Journal of Hydrology*, 144(1-4), 213-246.
- Davraz, A., Sener, E., & Sener, S. (2008). Temporal variations of fluoride concentration in Isparta public water system and health impact assessment (SW-Turkey). *Environmental Geology*, 56(1), 159-170.
- Dreher, T. (2003). Comment on Güler C, Thyne GD, McCray JE, Turner AK (2002): Evaluation of graphical and multivariate statistical methods for classification of water chemistry data (Hydrogeology Journal 10: 455-474). *Hydrogeology Journal*, 11(5), 605-606.
- Eltahir, E. A., & Yeh, P. J. F. (1999). On the asymmetric response of aquifer water level to floods and droughts in Illinois. *Water Resources Research*, 35(4), 1199-1217.
- Engel, M., Penna, D., Bertoldi, G., Vignoli, G., Tirler, W., & Comiti, F. (2019). Controls on spatial and temporal variability of streamflow and hydrochemistry in a glacierized catchment. *Hydrology and Earth System Sciences*, 23, 2041-2063.
- Erman, N. A., & Erman, D. C. (1995). Spring permanence, Trichoptera species richness, and the role of drought. *Journal of the Kansas Entomological Society*, 50-64.
- Erman, N. A. (2002). Lessons from a long-term study of springs and spring invertebrates (Sierra Nevada, California, USA) and implications for conservation and management. In *Conference proceedings. Springfed Wetlands: Important Scientific and Cultural Resources of the Intermountain Region*, Las Vegas, NV.
- Farnham, I. M., Johannesson, K. H., Singh, A. K., Hodge, V. F., & Stetzenbach, K. J. (2003). Factor analytical approaches for evaluating groundwater trace element chemistry data. *Analytica Chimica Acta*, 490(1-2), 123-138.
- Forster, C., & Smith, L. (1988). Groundwater flow systems in mountainous terrain: 2. Controlling factors. *Water Resources Research*, 24(7), 1011-1023.

- Friedman, I., Harris, J. M., Smith, G. I., & Johnson, C. A. (2002). Stable isotope composition of waters in the Great Basin, United States 1. Air-mass trajectories. *Journal of Geophysical Research: Atmospheres*, 107(D19), ACL-14.
- Friedman, I., Smith, G. I., Johnson, C. A., & Moscati, R. J. (2002). Stable isotope compositions of waters in the Great Basin, United States 2. Modern precipitation. *Journal of Geophysical Research: Atmospheres*, 107(D19), ACL-15.
- Frisbee, M. D., Phillips, F. M., Campbell, A. R., Liu, F., & Sanchez, S. A. (2011). Streamflow generation in a large, alpine watershed in the southern Rocky Mountains of Colorado: Is streamflow generation simply the aggregation of hillslope runoff responses?. *Water Resources Research*, 47(6).
- Frisbee, M. D., Wilson, J. L., & Sada, D. W. (2013). Climate Change and the Fate of Desert Springs: Innovation Working Group on the Response of Springs to the Effects of Climate Change; Jemez Springs, New Mexico, 1–3 October 2102. *Eos, Transactions American Geophysical Union*, 94(15), 144-144.
- Gardner, W. P., Jencso, K., Hoylman, Z. H., & Thiros, N. E. (2018, December). Mountain Water-The Role of Deep Groundwater in Mountain Watersheds. In AGU Fall Meeting Abstracts.
- Gleason, C. L., Frisbee, M. D., Rademacher, L. K., Sada, D. W., & Meyers, Z. P. (2020). Hydrogeology of desert springs in the Panamint Range, California, USA: Identifying the sources and amount of recharge that support spring flow. *Hydrological Processes*, 34(3), 730-748.
- Gleason, C. L., Frisbee, M. D., Rademacher, L. K., Sada, D. W., Meyers, Z. P., Knott, J. R., & Hedlund, B. P. (2020). Hydrogeology of desert springs in the Panamint Range, California, USA: Geologic controls on the geochemical kinetics, flowpaths, and mean residence times of springs. *Hydrological Processes*.
- Graham, C. B., Barnard, H. R., Kavanagh, K. L., & McNamara, J. P. (2013). Catchment scale controls the temporal connection of transpiration and diel fluctuations in streamflow. *Hydrological Processes*, 27(18), 2541-2556.
- Griffin, D., & Anchukaitis, K. J. (2014). How unusual is the 2012–2014 California drought?. *Geophysical Research Letters*, 41(24), 9017-9023.
- Halford, K. J., & Jackson, T. R. (2020). Groundwater characterization and effects of pumping in the Death Valley regional groundwater flow system, Nevada and California, with special reference to Devils Hole (No. 1863). US Geological Survey.
- Hem, J. D. (1985). Study and interpretation of the chemical characteristics of natural water (Vol. 2254). Department of the Interior, US Geological Survey.
- Hirt, W. H. (2007). Petrology of the Mount Whitney Intrusive Suite, eastern Sierra Nevada, California: Implications for the emplacement and differentiation of composite felsic intrusions. *Geological Society of America Bulletin*, 119(9-10), 1185-1200.

- Hogg, I. D., & Williams, D. D. (1996). Response of stream invertebrates to a global-warming thermal regime: An ecosystem-level manipulation. *Ecology*, 77(2), 395-407.
- Ingraham, N. L., & Taylor, B. E. (1991). Light stable isotope systematics of large-scale hydrologic regimes in California and Nevada. *Water Resources Research*, 27(1), 77-90.
- Iqbal, M. Z., Krothe, N. C., & Spalding, R. F. (1997). Nitrogen isotope indicators of seasonal source variability to groundwater. *Environmental Geology*, 32(3), 210-218.
- Irons, J. G., & Oswood, M. W. (1992). Seasonal temperature patterns in an arctic and two subarctic Alaskan (USA) headwater streams. *Hydrobiologia*, 237(3), 147-157.
- Jeelani, G. H., Bhat, N. A., & Shivanna, K. (2010). Use of $\delta^{18}\text{O}$ tracer to identify stream and spring origins of a mountainous catchment: A case study from Liddar watershed, Western Himalaya, India. *Journal of Hydrology*, 393(3-4), 257-264.
- Jeelani, G., Kumar, U. S., Bhat, N. A., Sharma, S., & Kumar, B. (2015). Variation of $\delta^{18}\text{O}$, δD and 3H in karst springs of south Kashmir, western Himalayas (India). *Hydrological Processes*, 29(4), 522-530.
- Jiang, Y. (2011). Strontium isotope geochemistry of groundwater affected by human activities in Nandong underground river system, China. *Applied Geochemistry*, 26(3), 371-379.
- Johannesson, K. H., Stetzenbach, K. J., Hodge, V. F., Kreamer, D. K., & Zhou, X. (1997). Delineation of Ground-Water Flow Systems in the Southern Great Basin Using Aqueous Rare Earth Element Distributions. *Groundwater*, 35(5), 807-819.
- Johnson, N. M., Likens, G. E., Bormann, F. H., Fisher, D. W., & Pierce, R. S. (1969). A working model for the variation in stream water chemistry at the Hubbard Brook Experimental Forest, New Hampshire. *Water Resources Research*, 5(6), 1353-1363.
- Johnson, T. M., Roback, R. C., McLing, T. L., Bullen, T. D., DePaolo, D. J., Doughty, C., ... & Murrell, M. T. (2000). Groundwater "fast paths" in the Snake River Plain aquifer: Radiogenic isotope ratios as natural groundwater tracers. *Geology*, 28(10), 871-874.
- Kattan, Z. (1997). Environmental isotope study of the major karst springs in Damascus limestone aquifer systems: case of the Figeih and Barada springs. *Journal of Hydrology*, 193(1-4), 161-182.
- Keery, J., Binley, A., Crook, N., & Smith, J. W. (2007). Temporal and spatial variability of groundwater-surface water fluxes: development and application of an analytical method using temperature time series. *Journal of Hydrology*, 336(1-2), 1-16.
- Kirchner, J. W. (2003). A double paradox in catchment hydrology and geochemistry. *Hydrological Processes*, 17(4), 871-874.
- Kreamer, D. K., Hodge, V. F., Rabinowitz, I., Johannesson, K. H., & Stetzenbach, K. J. (1996). Trace element geochemistry in water from selected springs in Death Valley National Park, California. *Groundwater*, 34(1), 95-103.

- Li, B., Rodell, M., & Famiglietti, J. S. (2015). Groundwater variability across temporal and spatial scales in the central and northeastern US. *Journal of Hydrology*, 525, 769-780.
- Lin, C. Y., Abdullah, M. H., Praveena, S. M., Yahaya, A. H. B., & Musta, B. (2012). Delineation of temporal variability and governing factors influencing the spatial variability of shallow groundwater chemistry in a tropical sedimentary island. *Journal of Hydrology*, 432, 26-42.
- Liñán Baena, C. L., Andreo, B., Mudry, J., & Cantos, F. C. (2009). Groundwater temperature and electrical conductivity as tools to characterize flow patterns in carbonate aquifers: The Sierra de las Nieves karst aquifer, southern Spain. *Hydrogeology Journal*, 17(4), 843-853.
- Liu, X., Song, X., Zhang, Y., Xia, J., Zhang, X., Yu, J., ... & Zhang, B. (2011). Spatio-temporal variations of $\delta^2\text{H}$ and $\delta^{18}\text{O}$ in precipitation and shallow groundwater in the Hilly Loess Region of the Loess Plateau, China. *Environmental Earth Sciences*, 63(5), 1105-1118.
- Manga, M. (1999). On the timescales characterizing groundwater discharge at springs. *Journal of Hydrology*, 219(1-2), 56-69.
- Manga, M. (2001). Using springs to study groundwater flow and active geologic processes. *Annual Review of Earth and Planetary Sciences*, 29(1), 201-228.
- Majumdar, N., Majumdar, R. K., Mukherjee, A. L., Bhattacharya, S. K., & Jani, R. A. (2005). Seasonal variations in the isotopes of oxygen and hydrogen in geothermal waters from Bakreswar and Tantloi, Eastern India: implications for groundwater characterization. *Journal of Asian Earth Sciences*, 25(2), 269-278.
- Manning, A. H., Clark, J. F., Diaz, S. H., Rademacher, L. K., Earman, S., & Plummer, L. N. (2012). Evolution of groundwater age in a mountain watershed over a period of thirteen years. *Journal of Hydrology*, 460, 13-28.
- Maulé, C. P., Chanasyk, D. S., & Muehlenbachs, K. (1994). Isotopic determination of snow-water contribution to soil water and groundwater. *Journal of Hydrology*, 155(1-2), 73-91.
- Mayer, J. (1999). Spatial and temporal variation of groundwater chemistry in Pettyjohns Cave, northwest Georgia, USA. *Journal of Cave and Karst Studies*, 61(3), 131-138.
- McCabe, D. J. (1998). Biological communities in springbrooks. Studies in crenobiology. The biology of springs and springbrooks. Backhuys Publishers, Leiden, The Netherlands, 221-228.
- Moreo, M. T., Senay, G. B., Flint, A. L., Damar, N. A., Lacznia, R. J., & Hurja, J. (2014). Hydroclimate of the Spring Mountains and Sheep Range, Clark County, Nevada. US Geological Survey, Scientific Investigations Report, 5142.
- Mote, P. W., Rupp, D. E., Li, S., Sharp, D. J., Otto, F., Uhe, P. F., ... & Allen, M. R. (2016). Perspectives on the causes of exceptionally low 2015 snowpack in the western United States. *Geophysical Research Letters*, 43(20), 10-980.

- Morvan, X., Mouvet, C., Baran, N., & Gutierrez, A. (2006). Pesticides in the groundwater of a spring draining a sandy aquifer: temporal variability of concentrations and fluxes. *Journal of Contaminant Hydrology*, 87(3-4), 176-190.
- Musgrove, M., & Banner, J. L. (2004). Controls on the spatial and temporal variability of vadose dripwater geochemistry: Edwards Aquifer, central Texas. *Geochimica et Cosmochimica Acta*, 68(5), 1007-1020.
- Musgrove, M., Stern, L. A., & Banner, J. L. (2010). Springwater geochemistry at Honey Creek State Natural Area, central Texas: Implications for surface water and groundwater interaction in a karst aquifer. *Journal of Hydrology*, 388(1-2), 144-156.
- Nagorski, S. A., Moore, J. N., McKinnon, T. E., & Smith, D. B. (2003). Geochemical response to variable streamflow conditions in contaminated and uncontaminated streams. *Water Resources Research*, 39(2).
- Peterman, Z. E., Stuckless, J. S., Mahan, S. A., Marshall, B. D., Gutentag, E. D., & Downey, J. S. (1992). Strontium isotope characterization of the Ash Meadows ground-water system, southern Nevada, USA (No. CONF-920761-Vol. 1). AA Balkema, Rotterdam (Netherlands).
- O'Driscoll, M. A., DeWalle, D. R., McGuire, K. J., & Gburek, W. J. (2005). Seasonal ^{18}O variations and groundwater recharge for three landscape types in central Pennsylvania, USA. *Journal of Hydrology*, 303(1-4), 108-124.
- Ozyurt, N. N. (2008). Analysis of drivers governing temporal salinity and temperature variations in groundwater discharge from Altug Submarine Karst Cave (Kas-Turkey). *Environmental Geology*, 54(4), 731-736.
- Paces, J. B., Peterman, Z. E., Futa, K., Oliver, T. A., & Marshall, B. D. (2007). Strontium Isotopic Composition of Paleozoic Carbonate Rocks in the Nevada Test Site Vicinity, Clark, Lincoln, and Nye Counties, Nevada and Inyo County, California (No. ds 2007 280). United States Geological Survey-Nevada, Henderson, Nevada.
- Pauwels, H., Lachassagne, P., Bordenave, P., Foucher, J. C., & Martelat, A. (2001). Temporal variability of nitrate concentration in a schist aquifer and transfer to surface waters. *Applied Geochemistry*, 16(6), 583-596.
- Penna, D., Engel, M., Mao, L., Dell'Agnese, A., Bertoldi, G., & Comiti, F. (2014). Tracer-based analysis of spatial and temporal variations of water sources in a glacierized catchment. *Hydrology and Earth System Sciences*, 18(12), 5271-5288.
- Pinder, G. F., & Jones, J. F. (1969). Determination of the ground-water component of peak discharge from the chemistry of total runoff. *Water Resources Research*, 5(2), 438-445.
- Plummer, L. N., Busenberg, E., Böhlke, J. K., Nelms, D. L., Michel, R. L., & Schlosser, P. (2001). Groundwater residence times in Shenandoah National Park, Blue Ridge Mountains, Virginia, USA: a multi-tracer approach. *Chemical Geology*, 179(1-4), 93-111.

- Pretti, V. A., & Stewart, B. W. (2002). Solute sources and chemical weathering in the Owens Lake watershed, eastern California. *Water Resources Research*, 38(8), 2-1.
- Rademacher, L. K., Clark, J. F., & Hudson, G. B. (2002). Temporal changes in stable isotope composition of spring waters: implications for recent changes in climate and atmospheric circulation. *Geology*, 30(2), 139-142.
- Resh, V. H. (1983). Spatial differences in the distribution of benthic macroinvertebrates along a springbrook. *Aquatic Insects*, 5(4), 193-200.
- Rossini, R. A., Tibbetts, H. L., Fensham, R. J., & Walter, G. H. (2017). Can environmental tolerances explain convergent patterns of distribution in endemic spring snails from opposite sides of the Australian arid zone?. *Aquatic Ecology*, 51(4), 605-624.
- Sada, D. W., & Herbst, D. B. (2001). Macroinvertebrates and environmental characteristics of Owens Valley springs, Inyo County, California. Bishop: City of Los Angeles Department of Water and Power.
- Sada, D. W., & Pohlmann, K. F. (2007). Environmental and Biological Characteristics of Springs in Death Valley National Park, California. Unpublished report to US National Park Service, Mojave Inventory and Monitoring Network, Boulder City, NV.
- Scheytt, T. (1997). Seasonal Variations in Groundwater Chemistry Near Lake Belau, Schleswig-Holstein, Northern Germany. *Hydrogeology Journal*, 5(2), 86-95.
- Shuster, E. T., & White, W. B. (1971). Seasonal fluctuations in the chemistry of lime-stone springs: A possible means for characterizing carbonate aquifers. *Journal of Hydrology*, 14(2), 93-128.
- Singleton, M. J., & Moran, J. E. (2010). Dissolved noble gas and isotopic tracers reveal vulnerability of groundwater in a small, high-elevation catchment to predicted climate changes. *Water Resources Research*, 46(10).
- Smith, G. I., Friedman, I., Klieforth, H., & Hardcastle, K. (1979). Areal distribution of deuterium in eastern California precipitation, 1968–1969. *Journal of Applied Meteorology*, 18(2), 172-188.
- Smith, G. I., Friedman, I., Veronda, G., & Johnson, C. A. (2002). Stable isotope compositions of waters in the Great Basin, United States 3. Comparison of groundwaters with modern precipitation. *Journal of Geophysical Research: Atmospheres*, 107(D19), ACL-16.
- Soulsby, C., Chen, M., Ferrier, R. C., Helliwell, R. C., Jenkins, A., & Harriman, R. (1998). Hydrogeochemistry of shallow groundwater in an upland Scottish catchment. *Hydrological Processes*, 12(7), 1111-1127.
- Springer, A. (2015, February 20). Springs: The Canary in a Coal Mine for Groundwater. *National Geographic Society Newsroom*. <https://blog.nationalgeographic.org/2015/02/20/springs-the-canary-in-a-coal-mine-for-groundwater/>

- Springer, A. E., & Stevens, L. E. (2009). Spheres of discharge of springs. *Hydrogeology Journal*, 17(1), 83.
- Stetzenbach, K. J., Farnham, I. M., Hodge, V. F., & Johannesson, K. H. (1999). Using multivariate statistical analysis of groundwater major cation and trace element concentrations to evaluate groundwater flow in a regional aquifer. *Hydrological Processes*, 13(17), 2655-2673.
- Stewart-Maddox, N. S., Frisbee, M. D., Andronicos, C. L., Genereux, D. P., & Meyers, Z. P. (2018). Identifying the regional extent and geochemical evolution of interbasin groundwater flow using geochemical inverse modeling and $^{87}\text{Sr}/^{86}\text{Sr}$ ratios in a complex conglomeratic aquifer. *Chemical Geology*, 500, 20-29.
- Suursoo, S., Hill, L., Raidla, V., Kiisk, M., Jantsikene, A., Nilb, N., ... & Isakar, K. (2017). Temporal changes in radiological and chemical composition of Cambrian-Vendian groundwater in conditions of intensive water consumption. *Science of The Total Environment*, 601, 679-690.
- Swanson, S. K., Bahr, J. M., Schwar, M. T., & Potter, K. W. (2001). Two-way cluster analysis of geochemical data to constrain spring source waters. *Chemical Geology*, 179(1-4), 73-91.
- Tallini, M., Parisse, B., Petitta, M., & Spizzico, M. (2013). Long-term spatio-temporal hydrochemical and ^{222}Rn tracing to investigate groundwater flow and water-rock interaction in the Gran Sasso (Central Italy) carbonate aquifer. *Hydrogeology Journal*, 21(7), 1447-1467.
- Tan, H., Wen, X., Rao, W., Bradd, J., & Huang, J. (2016). Temporal variation of stable isotopes in a precipitation-groundwater system: implications for determining the mechanism of groundwater recharge in high mountain-hills of the Loess Plateau, China. *Hydrological Processes*, 30(10), 1491-1505.
- Templ, M., Filzmoser, P., & Reimann, C. (2008). Cluster analysis applied to regional geochemical data: problems and possibilities. *Applied Geochemistry*, 23(8), 2198-2213.
- Tichomirowa, M., Heidel, C., Junghans, M., Haubrich, F., & Matschullat, J. (2010). Sulfate and strontium water source identification by O, S and Sr isotopes and their temporal changes (1997–2008) in the region of Freiberg, central-eastern Germany. *Chemical Geology*, 276(1-2), 104-118.
- Tóth, J. (1999). Groundwater as a geologic agent: an overview of the causes, processes, and manifestations. *Hydrogeology Journal*, 7(1), 1-14.
- Unland, N. P., Cartwright, I., Rau, G. C., Reed, J., Gilfedder, B. S., Atkinson, A. P., & Hofmann, H. (2013). Investigating the spatio-temporal variability in groundwater and surface water interactions: a multi-technique approach. *Hydrology and Earth System Sciences*, 17(9), 3437.
- Van der Hoven, S. J., Solomon, D. K., & Moline, G. R. (2005). Natural spatial and temporal variations in groundwater chemistry in fractured, sedimentary rocks: scale and implications for solute transport. *Applied Geochemistry*, 20(5), 861-873.
- Walker, J. F., Hunt, R. J., Bullen, T. D., Krabbenhoft, D. P., & Kendall, C. (2003). Variability of isotope and major ion chemistry in the Allequash Basin, Wisconsin. *Groundwater*, 41(7), 883-894.

- Warix, S. R., Rademacher, L. K., Meyers, Z. P., & Frisbee, M. D. (2020). Groundwater geochemistry and flow in the Spring Mountains, NV: Implications for the Death Valley Regional Flow System. *Journal of Hydrology*, 580, 124313.
- Wasserburg, G. J., Wetherill, G. W., & Wright, L. A. (1959). Ages in the precambrian terrane of Death Valley, California. *The Journal of Geology*, 67(6), 702-708.
- Wasserburg, G. J., Albee, A. L., & Lanphere, M. A. (1964). Migration of radiogenic strontium during metamorphism. *Journal of Geophysical Research*, 69(20), 4395-4401.
- Wilson, J. L., & Guan, H. (2004). Mountain-block hydrology and mountain-front recharge. Groundwater recharge in a desert environment: The Southwestern United States, 9.
- Winograd, I. J., & Friedman, I. (1972). Deuterium as a tracer of regional ground-water flow, southern Great Basin, Nevada and California. *Geological Society of America Bulletin*, 83(12), 3691-3708.
- Winograd, I. J., & Thordarson, W. (1975). Hydrogeologic and hydrochemical framework, south-central Great Basin, Nevada-California, with special reference to the Nevada Test Site.
- Winograd, I. J., Riggs, A. C., & Coplen, T. B. (1998). The relative contributions of summer and cool-season precipitation to groundwater recharge, Spring Mountains, Nevada, USA. *Hydrogeology Journal*, 6(1), 77-93.
- Wright, S. N., & Novakowski, K. S. (2019). Groundwater recharge, flow and stable isotope attenuation in sedimentary and crystalline fractured rocks: Spatiotemporal monitoring from multi-level wells. *Journal of Hydrology*, 571, 178-192.

CHAPTER 7. CONCLUSIONS AND RECOMMENDATIONS

7.1 Epilogue

In this dissertation I investigated a series of observable metrics (i.e., hydrogeologic, geochemical, and geomorphic, and ecological) in an attempt to quantify the *resistance* and/or *resilience* of desert springs in the southern Great Basin to perturbations related to climate change. In this investigation I examined which of these metrics are inherently linked, at what point do these relationships fail, and, which springs are the most vulnerable (e.g., lack resistance and/or resilience) hydrologically and ecologically (or both)? The following chapters were only possible due to collaborative, interdisciplinary sampling efforts of desert springs across a vast topographic gradient in the southern Great Basin.

In Chapter 2, I addressed a potential problem with the prevalent, most widely used workflow for generating geochemical clusters from major cation and anion data. In this chapter, I offer an alternative preprocessing methodology that combats some of the flaws of the “traditional preprocessing methodology” and may be more suitable for certain geochemical applications depending of the goals of the analyst. This chapter provides a methodology that is useful for linking hydrochemical patterns with ecological data.

In Chapter 3, I test, using field data, whether “old” groundwater can provide buffering to the immediate effects of climate change using a novel combination of remote sensing and groundwater residence time data. This chapter addresses the short-term resistance of springs and provides a potential avenue to investigate the subsequent resilience, or recovery, of groundwater-dependent ecosystems from the 2011-2017 California drought.

In Chapter 4, I use a multitracer approach to extend the classic works of Feth et al. (1964) and Garrels and Mackenzie (1967) from local to intermediate scales by investigating mountain front springs emerging along the eastern slope of the Sierra Nevada in Owens Valley (CA). This chapter explicitly tests whether a simple geochemical measurement such as electrical conductivity can be used as an indicator of groundwater residence time in a *relatively* geologically homogenous region (i.e., the Sierra Nevada Batholith). Additionally, work from this chapter provides the framework for Pordel et al. (*in prep.*) to test relationships with benthic macroinvertebrate

community structure and geochemistry at local to intermediate scales (i.e., a limited range in environmental characteristic such as EC and temperature).

In Chapter 5, I consider the role of spring landscape position, a combination of topographic position and landform type, and spring emergence mechanism as predictors of spring hydrochemical characteristics and ecological community structure. In this chapter I concatenated a large dataset from numerous studies on springs that have been conducted in the study area in order to: 1) examine regional spring hydrochemical patterns across a topographically, geologically, and structurally complex landscape and 2) shed light on a major knowledge gap, the factors controlling BMI community structure at the regional scale.

In Chapter 6, I investigate the temporal variability of springs sampled multiple times from 2016-2019. This chapter examines if dampened temporal variability across multiple geochemical analytes is indicative of metrics associated with hydrological stability (e.g., increased groundwater temperature, salinity, and residence time).

7.2 Synthesis and Recommendations

Springs in arid regions are often the only permanent sources of surface flow. As such, springs serve critical needs economically, recreationally, and, perhaps most importantly, ecologically. Springs have been described as “keystone features” (Perla and Stevens, 2008; Freed et al., 2019) and “aquatic archipelagos” (Minckley and Deacon, 1968; Unmack and Minckley, 2008) due to their immense ecological worth relative to their relatively small footprint on the land surface and “keystone features”. Unfortunately, desert springs and the ecological communities they support are threatened due to disturbance, groundwater extraction, and climate change. Increasing temperatures and decreasing annual snowpack in the southern Great Basin of the United States are currently being observed and are projected to worsen in the future as a consequence of climate change. However, in comparison to other groundwater-sourced features, e.g., wetlands or streamflow generation in mountainous settings, springs have been disproportionately ignored in the literature relative to their hydrological and ecological worth. Currently, there is not set of overarching metrics applied to springs that can potentially describe their vulnerability or relationship to characteristics indicative of vulnerability (e.g., groundwater residence time). This study addresses major knowledge gaps surrounding the vulnerability of aridland springs by 1) identifying several factors indicative of spring resistance, 2) identifying correlation factors

between different metrics, and 3) identifying types of springs that are potentially hydrologically or ecologically vulnerable.

7.2.1 Alternative preprocessing methodology for geochemical clustering

The “alternative data preprocessing” methodology presented in this study (Chapter 2) aims to combat weaknesses in the commonly used “traditional data preprocessing” methodology (e.g., Güler et al., 2002; Thyne et al., 2004; Güler and Thyne, 2004) used to generate geochemical clusters from major cation and anion data. For example, the “traditional data preprocessing” methodology tends to produce geochemical clusters more attuned to tracking changes in salinity rather than patterns of rock-water interaction. While both Dreher (2003) and Templ et al. (2008) raised potential concerns regarding the use of sequential workflows for generating geochemical clusters without a close examination of aquifer geology and geochemical kinetics, there have been few attempts to develop an alternative approach. The “alternative data preprocessing” methodology presented in this study utilizes the strengths of graphical approaches for analyzing major ion data and applies them in a hierarchical clustering analysis (HCA) for two case studies: 1) Owens Valley (CA) and 2) the Spring Mountains (NV). Compared with results obtained using the “traditional data preprocessing” methodology, results obtained from the methodology presented in this study more closely match prior conceptual models of groundwater evolution in specific geologic units (e.g., Warix et al., 2020). However, this work does not discount the work of Güler et al. (2002), Thyne et al., (2004), or Güler and Thyne, (2004). The “traditional preprocessing methodology” is likely more desirable in studies of water quality or regional evolution where the analyst is more interested in tracking changes in salinity. Use of the “alternative preprocessing” methodology is recommended in instances where the analyst is interested in tracking patterns of geochemical evolution through specific units (i.e., “geochemical fingerprints”). Development of this clustering method has helped to assist with other aspects of this project by providing geochemical groupings based on rock-water interaction that can be related back to ecological community structure (e.g., Pordel et al., *in prep*).

7.2.2 Metrics that describe spring resistance

In this part of my dissertation (Chapter 3), I utilized a novel combination of remote sensing and residence time data to evaluate spring hydroecological resistance to a historic drought and its relation to groundwater residence time. One conceptual model states that if a flowpath distribution supplying flow to a groundwater discharge location contains a substantial component of old groundwater (i.e., long residence-time groundwater), then this component will provide buffering to the effects of perturbations (e.g., major droughts) such that the effects may not immediately be felt. Conversely, this conceptual model also suggests that if a flowpath distribution contains a substantial component of young groundwater, then the effects of the perturbation may propagate more rapidly to the groundwater discharge point. In the case of groundwater-dependent ecosystems in the southern Great Basin, vibrant, green vegetation exists at groundwater discharge points that strongly contrasts with the surrounding landscape. Therefore, because testing of this conceptual model with field data is strongly lacking, I wanted to evaluate whether the responses of spring-dependent vegetation to a historic drought: 1) could provide a proxy for the overall hydrogeologic resistance of a spring, and 2) could be predicted by spring residence times.

Our results showed that springs discharging a substantial portion of old groundwater had resistant groundwater-dependent vegetation and possible desiccation over the course of the drought. In contrast, springs discharging a large portion of bomb-pulse or modern groundwater showed decreases in the health of groundwater-dependent vegetation. The results of this study have both theoretical and applied applications. The results from this chapter provide credence to the conceptual model and provide some of the first field evidence showing that a flowpath distribution consisting of old, stable groundwater flowpaths provides buffering to the immediate effects of climate change. Furthermore, the methodology presented in this study provides a remote sensing-based approach, provided the right conditions are met, to evaluate the health and/or hydrologic stability of groundwater-dependent ecosystems

The results of this study provide one major path for future work. While this study focuses on the hydroecological resistance of springs, the region underwent a rapid drought recovery following a record snowpack in 2017. Now that an appreciable amount of time has passed since the end of the drought, one could evaluate the vegetation recovery (or lack thereof) of spring-dependent vegetation. This type of analysis would allow for the evaluation of spring

hydrogeological resilience, or the ability of these systems to recover following a perturbation such as a major drought.

7.2.3 Metrics that are related to groundwater residence time

Following the results of Chapter 2 indicating that a significant component of old groundwater provides substantial buffering to the immediate effects of climate change, the next set of chapters aimed to find metrics associated with or correlated to groundwater residence time. Measurements of groundwater residence time are expensive and often require certain flow characteristics and emergence criteria for sampling.

7.2.3.1 Extending Feth et al. (1964) and Garrels and Mackenzie (1967)

In Chapter 3, I rigorously tested a commonly inferred relationship from the seminal work from Feth (1964) and Garrels and Mackenzie (1967), conducted at high elevation, local scales in the Sierra Nevada. The goal of this project was to investigate if a simple metric like electrical conductivity can serve as a proxy for groundwater residence time at intermediate flowpath lengths. This work was accomplished using a multi-tracer approach on mountain front springs primarily emerging on the frontal fault zone of the eastern Sierra Nevada in Owens Valley (CA). I used stable isotopes and noble gas recharge indicators to roughly delineate spring contributing areas and to identify the geologic units mostly likely supplying recharge contributing to spring discharge. Spring geochemistry and subsequent inverse geochemical models were used to understand the dominant weathering reactions contributing to spring geochemical compositions. A combination of environmental tracers (e.g., ^3H , $^{36}\text{Cl}/\text{Cl}$, $^3\text{H}-^3\text{He}$, $^3\text{He}/^4\text{He}$, and ^{14}C) were used to understand the groundwater flowpath distributions supporting springflow.

The results of this study showed that, even in a relatively geologically homogenous terrain like the Sierra Nevada batholith, the principal factor driving geochemical evolution with increased scale (i.e., distance, flowpath length, and residence time) is geologic heterogeneity. While this does not preclude the use of a simple metric like conductivity to make inferences about groundwater residence time, either the right conditions (i.e., a narrow range of petrologic compositions) should be met or derived results (e.g., mol transfers from inverse geochemical models) should be used. For example, springs reflecting a mixture of geochemical evolution

primarily through quartz monzonite/granodiorite and Penn-Permian metasedimentary roof pendants displayed a pattern of increasing conductivity (and geochemical fingerprint) and temperature with increasing residence time. Another contribution of this chapter was that disseminated calcite within granitic plutons constitutes a major component of solute fluxes out of granitic watersheds, not just in shallow groundwater, surface water (Pretti and Stewart, 2002), and glaciated catchments (Blum et al., 1994; Blum et al., 1998), but in deeper groundwater discharging at intermediate and regional flowpath lengths.

7.2.3.2 Spring landscape position and emergence mechanism

In Chapter 4, I investigated the role of spring landscape placement (i.e., topographic position and landform) as a predictor of spring hydrochemical characteristics and benthic macroinvertebrate (BMI) community structure across the high relief and regionally extended terrain of the southern Great Basin. This was accomplished by first creating a regional hydrochemical dataset of springs within the study area from governmental agency reports and databases, consultant reports, and academic studies from scientific journals and university dissertations. This dataset was utilized to test relationships of spring landscape placement and hydrochemical characteristics using qualitative topographic classifications and topographic indices (e.g., elevation, slope, Topographic Wetness Index, profile curvature, and relative elevation) derived from digital elevation models. Hydrochemical data from recent sampling efforts were examined against the regional dataset to determine if springs sampled for BMI were representative of the regional hydrochemical variance. Nonmetric multidimensional scaling (NMDS) analysis was used to examine patterns of benthic community composition in undisturbed or reference isolated desert springs. Ecological indices were calculated from BMI data to examine patterns of richness, diversity, and tolerance across the study area.

Our results showed that there are systematic relationships with spring landscape placement and hydrochemical characteristics, i.e., moving from high topographic positions (e.g., Nival & High Mountain) to lower topographic positions (e.g., Low Mountain & Valley Floor) there are clear patterns of increasing discharge temperature, groundwater salinity, and groundwater residence time. This continuum does not extend to springs emerging in “Playa” settings, where there is a significant increase in groundwater salinity, a decrease in discharge temperature, and a decrease in groundwater residence time from springs emerging in “Valley Floor” settings. This

environmental harshness gradient corresponds to increasing benthic macroinvertebrate community tolerance, decreasing richness, and decreasing diversity from high topographic positions to low topographic positions. This work corroborates prior work by Sada and Thomas (2015) purporting the influence of hydrogeology and landscape setting in controlling BMI community structure. The fact that our work shows opposing controls on BMI community structure compared with studies conducted at local scales indicates that the factors controlling BMI community structure change with increasing analysis scale. The summation of results from this chapter led to the development of a conceptual model of spring systems in the southern Great Basin.

The results of this chapter provide several future avenues for follow-up work. To start, it would be interesting to test different metrics associated with climate (e.g., precipitation and recharge) and ecology (e.g., distance from treeline, distance from pinyon-juniper ecotone, etc.). While the raw data needed to construct these metrics is not readily available, it is possible these types of analyses could be conducted via remote sensing approaches. Additionally, it would be interesting to focus more on spring emergence mechanism as this study only focused on “fault controlled” or “non-fault controlled” classification and how different types of structural features are informative of hydrochemical characteristics. The geological and structural complexity of this region makes it hard to distinguish spring emergence mechanism using a “big data approach”, however, with careful consideration of each spring I think this could be accomplished. Finally, there is considerable room to investigate other types of benthic community structure on isolated desert springs within the study area, e.g., the factors controlling microbial communities. Future work on these types of knowledge gaps would improve the conceptual model posited in this chapter.

7.2.3.4 Spring temporal variability

In the final chapter of this dissertation (Chapter 6), I investigated the relationship of geochemical temporal variability in springs to groundwater residence time. I wanted to understand whether bomb-pulse groundwater (e.g., 60-70 years) could potentially be distinguished from ancient groundwater (e.g., 4000 year +) on the basis of geochemical variability. In other words, are geochemical signals increasingly dampened (i.e., a dampening continuum) with increasing groundwater residence time? While other studies (e.g., Plummer et al., 2001) have shown that such a continuum exists at smaller spatial scales with younger residence time distributions, this concept

has not been rigorously tested at larger spatial scales with wide ranges in groundwater residence time (e.g., the southern Great Basin). In order to address this knowledge gap, I examined the geochemical variability of springs sampled up to 8 times between 2016-2019. I focused on temporal analysis of spring discharge temperature, major ion concentrations, strontium isotopes, water stable isotopes, and age-dating environmental tracers.

The major finding of this work was that the majority of springs (26/33) were very stable and exhibited no discernable geochemical variability over the sampling interval. We did not find a direct connection between geochemical variability and groundwater residence time other than with springs that incorporate a significant component of modern water into their flowpath distribution. Other types of springs that exhibited increased variability across multiple geochemical metrics were either associated with low discharge, specific spheres of discharge, or associated with spring disturbance that promoted increased variability (e.g., barrel-lined springs). A major implication of this work is the need to decouple ecological vulnerability from hydrogeological vulnerability. Our results show that ecological vulnerability is both a function of hydrogeological variability from subsurface processes and the effect of surface conditions that can be unrelated to groundwater residence time (e.g., discharge rate, sphere of discharge, spring disturbance).

The results of this study provide several potential pathways for future work. First off, a subset of these springs, preferably those with long historical records, should be selected for decadal sampling moving into the future. However, one of the major discussion points of this chapter was that the repeat springs analyzed in this study might not have captured the highest elevation “tail” of the spring distribution within the study area (e.g., Peak Spring or Jail Spring). Therefore, it would be interesting to incorporate repeat analysis of these types of springs and then reexamine the overarching questions of this chapter. Additionally, while BMI samples were not temporally sampled as a part of the IES project due to the destructive effect of BMI sampling on the aquatic community, microbiological samples were collected in tandem with the hydrochemical sampling. It would be very interesting to examine potential connections with geochemical temporal variability and microbial community composition.

7.2.4 An invaluable baseline

A hallmark of this work, and of the greater IES project, is the invaluable dataset created over the last five years. This dataset is unique in its breadth, collaborative efforts, and repeat sampling of hydrochemical analytes and environmental tracers. While a portion of my dissertation highlighted the remarkable hydrochemical stability of springs subjected to repeat sampling from 2016-2019, recent sampling efforts also noted the disappearance or transition from perennial to ephemeral flow of springs in the Spring Mountains, Panamint Range, and White-Inyo Mountains. This work represents a fixed baseline for the hydrogeologic and ecological health of isolated desert springs spanning a wide range of topographic positions and environmental harshness. With the effects of anthropogenically-induced climate change already affecting the region and recent work suggesting that large portions of the western United States are in the midst of a mega-drought (Williams et al., 2020), this baseline will be critical to evaluating the health of mountain-block and valley floor aquifers in the coming decades.

7.2.5 A synthesis of spring vulnerability metrics

The ultimate goal of this dissertation was to test and synthesize a series of metrics to assess spring vulnerability in the southern Great Basin. Based on the results of these chapters, I would expect more vulnerable springs to be associated with high elevation and mid-elevation local-scale springs discharging a substantial portion of bomb-pulse and modern recharge. This type of more vulnerable spring may also be associated with increased annual variability in groundwater-dependent vegetation (e.g., dying/drying susceptibility to droughts), geochemically unevolved discharge, a high relative topographic position and associated characteristics (increased profile concavity and slope), a lack of endemic BMI, and increased temporal geochemical variability. In comparison, our results indicate that hydrogeologically resistant springs may be associated with low mountain, bajada, and valley bottom (valley floor and playa) topographic settings where a significant amount of “old” groundwater (>100 years) or intermediate/regional groundwater flow is being discharged. These discharge zones are often associated with major structural features. This type of more resistant spring may be associated with decreased annual variability in groundwater-dependent vegetation (e.g., dampened vegetation fluctuations in response to multi-year events),

geochemically evolved discharge, a low relative topographic position, endemic or regionally dispersed non-vagile taxa, and decreased temporal geochemical variability.

7.3 References

- Blum, J. D., Erel, Y., & Brown, K. (1993). $^{87}\text{Sr}/^{86}\text{Sr}$ ratios of Sierra Nevada stream waters: Implications for relative mineral weathering rates. *Geochimica et Cosmochimica Acta*, 57(21-22), 5019-5025.
- Blum, J. D., Gazis, C. A., Jacobson, A. D., & Page Chamberlain, C. (1998). Carbonate versus silicate weathering in the Raikhot watershed within the High Himalayan Crystalline Series. *Geology*, 26(5), 411-414.
- Dreher, T. (2003). Comment on Güler C, Thyne GD, McCray JE, Turner AK (2002): Evaluation of graphical and multivariate statistical methods for classification of water chemistry data (Hydrogeology Journal 10: 455–474). *Hydrogeology Journal*, 11(5), 605-606.
- Freed, Z., Aldous, A., & Gannett, M. W. (2019). Landscape controls on the distribution and ecohydrology of central Oregon springs. *Ecohydrology*, 12(2), e2065.
- Garrels, R. M., & Mackenzie, F. T. (1967). Origin of the chemical compositions of some springs and lakes.
- Güler, C., Thyne, G. D., McCray, J. E., & Turner, K. A. (2002). Evaluation of graphical and multivariate statistical methods for classification of water chemistry data. *Hydrogeology Journal*, 10(4), 455-474.
- Güler, C., & Thyne, G. D. (2004). Hydrologic and geologic factors controlling surface and groundwater chemistry in Indian Wells-Owens Valley area, southeastern California, USA. *Journal of Hydrology*, 285(1-4), 177-198.
- Feth, J. H. F., Robertson, C. E., & Polzer, W. L. (1964). *Sources of mineral constituents in water from granitic rocks, Sierra Nevada, California and Nevada* (No. 1535-I). US Govt. Print. Off.,.
- Minckley, W. L., & Deacon, J. E. (1968). Southwestern Fishes and the Enigma of " Endangered Species". *Science*, 159(3822), 1424-1432.
- Perla, B. S., & Stevens, L. E. (2008). Biodiversity and productivity at an undisturbed spring in comparison with adjacent grazed riparian and upland habitats. *Aridland springs in North America: Ecology and conservation*, 230-243.
- Plummer, L. N., Busenberg, E., Böhlke, J. K., Nelms, D. L., Michel, R. L., & Schlosser, P. (2001). Groundwater residence times in shenandoah national park, blue ridge mountains, virginia, usa: a multi-tracer approach. *Chemical Geology*, 179(1-4), 93-111.

Pretti, V. A., & Stewart, B. W. (2002). Solute sources and chemical weathering in the Owens Lake watershed, eastern California. *Water Resources Research*, 38(8), 2-1.

Sada, D. W., Thomas, J. M. (2015). Aquifer provenance, flow pathways, landscape setting and BMI community relationships in Great Basin and Mojave Desert springs, *Nevada Water Resources Association Conference: Reno, NV, December 9, 2015-December 11, 2015*

Templ, M., Filzmoser, P., & Reimann, C. (2008). Cluster analysis applied to regional geochemical data: problems and possibilities. *Applied Geochemistry*, 23(8), 2198-2213.

Thyne, G., Güler, C., & Poeter, E. (2004). Sequential analysis of hydrochemical data for watershed characterization. *Groundwater*, 42(5), 711-723.

Unmack, P. J., & Minckley, W. L. (2008). The demise of desert springs. *Aridland springs in North America: ecology and conservation*. University of Arizona Press, Tucson, 11-34.

Warix, S. R., Rademacher, L. K., Meyers, Z. P., & Frisbee, M. D. (2020). Groundwater geochemistry and flow in the Spring Mountains, NV: Implications for the Death Valley Regional Flow System. *Journal of Hydrology*, 580, 124313.

Williams, A. P., Cook, E. R., Smerdon, J. E., Cook, B. I., Abatzoglou, J. T., Bolles, K., ... & Livneh, B. (2020). Large contribution from anthropogenic warming to an emerging North American megadrought. *Science*, 368(6488), 314-318.